Journal of Applied Mechanics

(Contributions of the ASME Applied Mechanics Division)

Bending of a Semicircular Plate . . . . . D. F. Mester and M. A. Sadowsky 329
Series Solutions for an Infinite Plate With Triangular Inlay . . . . . R. M. Beam-Isenwood 336
On Stresses and Deflections of Rectangular Beams . . . . . B. A. Boley and I. S. Tolins 339
Orthotropically Stiffened Plates . . . W. H. Hoppmann, 2nd, N. J. Huffington, Jr., and L. S. Magness 343
On the Strength of Thin-Walled Cylinders . . . . . G. D. Gallesty and E. Reed 351
Bending of Rectangular Plates . . . . . P. Shahabbi 359
On Loss of Excursion in Flexural Vibrations of Rings . . . . . L. L. Philipson 364
Wave Propagation in Ring Springs . . . . . E. H. Lee and A. J. Wang 367
On the Theory of the Acceleration Damper . . . . . Carl Grubin 375
Vibration of a Cascade System . . . . . D. C. Johnson and R. E. D. Bishop 379
Effect of Spring Mass on Contact-Accelerometer Response . . . . . T. H. Lin 385
Time-Dependent Tangent Modulus Applied to Column Creep Buckling . . . . . R. L. Carlson 390
An Electroplastic Thermal-Stress Analysis of a Free Plate . . . . . Jerome Weiner 395
On the Carrying Capacity of Redundant Structures . . . . . E. R. Masur and K. P. Millard 403
The Propagation of Fatigue Cracks . . . . . A. K. Head 407
Impact With Finite Acceleration Time of Elastic Beams . . . . . R. C. Abrams 411
Determination of a Viscoelastic Model . . . . . D. R. Bland and E. H. Lee 416
Analysis of Slip Damping . . . . . L. E. Goodman and J. H. Klumpp 421
Forced Vibrations of Rectangular Plates . . . R. D. Mindlin, A. Schacknow, and H. Deresiewicz 430
Aerodynamic Ventilation From a Slot Jet . . . . . A. S. Weinstein, J. F. Osterle, and W. Forstall 437
Studies on Plastic Flow of Anisotropic Metals . . . . . L. W. Hu 444
Method for Calculating Stress-Concentration Factors . . . . . M. Hetényi and T. D. Lin 451
Calculation of Thickness of Surface Film in Boundary Lubrication . . . I-Ming Feng and C. M. Chang 458
Plastic Twisting of Thick-Walled Ring Sectors . . . . . W. Freiberger and W. Prager 461

Design Data and Methods

Deflection of Straight Beam Subjected to Unsymmetrical Bending . . . . . J. C. Levy 464
Refined Analysis of Heat-Exchanger Tube-Sheet Stresses . . . . . Yi-Yuan Yu 468

Brief Notes

Theory of Fatigue Fracture . . . . . A. Ali Khodadin 473
On the Gage Factor of SR-4 Type Strain Gages . . . . . G. C. Kaczynski 474
On Buckling of Sandwich Cylinders . . . . . A. C. Eringen 476
The Complex Variable Approach to Stress Singularities—II . . . . . M. L. Williams 477
Stress-Concentration Factors in Bending of Shafts . . . . . H. Ōhashi and K. Tokui 478
Shear-Lag Effect on Columns . . . . . P. C. Pavia 479
Discussion on previously published papers by P. G. Hodge, Jr.; F. B. Hildreth; P. S. Theocaris; M. M. Frocht and J. D. Flynn; Yi-Yuan Yu; N. J. Huffington, Jr.; G. Horvay, C. B. Linhart, and J. S. Berg; and L. W. Hu, and H. H. Trimer 480
Book Reviews 490

SEPTEMBER, 1956

VOL. 23, No. 3

Transactions of The American Society of Mechanical Engineers

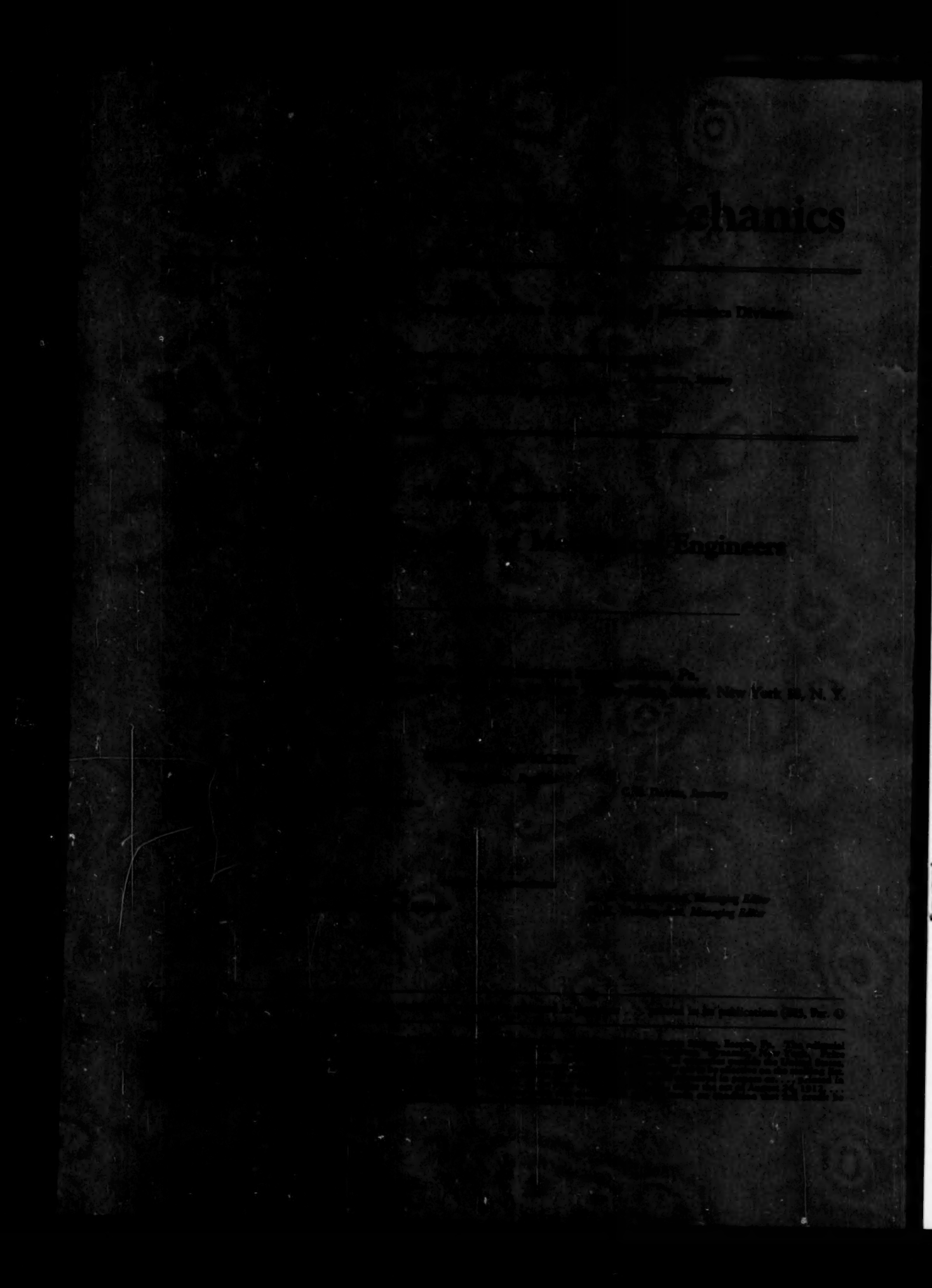

Bending of a Uniformly Loaded Semicircular Plate Simply Supported Around the Curved Edge and Free Along the Diameter

By D. F. MUSTER[1] and M. A. SADOWSKY[2]

Within the limits of classical plate theory, a solution is obtained in series form for the problem of a uniformly loaded, semicircular plate, simply supported around the curved edge and free along the diameter. The solution, although singular at the corners, is otherwise analytic and amenable to numerical evaluation by electronic calculators. The solution results are compared to those obtained experimentally by Robinson and Huggenberger. The agreement is reasonable, when account is taken of the manner in which their empirical results were obtained.

Nomenclature

The following nomenclature is used in the paper:

(r, θ, z) = cylindrical polar co-ordinates
$\rho = r/a$ = dimensionless radial co-ordinate
a = radius of plate
w = deflection
M_r, M_θ = bending moments per unit length
$M_{r\theta}$ = twisting moment per unit length
Q_r, Q_θ = shear forces per unit length
$\bar{Q}_r$, $\bar{Q}_\theta$ = Kirchhoff shear force per unit length
R = concentrated reaction at plate corners
p = lateral load intensity
ν = Poisson's ratio
h = plate thickness
E = Young's moduuls

Introduction

In what follows we seek to obtain, within the classical theory of thin plates, the deflections, moments, and shears of a semicircular plate under the action of a uniform lateral load. The curved edge of the plate is simply supported and the diametral edge is free.

The particular problem considered here is an idealization of one which occurs in the design of steam turbines. Turbine stages are separated by circular "diaphragms" split transversally along a horizontal diameter. Each of the semicircular sections contains a row of stator buckets and a concentric circular cutout which fits closely around the rotor shaft, Fig. 1. The curved edge of the diaphragm rests against a matching projection which is integral with the stator shell.

In an attempt to develop a rational design basis for the diaphragms, several analytical and experimental investigations have been conducted. In some, the diaphragm is idealized by considering it as a simply supported semicircular plate free along the diametral edge, but only approximate solutions have been reported.

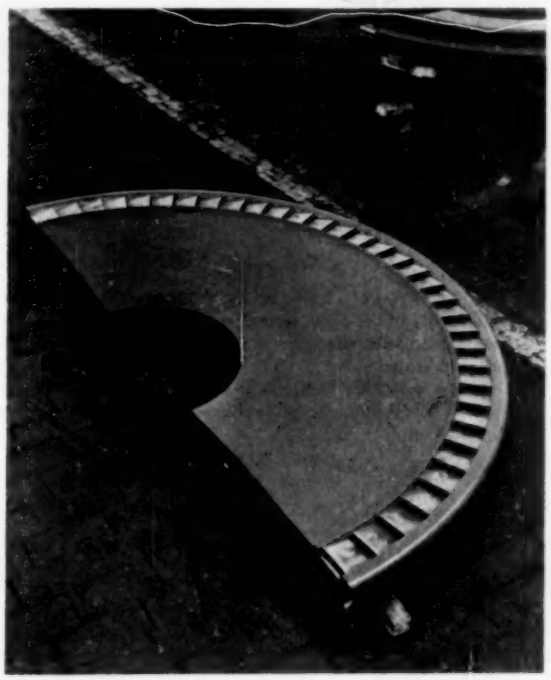

Fig. 1 Typical Steam-Turbine Diaphragm

In 1923 E. L. Robinson (1)[3] included in his unpublished experimental study of steam-turbine diaphragms a case similar to that which we present here. Huggenberger (2) published in 1926 the results of a similar, but more extensive study. Whereas Robinson did not attempt an analysis of the idealized problem, Huggenberger essayed to find a solution by energy methods. However, in several attempts he was not able to obtain a solution which would corroborate his carefully obtained experimental results.

Wahl (3) developed an approximate solution for the bending of a semicircular plate with a central cutout by considering it as an initially curved bar bent out of its plane of initial curvature. His analysis gave reasonable agreement with the experimental results only at the point of maximum stress; that is, at the inter-

[1] Engineer, General Engineering Laboratory, General Electric Company, Schenectady, N. Y. Assoc. Mem. ASME.

[2] Professor of Mechanics, Rensselaer Polytechnic Institute, Troy, N. Y. Mem. ASME.

Presented at the National Applied Mechanics Conference, Urbana, Ill., June 14–16, 1956, of The American Society of Mechanical Engineers.

Discussion of this paper should be addressed to the Secretary, ASME, 29 West 39th Street, New York, N. Y., and will be accepted until October 10, 1956, for publication at a later date. Discussion received after the closing date will be returned.

Note: Statements and opinions advanced in papers are to be understood as individual expressions of their authors and not those of the Society. Manuscript received by ASME Applied Mechanics Division, July 12, 1955. Paper No. 56—APM-7.

[3] Numbers in parentheses refer to the Bibliography at the end of the paper.

section of the inner edge of the circular cutout and the line of symmetry of the plate.

In a recent experimental study Taylor (4) used the results of Wahl's analysis to compute the stresses and deflections of two diaphragms (with blading and central cutouts) subjected to loads distributed uniformly along a semicircular arc. The arc was located so that the center of gravity of the load along it coincided with that of the same total load distributed uniformly over the entire surface of the diaphragm. His calculated results (using Wahl's analysis) agree well with his experimental results for maximum deflection and, after some adjustment, for the distribution of the support reaction.

Smith (5) published the results of another series of tests on diaphragms loaded in the same manner as Taylor. However, he gives no analysis, only results (stresses and deflections). Maximum stresses computed from his formulas agree very well with those of Huggenberger (2), but maximum deflections calculated from his results do not.

Statement of the Problem

According to the classical theory of thin plates, transverse deflections of the middle surface of a plate are characterized by

$$\nabla^4 w = p/D \quad \ldots\ldots [1]$$

where p and $D = Eh^3/12(1 - \nu^2)$ are the load intensity and the flexural rigidity of the plate, respectively. The plate we consider here is oriented with reference to a cylindrical polar co-ordinate system as indicated in Fig. 2. The corners of the plate are located at $r = a, \theta = \pm\pi/2$ and the upper and lower surfaces are given by $z = \pm h/2$. The boundary conditions are characterized by the requirements that

$$\left.\begin{aligned} &\text{for } r = a, \quad -\pi/2 \le \theta \le \pi/2: \\ &\qquad w = 0 \ldots\ldots (a) \\ &\qquad M_r = 0 \ldots\ldots (b) \\ &\text{for } 0 \le r \le a, \quad \theta = \pm\pi/2: \\ &\qquad \bar{Q}_\theta = Q_\theta + \frac{\partial M_{r\theta}}{\partial r} = 0 \ldots\ldots (c) \\ &\qquad M_\theta = 0 \ldots\ldots (d) \end{aligned}\right\} \ldots [2]$$

The Kirchhoff boundary conditions of the classical theory also produce concentrated reactions at supported corners of a polygonal plate. At the corners $r = a, \theta = \pm\pi/2$ we have then

$$R = \lim_{\theta \to \frac{\pi}{2} - 0} M_{r\theta}(a, \theta) + \lim_{r \to a - 0} M_{r\theta}\left(r, \pm\frac{\pi}{2}\right) = \lim_{\theta \to \frac{\pi}{2} - 0} M_{r\theta}(a, \theta) \ldots\ldots [3]$$

Particular Solutions in Plane Polar Co-Ordinates

Among the aggregates of solutions of the biharmonic equation in plane polar co-ordinates (6), we limit our attention to those which are even in the interval $-\pi/2 \le \theta \le \pi/2$ and regular at $r = 0$. These aggregates are

$$\left.\begin{aligned} &[A_n]: && w = r^{n+2}\cos(n+2)\theta \\ &[B_n]: && w = r^{n+2}\cos n\theta \\ &&& (n = 0, 1, 2 \ldots) \end{aligned}\right\} \ldots [4]$$

[4] Throughout this paper, capital letters in brackets denote the displacement, moment, and shear distributions associated with the corresponding solution.

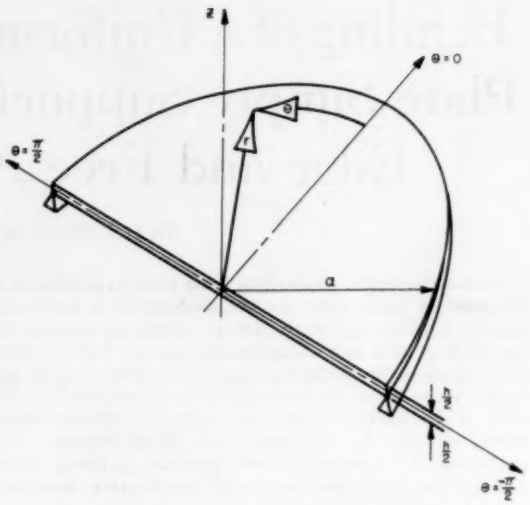

Fig. 2 Semicircular Plate Referred to a Cylindrical Polar Co-Ordinate System

Let us consider that portion of a uniformly loaded, simply supported circular plate enclosed in the region $0 \le r \le a, -\pi/2 \le \theta \le \pi/2$. Let $[S_1]$ denote the solution of the full circular plate (7), that is

$[S_1]$:

$$w = \frac{p}{64D}(a^2 - r^2)\left(\frac{5+\nu}{1+\nu}a^2 - r^2\right) \ldots\ldots [5]$$

In the half-plate portion we have chosen, $[S_1]$ satisfies conditions $[2a, b]$ around the simply supported edge $r = a$ and condition $[2c]$ along the diameter $\theta = \pm\pi/2$. However, it yields for the diameter, the bending moment

$$\bar{M}_\theta = \frac{p}{16}[(3+\nu)a^2 - (1+3\nu)r^2] \ldots\ldots [6]$$

From the aggregates $[A_n]$ and $[B_n]$ we look for a linear combination to be added to the solution $[S_1]$ which will free the boundary $\theta = \pm\pi/2$ of the bending moment M_θ given in Equation [6], but will not violate conditions $[2c]$. In the aggregate

$$[R] = [S_1] + \frac{pa^2}{32D}\{[A_0] + 2[B_0]\} + \frac{p}{192D}\{[A_2] \ldots + 4[B_2]\} \ldots\ldots [7]$$

we have such a linear combination. However, on the curved boundary $r = a$, $[R]$ yields

$$\left.\begin{aligned} w &= \frac{pa^4}{192D}(12 + 10\cos 2\theta + \cos 4\theta) \\ M_r &= \frac{-pa^2}{16}[2(1+\nu) + (5-\nu)\cos 2\theta + (1-\nu)\cos 4\theta] \end{aligned}\right\} \ldots [8]$$

If we are to satisfy conditions $[2a, b]$ we must find a solution $[U]$ for the residual problem characterized by Equation [8] which also will include the effect of rigid-body translation of the plate in the z-direction and rigid-body rotation about the axis $\theta = \pm\pi/2$. The latter effects are given by the solutions

$$\left.\begin{aligned} &[A_{-2}]: && w = 1 \\ &[A_{-1}]: && w = a\rho\cos\theta \end{aligned}\right\} \quad \ldots\ldots [9]$$

respectively. Thus the solution $[U]$ takes the form

$$[U] = c_{-2}[A_{-2}] + c_{-1}[A_{-1}] + \sum_{n=0}^{\infty} c_n[C_n] \quad \ldots\ldots [10]$$

The solutions $[A_{-2}]$ and $[A_{-1}]$ satisfy conditions [2c, d]. The $[C_n]$ must be chosen so that $[U]$ will clear the simply supported edge of the residual bending moment M_r and deflection w and not contribute to the value of M_θ and $\bar{Q}_\theta$ along the free diameter. With this in mind we consider M_θ and $\bar{Q}_\theta$, which are evaluated along the diameter

for $n = 2k\ (k = 0, 1, 2, \ldots)$

$$\left.\begin{aligned} &[A_{2k}]: && M_\theta = (-)^{k+1}(2k+1)(2k+2)(1-\nu)r^{2k} \\ & && \bar{Q}_\theta = 0 \\ &[B_{2k}]: && M_\theta = (-)^k 2(2k+1)[k-1-(k+1)\nu]r^{2k} \\ & && \bar{Q}_\theta = 0 \end{aligned}\right\} \quad \ldots [11]$$

for $n = 2k + 1$

$$\left.\begin{aligned} &[A_{2k+1}]: && M_\theta = 0 \\ & && \bar{Q}_\theta = (-)^{k+1}(2k+1)(2k+2)(2k+3)(1-\nu)r^{2k} \\ &[B_{2k+1}]: && M_\theta = 0 \\ & && \bar{Q}_\theta = (-)^k(2k+1)(2k+2)[2k+5-(2k+1)\nu]r^{2k} \end{aligned}\right\} \quad \ldots [12]$$

The coefficients of r^n in $[C_n]$ must vanish for $\theta = \pm\pi/2$. In view of this and Equations [11] and [12], the aggregate $[C_n]$ must consist of two parts

$$[C_{2k}] = \alpha_{2k+2}[A_{2k}] + \beta_{2k}[B_{2k}] \quad \ldots\ldots [13]$$

from Equations [11], and

$$[C_{2k+1}] = \alpha'_{2k+3}[A_{2k+1}] + \beta'_{2k+1}[B_{2k+1}] \quad \ldots\ldots [14]$$

from Equations [12], where

$$\left.\begin{aligned} \alpha_{2k+2} &= \frac{-k+1+(k+1)\nu}{(k+1)(2k+1)} \\ \beta_{2k} &= -\frac{1-\nu}{k+1} \\ \alpha'_{2k+3} &= \frac{2k+5-(2k+1)\nu}{(2k+2)(2k+3)} \\ \beta'_{2k+1} &= \frac{1-\nu}{2k+2} \end{aligned}\right\} \quad \ldots\ldots [15]$$

In the interval $-\pi/2 \le \theta \le \pi/2$, the set $\cos 2k\theta$ used in Equations [13] is complete relative to even functions of θ. The functions $\cos(2k+1)\theta$ used in Equation [14] consequently should be expanded as series in $\cos 2k\theta$. We apply the relation

$$\cos(2k+1)\theta = (-)^k\frac{4}{\pi}\left[\frac{1}{2(2k+1)} + (2k+1)\sum_{p=1}^{\infty}\frac{(-)^p}{(2k+1)^2-4p^2}\cos 2p\theta\right] \quad \ldots\ldots [16]$$

to Equation [14], which yields

$[C_{2k+1}]$:

$$w = (-)^k\frac{4(a\rho)^{2k+3}}{\pi(k+1)}\left[\alpha_{2k+3} + \sum_{p=1}^{\infty}\beta_{2k+1}\cos 2p\theta\right] \quad \ldots [17]$$

where

$$\left.\begin{aligned} \alpha_{2k+3} &= \frac{1-(2k+2)\nu}{(2k+1)(2k+3)^2} \\ \beta_{2k+1} &= (-)^p\frac{(4k+2)[1-(2k+2)\nu]+8p^2}{[(2k+1)^2-4p^2][(2k+3)^2-4p^2]} \end{aligned}\right\} \quad \ldots [18]$$

and $[U]$ becomes

$$[U] = c_{-2}[A_{-2}] + c_{-1}[A_{-1}] + \sum_{k=0}^{\infty}\{c_{2k}[C_{2k}] + c_{2k+1}[C_{2k+1}]\} \quad \ldots\ldots [19]$$

where the aggregates $[A_{-2}]$, $[C_{2k}]$, $[C_{2k+1}]$ are given by Equations [9], [13], [17], respectively, and $[A_{-1}]$ is given by

$[A_{-1}]$:

$$w = \frac{4}{\pi}(a\rho)\left[\frac{1}{2} + \sum_{p=1}^{\infty}\frac{(-)^p}{1-4p^2}\cos 2p\theta\right] \quad \ldots\ldots [20]$$

Solution of the Problem

The solution to the problem characterized by the boundary conditions [2] is of the form

$$[S] = [R] + [U] \quad \ldots\ldots [21]$$

Solution $[R]$ cleared the diameter $\theta = \pm\pi/2$ of tractions, leaving a residual problem on the boundary $r = a$ stated implicitly in Equation [8]. Thus $[U]$ the solution of the residual problem is characterized by the boundary conditions

$$\left.\begin{aligned} &\text{for } \theta = \pm\pi/2, \quad 0 \le r \le a: \\ &\qquad \bar{Q}_\theta = 0 && (a) \\ &\qquad M_\theta = 0 && (b) \\ &\text{for } -\pi/2 \le \theta \le \pi/2, \quad r = a: \\ &w = -\frac{pa^4}{192D}[12 + 10\cos 2\theta + \cos 4\theta] && (c) \\ &M_r = \frac{pa^2}{16}[2(1+\nu) + (5-\nu)\cos 2\theta + (1-\nu)\cos 4\theta] && (d) \end{aligned}\right\} \quad \ldots [22]$$

Since each of the solutions $[C_{2k}]$ and $[C_{2k+1}]$ was constructed so as to satisfy Equations [22a, b], and since $[A_{-2}]$ and $[A_{-1}]$ do the same identically, then so must $[U]$, provided the series

$$\sum_{k=0}^{\infty} c_{2k}[C_{2k}] \quad \text{and} \quad \sum_{k=0}^{\infty} c_{2k+1}[C_{2k+1}]$$

are suitably convergent.

If we apply the boundary conditions [22] to [U] in Equation [19] we obtain

$$c_{-2} + c_{-1}\left(\frac{4}{\pi}\right)\left[\frac{1}{2} + \sum_{p=1}^{\infty}\frac{(-)^p}{1-4p^2}\cos 2p\theta\right] + \sum_{k=0}^{\infty}[\alpha_{2k+2}\cos(2k+2)\theta + \beta_{2k}\cos 2k\theta]c_{2k} + \sum_{k=0}^{\infty}\frac{4}{\pi}\frac{(-)^k}{k+1}\left(\alpha_{2k+3} + \sum_{p=1}^{\infty}\beta_{2k+1}\cos 2p\theta\right)c_{2k+1} = -12 - 10\cos 2\theta - \cos 4\theta \quad [23]$$

$$\sum_{k=0}^{\infty} 2(1-\nu)[\gamma_{2k+2}\cos(2k+2)\theta + \delta_{2k}\cos 2k\theta]c_{2k} + \sum_{k=0}^{\infty}\frac{(-)^{k+1}}{\pi}\left[\gamma_{2k+3} + \sum_{p=1}^{\infty}\delta_{2k+1}\cos 2p\theta\right]c_{2k+1} = 24(1+\nu) + 12(5-\nu)\cos 2\theta + 12(1-\nu)\cos 4\theta \quad [24]$$

where α_{2k+2}, β_{2k} are given by Equations [15]; α_{2k+3}, β_{2k+1} are given by Equations [18], and

$$\left.\begin{aligned}\gamma_{2k+2} &= k - 1 - (k+1)\nu \\ \delta_{2k} &= k + 1 - (k-1)\nu \\ \gamma_{2k+3} &= \frac{8(1-\nu)}{(2k+1)(2k+3)} \\ \delta_{2k+1} &= (-)^p 16(1-\nu)\frac{(2k+1)(2k+3)(1-\nu) + [2k+3-(2k+1)\nu]4p^2}{[(2k+1)^2-4p^2][(2k+3)^2-4p^2]}\end{aligned}\right\} \quad [25]$$

If the boundary conditions [22] are to be satisfied, then Equations [23] and [24] must be identities in θ. We obtain from Equations [23] and [24] an infinite system of linear equations in the coefficients of superposition c_s

$$\left.\begin{aligned}&\omega_s^r c_s = e_r \\ &(r = 0, 1, 2, \ldots) \\ &(s = -2, -1, 0, 1, 2, \ldots)\end{aligned}\right\} \quad [26]$$

where column matrices $\omega_s^r c_s$ and e_r represent the coefficients of the terms in $\cos 2k\theta$.

The values of the coefficients c_s used in Equation [19] with Equations [9], [13], [15], [17], [18], and [20] constitute the solution of the residual problem. This, added to the solution [R] given in Equation [7], comprises the complete solution of the problem [S].

The solution [S] is analytic everywhere in the region $0 \leq r \leq a$, $-\pi/2 \leq \theta \leq \pi/2$, except at the points $r = a$, where it is singular. In general, the isolation of a singularity in an individual term and application of the series expansions to the regular remainder of a solution is desirable. Preliminary investigations for possible solutions which would isolate the singularity, led in each case to residual problems with greatly increased computational difficulties. Under these conditions, it is felt that the present solution, which is amenable to numerical evaluation, is adequate.

Evaluation of Deflections, Moments, and Shears—Discussion of Numerical Results

The numerical solution of Equation [26] for the coefficients of superposition c_s was carried out for leading minors of the infinite matrix ω_s^r of orders 15, 20, 25, 30, and 40. In each case, the Gauss elimination method (8, 9) was used to obtain a solution. The results of these computations show that as the order of the leading minors used in Equation [26] increases, the resulting values of c_s evidently approach asymptotic values.

The complete set of values for c_s obtained from the solution of Equation [26] for the leading minor of order 40 is shown in Table 1. These values were used in subsequent calculation of the deflections, moments, and shears.

TABLE 1 NUMERICAL VALUES OF c_s (ν = 0.3) FROM 40TH ORDER MATRIX

s	c_s	s	c_s
−2	16.015295	−1	−9.5886852
0	11.614035	1	−4.0134271
2	12.523605	3	0.23470183
4	−0.19597221	5	−0.46634303
6	0.13212126	7	0.39226295
8	−0.095160004	9	−0.32592533
10	0.071916055	11	0.27495312
12	−0.056341752	13	−0.23542071
14	0.045359209	15	0.20390848
16	−0.037358305	17	−0.17810880
18	0.031230487	19	0.15639302
20	−0.026661646	21	−0.13777202
22	0.022883763	23	0.12138329
24	−0.019933808	25	−0.10670159
26	0.017495709	27	0.093257058
28	−0.015469230	29	−0.080660535
30	0.013797344	31	0.068557733
32	−0.012369751	33	−0.056526898
34	0.011136245	35	0.043972138
36	−0.010097187	37	−0.030164126

Expressions for the deflection, moments, and shears of the plate are obtained from [S]:

$$w = \frac{pa^4}{192D}\left\{3\frac{5+\nu}{1+\nu} + 6\left(\cos 2\theta - \frac{1-\nu}{1+\nu}\right)\rho^2 + (3 + 4\cos 2\theta + \cos 4\theta)\rho^4 + c_{-2} + c_{-1}\frac{4\rho}{\pi}\left[\frac{1}{2} + \sum_{p=1}^{18}\frac{(-)^p}{1-4p^2}\cos 2p\theta\right] + \sum_{k=0}^{18}\rho^{2k+2}[\alpha_{2k+2}\cos(2k+2)\theta + \beta_{2k}\cos 2k\theta]c_{2k} + \sum_{k=0}^{18}(-)^k\frac{4\rho^{2k+3}}{\pi(k+1)}\left[\alpha_{2k+3} + \sum_{p=1}^{18}\beta_{2k+1}\cos 2p\theta\right]c_{2k+1}\right\} \quad [27]$$

where α_{2k+2}, β_{2k} are given by Equations [15]; α_{2k+3}, β_{2k+1} by Equations [18]; and the coefficients of superposition c_s in Table 1. These expressions are evaluated for $\nu = 0.3$ and the following grid in (ρ, θ)

$$\rho = 0(0.15)0.90(0.02)1.00$$

$$\theta = 0(10°)80°(1°)90°$$

The results of this computation are shown in Figs. 3 through 8.

The computed values of w and M_r serve as a check on the satisfaction of the Boundary Conditions [2a, b]. Within the number of terms considered in the numerical evaluation of the series solution established earlier, these values of w and M_r, which should vanish, were both found to be less than $\pm 10^{-4}$.

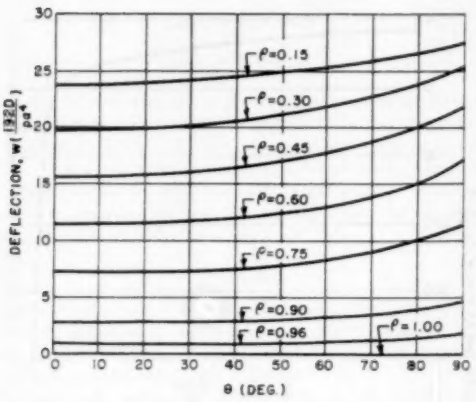

FIG. 3 VARIATION OF DEFLECTION w WITH θ FOR SEVERAL ρ-VALUES

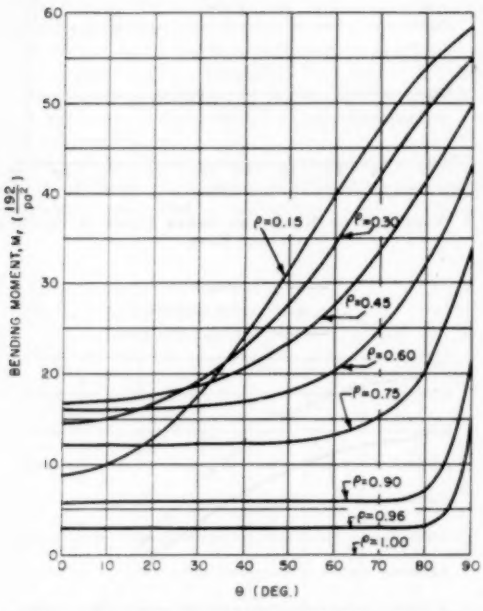

FIG. 4 VARIATION OF BENDING MOMENT M_r WITH θ FOR SEVERAL ρ-VALUES

COMPARISON OF NUMERICAL RESULTS WITH EXPERIMENTAL RESULTS OF ROBINSON AND HUGGENBERGER

The variation of the Kirchhoff shear force $\overline{Q}_r$ along the edge $r = a$ is shown in Fig. 9. Unfortunately, the available experimental results do not permit direct comparison of this distribution with that of an actual plate. Robinson (1) supported his test plates on springs arranged around the curved boundary. The springs were adjusted to exert sufficient force upward to bring the edge back to the original position it occupied before the plate was loaded. There was no provision to exert a similar downward force which is required on a part of the boundary if $w = 0$ along the curved edge. However, the distribution of spring forces reported by Robinson is similar in shape to the negative portion of the curve in Fig. 9.

The variation of the deflection along the diameter $\theta = \pm\pi/2$

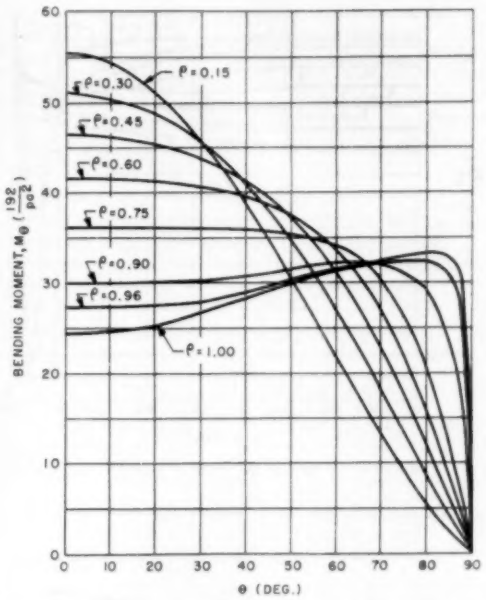

FIG. 5 VARIATION OF BENDING MOMENT M_θ WITH θ FOR SEVERAL ρ-VALUES

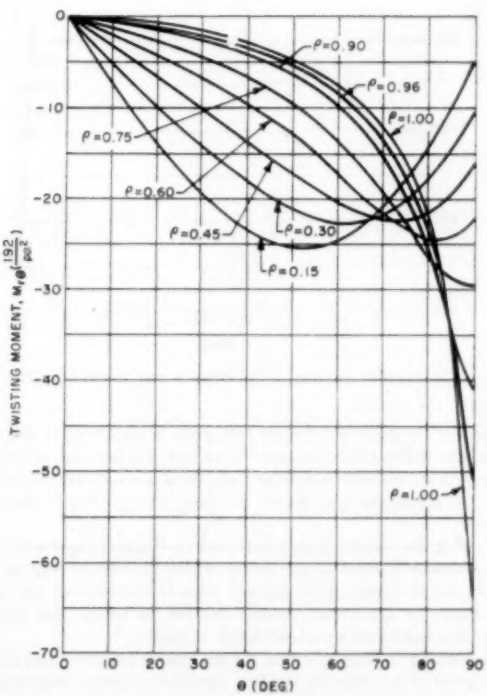

FIG. 6 VARIATION OF TWISTING MOMENT $M_{r\theta}$ WITH θ FOR SEVERAL ρ-VALUES

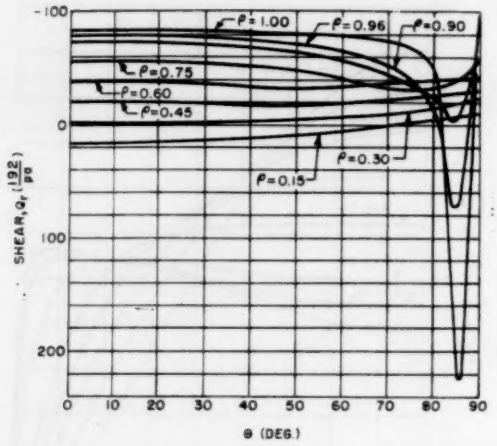

FIG. 7 VARIATION OF SHEAR Q_r WITH θ FOR SEVERAL ρ-VALUES

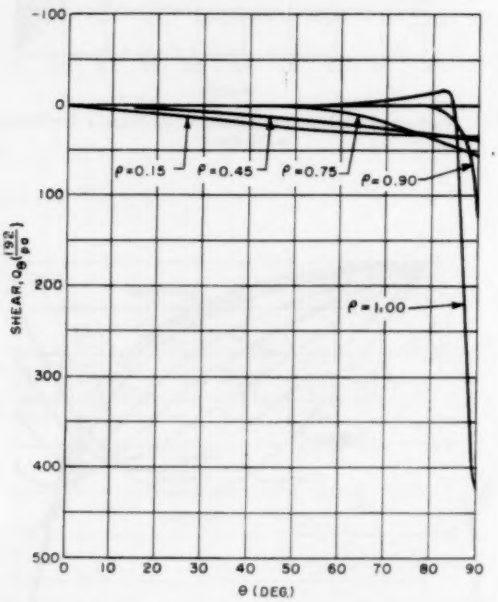

FIG. 8 VARIATION OF SHEAR Q_θ WITH θ FOR SEVERAL ρ-VALUES

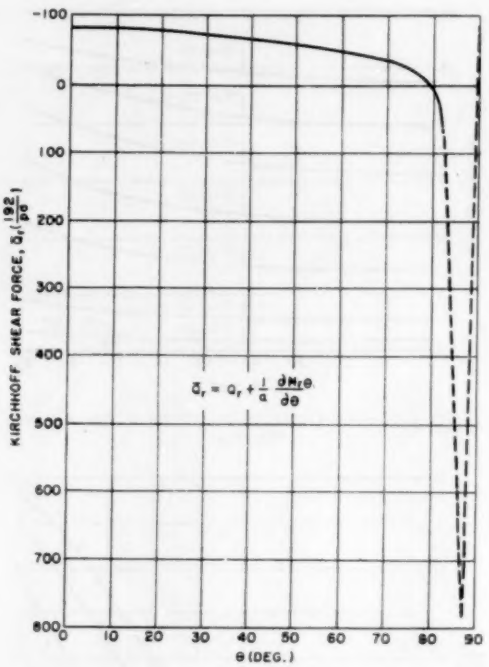

FIG. 9 VARIATION OF KIRCHHOFF SHEAR FORCE $\bar{Q}_r$ ALONG THE CURVED EDGE

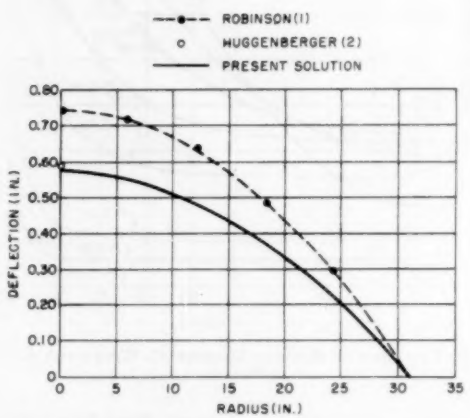

FIG. 10 VARIATION OF DEFLECTION ALONG FREE DIAMETER OF A 62-IN-DIAM, 1/4-IN-THICK SEMICIRCULAR STEEL PLATE FROM OTHER SOURCES AND PRESENT SOLUTION

measured by Robinson for his test plate is compared in Fig. 10 with the deflections computed from our solution for a similar plate. The differences in edge conditions and method of loading the two plates can account for the discrepancy between the two curves.

Among the series of tests conducted by Huggenberger were two of particular interest to us; one in which the curved edge of the plate simply rested on a support (this is identical to the edge condition in Robinson's tests), another in which the curved edge was restrained by a true simple support.

According to Huggenberger, the maximum deflection and bending stress of a uniformly loaded, simply supported semicircular plate is given by (2)

$$w_{max}' = 2.37\, w_{max}'' \quad \ldots\ldots\ldots\ldots\ldots\ldots [28]$$

$$\sigma_{rmax}' = 1.54\, \sigma_{rmax}'' \quad \ldots\ldots\ldots\ldots\ldots\ldots [29]$$

where the single and double primes refer to the half and full-circular plates, respectively.[5] Equation [28] was used to determine the maximum deflection of the same steel plate considered earlier with reference to Robinson's results. The value from Equation [28], which is 3 per cent greater than that calculated by our solution, is shown in Fig. 10. The expressions analogous to Equations [28] and [29] obtained from our solution for $r = 0$, $\theta = \pm\pi/2$ are

[5] These expressions appear in (10) in modified form.

$$w_{max}' = 2.31\, w_{max}'' \quad [30]$$

$$\sigma_{rmax}' = 1.49\sigma_{rmax}'' \quad [31]$$

where the primes have the same significance as in the foregoing.

Huggenberger also measured experimentally the magnitude of the concentrated force at each corner of the plate and reports that ". . . . it amounts to about one quarter of the entire pressure" (2). By Equation [3], with the appropriate value of $M_{r\theta}$ given in Fig. 6, we compute the magnitude of each force to be approximately 22 per cent of the total load.

Summary

In this paper, within the limits of classical thin-plate theory, a solution is obtained in series form for the problem of a uniformly loaded semicircular plate, simply supported around the curved edge and free along the diameter.

The principal conclusions may be summarized as follows:

1 The numerical results agree reasonably well with the available evidence.

2 The solution has singularities at the corners corresponding to concentrated forces.

3 The concentrated reactions at the corners each have magnitude equal to about 22 per cent of the total load on the plate.

4 The maximum deflection of the semicircular plate is 2.31 times the maximum deflection of a uniformly loaded, simply supported circular plate.

5 The maximum bending stress of the semicircular plate (at $r = 0$) is 1.49 times the maximum bending stress of a uniformly loaded, simply supported circular plate.

Acknowledgment

The authors are particularly indebted to Mr. E. E. Zwicky and Miss J. King (both of Large Steam Turbine-Generator Department, General Electric Company) for their enthusiastic co-operation in the computational phase of this investigation. The extensive computations were performed on electronic calculators in General Electric Company.

BIBLIOGRAPHY

1 "Strength of Steam Turbine Diaphragms," by E. L. Robinson, General Electric Company Report No. 16380, 1923, 43 pages.

2 "Festigkeit Halbreisförmiger Platten und Dampfturbinen-Leiträder," by A. Huggenberger, *Forschungsarbeiten auf dem Gebiete des Ingenieurwesens*, Heft 280, VDI-Verlag, Berlin, Germany, 1926, 74 pages.

3 "Strength of Semicircular Plates and Rings Under Uniform External Pressure," by A. M. Wahl, Trans. ASME, vol. 54, 1932, pp. 311–320.

4 "Stress and Deflection Tests of Steam-Turbine Diaphragms." by V. C. Taylor, Trans. ASME, vol. 73, 1951, p. 877.

5 "Deflection and Stress in Built-Up Half Diaphragm," by D. M. Smith, Proceedings of the Fifth International Congress of Applied Mechanics, Cambridge, Mass., 1938, p. 62.

6 "Theory of Plates and Shells," by S. Timoshenko, McGraw-Hill Book Company, Inc., New York, N. Y., 1940, 492 pages.

7 "Theory of Elasticity," by R. V. Southwell, Oxford University Press, London, England, second edition, 1941, 509 pages.

8 "Linear Computations," by P. S. Dwyer, John Wiley & Sons, Inc., New York, N. Y., 1951, p. 103.

9 "Practical Solution of Linear Equations and Inversion of Matrices," by L. Fox, Contributions to the Solution of Systems of Linear Equations and the Determination of Eigenvalues, National Bureau of Standards AMS No. 39, 1954, p. 8.

10 "Steam and Gas Turbines," by A. Stodola, Peter Smith, New York, N. Y., 1945, p. 511.

Stress Solutions for an Infinite Plate With Triangular Inlay[1]

By R. M. EVAN-IWANOWSKI,[2] SYRACUSE, N. Y.

The method of solving two-dimensional problems in elasticity by means of the functions of complex variable, essentially developed by É. Goursat (1),[3] and N. I. Muskhelishvili (2–4), has been applied to the following cases: (*a*) An infinite plate with a rigid triangular inlay under uniform tension at infinity; (*b*) A concentrated force; and (*c*) a moment acting on a triangular inlay in an infinite plate. All these problems are second boundary-value problems; i.e., the displacements are prescribed on the boundary. The first boundary-value problem for a triangular opening in an infinite plate was treated by Hu-Nan Chu (7). The mapping function used in this paper is $z = \omega(\zeta) = K\left(\zeta + \frac{n}{\zeta^2}\right)$, K is real, $0 < n < 1/3$ and real, and it maps an exterior of a triangle with rounded corners, Fig. 1, in the z-plane into an exterior of a unit circle in the ζ-plane [for detailed discussion of this mapping refer to (4)[4]].

Nomenclature

The following nomenclature is used in the paper:

$z = x + iy$
$\zeta = re^{i\theta}$
$\sigma = e^{i\theta}$
n, m, K = constants
E = Young's modulus
G = shear modulus
ν = Poisson's ratio
$\kappa = \dfrac{3 - \nu}{1 + \nu}$
σ_1, σ_2 = principal stresses at infinity
σ_r, σ_θ = radial and tangential components of stress
$\tau_{r\theta}$ = shear stress
u, v = radial and tangential components of dispalcement
g_1, g_2 = components of displacements on boundary
p = distributed load
P = concentrated load
M = moment
α = angle between x-axis and given direction
ϵ = small angle of rotation
$B = \dfrac{\sigma_1 + \sigma_2}{4}$
$B' = -\dfrac{\sigma_1 - \sigma_2}{2}\cos 2\alpha$
$C' = \dfrac{\sigma_1 - \sigma_2}{2}\sin 2\alpha$
$C = \dfrac{E\epsilon^*}{4}$
ϵ^* = angle of rotation at infinity
X, Y = rectangular components of resultant force

Introduction

Muskhelishvili's method has been extensively applied to the problems of infinite plates with openings or inlays. In (4) several examples are given related to the general use of mapping functions of the type

$$z = \omega(\zeta) = K\left(\zeta + \frac{n}{\zeta^m}\right)$$

$K > 0$, $0 < n < 1/m$, m positive integer, selected from various workers, among them G. N. Savin (1936), A. N. Dinnik and others (1938), and G. S. Shapiro (1941). There is no need, therefore, to publish another description of the method itself or to give a derivation of intermediate functions and expressions entering into these problems. It is sufficient to present the final results for the specific cases treated in this paper.

An Infinite Plate With Rigid Triangular Inlay Under Action of Uniform Tension at Infinity

Consider the uniform stress p acting as shown in Fig. 1. X, Y, and C are zero, since there is no body force and no rotation at infinity, i.e., $\epsilon^* = 0$; also $\sigma_1 = p$, $\alpha = 0$, $B = P/4$, $B' = -P/2$, $C' = 0$ (for general relationships see reference 4).[5] On the boundary of contact between the inlay and the plate

$$g_1 = u = -y\epsilon; \quad g_2 = v = ix\epsilon$$

or

$$g_1 + ig_2 = i\epsilon z = i\epsilon K\left(\sigma + \frac{n}{\sigma^2}\right)$$

The small angle of rotation ϵ is computed from the moment M_0 about the origin

$$M_0 = 4\pi\epsilon GK^2\left(1 + \frac{2n^2}{\kappa}\right) \quad \ldots\ldots\ldots\ldots [1]$$

ϵ is independent from the stresses at infinity. If M_0 is zero, as it is in this case, so is ϵ. This is not generally true;[6] e.g., for an elliptic inlay ϵ is treated in (3).

Since the inlay remains rigid and is assumed rigidly attached to the plate, there is no relative displacement of adjacent points in the tangential direction (8). Thus on the boundary

$$e_\theta = \frac{1}{E}(\sigma_\theta - \nu\sigma_r) = 0; \quad \sigma_\theta = \nu\sigma_r \quad \ldots\ldots\ldots [2]$$

Hence the normal and tangential stresses on the boundary are found to be

---

[1] Results are based on a part of a doctorate thesis, Department of Engineering Mechanics and Materials, Cornell University, Ithaca, N. Y., 1954.

[2] Assistant Professor, Department of Mechanical Engineering, Syracuse University.

[3] Numbers in parentheses refer to the Bibliography at end of paper.

[4] Reference (4), pp. 177–178.

Presented at the National Applied Mechanics Conference, Urbana, Ill., June 14–16, 1956, of The American Society of Mechanical Engineers.

Discussion of this paper should be addressed to the Secretary, ASME, 29 West 39th Street, New York, N. Y., and will be accepted until October 10, 1956, for publication at a later date. Discussion received after the closing date will be returned.

Note: Statements and opinions advanced in papers are to be understood as individual expressions of their authors and not those of the Society. Manuscript received by ASME Applied Mechanics Division, May 9, 1955. Paper No. 56—APM-4.

[5] Reference (4), p. 126.

[6] I.e., when angle α is different from zero.

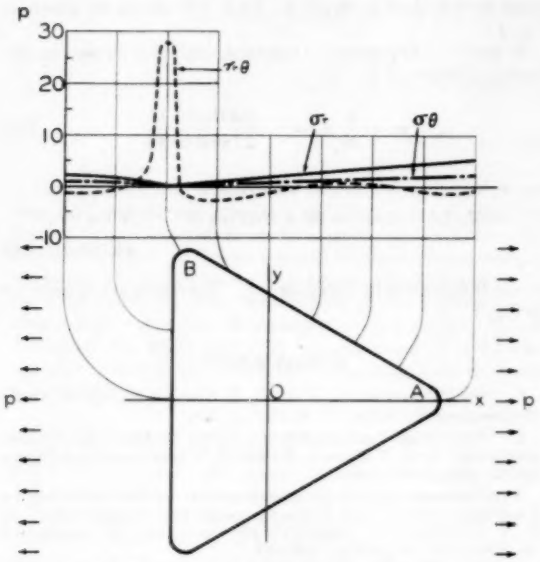

FIG. 1 STRESS DISTRIBUTION AROUND THE BOUNDARY OF AN INFINITE PLATE WITH A TRIANGULAR INLAY UNDER ACTION OF UNIFORM TENSION p AT INFINITY

$$(1+\nu)\sigma_r = \mathrm{Re}\left\{\frac{4K}{\kappa(\sigma^3-2n)}\,[3nB + B'\sigma + \kappa B\sigma^3]\right\} \quad \ldots\ldots [3]$$

The shear stress there is obtained from

$$\begin{aligned}(1-\nu)\sigma_r + 2i\tau_{r\theta} = 2\{&(1+n\sigma^3)[6nB(K-2) \\ &+ 2B'(K-3n)\sigma + 6\kappa nB\sigma^3] \\ &+ \sigma^2[4\kappa n^2B + 4\kappa nBK\sigma + 6nBB'(1+2n^2)\sigma^2 \\ &+ 8\kappa nB(1+n^2)\sigma^3 - \kappa K(1+10n^2)\sigma^4 + 2\kappa n^2\sigma^6 + 2\kappa nK\sigma^7] \\ &+ \kappa K(\sigma^3-2n)[B'\sigma - B(\kappa+2n\sigma^3)]\}/D(\sigma) \quad \ldots\ldots [4]\end{aligned}$$

where

$$D(\sigma) = \kappa K(1-2n\sigma^3)(\sigma^3-2n) \quad \ldots\ldots [5]$$

A CONCENTRATED FORCE ACTING ON A RIGID INLAY IN AN INFINITE PLATE

This situation is shown in Fig. 2. It is obvious that the inlay does not rotate in this case, hence $\epsilon = 0$, $g_1 + ig_2 = 0$, also $C = B = B' = C' = 0$; $X = P$, $Y = 0$, and thus the normal, tangential, and shear stresses on the boundary of the plate are given by

$$\sigma_\theta + \sigma_r = (1+\nu)\sigma_r = \mathrm{Re}\left[\frac{2P\sigma(n-\kappa\sigma)}{\pi\kappa K(\kappa+1)(\sigma^3-2n)}\right] \quad \ldots [6]$$

$$\begin{aligned}(1-\nu)\sigma_r + 2i\tau_{r\theta} = P\sigma[&(1+n\sigma^3)(-2n^3+2\kappa n\sigma-2n\sigma^3+\kappa\sigma^4) \\ &+ \kappa^2(\sigma^3-2n)^2 + 3(n-\kappa)(1+2n^3)\sigma - \kappa n\sigma \\ &(\sigma^3-2n)^2]/D(\sigma) \quad \ldots\ldots [7]\end{aligned}$$

where $$D(\sigma) = \pi\kappa K(\kappa+1)(1-2n\sigma^3)(\sigma^3-2n)^2 \quad \ldots\ldots [8]$$

A MOMENT ACTING ON A RIGID TRIANGULAR INLAY IN AN INFINITE PLATE

Consider a problem shown in Fig. 3. In this case clearly $B = B' = C' = 0$; $X = Y = 0$. The normal, tangential, and shear stresses on the boundary of the plate are

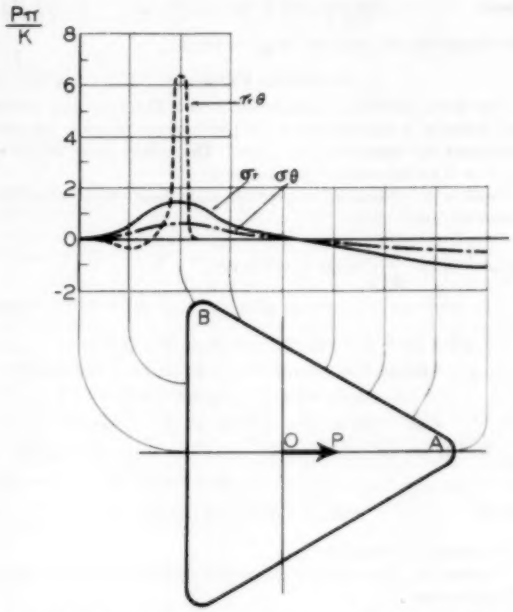

FIG. 2 STRESSES ON THE BOUNDARY OF AN INFINITE PLATE[7] WITH TRIANGULAR INLAY UNDER ACTION OF A CONCENTRATED FORCE P

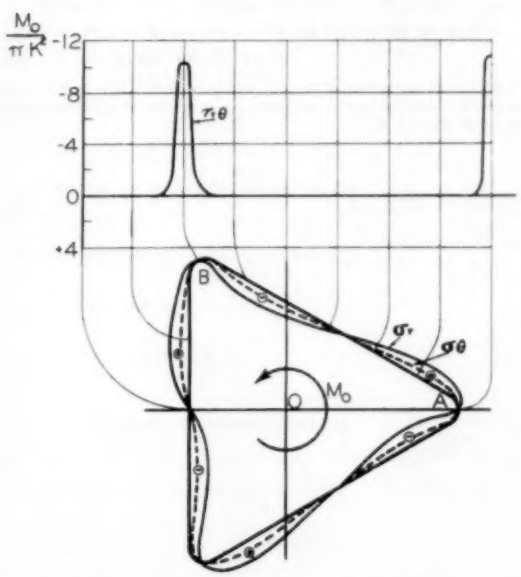

FIG. 3 STRESSES ON THE BOUNDARY OF AN INFINITE PLATE WITH TRIANGULAR INLAY UNDER ACTION OF A MOMENT M_0

$$\sigma_\theta + \sigma_r = (1+\nu)\sigma_r = \mathrm{Re}\left\{\frac{16iGen}{\kappa(\sigma^3-2n)}\right\} \quad \ldots\ldots [9]$$

$$\begin{aligned}(1-\nu)\sigma_r + 2i\tau_{r\theta} = 4iGen[&4n(1-n^3) - 4(2+n^3)\sigma^3 + 3n\sigma^6] \\ &/D(\sigma) \quad \ldots\ldots [10]\end{aligned}$$

[7] More detailed graphs are available from the author.

where $D(\sigma) = \kappa\sigma(1 - 2n\sigma^3)(\sigma^3 - 2n)$ ..... [11]

ϵ in Equations [9] and [10] is given by [1].

Numerical Examples

The three problems enumerated in the Abstract and whose final solution is represented in the previous paragraphs, are now illustrated by numerical examples. The values $n = 0.3$, $\nu = 1/3$, $\alpha = 0$ are selected for this purpose.[8]

Problem 1. Normal, tangential, and shear stresses on the boundary are

$$\sigma_\theta = \frac{1}{3}\,\sigma_r = \frac{p}{2}\,[-0.59 + 0.3\cos\theta - 0.5\cos 2\theta + 0.45\cos 3\theta]/D(\theta) \quad [12]$$

$$\tau_{r\theta} = p[0.3\sin\theta + 0.5\sin 2\theta + 0.15\sin 3\theta]/D(\theta) + p[-0.09\sin\theta - 0.8\sin 2\theta + 0.31\sin 3\theta - 0.09\sin 4\theta + 0.3\sin 5\theta - 0.14\sin 6\theta]/D^2(\theta) + p[-1.28\sin\theta - 1.12\sin 2\theta + 0.41\sin 3\theta + 0.37\sin 4\theta - 0.16\sin 5\theta + 0.17\sin 6\theta - 0.27\sin 8\theta - 0.19\sin 9\theta]/D^3(\theta) \quad [13]$$

where $D(\theta) = 1.36 - 1.2\cos 3\theta$ ..... [14]

The results are shown in Fig. 1.

Problem 2. The normal, tangential, and shear stresses on the boundary are

$$\sigma_\theta = \frac{1}{3}\,\sigma_r = P\,(-0.72\cos\theta + 0.5\cos 2\theta)/\pi K D(\theta)\,. \quad [15]$$

$$\tau_{r\theta} = P[3.64\sin\theta + 1.8\sin 2\theta]/\pi K D(\theta) + P[-8.89\sin\theta - 3.86\sin 2\theta + 7.87\sin 4\theta + 0.05\sin 5\theta - 2.24\sin 7\theta + 0.11\sin 8\theta]/\pi K D^2(\theta) \quad [16]$$

[8] Radius of curvature at the corners is $R = 0.1\,K$; and the distances from point 0 to the intersections of a triangle with the x-axis are $0.3\,K$ and $1.7\,K$.

where $D(\theta)$ is given by Equation [14]. The results are shown in Fig. 2.

Problem 3. The normal, tangential, and shear stresses on the boundary are

$$\sigma_\theta = \frac{1}{3}\,\sigma_r = -\frac{0.3M_0\sin 3\theta}{2.18\pi K^2 D(\theta)} \quad [17]$$

$$\tau_{r\theta} = M_0(-1 + 0.6\cos 3\theta)/4.36\pi K^2 D(\theta) + M_0(1.0 - 1.41\cos 3\theta + 0.62\cos 6\theta - 0.36\cos 9\theta)/\pi K^2 D^2(\theta) \quad [18]$$

where $D(\theta)$ is given by Equation [14]. The results are represented in Fig. 3.

BIBLIOGRAPHY

1 "Sur l'Équation $\Delta\Delta u = 0$," by É. Goursat, *Bulletin de Societé Mathématique de France*, vol. 26, 1898, p. 236.

2 "Über einige Eigenschaften des ebenen Problems der Elastizitätstheorie," by G. V. Kolosov, *Zeitschrift für Mathematik und Physik*, vol. 62, 1914, p. 383–409.

3 "Praktische Lösung der fundamentalen Randwertaufgaben der Elastizitätstheorie in der Ebene für einige Berandungsformen," by N. I. Muskhelishvili, *Zeitschrift für angewandte Mathematik und Mechanik*, vol. 13, 1933, pp. 264–282.

4 "Some Basic Problems of the Theory of Elasticity," by N. I. Muskhelishvili, P. Noordhoff, Editor, Groningen, Holland, 1953.

5 "Beiträge zur Theorie des Cauchyschen Integrals," by A. Harnack, *Mathematische Annalen*, vol. 35, 1899, pp. 1–18.

6 "Conformal Mapping of Simply- and Multiply-Connected Regions," by V. I. Smirnov, Editor, Moscow, USSR, 1936, 112 pp.

7 "Some Problems in Two-Dimensional Elasticity," by Hu-Nan Chu, Doctorate Dissertation, Cornell University, Ithaca, N. Y., 1953.

8 "Solutions for Exterior of General Ovaloid Under Arbitrary Loading and Its Application to Square Rigid Core Problems," by Yi-Yuan Yu, Doctorate Dissertation, Northwestern University, Proceedings of the First National Congress of Applied Mechanics, 1952, pp. 227–236.

On the Stresses and Deflections of Rectangular Beams

By B. A. BOLEY[1] and I. S. TOLINS,[2] NEW YORK, N. Y.

The stresses and deflections in rectangular beams and bars are calculated from the two-dimensional elasticity theory by an iterative procedure previously derived. The loading consists of either normal or shear forces varying smoothly along the span. The results are obtained in the form of infinite series, whose first terms represent the elementary solutions of strength of materials; the accuracy of the *Mc/I* and *P/A* formulas can thus be estimated. A comparison with the Timoshenko beam theory is included.

Introduction

THE remarkably wide range of practical applicability of the formulas of elementary beam theory stems from the fact that these formulas provide excellent approximations to the actual beam behavior even in a large number of problems in which they do not represent the true solution according to the theory of elasticity. The reason for this is perhaps most clearly seen from an examination of the results of von Karman (1)[3] and Seewald (2), who were respectively concerned with the validity of the familiar formulas

$$\frac{1}{\rho} = \frac{-M}{EI} \quad \ldots\ldots [1a]$$

and

$$\sigma_x = \frac{My}{I} \quad \ldots\ldots [1b]$$

where $(1/\rho)$ is the curvature, and the other symbols have the usual meanings. Taking, for example, Equation [1*a*], it was shown by von Karman that a more general equation for a rectangular beam transversely loaded is

$$\frac{1}{\rho} = \frac{-M}{EI} + \frac{1}{EI}\frac{d^2M}{dx^2}\left(\frac{4c^2}{5} + \frac{\nu c^2}{2}\right) + (\text{terms containing higher derivatives of } M \text{ with respect to } x) \ldots [1c]$$

If the spanwise variation of the bending moment is smooth (that is, if M is expressible either as a polynomial or as a rapidly converging power series in x), then the series of Equation [1*c*] will converge very rapidly, and, in fact, the first term of the right-hand side (and therefore also Equation [1*a*]) will yield a good approximation to the correct result. Seewald has shown that an expansion, similar to that of Equation [1*c*], in terms of successively higher derivatives of the bending moment, also can be written for the stress σ_x; Equation [1*b*] has therefore a range of validity similar to that of Equation [1*a*].

The work of von Karman and Seewald is limited to rectangular beams under distributed loads perpendicular to the spanwise direction, i.e., to Case I of Fig. 1. The present work shows that similar results hold in the case of beams under smoothly distributed shear loads, parallel to the spanwise direction. It was found convenient to investigate this type of loading by considering the antisymmetric and symmetric loading conditions of Cases II and III of Fig. 1, respectively.

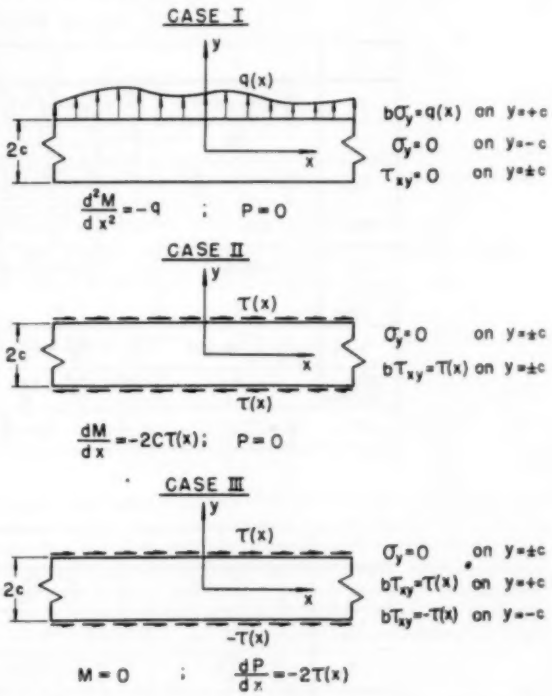

FIG. 1 NOMENCLATURE, BOUNDARY CONDITIONS, AND BASIC RELATIONS FOR EACH OF THE THREE CASES OF LOADING

The stresses predicted by the elementary theory for Case III of Fig. 1 are given by the formula

$$\sigma_x = \frac{P}{A} \quad \ldots\ldots [2]$$

rather than by Equation [1*b*]. The present work shows that the

[1] Associate Professor of Civil Engineering, Institute of Flight Structures, Columbia University.

[2] Research Associate, Institute of Flight Structures, Department of Civil Engineering and Engineering Mechanics, Columbia University.

[3] Numbers in parentheses refer to the Bibliography at the end of the paper.

Presented at the National Applied Mechanics Conference, Urbana, Ill., June 14–16, 1956, of THE AMERICAN SOCIETY OF MECHANICAL ENGINEERS.

Discussion of this paper should be addressed to the Secretary, ASME, 29 West 39th Street, New York, N. Y., and will be accepted until October 10, 1956, for publication at a later date. Discussion received after the closing date will be returned.

NOTE: Statements and opinions advanced in papers are to be understood as individual expressions of their authors and not those of the Society. Manuscript received by ASME Applied Mechanics Division, September 6, 1955. Paper No. 56—APM-1.

TABLE 1 SOLUTION FOR CASE I

i	1	2	3
ϕ	$\frac{M}{I}\left(\frac{y^3}{6}-\frac{c^2y}{2}-\frac{c^3}{3}\right)$	$-\frac{M''}{I}\left(\frac{y^5}{60}-\frac{c^2y^3}{30}+\frac{c^4y}{60}\right)$	$\frac{M^{III}}{I}\left(\frac{y^7}{1680}+\frac{c^2y^5}{1200}+\frac{c^3y^4}{72}-\frac{87c^4y^3}{25200}-\frac{c^5y^2}{36}+\frac{17c^6y}{8400}+\frac{c^7}{72}\right)$
σ_x	$\frac{M_y}{I}$	$-\frac{M''}{I}\left(\frac{y^3}{3}-\frac{c^2y}{5}\right)$	$\frac{M^{III}}{I}\left(\frac{y^5}{40}+\frac{c^2y^3}{60}+\frac{c^3y^2}{6}-\frac{87c^4y}{4200}-\frac{c^5}{18}\right)$
τ_{xy}	$-\frac{M'}{I}\left(\frac{y^2}{2}-\frac{c^2}{2}\right)$	$\frac{M''}{I}\left(\frac{y^4}{12}-\frac{y^2c^2}{10}+\frac{c^4}{60}\right)$	$-\frac{M^{III}}{I}\left(\frac{y^6}{240}+\frac{y^4c^2}{240}+\frac{y^3c^3}{18}-\frac{87y^2c^4}{8400}-\frac{yc^5}{18}+\frac{17c^6}{8400}\right)$
EIu	$y\int M\,dx$	$-M'\left[\frac{y^3}{3}-\frac{c^2y}{5}+\right.$ $\left.+\nu\left(\frac{y^3}{6}-\frac{c^2y}{2}-\frac{c^3}{3}\right)\right]$	$+M'''\left[\frac{y^5}{40}+\frac{c^2y^3}{60}+\frac{c^3y^2}{6}-\frac{87c^4y}{4200}-\frac{c^5}{18}\right.$ $\left.+\nu\left(\frac{y^5}{60}-\frac{c^2y^3}{30}+\frac{c^4y}{60}\right)\right]$
EIv	$-\iint M\,dx\,dx$	$M\left[\frac{4c^2}{5}+\left(c^2-y^2\right)\frac{\nu}{2}\right]$	$M''\left[\frac{y^4}{24}-\frac{c^2y^2}{4}-\frac{c^3y}{3}+\frac{227c^4}{4200}+\right.$ $\left.+\nu\left(\frac{y^4}{12}-\frac{c^2y^2}{10}+\frac{c^4}{60}\right)\right]$
$u_{y=0}$	0	$+\frac{\nu M'c^3}{3EI}$	$-\frac{c^5M'''}{18EI}$
$v_{y=0}$	$-\frac{1}{EI}\iint M\,dx\,dx$	$\frac{M}{EI}\left(\frac{4c^2}{5}+\frac{\nu c^2}{2}\right)$	$\frac{M''}{EI}\left[\frac{227c^4}{4200}+\frac{\nu c^4}{60}\right]$
$\left(\frac{d^2v}{dx^2}\right)_{y=0}$	$-\frac{M}{EI}$	$\frac{M''}{EI}\left(\frac{4c^2}{5}+\frac{\nu c^2}{2}\right)$	$\frac{M''}{EI}\left[\frac{227c^4}{4200}+\frac{\nu c^4}{60}\right]$
NOTE;	$\phi=\sum\phi_i$; $'\equiv\frac{\partial}{\partial x}$; $\sigma_y=-\frac{\partial^2\phi}{\partial x^2}$; $I=\frac{2bc^3}{3}$; $A=2bc$		

TABLE 2 SOLUTION FOR CASE II

i	1	2	3
ϕ	$\frac{M}{I}\left(\frac{y^3}{6}-\frac{c^2y}{6}\right)$	$\frac{M''}{I}\left(-\frac{y^5}{60}+\frac{c^2y^3}{30}-\frac{c^4y}{60}\right)$	$\frac{M^{III}}{I}\left(\frac{y^7}{1680}-\frac{7y^5c^2}{3600}+\frac{53c^4y^3}{25200}-\frac{19c^6y}{25200}\right)$
σ_x	$\frac{M_y}{I}$	$-\frac{M''}{I}\left(\frac{y^3}{3}-\frac{yc^2}{5}\right)$	$\frac{M^{III}}{I}\left(\frac{y^5}{40}-\frac{7y^3c^2}{180}+\frac{53yc^4}{4200}\right)$
τ_{xy}	$-\frac{M'}{I}\left(\frac{y^2}{2}-\frac{c^2}{6}\right)$	$\frac{M''}{I}\left(\frac{y^4}{12}-\frac{y^2c^2}{10}+\frac{c^4}{60}\right)$	$-\frac{M^{I}}{I}\left(\frac{y^6}{240}-\frac{7y^4c^2}{720}+\frac{53c^4y^2}{8400}-\frac{19c^6}{25200}\right)$
EIU	$y\int M\,dx$	$M'\left[-\frac{y^3}{3}+\frac{yc^2}{5}-\frac{\nu y(y^2-c^2)}{6}\right]$	$M'''\left[\frac{y^5}{40}-\frac{7y^3c^2}{180}+\frac{53yc^4}{4200}+\frac{\nu y\left(y^2-c^2\right)^2}{60}\right]$
EIV	$-\iint M\,dx\,dx$	$M\left[\frac{2c^2}{15}+\nu\left(\frac{c^2}{6}-\frac{y^2}{2}\right)\right]$	$M''\left[\frac{y^4}{24}-\frac{c^2y^2}{12}+\frac{87c^4}{4200}+\nu\left(\frac{y^4}{12}-\frac{y^2c^2}{10}+\frac{c^4}{60}\right)\right]$
$u_{y=0}$	0	0	0
$v_{y=0}$	$-\frac{1}{EI}\iint M\,dx\,dx$	$\frac{M}{EI}\left(\frac{2c^2}{15}+\frac{\nu c^2}{6}\right)$	$\frac{M''}{EI}\left(\frac{87c^4}{4200}+\frac{\nu c^4}{60}\right)$
$\left(\frac{d^2v}{dx^2}\right)_{y=0}$	$-\frac{M}{EI}$	$\frac{M''}{EI}\left(\frac{2c^2}{15}+\frac{\nu c^2}{6}\right)$	$\frac{M''}{EI}\left(\frac{87c^4}{4200}+\frac{\nu c^4}{60}\right)$
NOTE;	$\phi=\sum\phi_i$; $'\equiv\frac{\partial}{\partial x}$; $\sigma_y=\frac{\partial^2\phi}{\partial x^2}$; $I=\frac{2bc^3}{3}$; $A=2bc$		

TABLE 3 SOLUTION FOR CASE III

i	1	2	3
ϕ	$\frac{P}{A}\left(\frac{y^2}{2}-\frac{c^2}{2}\right)$	$\frac{P''}{A}\left(-\frac{y^4}{12}+\frac{y^2c^2}{6}-\frac{c^4}{12}\right)$	$\frac{P^{III}}{A}\left(\frac{y^6}{240}-\frac{y^4c^2}{144}+\frac{c^4y^2}{720}+\frac{c^6}{720}\right)$
σ_x	$\frac{P}{A}$	$-\frac{P''}{A}\left(y^2-\frac{c^2}{3}\right)$	$\frac{P^{III}}{A}\left(\frac{y^4}{8}-\frac{c^2y^2}{12}+\frac{c^4}{360}\right)$
τ_{xy}	$-\frac{P'y}{A}$	$\frac{P''}{A}\left(\frac{y^3}{3}-\frac{yc^2}{3}\right)$	$-\frac{P^{I}}{A}\left(\frac{y^5}{40}-\frac{c^2y^3}{36}+\frac{c^4y}{360}\right)$
AEU	$\int P\,dx$	$-P'\left[y^2\frac{c^2}{3}-\frac{\nu}{2}\left(y^2-c^2\right)\right]$	$P'''\left[\frac{y^4}{8}-\frac{c^2y^2}{12}+\frac{c^4}{360}+\frac{\nu}{12}\left(y^2-c^2\right)^2\right]$
AEV	$-\nu Py$	$P''\left[\frac{y^3}{6}-\frac{c^2y}{2}+\frac{\nu}{3}\left(y^3-c^2y\right)\right]$	$P^{III}\left[-\frac{y^5}{60}+\frac{c^2y^3}{18}-\frac{c^4y}{12}-\nu\left(\frac{y^5}{40}-\frac{c^2y^3}{36}+\frac{c^4y}{360}\right)\right]$
$u_{y=0}$	$\frac{1}{AE}\int P\,dx$	$\frac{c^2P'}{AE}\left(\frac{1}{3}-\frac{\nu}{2}\right)$	$\frac{c^4P'''}{AE}\left[\frac{1}{360}+\frac{\nu}{12}\right]$
$v_{y=0}$	0	0	0
$\left(\frac{d^2v}{dx^2}\right)_{y=0}$	0	0	0
NOTE:	$\phi=\sum\phi_i$; $'\equiv\frac{\partial}{\partial x}$; $\sigma_y=\frac{\partial^2\phi}{\partial x^2}$; $I=\frac{2bc^3}{3}$; $A=2bc$		

corresponding more accurate expression for the stress can be written, analogously to Equation [1c], in terms of successively higher derivatives of P with respect to x. As above, therefore, Equation [2] is very accurate for smooth loadings.

The results are collected in Tables 1, 2, and 3, respectively, for Cases I, II, and III of Fig. 1. The first of these is the same as was considered in references (1, 2), but is, nevertheless, included so as to correct some numerical inaccuracies present in the latter.[4] It also should be noted that the method of solution described in the following is different from that of references (1, 2).

Method of Solution

The results obtained by von Karman and Seewald were derived with the aid of an integral transform technique, and by then expanding the bending-moment distribution in a Taylor series along the span. Such a technique has the advantage that it yields a solution not only in the case of smoothly varying loads, but it also can describe the behavior of the beam in the neighborhood of concentrated loads. If the investigation is restricted to the former type of loading, however, it is desired to use a simpler procedure, such as that developed in reference (3). This procedure consists of a step-by-step solution of the governing linear partial differential equation and was found in reference (3) to be of wide applicability. It was, in fact, used there in the solution of the heat-conduction equation as well as for the equations of two-dimensional thermoelasticity. It is interesting to note that in both of these applications the results were expressible in terms of series of the same general nature as that of Equation [1c], and therefore could be used as the basis of approximate theories in those fields.

The proposed method of solution was discussed in detail in reference (3); only the steps strictly necessary for the present solutions will be outlined here. It is desired to obtain an expression for the Airy stress function φ (4), related to the stresses by the relations

$$\sigma_x = \frac{\partial^2\varphi}{\partial y^2}; \quad \sigma_y = \frac{\partial^2\varphi}{\partial x^2}; \quad \tau_{xy} = -\frac{\partial^2\varphi}{\partial x \partial y} \dots\dots [3]$$

and satisfying the differential equation

$$\frac{\partial^4\varphi}{\partial x^4} + 2\frac{\partial^4\varphi}{\partial x^2\partial y^2} + \frac{\partial^4\varphi}{\partial y^4} = 0 \dots\dots [3a]$$

as well as the boundary conditions listed in Fig. 1 for each loading considered.

The solution is written in the form

$$\varphi = \varphi_1 + \varphi_2 + \varphi_3 + \dots\dots [4]$$

where the functions φ_i satisfy the following equations

$$\frac{\partial^4\varphi_i}{\partial y^4} = -2\frac{\partial^4\varphi_{i-1}}{\partial x^2\partial y^2} - \frac{\partial^4\varphi_{i-2}}{\partial x^4}; \quad \varphi_i = 0 \text{ for } i < 1 \dots [4a]$$

The boundary conditions for the function φ_1 are identical with those given in Fig. 1; those for the other functions φ_i state that the stresses σ_y and τ_{xy} must vanish at $y = \pm c$ and can be shown to be reducible to

$$\varphi_i = \frac{\partial\varphi_i}{\partial y} = 0 \quad \text{at } y = \pm c; \; i > 1 \dots\dots [4b]$$

Inspection of Equations [3a], [4], [4a], and [4b] shows that the function φ obtained in this manner will satisfy all the conditions of the problem. Furthermore, each function φ_i will contain derivatives with respect to x of a single order only, the order increasing with i, so that the result is obtained in the desired form.

The function φ_1 depends on the particular case considered; however, the relation between φ_i, φ_{i-1}, and φ_{i-2} does not, and can be found readily by solving Equations [4a] under the boundary conditions [4b]. The final result is, after several integrations by parts, as follows

$$\begin{aligned}
\varphi_i = &-2y\int_{-c}^{y}\varphi''_{i-1}\,dy + 2\int_{-c}^{y}\varphi''_{i-1}\,y\,dy - \frac{y^3}{6}\int_{-c}^{y}\varphi^{(IV)}{}_{i-2}\,dy \\
&+ \frac{y^2}{2}\int_{-c}^{y}\varphi^{(IV)}{}_{i-2}\,y\,dy - \frac{y}{2}\int_{-c}^{y}\varphi^{(IV)}{}_{i-2}\,y^2\,dy \\
&+ \frac{1}{6}\int_{-c}^{y}\varphi^{(IV)}{}_{i-2}\,y^3\,dy + \left[\frac{c}{2} + y + \frac{y^2}{2c}\right]\int_{-c}^{c}\varphi''_{i-1}\,dy \\
&+ \left[\frac{y^3}{2c^3} - \frac{3y}{2c} - 1\right]\int_{-c}^{c}\varphi''_{i-1}\,y\,dy + \left[\frac{y^3}{12} + \frac{cy^2}{8} - \frac{c^3}{24}\right]\times \\
&\int_{-c}^{c}\varphi^{(IV)}{}_{i-2}\,dy + \left[-\frac{y^3}{8c} - \frac{y^2}{4} - \frac{cy}{8}\right]\int_{-c}^{c}\varphi^{(IV)}{}_{i-2}\,y\,dy \\
&+ \left[\frac{y^2}{8c} + \frac{y}{4} + \frac{c}{8}\right]\int_{-c}^{c}\varphi^{(IV)}{}_{i-2}\,y^2\,dy + \left[\frac{y^3}{24c^3}\right. \\
&\left. - \frac{y}{8c} - \frac{1}{12}\right]\int_{-c}^{c}\varphi^{(IV)}{}_{i-2}\,y^3\,dy \dots\dots [5]
\end{aligned}$$

With the foregoing formulas, the results of Tables 1, 2, and 3 pertaining to the stress function and the stresses are readily derived.

Calculation of Displacements

The displacements u and v, in the x and y-directions, respectively, must satisfy the equations (4)

$$\left.\begin{aligned}
E\frac{\partial u}{\partial x} &= \sigma_x - \nu\sigma_y \\
E\frac{\partial v}{\partial y} &= \sigma_y - \nu\sigma_x \\
E\left(\frac{\partial u}{\partial y} + \frac{\partial v}{\partial x}\right) &= 2(1+\nu)\tau_{xy}
\end{aligned}\right\} \dots\dots [6]$$

where ν is Poisson's ratio and where the stresses are obtained from Tables 1, 2, or 3. The displacements are obtained by integrating the first and second of Equations [6] with respect to x and y, respectively, and then adjusting the arbitrary functions which arise during this process so as to satisfy the third of Equations [6]. The final results for Cases I, II, and III of Fig. 1 are collected in Tables 1, 2, and 3. It should be noted that in all cases rigid body displacements given by

$$u_{RB} = c_1 + c_2 y; \quad v_{RB} = c_3 - c_2 x \dots\dots [6a]$$

have been omitted.

For comparison with the deflection formulas of elementary theory, the expression for u, v, and $(\partial^2 v/\partial x^2)$ on the line $y = 0$ have also been included in Tables 1, 2, and 3. Similar expressions could have been obtained on the basis of average displacements defined by

$$u_{avg} = \frac{1}{2c}\int_{-c}^{c} u\,dy; \quad v_{avg} = \frac{1}{2c}\int_{-c}^{c} v\,dy \dots\dots [7]$$

[4] The authors wish to thank one of the reviewers of this paper for bringing to their attention reference (7) in which the inaccuracies of reference (2) are corrected. Some of the results of Table 1 are, in fact, the same (with a different sign convention) as those of reference 7.

Importance of Correction to Elementary Formulas

Discussions of the importance, for Case I of Fig. 1, of the correction required to the elementary formulas have been given in the Introduction and in the works cited there. Briefly, it may be stated that the magnitude of the correction will be in the smaller, for a given beam, the smoother the bending-moment variation. Comparison of Tables 1, 2, and 3 shows that the results are of similar form in all three cases of loading considered in this paper and therefore the foregoing conclusion may be extended to apply to Cases II and III as well.

A different viewpoint may be obtained by considering the same loading distribution to be applied to beams of different dimensions, and by comparing the magnitude of the correction to the elementary theory in these cases. This may be done by expressing the results in nondimensional form. With the nondimensional variables

$$\varphi_1 = \frac{\varphi I}{c^3 M_0}; \quad M_1 = \frac{M}{M_0}; \quad x_1 = \frac{x}{L}; \quad y_1 = \frac{y}{c} \qquad [8]$$

where M_0 is a constant reference moment, the stress function of Case II, for example, becomes

$$\varphi_1 = M_1\left(\frac{y_1^3}{6} - \frac{y_1}{6}\right) - \left(\frac{c}{L}\right)^2 \frac{d^2M_1}{dx_1^2}\left(\frac{y_1^5}{60} - \frac{y_1^3}{30} + \frac{y_1}{60}\right) + \left(\frac{c}{L}\right)^4 \frac{d^4M_1}{dx_1^4}\left(\frac{y_1^7}{1680} - \frac{7y_1^5}{3600} + \frac{53y_1^3}{25{,}200} - \frac{19y_1}{25{,}200}\right) + \cdots \qquad [8a]$$

Similar results hold for the other cases of loading. Inspection of Equation [8a] shows that the correction terms to the elementary theory are proportional to successively higher powers of the aspect ratio (c/L) of the beam. It may then be concluded that, for a given loading on a given span length, the importance of the correction terms will be smaller for thinner beams.

Relation to the Timoshenko Theory of Beams

An improvement on the elementary beam theory was introduced by Timoshenko (5), who considered the shearing deformations of the beam. Assuming the beam deflections to be made up of two parts, caused by bending and shear and denoted by v_b and v_s, respectively (6), one may write the relation between bending moment and curvature, analogous to Equation [1a], as

$$\frac{d^2v_b}{dx^2} = -\frac{M}{EI} \qquad [9a]$$

The governing equations of Timoshenko beams are, for static loadings

$$\left.\begin{aligned} V &= (GA/N)(v' - v'_b) \\ M' - V + 2c\tau &= 0 \\ V' + q &= 0 \end{aligned}\right\} \qquad [9b]$$

in addition to Equation [9a]. V denotes the shear force at any cross section, G the shear modulus, v the total deflection (i.e., $v = v_b + v_s$), and primes, differentiation with respect to x. The terms q and τ again refer to the loadings for Cases I and II, respectively.

Elimination of V and v''_b from Equations [9a] and [9b] gives the following relation between the total curvature v'' and the bending moment M

$$v'' = -\frac{M}{EI} + \frac{N}{GA}(M'' + 2c\tau') \qquad [10]$$

Comparison with Case II of Fig. 1 shows that in this case the term in parentheses vanishes, and that therefore no improvement in the curvature results from Timoshenko's theory. In Case I, however, the results of Table 1 and of Equation [10] are of a similar form. The coefficient of M'' in Equation [10] is, in fact, identical with the coefficient of M'' in the expression for the curvature of Table 1 if the value of N is taken to be

$$N = \frac{24 + 15\nu}{20(1 + \nu)} \qquad [11]$$

For $\nu = 0$ the familiar value $N = 1.2$ of course results.

BIBLIOGRAPHY

1 "Über die Grundlagen der Balkentheorie," by Th. von Karman, Abh. Aerodynam. Inst., Technische Hochschule, Aachen, Germany, vol. 7, 1927, pp. 3–10.

2 "Die Spannungen und Formänderungen von Balken mit rechteckigem Querschnitt," by F. Seewald, Abh. Aerodynam. Inst., Technische Hochschule, Aachen, Germany, vol. 7, 1927, pp. 11–33.

3 "The Determination of Temperature, Stresses and Deflections in Two-Dimensional Thermo-Elastic Problems," by B. A. Boley, *Journal of the Aeronautical Sciences*, vol. 23, no. 1, January, 1956, pp. 67–75.

4 "Theory of Elasticity," by S. Timoshenko and J. N. Goodier, McGraw-Hill Book Company, Inc., New York, N. Y., second edition, 1951.

5 "Vibration Problems in Engineering," by S. Timoshenko, D. Van Nostrand Company, Inc., New York, N. Y., third edition, 1955, p. 329.

6 "An Approximate Theory of Lateral Impact on Beams," by B. A. Boley, Journal of Applied Mechanics, Trans. ASME, vol. 77, 1955, pp. 69–76.

7 "Bending of Rectangular Beams," by L. H. Donnell, Journal of Applied Mechanics, Trans. ASME, vol. 74, 1952, p. 123.

A Study of Orthogonally Stiffened Plates

By W. H. HOPPMANN, 2ND,[1] N. J. HUFFINGTON, JR.,[2] AND L. S MAGNESS[3]

A previous theory and method for the analysis of orthogonally stiffened plates (1)[4] has been extended to include additional study of theoretical and experimentally determined frequencies of vibration and strain distributions. Some details of calculations based on the theory as well as experimental results are provided in curves and tables. Sufficient verification of the theory is obtained to warrant serious consideration of possible use of the method for design purposes.

Nomenclature

The following nomenclature is used in the paper:

ϵ_i = extensional strain
γ = shear strain
σ_j = extensional stress
τ = shear stress
S_{ij} = elastic constants ($S_{ij} = S_{ji}$)
$E_x = \frac{1}{S_{11}}$ = Young's modulus
$E_y = \frac{1}{S_{22}}$ = Young's modulus
$G_{xy} = \frac{1}{S_{66}}$ = rigidity or shear modulus
$\nu_{xy} = -E_x S_{12}$ = Poisson's ratio
$\nu_{yx} = -E_y S_{12}$ = Poisson's ratio
M_x = bending couple per unit length on edges parallel to y-axis
M_y = bending couple per unit length on edges parallel to x-axis
w = deflection of plate
h^* = thickness of plate (equivalent orthotropic plate)
a = width of plate
b = length of plate
x, y = co-ordinates of point on surface of plate
A_x, A_y, A_{xy} = constants in differential equations of plate and are expressions in terms of the elastic constants S_{ij}
$F(x, y, t)$ = force applied normally to face of plate
ρ = mass density
t = time
p_{mn} = circular frequency of m-, n-mode of vibration of rectangular plate
m, n = mode numbers corresponding to x-direction and y-direction, respectively
P_0 = amplitude of driving force
ω = circular frequency of driving force
D_x, D_y, H = elastic plate moduli in terms of A_x, A_{xy}, A_y

Introduction

The technological importance of the mechanics of stiffened plates is sufficiently well established to require no elaboration. However, it may be worth while to emphasize the growing importance of panels with integrally attached stiffeners, especially in aeronautical engineering. The new industrial approaches to such design matters increases the need for fresh concepts and methods in analyzing the performance of stiffened structures subjected to static or dynamic loads. The principal methods of analysis of deformation of stiffened structures are generally still based on a treatment of the plate as separate from the stiffener system. As an exception, several technical papers have described analysis for treating the stiffened plate as an equivalent plate of homogeneous, uniformly thick, anisotropic material. However, the investigators who have done this work have invariably attempted to estimate the bending and twisting compliances for the stiffened plates on a theoretical basis, using beam theory as a guide. In a recent paper (1) by one of the authors, a method of systematically determining elastic compliances of stiffened plates by a set of consistent experiments was proposed. Results of the analysis and experimentation were very encouraging.

In the present paper further experimentation based on the method is described and discussed. In particular, the distribution of strain is studied along with frequency of flexural vibration. For the purpose, two different designs of stiffened plates were investigated. Proper determination of frequencies of vibration of the stiffened plates is essential for analysis of the dynamic response of such plates. Furthermore, strain studies are needed in order to evaluate properly the effect of strain concentration associated with the stiffeners.

Résumé of the Theory of Compliances of a Stiffened Plate

In a paper already mentioned (1) the theory and method for determining elastic compliances of stiffened plates have been described at some length. For the present purpose only a brief résumé will be given here. A stiffened plate is considered as if it were approximately a plate of homogeneous orthotropic material of some definite thickness. It is further assumed that the elastic constants of this equivalent orthotropic plate can be chosen in such a manner that it will have approximately the bending and twisting stiffnesses or compliances of the given orthogonally stiffened plate.

Now suppose that conveniently sized but sufficiently representative rectangular and square test plates are machined just like sections from the stiffened prototype. These test plates may themselves be looked upon as small orthotropic plates. The rectangular plates serve for bending tests and the square ones for twisting tests. The elastic constants determined from tests on these model plates will be assumed to be sufficiently close approximations to those of the stiffened material of which the prototype is made. It is assumed further that the plates are effectively homogeneous and orthotropic and therefore have three axes of symmetry for the elasticity at each point. The edges of the test

[1] Associate Professor of Mechanical Engineering, The Johns Hopkins University, Baltimore, Md. Mem. ASME.
[2] Associate Professor of Applied Mechanics, Virginia Polytechnic Institute, Blacksburg, Va. Assoc. Mem. ASME.
[3] Graduate Student, The Johns Hopkins University, Baltimore, Md. Assoc. Mem. ASME.
[4] Numbers in parentheses refer to the Bibliography at the end of the paper.

Presented at the National Applied Mechanics Conference, Urbana, Ill., June 14–16, 1956, of The American Society of Mechanical Engineers.
Discussion of this paper should be addressed to the Secretary, ASME, 29 West 39th Street, New York, N. Y., and will be accepted until October 10, 1956, for publication at a later date. Discussion received after the closing date will be returned.
Note: Statements and opinions advanced in papers are to be understood as individual expressions of their authors and not those of the Society. Manuscript received by ASME Applied Mechanics Division, August 19, 1955. Paper No. 56—APM-11.

plates are parallel to the stiffeners and hence parallel to the principal directions of stiffness, respectively.

The stress-strain relation in the usual notation of the equivalent orthotropic material may be written for strains in terms of the elastic constants and stresses as

$$\left.\begin{aligned} \epsilon_i &= S_{ij}\sigma_j \qquad (i, j = 1, 2) \\ \gamma &= S_{66}\tau \end{aligned}\right\} \ldots\ldots\ldots [1]$$

Three planes of symmetry are assumed and there are four independent constants of elasticity $S_{ij}(S_{12} = S_{21})$.

It may be recalled that the differential equation for forced flexural vibrations can be written as

$$A_x \frac{\partial^4 w}{\partial x^4} + A_{xy} \frac{\partial^4 w}{\partial x^2 \partial y^2} + A_y \frac{\partial^4 w}{\partial y^4} + \rho h^* \frac{\partial^2 w}{\partial t^2} = F(x, y, t) \ldots [2]$$

The constants A_x, A_{xy}, and A_y can readily be put in terms of the elastic constants S_{ij} (see the nomenclature for definition of terms). Apparatus for determination of S_{ij} is described in reference (2).

In order to determine the effective elastic constants S_{ij} for the stiffened plates we take the acceleration and applied force F identically zero in Equation [2]. The equation can then be solved for certain simple boundary conditions which can be approximated by bending and twisting experiments.

Experiments for the purpose, as applied to our particular designs of stiffened steel plates, will be described shortly.

If the driving force F is taken identically zero the resulting equation can be solved subject to given boundary conditions so that the frequency of flexural vibrations is determined. For the case of simply supported rectangular plates the circular frequencies p_{mn} are given as follows (1)

$$p_{mn} = \frac{\pi^2}{\sqrt{\rho h^*}} \sqrt{D_x \frac{m^4}{a^4} + 2H \frac{m^2 n^2}{a^2 b^2} + D_y \frac{n^4}{b^4}} \ldots [3]$$

Bending Strains

The extension of the previous work on the bending of orthogonally stiffened plates (1) to include a study of flexural strains will now be considered. It is quite clear that stiffeners on a plate introduce stress concentrations in the regions where stiffener is attached to plate. This fact greatly complicates the problem of determining strain at every point of such a plate. In view of this, it seems useful to study the bending strains calculated for the equivalent homogeneous orthotropic plate and compare them with strains measured on actual plates. For the purpose of experimentation a force for producing the strain is required. This force may be useful both in the determination of natural frequencies of vibration as well as strain distribution. Consequently it should preferably be a driving force of the following type

$$F(x, y, t) = 0$$

at any point except

$$\left.\begin{aligned} &\left(\frac{a}{2}, \frac{b}{2}\right) \text{ and} \\ F&\left(\frac{a}{2}, \frac{b}{2}, t\right) = P_0 \sin \omega t \end{aligned}\right\} \ldots\ldots\ldots [4]$$

This force can be approximated by a magnetic drive and it is associated with a relatively simple solution to the differential equation of motion, Equation [2], for simple-supported boundary conditions.

Such boundary conditions for a rectangular plate may be expressed as follows

$$\left.\begin{aligned} M_x &= 0 \quad \text{for boundary perpendicular to } x\text{-axis} \\ M_y &= 0 \quad \text{for boundary perpendicular to } y\text{-axis} \\ w &= 0 \quad \text{entire boundary} \end{aligned}\right\} \ldots [5]$$

The Lagrangian technique, illustrated by Timoshenko for the vibrations of a bar (7), may readily be used to obtain a solution to the plate equation assuming a force given by Equation [4].

The characteristic functions in the space variables are obviously sine functions and the solution may be written

$$w = \sum_1^\infty \sum_1^\infty \sin \frac{m\pi x}{a} \sin \frac{n\pi y}{b} q_n(t) \ldots\ldots [6]$$

This equation obviously satisfies the boundary conditions.

Using the Lagrangian equations of motion the functions $q_n(t)$ can be determined readily, and the final solution is

$$w = \Sigma\Sigma \frac{4P_0}{\rho a^2 h^*} \sin \frac{m\pi}{2} \sin \frac{n\pi}{2} \sin \frac{m\pi x}{a} \sin \frac{n\pi y}{b} \left[\frac{1}{p_{mn}^2 - \omega^2}\left(\sin \omega t - \frac{\omega}{p_{mn}} \sin p_{mn} t\right)\right] \ldots\ldots [7]$$

The frequencies p_{mn} turn out to be again those given by Equation [3].

It may be noted that in the equation for the displacement w, thickness of the plate does not explicitly occur. The reason for this is clear when we appreciate the fact that the circular frequencies p_{mn} depend on the measured stiffnesses but are independent of the explicit thickness h. The fact has been extensively discussed in a previous paper (1).

The elastic bending strains may now be readily represented by (8)

$$\left.\begin{aligned} \epsilon_x &= -z \frac{\partial^2 w}{\partial x^2} \\ \epsilon_y &= -z \frac{\partial^2 w}{\partial y^2} \end{aligned}\right\} \ldots\ldots\ldots [8]$$

The strains depend on some z which it will be necessary to specify.

Experiments to Determine Natural Frequencies of Vibration and Bending Strains

For the purpose of the investigation, two designs of stiffened plates were more or less arbitrarily chosen. No special significance attaches to these designs except that they are relatively economical to manufacture and do provide stiffeners machined onto the plates. A symmetrical design with stiffeners on both sides was decided upon partly to provide data for testing various methods of calculating rigidity factors proposed by one of the authors (3). Details of the stiffeners on these plates are shown in Table 1.

For each design three plates are required for determination of elastic constants (1): Two rectangular plates for bending tests each 6 in. × 18 in., and one square plate for twisting test 12 in. × 12 in. The square plates were also used in vibration tests. The bending and twisting test apparatus is shown in Fig. 1 and Fig. 2, respectively. A set of the experimental plates is shown in Fig. 3. A schematic diagram of the actual loading of plates to determine S_{ij} is shown in Fig. 4(*a* and *b*).

The vibration test stand on which the square plates were mounted for the study of natural frequencies and strain distribution is shown in Fig. 5. It is solid steel and quite massive. As may be noted, a rigid holding frame with large bolts is used to clamp the periphery of test plate to the stand. Since the theoretical solution derived is for simply supported plates, a method pre-

TABLE 1 DIMENSIONS OF REPEATING CROSS SECTIONS OF TEST SPECIMENS

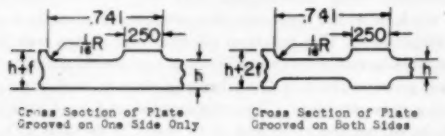

Cross Section of Plate Grooved on One Side Only

Cross Section of Plate Grooved on Both Sides

PLATES GROOVED ON ONE SIDE ONLY

SPECIMEN	h, inches	h+f, inches
Longitudinally Grooved Bending Specimen	.1945	.2584
Transversely Grooved Bending Specimen	.1949	.2606
Twisting Specimen	.1946	.2568

PLATES GROOVED ON BOTH SIDES

SPECIMEN	h, inches	h+2f, inches
Longitudinally Grooved Bending Specimen	.1323	.2559
Transversely Grooved Bending Specimen	.1355	.2606
Twisting Specimen	.1378	.2630

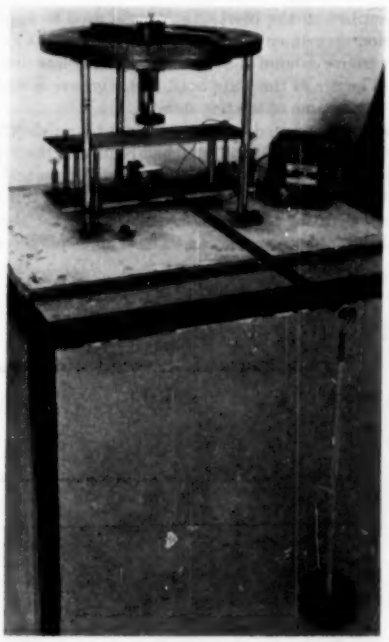

FIG. 1 BENDING TEST

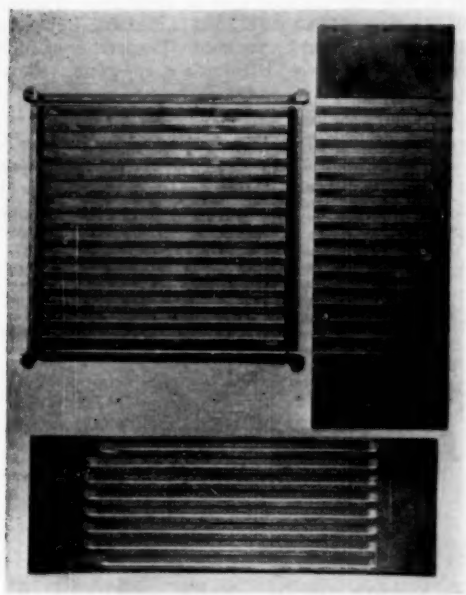

FIG. 3 SET OF THREE TEST PLATES

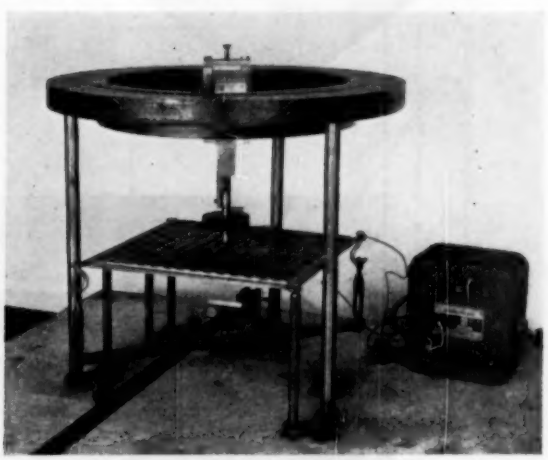

FIG. 2 TWISTING TEST

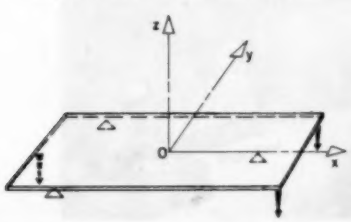

FIG. 4(a) BENDING PLATE

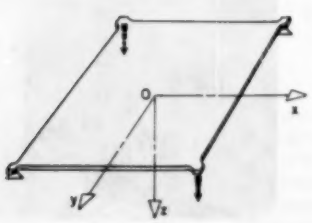

FIG. 4(b) TWISTING PLATE

viously described in the literature (4) was used to approximate this condition experimentally. Essentially it consists in machining a deep groove around the boundary of the plate and close to the edge. The rim of the plate outside this groove is then rigidly attached to the frame of the test stand.

Vibrations were excited in the test plate by an electromagnet located beneath the plate and attached rigidly to the supporting stand. It was necessary to design a special circuit to get the most effective use out of the magnetic drive. To do this the magnetic circuit operating off an audio oscillator has variable capacitance and variable resistance for matching purposes. This method was proposed by H. S. McDonald who constructed the circuit actually used. The circuit was a very effective one in the type of work in which resonance frequencies are actually excited in test structures. The practical effect of the design was to increase strains to easily measurable levels but also it amplified the acoustical power output of the vibrating plate to such a point as to create a noise problem. The measured sound level at a point about 6 in. above the vibrating plate was 125 decibels as measured on the flat C scale of a General Radio sound-level meter. Comparative noise levels characteristic of various human occupations are given in the literature (6).

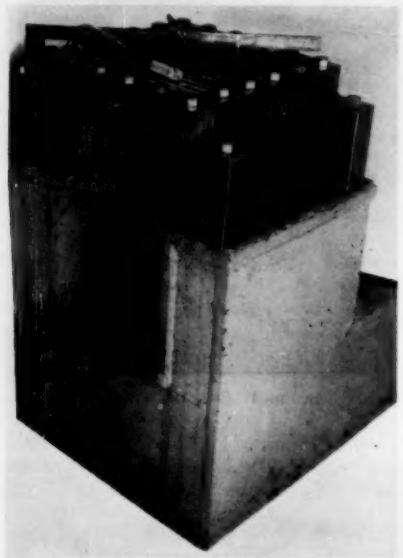

FIG. 5 VIBRATION TEST APPARATUS

To solve the noise problem it was necessary to build an acoustic hood which was essentially a three-sided box with a top made to fit over the test stand and sealing the fourth side against a fixed bulkhead. The bottom was fitted tightly against the floor. The resulting test cubicle was about 38 in. × 38 in. × 49 in. The hood was constructed of $^3/_4$-in. plywood with 6-in. × $^3/_4$-in. extra apron around the bottom. The inside was lined with 1-in-thick phenolic-base fiberglas faced with glass cloth. Air space of about $1^1/_2$ in. was provided everywhere except on the fixed-end bulkhead and the bottom.

The design principles for such soundproofed spaces are well known (5, 6) and will not be discussed here. It may be recalled, however, that the absorbent material reduces the sound in the enclosures and therefore less insulating material is necessary to reduce transmission from the enclosure to the outside. It may be of interest to note that the hood gave an attenuation of about 28 decibels as measured at a control point in the laboratory but outside of the space covered by the hood. The level dropped from 121 decibels to 93 decibels. Experimental apparatus is shown in Fig. 5(a).

Strains were measured with standard equipment using resistance-type strain gages. The gages actually used were SR-4 gages numbered C-5, A-7, and A-8. The shorter gages were essential in measuring strains on the surface of the stiffeners in a direction normal to length of stiffeners. The width of stiffener is only 0.250 in.

FIG. 5(a) EXPERIMENTAL APPARATUS

Resonances in the vibration tests used to determine natural frequencies of vibration were indicated by these strain measurements shown on a cathode-ray oscilloscope as well as by crystal-type pickup output which was also observed on the oscilloscope. The audio oscillator, feeding into a power amplifier, excited an electromagnet which vibrated the plate. In this manner the natural frequencies of the plate were determined at resonance.

Amplitudes of vibration at the center of the plate were measured with a sensitive displacement meter.

Experimental Results and Theoretical Calculations

The elastic compliances defined in this paper as load per unit deflection, were based on load-deflection curves such as those shown in Figs. 6–8.

TABLE 2 ELASTIC CONSTANTS

	ELASTIC CONSTANTS				
	$\frac{S_{11}}{h^3}\times10^6$, $(lb.in.)^{-1}$	$\frac{S_{12}}{h^3}\times10^6$, $(lb.in.)^{-1}$	$\frac{S_{21}}{h^3}\times10^6$, $(lb.in.)^{-1}$	$\frac{S_{22}}{h^3}\times10^6$, $(lb.in.)^{-1}$	$\frac{S_{66}}{h^3}\times10^6$, $(lb.in.)^{-1}$
Plate grooved on one side	2.67	-0.76	-0.73	3.37	9.34
Plate grooved on both sides	3.96	-1.77	-1.69	7.90	12.85

TABLE 3 ELASTIC MODULI AND POISSON'S RATIOS

	ELASTIC MODULI AND POISSON'S RATIOS				
	$E_x h^3$, lb.in.	$E_y h^3$, lb.in.	$G_{xy} h^3$, lb.in.	ν_{xy}	ν_{yx}
Plate grooved on one side	375000	296000	107000	0.28	0.22
Plate grooved on both sides	252000	126500	77800	0.44	0.22

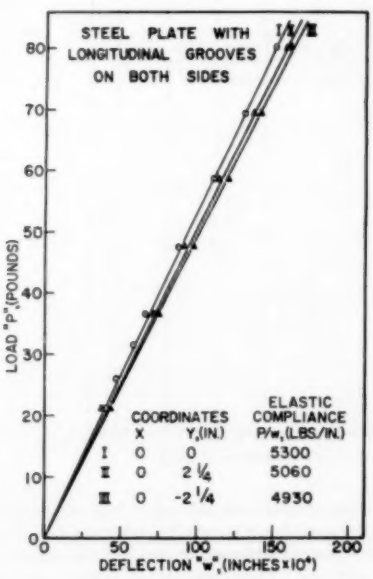

Fig. 6 Bending Test

The calculated elastic constants S_{ij} based on the experimentally determined compliances are given in Table 2. In Table 3 the corresponding elastic moduli and Poisson ratios are shown.

TABLE 4 ELASTIC PLATE MODULI

	ELASTIC PLATE MODULI				
	D_x, lb.in.	D_y, lb.in.	D_{xy}, lb.in.	D_1, lb.in.	H, lb.in.
Plate grooved on one side	33300	26300	8920	7370	25210
Plate grooved on both sides	23250	11660	6480	5090	18050

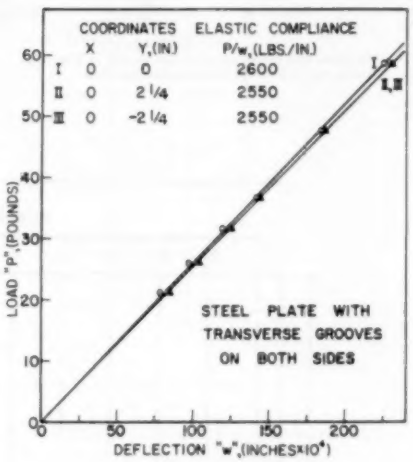

Fig. 7 Bending Test

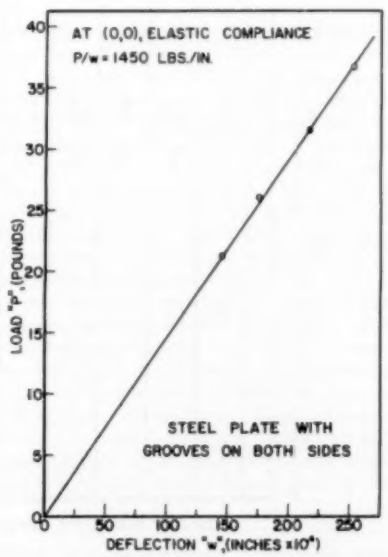

Fig. 8 Twisting Test

Elastic plate moduli, or more specifically, the constants D_x, D_y, and H occurring in the frequency equation are given in Table 4.

For the present purpose, strain measurements were limited to points along the two principal axes through the center of the plate. One of these center lines is along the top of a stiffener. The other center line is transverse to the direction of the stiffeners. Strain gages were placed atop the stiffeners (Fig. 9) as well as on the

TABLE 5 MEASURED STRAINS AT VARIOUS LOCATIONS ON PLATE WITH STIFFENERS ON BOTH SIDES

Location	Strain	Location	Strain
A	22	N	118
B	42	O	...
C	65	P	36
D	80	Q	25
E	94	R	Negligible
F	169	S	Negligible
G	101	T	Negligible
H	107	U	178
I	186	V	122
J	182	W	45
K	159	X	98
L	Negligible	Y	Negligible
M	...	Z	169

NOTE: 1 Locations and direction of strain shown in Fig. 10.
2 Strains are in units of microinches per inch.

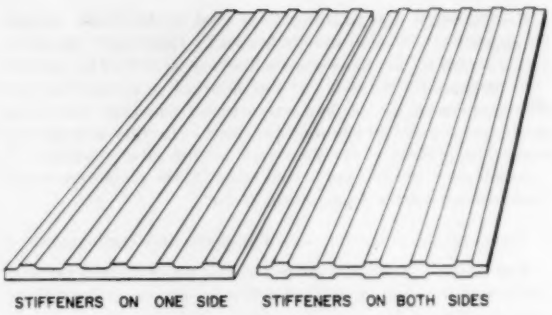

FIG. 9 STIFFENED EXPERIMENTAL PLATES

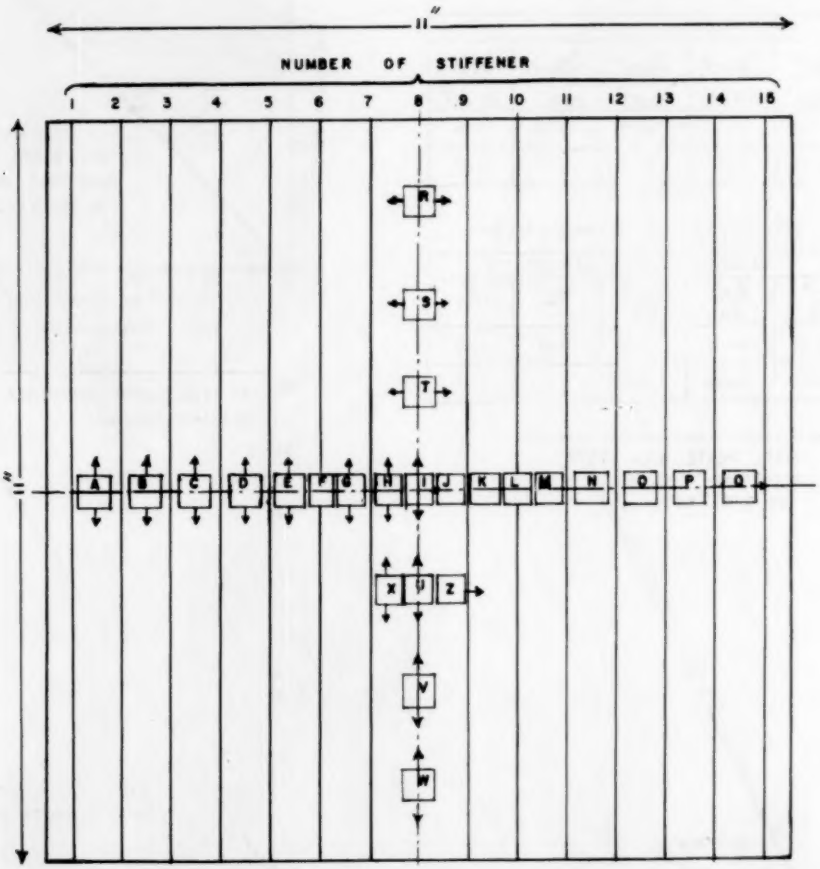

FIG. 10 SCHEMATIC ARRANGEMENT OF STRAIN GAGES ON STIFFENED PLATES

plate between successive stiffeners. The locations of the strain gages are shown in Fig. 10. It may be observed that the measured strains atop a stiffener in the direction normal to its length are relatively very small. All of the gages are recorded in Table 5 with code letters corresponding to those in Fig. 10. The experimentally determined strains correspond to a measured amplitude of vibration at the center of the plate. The amplitude was 0.0174 in.

Curves of theoretically determined bending strains are shown in Fig. 11. These strains were calculated from Equations [8] using a value of the co-ordinate z equal to either one half the thickness of the plate between stiffeners or one half the thickness through plate and stiffener. The experimentally determined strains and calculated strains were limited to the case of plate with stiffeners on both sides. Consequently it is natural to choose the plane of symmetry as the middle surface and measure the z-co-ordinate as we have done. The corresponding measured strains are plotted for comparison with those given by the theoretical curves.

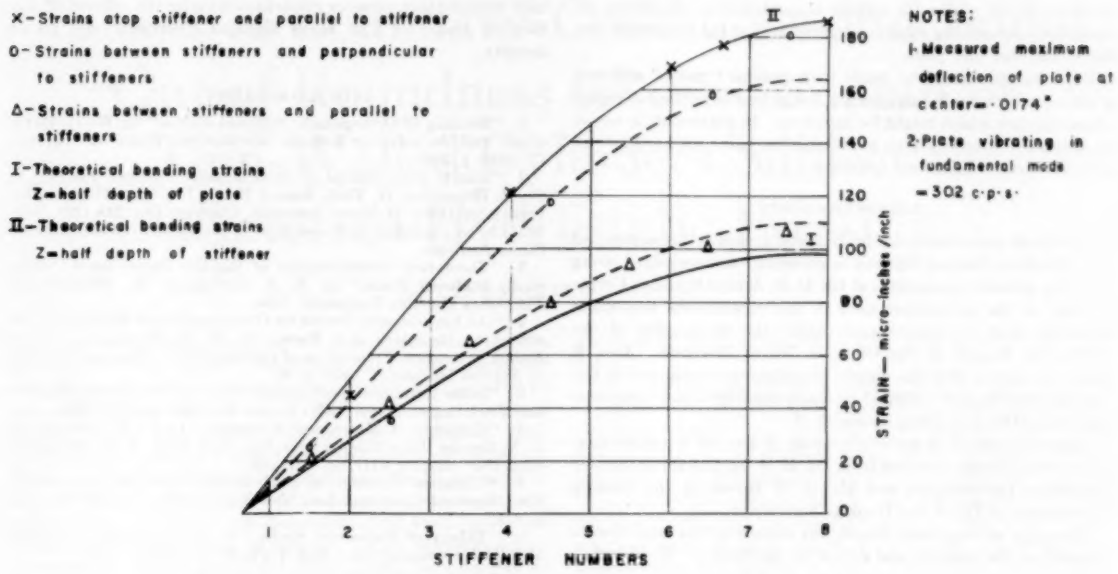
X-Strains atop stiffener and parallel to stiffener
O-Strains between stiffeners and perpendicular to stiffeners
Δ-Strains between stiffeners and parallel to stiffeners
I-Theoretical bending strains Z=half depth of plate
II-Theoretical bending strains Z=half depth of stiffener
NOTES:
1-Measured maximum deflection of plate at center=.0174"
2-Plate vibrating in fundamental mode =302 c.p.s.
STRAIN — micro-inches/inch
STIFFENER NUMBERS

FIG. 11 COMPARISON BETWEEN EXPERIMENTAL AND THEORETICAL BENDING STRAINS

The agreement between measured strains and calculated strains is reasonably good. The strains measured at the top of a stiffener and in the direction of the stiffener agree excellently with the predicted theoretical bending strains. Of course the strains at the top of stiffeners but in a direction normal to the length of the stiffener are negligible in magnitude. No doubt this should be expected. The strains measured on the surface of the plate between stiffeners and parallel to the direction of the stiffeners agree well with theory. However, the strains measured at this surface and in a direction perpendicular to the length of stiffeners are considerably larger than the theoretical bending strains. It is considered that ends of the strain gages are too close to stiffeners and in fields of relatively high stress gradients. The only sound theoretical approach to the prediction of these particular strains is to allow for strain concentrations on the basis of the general theory of elasticity.

There is excellent agreement between the theoretically determined frequencies of vibration and those determined by experiment. This can be seen clearly from the comparison given in Table 6 and Table 7. The reason for this, of course, is that the mass of the plate and the elastic compliances which are the controlling factors can be measured accurately. The frequencies are computed from Equation [3] in which all of the quantities are readily determined. It may be observed that the agreement exists even though rotatory inertia and shear deformation have been neglected in the theory. Undoubtedly there will be greater discrepancy at higher frequencies and there must be restrictions in terms of stiffener-thickness-to-plate-thickness ratios.

It might be noted that since the air gap between magnet and driven plate varies sensibly during the vibrations, the driving force is somewhat space-dependent and hence nonlinear vibrations may be excited. During the experiment several subharmonics were identified as well as a few quasi-resonant frequencies above the fundamental frequency of the plate. These vibrations can be identified readily by wave form on the cathode-ray oscilloscope. When the plate is driven at its natural frequencies corresponding to linear elasticity, these frequencies also are readily verifiable.

TABLE 6 FREQUENCIES OF FLEXURAL VIBRATION—STIFFENERS ON ONE SIDE OF PLATE

m \ n	1	2	3
1	366 / 336	820 / 821	1620 / 1640
2	870 / 884	1330 / 1345	2100 / 2145
3	1700 / 1806	2180 / 2251	2900 / 3026

NOTES: 1 Theoretical frequency is in lower half of box and experimental frequency is in upper half of box.
2 Frequencies are in cycles per second.

TABLE 7 FREQUENCIES OF FLEXURAL VIBRATION—STIFFENERS ON BOTH SIDES OF PLATE

m \ n	1	2	3
1	302 / 294	644 / 657	1216 / 1250
2	812 / 799	1152 / 1175	1760 / 1782
3	1580 / 1643	2040 / 2022	2570 / 2645

NOTES: 1 Theoretical frequency is in lower half of box and experimental frequency is in upper half of box.
Frequencies are in cycles per second.

CONCLUSION

The preliminary study described in this paper provides considerable grounds for expecting success with the proposed methods of determining strain and vibration characteristics of stiffened plates.

Excellent predictions of frequencies of flexural vibrations based on theory seem possible at least for the lower frequencies. Knowledge of such physical characteristics is essential in any consideration of the dynamic response of stiffened plates in the elastic range.

Flexural strains apparently can be predicted with considerable

accuracy if one allows for certain understandable qualifying assumptions concerning strain concentrations at the connection between stiffener and plate.

Experiments should be made with general types of stiffened plate actually used in engineering design and over the full range of parameters which might be involved. In particular, it would be extremely interesting to know at what point rotatory inertia would become a significant influence.

Acknowledgments

Technical sponsorship of the Ballistic Research Laboratory of the Aberdeen Proving Ground is gratefully acknowledged along with the general sponsorship of the U. S. Army Ordnance Corps.

Some of the equipment used in the experiments was made available from an investigation under the sponsorship of the Mechanics Branch of the Office of Naval Research. Also, it should be noted that the elastic compliances determined in the present investigation followed methods developed under sponsorship of the Office of Naval Research (1).

Acknowledgment is gratefully made of the aid in electromagnetic circuit design received from Dr. H. S. McDonald of the Bell Telephone Laboratories, and Mr. R. G. Roush of the research laboratories at The Johns Hopkins University.

Although we sometimes forget, any success in this kind of work depends on the patience and skill of the mechanics. We therefore take considerable pleasure in acknowledging the efforts of Mr. Bernard Baker of The Johns Hopkins University and his assistants.

BIBLIOGRAPHY

1 "Bending of Orthogonally Stiffened Plates," by W. H. Hoppmann, 2nd, JOURNAL OF APPLIED MECHANICS, Trans. ASME, vol. 77, 1955, p. 267.

2 "Elastic Compliances of Orthogonally Stiffened Plates," by W. H. Hoppmann II, Tech. Report No. 9, The Johns Hopkins University for Office of Naval Research, Contract Onr 248 (12), July, 1955, to be published in Proceedings of the Society for Experimental Stress Analysis.

3 "Theoretical Determination of Rigidity Properties of Orthogonally Stiffened Plates," by N. J. Huffington, Jr., dissertation—The Johns Hopkins University, 1954.

4 "An Experimental Device for Obtaining Elastic Rotational Constraint on Boundary of a Plate," by W. H. Hoppmann II and Joshua Greenspon, Proceedings of the Second U. S. National Congress of Applied Mechanics, 1955, p. 87.

5 "Noise Ratings of Ventilating Fans," by W. H. Hoppmann II and Fred Lager, Trans. ASHVE, vol. 51, 1945, pp. 271–284.

6 "Elements of Mechanical Vibration," by C. R. Freberg and E. N. Kemler, John Wiley & Sons, Inc., New York, N. Y., second edition, 1949, chapter VIII, pp. 151–169.

7 "Vibration Problems in Engineering," by S. Timoshenko, D. Van Nostrand Company, Inc., New York, N. Y., first edition, 1928, p. 238.

8 "Theory of Plates and Shells," by S. Timoshenko, McGraw-Hill Book Company, Inc., New York, N. Y., 1940, p. 40.

Effects of Boundary Conditions and Initial Out-of-Roundness on the Strength of Thin-Walled Cylinders Subject to External Hydrostatic Pressure

By G. D. GALLETLY[1] AND R. BART[2]

Using classical small-deflection theory, an investigation was made of the effects of boundary conditions and initial out-of-roundness on the strength of cylinders subject to external hydrostatic pressure. The equations developed in this paper for initially out-of-round cylinders with clamped ends, and a slightly modified form of the equations previously derived by Bodner and Berks for simply supported ends, were applied to some actual test results obtained from nine steel cylinders which had been subjected to external hydrostatic pressure. Three semiempirical methods for determining the initial out-of-roundness of the cylinders also were investigated and these are described in the paper. The investigation indicates that if the initial out-of-roundness is determined in a manner similar to that suggested by Holt then the correlation between the experimental and theoretical results is quite good. The investigation also indicates that while the difference in collapse pressures for clamped-end and simply supported perfect cylinders may be quite considerable, this does not appear to be the case when initial out-of-roundnesses of a practical magnitude are considered.

Introduction

SEVERAL analyses have appeared in the literature for the elastic buckling of a thin cylindrical shell subject to external hydrostatic pressure (1).[3] The majority of these analyses have been based upon the classical small-deformation theory of thin shells and have assumed a geometrically perfect, stress-free structure prior to loading. The correlation obtained between these theories and experimental results has been good for long cylinders but rather poor for short cylinders. Efforts are currently being made by several investigators to explain the discrepancy between theory and experiment in the short-cylinder range by the use of large-deflection theory. At this date, however, it is not known by how much this discrepancy will be reduced as all the final reports on their work have not been published.

One possible cause for the discrepancy between theoretical and experimental results can be ascribed to the initial out-of-roundness of the cylinders, and a number of investigations, using small-deflection theory, already have been made on the effect of initial irregularities on the collapse pressure of cylinders subject to external hydrostatic pressure (2, 3, 4). As was to be expected, these analyses showed that the initial irregularities reduced the failure pressures below those of the perfect cylinders. However, when these analyses were applied to some models which had been tested experimentally, they predicted failure pressures which were less than three quarters of those observed experimentally. Since these analyses had assumed simple supports at the ends of the cylinders and it was probable that the boundary conditions of the models were somewhere between the extremes of simple supports and clamped ends, it was of interest to investigate the reduction in collapse pressure of clamped-end cylinders due to initial irregularities, to see if the assumed boundary conditions would explain the discrepancy between experiment and theory. Also, the analyses assume that the initial out-of-roundness in the cylinders is similar to one of the modes into which a perfectly circular cylinder of the same dimensions would buckle, and actual shells never satisfy this condition. It thus seemed desirable to investigate the various simplified methods that have been suggested for determining the initial out-of-roundness of the cylinders to see what effect these had upon the computed failure pressure. These methods are described in the paper.

It is also of interest to note that there are other limitations in the existing linearized theories. These are:

(*a*) The fact that in these problems there usually exist other buckling pressures close to the minimum buckling pressure. Thus, use of only that mode of initial out-of-roundness which corresponds to the minimum buckling pressure is really only defensible at pressures very close to the minimum buckling pressure.

(*b*) The simple yield criterion used to predict failure.

This point is discussed under the section entitled "Assumptions Made in Analysis."

The authors have not investigated the foregoing factors but hope to do so in the future.

The approach used in this paper is similar to that of Bodner and Berks (3), except that instead of using a Donnell type equation Galerkin's method was employed in conjunction with a modified Donnell type equation. The initial out-of-roundness pattern assumed by Bodner and Berks was of the form

$$w_0 = e \sin m\theta \cos \frac{\pi x}{L}$$

(origin at mid-length) while that assumed by the present authors was

[1] Shell Development Company, Emeryville, Calif. Assoc. Mem. ASME; formerly Head, Plates and Shells Section, David Taylor Model Basin, Washington, D. C.

[2] Structural Research Engineer, David Taylor Model Basin, Washington, D. C.

[3] Numbers in parentheses refer to the Bibliography at the end of the paper.

Presented at the National Applied Mechanics Conference, Urbana, Ill., June 14–16, 1956, of THE AMERICAN SOCIETY OF MECHANICAL ENGINEERS.

Discussion of this paper should be addressed to the Secretary, ASME, 29 West 39th Street, New York, N. Y., and will be accepted until October 10, 1956, for publication at a later date. Discussion received after the closing date will be returned.

NOTE: Statements and opinions advanced in papers are to be understood as individual expressions of their authors and not those of the Society. Manuscript received by ASME Applied Mechanics Division, May 31, 1955. Paper No. 56—APM-9.

$$w_0 = \frac{e}{2} \sin m\theta \left[1 - \cos \frac{2\pi x}{L}\right]$$

(origin at one end of the cylinder). Thus, in both cases, the initial out-of-roundness satisfied the relevant boundary conditions and was also similar in form to one of the assumed buckling modes. The magnitude of the initial out-of-roundness at the ends and center of the cylinder was also the same in both cases.

The Bodner-Berks solution and that presented herein thus represent lower and upper bounds for the effect of initial eccentricities on the collapse pressures of elastically supported unstiffened cylinders, when the initial eccentricities have the same shape as one of the assumed buckling modes of the perfect cylinder. While the two solutions are not exact, they should provide good approximations to the exact solutions. One of the limitations of using Donnell's equation is that the number of circumferential lobes should be fairly high, and thus the results will be slightly in error for very long cylinders which buckle into two or three circumferential lobes.

The final results of the investigation are given in Fig. 2 and in Tables 2, 4, and 5. It can be seen that the correlation between experiment and theory is quite good when method (*c*) is used to determine the initial out-of-roundness of the models. [Method (*c*) is similar to that suggested by Holt (5).] However, it is not claimed that the results give a complete answer to the problem and more work of both an experimental and theoretical nature is required.

Method of Analysis

The modifications to Donnell's equation brought about by initial eccentricities in the shell have been presented by Bodner and Berks (3) and, prior to them, by Cicala (6). The equations also have been derived by the authors in the Appendix, using a somewhat different approach to that adopted by the previously mentioned authors. For the case of uniform external hydrostatic pressure applied on all sides of an imperfect cylinder the relevant equations are, from Equations [19*a*], [19*b*], [21], and [24] in the Appendix

$$\left.\begin{aligned}
&D\nabla^4 w + \frac{Eh}{R^2}\nabla^{-4} w_{xxxx} + pR\left[1/2(w + w_0)_{xx} + \frac{1}{R^2}(w + w_0)_{\theta\theta}\right] - p = 0 \quad \ldots\ldots (a)\\
&\nabla^4 u = \frac{1}{R}\left[\nu w_{xxx} - \frac{1}{R^2} w_{x\theta\theta}\right] \quad \ldots\ldots\ldots\ldots (b)\\
&\nabla^4 v = \frac{1}{R^2}\left[(2 + \nu) w_{xx\theta} + \frac{1}{R^2} w_{\theta\theta\theta}\right] \quad \ldots\ldots (c)\\
&\nabla^4 F = -\frac{E}{R} w_{xx} \quad \ldots\ldots\ldots\ldots\ldots\ldots\ldots (d)
\end{aligned}\right\} \ldots [1]$$

where

h = thickness of shell
R = mean radius of shell
p = applied hydrostatic pressure
E = modulus of elasticity
D = $Eh^3/12(1 - \nu^2)$
ν = Poisson's ratio
F = stress function of the total membrane stresses
$\nabla^4 = \left(\frac{\partial^2}{\partial x^2} + \frac{1}{R^2}\frac{\partial^2}{\partial \theta^2}\right)^2$; $\nabla^4 \nabla^{-4} f = f$
w_0 = initial radial out-of-roundness (+ inwards)
u, v, w = elastic axial, tangential, and radial (+ inwards) displacements of the imperfect cylinder minus the uniform compression experienced by a perfect cylinder (see Equation [18] in the Appendix).

The subscripts x and θ indicate partial differentiations with respect to those variables.

The patterns assumed for w and w_0, and which satisfy the boundary conditions for clamped-end cylinders, were as follows

$$\left.\begin{aligned}
w &= B \sin m\theta \left[1 - \cos \frac{2\pi x}{L}\right]\\
w_0 &= \frac{e}{2} \sin m\theta \left[1 - \cos \frac{2\pi x}{L}\right]
\end{aligned}\right\} \quad \ldots\ldots\ldots [2]$$

where

B = half amplitude of w-displacement
e = maximum value of initial radial out-of-roundness
m = number of circumferential waves
L = unsupported length of shell
x, θ = axial and angular co-ordinates

If the Expressions [2] happen to be an exact solution of the problem, then they will satisfy the differential equation of equilibrium, Equation [1*a*], exactly. However, as both w and w_0 were chosen to satisfy the boundary conditions rather than the equilibrium equation, this, in general, will not be the case. The resulting expression will be a function of x and θ which we shall denote by Q. Galerkin's equation for determining the relations between the coefficients B and e is then

$$\int_0^{2\pi}\int_0^L Q \sin i\theta \left[1 - \cos \frac{2\pi x}{L}\right] R\, d\theta\, dx = 0 \ldots\ldots [3]$$

where i assumes the values 1, 2, 3 .....
For $i \neq m$ Equation [3] will be found to be zero identically. For $i = m$ the following relation between B and e, obtained from Equation [3], will be found to hold

$$B = \frac{e}{2} \frac{p}{p_{cr} - p} \quad \ldots\ldots\ldots\ldots\ldots [4]$$

where p_{cr} is given by the expression

$$p_{cr} = \frac{E\left\{\dfrac{\left(\frac{h}{R}\right)^2 [3m^4 + 2m^2\Delta^2 + \Delta^4]}{12(1 - \nu^2)} + \dfrac{\left(\frac{h}{R}\right)\Delta^4}{(m^2 + \Delta^2)^2}\right\}}{(3m^2 + 1/2\Delta^2)} \quad \ldots\ldots [5]$$

and

$$\Delta = \frac{2\pi R}{L}$$

The smallest value of the buckling pressure of the perfect cylinder p_{cr} is found by minimizing Equation [5] with respect to m. A relation similar to that expressed by Equation [5] has recently been presented by Nash (7) using an energy method. A relation similar to Equation [4] was also obtained by Bodner and Berks for simply supported imperfect cylinders.

Thus, from Equations [2] and [4], we obtain the following expression for w

$$w = \frac{e}{2} \frac{p}{p_{cr} - p} \sin m\theta \left[1 - \cos \frac{2\pi x}{L}\right] \quad \ldots\ldots [6]$$

The bending moments in the shell can then be calculated from the relations

$$\left.\begin{aligned} M_x &= -D\left[w_{xx} + \frac{\nu}{R^2}\,w_{\theta\theta}\right] \\ M_\theta &= -D\left[\frac{1}{R^2}\,w_{\theta\theta} + \nu w_{xx}\right] \end{aligned}\right\} \quad \ldots\ldots\ldots [7]$$

The maximum bending stresses are then given by

$$\sigma_{bx} = \pm\frac{6}{h^2}\,(M_x)_{max}; \qquad \sigma_{b\theta} = \pm\frac{6}{h^2}\,(M_\theta)_{max} \ldots\ldots [8]$$

To obtain the total normal stresses we now have to add the membrane stresses to Equation [8]. To determine these latter we solve Equations [1*d*] and [6] for the stress function F (periodic terms only). The total membrane stresses are then given by

$$\sigma_{mx} = -\frac{pR}{2h} + \frac{F_{\theta\theta}}{R^2}; \qquad \sigma_{m\theta} = -\frac{pR}{h} + F_{xx} \ldots\ldots [9]$$

The total normal stresses are obtained by adding algebraically Equations [8] and [9]. The greatest normal stresses occur at mid-length of the cylinder ($x = L/2$) and where $\sin m\theta = \pm 1$ (trough and crest points of the lobes). At these points the twisting moment $M_{x\theta}$ is zero and thus the normal stresses are principal stresses. The absolute maximum normal stresses occur at the outer shell wall for the trough points.

Having obtained the maximum principal stresses σ_x and σ_θ in terms of the initial out-of-roundness, the geometric parameters, and the applied external hydrostatic pressure, we now employ the octahedral shear-stress criterion of failure (which gives the same results as the Hencky-von Mises criterion of failure), viz.

$$\sigma_y^2 = \sigma_\theta^2 + \sigma_x^2 - \sigma_\theta\sigma_x \ldots\ldots\ldots\ldots [10]$$

where σ_y is the yield point of the material. Substitution of the maximum principal stresses σ_x and σ_θ in Equation [10] then gives an equation relating the initial out-of-roundness, the geometric parameters of the shell, the yield point of the material, and the pressure at which the shell begins to yield p_y.

It should be noted that instead of using the yielding criterion given by Equation [10] where σ_x and σ_θ are principal stresses, it is more accurate to use the expression

$$\sigma_y^2 = \sigma_\theta^2 + \sigma_x^2 - \sigma_\theta\sigma_x + 3\tau_{x\theta}^2 \ldots\ldots\ldots [10a]$$

where now σ_x, σ_θ, and $\tau_{x\theta}$ are the normal and shear stresses at any point and which are functions of x and θ. Yielding will first occur in the cylinder for those values of x and θ which maximize the right-hand side of Equation [10*a*]. However, to compute these values of x and θ by differentiation of Equation [10*a*] involves more complications than seem warranted. Trials indicate that the stress condition at the outer shell wall for trough points of a lobe is probably as unfavorable as anywhere else. As mentioned earlier, the twisting moment $M_{x\theta}$ is zero at these points and thus Equation [10*a*] reduces to Equation [10].

As we shall later present curves of p_y, the pressure at which shell yielding commences, versus e/h, the initial eccentricity-shell thickness ratio, for both simply supported and clamped-end cylinders, we have summarized the results obtained in this paper and those obtained by Bodner and Berks in Table 1. (We have added a few terms to the latter solution, as Bodner and Berks neglected the periodic terms in Equation [9]). Also, we used the expression $w_{\theta\theta}/R^2$ for the circumferential change in curvature instead of $(w_{\theta\theta}/R^2 + v_\theta/R)$ which was used by Bodner and Berks when computing the bending stresses due to initial out-of-roundness. Our expression is consistent with the expression used in deriving the approximate equations of equilibrium for an initially out-of-round cylinder (see Appendix) and also is the same as that used by Donnell in his work on perfect cylinders (8). The effect of using $w_{\theta\theta}/R^2$ instead of $(w_{\theta\theta}/R^2 + v_\theta/R)$ is to eliminate the quantity f which appears in the equations developed by Bodner and Berks.) It can be seen that the final equation (Equation [12] in Table 1) relating the initial out-of-roundness and the pressure to cause first yielding is essentially the same for both clamped-end and simply supported cylinders, except for the factor of 2 required by the definition of e as the maximum initial out-of-roundness and the slight changes in definition of the quantities K and β appearing in that equation.

TABLE 1 COMPARISON OF EQUATIONS AND PARAMETERS FOR SIMPLY SUPPORTED AND CLAMPED-END CYLINDERS HAVING AN INITIAL OUT-OF-ROUNDNESS SIMILAR IN SHAPE TO ONE OF THE ASSUMED BUCKLING MODES

	Simple supports	Clamped ends	Equation no.
Assumed w and w_0	$w = A \sin m\theta \cos \frac{\pi x}{L}$; $w_0 = e \sin m\theta \cos \frac{\pi x}{L}$ (Origin at mid-length)	$w = B \sin m\theta \left[1 - \cos \frac{2\pi x}{L}\right]$; $w_0 = e/2 \sin m\theta \left[1 - \cos \frac{2\pi x}{L}\right]$ (Origin at one end)	
p_{cr}	$\dfrac{E\left\{\frac{\left(\frac{h}{R}\right)^2 [m^2 + \delta^2]^2}{12(1-\nu^2)} + \frac{\left(\frac{h}{R}\right)\delta^4}{[m^2+\delta^2]^2}\right\}}{\left[m^2 + \frac{1}{2}\delta^2\right]}$; $\delta = \frac{\pi R}{L}$;	$\dfrac{E\left\{\frac{\left(\frac{h}{R}\right)^2 [3m^4 + 2m^2\Delta^2 + \Delta^4]}{12(1-\nu^2)} + \frac{\left(\frac{h}{R}\right)\Delta^4}{[m^2+\Delta^2]^2}\right\}}{\left[3m^2 + \frac{1}{2}\Delta^2\right]}$; $\Delta = \frac{2\pi R}{L}$	[11]
Equation relating p_y and e	$\frac{e}{h} = \left(1 - \frac{p_y}{p_{cr}}\right)\left\{\frac{-3 + [9 - 4(1-\beta+\beta^2)H]^{1/2}}{4(1-\beta+\beta^2)K}\right\} \times \begin{cases} 1 & \text{for simple supports} \\ 2 & \text{for clamped ends} \end{cases}$		[12]
$\frac{2p_{cr}(1-\nu^2)}{E}\left(\frac{R}{h}\right)^2 K$	$m^2 + \nu\delta^2 + 2(1-\nu^2)\frac{R}{h}\frac{\delta^4}{[m^2+\delta^2]^2}$	$2m^2 - 1 + \nu\Delta^2 + 2(1-\nu^2)\frac{R}{h}\frac{\Delta^4}{[m^2+\Delta^2]^2}$	
β	$\left\{\frac{\nu m^2 + \delta^2 + 2(1-\nu^2)\frac{R}{h}\frac{m^2\delta^2}{[m^2+\delta^2]^2}}{m^2 + \nu\delta^2 + 2(1-\nu^2)\frac{R}{h}\frac{\delta^4}{[m^2+\delta^2]^2}}\right\}$	$\left\{\frac{\nu[2m^2-1] + \Delta^2 + 2(1-\nu^2)\frac{R}{h}\frac{m^2\Delta^2}{[m^2+\Delta^2]^2}}{2m^2 - 1 + \nu\Delta^2 + 2(1-\nu^2)\frac{R}{h}\frac{\Delta^4}{[m^2+\Delta^2]^2}}\right\}$	
H	$\left[3 - \left(\frac{2h\sigma_y}{Rp_y}\right)^2\right]$		

Assumptions Made in Analysis

Besides the approximate strain and change in curvature-displacement relations used in the derivation of the Donnell equation for an initially out-of-round cylinder, and the assumption that it is initially stress free, it might be useful to list some of the other assumptions that have been made both in the analysis of this paper and that of Bodner and Berks. These are as follows:

1 That the circumferential membrane stress in the shell is constant along its length and equal to $-pR/h$, whereas this is actually not the case.

2 The assumption that the initial out-of-roundness is small (with an order of magnitude of one shell thickness) is symmetric with respect to the center line of the shell, and has the same form as one of the buckling modes of a perfect cylinder with the same shell dimensions. Actual shells rarely, if ever, satisfy the last two requirements and so the question arises as to how the initial out-of-roundness should be measured.

3 The assumption that failure occurs (appearance of visible lobes) when the most highly stressed points in the cylinder start to yield. Actually, failure does not occur until plastic regions form at the trough and crest points of the lobes. The pressure required to produce these yield zones is greater than that at which the most highly stressed points begin to yield, and neglect of this effect therefore underestimates the strength of the shells. An adequate theory to take this effect into account has not been developed as yet, but, as for beams, presumably the ratio of the pressure to cause first yielding to the pressure required for the formation of plastic regions depends on the relative magnitudes of the direct stresses in the cylinder wall and the bending stresses resulting from initial out-of-roundness.

4 The assumption that Poisson's ratio is a constant and equals 0.3.

As it is intended to apply the analyses developed for unstiffened cylinders to stiffened cylinders which failed by buckling between ring stiffeners, it would be well if we enumerated the additional assumptions that were made. These are:

5 That the stiffening rings at the ends of any bay are perfectly circular; i.e., they do not have any initial out-of-roundness. This never occurs in practice, of course, but should not be too serious if the circularity of the stiffening rings is very much better than that of the shell, or if the predominant mode of initial out-of-roundness in the rings is very different from the predominant mode in the shell.

6 As for unstiffened cylinders, the circumferential membrane stress in the perfect cylinder is assumed to be $-pR/h$, whereas it actually varies along the length of the shell. A more correct representation of the stress distribution would be obtained by using the analysis of von Sanden and Günther (9), or more accurately still, that of Salerno and Pulos (10).

Methods of Determining Initial Out-of-Roundness

As mentioned hitherto, the analyses assume that the initial out-of-roundness is symmetrical about the mid-length of the shell and that its circumferential variation is in the shape of one of the buckling modes of a perfect cylinder. Actual shells do not meet either of these requirements. If we do not make a harmonic analysis of the initial out-of-roundness, and also extend the theory to account for the various harmonic components, the question arises as to how we shall measure the quantity e, which is defined in the analysis as the maximum initial out-of-roundness when its shape is similar to one of the buckling modes. As far as the authors are aware, three simplified, semiempirical methods for determining the initial out-of-roundness have been proposed in the literature so far. These are (see Fig. 1):

(a) The centroid of the initial circularity contour is first determined. Then the angle π/m, where m is the number of lobes into which the perfect cylinder would buckle, is calculated. A sector of a circle, subtending this angle π/m is then drawn on transparent paper and placed with its apex at the centroid of the initial circularity contour. The sector is then rotated so that it traverses the entire circumference of the circularity contour until the location is found at which the maximum difference between the two sector radii occurs. The initial out-of-roundness is then taken as this maximum difference. This method of determining the initial out-of-roundness is essentially that proposed by Saunders, Trilling, and Windenburg (11, 12).

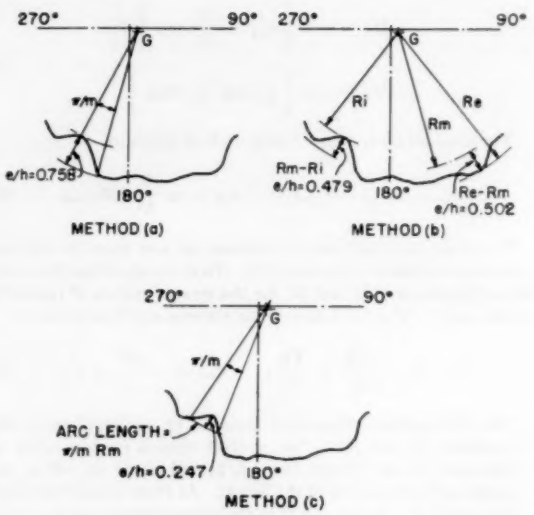

Fig. 1 Illustrations of Three Methods for Determining Initial Out-of-Roundness of Cylinders at Station 4 of Model BR-5

(b) Both the centroid and the area of the initial circularity contour are determined. The radius R_m of the circle whose area is the same as that of the initial circularity contour is then determined. A circle, with center at the centroid of the initial circularity contour and of radius R_m, is then drawn. The initial out-of-roundness is then taken as the maximum value of $[R_e - R_m]$ and $[R_m - R_i]$, where R_e and R_i are the radius vectors from the centroid to points on the initial circularity contour which are exterior and interior, respectively, to the circle of radius R_m. A method for determining the initial out-of-roundness similar to the foregoing has been suggested, among others, by Bodner and Berks (3).

(c) As in (b) both the centroid of the initial circularity contour and the radius R_m of the mean circle are determined. Also, as in (a), the angle π/m is calculated. The arc length of one half-lobe is then obtained as $(\pi/m)R_m$. This arc is then moved around the initial circularity contour with its end points always in contact with the contour. The initial out-of-roundness is then taken as the maximum radial distance between the circularity contour and the arc. This method for determining the initial out-of-roundness is somewhat similar to the method proposed by Holt (5).

Numerical Results

In this section we present the results obtained by applying the analysis developed for simply supported imperfect cylinders (3), and its extension to clamped ends, to nine steel welded cylinders that have been tested at the Taylor Model Basin. At failure, all these models had lobes which partially covered the circumference

TABLE 2 GEOMETRIC RATIOS, YIELD POINTS, EXPERIMENTAL AND THEORETICAL COLLAPSE PRESSURES FOR STEEL CYLINDERS

(1) Model no.	(2) $\frac{L}{2R}$	(3) $\frac{h}{2R}$	(4) σ_y (psi)	(5) Number of stiffeners	(6) Expt. buckling pressure, psi	(7) Maximum sustaining pressure, psi	(8) Theoretical elastic buckling pressure from Eq. [11] of Table 1, psi — Simple supports		(9) Clamped ends		(10) Pressure to cause axisymmetric yielding of stiffened cylinders [c]
50	0.125	0.0028	39000	2 internal	175	195 (18, 19)[a]	301	(17)	451.5	(18)	264
33	0.250	0.0032	31000	2 internal	133	139 (13, 14)	192.5	(12)	262	(14)	225
66	0.500	0.0048	40000	none	235[b]	235 (8, 9)	283	(8)	395	(10)	...
71	0.500	0.0065	44000	none	327[b]	327 (?)	586	(8)	804	(9)	...
42	1.000	0.0033	43000	none	58	59 (8)	51.2	(7)	73.4	(8)	...
61	2.000	0.0040	39000	none	48[b]	48 (5, 6)	41.1	(5)	60.2	(6)	...
BR-1	0.184	0.0024	61700	5 external	80	107 (15)	135	(15)	186	(17)	322
BR-4	0.250	0.0049	50600	5 external	390	390 (10)	613	(11)	848	(12)	560
BR-5	0.184	0.0023	54400	5 external	80	95 (14)	120	(15)	165	(17)	284

[a] Numbers in parentheses are the number of lobes at failure.
[b] No distinction made in Windenburg's notes between buckling and maximum sustaining pressures for these models; hence, they were assumed to be equal in the above table.
[c] Calculated for median surface of shell at mid-bay length using analysis of von Sanden and Günther in conjunction with octahedral shear stress criterion.

TABLE 3 MAXIMUM e/h-VALUES OBTAINED BY DIFFERENT METHODS FOR DETERMINING INITIAL OUT-OF-ROUNDNESS

(1) Model no.	(2) Method (a) C.E.	(2) Method (a) S.S.	(3) Method (b)	(4) Method (c) (i) Outward C.E.	(4) Method (c) (i) Outward S.S.	(5) Method (c) (ii) Inward C.E.	(5) Method (c) (ii) Inward S.S.	(6) Max. of (i) and (ii) C.E.	(6) Max. of (i) and (ii) S.S.
50	0.136[a]	0.140	0.175	0.016	0.017	0.074	0.078	0.074	0.078
33	0.097	0.104	0.068	0.067	0.078	0.085	0.093	0.085	0.093
66	0.043	0.047	0.041	0.041	0.045	0.032	0.037	0.041	0.045
71	0.139	0.143	0.118	0.008	0.011	0.090	0.098	0.090	0.098
42	0.267	0.272	0.191	0.080	0.091	0.114	0.121	0.114	0.121
61	0.125	0.130	0.082	0.027	0.033	0.022	0.027	0.027	0.033
BR-1 [6, 8][b]	0.575(6)[b]	0.615(8)	0.554(2)	0.319(6)	0.375(6)	0.267(6)	0.302(6)	0.319(6)	0.375(6)
BR-4 [4, 10]	0.164(4)	0.176(4)	0.128(2)	0.063(4)	0.068(4)	0.073(4)	0.082(4)	0.073(4)	0.082(4)
BR-5 [4, 6, 10]	0.741(4)	0.758(4)	0.502(4)	0.236(10)	0.285(10)	0.210(4)	0.247(4)	0.236(10)	0.285(10)

[a] Tabulated values accurate to approximately ±5 per cent.
[b] Numbers in square brackets indicate the stations at which lobes first appeared in the multibay stiffened cylinders. Numbers in parentheses are the stations at which the maximum e/h-values occurred, according to the method used.

TABLE 4 COMPARISON OF PREDICTED PRESSURES (PSI) FOR OCCURRENCE OF A VISIBLE LOBE—USING THE DIFFERENT METHODS FOR DETERMINING INITIAL OUT-OF-ROUNDNESS—WITH THE EXPERIMENTAL PRESSURES (PSI)

(1) Model no.	(2) Method (a) C.E.	(2) Method (a) S.S.	(3) Method (b) C.E.	(3) Method (b) S.S.	(4) Method (c) C.E.	(4) Method (c) S.S.	(5) Expt.	(6) Col. (2)/Col. (5) C.E.	(6) Col. (2)/Col. (5) S.S.	(7) Col. (3)/Col. (5) C.E.	(7) Col. (3)/Col. (5) S.S.	(8) Col. (4)/Col. (5) C.E.	(8) Col. (4)/Col. (5) S.S.
50	151	134	137	125	160	160	175	0.863	0.766	0.784	0.715	1.03	0.915
33	130	115	128	116	135	120	133	0.978	0.866	0.964	0.873	1.01	0.903
66	278	228	262	234	283	230	235	1.18	0.971	1.20	0.996	1.20	0.980
71	332	297	352	317	384	333	327	1.02	0.910	1.08	0.970	1.18	1.02
42	56	41.5	60	44	65	46	58	0.965	0.716	1.03	0.759	1.12	0.793
61	55	38	56	39	59	40.5	48	1.14	0.793	1.17	0.813	1.23	0.845
BR-1	74	63	75	67.5	98	80	80	0.922	0.788	0.938	0.844	1.22	1.00
BR-4	304	267	331	298	390	340	390	0.780	0.686	0.850	0.765	1.00	0.872
BR-5	57	50	68	61	92.5	76	80	0.713	0.625	0.850	0.763	1.16	0.950

of the shell. The geometric ratios, yield points, experimental and theoretical collapse pressures for these cylinders are given in Table 2. The first six models in this table were tested some 20 years ago by Windenburg and Trilling (12), although they did not investigate theoretically the effect of initial out-of-roundness on the collapse pressure. The last three models, which are multibay cylinders, have been tested recently at the Taylor Model Basin (13, 14).

A comparison of columns 6 and 8 in Table 2 shows a considerable discrepancy between the experimental and theoretical buckling pressures for even the simply supported cylinders. For some models, it would also appear that axisymmetric yielding rather than buckling was the controlling mode of failure. This can be seen by comparing columns 8 and 10 in Table 2. However, it will be seen later when out-of-roundness is taken into account that the theoretical pressures for buckling-type failures are lower than the axisymmetric yield pressures. It is also of interest to note that Models 42 and 61 are the only models for which the experimental buckling pressures are higher than those predicted theoretically for simply supported cylinders, although the same supports were used for these two models as for the four models preceding them.

Using the geometric ratios and yield points shown in Table 2 and Equations [11] and [12] in Table 1, it is possible to construct curves showing the relation between the pressure at which yielding first occurs in the cylinder wall p_y, and the ratio of the initial out-of-roundness to the shell thickness e/h. Two such curves are shown in Fig. 2 for illustrative purposes. In constructing these curves, the value of m used in Equation [12] was the value of m which minimized Equation [11] in Table 1. These values of m are listed in parentheses in columns 8 and 9 of Table 2. These values of m do not actually give the minimum p_y for a given e/h. This point will be discussed later. It also should be noted that for $e/h = 0$ some of the curves in Fig. 2 do not attain the elastic buckling pressures tabulated in columns 8 and 9 of Table 2. When this is found to occur it means that the pressure to cause axisymmetric yielding of the shell is lower than the elastic buckling pressure.

In Table 3 are tabulated the maximum e/h-values obtained using the different methods for determining the initial out-of-roundness described earlier. The e/h-values were determined at mid-length for the unstiffened cylinders and at mid-length of the bays for the multibay cylinders. Two values are listed for each model under methods (*a*) and (*c*) because, in these methods, the number of lobes into which the perfect cylinder would buckle is used and this number is usually different for simply supported and clamped ends.

Now, selecting the experimental buckling pressures listed in column 6 of Table 2 in conjunction with their corresponding eccentricities listed in columns 2, 3, and 6 of Table 3, one can plot points on curves similar to Fig. 2 which represent values determined experimentally. In Table 4 we also give a numerical comparison of the theoretical and experimental pressures at which visible lobes first occur. The theoretical values in this table

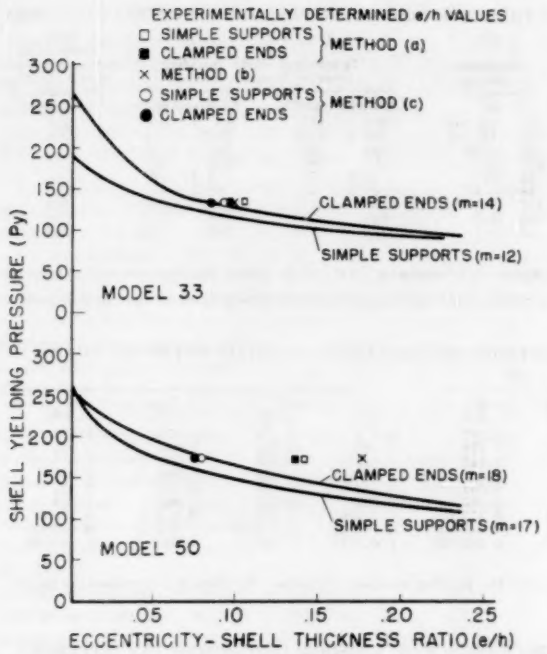

FIG. 2 SHELL YIELDING PRESSURE FOR MODELS 33 AND 50 VERSUS ECCENTRICITY: SHELL-THICKNESS RATIO

TABLE 5 AVERAGE VALUES OF COLUMNS (6), (7), AND (8) IN TABLE 4, CLASSIFIED ACCORDING TO CYLINDER TYPE

Cylinder type	Method (a) C.E.	Method (a) S.S.	Method (b) C.E.	Method (b) S.S.	Method (c) C.E.	Method (c) S.S.
Unstiffened.....	1.08	0.85	1.12	0.89	1.18	0.91
Stiffened.....	0.85	0.75	0.88	0.79	1.08	0.93

were obtained from the e/h-values listed in Table 3 in conjunction with the theoretical p_y versus e/h curves similar to Fig. 2. The last three columns in Table 4 show the ratios of theoretically predicted pressures for the occurrence of a visible lobe to those obtained experimentally, according to the various methods used for determining the initial out-of-roundness. The average values of these last three columns, classified according to whether the cylinders were stiffened or not, are tabulated in Table 5. It can be seen from Tables 4 and 5 that use of method (a), with the assumption of simply supported ends, was the most conservative in most cases and predicted pressures which were always below those obtained experimentally. However, the best correlation between the experimental results and the simplified theories discussed in this paper appears to be obtained when method (c) is used for determining the initial out-of-roundness and the cylinders are assumed to be simply supported.

It was mentioned earlier that for a given e/h the value of m that would give the lowest p_y was not necessarily the value of m which minimized the expression for p_{cr} (Equations [11] in Table 1). It was also noted at that time, however, that the error obtained by assuming this to be so was not very great and also greatly reduced the computational labor. Some idea of the error involved can be obtained by referring to Fig. 3. The curves in this figure are plots of m which minimize e/h for a given p_y. For a p_y of 80 psi it can be seen that the minimum value of e/h is 0.34 at $m = 18$, while at $m = 15$ (the value which minimizes p_{cr}) the value of e/h is 0.4. However, if we now fix the value of e/h at 0.4, then the minimum value of p_y is 75 psi and occurs at $m = 19$. Similar

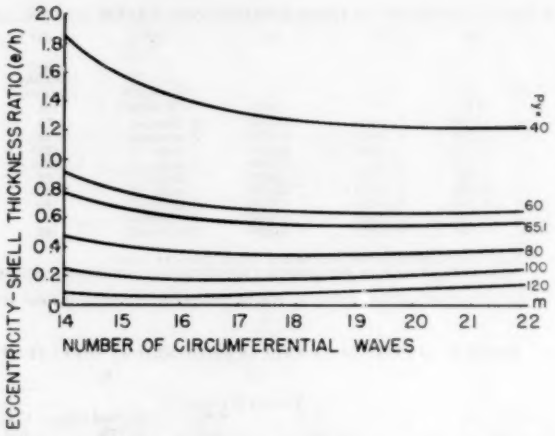

FIG. 3 INITIAL ECCENTRICITY-SHELL THICKNESS RATIO VERSUS NUMBER OF CIRCUMFERENTIAL WAVES FOR MODEL BR-1 (ASSUMED SIMPLY SUPPORTED)

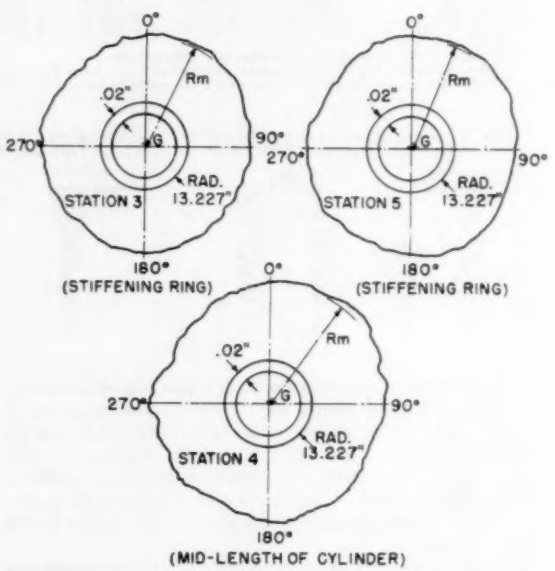

FIG. 4 TYPICAL INITIAL CIRCULARITY CONTOURS FOR MODEL BR-4

results are obtained with the other curves and also with the m versus e/h curves for clamped-end cylinders which we have not included here. It is thus seen that assuming the value of m which minimizes p_{cr} will also minimize p_y for a given e/h is slightly on the unsafe side, the magnitude of the error depending on the value of e/h taken. However, owing to the fact that actual cylinders under hydrostatic pressure collapse in substantially the same number of lobes as is predicted by theory for the perfect cylinder, and also for simplicity in calculations, we have ignored this discrepancy.

It also will be remembered that in applying the analyses to stiffened cylinders we made the assumption that the stiffening rings were perfectly circular. This, of course, never occurs in practice. Some idea of the degree of circularity actually present can be obtained by reference to Fig. 4. This figure shows the initial circularity contours of the stiffening rings bordering, and the

shell at the center of one of the bays in which lobes first appeared in Model BR-4. If we adopt method (*c*) described earlier as our criterion for initial out-of-roundness, then the stiffening rings of this model had about one tenth the out-of-roundness of the shell. Similar results also were obtained for the other models. Thus, for the problem of inter-ring collapse of stiffened cylinders, the assumption of zero initial out-of-roundness of the stiffening rings appears to be a reasonable one.

It might be thought that a harmonic analysis of the initial out-of-roundness would show that the amplitude of the harmonic component corresponding to the value of m which minimized p_{cr} (Equation [11] in Table 1) was many times that of the other components. To investigate this point a harmonic analysis, using 72 subdivisions of the circumference, was made of the initial circularity contour at Station 4 of Model BR-4 using Filon's method (15). The number of waves into which a perfect cylinder with shell dimensions similar to BR-4 would buckle is, according to the linear theory used herein, 11 for simply supported ends and 12 for clamped ends. From the harmonic analysis it was found that there were nine harmonics with amplitudes greater than the eleventh and two greater than the twelfth. It also was found that the amplitude of the largest harmonic ($m = 8$) was more than twice that of the twelfth mode and more than five times that of the eleventh mode. Further, even this largest amplitude was much too small to effect a reasonable correlation between theory and experiment. Thus the harmonic analysis of the BR-4 initial out-of-roundness contour did not produce any results which might be useful in practice.

In conclusion, it might be of interest to mention that some attempts have been made to determine experimentally the longitudinal form of the buckling displacemnts in the multibay cylinders. The results of these few investigations are summarized in reference (14). However, more experimental work still remains to be done before any conclusions regarding the shape of the buckling displacement can be made.

Summary

In the preceding sections an attempt has been made to explain some of the discrepancies that exist between experimental and theoretical results for cylinders subjected to external hydrostatic pressure. To do this it was assumed that (*a*) the actual boundary conditions were somewhere between the extremes of simple supports and clamped ends; (*b*) the initial out-of-roundness was similar in form to one of the modes into which a perfect cylinder would buckle; (*c*) the stress distribution in the equilibrium problem for the perfect cylinder could be represented by the membrane stresses; and (*d*) the linear small-deformation equations of equilibrium would describe the problem adequately. Any cold-working, residual, or welding stresses, or any elastic nonhomogeneity that might have been present were neglected. It also was assumed that failure (formation of a lobe) would occur when the stresses at the most highly stressed point satisfied the octahedral shear-stress criterion. Three simplified methods of measuring the initial out-of-roundness were also investigated. The simplified analyses, together with the different methods of measuring out-of-roundness, were applied to nine steel welded cylinders with length-diameter ratios of $^1/_4$ to 2, thickness-diameter ratios of 0.0025 to 0.0065, and yield points of the steel of 30,000 to 60,000 psi. The correlation between experimental and theoretical results was quite good, when method (*c*) was used for determining the initial out-of-roundness of the cylinders.

Acknowledgment

The authors wish to express their sincere appreciation to Taylor Model Basin staff members Messrs. R. F. Keefe, A. F. Kirstein, and R. C. Slankard for their able assistance in performing the numerical computations and determining the initial out-of-roundness of the models, and to Mr. R. Stuckey in executing the drafting work.

They also wish to thank Dr. S. R. Bodner of the Polytechnic Institute of Brooklyn for his constructive comments on the authors' work.

Bibliography

1 "Buckling of Multiple-Bay Ring-Reinforced Cylindrical Shells Subject to Hydrostatic Pressure," by W. A. Nash, Journal of Applied Mechanics, Trans. ASME, vol. 75, 1953, pp. 469–474. [See also reference (7) in Bibliography; (also, DTMB Report 785, April, 1954).

2 "A Study of the Collapsing Pressure of Thin-Walled Cylinders," by R. G. Sturm, University of Illinois Engineering Experiment Station, Bulletin No. 329, 1941.

3 "The Effect of Imperfections on the Stresses in a Circular Cylindrical Shell Under Hydrostatic Pressure," by S. R. Bodner and W. Berks, PIBAL Report No. 210, Polytechnic Institute of Brooklyn, Brooklyn, N. Y., December, 1952.

4 "Effect of Small Initial Irregularities on the Stresses in Cylindrical Shells," by T. S. Wu, L. E. Goodman, and N. M. Newmark, University of Illinois, N6ori-071(06), T. O. VI, Structural Research Series No. 50, April, 1953.

5 "A Procedure for Determining the Allowable Out-of-Roundness for Vessels Under External Pressure," by M. Holt, Trans. ASME, vol. 74, 1952, pp. 1225–1230.

6 "The Effect of Initial Deformations on the Behavior of a Cylindrical Shell Under Axial Compression," by P. Cicala, *Quarterly of Applied Mathematics*, vol. 9, 1951, pp. 273–293.

7 "Buckling of Thin Cylindrical Shells Subject to Hydrostatic Pressure," by W. A. Nash, *Journal of the Aeronautical Sciences*, vol. 21, 1954, pp. 354–355.

8 "Stability of Thin-Walled Tubes Under Torsion," by L. H. Donnell, NACA TR 479, 1933.

9 "The Strength of Cylindrical Shells, Stiffened by Frames and Bulkheads, Under Uniform External Pressure on All Sides," by K. von Sanden und K. Günther, Werft und Reederei, vol. 1, nos. 8, 9, and 10, 1920; vol. 2, no. 17, 1921; DTMB Translation 38, March, 1952.

10 "Stress Distribution in a Circular Cylindrical Shell Under Hydrostatic Pressure Supported by Equally Spaced Circular Ring Frames, Part I—Theory," by V. L. Salerno and J. Pulos, PIBAL Report No. 171-A, Polytechnic Institute of Brooklyn, Brooklyn, N. Y., June, 1951.

11 "The Use of Models in Determining the Strength of Thin-Walled Structures," by H. E. Saunders and D. F. Windenburg, Trans. ASME, vol. 54, Paper APM-54-25, 1932.

12 "Collapse by Instability of Thin Cylindrical Shells Under External Pressure," by D. F. Windenburg and C. Trilling, Trans. ASME, vol. 56, Paper APM-56-20, 1934; DTMB Report 385, July, 1934.

13 "Tests of the Elastic Stability of a Ring-Stiffened Cylindrical Shell, Model BR-5 ($\lambda = 1.705$), Subjected to Hydrostatic Pressure," by R. C. Slankard and W. A. Nash, DTMB Report No. 822, May, 1953.

14 "Tests of the Elastic Stability of a Ring-Stiffened Cylindrical Shell, Model BR-4 ($\lambda = 1.103$), Subjected to Hydrostatic Pressure," by R. C. Slankard, DTMB Report 876, February, 1955.

15 "Integral Transforms in Mathematical Physics," by C. J. Tranter, Methuen and Company Ltd., London, England, and John Wiley & Sons, Inc., New York, N. Y., 1951, section 5.4.

16 "An Expression for the Volume Change of a Cylindrical Shell," by R. Bart, DTMB Memorandum to Head, Structures Division, dated February 28, 1955.

Appendix

Approximate Equations of Equilibrium for an Initially Out-of-Round Cylinder

These equations have been derived previously by Bodner and Berks (3) using a different approach. Our reason for this new derivation is to make clear what approximations and assumptions are involved in the simplified equations of equilibrium.

Consider a cylinder of mean radius R which has a small radial initial out-of-roundness w_0. Selecting x, θ, and z as co-ordinate axes and denoting the longitudinal, tangential, and radial elastic displacements by U, V, and W, it is then possible to show that the strains at the middle surface are given by

$$\left.\begin{aligned}
\epsilon_x &= U_x + \frac{1}{2}\,[V_x^2 + W_x^2] + W_x w_{0x} \\
\epsilon_\theta &= \frac{1}{R}\,[V_\theta - W] + \frac{1}{2R^2}\,[V + W_\theta]^2 + \frac{U_\theta^2}{2R^2} \\
&\quad + \frac{w_{0\theta}}{R^2}\,[V + W_\theta] + \frac{w_0}{R^2}\,[V_\theta - W] \\
\gamma_{x\theta} &= \frac{U_\theta}{R} + V_x + \frac{W_x W_\theta}{R} + \frac{W_x V}{R} - U_x V_x + \frac{U_\theta W}{R^2} \\
&\quad - \frac{U_\theta V_\theta}{R^2} + \frac{W_\theta w_{0x}}{R} + \frac{V w_{0x}}{R} + \frac{W_x w_{0\theta}}{R} + \frac{U_\theta w_0}{R^2}
\end{aligned}\right\} \quad [13]$$

We shall simplify these complicated expressions to the following

$$\left.\begin{aligned}
\epsilon_x &= U_x + \frac{1}{2}\,W_x^2 + W_x w_{0x} \\
\epsilon_\theta &= \frac{1}{R}\,[V_\theta - W] + \frac{W_\theta^2}{2R^2} + \frac{W_\theta w_{0\theta}}{R^2} \\
\gamma_{x\theta} &= \frac{U_\theta}{R} + V_x + \frac{W_\theta W_x}{R} + \frac{W_\theta w_{0x}}{R} + \frac{W_x w_{0\theta}}{R}
\end{aligned}\right\} \quad [14]$$

For the changes in curvature, we shall use the quantities previously used by Donnell (8) for perfect cylinders, viz.

$$\chi_x = W_{xx}, \quad \chi_\theta = \frac{W_{\theta\theta}}{R^2}, \quad \chi_{x\theta} = \frac{W_{x\theta}}{R} \quad [15]$$

The work done W_D by the uniform external pressure acting on all sides of the cylinder is given by the product of the pressure and the change in volume of the cylinder. Thus there follows (16)

$$\left.\begin{aligned}
W_D = p \int_0^{2\pi} \int_0^L \Bigg[& W - \frac{V_\theta}{2} - \frac{RU_x}{2} \\
& + \frac{2}{3}\,U_x(W + w_0) - \frac{1}{3}\,U(W_x + w_{0x}) \\
& + \frac{1}{3}\,U'(W_x + w_{0x}) + \frac{1}{3}\,U_x'(W + w_0) - \frac{Ww_0}{R} \\
& - \frac{W^2}{2R} + \frac{V_\theta}{R}(W + w_0) - \frac{V^2}{2R} - \frac{1}{3}\,U_x V_\theta \\
& - \frac{1}{3}\,UV_{x\theta} - \frac{1}{6}\,U_x' V_\theta - \frac{1}{6}\,U' V_{x\theta} \Bigg] R\,dx\,d\theta
\end{aligned}\right\} \quad [16]$$

where

$$U' = \frac{\int_0^{2\pi} U\,d\theta}{2\pi}, \quad U_x' = \frac{\int_0^{2\pi} U_x\,d\theta}{2\pi}$$

We shall simplify this complicated expression for W_D to the following

$$W_D = p \int_0^{2\pi} \int_0^L \left[W - \frac{V_\theta}{2} - \frac{RU_x}{2} \right] R\,dx\,d\theta \quad [17]$$

It is also convenient to consider the U, V, and W displacements to be made up of two parts

$$\left.\begin{aligned}
U &= \bar{U} + u \\
V &= \bar{V} + v \\
W &= \bar{W} + w
\end{aligned}\right\} \quad [18]$$

where $\bar{U}$, $\bar{V}$, and $\bar{W}$ are the displacements which would occur in the equilibrium problem of a perfectly circular cylinder under uniform external pressure.

The total potential of the system U_T is then obtained by adding the extensional and bending-strain energies of the shell and subtracting the work done by the external pressure. In calculating the extensional energy, we retained the terms in u, v, w, w_0 through the second order and the terms in $\bar{U}$, $\bar{V}$, $\bar{W}$ (directly proportional to the applied pressure) through the first order only; also, we neglected the effect of the deflection of the shell between supports on the displacements and stresses of the perfect cylinder.

Variation of U_T with respect to u, v, and w then gives the differential equations of the problem. Further manipulation of these equations results in the following

$$\left.\begin{aligned}
\nabla^4 u &= \frac{\nu}{R}\,w_{xxx} - \frac{w_{x\theta\theta}}{R^2} \quad (a) \\
\nabla^4 v &= \frac{(2+\nu)}{R^2}\,w_{xx\theta} + \frac{w_{\theta\theta\theta}}{R^4} \quad (b) \\
D\nabla^4 w + \frac{Eh}{R^2}\,\nabla^{-4} w_{xxxx} &= p + h\left[\bar{\sigma}_x (w + w_0)_{xx} \right. \\
&\quad \left. + \frac{2\bar{\tau}_{x\theta}}{R}\,(w + w_0)_{x\theta} + \frac{\bar{\sigma}_\theta}{R^2}\,(w + w_0)_{\theta\theta} \right] \quad (c)
\end{aligned}\right\} \quad [19]$$

where $\bar{\sigma}_x$, $\bar{\sigma}_\theta$, and $\bar{\tau}_{x\theta}$ are the membrane stresses which would occur in a perfectly circular cylinder and which were assumed to be constant in deriving the foregoing equations.

For the case of uniform external hydrostatic pressure applied on all sides of a perfectly circular cylinder, and neglecting the deflection of the shell between supports, there results

$$\bar{\sigma}_\theta = -\frac{pR}{h}, \quad \bar{\sigma}_x = -\frac{pR}{2h}, \quad \bar{\tau}_{x\theta} = 0 \quad [20]$$

Substituting the Relations [20] into Equation [19c] yields

$$D\nabla^4 w + \frac{Eh}{R^2}\,\nabla^{-4} w_{xxxx} + pR\left[\frac{1}{2}\,(w + w_0)_{xx} + \frac{1}{R^2}\,(w + w_0)_{\theta\theta} \right] - p = 0 \quad [21]$$

Now define a stress function of the total membrane stresses F such that

$$\frac{N_x}{h} = \frac{F_{\theta\theta}}{R^2}, \quad \frac{N_\theta}{h} = F_{xx}, \quad \frac{N_{x\theta}}{h} = -\frac{F_{x\theta}}{R} \quad [22]$$

Using Equation [14] and the stress-strain relations it is then easy to show that

$$\nabla^4 F = E\left\{ -\frac{1}{R}\,W_{xx} + \frac{W_{x\theta}^2}{R^2} - \frac{W_{xx}W_{\theta\theta}}{R^2} + \frac{2W_{x\theta}w_{0x\theta}}{R^2} - \frac{W_{xx}w_{0\theta\theta}}{R^2} - \frac{W_{\theta\theta}w_{0xx}}{R^2} \right\} \quad [23]$$

As we are interested here in the linear problem, and as we have previously neglected the deflection of the shell between supports, Equation [23] reduces to

$$\nabla^4 F = -\frac{E}{R}\,w_{xx} \quad [24]$$

Equations [19a], [19b], [21], and [24] together with the appropriate boundary conditions define the problem.

Buckling of Rectangular Plates Uniformly Compressed in Two Perpendicular Directions With One Free Edge and Opposite Edge Elastically Restrained

By P. SHULESHKO,[1] SYDNEY, AUSTRALIA

A short history of the buckling of elastic plates was considered by the author in previous papers (1, 2).[2] The present paper deals with specific cases. Only those papers which directly concern this problem will be quoted.

Introduction

ASSUME a rectangular thin elastic plate which has two opposite edges $x = 0$ and $x = a$ simply supported, the edge $y = b$ elastically built into a medium which is characterized by the coefficient r_1 (Fig. 1) and the edge $y = 0$ free. The plate is compressed in its middle plane by means of uniformly distributed forces of intensity P_1 along edges $x = 0$ and $x = a$ and P_2 along the edges $y = 0$ and $y = b$ where

$$P_1 = \nu P_2 \quad \text{and} \quad 0 \leq \nu \leq \infty$$

By gradually increasing P_2 the condition will be reached at which the flat form of equilibrium of the compressed plate will become unstable and a slight lateral force will produce a lateral deflection which does not disappear when the lateral force is removed. Then the axial load which is sufficient to keep the plate in the slightly bent form is called the "critical load" or the "critical force" P_{cr} and such a condition of the plate, the "critical condition."

The critical force P_{cr} will be presented in the form

$$P_{cr} = k \frac{m^2 \pi^2 D}{a^2} \qquad [1]$$

where

k = nondimensional coefficient that depends upon conditions of edge restraint, loading, and shape of plate; i.e., depends upon ratio mb/a and coefficients r_1 and ν

D = flexural rigidity of plate $= \dfrac{Eh^3}{12(1 - \mu^2)}$

E = modulus of elasticity in tension and compression

h = thickness of plate

μ = Poisson's ratio

m = whole number of half waves in x-direction

a = length of plate (see Fig. 1)

b = width of plate

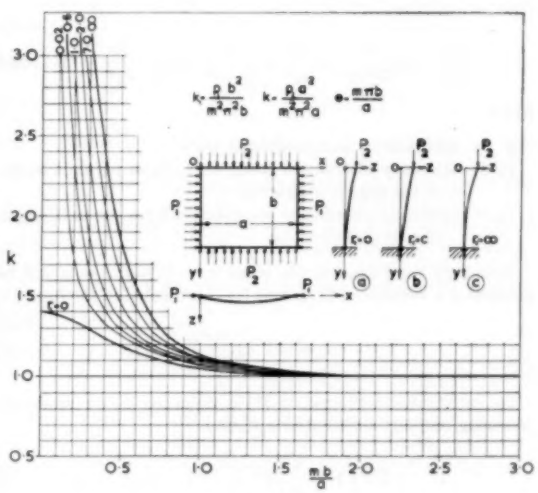

Fig. 1

From the general solution the four separate cases of buckling of rectangular plates will be derived.

(a) Buckling of plates uniformly compressed in two perpendicular directions in which the edges $x = 0$, $x = a$, and $y = b$ are simply supported but edge $y = 0$ is free, Fig. 1(a). For this case, $r_1 = 0$ and $P_1 = P_2 = P$ (i.e., $\nu = 1$).

(b) The same as (a) but with the edge $y = b$ rigidly built-in, Fig. 1(c). For this case, $r_1 = \infty$, and $P_1 = P_2 = P$ (i.e., $\nu = 1$).

(c) Buckling of plates uniformly compressed only in the y-direction in which the edges $x = 0$, $x = a$ are simply supported, edge $y = 0$ is free, and edge $y = b$ elastically built into a medium which is characterized by the coefficient r_1, Fig. 2. For this case, $P_1 = 0$, $P_2 = P$, and r_1 may have any value between 0 and ∞.

(d) The same as (c) but compression is in the x-direction only, Figs. 3 and 4. For this case, $P_1 = P$, $P_2 = 0$, and r_1, as before, may have any value between 0 and ∞.

Differential Equation of the Problem and Its Solution

The differential equation for the deflected plate is

---

[1] Lecturer of Civil Engineering, N.S.W. University of Technology; formerly, Professor of Theoretical and Applied Mechanics, Ukrainian Technical University, Regensburg, Germany.

[2] Numbers in parentheses refer to the Bibliography at the end of the paper.

Presented at the National Applied Mechanics Conference, Urbana, Ill., June 14–16, 1956, of The American Society of Mechanical Engineers.

Discussion of this paper should be addressed to the Secretary, ASME, 29 West 39th Street, New York, N. Y. and will be accepted until October 10, 1956, for publication at a later date. Discussion received after the closing date will be returned.

Note: Statements and opinions advanced in papers are to be understood as individual expressions of their authors and not those of the Society. Manuscript received by ASME Applied Mechanics Division, December 29, 1954. Paper No. 56—APM-20.

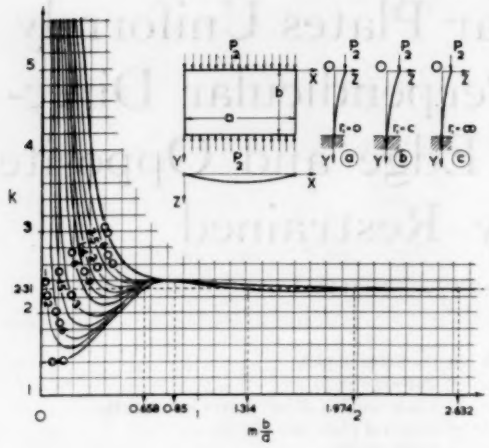

FIG. 2

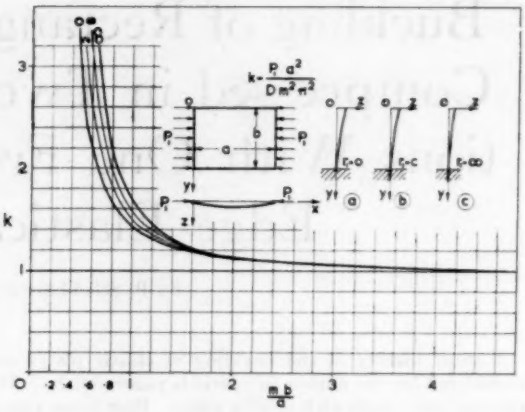

FIG. 3

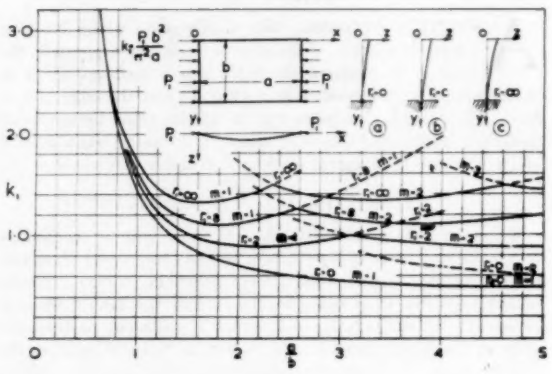

FIG. 4

$$\frac{\partial^4 w}{\partial x^4} + 2\frac{\partial^4 w}{\partial x^2 \partial y^2} + \frac{\partial^4 w}{\partial y^4} + \frac{P_1}{D}\frac{\partial^2 w}{\partial x^2} + \frac{P_2}{D}\frac{\partial^2 w}{\partial y^2} = 0 \ldots [2]^1$$

where

w = deflection of middle plane of plate
P_1 = uniformly distributed compressive force per unit length of the edge in x-direction
P_2 = uniformly distributed compressive force per unit length of edge in y-direction

Boundary conditions at the edges $x = 0$ and $x = a$ will be satisfied if a solution of Equation [2] is presented in the form (1)

$$w = AY \sin\frac{m\pi x}{a} \ldots\ldots\ldots\ldots\ldots [3]$$

On substitution of Equation [3] in Equation [2] we obtain the following ordinary differential equation

$$Y^{iv} - 2\lambda^2\left(1 - \frac{k}{2}\right)Y'' + \lambda^4(1 - k_1)Y = 0 \ldots\ldots [4]$$

where

$$\lambda = \frac{m\pi}{a}, \quad k_1 = \frac{P_1 a^2}{m^2\pi^2 D}, \quad k = \frac{P_2 a^2}{m^2\pi^2 D} \ldots\ldots\ldots [5]$$

The general solution of Equation [4] can be presented in the following form

$$Y = C_1 \sinh \alpha y + C_2 \cosh \alpha y + C_3 \sinh \beta y + C_4 \cosh \beta y \ldots [6]$$

where

$$\left.\begin{aligned} \alpha &= \lambda\sqrt{k_2 + \sqrt{k_2^2 - (1 - k_1)}}, \\ \beta &= \lambda\sqrt{k_2 - \sqrt{k_2^2 - (1 - k_1)}} \\ k_2 &= 1 - \frac{k}{2} \end{aligned}\right\} \ldots [7]$$

The constants of integration can be obtained from the following boundary conditions:

(*a*) For a free edge (1, 2) (i.e., $y = 0$)

$$\frac{\partial^2 w}{\partial y^2} + \mu\frac{\partial^2 w}{\partial x^2} = 0, \text{ and } D\left[\frac{\partial^3 w}{\partial y^3} + (2 - \mu)\frac{\partial^3 w}{\partial y \partial x^2}\right] + P_2\frac{\partial w}{\partial y} = 0 \ldots [8]$$

The second Boundary Condition [8] is different from that given by Kirchhoff, because it includes the additional term

$$P_2\frac{\partial w}{\partial y}$$

which occurs when the edge of plate is free and loaded by the force P_2, Fig. 1.

(*b*) For an elastically restrained edge ($y = b$) (4 to 7)

$$w = 0, \text{ and } -D\left(\frac{\partial^2 w}{\partial y^2} + \mu\frac{\partial^2 w}{\partial x^2}\right) = 4S\frac{\partial w}{\partial y} \ldots\ldots [9]$$

where S is the stiffness per unit length of the elastic restraining medium at the edge of the plate, or moment required to rotate a unit length of the medium through one fourth of radian (4 to 6).

By substituting Equation [3] in Equations [8] and [9] these boundary conditions can be written in the following form

$$Y'' - \lambda^2\mu Y = 0, \quad \text{and } Y''' - \lambda^2(2k - \mu)Y' = 0 \text{ (for } y = 0) \ldots [10]$$

[1] The classical theory of the buckling of plates is used here.

and

$$Y = 0, \quad \text{and} \quad Y'' + \frac{r_1}{b} Y' = 0, \quad (\text{for } y = b) \ldots\ldots [11]$$

where

$$r_1 = \frac{4Sb}{D} \ldots\ldots [12]$$

$S = 0$ for a simply supported edge
$S = \infty$ for a rigidly built-in edge
$S = C$ for some intermediate case of edge restraint

This constant C can be calculated by using a method given by E. E. Lundquist and E. Z. Stowell (6), or by S. Timoshenko.[4]

S. Timoshenko in his book[4] gives instead of Equation [9] the following boundary conditions

$$D\left(\frac{\partial^2 w}{\partial y^2} + \mu \frac{\partial^2 w}{\partial x^2}\right) = C \frac{\partial^2 w}{\partial x^2 \partial y} \ldots\ldots [9a]$$

which, after substitution of Equation [3], becomes

$$Y'' + \lambda^2 \frac{C}{D} Y' = 0 \quad (\text{for } y = b) \ldots\ldots [11a]$$

Equating [11] to [11a], we have

$$r_1 = \lambda^2 \frac{Cb}{D} \ldots\ldots [12a]$$

Equating [12] to [12a], we obtain

$$C = \frac{4S}{\lambda^2} \ldots\ldots [13]$$

i.e., if the edges $x = 0$ and $x = a$ are simply supported, it does not matter which boundary condition for edge $y = b$ is used, Equation [9] or [9a].

Substituting Equation [6] into [10] and simplifying, the following expressions are obtained

$$-C_3 = \frac{\alpha B}{\beta A} C_1, \quad \text{and} \quad -C_4 = \frac{A}{B} C_2 \ldots\ldots [14]$$

where

$$A = \alpha^2 - \lambda^2\mu, \quad B = \beta^2 - \lambda^2\mu \ldots\ldots [15]$$

The function Y after substitution of Equations [14] into [6], can then be written in the form

$$Y = C_1'[\beta A \sinh \alpha y - \alpha B \sinh \beta y] + C_2'[B \cosh \alpha y - A \cosh \beta y] \ldots [16]$$

where C_1', and C_2', are new arbitrary constants.

[4] Reference (3d), p. 257.
[5] Reference (3c), p. 343.

Substituting Equations [15] into [11], two homogeneous linear equations in C_1' and C_2' are obtained. The critical value of the compressive force P_{cr} is now determined by equating to zero the determinant of these equations, which gives

$$[\beta^2 - \alpha^2][\alpha B^2 \sinh \beta b \cosh \alpha b - \beta A^2 \sinh \alpha b \cosh \beta b] + \frac{r_1}{b}[-(\alpha^2 B^2 + \beta^2 A^2) \sinh \alpha b \sinh \beta b + \alpha\beta(A^2 + B^2) \cosh \alpha b \cosh \beta b - 2\alpha\beta AB] = 0 \ldots [17]$$

The numerical factor k which determines the critical load P_{cr} is obtained as the least root of Equation [17].

The two limiting cases, given by $r_1 = 0$ and $r_1 = \infty$ are considered here before the general, for which r_1 may have any value between 0 and ∞.

Buckling of Rectangular Plates Uniformly Compressed in x and y-Directions in Which Edges $x = 0$, $x = a$, and $y = b$ Are Simply Supported and Edge $y = 0$ Is Free

The transcendental equation for this case is obtained by substituting $r_1 = 0$ and $\nu = 1$ into Equation [17]. Thus

$$(\beta^2 - \alpha^2)[\alpha B^2 \sinh \beta b \cosh \alpha b - \beta A^2 \sin \alpha b \cosh \beta b] = 0 \ldots [18]$$

where

$$\nu = 1, k_1 = k, \alpha = \lambda, \beta = i\lambda\sqrt{(k-1)}, i = \sqrt{-1} \ldots\ldots [19]$$

$$A = \lambda^2\delta, B = -\lambda^2(k - \delta), \delta = 1 - \mu \ldots\ldots [20]$$

After substituting the values [19] and [20] into Equation [18] and simplifying, the following equation is obtained

$$\delta^2 \gamma \cos \gamma \sinh \theta - (k + \delta)^2 \theta \cosh \theta \sin \gamma = 0 \ldots\ldots [21]$$

where

$$\theta = \alpha b = \lambda b = \frac{m\pi b}{a}, \gamma = -i\beta b = \theta\sqrt{k-1} \ldots [22]$$

The first line of Table 1 gives values of the least root of Equation [21] for various values of the ratio mb/a, for which the problem has any physical significance. The value of 0.3 has been adopted for μ.

The same values also are represented by the lowest curve ($r_1 = 0$) in Fig. 1.

From the table and graph it can be seen that the roots for ratios $mb/a \geq 1.71$ are constant, and equal unity; i.e., $k = 1$. If the coefficient k is known, the critical force P_{cr} can be determined for every ratio mb/a by using Equation [1].

Trial calculations show that the smallest value of P_{cr} for all values of b/a will be when $m = 1$; i.e., the buckled plate will have only one half wave in the x-direction.

TABLE 1

mb/a	0.0	0.05	0.10	0.15	0.20	0.25	0.30	0.35	0.40	0.45	0.50	0.55	0.60	0.65	0.70	0.75	0.80	0.85
k at $r_1 = 0$	1.40	1.39	1.38	1.36	1.34	1.31	1.28	1.26	1.24	1.21	1.19	1.17	1.15	1.13	1.11	1.10	1.09	1.08
k at $r_1 = 0.02$	—	6.80	3.00	2.22	1.75	1.60	1.45	1.388	1.33	1.294	1.26	1.223	1.20	1.172	1.15	1.138	1.12	1.10
k at $r_1 = 0.5$	—	18.0	6.00	3.333	2.34	1.872	1.66	1.486	1.41	1.358	1.30	1.263	1.23	1.207	1.18	1.159	1.135	1.116
k at $r_1 = 1$	—	30.0	8.5	4.444	3.0	2.24	1.87	1.633	1.53	1.432	1.36	1.306	1.26	1.235	1.20	1.182	1.16	1.135
k at $r_1 = 2$	—	52.0	14.0	6.844	4.25	3.04	2.34	1.959	1.72	1.565	1.45	1.378	1.32	1.278	1.24	1.209	1.18	1.158
k at $r_1 = 7$	—	76.0	20	9.556	5.75	3.92	3.00	2.408	2.06	1.793	1.64	1.521	1.42	1.337	1.28	1.244	1.20	1.176
k at $r_1 = \infty$	∞	100	26	12.0	7.0	4.80	3.56	2.816	2.36	2.035	1.83	1.663	1.55	1.456	1.37	1.298	1.24	1.204

mb/a	0.90	0.95	1.00	1.10	1.20	1.30	1.40	1.50	1.60	1.70	1.80	190	2.00	2.055	2.50	3.00	∞
k at $r_1 = 0$	1.07	1.06	1.05	1.04	1.03	1.02	1.01	1.004	1.00	1.00	1.00	1.00	1.00	1.00	1.00	1.00	1.00
k at $r_1 = 0.02$	1.09	1.080	1.07	1.0496	1.03	1.024	1.017	1.013	1.005	1.003	1.002	1.002	1.00	1.00	1.00	1.00	1.00
k at $r_1 = 0.5$	1.10	1.093	1.08	1.058	1.04	1.03	1.02	1.018	1.010	1.007	1.003	1.004	1.00	1.00	1.00	1.00	1.00
k at $r_1 = 1$	1.12	1.105	1.09	1.074	1.05	1.035	1.03	1.022	1.016	1.011	1.005	1.0044	1.00	1.00	1.00	1.00	1.00
k at $r_1 = 2$	1.14	1.119	1.10	1.083	1.06	1.047	1.04	1.031	1.022	1.014	1.006	1.0055	1.00	1.00	1.00	1.00	1.00
k at $r_1 = 7$	1.16	1.13	1.12	1.091	1.07	1.056	1.04	1.036	1.027	1.017	1.009	1.0069	1.00	1.00	1.00	1.00	1.00
k at $r_1 = \infty$	1.17	1.152	1.13	1.107	1.08	1.065	1.05	1.04	1.03	1.021	1.012	1.0083	1.00	1.00	1.00	1.00	1.00

Buckling of Rectangular Plates Uniformly Compressed in x and y-Directions in Which Edges $x = 0$ and $x = a$ Are Simply Supported, Edge $y = 0$ Is Free But Edge $y = b$ Is Rigidly Built-In

The transcendental equation for this case, Fig. 1(c), is obtained if $\nu = 1$ and $r_1 = \infty$ are substituted in Equation [17]. Thus

$$-(\alpha^2B^2 + \beta^2A^2)\sinh \alpha b \sinh \beta b + \alpha\beta(A^2 + B^2)\cosh \alpha b \cosh \beta b - 2\alpha\beta AB = 0 \quad [23]$$

where

$$\left.\begin{aligned} &\alpha = \frac{m\pi}{a},\ \beta = i\frac{m\pi}{a}\sqrt{(k-1)},\ \lambda = \frac{m\pi}{a} \\ &\alpha\beta = i\lambda^2\sqrt{k-1} \\ &AB = -\lambda^4\delta(k-\delta) \\ &A^2 + B^2 = \lambda^4[\delta^2 + (k-\delta)^2] \\ &\alpha^2B^2 + \beta^2A^2 = \lambda^4[(k-\delta)^2 - (k-1)\delta^2] \\ &\alpha\beta(A^2 + B^2) = i\lambda^6\sqrt{(k-1)}\,[\delta^2 - (k-\delta)^2] \\ &2\alpha\beta AB = -2\lambda^4\delta i(k-\delta)\sqrt{(k-1)} \end{aligned}\right\} \quad [24]$$

After substituting the values, given in Equations [24] into [23] and simplifying, the following equation is obtained

$$-[(k-\delta)^2 - \delta^2(k-1)]\theta \sinh \theta \sin \gamma + [\delta^2 + (k-\delta)^2]\gamma \cos \gamma \cosh \theta + 2\delta\gamma(k-\delta) = 0 \quad [25]$$

where

$$\theta = \frac{m\pi b}{a},\quad \gamma = \theta\sqrt{(k-1)} \quad [26]$$

The last line of Table 1 gives values of the least root of Equation [25] for various values of mb/a, for which the problems have physical significance ($\mu = 0.30$). The same values are also represented by the highest curve ($r_1 = \infty$) in Fig. 1.

From this table and graph it can be seen that the roots for the ratio $mb/a \geq 2.06$ are constant and equal to unity; i.e., $k = 1$.

Whole numbers m of half-wave lengths must be chosen so that the critical force P_{cr} shall have its least value.

Buckling of Rectangular Plates Uniformly Compressed in Two Perpendicular Directions With One Free Edge and Elastically Restrained Against Rotation Along Opposite Edge

In this case the value of the coefficient r_1 can range from $r_1 = 0$ to $r_1 = \infty$ and accordingly the roots of Equation [17] will vary between the roots of Equation [21] and those of Equation [25]. Consequently, the curves for different values of r_1 will be disposed between the lowest curve of k for $r_1 = 0$ and the highest curve of k for $r_1 = \infty$, Fig. 1. By comparing the curves for those two extreme cases and the values of Table 1, it can be seen that for plates with ratio mb/a between 2.06 and ∞, ($2.06 < mb/a < \infty$), the boundary conditions at the edge $y = b$ do not substantially affect the critical forces P_{cr}. Consequently, in practice, k may be taken as 1 for all plates with $mb/a \geq 2.06$. We must obtain the roots k for different values of r_1 only in the interval $0 \leq mb/a \leq 2.06$. These roots are obtained from Equation [17] and are given in Table 1.

The same values are also represented in Fig. 1 by the curves for $r_1 = 0$, $r_1 = 0.02$, $r_1 = 0.5$, $r_1 = 1.0$, $r_1 = 2.0$, $r_1 = 7.0$, and $r_1 = \infty$.

From the family of curves it can be seen, as stated previously, that the boundary conditions on the edge $y = b$ only affect plates with the ratio $mb/a < 2.06$. For plates with the ratio $mb/a \geq 2.06$ the value of the root k can be taken as unity for all plates irrespective of the boundary conditions on the edge $y = b$, and P_{cr} can be represented by the formula

$$P_{cr} = \frac{\pi^2 D}{a^2},\quad (m = 1)$$

Calculations show that the smallest value of P_{cr} for plates with ratio, say, $b/a > 0.5$ for all values of r_1 and $0 \leq \nu \leq 1$ is obtained by taking $m = 1$; i.e., by assuming that the buckled plate has only one half wave in the x-direction.

If $\nu > 1$, i.e., $P_1 > P_2$, it is possible to have more than one half wave in the x-direction. In the particular case when $\nu = \infty$, i.e., $P_1 = P$, $P_2 = 0$, the buckled plate can have several half waves depending on the ratio a/b, Fig. 4.

Specific Cases

Case 1. Buckling of Rectangular Plate Uniformly Compressed in y-Direction With Edge $y = 0$ Free and $y = b$ Elastically Restrained; Edges $x = 0$ and $x = a$ Are Simply Supported, Fig. 2. The transcendental equation for this case is obtained if $\nu = 0$ is substituted in Equation [17] and the values αb and βb are represented in the form

$$\alpha b = p + iq,\ \text{and}\ \beta b = p - iq$$

where

$$p = \frac{\theta}{2}\sqrt{(4-k)},\ q = \frac{\theta}{2}\sqrt{k},\ i = \sqrt{-1},\ k = \frac{Pa^2}{m^2\pi^2 D} \quad [27]$$

Then Equation [17] will be transformed into the form (1)

$$[ps\cos 2p + qt \sin 2q] + r_1[s\sinh^2 p + t\sin^2 q - u] = 0 \quad [28]$$

where

$$\left.\begin{aligned} &s = k(k - 4\delta + \delta^2),\quad t = (k-\delta^2)(4-k) \\ &u = k(4-k),\ \text{and}\ \delta = (1-\mu) \end{aligned}\right\} \quad [29]$$

The smallest root k of Equation [28] for various values of r_1 and ratio mb/a is given in Table 2 and the same values are represented in Fig. 2 by the curves.

From the family of curves it can be seen that the boundary conditions on the edge $y = b$ do not have any appreciable effect on the value of k, for ratios $mb/a > 0.80$, and for all values of $mb/a > 1.80$, with $\mu = 0.30$, k may be taken as equal to 2.31, irrespective of the boundary conditions on the edge $y = b$. If μ differs from 0.30 and $mb/a > 0.80$, k may be represented as follows

$$k = 3 - 2\mu - \mu^2 \quad [30]$$

Case 2. Buckling of Rectangular Plates Uniformly Compressed in x-Direction With Edge $y = 0$ Free and $y = b$ Elastically Restrained. Edges $x = 0$ and $x = a$ Are Simply Supported, Figs. 3 and 4. This is the case when $\nu = \infty$; i.e., $P_1 = P$ and $P_2 = 0$, Fig. 3. If these values are substituted in Equation [17] and αb and βb represented in the form

$$\alpha b = \alpha_1 = \theta\sqrt{(1 + \sqrt{k})},\ \beta b = \beta_1 i = \theta i\sqrt{(-1 + \sqrt{k})} \quad [31]$$

then Equation [17] will be transformed into the form

$$\sqrt{k}[-(\delta + \sqrt{k})^2\beta_1 \cos \beta_1 \sinh \alpha_1 + (\delta - \sqrt{k})^2\alpha_1 \cosh \alpha_1 \sin \beta_1] + r_1\{[\delta^2 + k(1-2\delta)]\sinh \alpha_1 \sin \beta_1 - (\delta^2 + k)\sqrt{(k-1)}\cosh \alpha_1 \cos \beta_1 + (\delta^2 - k)\sqrt{(k-1)}\} = 0 \quad [32]$$

The least root k of Equation [32] for various values of the ratio

TABLE 2

mb/a / k at r_1 =	0	0.05	0.20	0.40	0.60	0.80	1.00	1.20	1.40	1.60	1.80	2.0	∞
0	1.40	1.402	1.516	1.84	2.23	2.397	2.366	2.314	2.31	2.31	2.31	2.31	2.31
0.04		3.00	1.635	1.86	2.231	2.398	2.368	2.316					2.31
0.06		3.85	1.67	1.87	2.234	2.40	2.37	2.317					2.31
0.10		5.45	1.76	1.89	2.238	2.40	2.37	2.318					2.31
0.20		9.10	1.98	1.93	2.245	2.40	2.37	2.32					2.31
0.30		12.60	2.19	1.97	2.252	2.40	2.37	2.322					2.31
0.40		15.80	2.37	2.015	2.258	2.40	2.37	2.324					2.31
0.50		18.90	2.54	2.05	2.265	2.40	2.37	2.326					2.31
0.60		21.50	2.71	2.08	2.271	2.40	2.372	2.328					2.31
0.70		24.40	2.87	2.116	2.277	2.40	2.374	2.328					2.31
0.80		27.00	3.03	2.15	2.283	2.40	2.376	2.33					2.31
0.90		29.30	3.18	2.18	2.288	2.40	2.378	2.33					2.31
1.00		31.50	3.31	2.20	2.293	2.40	2.38	2.33	2.31	2.31	2.31	2.31	2.31
1.20		35.60	3.56	2.25	2.302	2.40	2.38	2.332	2.312	2.311			2.31
1.40		39.60	3.77	2.29	2.311	2.40	2.38	2.334	2.314	2.312			2.31
1.60		43.0	3.99	2.33	2.318	2.40	2.38	2.336	2.316	2.313			2.31
1.80		46.80	4.18	2.37	2.325	2.40	2.38	2.338	2.318	2.314			2.31
2.00		47.75	4.34	2.40	2.331	2.40	2.381	2.34	2.32	2.315			2.31
2.50		53.50	4.68	2.47	2.344	2.40	2.382	2.342	2.322	2.316			2.31
3.00		58.20	4.98	2.53	2.354	2.40	2.383	2.344	2.324	2.318			2.31
3.50		62.50	5.20	2.57	2.36	2.40	2.384	2.346	2.326	2.32			2.31
4.00		66.00	5.37	2.62	2.366	2.40	2.384	2.347	2.328	2.32			2.31
5.00		71.50	5.70	2.68	2.378	2.40	2.385	2.35	2.33	2.32			2.31
10.00		83.80	6.53	2.85	2.415	2.40	2.39	2.36	2.33	2.32			2.31
20.00		92.10	7.00	2.942	2.436	2.40	2.39	2.36	2.33	2.32			2.31
30.00		95.00	7.13	2.98	2.444	2.40	2.39	2.36	2.33	2.32			2.31
40.00		96.20	7.22	3.00	2.448	2.40	2.39	2.36	2.33	2.32			2.31
60.00		97.40	7.35	3.014	2.452	2.40	2.39	2.36	2.33	2.32			2.31
100.00		99.0	7.46	3.034	2.455	2.41	2.39	2.36	2.33	2.32	2.31	2.31	2.31
170.00		100.0	7.56	3.049	2.456	2.41	2.39	2.36	2.33	2.32	2.312	2.3106	2.31
∞	∞	101.0	7.62	3.08	2.46	2.41	2.39	2.36	2.33	2.32	2.312	2.3106	2.31

TABLE 3

mb/a	0.10	0.20	0.30	0.40	0.50	0.60	0.70	0.80	0.90	1.00	1.20	1.40	1.60	1.80	2.00	2.50	3.00	∞
k at $r_1 = 0$	46.7	12.65	6.11	3.81	2.79	2.22	1.90	1.68	1.54	1.44	1.35	1.25	1.193	1.14	1.10	1.06	1.04	1.00
k at $r_1 = 2$	9.0	22.5	11.2	5.62	3.60	2.61	2.14	1.84	1.64	1.49	1.37	1.265	1.20	1.15	1.10	1.06	1.04	1.00
k at $r_1 = 8$	12.3	30.7	12.4	7.65	4.48	3.08	2.42	2.01	1.75	1.58	1.40	1.272	1.215	1.16	1.105	1.062	1.04	1.00
k at $r_1 = \infty$	14.3	35.8	14.6	8.93	5.42	3.66	2.75	2.24	1.90	1.70	1.435	1.29	1.24	1.17	1.11	1.066	1.04	1.00

TABLE 4

a/b	0	0.05	0.10	0.20	0.30	0.40	0.50	0.60	0.70	0.80	0.90	1.00	1.10	1.20	1.30
k at $r_1 = 0$	∞	400	101	25.4	11.5	6.63	4.40	3.26	3.26	2.53	2.06	1.72	1.44	1.27	1.135
k at $r_1 = 2$	∞	400	101	25.4	11.5	6.64	4.41	3.27	2.57	2.10	1.76	1.49	1.35	1.23	1.13
k at $r_1 = 8$	∞	400	101	25.4	11.5	6.65	4.43	3.29	2.65	2.19	1.85	1.58	1.44	1.34	1.25
k at $r_1 = \infty$	∞	400	101	25.4	11.56	6.67	4.45	3.34	2.70	2.30	1.97	1.70	1.56	1.47	1.41

a/b	1.40	1.50	1.60	1.70	1.80	1.90	2.00	2.10	2.20	2.30	2.40	2.50	3.0	4.0	5.0
k at $r_1 = 0$	1.03	0.952	0.835	0.79	0.755	0.72	0.698	0.67	0.65	0.635	0.624	0.610	0.553	0.516	0.506
k at $r_1 = 2$	1.06	1.01	0.97	0.936	0.92	0.905	0.90	0.90	0.895	.89	0.895	.90	0.98	0.90_2	0.90_2
k at $r_1 = 8$	1.20	1.16	1.13	0.115	1.11	0.115	1.12	1.13	1.15	1.18	1.20	1.23	1.16_2	1.12_2	1.23_2
k at $r_1 = \infty$	1.36	1.34	1.33	1.33	1.34	1.36	1.38	1.41	1.45	1.49	1.47_2	1.43_2	1.34_2	1.38_2	1.43_2

NOTE: Indexes 2 and 3 show that roots of k are calculated for $m = 2$ and $m = 3$.

mb/a and $\mu = 0.25$ is given in Table 3 and the same values are also represented by the curves in Fig. 3.

From the curves and Table 3 it can be seen that the coefficient k has significance for plates with ratios mb/a less than 2.00. When $mb/a > 2.0$ the coefficient k approaches unity.

For a long plate with $a \gg b$ the coefficient k_1 instead of k represented in the form

$$k_1 = \frac{Pb^2}{D\pi^2} \quad \ldots\ldots\ldots\ldots\ldots\ldots\ldots\ldots [33]$$

can be used as reference (3).

The least root k_1 for various values of the ratio a/b and various values of the coefficient r_1, and m are represented in Table 4 and graphically in Fig. 4. Most of the values of roots k_1 for this case were taken from the work of Prof. S. P. Timoshenko (3), who was the first to consider this case.[6]

From the family of curves it can be seen that the whole number of half-wave lengths m depends upon the values of the ratio a/b and of the coefficient r_1. The coefficient r_1, as can be seen from Table 4, has appreciable significance for plates with the ratio a/b greater than 0.50.

ACKNOWLEDGMENTS

The author is grateful to Mr. A. S. Hall, Head of the Structural Division, and to Messrs. F. E. Archer and E. M. Kitchen, Lecturers at the N.S.W. University of Technology, for helpful advice in preparation of this paper and checking the manuscript.

[6] After Prof. S. P. Timoshenko this case was considered in detail by E. E. Lundquist and E. Z. Stowell (7).

BIBLIOGRAPHY

1 "Buckling of Rectangular Plates Uniformly Compressed in the Vertical Direction With Upper Edge Free," by P. Shuleshko, *The Journal of the Institution of Engineers*, Australia, vol. 25, nos. 4–5, 1953.

2 "Stability of Thin Plates, Which Have Part of the Contour Free," by P. Shuleshko, Scientific Memoirs of Ukrainian Technical University at Regensburg, Germany (in Ukrainian), 1948.

3 (*a*) "On Buckling of Compressed Plates," by S. P. Timoshenko, Bull. Polytech. Institute Kiev, Ukraina (in Russian), 1907, p. 343.

(*b*) "The Collected Papers of S. P. Timoshenko," by S. P. Timoshenko, McGraw-Hill Publishing Company, Ltd., 1953, pp. 11–20.

(*c*) "Theory of Elastic Stability," by S. P. Timoshenko, McGraw-Hill Book Company, Inc., New York, N. Y., 1936, pp. 337–345.

(*d*) "Theory of Elasticity," by S. P. Timoshenko, St. Petersburg, Russia, vol. 2, 1916.

4 "Critical Compressive Stress for Flat Rectangular Plates Supported Along All Edges and Elastically Restrained Against Rotation Along Unloaded Edges," by E. E. Lundquist and E. Z. Stowell, NACA Report 733, 1942, pp. 99–109.

5 "Critical Bending Stress for Flat Rectangular Plates Supported Along All Edges and Elastically Restrained Against Rotation Along Unloaded Compression Edge," by T. H. Johnson and R. G. Noel, *Journal of the Aeronautical Sciences*, vol. 20, 1953, pp. 535–540.

6 "Restraint Provided a Flat Rectangular Plate by Sturdy Stiffener Along an Edge of the Plate," by E. E. Lundquist and E. Z. Stowell, NACA Report 735, 1953.

7 "Critical Compressive Stresses for Outstanding Flanges," by E. E. Lundquist and E. Z. Stowell, NACA Report 734, 1942.

On the Role of Extension in the Flexural Vibrations of Rings

By L. L. PHILIPSON,[1] CULVER CITY, CALIF.

In a generalization of the classical analysis of A. E. H. Love,[2] equations describing the flexural vibrations of thin rings are derived without making use of the usual assumption of no extension of the central line. Direct comparison with the nonextensional formulas of Love leads to a criterion for the validity of the assumption. In the process, the forced-vibration problem is shown to require the possibility of extension in certain cases in which its neglecting in a free-vibration analysis is valid.

Introduction

IN THE usual linear theory of the elastic behavior of naturally curved rods[3] it is assumed that during linear strains the length of the "central line" (locus of centroids of the cross sections) remains invariant; that is, there is no "extension." This assumption is a carry-over from the case of an initially straight rod, but its validity for curved rods apparently has not been established completely.

Our interest is primarily in the elastic vibrations of a ring segment whose central line initially describes an arc of a plane circle. In its treatment additional confusion seems to have arisen due to Love's derivation of his equations of equilibrium with several uses of the nonextension assumption, oddly followed[2] (Sec. 293[c]) by the application of the equations to a case where it is not valid. We shall find that the form of Love's equilibrium equations is actually correct even when extension is permitted, but the "stress components" and "couples" in the equations have different expressions in terms of the displacement components. We shall establish the more complete equations for the radial and tangential displacement components of "flexural vibrations," and then show under what conditions these specialize to the nonextensional equations. These conditions will therefore be sufficient, to our order of approximation, for the validity of the nonextension assumption.

Waltking[3] previously attempted to clarify these conditions. However, as we shall see later, his preliminary (and also common) neglecting of the "rotatory inertia" of the ring results in the omission of terms in the final differential equations for the strain components which are of the same magnitude as those he gains by allowing the length of the central line to vary.

Since our results are obtained through straightforward modifications of Love's analysis, the derivation will be detailed only where these modifications should be emphasized. Because it is practically important, e.g., in the study of aircraft structural rings, as well as due to the fact that it aids in the enlightenment of the problem of extension, we shall include also a radially directed applied force, sinusoidal in time, and variable in amplitude.

Definitions and Co-Ordinates

Consider first a thin homogeneous isotropic rod which may have arbitrary curvature and twist in the unstrained state, but which has a uniform cross section, a principal axis of which makes a constant angle $\pi/2 - f_0$, with the radius of curvature of the central line. Let C_0 denote the unstrained central line of the rod and s_0 measure arc length along it.

At an arbitrary point P_0 on C_0 construct a co-ordinate frame (x_0, y_0, z_0), where x_0 is in the direction of the principal axis mentioned previously, z_0 is in the direction tangential to C_0, positive in the direction of increasing s_0. The y_0-axis is then chosen to complete a right-handed rectangular co-ordinate system.

Similarly, construct a frame (x_1, y_1, z_1) at P_1 on the "strained" central line C_1, where P_1 is the image of P_0 under the strain. The z_1-axis is to be tangential to C_1 in the direction of increasing arc length s_1; the x_1-axis lies on the plane with z_1 which is tangent at P_1 to the strained rod material originally in the (x_0, z_0) plane; y_1 is again chosen to complete a right-handed rectangular frame. Let $\pi/2 - f_1$ be the angle (generally different at different P_1) between the x_1-axis and the radius of curvature of C_1.

Define the extension of C_0 to be $\epsilon = ds_1/ds_0 - 1$. Evidently, $\epsilon = 0$ if, and only if, the length of the central line remains invariant in its transformation from C_0 into C_1.

The co-ordinate frames at P_0 on C_0 and P_1 on C_1 can be related by a matrix of direction cosines L_i, M_i, N_i as indicated by the following

	x_0	y_0	z_0
x_1	L_1	M_1	N_1
y_1	L_2	M_2	N_2
z_1	L_3	M_3	N_3

..... [1]

Finally let β be the cosine of the angle between the x_1 and y_0-axes (so $\beta = M_1$). For small deformations, β is approximately the angle of rotation of the (x_0, y_0, z_0) frame about an axis parallel to z_0 in its transformation into the (x_1, y_1, z_1) frame.

Geometrical Components of C_0 and C_1

If P_0 moves along C_0 in the direction of increasing s_0 with unit speed, the (x_0, y_0, z_0) frame will rotate about C_0 with a vector angular velocity whose components κ_0, κ_0', τ_0 are, respectively, the "curvatures" at P_0 of C_0's projection onto the (y_0, z_0) and (x_0, z_0) planes, and the "twist." If ρ_0 is the radius of curvature of C_0 at P_0, then

$$\kappa_0 = -(\cos f_0)/\rho_0, \quad \kappa_0' = (\sin f_0)/\rho_0$$

Similarly, define the geometrical components κ_1, κ_1', τ_1 of C_1

---

[1] Hughes Research Laboratories.

[2] "A Treatise on the Mathematical Theory of Elasticity," by A. E. H. Love, Dover Publications, New York, N. Y., fourth edition, chapters 18–22, 1944.

[3] "Schwingungszahlen und Schwingungsformen von Kreisbogentragern," by F. W. Waltking, *Ingenieur-Archiv*, vol. 5, 1934, pp. 429–449.

Presented at the National Applied Mechanics Conference, Urbana, Ill., June 14–16, 1956, of The American Society of Mechanical Engineers.

Discussion of this paper should be addressed to the Secretary, ASME, 29 West 39th Street, New York, N. Y., and will be accepted until October 10, 1956, for publication at a later date. Discussion received after the closing date will be returned.

Note: Statements and opinions advanced in papers are to be understood as individual expressions of their authors and not those of the Society. Manuscript received by ASME Applied Mechanics Division, July 12, 1955. Paper No. 56—APM-2.

Static Equilibrium Equations

Let X_s, Y_s, Z_s be the components of the stress tensor acting on the cross section at P_1 of the deformed rod in the x_1, y_1, z_1 directions, respectively. These three "tractions" integrated over the cross section result in the "shearing" and "tensile" forces

$$N = \int\int X_s dA, \quad N' = \int\int Y_s dA, \quad T = \int\int Z_s dA \ldots [2]$$

and the couples

$$G = \int\int y_1 Z_s dA, \quad G' = \int\int x_1 Z_s dA,$$
$$H = \int\int (x_1 Y_s - y_1 X_s) dA \ldots [3]$$

Under the application of body forces X, Y, Z and couples $K, K', \mathfrak{H}$, per unit length of C_1, the conditions for static equilibrium of the deformed rod may then be derived exactly as in Love[2] (Sec. 259), except for the retention of extension, to be

$$\left.\begin{aligned} &dN/ds_1 - \tau_1 N' + \kappa_1' T + X = 0 \\ &dN'/ds_1 - \kappa_1 T + \tau_1 N + Y = 0 \\ &dT/ds_1 - \kappa_1' N + \kappa_1 N' + Z = 0 \\ &dG/ds_1 - \tau_1 G' + \kappa_1' H - N' + K = 0 \\ &dG'/ds_1 - \kappa_1 H + \tau_1 G + N + K' = 0 \\ &dH/ds_1 - \kappa_1' G + \kappa_1 G' + \mathfrak{H} = 0 \end{aligned}\right\} \ldots [4]$$

Evaluation of κ_1, κ_1', τ_1

Again, consider P_0 as moving with unit speed along C_0, so that the (x_0, y_0, z_0) frame has angular velocity $(\kappa_0, \kappa_0', \tau_0)$. Let P_0^* be an arbitrary but fixed point on C_0 and let l_i, m_i, n_i be the direction cosines of the (x_1, y_1, z_1) frame at P_1 relative to the (x_0^*, y_0^*, z_0^*) frame at P_0^*. Then when P_0 coincides with P_0^*, $l_1 = L_1$, etc., and

$$dl_1/ds_0 = dL_1/ds_0 - M_1\tau_0 + N_1\kappa_0' \ldots [5]$$

with similar relationships holding for the other cosines (c.f., Love,[2] Sec. 290). Furthermore (Love,[2] Sec. 253) equations of the nature of

$$dl_1/ds_1 = l_2\tau_1 - l_3\kappa_1' \ldots [6]$$

also hold. Hence, for the cosines of a moving frame relative to a fixed one, recalling from the section Definitions that $ds_1 = ds_0(1+\epsilon)$, we have, when $P_0 = P_0^*$, a set of equations typified by

$$dL_1/ds_0 - M_1\tau_0 + N_1\kappa_0' = (L_2\tau_1 - L_3\kappa_1')(1+\epsilon) \ldots [7]$$

This can be solved for κ_1, κ_1', τ_1 following a preliminary evaluation of L_i, M_i, N_i.

Let (u, v, w) represent the displacement vector of P_1 relative to the (x_0, y_0, z_0) frame at P_0. Let P_0' be a point on C_0 distant δs_0 from P_0, P_1' on C_1 the image of P_0' under the strain and distant δs_1 from P_1. Let (ξ, η, ζ) be the co-ordinates of P_1' relative to the (x_0, y_0, z_0) frame. Then, as a simple sketch makes clear, we have

$$N_3 = \cos(z_0, z_1) = \lim_{\delta s_1 \to 0} \frac{\zeta - w}{\delta s_1} \ldots [8]$$

and similar expressions for L_3, M_3. But (Love,[2] Sec. 289)

$$\left.\begin{aligned} &\lim_{\delta s_0 \to 0} \frac{\xi - u}{\delta s_0} = \frac{du}{ds_0} - v\tau_0 + w\kappa_0' \\ &\lim_{\delta s_0 \to 0} \frac{\eta - v}{\delta s_0} = \frac{dv}{ds_0} - w\kappa_0 + u\tau_0 \\ &\lim_{\delta s_0 \to 0} \frac{\zeta - w}{\delta s_0} = 1 + \frac{dw}{ds_0} - u\kappa_0' + v\kappa_0 \end{aligned}\right\} \ldots [9]$$

Equations [8] and [9] combine, using $ds_1 = ds_0(1+\epsilon)$, to give as expressions for L_3, M_3, N_3 the right sides of Equations [9] multiplied by $(1+\epsilon)^{-1}$. To the first order in the "displacement components" u, v, w, and their derivatives, the identity $L_3^2 + M_3^2 + N_3^2 = 1$ leads to an expression for the extension

$$\epsilon = dw/ds_0 - u\kappa_0' + v\kappa_0 \ldots [10]$$

whence it follows that

$$\left.\begin{aligned} L_3 &= du/ds_0 + w\kappa_0' - v\tau_0 \\ M_3 &= dv/ds_0 + u\tau_0 - w\kappa_0 \\ N_3 &= 1 \end{aligned}\right\} \ldots [11]$$

to the first order. As noted by Waltking,[3] the anomaly $\epsilon \leq 0$, apparently required by Love's results in Section 289,[2] is now seen to be due to his neglecting the $(1+\epsilon)^{-1}$ factor in the L_3, M_3, N_3 expressions, obtained from Equations [9]. This results in $N_3 = 1 + \epsilon$, which coupled with the fact $N_3 \leq 1$, seems to require nonpositive ϵ.

Next, employing Equations [11], the identity $M_1 = \beta$, the orthogonality of the rows and columns in the array, [1], and the fact that the determinant of that array is unity one can directly obtain, to the first order

$$L_1 = 1, \quad M_1 = \beta, \quad N_1 = -L_3, \quad L_2 = -\beta,$$
$$M_2 = 1, \quad N_2 = -M_3 \ldots [12]$$

Finally inserting Equations [11] and [12] into [7] we may solve for C_1's geometrical components

$$\kappa_1 = \bar{\kappa}_1(1-\epsilon), \quad \kappa_1' = \bar{\kappa}_1'(1-\epsilon), \quad \tau_1 = \bar{\tau}_1(1-\epsilon) \ldots [13]$$

where

$$\left.\begin{aligned} \bar{\kappa}_1 &= \kappa_0 + \beta\kappa_0' - dM_3/ds_0 - \tau_0 L_3 \\ \bar{\kappa}_1' &= \kappa_0' - \beta\kappa_0 + dL_3/ds_0 - \tau_0 M_3 \\ \bar{\tau}_1 &= \tau_0 + d\beta/ds_0 + \kappa_0 L_3 + \kappa_0' M_3 \end{aligned}\right\} \ldots [14]$$

L_3, M_3 being given by Equations [11]. The barred quantities are Love's components. If κ_1, κ_1', τ_1 are now inserted into the Equations of Equilibrium [4] and s_1 is eliminated, we arrive at

$$\left.\begin{aligned} &dN/ds_0 - \bar{\tau}_1 N' + \bar{\kappa}_1' T + \bar{X} = 0 \\ &dN'/ds_0 - \kappa_1 T + \bar{\tau}_1 N + \bar{Y} = 0 \\ &dT/ds_0 - \bar{\kappa}_1' N + \bar{\kappa}_1 N' + \bar{Z} = 0 \\ &dG/ds_0 - \bar{\tau}_1 G' + \bar{\kappa}_1' H - N'(1+\epsilon) + \bar{K} = 0 \\ &dG'/ds_0 - \bar{\kappa}_1 H + \bar{\tau}_1 G + N(1+\epsilon) + \bar{K}' = 0 \\ &dH/ds_0 - \bar{\kappa}_1' G + \bar{\kappa}_1 G' + \bar{\mathfrak{H}} = 0 \end{aligned}\right\} \ldots [15]$$

where $\bar{X} = X(1+\epsilon)$, etc., are the body forces and torques per unit length of C_0. Equations [15] have the same form as Love's equations, except for the factor $1+\epsilon$ in the fourth and fifth. When the body forces are of first order in the displacement components, however (as we shall see specifically later), so are N and N', and consequently the factor can be dropped and Love's equations obtained. Nevertheless, we shall next find that Equations [15] are not identical to Love's when they are expressed in terms of u, v, w, β.

Dynamical Equilibrium Equations in Terms of Displacement Components

The fundamental formal difference between the present analysis and Love's now arises. The usual assumptions of the "ordinary theory" of elasticity (c.f., Love,[2] Sec. 259, where it is shown that these remain valid when extension is included) for the stress couples and the tension are

$$\left.\begin{aligned} G &= EJ_x(\kappa_1 - \kappa_0) \\ G' &= EJ_y(\kappa_1' - \kappa_0) \\ H &= C(\tau_1 - \tau_0) \\ T &= EA\epsilon \end{aligned}\right\} \quad \ldots\ldots\ldots\ldots [16]$$

where E is Young's modulus, A is the (uniform) cross-section area, C is the "torsional rigidity," and J_x, J_y are the moments of inertia of the cross section about the x_0 and y_0-axes, respectively. Because $\kappa_1 = \bar{\kappa}_1(1 - \epsilon)$, etc., the quantities in Equations [16] have basically different expressions from Love's when the displacement components are introduced. Specializing to a ring whose central line initially is an arc of a plane circle of radius a with the positive x_0-axis inward along the radius, we take $f_0 = \pi/2$, whence $\kappa_0 = 0$, $\kappa_0' = 1/a$, $\tau_0 \doteq 0$. Then, with $s_0 = a\theta$, we have

$$\left.\begin{aligned} G &= EJ_x a^{-2}(a\beta - d^2v/d\theta^2) \\ G' &= EJ_y a^{-2}(u + d^2u/d\theta^2) \\ H &= Ca^{-2}(ad\beta/d\theta + dv/d\theta) \\ T &= EAa^{-1}(dw/d\theta - u) \end{aligned}\right\} \quad \ldots\ldots\ldots [17]$$

We may substitute these evaluations into Equations [15], together with those of $\bar{\kappa}_1$, $\bar{\kappa}_1'$, $\bar{\tau}_1$ from [14]. Let us furthermore obtain the dynamical equations of equilibrium from Equations [15] by application of d'Alembert's principle in the usual way. Considering also a radially directed force per unit length of C_0, $f(\theta, t)$, and writing m for the mass of the rod per unit length of C_0, we arrive at

$$\left.\begin{aligned} \partial N/\partial\theta + T &= ma\partial^2u/\partial t^2 - f \\ \partial T/\partial\theta - N &= ma\partial^2w/\partial t^2 \\ \partial G'/\partial\theta + aN(1 + \epsilon) &= I_y\partial^2\varphi_y/\partial t^2 \end{aligned}\right\} \quad \ldots\ldots [18]$$

and three other equations involving v, β, and N' only. The quantities φ_y, I_y are the angle of rotation and (mass) moment of inertia per unit length of C_0, respectively, about the y_0-axis; thus

$$\left.\begin{aligned} \varphi_y &\doteq \sin\varphi_y = \cos(\pi/2 - \varphi_y) = L_3 \\ I_y &= m\gamma^2 \end{aligned}\right\} \quad \ldots\ldots [19]$$

where γ is the radius of gyration of the cross section about the y_0-axis (perpendicular to the plane of the central line of the ring).

The separation of the equilibrium equations into two sets for u, w, and v, β, is possible because the angle $f_0 = \pi/2$. The u, w set given by Equations [18] describes the flexural vibrations in which our interest lies; the v, β set is identically satisfied by $v = \beta = 0$.

Inserting Equations [19], and using Equations [11] and [17], the third equation in [18] gives

$$N(1 + \epsilon) = \frac{-EJ_y}{a^3}\left(\frac{\partial u}{\partial\theta} + \frac{\partial^3 u}{\partial\theta^3}\right) + \frac{I_y}{a}\frac{\partial^2}{\partial t^2}\left(\frac{\partial u}{\partial\theta} + w\right) \quad \ldots\ldots [20]$$

This explicitly indicates that, to the first order, the $1 + \epsilon$ factor might have been dropped in Equations [15]. Assuming steady sinusoidal time variation with frequency ω

$$f(\theta, t) = F(\theta)e^{i\omega t}, \quad u(\theta, t) = U(\theta)e^{i\omega t}, \quad w(\theta, t) = W(\theta)e^{i\omega t}$$

we may eliminate to obtain an equation for U alone and another for W

$$U^{(6)} + 2(1 + pq)U^{(4)} + (1 - q + 3pq + p^2q^2)U'' + q(1 + p - pq - p^2q)U - [F'' + pq(1 + p)F]a^4/EJ_y = 0 \quad \ldots [21]$$

$$W^{(6)} + 2(1 + pq)W^{(4)} + (1 - q + 3pq + p^2q^2)W'' + q(1 + p - pq - p^2q)W + [F'(1 - p - p^2q) + pF''']a^4/EJ_y = 0 \quad \ldots [22]$$

where

$$p = J_y/a^2A = (\gamma/a)^2, \quad q = ma^4\omega^2/EJ_y$$

and differentiation is with respect to θ. Note that the homogeneous parts of Equations [21] and [22] are identical.

Conclusions

Equation [22], with $F = 0$, compared with Waltking's equation[3]

$$W^{(6)} + (2 + pq)W^{(4)} + (1 - q - pq)W'' + q(1 - pq)W = 0 \quad \ldots [23]$$

indicates, as stated in the Introduction, that his analysis, neglecting the rotatory inertia, has lost terms of the order of pq, significant when extension is considered.

Both Equations [22], with $F = 0$, and [23] reduce to Love's nonextensional equation[2] (Sec. 293[a])

$$W^{(6)} + 2W^{(4)} + (1 - q)W'' + qW = 0 \quad \ldots\ldots [24]$$

whence it follows that the nonextension assumption is valid, when $pq \ll 1$. This condition is implied when q is not too large and the thickness of the ring in the radial direction is small relative to its radius. However, if the frequency is increased, q becomes large and thinness of the ring is not sufficient for the validity of the assumption. Generally, for $pq \ll 1$, we must have $\omega \ll \omega^*$, where

$$\omega^* = (AE/ma^2)^{1/2} \quad \ldots\ldots\ldots\ldots [25]$$

This last is just the natural frequency of pure radial vibration[4] (Sec. 68), as is seen from Equations [21] and [22] with F and U equal to constants, $W = 0$

$$U_0 = a^2F_0/[AE(1 - pq)] = F_0/m(\omega^{*2} - \omega^2) \quad \ldots [26]$$

Since this mode of vibration is inherently extensional, it is of course not surprising that ω^* limits the validity of nonextension.

A feature of the forced-vibration problem which may not be generally appreciated when an a priori nonextension assumption is made is evidenced in Equation [21]. When $pq \ll 1$, so that the assumption is valid for "free" vibrations as we have shown, it is valid for "forced" vibrations as well only if there are no values of θ where $F'' = 0$, $F \neq 0$ (e.g., F cannot be constant). For, near such values, the expression $F'' + pq(1 + p)F$ is no longer dominated by F'', so that the usual form for the forcing term obtains,[4] but by pqF even though pq is small. The results of the extensional analysis presented here thus may be required even when $\omega \ll \omega^*$.

[4] "Vibration Problems in Engineering," by S. Timoshenko, D. Van Nostrand Company, Inc., New York, N. Y., third edition, 1955.

Wave Propagation in an Elastic Rod Exhibiting Internal Coulomb Friction, Considered as a Model for a Ring Spring[1]

By E. H. LEE[2] and A. J. WANG[3]

The problem of stress-wave propagation in a ring spring is considered. A ring spring consists of rings placed normal to the spring axis with alternate internal and external conical bearing surfaces. The friction between these surfaces causes a loading-unloading relation which is strongly irreversible, leading to marked energy absorption for oscillatory stressing. The attenuation of a pulse of stress is analyzed in detail as it is propagated down a spring of infinite length. The influence of certain spring characteristics is evaluated. Concentration of the absorption of the total input energy is found in the region of the impact end of the spring, and particular examples are presented.

Introduction

A RING spring consists of a series of rings having conical surfaces assembled as shown in Fig. 1. A general description and the method of design of such springs are given by A. M. Wahl (1).[4] When an axial compressive load is applied, sliding occurs along the conical surfaces with the result that the inner rings are compressed and the outer rings extended radially. When the load is removed, the friction between the rings has to change sign before sliding can occur in the opposite direction. A typical load-deflection curve is shown in Fig. 2. The curve deviates from a straight line only when the gap δ in Fig. 1 approaches zero. After each cycle of loading and unloading, a large hysteresis loop is obtained with correspondingly high energy dissipation. The spring constants of the loading and unloading strokes depend on the dimensions and material of the rings, the angle of taper of the conical surfaces, and the coefficient of friction at these surfaces.

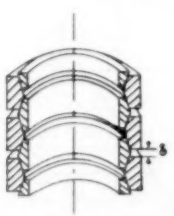

Fig. 1 Segment of a Ring Spring

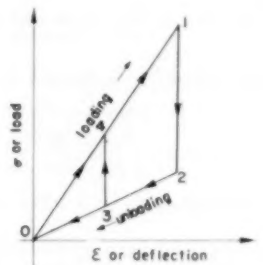

Fig. 2 Load-Deflection Relation for a Ring Spring, Which Represents Stress-Strain Relation for the Equivalent Rod Considered as a Continuous Model for Wave-Propagation Studies

In the present paper we consider a semi-infinite ring spring subject to a pulse of load at one end. We are concerned with the motion of the spring and the forces between the conical surfaces. The stress distribution within the ring itself is not considered. However, the stress can be found by the method described in reference (1), since the forces on the conical surfaces are known, and the lateral inertia effects in general will be negligible.

Similar to the treatment of wave propagation in helical compression springs (2), we may consider for a spring with many rings an equivalent continuum problem. This is a one-dimensional wave-propagation problem for a material that obeys the stress-strain relation shown in Fig. 2. By formally associating unit cross-sectional area with the spring, the total spring force is written as the stress σ. The Young's moduli E_1 and E_2 of the loading and unloading processes, respectively, correspond to the spring constants per unit spring length for the same processes for the ring spring. By adopting this analogy we can make use of the methods developed in plastic-wave-propagation problems; for example see (3 to 5).

The case of a ring spring of finite length involves reflection and wave interaction. It presents a more complicated problem and will be treated in a subsequent paper.

[1] This work was sponsored by the Ballistic Research Laboratories, Aberdeen Proving Ground, under Contract DA-19-020-ORD-798, with Brown University. Permission to publish is gratefully acknowledged.

[2] Professor of Applied Mathematics, Brown University, Providence, R. I.

[3] Formerly Research Associate in the Division of Applied Mathematics, Brown University, Providence, R. I.

[4] Numbers in parentheses refer to the Bibliography at the end of the paper.

Presented at the National Applied Mechanics Conference, Urbana, Ill., June 14–16, 1956, of The American Society of Mechanical Engineers.

Discussion of this paper should be addressed to the Secretary, ASME, 29 West 39th Street, New York, N. Y., and will be accepted until October 10, 1956, for publication at a later date. Discussion received after the closing date will be returned.

Note: Statements and opinions advanced in papers are to be understood as individual expressions of their authors and not those of the Society. Manuscript received by ASME Applied Mechanics Division, June 13, 1955. Paper No. 56—APM-5.

Mathematical Problem

We consider a semi-infinite rod of uniform cross section made of material that obeys the stress-strain relation shown in Fig. 2. In the figure, σ, ϵ denote the nominal compressive stress and strain, respectively, and these correspond to the total spring force and the deflection per unit initial length. The material will follow the path 01 during loading and paths 12, 20 during unloading. A reloading at point 3 will follow 34 and then 41. The rod is subjected to an impact at the end causing a constant stress σ_0 from time $t = 0$ to $t = t_0$. The stress and strain distributions in the rod are studied. These results can then be interpreted directly as the force and the displacement distribution in the ring spring.

Let x be the distance measured from the impact end along the initially unstrained rod, m be the mass per unit length of the rod, E_1 and E_2 be the slopes of the lines 01 and 02 in Fig. 2, respectively, u be the displacement of a section measured from its undeformed position, and v be the section velocity. This represents the so-called Lagrangian choice of variables. We shall consider compressive stress and strain as positive. The one-dimensional equation of motion is

$$\frac{\partial \sigma}{\partial x} = -m\frac{\partial^2 u}{\partial t^2} = -m\frac{\partial v}{\partial t} \quad \ldots\ldots [1]$$

The stress-strain relation is represented by three different equations

$$\left.\begin{array}{lll} \text{Along 01,} & \sigma = E_1\epsilon = -E_1\dfrac{\partial u}{\partial x} & \\ \text{Along 12,} & \epsilon = \text{const} & \\ \text{Along 20,} & \sigma = E_2\epsilon = -E_2\dfrac{\partial u}{\partial x} & \end{array}\right\} \quad \ldots\ldots [2]$$

Combining Equations [1] and [2], we have the following equations

$$\text{Along 01,} \qquad \frac{\partial^2\sigma}{\partial x^2} = \frac{1}{c_1^2}\frac{\partial^2\sigma}{\partial t^2} \quad \ldots\ldots [3a]$$

$$\text{Along 12,} \qquad \frac{\partial^2\sigma}{\partial x^2} = 0 \quad \ldots\ldots [3b]$$

$$\text{Along 21,} \qquad \frac{\partial^2\sigma}{\partial x^2} = \frac{1}{c_2^2}\frac{\partial^2\sigma}{\partial t^2} \quad \ldots\ldots [3c]$$

where $mc_1^2 = E_1$ and $mc_2^2 = E_2$.

The boundary conditions are as follows

At $x = 0$

$$\left.\begin{array}{ll} \sigma = \sigma_0 & 0 < t < t_0 \\ \sigma = 0 & t_0 < t \end{array}\right\} \quad \ldots\ldots [4]$$

At $x = \infty$

$$\sigma = 0 \quad \ldots\ldots [5]$$

The initial conditions are

At

$$t = 0, \quad \sigma = v = \epsilon = 0 \text{ for all } x \quad \ldots\ldots [6]$$

All of Equations [3] may be regarded as hyperbolic and they can best be solved by the method of characteristics. Thus the entire problem is solved by matching the different solutions in the different regions. Basic concepts of the application of the theory of characteristics in one-dimensional problems are given in reference (6). Here, we shall recall the following relations:

Equations [3a] and [3c] have the sets of characteristics $dx/dt = \pm c_1$ and $dx/dt = \pm c_2$, respectively. Along these characteristics, the following relations hold

$$\left.\begin{array}{l} mc_iv + \sigma = \text{const along } dx/dt = +c_i \\ mc_iv - \sigma = \text{const along } dx/dt = -c_i \end{array}\right\} \quad \ldots\ldots [7]$$

where the subscript i takes on values 1 or 2.

Equation [3b] can be integrated directly, giving

$$\sigma = f(t)x + g(t) \quad \ldots\ldots [8]$$

Thus, along a line $t = \text{const}$, $\sigma = ax + b$; i.e., the stress varies linearly with x. The line $t = \text{const}$ can be regarded as a degenerate characteristic with $dx/dt \to \infty$ and $\sigma = ax + b$ as the relation along it.

If lines of stress discontinuity occur, the following similar relations are obtained from the equations of continuity and momentum change. For a stress discontinuity traveling in the $+c$ direction, we have

$$(mcv - \sigma)_a = (mcv - \sigma)_b \quad \ldots\ldots [9]$$

where the subscripts b and a denote points just before and after the stress discontinuity (stress-wave front). For a stress discontinuity traveling in the $-c$-direction, the following holds

$$(mcv + \sigma)_a = (mcv + \sigma)_b \quad \ldots\ldots [10]$$

Solution of Problem

We shall make use of the $x - t$ plane shown in Fig. 3. The stress $\sigma = \sigma_0$ is applied at $x = 0$ from $t = 0$ to $t = t_0$, represented

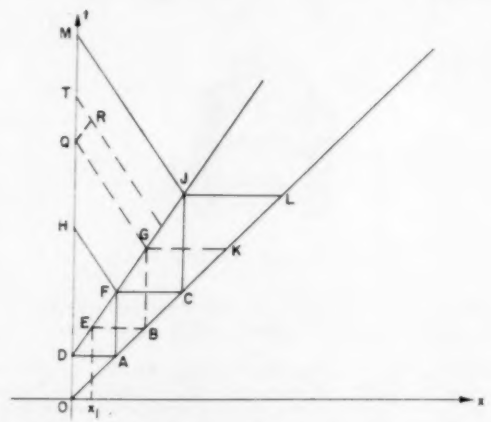

Fig. 3 Configuration of Wave Fronts in (x, t)-Plane
(Loading occurs at impact end along OD, OL is the loading wave front, and DJ the boundary across which slippage in unloading commences.)

by the interval OD. For $t > t_0$, the stress is removed, $\sigma = 0$ along DM. OL is the loading wave front traveling with velocity $dx/dt = c_1$. Ahead of this line, the rod is unstrained, and OL is a line of stress discontinuity. Since loading always follows the path 01, Fig. 2, the line OL remains straight until the stress discontinuity across it vanishes. DA is the instantaneous unloading wave corresponding to the path 12 in Fig. 2. DJ is the unloading wave corresponding to the path 20, having a slope of $dx/dt = c_2$. Between OL and DJ, each section undergoes unloading at con-

stant strain. Above DJ, the unloading takes place with the stress-strain ratio equal to E_2. The propagation of unloading waves for the ring spring is closely related to that in a plastic material (3, 5).

To solve the problem by the characteristic method, we start from the boundary and initial conditions, Equations [4] and [6]; i.e., we solve the region ODA first. The jump condition [9] across OA and the boundary condition along OD are sufficient to determine the stress and strain distributions inside this region. With stress along OA known, the stress along DF is obtained by multiplying it by the factor (E_2/E_1); because a vertical line in the $x - t$ plane represents the same section in our Lagrangian representation, and the section unloads with constant strain. Along DA, we may regard c as being infinite, according to Equation [9] for finite stress jump across DA, the velocity should then be continuous. The region $FDAC$ can thus be solved by using the condition along DA as initial condition and the jump condition across AC and the stress along DF as boundary conditions. With the stress along AC known, multiplication by the factor (E_2/E_1) gives the stress along FJ. For the same reason as before, there is no velocity discontinuity across CF. The same process is repeated for the next region $JFCL$. The solution in the entire region between the loading and the unloading waves can be built up in this manner.

The region behind DJ is solved from the boundary condition along DM and the jump condition across DJ.

We shall follow the foregoing procedure to find the stress and strain distribution in the rod. For convenience, we shall introdue the following dimensionless variables: Let

$$\left.\begin{aligned} \frac{x}{c_1 t_0} &= x^*, \qquad \frac{t}{t_0} = t^* \\ \frac{\sigma}{\sigma_0} &= \sigma^*, \qquad \frac{v}{\sigma_0/mc_1} = v^* \end{aligned}\right\} \quad \ldots\ldots\ldots [11]$$

also denote

$$\gamma^2 = E_2/E_1, \qquad v_0 = \sigma_0/mc_1$$

then

$$\gamma = c_2/c_1 \quad \ldots\ldots\ldots [12]$$

The relations [7] become

$$v^* \pm \sigma^* = \text{const along } dx^*/dt^* = \pm 1 \quad \ldots\ldots [13]$$

and

$$\gamma v^* \pm \sigma^* = \text{const along } dx^*/dt^* = \pm\gamma \quad \ldots\ldots [14]$$

The jump conditions [9] and [10] become

$$(v^* \mp \sigma^*)_a = (v^* \mp \sigma^*)_b \quad \text{across} \quad dx^*/dt^* = \pm 1. \quad [15]$$

$$(\gamma v^* \mp \sigma^*)_a = (\gamma v^* \mp \sigma^*)_b \quad \text{across} \quad dx^*/dt^* = \pm\gamma. \quad [16]$$

$$(v_a^* - v_b^*) = 0 \quad \text{across} \quad dx^*/dt^* = \infty \ldots [17]$$

For convenience, we shall drop the asterisks in the following. *In the region* OAD, $\sigma = 1$ along OD; the jump condition [15] across OA gives $v = \sigma$ for any point on OA. Using the relation $v - \sigma = \text{const}$ in Equation [13] we obtain $v = 1$ along OD. The relations [13] give $\sigma = v = 1$, $\epsilon = \epsilon_0 = (\sigma_0/E_1)$ uniform in the entire region. Since no unloading is considered up to this stage, the foregoing solution is identical with that for a linearly elastic material with stress-strain relation 01 in Fig. 2.

In the regions between the two lines OL *and* DJ, all vertical lines represent an unloading going on at each section with constant strain (e.g., along 12 in Fig. 2). The strains along such lines are independent of time. From the definitions of strain and velocity, one can show that the velocity inside the region is independent of x. Hence the velocity along a horizontal line is constant and that segment is moving as a rigid body.

In the region $FDAC$, the stress along $DF = \gamma^2$, the stress along $AC = v$. The rigid-body motion for a horizontal segment EB between AC and DF is therefore governed by the following equation

$$(x_B - x_E)\frac{dv}{dt} = (\sigma_{Eb} - \sigma_{Ba}) \quad \ldots\ldots\ldots [18]$$

The length of the segment $EB = x_B - x_E = (1 - \gamma)t + \gamma$. Substituting the known values for stresses, we get

$$[(1 - \gamma)t + \gamma]\frac{dv}{dt} = \gamma^2 - v \quad \ldots\ldots\ldots [19]$$

Equation [19] is integrated to give

$$(v - \gamma^2)[(1 - \gamma)t + \gamma]^{1/(1-\gamma)} = \text{const}$$

Since the velocity is continuous across AD, for which $t = 1$, $v = 1$, the integration constant is determined. The velocity inside this region is therefore

$$v = \gamma^2 + (1 - \gamma^2)[(1 - \gamma)t + \gamma]^{-[1/(1-\gamma)]} \ldots [20]$$

This is also the stress σ_{Ba} along AC.

Along CF, $t = 1 + 1/\gamma$

$$v_F = \gamma^3 + (1 - \gamma^2)\gamma^{1/(1-\gamma)} \quad \ldots\ldots\ldots [21]$$

This is used as an initial condition to determine velocities in the next region.

The stress varies linearly along BE from σ_{Ba} represented by Equation [20] to $\sigma_{Bb} = \gamma^2$. For the section $x = x_1$ the stress at time t is

$$\begin{aligned} \sigma_{x1} &= \gamma^2 + \frac{x_1 - x_E}{x_B - x_E}(1 - \gamma^2)[(1 - \gamma)t + \gamma]^{-[1/(1-\gamma)]} \\ &= \gamma^2 + \frac{x_1 - (t-1)\gamma}{t - (t-1)\gamma}(1 - \gamma^2)[(1 - \gamma)t + \gamma]^{-[1/(1-\gamma)]} \\ &= \gamma^2 + (1 - \gamma^2)[x_1 - (t-1)\gamma] \\ &\qquad [(1 - \gamma)t + \gamma]^{-(2-\gamma)/(1-\gamma)} \ldots\ldots [22] \end{aligned}$$

Equation [22] also represents the stress history between AD and CF for any section x_1.

In the region $JFCL$, the stress along $FJ = \gamma^2\sigma_{Ba}$; along CL it is again v according to the jump condition. The rigid-body motion for a horizontal segment GK between CL and FJ is governed by

$$\begin{aligned} [(1 - \gamma)t_G + \gamma]\frac{dv}{dt} &= \gamma^2\{\gamma^2 + (1 - \gamma^2) \\ &\qquad [(1 - \gamma)t_B + \gamma]^{-[1/(1-\gamma)]}\} - a \end{aligned}$$

Note that t_B appears on the right-hand side; it must be changed to t_G, according to $t_B = \gamma(t_G - 1)$, before integration. Accordingly, we must integrate

$$\begin{aligned} &[(1 - \gamma)t + \gamma]\frac{dv}{dt} \\ &\qquad + v = \gamma^2\{\gamma^2 + (1 - \gamma^2)[\gamma(1 - \gamma)t + \gamma^2]^{-[1/(1-\gamma)]}\} \end{aligned}$$

and obtain

$$\begin{aligned} &(v - \gamma^4)[\gamma(1 - \gamma)t + \gamma^2]^{1/(1-\gamma)} \\ &\qquad = \gamma^3(1 + \gamma)\ln[(1 - \gamma)t + \gamma] + \text{const} \end{aligned}$$

The integration constant is determined by Equation [21] and equals

$$[\gamma^2 + (1 - \gamma^2)\gamma^{1/(1-\gamma)} - \gamma^4] + \gamma^2(1 + \gamma) \ln \gamma$$

Hence

$$(v - \gamma^4)[\gamma(1 - \gamma)t + \gamma^2]^{1/(1-\gamma)} = \gamma^2(1 + \gamma) \ln [\gamma(1 - \gamma)t + \gamma^2] + (1 - \gamma^2)[\gamma^2 + \gamma^{1/(1-\gamma)}]$$

or

$$v = \gamma^4 + [\gamma(1 - \gamma)t + \gamma^2]^{-[1/(1-\gamma)]} \{\gamma^2(1 + \gamma) \ln [\gamma(1 - \gamma)t + \gamma^2] + (1 - \gamma^2)[\gamma^2 + \gamma^{1/(1-\gamma)}]\} \quad [23]$$

This is also the stress σ_{Ka} along CL.

Along JL

$$t = 1 + \frac{1}{\gamma} + \frac{1}{\gamma^2}$$

$$v_J = \gamma^4 + \gamma^{1/(1-\gamma)} \{-\gamma^2(1 + \gamma) \ln \gamma + (1 - \gamma^2)[\gamma^2 + \gamma^{1/(1-\gamma)}]\} \quad [24]$$

This is used as an initial condition to determine velocities in the next region.

In the next region the stress along DJ produced is $\gamma^2\sigma_{Ka}$ and the stress along OL produced is still v. As we can see, the equation for determining v becomes progressively more complicated, and numerical analysis is needed.

The stress variation along the loading wave OL up to

$$t = 1 + \frac{1}{\gamma} + \frac{1}{\gamma^2}$$

is plotted in Fig. 4 for $\gamma^2 = 1/2$ and $1/4$. The case $\gamma = 0$ will consist of region AC only, Equation [20] gives $\sigma = 1/t$; thus the stress discontinuity along the leading wave does not vanish in finite time. This is also true for all other cases.

In the region DJM, we shall make use of the boundary condition $\sigma = 0$ along DM and the jump condition along DJ. First we have to find out the conditions at D. Equation [16] across DJ at D gives

$$\gamma v_{Da} - \sigma_{Da} = \gamma v_{Db} - \sigma_{Db}$$

Since $\sigma_{Da} = 0$ is given, $v_{Db} = 1$, $\sigma_{Db} = \gamma^2$, we get

$$v_{Da} = 1 - \gamma \quad [25]$$

For any point P along DJ, Equation [14] provides

$$\gamma v_{Pa} + \sigma_{Pa} = \gamma(1 - \gamma) \quad [26]$$

Across DJ Equation [16] provides

$$\gamma v_{Pa} - \sigma_{Pa} = v_{Pb} - \sigma_{Pb} \quad [27]$$

Since v_{Pb} and σ_{Pb} are found in the previous discussion, Equations [26] and [27] give the stress and velocity variation along DJ. These equations continue to be valid as long as $\sigma_{Pa} \leq \sigma_{Pb}$; i.e., before the stress discontinuity across DJ vanishes. After such a point, if we still use these equations, we shall find $\sigma_{Pa} > \sigma_{Pb}$ which means that the section is subjected to loading again. However, loading has to follow a different path, namely, 34 and then 41 in Fig. 2, and the foregoing equations are not applicable.

Along DJ produced after the point P where $\sigma_{Pa} = \sigma_{Pb}$ there are two possibilities; i.e., the section will or will not have a stress discontinuity. Stress discontinuity can only occur in loading along the path 34. It can be shown that this possibility leads to incompatibility in the velocity solution. Hence our problem is to determine the trajectory PY (Fig. 5) across which the stress is

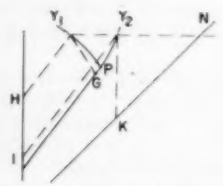

FIG. 5 DETAIL OF CONFIGURATION IN (x, t)-PLANE AT TERMINATION OF UNLOADING SHOCK WAVE

continuous. An analogous problem arises in determining the plastic-unloading boundary in the plastic-wave problems (5).

The section after crossing PY may still load along 34 in which case it is PY_1 or unload along 30, in which case it is PY_2. The general method of solution is the same, but one of these alternatives will lead to a contradiction. In each case we have a set of three equations to determine the locus of Y. In the case of Y_1, i.e., loading, these are one equation of motion of the rigid body Y_1N and the two relations along the characteristics Y_1H and Y_1G. These equations suffice to determine the stress, the velocity, and the position of Y_1. In the case of Y_2, there are one equation of motion of the rigid body Y_2N, one relation along the characteristic Y_2I, and the relation giving $\sigma_{Y_2} = \gamma^2\sigma_K$. The equations also suffice to determine the stress, the velocity, and

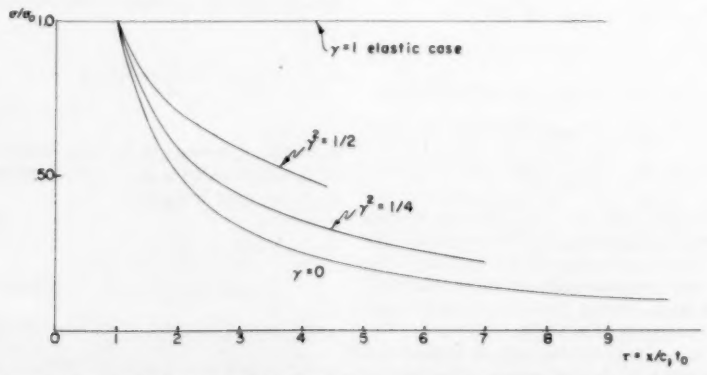

FIG. 4 FORCE VARIATION AT THE LOADING WAVE FRONT FOR DIFFERENT SPRING DESIGNS
(Small γ is associated with high friction and widely separated loading and unloading lines in Fig. 2.)

the position of Y_4. For actual illustration, we refer the reader to "Wave Propagation in a Finite Ring Spring," by E. H. Lee and A. J. Wang, Brown University Report DA-798/21 not yet published.

To find the stress and velocity distribution inside the region DMJ by the characteristic method, we still have to find the velocity at the impact end.

Along GQ in Fig. 3, Equations [14] give

$$\gamma v_Q = \gamma v_{Ga} - \sigma_{Ga} = \gamma v_{Gb} - \sigma_{Gb}$$

$$v_Q = v_{Gb} - \sigma_{Gb}/\gamma \quad [28]$$

$$= \sigma_{Ka} - \gamma \sigma_{Ba} \quad [29]$$

Note, however, that each of these points is at a different time; they are related to t_Q by

$$\left.\begin{aligned} t_G = t_K &= (t_Q + 1)/2 \\ t_B &= \gamma(t_Q - 1)/2 \end{aligned}\right\} \quad [30]$$

With the help of Fig. 4, v_Q is obtained from Equation [29] and it is plotted for the cases $\gamma^2 = 0, 1/4, 1/2, 1$ in Fig. 6. Integration of v_Q with respect to time gives the displacement of the impact end. This is also shown in Fig. 6. The displacement at the impact end for the elastic case is $v_0 t_0$, while for the cases $\gamma^2 = 1/2$ and $1/4$, the part of the solution carried out appears to indicate approach to a greater value.

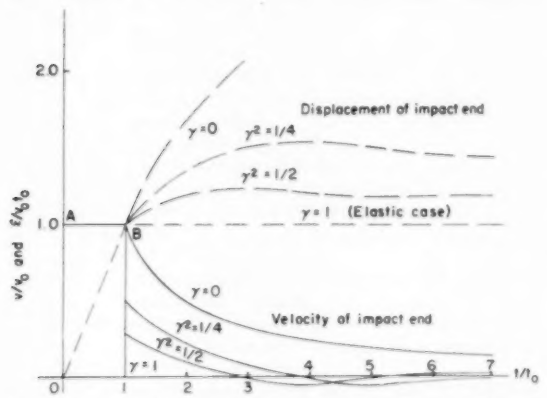

FIG. 6 PLOTS OF DISPLACEMENT AND VELOCITY AT IMPACT END FOR SEVERAL SPRING DESIGNS

For any point R in the region, Fig. 3, Equations [14] give

$$\gamma v_R - \sigma_R = \gamma v_T$$

$$\gamma v_R + \sigma_R = \gamma v_Q$$

or

$$\left.\begin{aligned} \sigma_R &= \gamma(v_Q - v_T)/2 \\ v_R &= (v_Q + v_T)/2 \end{aligned}\right\} \quad [31]$$

If the co-ordinate of R is represented by (x_R, t_R), those for the points Q and T are

$$\left.\begin{aligned} t_Q &= t_R - x_R/\gamma, \quad x_Q = 0 \\ t_T &= t_R + x_R/\gamma, \quad x_T = 0 \end{aligned}\right\} \quad [32]$$

With the help of Fig. 6, Equation [31] is readily solved.

ENERGY DISSIPATION

The work done by the external force is equal to $\sigma_0 v_0 t_0 = W_0$. At each section, after a complete cycle of loading and unloading, the enclosed area 012 in Fig. 2 represents the dissipated energy per unit length of spring. The dissipation process goes on indefinitely because the stress discontinuity along the loading wave front OL does not vanish. From the known stress distribution along the rod, however, we find that the major part of the dissipation takes place near the impact end of the rod.

Energy dissipation in the section between $x = 0$ to $x = x_A$

$$= \frac{1}{2}(\sigma_0 - \gamma^2\sigma_0)\epsilon_0 c_1 t_0$$

$$= \frac{1}{2} W_0(1 - \gamma^2)$$

This assumes a single loading cycle, so that this value represents a minimum. If the stress oscillates as a result of reflection from the wave front, the energy dissipated will be greater. This consideration also applies to the analysis which follows.

Energy dissipation in the section between $x = x_A$ to $x = x_C$

$$= \frac{1}{2}\int_{x_A}^{x_C} \sigma(1 - \gamma^2)\epsilon \, dx$$

$$= \frac{1}{2}(1 - \gamma^2)\frac{\sigma_0^2}{mc_1} t_0 \int_1^{1+(1/\gamma)} \left\{\gamma^2 + (1 - \gamma^2)[(1 - \gamma)\tau + \gamma]^{-\frac{1}{1-\gamma}}\right\}^{\frac{1}{2}} d\tau$$

$$= \frac{1}{2}(1 - \gamma^2)W_0 \left\{1 + \gamma - \gamma^2 - (1 - \gamma^2)\gamma^{\frac{\gamma}{1-\gamma}}\left[2\gamma + (1 - \gamma)\gamma^{\frac{1}{1-\gamma}}\right]^{\frac{1}{2}}\right\}$$

The expressions for the remaining sections can be obtained in a straightforward manner, but they are algebraically complicated.

For $\gamma^2 = 1/2$ the first section dissipates 25 per cent of the input, the next section 22 per cent of the input. For $\gamma^2 = 1/3$, the first section dissipates 33 per cent and the next section 28 per cent of the input.

DISCUSSION

The solutions discussed in the paper illustrate the internal reflections associated with the propagation of an unloading wave in a ring spring. These are caused by the theoretically infinite velocity of propagation associated with the initially constant strain unloading path in Fig. 2, and the speed of propagation of the subsequent unloading process which is less than the initial loading wave speed.

Fig. 4 shows the influence of the unloading process on the magnitude of the loading wave front. In the elastic case ($\gamma = 1$) the unloading process is propagated at exactly the loading wave speed, and so the unloading wave never overtakes the loading wave, and the amplitude of the latter remains constant. For other values of γ, the unloading caused by the removal of the stress at the impact surface is propagated in part at theoretically infinite speed and produces a gradual reduction of the amplitude of the loading wave front. For smaller values of γ, the magnitude of the stress decrease which is propagated at high velocity increases, with a consequent enhanced attenuation of the loading wave front. For $\gamma = 0$, the value which can be expected to produce the maximum attenuation, the stress at the loading wave front decreases as $1/t$.

The decrease in stress at the loading wave front is not the only measure of the effectiveness of the unloading process. The distribution of stress behind the wave front determines the distribution of strain and so the motion of the impacted end. While the

stress is applied, springs for all values of γ behave as does the elastic case; the velocity of the impacted end maintains the constant value v_0 as shown by AB in Fig. 6, and the end displacement increases linearly with the time as shown by OB. When the stress is removed the motions of the impact end depicted in Fig. 6 arise. In the elastic case, $\gamma = 1$, the unloading wave reduces the stress to zero, and it maintains the value zero for all sections across which the unloading wave has passed. The velocity of the unloaded material is zero; and the impact end remains at rest. As γ decreases, the velocity reduction decreases, so that the end displacement continues to increase for a period as shown in Fig. 6. Thus the decreased attenuation at the loading wave front with increasing γ discussed in the previous paragraph is compensated by an enhanced unloading behind the wave front which causes a reduced end displacement with increasing γ. For $\gamma = 0$, no recovery of strain occurs, and the velocity decreases as $1/t$ with a consequent unbounded increase in end displacement. The end displacements for other values of γ fall between these two extremes, and appear to be asymptotic to values greater than that for the elastic case. However, it was not possible to determine this limit analytically. For $\gamma = 0$, recovery of strain would only occur at zero stress which is not reached in the present example. The strain produced is therefore effectively permanent and the problem closely resembles a plastic-wave problem.

The finite displacements after unloading exhibited by the foregoing solutions arise because of the infinite extent of the spring and the ever-increasing length of the spring subjected to stress. For a finite spring subjected to a cycle of loading which falls to zero after a certain duration, the load-deformation relation depicted in Fig. 2 demands that the displacement must also reduce finally to zero. This is in contrast to the present solution.

It might be mentioned that the present analysis assumes that the gap δ shown in Fig. 1 does not close. For larger strains resulting in closure, an analysis similar to that discussed in (2) will be necessary to allow for the effective increase in stiffness associated with closure waves.

BIBLIOGRAPHY

1 "Mechanical Springs," by A. M. Wahl, Penton Publishing Company, Cleveland, Ohio, 1944, pp. 348–358.

2(a) "Wave Propagation in Helical Compression Springs," by E. H. Lee, Proceedings of the Fifth Symposium of Applied Mathematics of the American Mathematical Society, June, 1952, McGraw-Hill Book Company, Inc., New York, N. Y., 1954.

2(b) "Dynamic Loading of Compression Springs," by K. W. Maier, *Product Engineering*, vol. 25, January, 1954, pp. 162–167.

3 "The Permanent Strain in a Uniform Bar Due to Longitudinal Impact," by M. P. White and L. Griffis, JOURNAL OF APPLIED MECHANICS, Trans. ASME, vol. 69, 1947, pp. A-337–A-343.

4 "The Propagation of Plastic Deformation in Solids," by Th. von Kármán and P. Duwez, *Journal of Applied Physics*, vol. 21, 1950, p. 987.

5 "A Boundary Value Problem in the Theory of Plastic Wave Propagation," by E. H. Lee, *Quarterly of Applied Mathematics*, vol. 10, 1953, pp. 335–346.

6 "Supersonic Flow and Shock Waves," by R. Courant and K. O. Friedrichs, Interscience Publishers, New York, N. Y., 1948.

On the Theory of the Acceleration Damper[1]

By CARL GRUBIN,[2] SANTA MONICA, CALIF.

The acceleration damper reduces the vibration of a mechanical system through momentum transfer by collision and conversion of mechanical energy into heat. A typical unit consists of a mass particle moving in a container fixed to the primary vibrating system. The direct problem is to determine the motion of a single-degree-of-freedom system with a damper, when the driving force is simple harmonic. The inverse is to determine the characteristics of a damper for reducing the vibration of the same system to a prescribed value. Numerical results indicate that the damper is most effective at resonance.

Nomenclature

The following nomenclature is used in the paper:

M = primary mass
m = particle mass
μ = m/M
X = absolute co-ordinate of M
x = co-ordinate of m relative to M
t = time
θ = nondimensional time varying from 0 to 1
t_0 = initial time
$t_1, t_2, \ldots$ = time of first collision, second collision, etc.
t_s = arbitrary initial time for steady state
e = coefficient of restitution between M and m
d = container length
K = spring constant
C = viscous-damping coefficient
ω = natural frequency of primary system
Ω = frequency of sinusoidal driving force
δ = C/C_{cr}
η = $(1 - \delta^2)^{1/2}$
A = steady-state amplitude of primary system without acceleration damper
ψ = steady-state phase angle between motion of primary system and driving force without acceleration damper
$\Delta(dX/dt)$ = velocity discontinuity of M due to collision; varies with each collision but assumed constant in second section
ρ = d/A

$$\lambda = \frac{\pi}{\Omega/\omega}$$

$$Q(\theta) = \{\exp[\delta\lambda(1-\theta)] \sin \eta\lambda\theta - \exp(-\delta\lambda\theta) \sin \eta\lambda(1-\theta)\}$$

Introduction

The acceleration damper is a device for reducing the vibration amplitude of a mechanical system through the mechanism of momentum transfer by collision and the conversion of mechanical energy into heat. A typical unit consists of a mass particle constrained to move in a container fixed to the primary vibrating system.

The use of this device was conceived and first investigated by Lieber and Jensen.[3] In their analysis they assume that the motion of the primary system is simple harmonic and the coefficient of restitution is zero. They determine that maximum energy will be dissipated in a cycle when the container length is π times the amplitude. In the present paper no a priori assumptions are made and the coefficient of restitution is finite.

The paper investigates the motion of the classical single-degree-of-freedom system subjected to the action of a single container damper. The objectives of the analysis are twofold:

1 Determine the motion of a given system with a given damper (direct problem).

2 Determine the damper parameters necessary for reducing the vibration amplitude of a given system to a prescribed value (inverse problem).

Two solutions are obtained for the equations governing the motion of the primary mass and the particle. The first, the complete solution, satisfies the initial conditions and determines the motion of the system from collision to collision. This calculation is tedious and does not lend itself toward solving the inverse problem defined in the foregoing. The second solution is developed by assuming the motion to be steady state. This solution is simple from the aspect of computation and permits a solution of the inverse problem. For a sufficiently large number of collisions it is found numerically that the motions predicted by the complete and steady-state solutions are in excellent agreement. The calculations also indicate that the damper is most effective at the resonant condition.

Analysis

Complete Solution. A model of the system considered is shown in

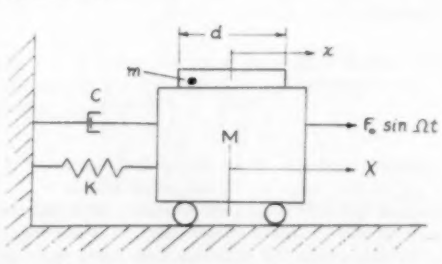

Fig. 1 Model of System

[1] This paper is based on the dissertation submitted by the author to the Polytechnic Institute of Brooklyn in partial fulfillment of the requirements for the PhD degree in Applied Mechanics. The work was carried out under the sponsorship of the Office of Naval Research, first at the Polytechnic Institute of Brooklyn, and later at Rensselaer Polytechnic Institute. A short version of the paper was read before the Eighth International Congress of Applied Mechanics in Istanbul, Turkey, August, 1952, by the dissertation adviser, Prof. Paul Lieber.

[2] Designer, Automatic Controls Section, Douglas Aircraft Company, Inc.

Presented at the National Applied Mechanics Conference, Urbana, Ill., June 14–16, 1956, of The American Society of Mechanical Engineers.

Discussion of this paper should be addressed to the Secretary, ASME, 29 West 39th Street, New York, N. Y., and will be accepted until October 10, 1956, for publication at a later date. Discussion received after the closing date will be returned.

Note: Statements and opinions advanced in papers are to be understood as individual expressions of their authors and not those of the Society. Manuscript received by ASME Applied Mechanics Division, June 13, 1955. Paper No. 56—APM-10.

[3] "An Acceleration Damper: Development, Design, and Some Applications," by P. Lieber and D. P. Jensen, Trans. ASME, vol. 67, 1945, pp. 523–530.

Fig. 1. The equations of motion for M and m, assuming no friction between m and its container, are

$$\left.\begin{aligned} M\frac{d^2X}{dt^2} + C\frac{dX}{dt} + KX &= F_0 \sin \Omega t \\ \frac{d^2x}{dt^2} &= -\frac{d^2X}{dt^2} \end{aligned}\right\} \quad \ldots\ldots [1]$$

where x is the co-ordinate of m relative to M.

The initial conditions are at

$$t = t_0 \left\{\begin{aligned} X &= X_0 \\ \frac{dX}{dt} &= \left(\frac{dX}{dt}\right)_0 \end{aligned}\right. \qquad \left\{\begin{aligned} x &= x_0 \\ \frac{dx}{dt} &= \left(\frac{dx}{dt}\right)_0 \end{aligned}\right\} \quad \ldots\ldots [2]$$

The solutions to Equation [1] satisfying [2] are

$$X = \exp\left[-\delta(\omega t - \omega t_0)\right]\left[\frac{A_0}{\eta}\sin \eta(\omega t - \omega t_0) + B_0 \cos \eta(\omega t - \omega t_0)\right] + A \sin(\Omega t - \psi)$$

$$x = -X + X_0 + x_0 + \left[\left(\frac{dX}{dt}\right)_0 + \left(\frac{dx}{dt}\right)_0\right](t - t_0) \ldots [3]$$

where

$$\omega = \left(\frac{K}{M}\right)^{1/2}$$

$$\delta = C/C_{cr}$$

$$C_{cr} = 2(KM)^{1/2}$$

$$A_0 = \delta B_0 + \frac{1}{\omega}\left(\frac{dX}{dt}\right)_0 - A\frac{\Omega}{\omega}\cos \tau_0$$

$$B_0 = X_0 - A \sin \tau_0$$

$$\tau_0 = \Omega t_0 - \psi$$

$$\eta = (1 - \delta^2)^{1/2}$$

$$A = \frac{F_0}{K}\left[\left(1 - \frac{\Omega^2}{\omega^2}\right)^2 + 4\delta^2\frac{\Omega^2}{\omega^2}\right]^{-1/2}$$

$$\tan \psi = \frac{2\delta(\Omega/\omega)}{1 - (\Omega^2/\omega^2)} \qquad 0 < \psi < \pi$$

Solutions [3] are valid till t_1, time of the first collision. The collision is assumed ideal in that the positions of M and m remain fixed while their velocities are discontinuous. Therefore new solutions are required for X and x after t_1.

The time t_1 is obtained by setting x equal to the co-ordinate of either end of the container. Thus, taking the position $x = 0$ as midway between the ends of the container, the equation for t_1 is, from Equations [3]

$$\pm\frac{d}{2} = -X(t_1) + X_0 + x_0 + \left[\left(\frac{dX}{dt}\right)_0 + \left(\frac{dx}{dt}\right)_0\right](t_1 - t_0) \ldots\ldots [4]$$

In Equation [4] the + or − sign is used according to which yields the smaller value for t_1, consistent with $t_1 > t_0$. Now a fundamental difficulty occurs, for Equation [4] is transcendental in t_1 and can only be solved numerically. It is precisely this difficulty which prevents the solutions from being developed analytically beyond the first collision.

With t_1 determined numerically, the solutions for X and x in the region $t_1 < t < t_2$ (t_2 = time of second collision) are obtained as the solutions to Equations [1] with the initial conditions at

$$t = t_1 \left\{\begin{aligned} X &= X_1 \\ \frac{dX}{dt} &= \left(\frac{dX}{dt}\right)_{1+} \end{aligned}\right. \qquad \left\{\begin{aligned} x &= \pm\frac{d}{2} \\ \frac{dx}{dt} &= \left(\frac{dx}{dt}\right)_{1+} \end{aligned}\right\} \quad \ldots [5]$$

In Equations [5] the value of X_1 is obtained from [3] by substituting $t = t_1$, while + or $-d/2$ is used for x according to which value has been used in Equation [4] (continuity of displacement). However, for the velocities

$$\left.\begin{aligned} \left(\frac{dX}{dt}\right)_{1+} &= \left(\frac{dX}{dt}\right)_{1-} + \Delta\left(\frac{dX}{dt}\right)_1 \\ &= \left(\frac{dX}{dt}\right)_{1-} + \gamma\left(\frac{dx}{dt}\right)_{1-} \\ \left(\frac{dx}{dt}\right)_{1+} &= -e\left(\frac{dx}{dt}\right)_{1-} \end{aligned}\right\} \quad \ldots [6]$$

where $\Delta(dX/dt)_1$ = velocity discontinuity of M at t_1

$$\gamma = \frac{\mu}{(1 + \mu)}(1 + e)$$

$$\mu = m/M$$

e = coefficient of restitution

The − and + subscripts designate time immediately preceding and following the collision at t_1. The second of Equations [6] is the definition of the coefficient of restitution, while the expression for the velocity discontinuity is obtained from simple collision theory.[4] The values of $(dX/dt)_{1-}$ and $(dx/dt)_{1-}$ are obtained from Equation [3] with $t = t_1$.

With the motion determined for $t_1 < t < t_2$, the time t_2 is determined similarly to t_1. The procedure can be continued and the motion determined from collision to collision. In general, this will be impractical computationally, for many collisions may have to be considered before the motion settles to an average value, if it does at all.

Steady-State Solution. It is possible to develop an exact steady-state solution from the foregoing equations. This stems from the observation that after n collisions ($n = 1, 2, \ldots$) the solution can be written as

$$\left.\begin{aligned} X = X^{(0)} + \frac{1}{\eta\omega}\sum_{j=1}^{n}\left[\Delta\left(\frac{dX}{dt}\right)_j\right]\exp\left[-\delta(\omega t - \omega t_j)\right] \\ \times \sin \eta(\omega t - \omega t_j) \qquad t_n < t < t_{n+1}\ (n = 1, 2, \ldots) \end{aligned}\right\} \quad \ldots [7]$$

where $X^{(0)}$ is the motion of M in the absence of the damper and is given by Equation [3], $\Delta(dX/dt)_j$ is the velocity discontinuity of M at t_j, and t_j is the time of the jth collision.

Solution [7] satisfies the equation of motion of M and the appropriate initial conditions at each t_j, for the displacements are continuous while the velocity is discontinuous by the amount $\Delta(dX/dt)_j$. Each term in the summation represents the effect of a collision so that [7] is the complete solution with the identity of each collision preserved. Formally, therefore, Equation [7] describes the motion of M between the n and $(n + 1)$th collisions. However, it is useless for calculation since $\Delta(dX/dt)_j$

[4] See, for example, "Applied Mechanics-Dynamics," by G. W. Housner and D. E. Hudson, D. Van Nostrand Company, New York, N. Y., first edition, 1950, pp. 79–81.

and t_j are unknown, and must be determined by the collision-to-collision calculation discussed previously.

Now the steady-state solution will be obtained as the value approached by Equation [7] as $t \to \infty$. For the first term this presents no difficulty since $\underset{t\to\infty}{X^{(0)}}$ approaches the well-known steady-state solution for a single-degree-of-freedom system. However, the behavior of the summation term for $t \to \infty$ (hence also $n \to \infty$) is unknown, although it is clear that for the damper to be effective, its limiting value must substantially cancel that of $\underset{t\to\infty}{X^{(0)}}$. It is interesting to note that as $t, n \to \infty$ the effect of the collisions which occurred relatively early in the motion becomes less and less significant owing to the attenuation factor $\exp[-\delta(\omega t - \omega t_j)]$ (t increasing, t_j fixed). Only those collisions which occurred relatively near to the time under consideration contribute significantly to the damping action. Therefore, although the effect of an individual collision is attenuated, another effect arises with every collision, and the damping action, if indeed there is any, remains essentially continuous.

The assumption of a steady state implies that the period is that of the forcing function $T = 2\pi/\Omega$. In addition, it is assumed that during the period two collisions occur at equal time intervals, one at each end of the container.[5] This implies that the velocity discontinuities are of equal magnitude but alternate in sign. Thus

$$\left.\begin{aligned} \omega t_{j+1} - \omega t_j &= \frac{\omega\pi}{\Omega} \equiv \lambda \\ \Delta\left(\frac{dX}{dt}\right)_j &= (-1)^j \Delta\left(\frac{dX}{dt}\right) \\ (j &= 1, 2, \ldots) \end{aligned}\right\} \quad \ldots\ldots\ldots [8]$$

where $\Delta(dX/dt)$ is to be determined.

In Equation [7], let the summation term be defined as $X^{(n)}$. Noting by Equations [8] that

$$\left.\begin{aligned} \omega t_1 &= \omega t_0 + \lambda \\ \omega t_2 &= \omega t_1 + \lambda = \omega t_0 + 2\lambda \\ &\cdots\cdots\cdots \\ \omega t_j &= \omega t_0 + j\lambda \end{aligned}\right\} \quad \ldots\ldots\ldots [9]$$

and further that

$$\sin \eta(\omega t - \omega t_j) = \frac{1}{2i}\left\{\exp[i\eta(\omega t - \omega t_j)] - \exp[-i\eta(\omega t - \omega t_j)]\right\} \quad \ldots\ldots [10]$$

$X^{(n)}$ can be expressed as

$$\frac{2iX^{(n)}\eta\omega}{\Delta(dX/dt)} = \exp[-(\delta - i\eta)\xi] \sum_{j=1}^{n} [-\exp(\delta - i\eta)\lambda]^j - \exp[-(\delta + i\eta)\xi] \sum_{j=1}^{n} [-\exp(\delta + i\eta)\lambda]^j \quad \ldots\ldots [11]$$

where

$$\xi = (\omega t - \omega t_0)$$

The series in Equation [11] may be summed, and afterward we may allow $t, n \to \infty$.

[5] This appears reasonable intuitively, although steady states with a greater number of collisions may also exist.

The sum of a geometric series is

$$\sum_{j=1}^{n} Z^j = \frac{Z(1 - Z^n)}{1 - Z} \qquad Z \neq 1 \quad \ldots\ldots\ldots [12]$$

where Z may be a complex number.

Applying Equations [12] to [11] and simplifying gives

$$\frac{X^{(n)}\eta\omega\Lambda \exp[\delta(\xi - n\lambda)]}{\Delta(dX/dt)} = -\exp(\delta\lambda)\left\{\exp(-n\delta\lambda)\sin\eta\xi \mp \sin\eta(\xi - n\lambda)\right\} - \left\{\exp(-n\delta\lambda)\sin\eta(\xi - \lambda) \mp \sin\eta[\xi - (n+1)\lambda]\right\} \quad \ldots\ldots [13]$$

where

$$\Lambda = 2(\cos\eta\lambda + \cosh\delta\lambda)$$

The upper and lower signs in Equation [13] are associated with even and odd values of n, respectively. It can be shown that ultimately the choice of signs is immaterial. Before allowing $n \to \infty$, we note that by the first of Equations [8]

$$\left.\begin{aligned} \xi &\equiv \omega t - \omega t_0 \\ &= \omega t - \omega t_1 + \lambda \\ &= \omega t - \omega t_2 + 2\lambda \\ &\cdots\cdots\cdots \\ &= \omega t - \omega t_n + n\lambda \end{aligned}\right\} \quad \ldots\ldots\ldots [14]$$

In Equation [7] the range of t is $t_n < t < t_{n+1}$. Inspection of Equations [14] then suggests that a new independent variable θ be introduced, such that

$$\omega t - \omega t_n = \theta\lambda \qquad 0 < \theta < 1 \quad \ldots\ldots\ldots [15]$$

Using Equations [15] and [14] in [13] and allowing $n \to \infty$ gives

$$\underset{n\to\infty}{X^{(n)}} = \pm\frac{\Delta(dX/dt)}{\eta\omega\Lambda}\left\{\exp[\delta\lambda(1-\theta)]\sin\eta\lambda\theta - \exp(-\delta\lambda\theta)\sin\eta\lambda(1-\theta)\right\} \equiv \pm\frac{\Delta(dX/dt)}{\eta\omega\Lambda}Q(\theta) \quad \ldots\ldots [16]$$

Combining Equation [16] with $\underset{t\to\infty}{X^{(0)}}$ the steady-state motion of M is

$$X \sim A\sin(\Omega t - \psi) \pm \frac{\Delta(dX/dt)}{\eta\omega\Lambda}Q(\theta) \quad \ldots\ldots [17]$$

where the symbol $\sim$ is used to indicate "behaves as" since it remains to show how the variables t and θ are related.

From the definition of θ it is seen that a collision occurs when $\theta = 0$ and the succeeding one occurs when $\theta = 1$. Designating t_s as the (arbitrary) initial time of the steady state, the relation between t and θ is therefore

$$\theta = \frac{\Omega}{\pi}(t - t_s) \quad \ldots\ldots\ldots [18]$$

since for $\theta = 0$, $t = t_s$ and for $\theta = 1$, $t = t_s + \pi/\Omega$. Equation [18] prevails for the first half cycle of the steady state, while for the second

$$\theta = \frac{\Omega}{\pi}\left[t - \left(t_s + \frac{\pi}{\Omega}\right)\right] \quad \ldots\ldots\ldots [19]$$

Using Equations [18] and [19] in [17] and defining $(\Omega t_s - \psi) =$

τ_s, the motion for the two half cycles of the steady state becomes

$$X(\theta) = \left\{ \begin{array}{ll} A \sin(\pi\theta + \tau_s) \pm \dfrac{\Delta(dX/dt)}{\eta\omega\Lambda} Q(\theta) & 0 < \theta < 1 \\ -A \sin(\pi\theta + \tau_s) \mp \dfrac{\Delta(dX/dt)}{\eta\omega\Lambda} Q(\theta) & \end{array} \right\} \quad [20]$$

It is noted that the $\pm$ appearing in the first of Equations [20] is changed to $\mp$ because of the additional collision at $t = t_s + \pi/\Omega$.

Summarizing thus far, Equations [20] are exact steady-state solutions of the first of Equations [1]. In fact, $Q(\theta)$ is an exact solution to the homogeneous equation associated with Equations [1], while the first term in Equations [20] is, of course, a particular solution to the complete Equation [1]. In order to uniquely determine the motion it remains to calculate $\Delta(dX/dt)$, and $\sin \tau_s$, $\cos \tau_s$. The former is a measure of the intensity of the collisions, while the latter determines the "phase" between the two terms in Equations [20]. These unknowns are determined by enforcing the steady-state motion of the particle and its relation to the motion of M.

The motion of m is governed by the second of Equations [1], and the solutions to this equation, accounting for collisions on the left side of the container ($x = -d/2$) at $t = t_s$, and on the right side ($x = +d/2$) at $t = t_s + \pi/\Omega$, are

$$\left. \begin{array}{l} x^{(1)} = -X^{(1)} + X_0^{(1)} - \dfrac{d}{2} + \left[\left(\dfrac{dX}{dt} \right)_0^{(1)} + \left(\dfrac{dx}{dt} \right)_0^{(1)} \right] (t - t_s) \qquad t_s < t < t_s + \dfrac{\pi}{\Omega} \\ x^{(2)} = -X^{(2)} + X_0^{(2)} + \dfrac{d}{2} + \left[\left(\dfrac{dX}{dt} \right)_0^{(2)} + \left(\dfrac{dx}{dt} \right)_0^{(2)} \right] \left[t - \left(t_s + \dfrac{\pi}{\Omega} \right) \right] \\ \qquad\qquad t_s + \dfrac{\pi}{\Omega} < t < t_s + \dfrac{2\pi}{\Omega} \end{array} \right\} \quad [21]$$

In Equation [21] the solutions $X^{(1)}$ and $X^{(2)}$ refer to Solutions [20] for the two halves of the cycle, and $X_0^{(1)}$ and $(dX/dt)_0^{(1)}$ refer to the values of displacement and velocity obtained from $X^{(1)}$ by setting $\theta = 0$. The quantities $X_0^{(2)}$ and $(dX/dt)_0^{(2)}$ have similar meanings. The initial relative velocities $(dx/dt)_0^{(1)}$, $(dx/dt)_0^{(2)}$ remain to be determined.

The steady-state motion requires that the following conditions be satisfied

$$\left. \begin{array}{l} x_1^{(1)} = \dfrac{d}{2} \\ x_1^{(2)} = -\dfrac{d}{2} \\ \left(\dfrac{dx}{dt} \right)_0^{(1)} = -e \left(\dfrac{dx}{dt} \right)_1^{(2)} \\ -e \left(\dfrac{dx}{dt} \right)_1^{(1)} = \left(\dfrac{dx}{dt} \right)_0^{(2)} \end{array} \right\} \quad [22]$$

where the subscripts 0 and 1 refer to conditions at $\theta = 0$ and $\theta = 1$, respectively. The second and third of Equations [22] relate conditions at the beginning and end of the cycle, while the first and fourth relate to the intermediary collision. The final conditions to enforce are those which relate the velocity discontinuity to the relative velocity before collision. They are (c.f. first of Equations [6])

$$\left. \begin{array}{l} \Delta \left(\dfrac{dX}{dt} \right)_{t_s + \pi/\Omega} = \gamma \left(\dfrac{dx}{dt} \right)_1^{(1)} \\ \Delta \left(\dfrac{dX}{dt} \right)_{t_s + 2\pi/\Omega} = \gamma \left(\dfrac{dx}{dt} \right)_1^{(2)} \end{array} \right\} \quad [23]$$

Substituting Equations [20] and [21] into [22] and [23] reduces the six conditions to four independent ones for determining $\Delta(dX/dt)$, $\sin \tau_s$, $\cos \tau_s$, $(dx/dt)_0^{(1)}$, and $(dx/dt)_0^{(2)}$. By further manipulation the system may be reduced to a single equation in the unknowns $\sin \tau_s$, $\cos \tau_s$, viz.

$$\rho = 2 \sin \tau_s + H \cos \tau_s \quad [24]$$

where

$$\rho = \frac{d}{A}$$

$$H = \frac{\lambda\beta_2}{[(dQ/d\theta)_1 - \beta_1 (dQ/d\theta)_0]} \left[4\mu \frac{\Omega}{\omega} Q(0) - \pi\eta\Lambda \right]$$

$$\beta_1 = \frac{(2\mu + 1 - e)}{(2\mu e - 1 + e)}$$

$$\beta_2 = \frac{(1 + e)}{(2\mu e - 1 + e)}$$

$$Q(0) = -\sin \eta\lambda$$

$$(dQ/d\theta)_0 = \lambda[\eta \exp(\delta\lambda) + \delta \sin \eta\lambda + \eta \cos \eta\lambda]$$

$$(dQ/d\theta)_1 = \lambda[\eta \exp(-\delta\lambda) - \delta \sin \eta\lambda + \eta \cos \eta\lambda]$$

The solutions to Equation [24] are

$$\left. \begin{array}{l} \sin \tau_s = \dfrac{1}{(H^2 + 4)} [2\rho \pm H(H^2 + 4 - \rho^2)^{1/2}] \\ \cos \tau_s = \dfrac{1}{(H^2 + 4)} [\rho H \mp 2(H^2 + 4 - \rho^2)^{1/2}] \end{array} \right\} \quad [25]$$

where either set of signs may be chosen. (These have no relation to the double signs appearing in Equation [13].) Equations [25] show that the container length d cannot be arbitrarily large, in fact, $0 < \rho^2 \leq H^2 + 4$, at risk of having $\sin \tau_s$, $\cos \tau_s$ become complex numbers. Physically this means that if the container length is too long a two-collision-per-cycle steady-state motion is not possible.

With $\cos \tau_s$ determined the value of $\Delta(dX/dt)$ is found from the relation

$$\frac{\Delta(dX/dt)}{A\eta\omega\Lambda} \equiv h = \pi \frac{(1 + \beta_1)}{[(dQ/d\theta)_1 - \beta_1 (dQ/d\theta)_0]} \cos \tau_s \quad [26]$$

Expressions for $(dx/dt)_0^{(1)}$ and $(dx/dt)_0^{(2)}$ also can be obtained. They are useful for computing the relative motion, and are given by

$$\left. \begin{array}{l} \left(\dfrac{dx}{dt} \right)_0^{(1)} = -\left(\dfrac{dx}{dt} \right)_0^{(2)} = -\Omega A \dfrac{e}{(1 - e)} \times \\ \left\{ 2 \cos \tau_s + \dfrac{h}{\pi} [(dQ/d\theta)_0 - (dQ/d\theta)_1] \right\} \qquad e \neq 1 \end{array} \right\} \quad [27]$$

It remains to discuss the double set of signs appearing in Equations [25]. Either set may be chosen, and associated with each

value of $\cos \tau_s$ will be a value of h. Thus it appears there are two possible steady-state motions. No analytical criterion has been found as yet for deciding which of these occurs in practice, if indeed either. However, numerical results obtained from the steady-state solutions are in excellent agreement with the complete solution if the lower set of signs is chosen in Equations [25]. Thus we may accept the "empirical" result (comparison with the complete solution) that the lower set of signs is valid.

The results of the steady-state analysis may now be summarized:

The motion of M for a half cycle is by Equation [20], choosing upper signs (here the choice is immaterial)

$$\frac{X}{A} = \sin (\pi\theta + \tau_s) + hQ(\theta) \quad [28]$$

where $\sin \tau_s$, $\cos \tau_s$ are given by Equations [25], choosing the lower signs, and h is given by Equation [26]. For the second half cycle the motion is given by the negative of Equation [28]. A numerical calculation is simple and one can determine the amplitude X_{max} graphically. The effectiveness of the acceleration damper is the extent to which (X_{max}/A) is less than 1 for, in the absence of the damper, the amplitude is A.

For the important case of resonance $(\Omega/\omega) = 1$ and small damping $(\delta \ll 1)$ it is found that the expressions H and $Q(\theta)$ involve small differences of relatively large numbers. Expanding in power of δ, one obtains to the first order

$$\left.\begin{aligned} H &= \delta\left(1 + \frac{\pi^2}{2\mu}\right) \\ Q(\theta) &= \pi\delta \exp(-\pi\delta\theta) \sin \pi\theta \end{aligned}\right\} \quad [29]$$

The Inverse Problem. The inverse problem is to determine the characteristics of a single damper which reduces the amplitude of the primary system to a prescribed value. The steady-state solution will be used to solve this problem. However, a difficulty is encountered, for it is not possible to obtain X_{max} as an explicit function of the damper parameters, for by Equation [28], X is a transcendental function of θ.

From a practical viewpoint it is desirable to reduce X_{max} to a minimum value. Since this cannot be done directly, it was decided to minimize the integral of the square of X. Further, of the three damper parameters, m, e, and d, the minimum is taken with respect to d only, since the steady-state solution is a complicated function of m and e.

For this purpose define

$$F = \int_0^1 \left(\frac{X}{A}\right)^2 d\theta \quad [30]$$

The minimum condition then gives

$$dF/d\rho = 0 \quad [31]$$

Using Equation [30] in [31], substituting for X and evaluating the simple integrals, gives

$$\left(\frac{1}{2} + 2h_1 I_1 + h_1^2 J\right) \cos \tau_s (\cos \tau_s)_\rho + \frac{1}{2} \sin \tau_s (\sin \tau_s)_\rho + h_1 I_2 [\sin \tau_s (\cos \tau_s)_\rho + \cos \tau_s (\sin \tau_s)_\rho] = 0 \quad [32]$$

where

$$h_1 = \frac{h}{\cos \tau_s}$$

$$(\ )_\rho \equiv \frac{d(\ )}{d\rho}$$

$$I_1 = \int_0^1 Q(\theta) \sin \pi\theta d\theta$$

$$I_2 = \int_0^1 Q(\theta) \cos \pi\theta d\theta$$

$$J = \int_0^1 [Q(\theta)]^2 d\theta$$

Evaluating the foregoing integrals and making the appropriate substitutions in Equation [32] leads to a rather complicated equation for determining ρ. For the resonance case the equation simplifies to

$$\cos \tau_s (\cos \tau_s)_\rho = 0 \quad [33]$$

which has the solutions, denoting these by ρ_1^* and ρ_2^*

$$\left.\begin{aligned} \rho_1^* &= (H)_{(\Omega/\omega)=1} \\ \rho_2^* &= -2 \end{aligned}\right\} \quad [34]$$

The second solution is rejected since ρ is necessarily positive. Hence the container length that minimizes $F(\rho)$ at resonance is, dropping the subscript 1

$$\rho^* = (H)_{(\Omega/\omega)=1} \quad [35]$$

The associated motion is

$$\left(\frac{X}{A}\right)_{\rho=\rho^*} = \sin \pi\theta + [hQ(\theta)]_{(\Omega/\omega)=1} \quad [36]$$

Equations [35] and [36] are the solution to a modified inverse problem for the resonance case. If the (minimum) amplitude, as determined by Equation [36], is not sufficiently small, larger values of m, and perhaps e, may be chosen, and the calculation repeated until the desired amplitude of M is obtained. In this manner, one has a procedure for designing the acceleration damper for a specific purpose.

Numerical Results

Two numerical examples have been calculated to determine the predictions of the theory. For convenience they are designated as Cases 1 and 2 and are defined by the following arbitrary values of the parameters:

Case 1

$$\frac{\Omega}{\omega} = 1 \qquad \mu = 0.401$$

$$\delta = 0.1 \qquad e = 0.2$$

$$\rho = 1.013$$

Case 2

$$\frac{\Omega}{\omega} = 1.25 \qquad \mu = 0.401$$

$$\delta = 0.1 \qquad e = 0.2$$

$$\rho = 1.013$$

In addition, the initial conditions, required for the complete solution, are all chosen zero. The only difference between the two cases is the frequency ratio Ω/ω so that we can compare the performance of the damper at and off resonance.

Using the complete solution the calculations were terminated after thirteen collisions when the motions settled to steady values. By extracting the motion between three consecutive collisions one "cycle" is obtained. For Case 1 the cycle is chosen as the interval from the 10th to 12th collisions, and for Case 2, from the 9th

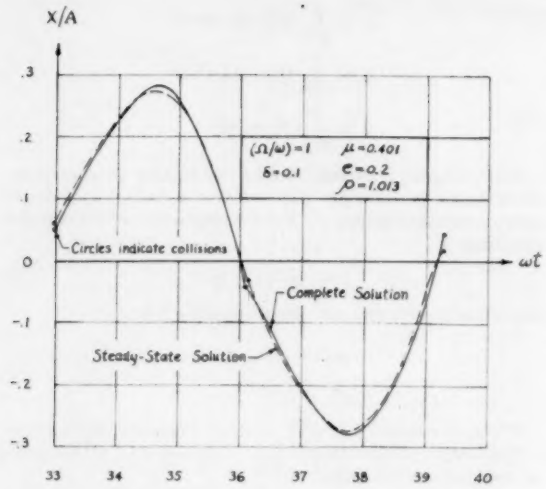

FIG. 2 MOTION OF M FOR CASE 1

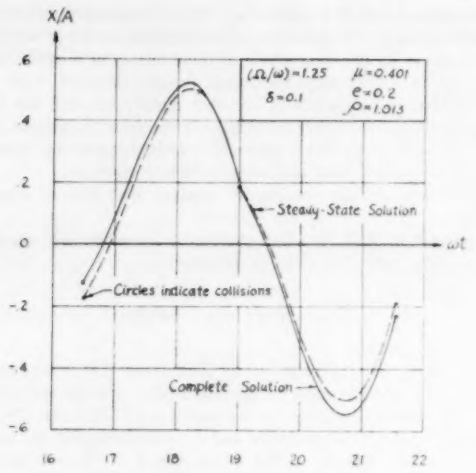

FIG. 3 MOTION OF M FOR CASE 2

to 11th. These results are shown in Figs. 2 and 3. Superimposed on these curves is one cycle of the motion calculated from the steady-state solution. The procedure for relating the complete and steady-state motions is, for Case 1, to let ωt_{10} (= 33.0) correspond to $\theta = 0$ and ωt_{11} (= 36.1) to $\theta = 1$. For the second half cycle, ωt_{11} corresponds to $\theta = 0$ and ωt_{12} (= 39.3) to $\theta = 1$. A similar procedure is followed for Case 2. These calculations indicate the following:

At resonance the damper can be quite effective, for according to Case 1, the amplitude is reduced to about 0.28 of its value without the damper. The mass ratio is large, however, and in a practical case this may not be feasible. However, the restitution coefficient is relatively low, and it appears that increasing e at resonance would increase the efficiency of the damper. This is suggested by Equation [6], since the velocity discontinuity, which is a measure of the damping, is proportional to $(1 + e)$.

Off resonance the damper is not as effective for, according to Case 2, the amplitude is reduced to only 0.54 of its value without the damper. It is thought that, in general, the further the system is off resonance the poorer will be the efficiency of the damper since the collisions produce motions which have the (damped) natural frequency of the system (see Equation [7]). Thus, at or near resonance, these motions, if properly phased (as determined by the container length), can nullify to a large extent the motion produced by the driving force, whereas off resonance this possibility does not exist. An important conclusion of this study is, therefore, that the damper appears to be most efficient at the critical condition (resonance).

The calculations also show the excellent agreement between the complete solution and the steady-state solution when the lower set of signs in Equation [25] is used. It is found in both cases that with the upper set of signs the particle exceeds the container extremities during the cycle, a result which is physically meaningless and which indicates that this solution must be rejected.

The solution to the inverse problem has been used for Case 1. It is found that Equation [35] yields a value $\rho^* = 0.965$ which is quite close to the value 1.013 already used. Then using Equation [36] a value of X_{max} is obtained which is nearly the same as in Fig. 2.

CONCLUSIONS

The theory of the acceleration damper has been developed for a single unit, when the primary single-degree-of-freedom system is subjected to a simple harmonic driving force. Two solutions for the equations of motion have been developed. In the first, by starting with prescribed initial conditions, the motion can be determined from collision to collision. This is not practical, however, for it may be necessary to consider many collisions to obtain the motion accurately (in this respect an analog-computing machine may be useful). In the second, steady-state solution, the motion is determined for only a half cycle. This solution is simple computationally, and offers a solution to the inverse problem.

Numerical calculations indicate that the damper may be quite effective in particular applications, especially at resonance. The agreement between the complete and steady-state solutions in the two cases considered strongly suggests the validity of the latter solution. In this connection, an interesting problem would be to prove analytically that for a specified range of parameters and arbitrary initial conditions, the complete solution, for large values of time, oscillates about the steady-state solution.

ACKNOWLEDGMENT

The author wishes to acknowledge the suggestions and encouragement of his adviser, Prof. Paul Lieber of Rensselaer Polytechnic Institute. He is also grateful to the Office of Naval Research whose support made the work possible.

The Modes of Vibration of a Certain System Having a Number of Equal Frequencies

By D. C. JOHNSON[1] and R. E. D. BISHOP,[2] CAMBRIDGE, ENGLAND

This paper is concerned with a conservative system, which represents an idealized bladed rotor, whose principal modes are indeterminate. The dynamical behavior of the system is discussed and a method of selecting suitable principal modes and co-ordinates is explained.

Nomenclature

The following nomenclature is used in the paper:

a = inertia coefficient in expression for kinetic energy (see Equations [21] and [39])
c = stability coefficient in expression for potential energy (see Equations [21] and [39])
F = amplitude of applied force
i = $\sqrt{(-1)}$
j = pair number specifying equal frequency modes (see Equations [14] and [15])
k = spring stiffness (see Fig. 1)
M = mass (see Fig. 1)
m = mass (see Fig. 1)
n = number of small masses
$p_0, p_1, \ldots p_n$ = principal co-ordinates
$q_0, q_1, \ldots q_n$ = co-ordinates (see Fig. 1); a prefixed subscript indicates a displacement in a given mode
r, s = subscripts representing specific small masses (= 1, 2, . . . n)
T = kinetic energy
u, v = subscripts representing specific masses (= 0, 1, 2, . . .n)
V = potential energy
y, z = subscripts representing modal numbers (= 0, 1, 2, . . . n)
α = receptance
Δ = determinant (see Equation [4])
ω = frequency

Introduction

The mechanical system discussed in this paper consists of a single mass M to which is attached a number n of masses all of a magnitude m; the masses m are connected to M by springs, all the springs having the same stiffness k. The masses are free to move in one direction only and the axes of all the springs are parallel to this direction. The arrangement is shown in Fig. 1, the direction of motion being indicated by the arrow.

The analysis of the vibration of the system has been found by the authors to help in the understanding of the behavior of a turbine disk which carries a large number of similar blades. The disk motion may then be angular about its axis or translational and perpendicular to its plane or a combination of these. The analysis is also of general interest because it concerns a system which has a large number of equal frequencies. The analysis for such a system is slightly different from that for a normal system and some discussion of the theory is given by Rayleigh,[3] who refers specifically to the vibration of membranes.

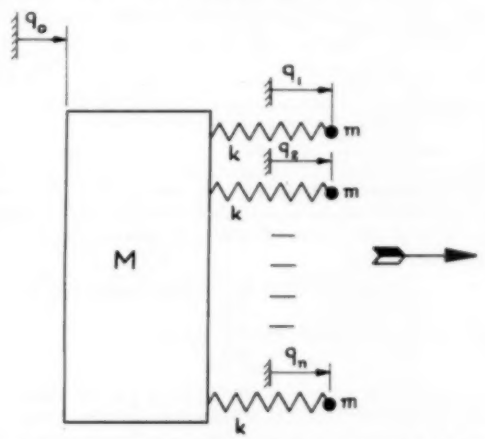

Fig. 1 Mechanical System Having (n — 1) Equal Natural Frequencies

The system of Fig. 1 has (n + 1) degrees of freedom and therefore (n + 1) principal modes of vibration, each with its corresponding frequency. Because many of these frequencies are the same, the principal modes are arbitrary although, when choosing them, certain restrictions must be complied with. The modal shapes which are suggested in this paper are those which remain valid if the system is modified by the introduction of n additional springs, each having some stiffness λ and one being placed between each of the masses m. When the system is modified in this way the natural frequencies are no longer all equal but consist of a number of equal pairs, though the frequencies of different pairs may remain very close; the modified system is also of interest in connection with bladed rotors.

The Lowest and Highest Principal Modes

The kinetic and potential energies of the system of Fig. 1 are given by

$$2T = M\dot{q}_0^2 + m\dot{q}_1^2 + m\dot{q}_2^2 + \ldots\ldots\ldots + m\dot{q}_n^2 \quad [1]$$

[1] Professor of Mechanical Engineering, University of Leeds, Leeds, England; formerly, University Lecturer in Engineering and Fellow of Trinity Hall, Cambridge, England.

[2] University Lecturer in Engineering and Fellow of Pembroke College, Cambridge; Engineering Laboratory, Cambridge University.

Presented at the National Applied Mechanics Conference, Urbana, Ill., June 14–16, 1956, of The American Society of Mechanical Engineers.

Discussion of this paper should be addressed to the Secretary, ASME, 29 West 39th Street, New York, N. Y., and will be accepted until October 10, 1956, for publication at a later date. Discussion received after the closing date will be returned.

Note: Statements and opinions advanced in papers are to be understood as individual expressions of their authors and not those of the Society. Manuscript received by ASME Applied Mechanics Division, June 8, 1955. Paper No. 56—APM-16.

[3] "Theory of Sound," by Lord Rayleigh, The Macmillan Company, London, England, 1894.

$$2V = k(q_0 - q_1)^2 + k(q_0 - q_2)^2 + \ldots\ldots + k(q_0 - q_n)^2$$
$$= nkq_0^2 + kq_1^2 + kq_2^2 + \ldots + kq_n^2 - 2kq_0q_1 - 2kq_0q_2 - \ldots\ldots - 2kq_0q_n \ldots\ldots [2]$$

These expressions may be used in Lagrange's equations to set up the equations of free vibration; they are

$$\left.\begin{aligned} M\ddot{q}_0 + nkq_0 - kq_1 - kq_2 - \ldots\ldots - kq_n &= 0 \\ m\ddot{q}_1 + kq_1 - kq_0 &= 0 \\ m\ddot{q}_2 + kq_2 - kq_0 &= 0 \\ \ldots\ldots & \\ \ldots\ldots & \\ m\ddot{q}_n + kq_n - kq_0 &= 0 \end{aligned}\right\} \ldots [3]$$

The frequency equation may now be obtained in the usual way. That is to say, the condition may be written down under which harmonic solutions of Equations [3] may be found. It is, in determinantal form

$$\Delta \equiv \begin{vmatrix} nk - M\omega^2 & -k & -k & \ldots & -k \\ -k & k - m\omega^2 & 0 & \ldots & 0 \\ -k & 0 & k - m\omega^2 & \ldots & 0 \\ \ldots & \ldots & \ldots & \ldots & \ldots \\ \ldots & \ldots & \ldots & \ldots & \ldots \\ -k & 0 & 0 & \ldots & k - m\omega^2 \end{vmatrix} = 0 \ldots [4]$$

The determinant Δ contains $(n + 1)$ rows and $(n + 1)$ columns and its roots $\omega_0^2, \omega_1^2, \ldots\ldots \omega_n^2$ are the squares of the natural frequencies of the system. Equation [4] can be reduced to the form

$$\omega^2(k - m\omega^2)^{n-1}[Mm\omega^2 - (M + nm)k] = 0 \ldots\ldots [5]$$

Thus the natural frequencies are given by

$$\left.\begin{aligned} \omega_0^2 &= 0 \\ \omega_1^2 = \omega_2^2 = \ldots\ldots = \omega_{n-1}^2 &= \frac{k}{m} \\ \omega_n^2 &= \frac{k(M + nm)}{Mm} \end{aligned}\right\} \ldots [6]$$

The principal mode corresponding to $\omega_0^2 = 0$ is a rigid-body motion since the system is unanchored. If, then, a prefixed subscript is used to indicate the modal number, the 0th modal shape is given by

$${}_0q_0 : {}_0q_1 : {}_0q_2 : \ldots : {}_0q_n :: 1:1:1: \ldots\ldots : 1 \ldots\ldots [7]$$

Not only the lowest principal mode, but also the highest (corresponding to the natural frequency ω_n) can be found by inspection, for the system will be seen to have a mode in which all the small masses move together in phase with equal amplitudes, the large mass moving in antiphase with them. If the small masses are thought of as being connected by a light rigid link, the system may be treated as if it consists of two masses, M and nm, connected by a spring whose stiffness is nk; the nonzero natural frequency of this two-degree-of-freedom system is found to be given by

$$\omega_n^2 = \frac{(nk)(M + nm)}{M(nm)} = \frac{k(M + nm)}{Mm} \ldots\ldots [8]$$

Moreover, the amplitude of the mass M is nm/M of that of the mass nm so that the modal shape is given by

$${}_nq_0 : {}_nq_1 : {}_nq_2 : \ldots\ldots : {}_nq_n :: -\frac{nm}{M} : 1:1: \ldots : 1 \ldots [9]$$

The 0th and nth principal modes which have been found are, of course, orthogonal. This may be checked readily and a convenient way of doing this is by the use of Equations [42] and [43] which are derived in the Appendix and which will be used later on.

The "Equal-Frequency" Modes

According to Equation [6] the system of Fig. 1 has $(n - 1)$ principal modes, all having the same frequency. But as the springs and small masses are all identical, these modes are indeterminate. The relevant natural frequency is $\sqrt{(k/m)}$ and, as it is that of a motion in which the large mass remains stationary, the conditions which must be fulfilled by principal modes in which $q_0 = 0$ will now be written down. Now if the large mass is to remain still, it must experience zero net reaction at all instants and, since the force exerted on it through the rth spring is kq_r in one of these equal-frequency modes, it follows that (on cancelling the factor k)

$$\sum_{r=1}^{n} {}_1q_r = 0; \quad \sum_{r=1}^{n} {}_2q_r = 0; \quad \ldots\ldots\ldots\ldots \quad \sum_{r=1}^{n} {}_{n-1}q_r = 0 \ldots [10]$$

There are thus $(n - 1)$ of these conditions.

Equations [10] ensure the orthogonality of the equal-frequency modes with the 0th and nth and the reader may regard this as being physically evident. That this is so may be demonstrated algebraically, by writing down the orthogonality relations (see Appendix) remembering that q_0 has been taken as zero in the equal-frequency modes; thus

$$\left.\begin{aligned} &\sum_{r=1}^{n} {}_0q_r \cdot {}_1q_r = 0; \quad \sum_{r=1}^{n} {}_0q_r \cdot {}_2q_r = 0; \quad \ldots; \quad \sum_{r=1}^{n} {}_0q_r \cdot {}_{n-1}q_r = 0 \\ &\sum_{r=1}^{n} {}_nq_r \cdot {}_1q_r = 0; \quad \sum_{r=1}^{n} {}_nq_r \cdot {}_2q_r = 0; \quad \ldots; \quad \sum_{r=1}^{n} {}_nq_r \cdot {}_{n-1}q_r = 0 \end{aligned}\right\} \ldots [11]$$

The factors ${}_0q_r$ and ${}_nq_r$ are the same for all the small masses so that both sets of equations reduce identically to Equation [10].

The equal-frequency modes must be orthogonal between themselves so it is necessary that

$$\left.\begin{aligned} &\sum_{r=1}^{n} {}_1q_r \cdot {}_2q_r = 0; \quad \sum_{r=1}^{n} {}_1q_r \cdot {}_3q_r = 0; \quad \ldots; \quad \sum_{r=1}^{n} {}_1q_r \cdot {}_{n-1}q_r = 0 \\ &\sum_{r=1}^{n} {}_2q_r \cdot {}_3q_r = 0; \quad \sum_{r=1}^{n} {}_2q_r \cdot {}_4q_r = 0; \quad \ldots \text{ etc.} \end{aligned}\right\} \ldots [12]$$

There are $(n - 1)(n - 2)/2$ of these conditions.

Equations [10] and [12] show that, in all, the equal-frequency modes have to satisfy $n(n - 1)/2$ conditions. The total number of quantities which have to be chosen when selecting these modes is $(n - 1)$ sets of the $(n - 1)$ ratios between the n displacements. Therefore there are $n(n - 1)/2$ equations and $(n - 1)^2$ quanti-

ties; hence there is an infinite choice of equal-frequency modes in which the large mass remains still provided that $n \geqslant 3$.

If an arbitrary shape were taken for the first mode, then it would be possible to construct a second which was orthogonal to it; a third could then be found which was orthogonal to the first and the second, and so on. The algebra of such a process would become prohibitive if n were large. An alternative approach will now be explained by which the modal shapes are obtained from a suitable set of functions which give all of them. One such set of functions are the sines and cosines of suitable fractions of 2π. These give modal shapes which are defined by

$$\left.\begin{aligned}
&{}_1q_1 : {}_1q_2 : \ldots : {}_1q_n :: \sin\frac{2\pi}{n} : \sin\frac{4\pi}{n} : \ldots : \sin 2\pi \\
&{}_2q_1 : {}_2q_2 : \ldots : {}_2q_n :: \cos\frac{2\pi}{n} : \cos\frac{4\pi}{n} : \ldots : \cos 2\pi \\
&{}_3q_1 : {}_3q_2 : \ldots : {}_3q_n :: \sin\frac{4\pi}{n} : \sin\frac{8\pi}{n} : \ldots : \sin 4\pi \\
&{}_4q_1 : {}_4q_2 : \ldots : {}_4q_n :: \cos\frac{4\pi}{n} : \cos\frac{8\pi}{n} : \ldots : \cos 4\pi
\end{aligned}\right\} \ldots [13]$$

and so on.

These modes will be seen to be a set of pairs. If the pair number is denoted by j, so that the corresponding mode numbers may be denoted by $(2j-1)$ and $2j$, and the mass number (as before) by r then the terms concerning the rth small mass in the jth pair of modes will be given by

$${}_{(2j-1)}q_r \propto \sin\frac{2\pi jr}{n} \ldots\ldots [14]$$

and

$${}_{(2j)}q_r \propto \cos\frac{2\pi jr}{n} \ldots\ldots [15]$$

It is now necessary to check that these modal shapes satisfy the Conditions [10] and [12] of orthogonality.

It can be seen by geometry that these modes satisfy Equations [10]. This is demonstrated by the vector diagram of Fig. 2 which is a closed polygon and so gives no resultant projection. Therefore these modes are orthogonal to the 0th and nth modes.

That these modes also satisfy the various orthogonality Equations [12] can be seen by considering separately the various forms that the relations may take. The orthogonality of the $(2j-1)$th and $(2j'-1)$th modes requires that

$$\sum_{r=1}^{n} \sin\frac{2\pi jr}{n} \sin\frac{2\pi j'r}{n} = 0 \ldots\ldots [16]$$

and this may be rewritten in the form

$$\frac{1}{2}\sum_{r=1}^{n}\left[\cos\frac{2\pi(j-j')r}{n} - \cos\frac{2\pi(j+j')r}{n}\right] = 0 \ldots [17]$$

These terms can be represented, as before, by closed polygons provided that $j \neq j'$. By the same process, the equation

$$\sum_{r=1}^{n} \cos\frac{2\pi jr}{n} \cos\frac{2\pi j'r}{n} = 0 \ldots\ldots [18]$$

may be written as

$$\frac{1}{2}\sum_{r=1}^{n}\left[\cos\frac{2\pi(j-j')r}{n} + \cos\frac{2\pi(j+j')r}{n}\right] = 0 \ldots [19]$$

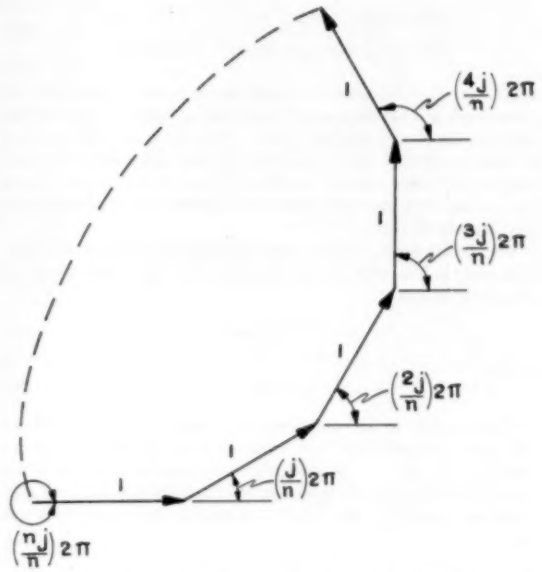

FIG. 2 VECTOR DIAGRAM FOR SHOWING ORTHOGONALITY OF SELECTED EQUAL-FREQUENCY MODES

and so can be shown to hold by means of closed vector polygons, again provided $j \neq j'$; that is to say, the $2j$th and $2j'$th modes are orthogonal. Finally, the orthogonality of the $(2j-1)$th and $2j'$th modes is given by

$$\sum_{r=1}^{n} \sin\frac{2\pi jr}{n} \cos\frac{2\pi j'r}{n} = \frac{1}{2}\sum_{r=1}^{n}\left[\sin\frac{2\pi(j-j')r}{n} + \sin\frac{2\pi(j+j')r}{n}\right] = 0 \ldots\ldots [20]$$

which polygons show to hold whether $j = j'$ or not. Thus all the relations are satisfied which must be fulfilled if the selected equal-frequency modes are to be orthogonal to each other; for the orthogonality of any pair of the modes, Equations [13], is covered by Equation [16], [18], or [20].

If n is an odd number, so that $(n-1)$ is even, there will be $(n-1)/2$ pairs of modes, Equations [13], and the set of values $j = 1, 2, \ldots . (n-1)/2$ will be required. On the other hand, if n is even so that $(n-1)$ is odd, there will be $n/2$ pairs of modes [13] minus one; it is then necessary to take $j = 1, 2, \ldots . (n-2)/2$ and to take in addition the set of cosines corresponding to $j = n/2$ since the sines give a degenerate mode in which the entire system remains stationary.

It will be found that higher values of j than $n/2$ lead to repetition of the modes between $j = 1$ and $j = n/2$; thus $j = (n+1)/2$ gives the same modal shapes as $j = (n-1)/2$, etc. This follows because it is impossible to find more than $(n+1)$ different orthogonal modes for a system with $(n+1)$ degrees of freedom.

In addition to the lowest and highest modes, a suitable set of reactionless equal-frequency modes has been selected so making up the required total of $(n+1)$ principal modes. It will next be shown how, through the use of a principal co-ordinate for each mode, the response of the system of Fig. 1 to a given excitation may be deduced.

PRINCIPAL CO-ORDINATES

Principal co-ordinates $p_0, p_1, \ldots . p_n$ can now be defined in the usual way for the system of Fig. 1. The notation

$$\left.\begin{aligned} 2T &= a_0\dot{p}_0^2 + a_1\dot{p}_1^2 + \ldots\ldots\ldots + a_n\dot{p}_n^2 \\ 2V &= c_0p_0^2 + c_1p_1^2 + \ldots\ldots\ldots + c_np_n^2 \end{aligned}\right\} \ldots [21]$$

will be used. The principal co-ordinates possess a property by which each is a measure of the distortion of the system at any instant in one of its principal modes. This being so, it is necessary to choose a scale of these distortions by selecting a suitable meaning for unit value of each of the p's; upon this selection depend the values of the inertia coefficients a and the stability coefficients c of Equations [21].

For the 0th mode, let unit value of the 0th principal co-ordinate p_0 correspond to unit values of $q_0, q_1, \ldots . q_n$. This gives the energy functions

$$2T = (M + nm)\dot{p}_0^2;\ 2V = 0 \ldots\ldots\ldots\ldots [22]$$

so that

$$a_0 = M + nm,\quad c_0 = 0 \ldots\ldots\ldots\ldots [23]$$

Turning next to the equal-frequency modes, Equations [13], let the scale be such that unit value of each of the principal co-ordinates $p_1, p_2, \ldots . p_{n-1}$ corresponds to actual equality of the q's to the appropriate trigonometric functions in Equations [13]. Consider motion in the $(2j - 1)$th mode; the energy functions are

$$\left.\begin{aligned} 2T &= m\dot{p}_{(2j-1)}^2\sum_{r=1}^{n}\sin^2\frac{2\pi jr}{n} = \frac{nm}{2}\dot{p}_{(2j-1)}^2 \\ 2V &= kp_{(2j-1)}^2\sum_{r=1}^{n}\sin^2\frac{2\pi jr}{n} = \frac{nk}{2}p_{(2j-1)}^2 \end{aligned}\right\} \ldots [24]$$

The same energy expressions are found for the cosine terms of all the $2j$th modes except that in which $j = n/2$ (which is used when n is even) so that the energy coefficients are

$$\left.\begin{aligned} a_1 = a_2 = \ldots\ldots = a_{n-1} &= \frac{nm}{2} \\ c_1 = c_2 = \ldots\ldots = c_{n-1} &= \frac{nk}{2} \end{aligned}\right\} (n \text{ odd}) \ldots . [25]$$

When n is even, a mode is used for which $j = n/2$ and the corresponding energy functions are

$$\left.\begin{aligned} 2T &= m\dot{p}_{n-1}^2\sum_{r=1}^{n}\cos^2 r\pi = nm\dot{p}_{n-1}^2 \\ 2V &= kp_{n-1}^2\sum_{r=1}^{n}\cos^2 r\pi = nkp_{n-1}^2 \end{aligned}\right\} \ldots\ldots [26]$$

Thus, when n is even, the energy coefficients are

$$\left.\begin{aligned} a_1 = a_2 = \ldots\ldots = a_{n-2} &= \frac{nm}{2};\quad a_{n-1} = nm \\ c_1 = c_2 = \ldots\ldots = c_{n-2} &= \frac{nk}{2};\quad c_{n-1} = nk \end{aligned}\right\} (n \text{ even}). [27]$$

Finally, the nth principal co-ordinate p_n will here be chosen to have unit value when the small masses have unit displacement. For this mode then

$$\left.\begin{aligned} 2T &= \left[M\left(\frac{nm}{M}\right)^2 + nm\right]\dot{p}_n^2 = nm\left(1 + \frac{nm}{M}\right)\dot{p}_n^2 \\ 2V &= nk\left(1 + \frac{nm}{M}\right)^2 p_n^2 \end{aligned}\right\} \ldots [28]$$

so that

$$a_n = nm\left(1 + \frac{nm}{M}\right);\quad c_n = nk\left(1 + \frac{nm}{M}\right)^2 \ldots . [29]$$

These principal co-ordinates can be used in the usual way to find the response of the system to harmonic excitation. Suppose, for instance, that the response at the rth small mass is required when a force $Fe^{i\omega t}$ is applied to the sth. The displacements q_r and q_s are given, in terms of the chosen p's, by the relations

$$\left.\begin{aligned} q_r &= p_0 + \sum_{j=1}^{(n-1)/2} p_{(2j-1)}\sin\frac{2\pi jr}{n} + \sum_{j=1}^{(n-1)/2} p_{(2j)}\cos\frac{2\pi jr}{n} + p_n \\ q_s &= p_0 + \sum_{j=1}^{(n-1)/2} p_{(2j-1)}\sin\frac{2\pi js}{n} + \sum_{j=1}^{(n-1)/2} p_{(2j)}\cos\frac{2\pi js}{n} + p_n \end{aligned}\right\} \ldots [30]$$

where n is here assumed to be an odd number. By the use of these expressions the equations of motion governing the various principal co-ordinates may be written down in the form

$$a_yp_y + c_yp_y = F\frac{\partial q_s}{\partial p_y}e^{i\omega t}\ (y = 0, 1, 2, \ldots . n) \ldots [31]$$

This set of $(n + 1)$ equations can be solved to give those variations of the co-ordinates p which have the impressed frequency ω; these solutions, when substituted into the first of Equations [30] then give the variation of q_r. It is found, in fact, that

$$q_r = \alpha_{rs}Fe^{i\omega t} \ldots\ldots\ldots\ldots [32]$$

where

$$\alpha_{rs} = \frac{-1}{(M + nm)\omega^2} - \frac{1}{n(k - m\omega^2)} + \frac{1}{nk\left(1 + \frac{nm}{M}\right)^2 - nm\left(1 + \frac{nm}{M}\right)\omega^2} \ldots\ldots [33]$$

when $r \neq s$ and

$$\alpha_{rr} = \frac{-1}{(M + nm)\omega^2} + \frac{n - 1}{n(k - m\omega^2)} + \frac{1}{nk\left(1 + \frac{nm}{M}\right)^2 - nm\left(1 + \frac{nm}{M}\right)\omega^2} \ldots\ldots [34]$$

when $r = s$.

The "cross-receptance," Equation [33], and the "direct-receptance," Equation [34], are expressed as series of partial fractions. The properties of such series as these have been discussed by Johnson[4] and a complete list of them for the system of Fig. 1 is given in Table 1.

Derivations of the Receptance by Other Means

If a force $Fe^{i\omega t}$ acts upon any mass of the system of Fig. 1, the response at any mass may be expected in the form of Equation [32] and one method of finding the receptance α has been explained. Now the derivation which has been given demonstrates the use of arbitrarily selected principal modes and it may be

[4] "The Application of Admittance Methods in the Classical Theory of Small Oscillations," by D C. Johnson, *Engineering*. vol. 171, 1951, p. 650.

TABLE 1 RECEPTANCES OF A SIMPLIFIED BLADED ROTOR

	RECEPTANCE IN SERIES FORM	COMPLETE "CLOSED" FORM
α_{ss}	$\frac{-1}{(M+nm)\omega^2} + \frac{nm^2}{(M+nm)[k(M+nm)-Mm\omega^2]}$	$\frac{(k-m\omega^2)^n}{\omega^2(k-m\omega^2)^{n-1}[Mm\omega^2-k(M+nm)]}$
α_{ro}	$\frac{-1}{(M+nm)\omega^2} - \frac{Mm}{(M+nm)[k(M+nm)-Mm\omega^2]}$	$\frac{k(k-m\omega^2)^{n-1}}{\omega^2(k-m\omega^2)^{n-1}[Mm\omega^2-k(M+nm)]}$
α_{rr}	$\frac{-1}{(M+nm)\omega^2} + \frac{(n-1)}{n(k-m\omega^2)} + \frac{M^2}{n(M+nm)[k(M+nm)-Mm\omega^2]}$	$\frac{(k-m\omega^2)^{n-2}[k^2-k(M+nm)\omega^2+Mm\omega^4]}{\omega^2(k-m\omega^2)^{n-1}[Mm\omega^2-k(M+nm)]}$
α_{rs}	$\frac{-1}{(M+nm)\omega^2} - \frac{1}{n(k-m\omega^2)} + \frac{M^2}{n(M+nm)[k(M+nm)-Mm\omega^2]}$	$\frac{k^2(k-m\omega^2)^{n-2}}{\omega^2(k-m\omega^2)^{n-1}[Mm\omega^2-k(M+nm)]}$

$r = 1, 2, \ldots\ldots n$
$s = 1, 2, \ldots\ldots n$

checked by two alternative derivations. These latter methods also possess features which are of interest in themselves; they will, therefore, be described briefly.

(*a*) *Reduction of Number of Degrees of Freedom.* The simplest way of finding receptances for the system is to make use of one of its properties; for it will be seen that, when undergoing forced vibration, it will do so as if it possesses either two or three degrees of freedom. Suppose, for instance, that excitation is applied at the large mass; all the small masses will take up the same motion, since they are indistinguishable, so that they can be thought of as being connected by a light rigid link. It follows that the system behaves like that of Fig. 3(*a*).

On the other hand, if a harmonic force $Fe^{i\omega t}$ is applied to one of the small masses—the sth, say—the system behaves like that of Fig. 3(*b*). The remaining masses all acquire the same motion which differs, in general, from that of the sth. The system behaves as if it has three degrees of freedom.

The various receptances of these simplified systems may be calculated by elementary means. In fact, it is found that, for the system of Fig. 3(*a*)

$$\left.\begin{aligned}\alpha_{00} &= \frac{k - m\omega^2}{\omega^2[Mm\omega^2 - k(M + nm)]}\\ \alpha_{r0} &= \frac{k}{\omega^2[Mm\omega^2 - k(M + nm)]}\end{aligned}\right\} \quad \ldots\ldots [35]$$

and, for the system of Fig. 3(*b*)

$$\left.\begin{aligned}\alpha_{0s} &= \frac{k}{\omega^2[Mm\omega^2 - k(M + nm)]}\\ \alpha_{ss} &= \frac{k^2 - k(M + nm)\omega^2 + Mm\omega^4}{\omega^2(k - m\omega^2)[Mm\omega^2 - k(M + nm)]}\\ \alpha_{rs} &= \frac{k^2}{\omega^2(k - m\omega^2)[Mm\omega^2 - k(M + nm)]}\end{aligned}\right\} \quad \ldots [36]$$

It is found that these values agree with those listed in the series form in Table 1.

(*b*) *Direct Evaluation of Receptance From Equations of Motion.* If a harmonic force $Fe^{i\omega t}$ acts upon the vth mass of Fig. 1 where $v = 0, 1, 2, \ldots\ldots n$, the term $Fe^{i\omega t}$ will appear on the right-hand side of the vth equation of motion, Equation [3]. Solutions of the simultaneous equations may then be sought in which all the q's vary harmonically with the frequency ω. By this means it is found that the displacement of the uth mass (where $u = 0, 1, 2, \ldots\ldots n$) is given by

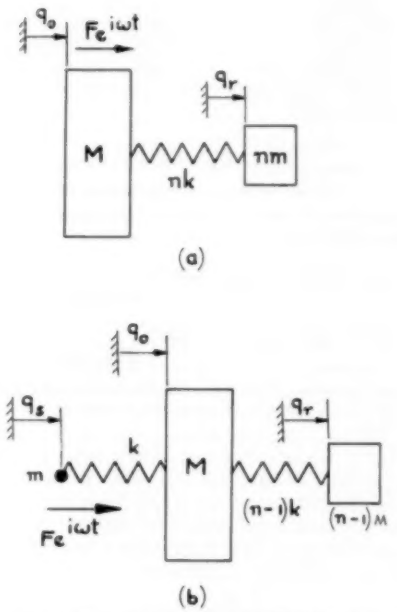

FIG. 3 SIMPLIFIED VERSIONS OF SYSTEM OF FIG. 1 WHICH SIMPLIFY CALCULATION OF RECEPTANCES

$$q_u = \alpha_{uv} F e^{i\omega t} \quad \ldots\ldots [37]$$

where

$$\alpha_{uv} = (-1)^{(u+v)} \frac{\Delta_{uv}}{\Delta} \quad \ldots\ldots [38]$$

In this expression Δ_{uv} is that determinant which is formed from Δ (see Equation [4]) by omitting its $(u + 1)$th column and its $(v + 1)$th row.

The evaluation of the various receptances by means of the Formula [38] is tedious and it is sufficient, here, merely to quote the results. They are listed in Table 1 as receptances in the "complete closed form" and they will be seen to possess repeated roots which are common to the numerator and denominator. In each case the receptance is the same as its series counterpart and

to the expressions of Equations [35] and [36] after cancellation of the factor $(k - m\omega^2)$ has been performed.

The appearance of the repeated factors $(k - m\omega^2)$ which are common to the numerators and denominators of these receptances is due to the fact that the frequency, Equation [6], has $(n - 1)$ repeated roots. This property of receptances has been treated previously[5] and so need not be dwelt upon here.

Conclusions

The system of Fig. 1 represents an idealized bladed rotor and, since all the "blades" are identical, it possesses indeterminate principal modes. This paper has been concerned with the dynamical behavior of this system and, in particular, with the treatment of these modes.

A method is shown of selecting principal modes such that the conditions of orthogonality are satisfied. By this means, principal co-ordinates may be chosen which are shown to give the receptances of the system by standard means.

Two other methods are outlined for finding the receptances of the system. The first of these makes use of the fact that the blades are identical and that, if they are excited only through their attachments to the rigid disk, their motions must all be the same. The second alternative method is by direct calculation from the equations of motion; while this method is tedious, it provides the receptances in a form which gives information on the nodal condition of the system.[6]

Appendix

The Orthogonality Principle

The kinetic and potential energies of the system of Fig. 1 may be written in the form

$$\left.\begin{aligned} 2T &= a_{00}\dot{q}_0^2 + a_{11}\dot{q}_1^2 + \ldots + a_{nn}\dot{q}_n^2 \\ &\qquad + 2a_{01}\dot{q}_0\dot{q}_1 + \ldots \\ 2V &= c_{00}q_0^2 + c_{11}q_1^2 + \ldots + c_{nn}q_n^2 \\ &\qquad + 2c_{01}q_0q_1 + \ldots \end{aligned}\right\} \ldots [39]$$

[5] "Some Properties of Nodes in Vibrating Systems," by R. E. D. Bishop and D. C. Johnson, *Aeronautical Quarterly*, vol. 6, February, 1955, p. 46

Suppose now that the system is made to oscillate in its yth and zth modes only. The energies will be given by

$$\left.\begin{aligned} 2T &= a_{00}({}_y\dot{q}_0 + {}_z\dot{q}_0)^2 + a_{11}({}_y\dot{q}_1 + {}_z\dot{q}_1)^2 + \ldots \\ &\quad + a_{nn}({}_y\dot{q}_n + {}_z\dot{q}_n)^2 + 2a_{01}({}_y\dot{q}_0 + {}_z\dot{q}_0)({}_y\dot{q}_1 + {}_z\dot{q}_1) + \ldots \\ 2V &= c_{00}({}_yq_0 + {}_zq_0)^2 + c_{11}({}_yq_1 + {}_zq_1)^2 + \ldots \\ &\quad + c_{nn}({}_yq_n + {}_zq_n)^2 + 2c_{01}({}_yq_0 + {}_zq_0)({}_yq_1 + {}_zq_1) + \ldots \end{aligned}\right\} \ldots [40]$$

Now, according to the principle of orthogonality, these energies are the sums of those due to each of the principal modes separately. It follows that

$$a_{00} \cdot {}_y\dot{q}_0 \cdot {}_z\dot{q}_0 + a_{11} \cdot {}_y\dot{q}_1 \cdot {}_z\dot{q}_1 + \ldots + a_{nn} \cdot {}_y\dot{q}_n \cdot {}_z\dot{q}_n + a_{01}({}_yq_0 \cdot {}_z\dot{q}_1 + {}_z\dot{q}_0 \cdot {}_y\dot{q}_1) + \ldots = 0 \ldots [41]$$

$$c_{00} \cdot {}_yq_0 \cdot {}_zq_0 + c_{11} \cdot {}_yq_1 \cdot {}_zq_1 + \ldots + c_{nn} \cdot {}_yq_n \cdot {}_zq_n + c_{01}({}_yq_0 \cdot {}_zq_1 + {}_zq_0 \cdot {}_yq_1) + \ldots = 0 \ldots [42]$$

This pair of equations represents a statement of the orthogonality condition. The first of them, however, may be simplified further by omitting the dots over the q's. This is because the co-ordinates q are linear functions of whatever set of principal co-ordinates is chosen. It follows that each term of Equation [41] contains the factor $\dot{p}_y\ \dot{p}_z$ and this may be cancelled out and replaced by $p_y\ p_z$ without interfering with the relation. That is to say

$$a_{00} \cdot {}_yq_0 \cdot {}_zq_0 + a_{11} \cdot {}_yq_1 \cdot {}_zq_1 + \ldots + a_{nn} \cdot {}_yq_n \cdot {}_zq_n + a_{01}({}_yq_0 \cdot {}_zq_1 + {}_zq_0 \cdot {}_yq_1) + \ldots = 0 \ldots [43]$$

Equations [42] and [43] are used in this paper as stating the condition of orthogonality. The energy coefficients a and c may be seen, on comparison of Equations [1], [2], and [39] to be given by

$$\left.\begin{aligned} a_{00} &= M;\quad a_{11} = a_{22} = \ldots = a_{nn} = m; \\ &\qquad a_{01} = a_{02} = \ldots = 0 \\ c_{00} &= nk;\quad c_{11} = c_{22} = \ldots = c_{nn} = k; \\ c_{01} &= c_{02} = \ldots = c_{0n} = -k;\quad c_{12} = c_{13} = \ldots = 0 \end{aligned}\right\} \ldots [44]$$

The Effect of Spring Mass on Contact-Accelerometer Responses

By T. H. LIN[1]

Theoretical responses of a contact-break accelerometer are analyzed for steady-state and some transient motions. The distributed mass of the spring is considered in the present analysis. For steady-state motions, viscous damping is assumed to exist between the spring and the case of the instrument. Responses to simple harmonic motions of different frequencies are shown. Responses to a single cosine wave and a step function of acceleration are analyzed. The main source of error in the contact-break accelerometer is shown to be due to the spring mass. An electromagnetic-contact accelerometer with no spring mass is proposed. Preliminary study of this accelerometer is shown.

Nomenclature

The following nomenclature is used in the paper:

a = velocity of wave propagation in an elastic medium
A = cross-section area of elastic rod
A_0 = amplitude of motion
B_1, B_n = constants
C = damping coefficient
E = Young's modulus of elasticity
e = compressive strain
e_0 = preset compressive strain
g = gravitational acceleration
L = length of spring or elastic rod
M_1 = top mass
M_2 = spring mass
n = an integral number
N_1, N_2 = constants
p_n = angular velocity
q_n = $\xi_n + i\eta_n$
R = ratio of preset compressive force to top mass plus one-half spring mass times acceleration for contact to break
S = force
t = time
u = displacement
V = nondimensional constant
x = distance from lower end of spring
x' = $L - x$
β = phase angle
γ = specific weight of elastic rod
η = constant with dimension of one over length
λ = nondimensional ratio
ξ = constant with dimension of one over length
ρ = density of elastic rod
Σ = summation
ω = angular velocity

Dots indicate differentiation with respect to time.

Introduction

The importance of acceleration measurement in the study of mechanics has been widely recognized. The ordinary spring-mass accelerometer has been used satisfactorily to measure steady-state accelerations with frequencies under 70 per cent of the natural frequency of the instrument (1).[2] The sensitivity of the instrument is inversely proportional to the square of the natural frequency of the accelerometer, so a high frequency usually results in a greatly reduced sensitivity (2). The responses to transient motions, like single sine wave, triangular and square pulses, have been analyzed for an accelerometer with the spring mass neglected (2, 3). In practice the spring-mass accelerometers, including crystal accelerometer (4), in certain instances, have not been able to give responses of adequate reliability for transient motions involving motions of high-frequency harmonics like impacts and shocks of very short duration.

Efforts have been made to develop peak accelerometers to record the maximum acceleration occurring during a transient motion. The commonly used peak accelerometers are the crusher gage, the contact accelerometer, the indenter gage, and so on (5). None of these has yet been able to respond, with adequate accuracy, to various transient accelerations. The crusher and the indenter types involve plastic deformation, which varies with rate of loading. Hence under different rate of loading, these two types will give different readings for the same maximum acceleration. The contact-break type (5) has no plastic deformation and has higher natural frequency than the contact-make type for the same spring and top mass and is, therefore, chosen for the present study.

The contact-break accelerometer consists of a mass on a spring attached to a case, Fig. 1. The case is fastened to the body whose acceleration is being measured. The top mass is pushed down by a setscrew preloading the spring. The break of contact indicates that the acceleration exceeds the preset value. By varying the preset value, the maximum acceleration of the motion can be determined. Although this instrument has been developed for some time, it is still rather unreliable for measuring transient accelerations of high frequencies. Contact-break accelerometers have been used to give acceleration-time curves (6). The application of the present study is not restricted to peak acceleration measurement but also may be applied to improve those contact accelerometers giving acceleration-time curves.

Analysis of Responses to Steady-State Motions

In the following analysis of contact-break accelerometers, the distributed mass of the spring is considered, so the dynamic sys-

[1] Professor of Aeronautical Engineering, University of Detroit; now Professor of Engineering, University of California, Los Angeles, Calif.

Presented at the National Applied Mechanics Conference, Urbana, Ill., June 14–16, 1956, of The American Society of Mechanical Engineers.

Discussion of this paper should be addressed to the Secretary, ASME, 29 West 39th Street, New York, N. Y., and will be accepted until October 10, 1956, for publication at a later date. Discussion received after the closing date will be returned.

Note: Statements and opinions advanced in papers are to be understood as individual expressions of their authors and not those of the Society. Manuscript received by ASME Applied Mechanics Division, January 3, 1955. Paper No. 56—APM-3.

[2] Numbers in parentheses refer to the Bibliography at the end of the paper.

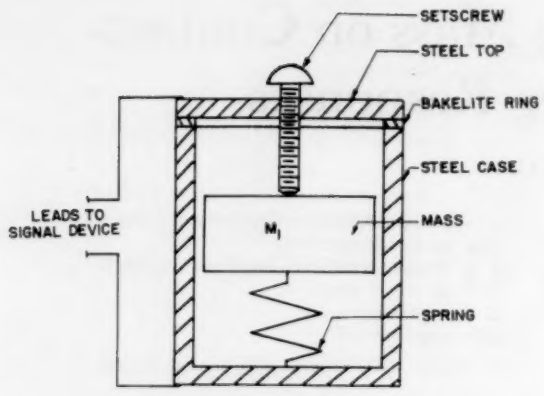

FIG. 1 CONTACT-BREAK ACCELEROMETER

tem no longer can be considered as having a single degree of freedom. In a contact-break accelerometer, there is no relative motion between the top mass and the instrument case, but different parts of the spring do have relative motion with respect to the case. Viscous damping (7) is assumed to exist between the spring and the case.

The differential equation of motion of a differential element of the spring can be written as

$$EA\frac{\partial^2 u}{\partial x^2}dx = \frac{\gamma A}{g}\frac{\partial^2 u}{\partial t^2}dx + c\left(\frac{\partial u}{\partial t} - \frac{\partial u_{x=0}}{\partial t}\right)dx \quad [1]$$

where the left-hand term corresponds to the differential stress in the spring and the right-hand terms correspond to the inertia and the viscous forces. This differential equation is linear, so the principle of superposition can be applied. The term $u_x = 0$ can be expressed in Fourier series if the series is differentiable to obtain

$$\frac{\partial u_{x=0}}{\partial t}$$

This requires the motion to be continuous and its derivative with respect to time to be sectionally continuous (8).

With this condition satisfied, the acceleration can be measured reliably if the following two conditions are fulfilled (9, 10): (*a*) The response to a simple harmonic motion must be proportional to the acceleration of this motion and the constant of proportionality must be the same for all the Fourier terms present in the steady-state motion. (*b*) The phase-angle lag of any particular frequency must be proportional to that frequency to give constant time lag for motions of all frequencies. In the following, these two conditions are used as a measure of the reliability of the instrument under steady-state motions.

Substituting $u_{x=0} = A_0 \sin \omega t$ for simple harmonic motions in Equation [1]

$$\frac{\partial^2 u}{\partial x^2} - \frac{\gamma}{Eg}\frac{\partial^2 u}{\partial t^2} - \frac{c}{EA}\frac{\partial u}{\partial t} = -\frac{c}{EA}A_0\omega\cos\omega t \quad [2]$$

The solution of Equation [2] (11) gives

$$u = \sum_{n=1}^{\infty} B_n(e^{ip_n t \pm q_n x} + e^{ip_n t \pm q_n x'}) + \frac{A_0}{1+V^2}\sin\omega t - \frac{A_0 V}{1+V^2}\cos\omega t \quad [3]$$

where

$$V = \frac{A\gamma\omega}{cg}, \quad x' = L - x \quad \text{and} \quad q_n = \xi_n + i\eta_n$$

Expressing Equation [3] in trigonometric series, and simplifying

$$u = F[e^{-\xi x}\sin(\omega t - \eta x) + e^{-\xi x'}\sin(\omega t - \eta x')] + G[e^{-\xi x}\cos(\omega t - \eta x) + e^{-\xi x'}\cos(\omega t - \eta x')] + \frac{A_0}{1+V^2}(\sin\omega t - V\cos\omega t) \quad [4]$$

where

$$F = \frac{A_0 V}{1+V^2}\,\frac{V(1+e^{-\xi L}\cos\eta L) - e^{-\xi L}\sin\eta L}{(1+e^{-\xi L}\cos\eta L)^2 + e^{-2\xi L}\sin^2\eta L}$$

$$G = \frac{A_0 V}{1+V^2}\,\frac{(1+e^{-\xi L}\cos\eta L) + Ve^{-\xi L}\sin\eta L}{(1+e^{-\xi L}\cos\eta L)^2 + e^{-2\xi L}\sin^2\eta L}$$

Differentiating Equation [4] $(\partial u/\partial x)_{x=L}$ can be expressed in the following form

$$\left(\frac{\partial u}{\partial x}\right)_{x=L} = N_1\sin\omega t + N_2\cos\omega t \quad [5]$$

The contact breaks when

$$EA\left[e_0 - \left(\frac{\partial u}{\partial x}\right)_{x=L}\right] \gtrless M_1\left(\frac{\partial^2 u}{\partial t^2}\right)_{x=L} \quad [6]$$

Before the contact breaks

$$\left(\frac{\partial^2 u}{\partial t^2}\right)_{x=L} = \left(\frac{\partial^2 u}{\partial t^2}\right)_{x=0} = -A_0\omega^2\sin\omega t$$

From Equations [5] and [6], the contact breaks when

$$EAe_0 \gtrless (EAN_1 - M_1A_0\omega^2)\sin\omega t + EAN_2\cos\omega t \gtrless Q\sin(\omega t - \beta) \quad [7]$$

where

$$Q = M_1A_0\omega^2\left[\left(\frac{EAN_2}{M_1A_0\omega^2}\right)^2 + \left(\frac{EAN_1}{M_1A_0\omega^2} - 1\right)^2\right]^{1/2}$$

$$\tan\beta = -\frac{EAN_2}{EAN_1 - A\omega^2M_1} \quad [8]$$

Let the ratio

$$R = \frac{EAe_0}{\left(M_1 + \frac{M_2}{2}\right)a_{peak}} \quad [9]$$

where a_{peak} is the minimum acceleration occurring in the given motion required to break the contact. For constant acceleration as given by a centrifuge in calibrating the accelerometer, R equals unity. For simple harmonic motions the ratio

$$R = \frac{EAe_0}{\left(M_1 + \frac{M_2}{2}\right)A_0\omega^2} \quad [10]$$

The deviation of R from unity is an indication of the error involved in measuring the peak acceleration of the motion.

The responses of a particular contact-break accelerometer, with distributed spring mass and distributed damping, to simple harmonic motions were calculated. The spring mass was taken to be equal to the top mass. The distributed damping for the whole spring length was taken to be equal to the critical damping

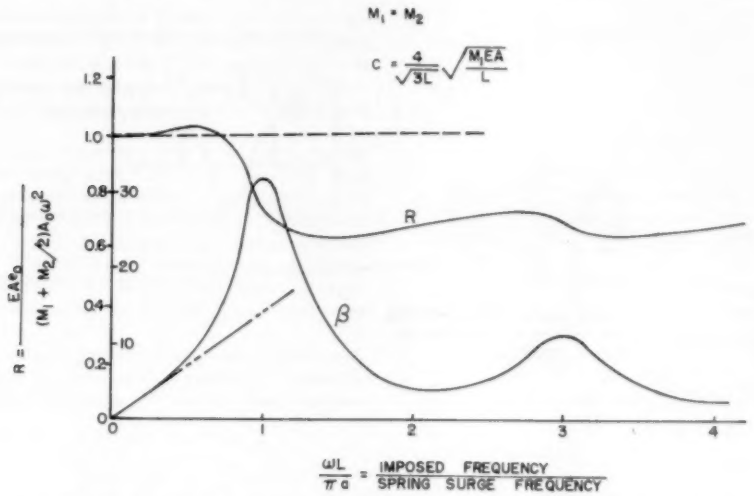

FIG. 2 RESPONSE CURVES OF A CONTACT ACCELEROMETER WITH DISTRIBUTED VISCOUS DAMPING UNDER SIMPLE HARMONIC MOTION

in a spring-mass system of single degree of freedom. The ratio R and the phase-lag angle β versus the ratio of the applied frequency to the spring-surge frequency are shown in Fig. 2. It is seen that, for this particular instrument, R is nearly constant and β varies linearly with the frequency ratio until this ratio reaches about 0.7. Therefore this instrument will indicate, with adequate accuracy, the peak accelerations of steady-state motions with the frequency ratios less than 0.7. Motions involving higher frequencies may introduce serious error. As the spring mass approaches zero, i.e., γ approaches zero, Equations [3] and [4] give V, F, and G all equal to zero. Equation [4] reduces to

$$u = A_0 \sin \omega t, \quad \left(\frac{\partial u}{\partial x}\right)_{x=0} = 0, \quad N_1 = N_2 = 0$$

Equations [7] and [8] give $R = 1$ and $\beta = 0$. This shows that the accuracy of the instrument improves as the spring mass is made small compared to the end mass.

RESPONSES TO TRANSIENT MOTIONS

In the analysis of responses to transient motions, no distributed damping between the spring and the case is considered, so Equation [2] reduces to

$$a^2 \frac{\partial^2 u}{\partial t^2} = \frac{\partial^2 u}{\partial x^2} \quad \ldots\ldots [11]$$

Transient acceleration of a single cosine wave, Fig. 3, is analyzed. This acceleration can be represented by the displacement function

$$u = 0 \quad \text{when} \quad 0 > t > \frac{2\pi}{\omega}$$

$$u = A_0(1 - \cos \omega t) \quad \text{when} \quad 0 < t < \frac{2\pi}{\omega}$$

Let $$u_{x=0} = u_{1(x=0)} + u_{2(x=0)} \quad \ldots\ldots [12]$$

where $$u_{1(x=0)} = -A_0(1 - \cos \omega t) \quad \text{for} \quad t \lesseqgtr 0$$

$$u_{1(x=0)} = 0 \quad \text{for} \quad t > 0 \quad \ldots\ldots [13]$$

$$u_{2(x=0)} = A_0(1 - \cos \omega t) \quad \text{for} \quad t \lesseqgtr \frac{2\pi}{\omega}$$

$$u_{2(x=0)} = 0 \quad \text{for} \quad t > \frac{2\pi}{\omega} \quad \ldots\ldots [14]$$

For $t \lesseqgtr 0$, the solution of Equation [11] with the end condition of $u_{1(x=0)} = -A_0(1 - \cos \omega t)$ gives

$$u_1 = -A_0 \left[1 - \left(\frac{1 - \cos \lambda}{\sin \lambda} \sin \frac{\lambda x}{L} + \cos \frac{\lambda x}{L}\right) \cos \omega t\right] \ldots [15]$$

where

$$\lambda = \frac{L\omega}{a}$$

If at $t = 0$ the applied motion suddenly ceases, $u_{1(x=0)} = 0$ for $t \geq 0$. The different parts of the spring, however, will still have motion after the applied motion ceases. The series satisfying the differential Equation [11] and the foregoing conditions are given as

$$u_1 = \sum_{n=1}^{\infty} A_n \sin \frac{n\pi x}{L} \cos \frac{n\pi a t}{L} \quad \ldots\ldots [16]$$

Equating Equation [15] to Equation [16] at $t = 0$

$$\Sigma A_n \sin \frac{n\pi x}{L} = -A_0 \left[1 - \left(\frac{1 - \cos \lambda}{\sin \lambda} \sin \frac{\lambda x}{L} + \cos \frac{\lambda x}{L}\right)\right] \ldots [17]$$

The coefficient A_n is found by multiplying Equation [11] by

$$\sin \frac{m\pi x}{L} \, dx$$

and integrating from 0 to L. Substituting A_n in Equation [16]

$$u_1 = -\Sigma 2A_0 \frac{[(-1)^n - 1]\lambda^2}{n\pi(n^2\pi^2 - \lambda^2)} \sin \frac{n\pi x}{L} \cos \frac{n\pi a t}{L} \quad \text{for} \quad t > 0 \ldots [18]$$

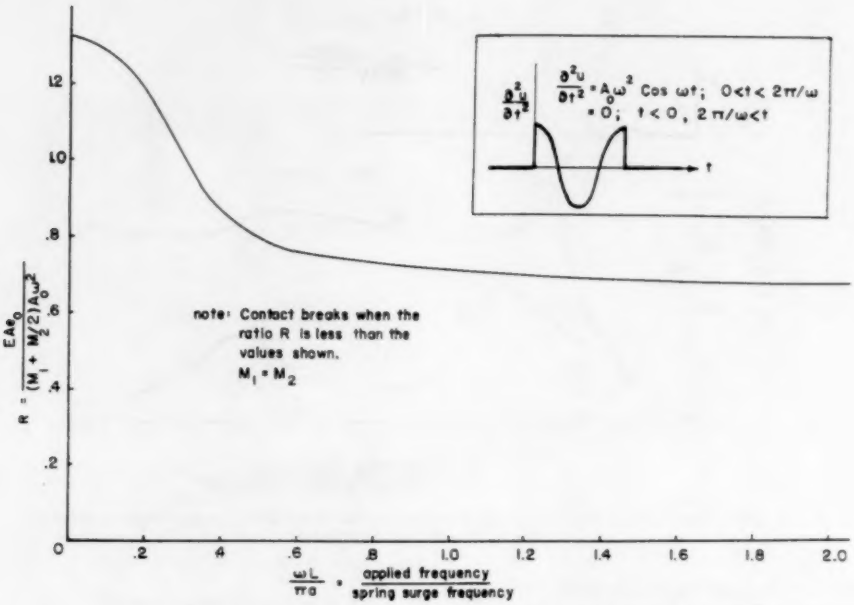

FIG. 3 RESPONSE TO TRANSIENT ACCELERATIONS OF SINGLE COSINE WAVES

Similarly

$$\left.\begin{aligned} u_2 &= A_0\left[1 - \left(\frac{1-\cos\lambda}{\sin\lambda}\sin\frac{\lambda x}{L} + \cos\frac{\lambda x}{L}\right)\cos\omega t\right] \quad \text{for} \quad t < \frac{2\pi}{\omega} \\ u_2 &= \Sigma 2A_0 \frac{[(-1)^n - 1]\lambda^2}{n\pi(n^2\pi^2 - \lambda^2)} \sin\frac{n\pi x}{L} \cos\frac{n\pi(\omega t - 2\pi)}{\lambda} \quad \text{for} \quad t > \frac{2\pi}{\omega} \end{aligned}\right\} \ldots [19]$$

$$u = u_1 + u_2$$

For $$0 < t < \frac{2\pi}{\omega}$$

$$u = -\Sigma 2A_0 \frac{[(-1)^n - 1]\lambda^2}{n\pi(n^2\pi^2 - \lambda^2)} \sin\frac{n\pi x}{L} \cos\frac{n\pi a t}{L} + A_0\left[1 - \left(\frac{1-\cos\lambda}{\sin\lambda}\sin\frac{\lambda x}{L} + \cos\frac{\lambda x}{L}\right)\cos\omega t\right] \ldots\ldots [20]$$

From Equations [6] and [20], the contact breaks when

$$\frac{EAe_0}{M_1A_0\omega^2} \leq \left(1 + \frac{M_2}{M_1\lambda}\tan\frac{\lambda}{2}\right)\cos\omega t - \frac{M_2}{M_1\pi^2}\sum_{1,3,5\ldots} \frac{4}{n^2 - \left(\frac{\lambda}{\pi}\right)^2}\cos\frac{n\pi\omega t}{\lambda} \ldots\ldots [21]$$

For $t > \frac{2\pi}{\omega}$

$$u = \Sigma 2A_0 \frac{[(-1)^n - 1]}{n\pi(n^2\pi^2 - \lambda^2)} \sin\frac{n\pi x}{L} \left[\cos\frac{n\pi(\omega t - 2\pi)}{\lambda} - \cos\frac{n\pi\omega t}{\lambda}\right] \ldots\ldots [22]$$

and the contact breaks when

$$\frac{EAe_0}{M_1A_0\omega^2} \geq \frac{M_2}{M_1}\frac{4}{\pi^2}\sum_{1,3,5\ldots} \frac{1}{n^2 - \left(\frac{\lambda}{\pi}\right)^2} \cdot \left[\cos\frac{n\pi(\omega t - 2\pi)}{\lambda} - \cos\frac{n\pi\omega t}{\lambda}\right] \ldots\ldots [23]$$

When ω approaches zero, the motion approaches to a step function of constant acceleration. The responses to this type of transient motions are shown in Fig. 3. It is seen that the ratio R deviates considerably from unity and hence will introduce considerable error in peak acceleration measurement. From Equation [21], as M_2 approaches zero, the ratio R approaches unity. Hence the accuracy of the instrument will be greatly increased if the spring mass is zero.

Transient acceleration of a damped free vibration also has been studied. A contact accelerometer was mounted on the free end of a long aluminum-alloy cantilever beam. The free end was raised and then released. This gives a free vibration with air damping. The acceleration-time curve was measured by a Statham accelerometer with a natural frequency much higher than that of the beam. The initial raising of the free end of the beam was adjusted so as to give break of contact only in the first cycle of vibration. The amount of damping was calculated from the acceleration-time curve given by the Statham accelerometer. Theoretical responses to these damped free vibrations were calculated (12). The discrepancy between the theoretical and the experimental values is about 10 per cent (12).

PRELIMINARY STUDY OF ELECTROMAGNETIC-CONTACT ACCELEROMETER

As shown in the foregoing, the errors in the responses of the contact-break accelerometer under steady-state and transient motions are mainly due to dynamic effects of the spring mass. In order to eliminate the spring mass, an electromagnetic type, Fig. 4, is proposed. An electromagnet replaces the mechanical

spring and the electromagnetic force replaces the spring compression. A permanent magnet is not used because its magnetic strength may change under shock. The electromagnetic force can be regulated by adjusting the current in the winding. This is equivalent to a massless spring, hence the error due to spring mass is eliminated.

The gap required to operate a neon bulb as an indicating device (6) has been found to be of the order of 10^{-4} in. This value can be reduced if a contact indicator with 6E5 "magic-eye" radio tube is used (5). As soon as the contact breaks, the magnetic force on the mass, instead of increasing as in the case of mechanical spring, decreases. This will help to accelerate the mass to obtain the required gap. Limited tests have been run on this type of electromagnetic accelerometer and the results are favorable as shown in Fig. 5.

It seems that the electromagnetic-contact accelerometer may be used to indicate the acceleration at a particular instant by rapidly decreasing the magnetizing current and hence the electromagnetic force. When the electromagnetic force is equal to or less than the inertia force of the mass, the contact breaks. This inertia force and hence the acceleration at the instant of break is indicated by the magnetizing current at that instant. This gives a single point in the acceleration-time curve. In order to get more points on the curve a number of units may be electrically controlled to work successively or a few units can be made to operate repeatedly. In this way, acceleration-time curves may be obtained. This gives the basic idea for this type of accelerometer. Considerable amount of study is required for its practical design and construction.

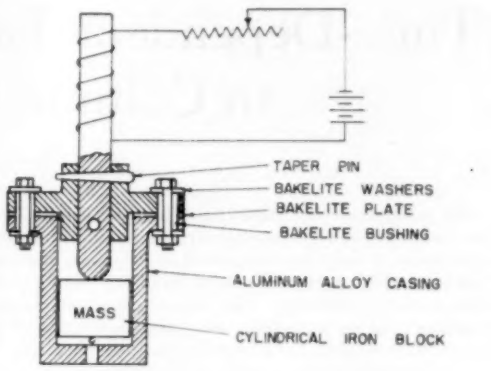

FIG. 4 MAGNETIC-TYPE CONTACT ACCELEROMETER

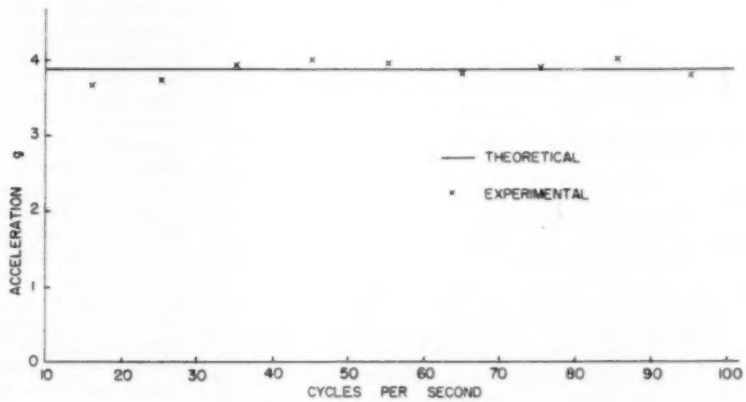

FIG. 5 EXPERIMENTAL RESPONSES OF ELECTROMAGNETIC-CONTACT ACCELEROMETER

ACKNOWLEDGMENT

The author wishes to express his gratitude to Prof. J. Ormondroyd of the University of Michigan for his invaluable advice, suggestions, and criticism.

BIBLIOGRAPHY

1 "An Instrument for Measuring Low Frequency Accelerations in Flight," by C. S. Draper and W. Wrigley, *Journal of the Aeronautical Sciences*, vol. 7, July, 1940, pp. 388–401.

2 "Design and Application of Accelerometers," by D. E. Weiss, Proceedings of the Society for Experimental Stress Analysis, vol. 4, no. 2, 1947, pp. 89–102.

3 "Response of Accelerometers to Transient Accelerations," by S. Levy and W. D. Kroll, *Journal of Research of National Bureau of Standards*, vol. 45, October, 1950, pp. 303–309.

4 "Anomalous Transient Response of a Crystal Pick-Up," by P. M. Honnell, *Journal of the Acoustical Society of America*, vol. 25, May, 1953, pp. 570–574.

5 "Handbook of Experimental Stress Analysis," by M. Hetényi, et al., John Wiley & Sons, Inc., New York, N. Y., 1950, pp. 368–377, 673.

6 "A Proposed Spring Accelerometer for Shock and Impact Measurements," by D. E. Hudson and O. D. Terrell, Proceedings of the Society for Experimental Stress Analysis, vol. 9, no. 1, 1950, pp. 1–10.

7 "Steady Forced Vibrations as Influenced by Damping," by L. S. Jacobsen, JOURNAL OF APPLIED MECHANICS, Trans. ASME, vol. 52 (1), 1930, Paper APM—52-15.

8 "Fourier Series and Boundary Value Problems," by R. V. Churchill, McGraw-Hill Book Company, Inc., New York, N. Y., 1941, p. 78.

9 "Significance of Mechanical Shock Measurements by Peak Reading Instruments," by I. Vigness, Symposium on Shock and Vibration Instrumentation at the Seventeenth Applied Mechanics Division Conference of THE AMERICAN SOCIETY OF MECHANICAL ENGINEERS, 1952.

10 "The Single Degree of Freedom System in Motion Measurement," by R. Rosenbaum, Symposium on Shock and Vibration Instrumentation at the Seventeenth Applied Mechanics Division Conference of THE AMERICAN SOCIETY OF MECHANICAL ENGINEERS, 1952.

11 "Partial Differential Equations," by H. Bateman, Dover Publications, New York, N. Y., 1944, p. 227.

12 "Response of a Contact Accelerometer Under Steady State and Transient Motions," by T. H. Lin, Doctoral Thesis at the University of Michigan, February, 1953.

Time-Dependent Tangent Modulus Applied to Column Creep Buckling

By R. L. CARLSON,[1] COLUMBUS, OHIO

The relation of the time-dependent tangent-modulus load—as conceived by Shanley—to actual column capacity is clarified. It may be interpreted as a limiting case of the "allowable-load capacity" which has been shown to be a conservative estimate. The time-dependent tangent-modulus load is, therefore, an approximation to a conservative estimate. The approximation, however, may be either conservative or nonconservative when applied to imperfect or real columns. Typical cases are discussed and experimental results for two alloys are cited.

Introduction

THE creep of engineering materials has been recognized for many years as a factor which must be considered in design. Numerous design rules and procedures have been advanced to account for effects of creep, and many machines and structures have been designed to operate at elevated temperatures. Designing to allow for creep is not, therefore, a new problem.

In recent years, this problem has, however, assumed a new importance. Formerly, this problem involved primarily stationary units for which a conservative design was not only desirable, but also allowable. With the advent of high-speed aircraft and missiles, however, it became apparent that a different philosophy of design was necessary. Added weight here meant decreased efficiencies, which could not be tolerated.

One of the high-temperature design problems that has become the subject of increasing interest during the past seven years is the creep buckling of columns. It is upon this problem that the investigation summarized by this paper was based.

Apparently the first treatment of the problem was given by Marin (1)[2,3] in 1947. His analysis was essentially based on earlier work by MacCullough (2) on the creep bending of beams, and it considered secondary or steady-state creep only.

Since that time, progress has evolved along two lines of approach. In the one approach, material response is described by the use of viscoelastic elements. Solutions of this type have been made by Freudenthal (3), Hilton (4), Rosenthal and Baer (5), and Kempner (6). The main advantage of this approach is that it results in mathematically solvable equations. The principal disadvantage is that many real materials do not obey the idealized response models. It is, nevertheless, quite possible that such solutions will prove useful for some materials, and they also may provide a starting point for the development of solutions for materials with more complex behaviors.

The second type of approach has consisted of attempts to devise methods that emphasize the use of real, rather than idealized, material-response behavior. Because this can often be done only by the use of complex empirical relations, simple mathematical solutions are possible only for a column with an idealized two-flange cross section. For solid cross sections, these methods require lengthy step-by-step-type computations.

Several methods of analyzing creep buckling according to this second type of approach have been presented within the past three years. Two of these methods, by Higgins (7) and by Libove (8), are devoted to attempts to determine the curve of deflection versus time. Although both utilize a deformation law suggested by Shanley (9), the procedures of the analyses are different. Essentially, however, both attempt to describe actual column-creep behavior.

In contrast to these methods, which are intended to be "exact" (this word is used with reservation, because engineering-type assumptions which made solution possible were made), a few attempts have been made to establish approximate methods that could be used to describe creep buckling. These methods have one common ingredient, and that is that they use isochronous stress-strain curves in some form. The first to suggest such an approach was Shanley (10). He reasoned that tangents to iso-stress-strain curves may be used as approximate stress distributions,[4] and that the time at which instability would occur for an initially perfect column might be estimated by the tangent-modulus load criterion, as interpreted by himself (11). Such a load, he anticipated, may be allowable or safe for the time for which the determination is made.

Independently, and by different means of analysis, the author (12) and Rosenthal (13) explored the possibility of using curve segments of, rather than tangents to, iso-stress-strain curves to represent approximate stress distributions.[5] The author (12) showed that these approximations were allowable or safe estimates. He also indicated that the time-dependent tangent-modulus load, as conceived by Shanley (10), would not necessarily always be allowable or safe for real columns. This fact was also noted by Rosenthal (13). Since there appears to be a need for a clearer interpretation on this point, this will be discussed in more detail in the body of this paper.

Discussion

Recently (12), the relation between approximate stress distributions derived from isochronous stress-strain curves and the actual stress distributions for columns subject to creep was discussed. Since some of the ramifications of this approximate approach were not explicity discussed, it is felt that a more detailed discussion is appropriate. Before beginning, however, a brief review of the basis for the method will be given. In this review,

[1] Assistant Chief, Metallurgical Engineering Division, Battelle Memorial Institute.

[2] Numbers in parentheses refer to the Bibliography at the end of the paper.

[3] Subsequent to the preparation of this paper, it was brought to the attention of the author that A. D. Ross, in *The Structural Engineer*, for August, 1946, discussed a possible method of accounting for creep effects in columns.

Presented at the National Applied Mechanics Conference, Urbana, Ill., June 14–16, 1956, of The American Society of Mechanical Engineers.

Discussion of this paper should be addressed to the Secretary, ASME, 29 West 39th Street, New York, N. Y., and will be accepted until October 10, 1956, for publication at a later date. Discussion received after the closing date will be returned.

Note: Statements and opinions advanced in papers are to be understood as individual expressions of their authors and not those of the Society. Manuscript received by ASME Applied Mechanics Division, August 8, 1955. Paper No. 56—APM-13.

[4] Shanley's discussion dealt with an idealized, two-flange column model.

[5] These considerations dealt with actual, rather than model columns.

reference to Fig. 1 will be helpful. The $t = 0$ line is the elastic stress-strain curve, and the t_i curve is the iso-stress-strain curve for the time t_i. That is, for example, the amount of creep occurring during the time t_i at the stress σ_D is given by D—G.

In discussing column stress distributions, it will be convenient to consider one cross section of a column of given dimensions and imperfection. The cases considered are only those for which the load has produced an initial stressing which is elastic throughout.

If a load is applied to the given column, the initial stress distribution can be illustrated by the use of the compression stress-strain diagram of column material. In Fig. 1, the ordinate B—A represents the stress on the convex side of the column, and D—C represents the stress on the concave side. The ordinates along B—D represent intermediate, initial-stress values.

As can be seen, the stresses are sufficiently large to cause creep. The nonuniform stress distribution will, moreover, cause nonuniform creep, which, in turn, will result in an increase in the column deflection. To maintain an internal and external-moment balance, the stresses must readjust. To satisfy the requirement for a larger internal moment, the stress σ_D will increase, and, since the external load remains constant, the stress σ_B will decrease. If, after a finite time t_i, σ_D increases to σ_D', and σ_B decreases to σ_B', the stress-strain points will move to D' and B', respectively. This can be shown to be true by using extreme paths of change. For σ_D, for example, these are D—G—E and D—H—F (reference 12).

Since D' and B' represent the end points of the stress distribution for the time t_i, a curve connecting them, such as shown dashed, describes the actual stress distribution at t_i.

As can be seen, the stress-distribution curve is more steeply inclined than the t_i curve in the region of the average stress σ_A. If, now, a segment of the t_i curve was to be used as an approximation[6] to the real stress distribution B'—D', it would appear as

[6] Force and moment balance requirements must, of course, be satisfied, and these would determine the end points of the approximate stress distribution.

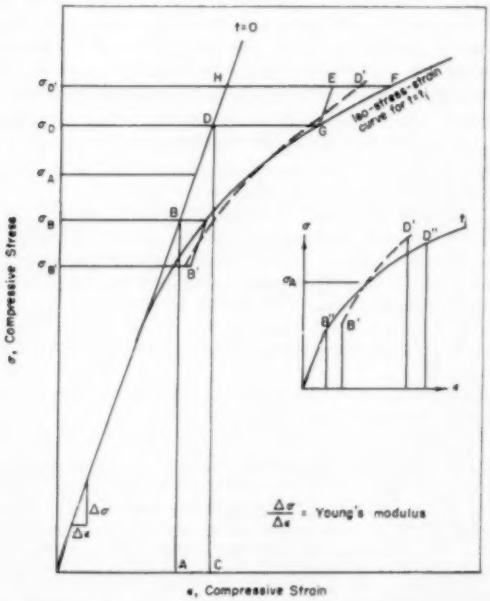

FIG. 1 GRAPHIC REPRESENTATION OF STRESS DISTRIBUTION ACTING ON A COLUMN CROSS SECTION

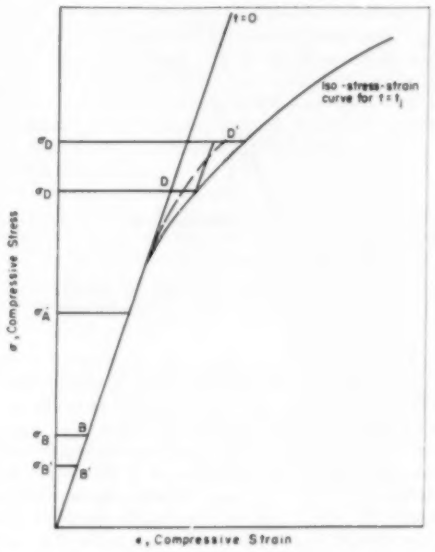

FIG. 2 GRAPHIC REPRESENTATION OF STRESS DISTRIBUTION

B''—D'' in the inset of Fig. 1. As can be seen, the use of the approximate stress distribution would indicate that the column was less stiff than it actually is. This property of the iso-stress-strain curves then forms the basis for a means of estimating allowable-column-load capacities.

Before proceeding, it should be emphasized that, whereas the use of the t_i segment will yield conservative estimates, the use of the tangent to the t_i curve will not necessarily be conservative, as anticipated by Shanley (10). To show this, an example advanced by Rosenthal (13) will be used. In Fig. 2, the diagram of Fig. 1 is repeated, except that the average column stress σ_A is now below the lowest stress for which creep can occur.[7] As can be seen, the tangent at σ_A remains unchanged, in spite of the fact that the column can creep under the stress σ_D on the concave face. As also can be seen, the t_i segment is, however, still less steep than the real stress distribution B'—D', and it can, hence, be used as a basis for a conservative estimate.

It should be noted that, in this example, it is probably necessary that the initial imperfection be sufficiently large for collapse to occur eventually. It may be that, for column imperfections normally encountered, the average stress of the example may be below values for which eventual collapse can occur.[8] Nevertheless, the example serves to indicate that the role of the time-dependent tangent-modulus load derived from iso-stress-strain curves should be more clearly interpreted. An attempt will be made in this paper to clarify this point.

Before discussing the relation of the time-dependent tangent-modulus load to actual creep-buckling loads, however, a review of the method for estimating these load capacities by the use of iso-stress-strain-curve segments will be given, because it is pertinent to the discussion.

Earlier in this discussion, it was indicated that such segments

[7] It may be argued that no such lower limit exists, and that creep will always occur for a finite stress. Even if this were true, however, cases in which the creep was not sufficient to modify the tangent significantly could certainly be found.

[8] Experimental evidence (12) indicates that there may be, for each column slenderness ratio and imperfection, a lower load limit below which collapse will not occur. This possibility needs to be examined more thoroughly, however.

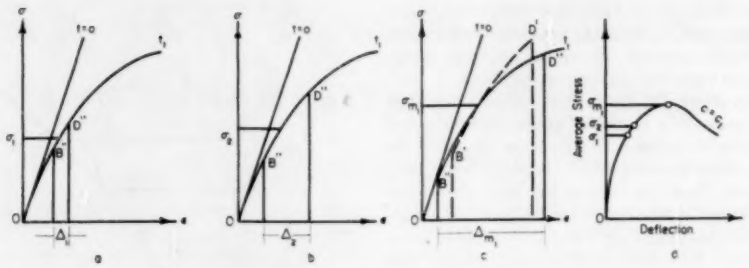

FIG. 3 GRAPHIC REPRESENTATION OF PROCEDURE FOR COMPUTING APPROXIMATE STRESS DISTRIBUTIONS FROM THE t_1 ISO-STRESS-STRAIN CURVE

could be used to obtain a conservative description of the creep behavior of columns. To illustrate how this actually may be accomplished, an answer to the following question will be given.

For a column of a given slenderness ratio $L/r = R_1$ and initial imperfection $c = c_1$, what is the maximum-load-capacity estimate that can be obtained for the time $t = t_1$ by using t_1 iso-stress-strain-curve segments as approximate stress distributions?[9]

A procedure which can be followed to obtain the foregoing value can best be illustrated by reference to Fig. 3 in the following discussion. Only the essential features will be considered here, as details of actual computations of this type can be found in references (12, 14, 15).

The basis for the computation is derived from a consideration of the condition for equilibrium; that is, force and moment balance requirements must be satisfied. These can be summarized for a given cross section by the equation

$$y = \frac{M}{P} \quad \ldots\ldots\ldots\ldots\ldots\ldots\ldots\ldots [1]$$

where y = total deflection resulting from initial imperfection and bending due to the column load, M = bending moment, P = column load.

The values of M and P can be shown (14, 15) to be given by integrals associated with the stress distribution, as illustrated in Fig. 1 by the curves B—D, B'—D', and B^v—D^v; M is the internal moment and P is the internal force associated with each distribution.

To find the maximum average stress for the given column from the t_1 curve, one can take a sequence of trial values $\sigma_1, \sigma_2, \ldots \sigma_a$ and satisfy Equation [1] for each value. In Fig. 3(*a*), for example, B^v—D^v illustrates a segment which satisfies Equation [1]. The location of B^v and D^v can be determined by evaluating Equation [1] for trial positions. Only correct locations will balance the equation.

Insets *a*, *b*, and *c* illustrate the process for successive values of average stress. In Fig. 3(*d*) the sequence of average stresses has been plotted as a function of the deflection due to the load.[10] As can be seen, the trial values of average stress rise to a maximum and then fall.[11] For the time t_1, then σ_{m_1} represents, for the given column, the highest average stress than can be obtained using a segment of the t_1 iso-stress-strain curve as an approximate stress distribution. For purposes of comparison, the actual stress distribution, B'—D', at the time t_1 for the average stress σ_{m_1} is shown dashed in Fig. 3(*c*).

[9] For reasons noted earlier, the actual column will be more "stiff" than indicated by the approximation for a given average stress.

[10] The deflection is a function of the strain difference Δ (references 14, 15).

[11] This characteristic behavior is to be expected, because the computation procedure followed is simply that used to compute maximum column loads (14, 15).

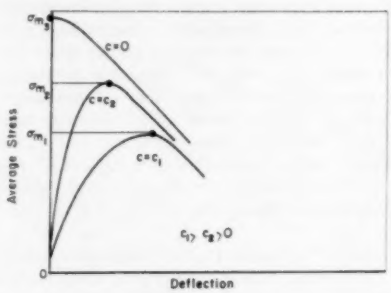

FIG. 4 VARIATION OF MAXIMUM ALLOWABLE AVERAGE STRESS WITH COLUMN IMPERFECTION FOR TIME t_1

The procedure just outlined can now be seen to have been merely a device by means of which it was possible to obtain the maximum allowable estimate of the load capacity of the given column for the time t_1.

To determine the relationship between these conservative or allowable-load-capacity estimates and the so-called time-dependent tangent-modulus load, it is useful to refer to a diagram similar to that of Fig. 3(*d*). For this purpose, Fig. 4 has been constructed. In addition, now, to the estimate σ_{m_1} for an imperfection of c_1, an estimate σ_{m_2} for an imperfection of c_2 has been included. As indicated, c_2 is less than c_1. Also, an estimate σ_{m_3} for an imperfection of $c = 0$ is included. The value of σ_{m_3} corresponds to the time-dependent tangent-modulus load, as derived from the iso-stress-strain curve for the time t_1.

It is thus seen that the time-dependent tangent-modulus method can be interpreted as a limiting case of the allowable-load-capacity method. As the initial imperfection approaches zero, the load-capacity estimate approaches the time-dependent tangent-modulus load. This follows, because, as B and D (see Fig. 1) approach one another, B^v and D^v become closer, and a tangent to the t_1 curve at σ_A approaches the curve segment at that point.

To illustrate more clearly the relationship between the load-capacity approximations and the actual load capacity, the graph of Fig. 5 has been prepared. The graph shown is a plot of column average stress as a function of failure time for a given column slenderness ratio. To serve as reference values, the relative positions of the reduced or double-modulus load and the tangent-modulus load have been indicated. As von Karman has indicated (16), these can be considered as the upper and lower limits, respectively, of the critical load for an initially straight, axially loaded column.

The result of using tangents to iso-stress-strain curves to derive approximate load-capacity estimates is illustrated by the indi-

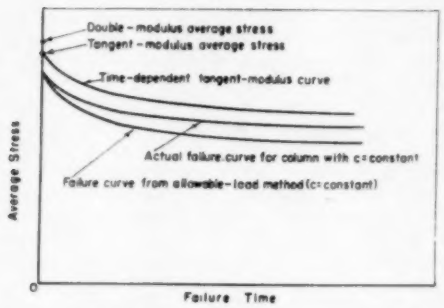

FIG. 5 RELATIVE POSITIONS OF ACTUAL AND APPROXIMATE COLUMN-FAILURE CURVES

cated curve. Since the time-zero iso-stress-strain curve coincides with the actual stress-strain curve, the curve intersects the average-stress axis at the value of the tangent-modulus load.

Consider, now, an imperfect column whose immediate-failure load is, as indicated, below the tangent-modulus load.[12] Since the time-failure curve corresponding to such a column starts below the tangent-modulus load, it seems reasonable to expect that, for a sufficiently large initial imperfection, it will remain below the time-dependent tangent-modulus time-failure curve throughout.

The lowest curve in the graph represents the time-failure curve obtained by using curve segments of the iso-stress-strain curve as approximate stress distributions. These estimates are, as indicated earlier, conservative for the given column. It should be noted that this curve intersects the actual time-failure curve on the average-stress axis. This again follows from the fact that zero-time iso-stress-strain curve coincides with the actual stress-strain curve.

The relationship between the two approximate methods of obtaining load-capacity estimates (the one using tangents and the other using curve segments) is made clear by Fig. 5. It also can be seen that the curves may lie fairly close to one another. The spacing will be established, of course, by the amount of imperfection present. In some instances, it is probable that the top two curves will intersect at some value of time. If this occurred, the time-dependent tangent-modulus load would be nonconservative up to that time, and conservative afterward.

APPLICATION

The mechanics of computing time-dependent tangent-modulus loads from isochronous stress-strain curves is quite simple. For ease of computation, the Euler formula

$$\sigma = \frac{\pi^2 E_T}{(L/r)^2}$$

where E_T is the time-dependent tangent modulus, can be rearranged to read

$$\frac{L}{r} = \pi \sqrt{\frac{E_T}{\sigma}}$$

To obtain a plot of stress σ versus slenderness ratio L/r for a given time, the most convenient procedure to follow is to construct a table in which the tangents corresponding to successive values of stress are entered. Using the foregoing formula, the slenderness ratio corresponding to each value of stress can then be computed. A curve of stress versus slenderness ratio for the given time can then be constructed by using the tabulated values. Curves for additional times can be constructed by the preparation of additional tables.

To illustrate the type of results that may be obtained by the use of the time-dependent tangent-modulus method, data from studies on two materials will be included in this discussion. The two materials are the aluminum alloy 2024-T4[13] in the "as-received" condition and the titanium alloy RC-130A. Since details of these studies are reported elsewhere (12, 19), only a summary of representative results will be given here.

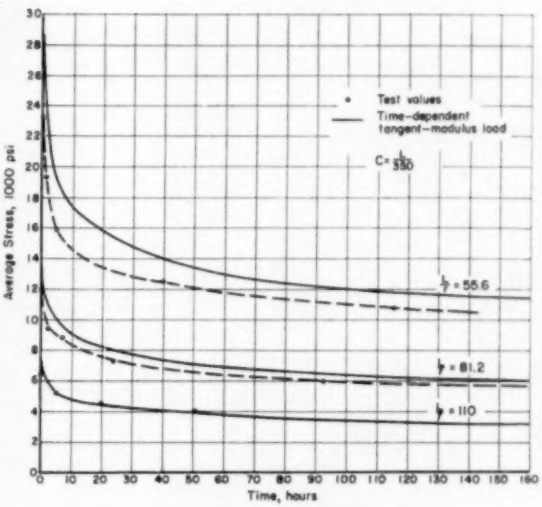

FIG. 6 AVERAGE STRESS VERSUS FAILURE TIME FOR 2024-T4 ALUMINUM ALLOY COLUMNS TESTED AT 450 F

Results for the aluminum alloy 2024-T4 are summarized in Fig. 6 by a plot of average stress versus failure time. The plotted points are test values for columns of rectangular cross section. The imperfection c of these columns was adjusted to be $c = L/350$. The solid curves in Fig. 6 were obtained by the use of the average stress versus slenderness ratio curves whose construction was described in the foregoing. It should be noted that tensile creep data were used to obtain the isochronous stress-strain curves from which the time-dependent tangent moduli were obtained. A limited number of compressive-creep tests (12) indicated, however, that for the temperature of 450 F, and the stress range of interest, the difference between tensile and compressive creep was not significant.

The results of Fig. 6 indicate that the predicted column capacities are greater for a given time than the test values. The possibility of such behavior is in accord with the interpretation given in the general discussion of the time-dependent tangent modulus. It will be remembered that it was indicated that predictions could be either conservative or nonconservative. It also is apparent, as indicated in that discussion, that if the value of imperfection had been smaller, say, $c = L/1000$, the experimental values would have been closer to, or perhaps above, the

[12] For imperfect "inelastic" columns, the immediate-failure load or maximum load can be greater than the tangent-modulus load (17, 18). As the column slenderness ratio increases, however, the maximum loads tend to become less than the tangent-modulus loads. The columns studied in this investigation were all within the "elastic" column range (large slenderness ratios), so the immediate-failure or maximum load can justifiably be picked to be less than the tangent-modulus load.

[13] This alloy was formerly identified as 24S-T4.

solid curve which does not, of course, reflect changes in values of imperfection and, therefore, remains fixed.

Results for the titanium alloy RC-130A are given in Fig. 7. In contrast to the results for the aluminum alloy, Fig. 7 indicates that the computed curve is conservative throughout. In comparing the experimental and computed curves, it should be noted that a significant part of the conservatism indicated can be attributed to error introduced by the use of tensile creep data. A limited amount of compression-creep data was obtained, and it was found that the resistance to creep is consistently less in tension than in compression (19). Estimates made by the use of the available compression-creep data indicate that approximately one half of the conservatism of the estimates is due to the use of tensile rather than compressive-creep data.

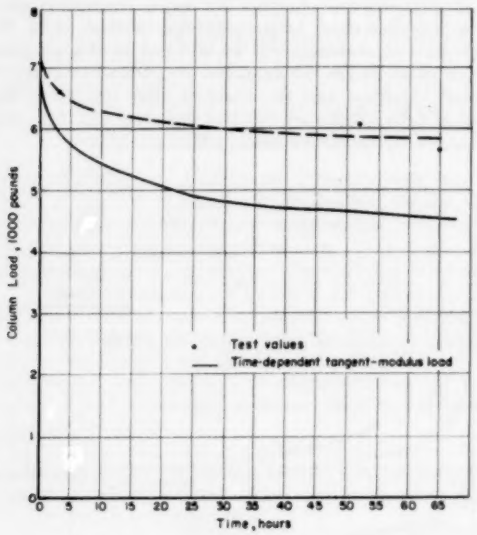

FIG. 7 COLUMN LOAD VERSUS FAILURE TIME AT 700 F FOR $L/r = 66$ (RC-130A)

In spite of the improvement that could be obtained by the use of compressive-creep data, the estimates of Fig. 7 would still be conservative. These data, then, are an example of the possible conservatism of the time-dependent tangent-modulus load estimates.

The imperfections of the test columns of Fig. 7 ranged from $e = 0.0010$ in. to $e = 0.0016$ in.[14] Had these values been larger, the curve for the experimental trend would have been lower, of course, and the conservatism would have been less. For sufficiently large values of imperfection, the experimental curve could drop below the computed curve in the manner observed in Fig. 6. This behavior is, as noted previously, in agreement with the interpretation given in the general discussion. The curves of Figs. 6 and 7 can, in fact, be recognized as possible variations of the corresponding curves of Fig. 5.

CONCLUSION

In this paper, the relation of the time-dependent tangent-modulus load—as conceived by Shanley—to actual column capacity has been clarified. It may be interpreted as a limiting case of the allowable-load capacity which has been shown to be a conservative estimate. The time-dependent tangent-modulus load is, therefore, an approximation to a conservative estimate. The approximation, however, may be either conservative or nonconservative.

Because the time-dependent tangent-modulus load is so easily computed, it offers promise as a means for obtaining engineering estimates of column-load capacity in spite of the fact that it may sometimes be nonconservative. It should be noted, moreover, that only a method that can account for column imperfection will be free of the possibility of nonconservatism. A method free from this possibility, however, will undoubtedly be relatively complex, so that its advantage will probably be at least partially offset.

[14] In terms of the definition previously used $e = L/860$ to $e = L/540$.

ACKNOWLEDGMENT

The work summarized in this paper was sponsored by the Materials Laboratory, Directorate of Research, Wright Air Development Center, under Contract No. AF 33(038)-9542.

BIBLIOGRAPHY

1 "Creep Deflections in Columns," by J. Marin, *Journal of Applied Physics*, vol. 18, January, 1947, pp. 103–109.

2 "An Experimental and Analytical Investigation of Creep in Bending," by G. H. MacCullough, JOURNAL OF APPLIED MECHANICS, Trans. ASME, vol. 55, 1933, Paper APM—55-9.

3 "The Inelastic Behavior of Engineering Materials and Structures," by A. M. Freudenthal, John Wiley & Sons, Inc., New York, N. Y., 1950.

4 "Creep Collapse of Viscoelastic Columns With Initial Curvature," by H. H. Hilton, *Journal of the Aeronautical Sciences*, vol. 19, 1952, p. 844.

5 "An Elementary Theory of Creep Buckling of Columns," by D. Rosenthal and H. W. Baer, Proceedings of the First U. S. National Congress of Applied Mechanics, ASME, 1952, pp. 603–611.

6 "Creep Bending and Buckling of Nonlinearly Viscoelastic Columns," by Joseph Kempner, NACA TN 3137, 1954.

7 "Weight-Strength Analysis of Aircraft Structures," by F. R. Shanley, McGraw-Hill Book Company, Inc., New York, N. Y., 1952, chapter 20, "Effect of Creep on Column Deflection," by T. P. Higgins, pp. 359–385.

8 "Creep-Buckling Analysis of Rectangular-Section Columns," by Charles Libove, NACA TN 2596, 1953.

9 F. R. Shanley, loc. cit., chapter 16.

10 F. R. Shanley, loc. cit., chapter 19.

11 F. R. Shanley, loc. cit., chapter 18.

12 "Investigation of Compressive-Creep Properties of Aluminum Columns at Elevated Temperatures, Part 2," by R. L. Carlson and G. K. Manning, WADC Technical Report 52-251, Part 2, 1954. See also "A Method for Estimating Allowable Load Capacities of Columns Subject to Creep," by R. L. Carlson and A. D. Schwope, Proceedings of the Second U. S. National Congress of Applied Mechanics, ASME, 1955, pp. 563–568.

13 WADC Technical Report 54-402 by D. Rosenthal and D. Hasanovitch, 1954.

14 "Theory of Elastic Stability," by S. Timoshenko, McGraw-Hill Book Company, Inc., New York, N. Y., 1936.

15 "Buckling Strength of Metal Structures," by F. Bleich, McGraw-Hill Book Company, Inc., New York, N. Y., 1952.

16 Discussion by Th. von Karman of "Inelastic-Column Theory," by F. R. Shanley, *Journal of the Aeronautical Sciences*, vol. 14, 1947, pp. 267–268.

17 "Bifurcation Criterion and Plastic Buckling of Plates and Columns," by C. E. Pearson, *Journal of the Aeronautical Sciences*, vol. 17, 1950, p. 417.

18 "The Effect of Initial Curvature on the Strength of an Inelastic Column," by T. W. Wilder, W. A. Brooks, and E. E. Mathauser, NACA TN 2872, 1953.

19 "Investigation of Compressive-Creep Properties of Aluminum Columns at Elevated Temperatures, Part 3," by R. L. Carlson and G. K. Manning, WADC Technical Report 52-251, 1955.

An Elastoplastic Thermal-Stress Analysis of a Free Plate[1]

By JEROME WEINER,[2] NEW YORK, N. Y.

The thermal stresses in a free plate of elastoplastic material subjected to a varying heat input over one face are determined. A heuristic solution is first found by suitable modifications of the known elastic solution. It is then verified that the solution satisfies all the conditions of the appropriate uniqueness theorem and represents therefore the unique solution to the problem. Residual stresses are determined and found to depend markedly on the peak magnitude of the heat input.

Introduction

THERMAL-stress calculations are usually based on an elastic stress-strain relationship. In some problems, however, inelastic effects may assume an important role as has been noted, for example, by Freudenthal (1),[3] who examines some simple problems with different types of inelastic stress-strain laws. The two types of inelastic behavior in their simplest form are represented by the linear viscoelastic and perfectly plastic bodies. Thus far, the majority of the papers concerned with inelastic thermal-stress analysis have dealt with linear viscoelastic solids; cf. Hilton, Hassan, and Russel (2) and Weiner and Mechanic (3). In the latter, it was noted that when thermal stresses are due solely to rapidly varying temperature transients, viscoelastic effects are negligible at practical temperature levels.

It therefore would seem to be of interest to perform some thermal-stress calculations in problems of this type using the elastoplastic idealization since the time scale does not affect the results with this idealization.

The elastoplastic theory utilized in this paper is based on the Prandtl-Reuss stress-strain relations with the von Mises yield condition. It is assumed in the analysis that all mechanical (and thermal) properties of the material are independent of temperature. With this assumption, the introduction of temperature effects into the usual elastoplastic theory presents no difficulties since it only affects the relationship between mean stress and strain. The elastoplastic theory used is outlined in Section 1 of this paper. Also included in this section is a statement of a uniqueness theorem applicable to the problem considered.

The particular problem considered is formulated mathematically in Section 2. It is that of a free plate subjected to a heat input uniformly distributed over one face, which increases monotonically from zero to a maximum value and then decays monotonically to zero. The other face and the edges of the plate are insulated. By restricting the analysis to heat inputs which do not vary too rapidly, it is possible to express the temperature distribution in the plate in a very simple form which facilitates further computations.

A heuristic solution to the problem is obtained in Section 3 by making suitable modifications of the elastic solution. It is found that plastic flow first starts at the outer faces of the plates and two plastic regions grow inward. As the heat input continues to increase, plastic flow also begins at the center of the plate and a plastic region forms there. After the heat input has decayed to zero, residual stresses remain in the plate. The nature of the residual-stress distribution depends markedly on the peak magnitude of the heat input.

In Section 4, it is verified that the heuristic solution satisfies all the conditions of the uniqueness theorem and therefore represents the unique solution to the problem. This verification is performed only for materials whose bulk modulus is infinite.

1 Formulation of Thermal Elastoplasticity

Thermal Prandtl-Reuss Theory. The following theory applies to a perfectly plastic solid in which there is a nonuniform temperature distribution. All mechanical properties are assumed independent of temperature; the only effect of temperature variation through the body is to alter the relation between mean stress and strain.

With these assumptions, the consideration of temperature variation using any of the theories of plasticity requires only slight modification of these theories since they are primarily concerned with the deviatoric stresses and strains. In this paper the Prandtl-Reuss stress-strain relations modified to include the effect of temperature variation and the von Mises yield condition will be used. These relations may be formulated mathematically as follows:

Let σ_{ij} and $\epsilon_{ij} (i, j = 1, 2, 3)$ denote the components of the tensors of stress and strain with respect to a Cartesian co-ordinate system x_i. The mean stress σ and the mean strain ϵ are defined as

$$\sigma = \frac{1}{3}\sigma_{ii}; \quad \epsilon = \frac{1}{3}\epsilon_{ii} \qquad [1]$$

where the usual summation convention is adopted.[4]

The deviatoric stress components s_{ij} and deviatoric strain components e_{ij} are then defined as

$$s_{ij} = \sigma_{ij} - \delta_{ij}\sigma; \quad e_{ij} = \epsilon_{ij} - \delta_{ij}\epsilon \qquad [2]$$

where δ_{ij} is the Kronecker delta

$$\delta_{ij} = \begin{cases} 0, & i \neq j \\ 1, & i = j \end{cases}$$

The von Mises condition for the occurrence of plastic flow is

---

[1] This research was performed under Air Force Contract No. AF 33(616)-2071 administered by the Aircraft Laboratory, Wright Air Development Center, Air Research and Development Command, Wright-Patterson Air Force Base, Ohio.

[2] Assistant Professor, Department of Civil Engineering and Engineering Mechanics, Institute of Air Flight Structures, Columbia University.

[3] Numbers in parentheses refer to the Bibliography at the end of the paper.

Presented at the National Applied Mechanics Conference, Urbana, Ill., June 14–16, 1956, of The American Society of Mechanical Engineers.

Discussion of this paper should be addressed to the Secretary, ASME, 29 West 39th Street, New York, N. Y., and will be accepted until October 10, 1956, for publication at a later date. Discussion received after the closing date will be returned.

Note: Statements and opinions advanced in papers are to be understood as individual expressions of their authors and not those of the Society. Manuscript received by ASME Applied Mechanics Division, July 11, 1955. Paper No. 56—APM-6.

[4] The reader who is unfamiliar with indicial notation is referred to reference (4).

$$J_2 = k^2 \quad [3]$$

where

$$J_2 = \frac{1}{2} s_{ij} s_{ij}$$

is the second invariant of the deviatoric stress tensor and k is the yield stress in pure shear.

The criterion for loading is expressed in terms of the sign of $\dot{J}_2$, a dot denoting differentiation of a quantity with respect to time; $\dot{J}_2 > 0$ indicates loading and $\dot{J}_2 < 0$ indicates unloading.

The stress-strain relations of the Prandtl-Reuss theory, with the addition of the temperature term, are as follows

$$\dot{\epsilon} = \frac{1}{3K} \dot{\sigma} + \alpha \dot{T} \quad [4]$$

$$\dot{e}_{ij} = \frac{1}{2G} \dot{s}_{ij} + \mu s_{ij} \quad [5]$$

where K is the elastic bulk modulus of its material, α is the coefficient of thermal expansion, T is the temperature, G is the elastic shear modulus, and μ is not a property constant but depends upon the local, instantaneous, state of stress and is defined as follows

$$\mu = \begin{cases} 0, \text{ whenever } J_2 < k^2, \text{ or } J_2 = k^2 \text{ but } \dot{J}_2 < 0 \\ \dfrac{s_{PS}\dot{e}_{PS}}{2k^2}, \text{ whenever } J_2 = k^2 \text{ and } \dot{J}_2 = 0 \end{cases} \quad [6]$$

Uniqueness Theorem. This paper is concerned with the determination of the stresses in a finite body of material which behaves according to the thermal Prandtl-Reuss theory just described, when the tractions at each point of the bounding surface and the temperature distribution throughout the body are given functions of space and time. For this class of problems, the following uniqueness theorem applies: ($\dot{S}_i$ denotes the rate of change of the traction at a given point of the bounding surface with normal n_i).

Theorem. Given, at any particular instant $t = t_0$, the values of σ_{ij}, for which $J_2 \leq k^2$, and $\dot{T}$ throughout a body occupying the region V and the values of $\dot{S}_i$ at each point of its bounding surface S. Then there exists at most one set of functions $\dot{\sigma}_{ij}$ defined throughout $V + S$ at $t = t_0$ which satisfy the following conditions:

(i) $\dot{\sigma}_{ij,j} = 0$ throughout V except possibly on certain surfaces, e.g., those separating the plastic from the elastic regions. The traction rates across these surfaces are required to be continuous.

(ii) $\dot{\sigma}_{ij} n_j = \dot{S}_i$ at each point of S.

(iii) $\dot{J}_2 = s_{ij}\dot{s}_{ij} \leq 0$ throughout the plastic region defined by $J_2 = k^2$.

(iv) There exists continuous velocity functions $\dot{u}_i$ (not necessarily unique) such that the corresponding strain rates, $\dot{\epsilon}_{ij} = \frac{1}{2}(\dot{u}_{i,j} + \dot{u}_{j,i})$, together with the σ_{ij} and $\dot{\sigma}_{ij}$, satisfy the Prandtl-Reuss stress-strain laws, Equations [4], [5], and [6] with $\mu \geq 0$.[5]

The proof of this theorem with $\dot{T} = 0$ is given in (4). The same proof applies when $\dot{T} \neq 0$ with only one trivial change. The formulation of the problem indicated by the foregoing theorem is an adequate representation of the physical process only if the displacements and their derivatives with respect to space and time are sufficiently small. This is assumed in what follows.

The theorem is used for demonstrating the uniqueness of a solution corresponding to a given thermal or loading process as follows: It is shown that the solution satisfies the conditions of the uniqueness theorem at every instant throughout the process, including the initial instant. It then follows from the theorem that $\dot{\sigma}_{ij}$ is determined uniquely throughout the process. Therefore, if the initial stress distribution is given, the stress distribution throughout the process is determined uniquely.

2 Formulation of Problem

Loading and Temperature Description. The problem studied is that of a free plate of thickness $2h$ and arbitrary shape oriented as shown in Fig. 1. The faces $\bar{x} = \pm h$ are free of traction while the tractions on the edges have zero resultant and zero moment.[6] The plate is initially free of stress.

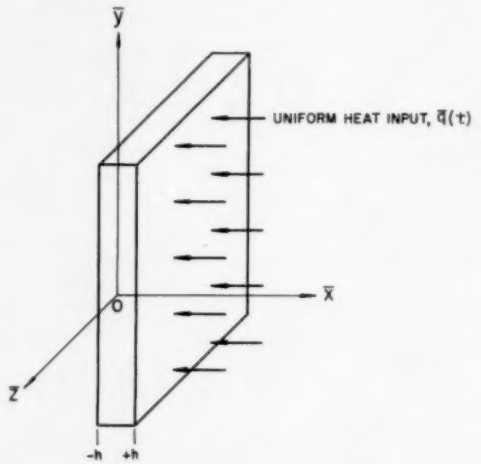

Fig. 1 Orientation of Plate

One face of the plate, initially at zero temperature throughout, is exposed to a uniform heat input which varies with time $\bar{q}(\bar{t})$, where $\bar{q}(0) = 0$, while the other face and all edges are perfectly insulated. The thermal properties of the plate are assumed independent of temperature. The temperature distribution in the plate may be written in the form (see Appendix)

$$T(\bar{x}, \bar{t}) = \frac{\bar{q}(\bar{t})}{\mathcal{K}} \left(\frac{\bar{x}^2}{4h} + \frac{\bar{x}}{2} - \frac{h}{12} \right) + \frac{1}{2h\rho c} \int_0^{\bar{t}} \bar{q}(\tau) d\tau - \mathcal{E}(\bar{x}, \bar{t}) \quad [7]$$

where $\mathcal{K}$ is the thermal conductivity, ρ the density, and c the specific heat of the plate.

It is shown in the Appendix that

$$|\mathcal{E}(\bar{x}, \bar{t})| \leq \frac{h^2 \dot{\bar{q}}_{\max}}{5\mathcal{K}\kappa} \quad [8]$$

where $\dot{\bar{q}}_{\max}$ is the maximum value of $|d\bar{q}/d\bar{t}|$ in the time interval

[5] The statement of the theorem is not rigorously complete. Conditions on the nature of V, certain subregions of V, and the functions involved which are necessary for the application of the divergence theorem are omitted. For the problem treated in this paper, these conditions are satisfied. The theorem is also not the most general which can be proved. For example, it may be modified, in the usual manner of elasticity theory, to include mixed boundary conditions. However, these generalizations are not required for the problem considered here.

[6] Barred symbols, such as $\bar{x}$, are used here for dimensional quantities. The unbarred symbols are reserved for corresponding nondimensional quantities.

$0 \leq \tau \leq t$ and κ is the thermal diffusivity. It is also shown in the Appendix that the maximum elastic stress produced by $\mathcal{E}(\bar{x}, t)$, $\sigma_{\mathcal{E}}$, has the following upper bound

$$|\sigma_{\mathcal{E}}| \leq \frac{0.046\, E\alpha h^2 \dot{\bar{q}}_{\max}}{(1-\nu)\mathcal{K}\kappa} \quad [9]$$

where E is the modulus of elasticity and ν is Poisson's ratio.

If the heat-input function $\bar{q}(t)$ is such that $\sigma_{\mathcal{E}}$ is negligible compared with the yield stress of the material, then the term $\mathcal{E}(\bar{x}, t)$ may be neglected in the elastoplastic analysis. This situation will be assumed in what follows. This assumption restricts the class of problems to which this analysis is directly applicable. However, the simplification it introduces allows explicit calculation of thermal stresses for these problems. The general methods used in the solution may be used as well when this simplification is not permissible, but the calculations become quite involved.

It is assumed further that $\bar{q}(t)$ increases monotonically to some maximum value $\bar{q}_M$ at time t_M and then decays monotonically to zero.

3 Heuristic Solution of Problem

In this section, a heuristic solution to the problem is obtained by modifications of the known elastic solution which seem physically reasonable. It will be shown in the following section, for materials with infinite K, that this solution satisfies all the requirements of the uniqueness theorem stated in Section 1 and is therefore the rigorous solution to the problem.

Elastic Solution of Problem. The solution of the problem formulated in Section 2 before any plastic flow occurs is well known, e.g. (6), and appears as follows for a general temperature distribution of the form $T(x, t)$

$$\sigma_{yy} = \sigma_{zz} = \frac{\alpha E}{1-\nu}\left\{\frac{1}{2h}\int_{-h}^{h} T(\bar{x}, t)\,d\bar{x} + \frac{3\bar{x}}{2h^3}\int_{-h}^{h} T(\bar{x}, t)\bar{x}\,d\bar{x} - T(\bar{x}, t)\right\} \quad [10]$$

$$\sigma_{xx} = \sigma_{xy} = \sigma_{xz} = \sigma_{yz} = 0$$

(The zero stress components listed in Equation [10] are assumed zero in the remainder of the analysis and will not be listed explicitly.)

If the temperature distribution of Equation [7], with $\mathcal{E}(\bar{x}, t)$ neglected, is substituted in Equation [10], the stress distribution before yielding occurs is given by the equation

$$\sigma_{yy} = \sigma_{zz} = \frac{\alpha E}{1-\nu}\left(\frac{\bar{q}}{4h\mathcal{K}}\right)\left(\frac{h^2}{3} - \bar{x}^2\right) \quad [11a]$$

The new symbol $\bar{\tau} = \sigma_{yy} = \sigma_{zz}$ is introduced. From Equations [1] and [2], for a state of stress as described by Equations [10]

$$\sigma = \frac{2}{3}\bar{\tau}; \quad s_{xx} = \frac{-2}{3}\bar{\tau}; \quad s_{yy} = s_{zz} = \frac{1}{3}\bar{\tau};$$

$$s_{xy} = s_{xz} = s_{yz} = 0 \quad [12a]$$

From Equation [3] it is seen that the condition for the occurrence of plastic flow is

$$J_2 = \frac{1}{3}\bar{\tau}^2 = k^2 \quad \text{or} \quad \bar{\tau} = \pm\sqrt{3}\,k \quad [12b]$$

By use of the dimensionless quantities

$$\tau = \frac{\bar{\tau}}{\sqrt{3}\,k}, \quad q = \frac{\alpha E \bar{q} h}{4\sqrt{3}\,(1-\nu)k\mathcal{K}}$$

and $x = \bar{x}/h$, Equation [11a] for the nonzero stress components $\bar{\tau}$ may be rewritten

$$\tau = q\left(\frac{1}{3} - x^2\right) \quad [11b]$$

It is seen from Equation [11b] that the maximum stress in the plate at any given instant is at $x = \pm 1$ and, for $q > 0$, is compressive. If $q(0) = 0$ (as is assumed in Equation [7]), and q increases monotonically with time, then plastic flow begins at the surfaces, $x = \pm 1$, when $\tau = -1$ there. From Equation [11b] this occurs when q reaches the value

$$q_1 = 3/2 \quad [13]$$

Growth of Two Plastic Regions. It seems reasonable to expect that as q continues to increase monotonically beyond q_1, two plastic regions will grow inward from each face and to a value of $q > q_1$, there will correspond a distance $\bar{\xi}$ such that the regions $\bar{\xi} \leq \bar{x} \leq h$ and $-h \leq \bar{x} \leq -\bar{\xi}$ will be completely plastic while the remainder of the plate still behaves elastically.

In the elastic region, $|\bar{x}| < \bar{\xi}$, it is assumed that the usual elastic solution, Equation [10] with h replaced by $\bar{\xi}$, applies with the addition of a uniform stress term to equilibrate the forces over the plastic region. (Since the stress distribution is symmetrical, there are no moments to equilibrate.) For the particular temperature distribution considered, the nonzero stress components then take the form

$$\left.\begin{aligned}\bar{\tau} &= \left(\frac{\alpha E}{1-\nu}\right)\left(\frac{\bar{q}}{4h\mathcal{K}}\right)\left\{\frac{\bar{\xi}^2}{3} - \bar{x}^2\right\} + \frac{\sqrt{3}\,k(h-\bar{\xi})}{\bar{\xi}}, \quad \text{for} \quad |\bar{x}| < \bar{\xi} \\ \bar{\tau} &= -\sqrt{3}\,k, \quad |\bar{x}| > \bar{\xi}\end{aligned}\right\} \quad [14a]$$

By use of the dimensionless quantities previously defined, and the dimensionless length, $\xi = \bar{\xi}/h$, Equation [14a] may be rewritten

$$\left.\begin{aligned}\tau &= q\left(\frac{\xi^2}{3} - x^2\right) + \frac{(1-\xi)}{\xi}, \quad 0 \leq |x| \leq \xi \\ \tau &= -1, \quad \xi \leq |x| \leq 1\end{aligned}\right\} \quad [14b]$$

The functional dependence of ξ on q is found by setting $x = \xi$ and $\tau = -1$. The result is

$$\xi = \sqrt[3]{\frac{3}{2q}} \quad [15]$$

The maximum tensile stress occurs at $x = 0$. To determine the value of q, q_2, when plastic flow will begin at the center of the plate, we set $x = 0$, $\tau = 1$, $q = q_2$, and

$$\xi = \sqrt[3]{\frac{3}{2q_2}}$$

in Equation [14b] and solve for q_2. The result is

$$q_2 = \frac{32}{9} \quad [16]$$

The value of ξ corresponding to this value of q is $\xi = 3/4$.

Growth of Three Plastic Regions. It seems reasonable to expect that as q continues to increase monotonically beyond q_2 a third plastic region will grow about the central plane of the plate. For a value of $q > q_2$, the regions $\xi \leq |x| \leq 1$, and $|x| \leq \zeta, 0 < \zeta < \xi < 1$, will be completely plastic while the remainder of the plate behaves elastically.

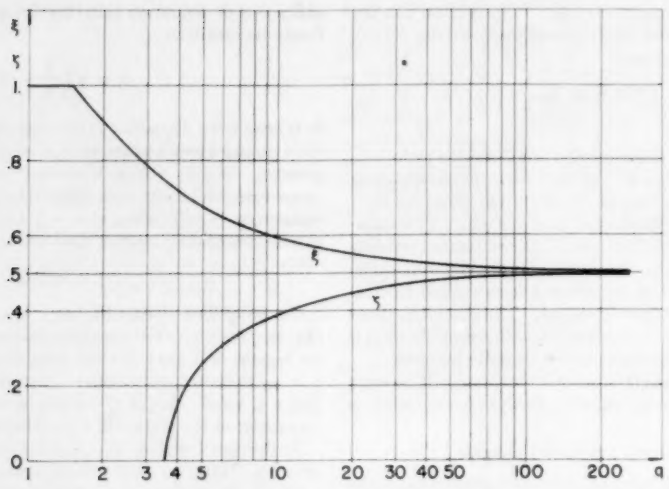

FIG. 2 GROWTH OF PLASTIC REGIONS

In the elastic regions, the elastic solution, Equation [10], is assumed to apply with the addition of a uniform stress term to equilibrate the forces over the plastic region. For the particular temperature distribution considered, the nonzero stress components then take the form

$$\left.\begin{aligned} &\tau = +1; \quad 0 \le |x| \le \zeta \\ &\tau = q\left\{\frac{\xi^3 - \zeta^3}{3(\xi - \zeta)} - x^2\right\} + \frac{(1 - \xi - \zeta)}{\xi - \zeta}; \quad \zeta \le x \le \xi \\ &\tau = -1; \quad \xi \le |x| \le 1 \end{aligned}\right\} \quad [17]$$

The functional dependence of ξ and ζ on q is obtained from the conditions that $\tau = -1$ for $x = \xi$ and $\tau = 1$ for $x = \zeta$. These conditions yield the two equations

$$-1 = q\left\{\frac{\xi^3 - \zeta^3}{3(\xi - \zeta)} - \xi^2\right\} + \frac{(1 - \xi - \zeta)}{\xi - \zeta} \quad [18a]$$

$$1 = q\left\{\frac{\xi^3 - \zeta^3}{3(\xi - \zeta)} - \zeta^2\right\} + \frac{(1 - \xi - \zeta)}{\xi - \zeta} \quad [18b]$$

After some algebraic manipulation, Equations [18a] and [18b] may be replaced by the equivalent system of equations

$$q^2 z^4 - 6qz + 12 = 0 \quad [19a]$$

$$\xi + \zeta = \frac{2}{qz} \quad [19b]$$

where

$$z = \xi - \zeta \quad [19c]$$

These equations are solved numerically most readily by first choosing a value of $z < 3/4$. The two roots of the resultant quadratic for q, Equation [19a], are then obtained. The simultaneous linear Equations [19b] and [19c] are then solved for ξ and ζ using the chosen value of z and each of the two roots for q. One root results in negative values for ζ and is therefore rejected, the other value of q yields the correct values of ξ and ζ which correspond to it. This process is repeated starting with other values of z. The results obtained in this manner are plotted in Fig. 2 in which is also plotted the variation of ξ for $q < q_2$ as given by Equation [15]. Fig. 2, therefore, describes completely the growth of plastic regions as q starts from zero and increases monotonically.

Decay of Heat Input and Residual Stresses. After $q(t)$ reaches q_M and starts to decay monotonically, it is assumed that unloading takes place in all the plastic regions. If this is the case, then the elastic stress-strain relations will apply throughout the plate. Therefore the rate of change of stress at the start of the decay is given by the time derivative of Equation [11b], that is

$$\dot{\tau} = \dot{q}\left(\frac{1}{3} - x^2\right) \quad [20]$$

Since $\dot{q} < 0$ during the decay of the heat input, it may be seen that unloading will in fact take place in all the plastic regions, if and only if $\xi_M > 1/\sqrt{3}$, where ξ_M is the value of ξ corresponding to q_M. From Fig. 2 it is seen that $\xi_M = 1/\sqrt{3}$ corresponds to $q_M = 13$ and the following analysis is restricted to smaller values of q_M. Numerical evaluation of the parameter q_M for practical conditions (Section 5 of reference 7) indicates, however, that values of $q_M > 13$ will seldom occur.

If $q_M < q_1$ there are, of course, no residual stresses. If $q_1 < q_M < q_2$ the stress distribution at the peak of the heat input, which is the initial stress distribution for the decay process, is given by Equation [14b]. If $q_M > q_2$, the stress distribution at the peak is given by Equation [17]. The rate of change of stress at and after the start of decay will be given by Equation [20] until yielding in the reverse direction occurs, when it must be replaced by the appropriate elastoplastic solution.

Four different types of residual-stress distribution are examined as listed in Table 1.

Typical stress distributions for each of the four ranges of q_M, as given in Table 1, together with the case in which no residual stress occurs, $q_M < 3/2$, are shown in Fig. 3. The formulas for the residual stresses for each of these four cases are derived in the following:

(i) $3/2 < q_M < 3$

Since no yielding in the reverse direction occurs during the decay of the heat input, Equation [20] applies for all of the decay period, and it is seen that the residual stresses are obtained by subtracting the elastic-stress distribution, Equation [11b] with

TABLE 1 TYPES OF RESIDUAL-STRESS DISTRIBUTION

q	Number of plastic regions at peak	Plastic flow during decay
$\frac{3}{2} - 3$	2	None
$3 - \frac{32}{9}$	2	At outer faces only
$\frac{32}{9} - \frac{64}{9}$	3	At outer faces only
$\frac{64}{9} - 13$	3	At outer faces and center

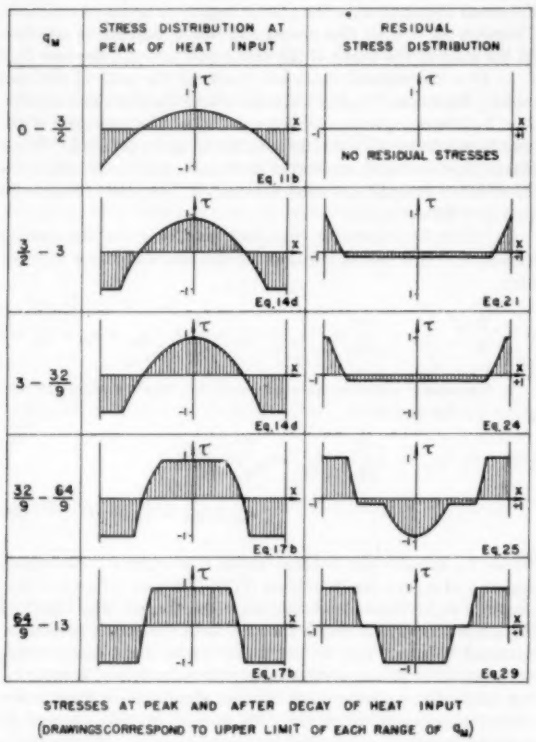

FIG. 3 TYPICAL PEAK AND RESIDUAL-STRESS DISTRIBUTIONS

q_M substituted for q, from Equation [14b]. The result is

$$\left.\begin{aligned} \tau &= \frac{q_M}{3}(\xi_M^2 - 1) + \frac{(1-\xi_M)}{\xi_M}; \quad 0 \le |x| \le \xi_M \\ \tau &= q_M\left(x^2 - \frac{1}{3}\right) - 1; \quad \xi_M \le |x| \le 1 \end{aligned}\right\} \quad [21]$$

where $$\xi_M = \sqrt[3]{\frac{3}{2q_M}}$$

is the value of ξ_M corresponding to q_M. It is seen that the maximum residual stress occurs at $x = \pm 1$ and that yielding in tension $\tau = 1$ will occur there when $q_M \ge q_a = 3$. Therefore Equations [21] apply only for $q_1 < q_M < q_a$.

(ii) $3 < q_M < \frac{32}{9}$

For $q_a \le q_M \le q_2$, it is seen that the equations to be subtracted from Equations [14b] are no longer those corresponding to the elastic solution but those corresponding to the elastoplastic solution with two plastic regions, Equations [14a], with k replaced by $2k$. In dimensionless terms, the equations to be subtracted are then

$$\left.\begin{aligned} \tau &= q_M\left(\frac{\delta^2}{3} - x^2\right) + \frac{2(1-\delta)}{\delta}; \quad 0 \le |x| \le \delta \\ \tau &= -2; \quad \delta \le |x| \le 1 \end{aligned}\right\} \quad [22]$$

where δ is determined from the condition that $\tau = -2$ for $x = \pm\delta$. This is seen to yield a relationship similar to Equation [15] with q replaced by $q_M/2$, that is

$$\delta = \sqrt[3]{\frac{3}{q_M}} \quad [23]$$

The residual streases for $q_a \le q_M \le q_2$ are obtained by subtracting Equations [22] from Equations [14b]. The result is

$$\left.\begin{aligned} \tau &= \frac{q_M}{3}(\xi_M^2 - \delta^2) + \frac{(1-\xi_M)}{\xi_M} - \frac{2(1-\delta)}{\delta}; \quad 0 \le |x| \le \xi_M \\ \tau &= q_M\left(x^2 - \frac{\delta^2}{3}\right) - \frac{2(1-\delta)}{\delta} - 1; \quad \xi_M \le |x| \le \delta \\ \tau &= 1; \quad \delta \le |x| \le 1 \end{aligned}\right\} \quad [24]$$

It is readily verified that no yielding occurs at $x = 0$ for the foregoing range of q_M.

(iii) $\frac{32}{9} < q_M < \frac{64}{9}$

For $q_2 \le q_M \le q_b$, with the upper limit still to be determined, the residual stresses are determined by subtraction of Equations [22] from Equations [17]. The result is

$$\left.\begin{aligned} \tau &= 1 - q_M\left(\frac{\delta^2}{3} - x^2\right) - \frac{2(1-\delta)}{\delta}; \quad 0 \le |x| \le \zeta_M \\ \tau &= \frac{q_M}{3}\left(\frac{\xi_M^3 - \zeta_M^3}{\xi_M - \zeta_M} - \delta^2\right) + \frac{(1-\xi_M-\zeta_M)}{\xi_M - \delta_M} - \frac{2(1-\delta)}{\delta}; \quad \zeta_M \le |x| \le \xi_M \\ \tau &= q_M\left(x^2 - \frac{\delta^2}{3}\right) - \frac{2(1-\delta)}{\delta} - 1; \quad \xi_M \le |x| \le \delta \\ \tau &= +1; \quad \delta \le |x| \le 1 \end{aligned}\right\} \quad [25]$$

It is next necessary to determine q_b, the value of q_M for which plastic flow at the center of the plate will just start upon complete decay of the heat input. This is determined from Equation [25] by setting $x = 0$, $\tau = +1$, $q_M = q_b$, and $\delta = \sqrt[3]{3/q_b}$ and solving for q_b. The result is

$$q_b = 2q_2 = \frac{64}{9} \quad [26]$$

(iv) $\frac{64}{9} < q_M < 13$

For $q_b \le q < q_c = 13$, the equations to be subtracted from Equations [17] are obtained in the same manner as these equations except that k is replaced by $2k$. They appear, therefore, as follows

$$\left.\begin{aligned} &\tau = +2; \quad 0 \le |x| \le \eta \\ &\tau = q_M \left\{ \frac{\delta^3 - \eta^3}{3(\delta - \eta)} - x^2 \right\} + \frac{2(1 - \delta - \eta)}{\delta - \eta}; \quad \eta \le |x| \le \delta \\ &\tau = -2; \quad \delta \le |x| \le 1 \end{aligned}\right\} \quad \ldots [27]$$

where the functional dependence of δ and η upon q_M is determined from the conditions that $\tau = -2$ for $x = \delta$ and $\tau = +2$ for $x = \eta$. It is seen, from the analogy between Equations [27] and [17], that

$$\left.\begin{aligned} \delta(q_M) &= \xi(q_M/2) \\ \eta(q_M) &= \zeta(q_M/2) \end{aligned}\right\} \quad \ldots [28]$$

where $\xi(q)$ and $\zeta(q)$ are the functions plotted in Fig. 2. From the nature of these graphs, it is seen that, for a given value of $q_M \ge q_b$

$$0 \le \eta < \zeta_M < \xi_M < \delta < 1$$

The residual stresses for $q_b \le q < q_c$ are obtained, then, by the subtraction of Equations [27] from Equations [17]. The result is

$$\left.\begin{aligned} &\tau = -1; \quad 0 \le |x| \le \eta \\ &\tau = 1 - q_M \left\{ \frac{\delta^3 - \eta^3}{3(\delta - \eta)} - x^2 \right\} - \frac{-2(1 - \delta - \eta)}{\delta - \eta}; \quad \eta \le |x| \le \zeta_M \\ &\tau = \frac{q_M}{3} \left\{ \frac{\xi_M^3 - \zeta_M^3}{\xi_M - \zeta_M} - \frac{\delta^3 - \eta^3}{\delta - \eta} \right\} + \frac{(1 - \xi_M - \zeta_M)}{\xi_M - \zeta_M} - \frac{2(1 - \delta - \eta)}{\delta - \eta}; \quad \zeta_M \le |x| \le \xi_M \\ &\tau = q_M \left\{ x^2 - \frac{\delta^3 - \eta^3}{3(\delta - \eta)} \right\} - \frac{2(1 - \delta - \eta)}{\delta - \eta} - 1; \quad \xi_M \le |x| \le \delta \\ &\tau = +1; \quad \delta \le |x| \le 1 \end{aligned}\right\} \quad \ldots [29]$$

In the foregoing equations, ξ_M and ζ_M are the values of ξ and ζ corresponding to q_M as given in Fig. 2. The values of δ and η corresponding to q_M are determined from the same figure by use of Equation [28].

As noted previously, this type of analysis does not apply for $q_M > 13$ since the assumption that unloading occurs throughout the plate at the start of the decay of the heat input no longer applies.

4 Rigorous Establishment of Solution

In order to establish rigorously the solution obtained heuristically in Section 3 it is necessary to show that the solution satisfies the conditions of the uniqueness theorem given in Section 2. These are examined in order as follows:

(i) It is clear from the form of stress-distribution determined

$$\sigma_{yy} = \sigma_{zz} = \bar{\tau}(\bar{x}, t) \text{ (independent of } \bar{y} \text{ and } \bar{z}) \text{ and } \sigma_{xx} = \sigma_{xy} = \sigma_{xz} = \sigma_{yz} = 0$$

that the equilibrium equations $\sigma_{ij,j} = 0$ are identically satisfied.

(ii) The stress-distribution obtained satisfies the conditions that the surfaces $\bar{x} = \pm h$ are free of traction for all time. The solution however corresponds to nonzero tractions on the edges of the plate which vary with time; if these tractions are considered the prescribed tractions, then this hypothesis of the uniqueness theorem is satisfied. It will be noted that the solution was obtained so that the tractions on the edges have zero resultant and zero moment. To the extent, therefore, that Saint Venant's principle applies to elastoplastic problems, the solution represents also the state of stress in a plate completely free of surface tractions at a sufficient distance from the edges of the plate.

(iii) For the first portion of the heat-pulse input, when $\dot{q} > 0$, the stress distribution in the plastic regions is assumed constant. Therefore $\dot{J}_2 = 0$ for this period and this hypothesis is satisfied. At the start of the decay of the heat input it is still the case that $J_2 = k^2$ in the regions which are plastic at the peak of the heat input. However, for the assumed stress-distribution variation $\dot{J}_2 < 0$ in these regions providing $q_M < q_c = 13$ at the start of the heat-input decay and this hypothesis is again satisfied. When plastic flow occurs at the end of the heat-input decay, the stress distribution is again assumed constant in the plastic regions so that $\dot{J}_2 = 0$ there again.

(iv) This hypothesis is examined here only for the case of infinite K. It is first noted that for the assumed stress distribution

$$\sigma = \frac{2}{3}\bar{\tau}, \quad s_{xx} = \frac{-2}{3}\bar{\tau}, \quad s_{yy} = s_{zz} = \frac{1}{3}\bar{\tau}, \quad s_{xy} = s_{xz} = s_{yz} = 0$$

In the elastic regions, the mean and deviatoric strains are then given by the equations

$$\epsilon = \alpha T, \quad e_{xx} = \frac{-\bar{\tau}_E}{3G}; \quad e_{yy} = e_{zz} = \frac{\bar{\tau}_E}{6G}; \quad e_{xy} = e_{xz} = e_{yz} = 0 \quad \ldots [30]$$

where $\bar{\tau}_E$ denotes the nonzero stress components in the elastic region, and is given by Equations [11b], [14b]$_1$, or [17]$_2$ when there are no, two, or three plastic regions, respectively. The functions, Equation [30] which define the strains in the elastic regions are assumed to apply also in the plastic regions and define strains there as well. These strains satisfy the equations of compatibility, so that there correspond to them displacement functions u_i which may be differentiated with respect to time to yield the velocity functions $\dot{u}_i$ required by hypothesis (iv). It remains to show that the calculated stresses, together with the foregoing strains, satisfy the Prandtl-Reuss stress-strain laws, Equations [4], [5], and [6] with $\mu \ge 0$.

The solution for the first portion of the heat pulse in which $\dot{q} > 0$ is considered first. Solutions have been obtained with either two or three plastic regions in which $J_2 = k^2$ and $\dot{J}_2 = 0$ and with the remainder of the plate elastic in which $J_2 < k^2$. It can be seen by direct substitution that the calculated stresses together with the assumed strains satisfy the Prandtl-Reuss equations for K infinite with $\mu = 0$ in the elastic regions and

$$\mu = \frac{s_{pq}\dot{e}_{pq}}{2k^2}$$

in the plastic regions, as required. It is only necessary, therefore, to show that $\mu \ge 0$. In the plastic regions

$$\mu = \frac{s_{pq}\dot{e}_{pq}}{2k^2} = \frac{\pm\dot{\tau}_E}{2G} \quad \ldots [31]$$

(+ in inner plastic region; — in outer plastic region). It is, therefore, sufficient to examine only $\dot{\tau}_E$.

For the case in which there are only two plastic regions, τ_E is given by Equation [14b], from which $\dot{\tau}_E$ is derived as

$$\dot{\tau}_E = \dot{q}\left(\frac{\xi^2}{3} - x^2\right) + q\left(\frac{2\xi\dot{\xi}}{3}\right) - \frac{\dot{\xi}}{\xi^2} \quad [32]$$

However, ξ satisfies Equation [15] from which $\dot{\xi}$ is derived as

$$\dot{\xi} = -\frac{1}{3}\sqrt[3]{\frac{3}{2q^4}}\,\dot{q} = \frac{-\xi\dot{q}}{3q} \quad [33]$$

Substitution from Equations [15] and [33] in Equation [32] yields

$$\dot{\tau}_E = \dot{q}\left(\frac{\xi^2}{3} - x^2\right) \quad [34]$$

Since $x \geq \xi$ in the outer plastic regions, $\dot{\tau}_E < 0$ and $\mu > 0$ there for $\dot{q} > 0$ as required.

For the case in which there are three plastic regions, τ_E is given by Equation [17]$_3$. By use of Equations [19a], [19b], and [19c] and some algebraic manipulation, it may be expressed in the following form which is more convenient for this analysis

$$\tau_E = q\left(\frac{z^2}{6} - x^2\right) + \frac{1}{2z} \quad [35]$$

Therefore

$$\dot{\tau}_E = \dot{q}\left(\frac{z^2}{6} - x^2\right) + q\left(\frac{z\dot{z}}{3}\right) - \frac{\dot{z}}{2z^2} \quad [36]$$

By differentiation of Equation [19a]

$$\frac{qz\dot{z}}{3} - \frac{\dot{z}}{2z^2} = \frac{\dot{q}}{2qz} - \frac{\dot{q}z^2}{6} \quad [37]$$

Substitution from Equation [37] in Equation [36] yields

$$\dot{\tau}_E = \dot{q}\left[\frac{(\xi + \zeta)}{4} - x^2\right] \quad [38]$$

From Equation [38] and the numerical results for ξ and ζ it is seen that for $\dot{q} > 0$, $\dot{\tau}_E < 0$ for $x > \xi$ and $\dot{\tau}_E > 0$ for $x < \zeta$. It is also noted that at the instant when the third plastic region starts to form, $\xi = 3/4$, $\zeta = 0$ and Equations [34] and [38] give the same value of $\dot{\tau}_E$ so that this derivative exists at this transition time also. Therefore $\mu > 0$ in the plastic regions as required. This completes the rigorous establishment of the solution for $0 < q < q_M$.

The solution for the second portion of the heat pulse in which $\dot{q} < 0$ is next considered. At time $t = t_M$, the start of the heat-input decay, it has been assumed that $\dot{J}_2 < 0$ in the regions which are plastic at that time. Therefore the first of Equations [6] applies and

$$\dot{J}_2 = s_{ij}\dot{s}_{ij} = \frac{2}{3}\bar{\tau}\dot{\bar{\tau}}_E = \frac{2}{3}\bar{\tau}\left[\sqrt{3}\;k\dot{q}\left(\frac{1}{3} - x^2\right)\right]$$

where $\bar{\tau}$ is the stress distribution at time $t = t_M$. It is seen that for $q_M \leq q_c$, $\xi_M > 1/\sqrt{3}$, and $\dot{J}_2 < 0$ as required in the regions plastic at $t = t_M$.

For $t > t_M$, the verification of the uniqueness of the solution proceeds in a completely analogous fashion to the analysis for $t < t_M$.

BIBLIOGRAPHY

1 "Effect of Rheological Behavior on Thermal Stresses," by A. M. Freudenthal, *Journal of Applied Physics*, vol. 25, 1954, pp. 1110–1117.

"On Inelastic Thermal Stresses in Flight Structures," by A. M. Freudenthal, *Journal of the Aeronautical Sciences*, vol. 21, 1954, pp. 772–778.

2 "Analytical Studies of Thermal Stresses in Media Possessing Temperature-Dependent Visco-Elastic Properties," by H. H. Hilton, H. A. Hassan, and H. G. Russel, WADC TR No. 53-322, September, 1953.

3 "Thermal Stresses in Free Plates Under Heat-Pulse Inputs," by J. H. Weiner and Harold Mechanic, Technical Report No. 4, Contract No. AF 33(616)-2071, assigned WADC TR No. 54-428.

4 "The Mathematical Theory of Plasticity," by R. Hill, Oxford University Press, London, England, first edition, 1950.

5 "Conduction of Heat in Solids," by H. S. Carslaw and J. C. Jaeger, Oxford University Press, London, England, first edition, 1947.

6 "Theory of Elasticity," by S. Timoshenko and J. N. Goodier, McGraw-Hill Book Company, Inc., New York, N. Y., second edition, 1951.

7 "An Elastoplastic Thermal Stress Analysis of a Free Plate," by J. H. Weiner, Technical Report No. 6, Contract No AF 33(616)-2071.

Appendix

Derivation of Approximate Temperature Distribution

The solution $T_1(\bar{x}, t)$ to the thermal problem stated in Section 2 for a unit step heat input is (5)

$$T_1(\bar{x}, t) = \frac{t}{2h\rho c} + \frac{1}{3\mathcal{K}}\left(\frac{\bar{x}^2}{4h} + \frac{\bar{x}}{2} - \frac{h}{12}\right) - \frac{4h}{\pi^2\mathcal{K}}\sum_{n=1}^{\infty}\frac{(-1)^n}{n^2}\,e^{\frac{-n^2\pi^2\kappa t}{4h^2}}\cos\frac{n\pi(\bar{x} + h)}{2h}$$

The temperature distribution $T(\bar{x}, t)$ for a varying heat input $\bar{q}(t)$, with $\bar{q}(0) = 0$ can be obtained from $T_1(\bar{x}, t)$ by use of the convolution integral as follows

$$T(\bar{x}, t) = \int_0^t \dot{\bar{q}}(\tau)T_1(\bar{x}, t - \tau)d\tau = \frac{\bar{q}(t)}{3\mathcal{K}}\left(\frac{\bar{x}^2}{4h} + \frac{\bar{x}}{2} - \frac{h}{12}\right) + \frac{1}{2h\rho c}\int_0^t \bar{q}(\tau)d\tau - \varepsilon(\bar{x}, t)$$

where

$$\varepsilon(\bar{x}, t) = \frac{4h}{\pi^2\mathcal{K}}\int_0^t \dot{\bar{q}}(\tau)\sum_{n=1}^{\infty}\frac{(-1)^n}{n^2}\,e^{\frac{-n^2\pi^2\kappa(t-\tau)}{4h^2}}\cos\frac{n\pi(\bar{x} + h)}{2h}\,d\tau$$

Let $\dot{\bar{q}}_{\max}$ be the maximum value of $|\dot{\bar{q}}(\tau)|$ in the time interval $0 \leq \tau \leq t$. Then it is seen that

$$|\varepsilon(\bar{x}, t)| \leq \frac{4h}{\pi^2\mathcal{K}}\,\dot{\bar{q}}_{\max}\int_0^t\sum_{n=1}^{\infty}\frac{1}{n^2}\,e^{\frac{-n^2\pi^2\kappa(t-\tau)}{4h^2}}\,d\tau = \frac{16h^2\dot{\bar{q}}_{\max}}{\pi^4}\sum_{n=1}^{\infty}\frac{1}{n^4}\left(1 - e^{\frac{-n^2\pi^2\kappa t}{4h^2}}\right) < \frac{16h^2\dot{\bar{q}}_{\max}}{\pi^4\mathcal{K}\kappa}\sum_{n=1}^{\infty}\frac{1}{n_4}$$

But

$$\sum_{n=1}^{\infty}\frac{1}{n^4} = \frac{\pi^4}{90}$$

Therefore

$$|\varepsilon(\bar{x}, t)| \leq \frac{h^2\dot{\bar{q}}_{\max}}{5\mathcal{K}\kappa}$$

as noted in Equation [8].

An upper bound for the elastic stress σ_ε due to $\varepsilon(\bar{x}, t)$, the neglected portion of the temperature distribution, is obtained by substituting $\varepsilon(\bar{x}, t)$ in Equation [10]

$$\sigma_\varepsilon = \frac{\alpha E}{1-\nu}\left\{\frac{1}{2h}\int_{-h}^{h}\varepsilon(\bar{x}, t)d\bar{x} + \frac{3\bar{x}}{2h^3}\int_{-h}^{h}\varepsilon(\bar{x}, t)\bar{x}d\bar{x} - \varepsilon(\bar{x}, t)\right\}$$

$$= \frac{4\alpha Eh}{(1-\nu)\pi^2\mathfrak{K}}\int_0^t \dot{q}(\tau)\sum_{n=1}^{\infty}\frac{(-1)^n}{n^2}\left\{\frac{6\bar{x}}{n^2\pi^2 h}[(-1)^n - 1] - \cos\frac{n\pi(\bar{x}+h)}{2h}\right\} e^{\frac{-n^2\pi^2\kappa(t-\tau)}{4h^2}}\, d\tau$$

Therefore

$$|\sigma_\varepsilon| \leq \frac{4\alpha Eh\dot{q}_{\max}}{(1-\nu)\pi^2\mathfrak{K}}$$

$$\int_0^t \sum_{n=1}^{\infty}\frac{1}{n^2}\left|\frac{6\bar{x}}{n^2\pi^2 h}[(-1)^n - 1] - \cos\frac{n\pi(\bar{x}+h)}{2h}\right| e^{\frac{-n^2\pi^2\kappa(t-\tau)}{4h^2}}\, d\tau$$

$$\leq \frac{16\alpha Eh^2\dot{q}_{\max}}{(1-\nu)\pi^4\mathfrak{K}\kappa}\sum_{n=1}^{\infty}\frac{1}{n^4}\left|\frac{6\bar{x}}{n^2\pi^2 h}[(-1)^n - 1] - \cos\frac{n\pi(\bar{x}+h)}{2h}\right| < \frac{16\alpha Eh^2\dot{q}_{\max}}{(1-\nu)\pi^4\mathfrak{K}\kappa} \times 0.278 = \frac{0.046\alpha Eh^2\dot{q}_{\max}}{(1-\nu)\mathfrak{K}\kappa}$$

where the upper bound of the rapidly convergent series was obtained by direct computation.

On the Carrying Capacity of Redundant Structures[1]

By E. F. MASUR[2] and K. P. MILBRADT[3]

It has been shown previously (1)[4] how the inclusion of certain nonlinear terms in the analysis of redundant trusses affects the predicted behavior of such structures in the postbuckling range. In particular, it was demonstrated that the nonlinear theory predicts states of axial stress corresponding to a general stiffening of the structure compared with the results of the classical linear analysis. After establishing a generalized minimum-strain-energy principle, this paper describes a series of tests which corroborates experimentally the predictions of the nonlinear theory. For example, the predicted (and measured) ultimate load of the test model amounts to about three times the load at which the linear theory predicts collapse through instability. A similar theory (2) dealing with the response of redundant trusses to primary bending moments is extended to certain types of singular cases which were excluded from the previous paper. It is shown analytically and verified by experiment that a constant ultimate state of axial stress may be reached already for finite applied couples. Elastic behavior is assumed throughout the paper.

Introduction

It is a well-known fact that a rigid-jointed truss generally becomes unstable if it is subjected to joint forces of large enough magnitude. If the members of the structure are relatively slender, that is, if the structure buckles in its own plane while still in the elastic range, these critical forces, according to the classical linear theory, represent the largest loads which the structure is able to sustain. The analytical or experimental determination of the loads corresponding to neutral equilibrium is therefore of great importance in the design of this type of structure and has been the subject of a number of papers, such as (3) and (4).

It can be demonstrated readily that a statically determinate truss does, in fact, collapse when subjected to loads associated with neutral equilibrium. Conversely, if its axial-force system is indeterminate, it has been shown (1) that the conventional linear analysis underestimates the total carrying capacity of the structure. In fact, the inclusion of certain nonlinear terms in the compatibility relations between the joint translations modifies the computed bar forces in such a way that a general stiffening of the structure takes place. As buckling progresses, the magnitude of the applied loads continues to increase. In general, an ultimate state of axial stress is approached asymptotically corresponding to an ultimate-load magnitude. If no prior yielding takes place, this ultimate load, rather than the conventional buckling load, represents the full carrying capacity of the truss. In what follows, a brief résumé is given of the basic equations governing the postbuckling range as developed in (1).

It is assumed that a redundant truss of the type shown in Fig. 1 is subjected to a set of given joint loads, which are multiplied by

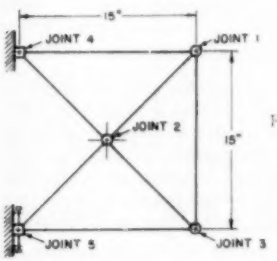

Fig. 1 Test Model—Schematic Drawing

the common parameter λ (factor of safety) to be determined later. In a structure of the mth degree of indeterminacy, the axial force S in a member can be represented by

$$S = \lambda S' + \lambda_\alpha S_\alpha \quad [1]$$

In Equation [1], S' represents the force system obtained through the customary analysis for the case of $\lambda = 1$, while the force systems $S_r (r = 1, 2 \ldots m)$ are internally self-equilibrated. The as yet undetermined multipliers λ_r, which of course vanish in the classical analysis for the unprestressed case, represent the influence of the nonlinear terms on the axial state of stress. Repeated Greek subscripts, as usual, denote summation over their range.

If now the n joints of the truss are subjected to externally applied couples represented by the column matrix $M = \{M_i\}$, the joint rotations $\theta = \{\theta_i\}$ are governed by the equations of equilibrium

$$A\theta = M \quad [2]$$

In this set of equations, the "stiffness matrix" $A = [a_{ij}]$ is symmetrical and a function of the axial bar forces and thus of the $m + 1$ multipliers λ and λ_r. Neutral equilibrium exists when the set of equations

$$A\theta = 0 \quad [3]$$

admits a nontrivial solution for θ; in that case

$$f(\lambda;\ \lambda_r) \equiv |A| = 0 \quad [4]$$

In the determinate case, the smallest value of λ satisfying Equation [4] represents the factor of safety since λ remains constant during buckling.

---

[1] The work described in this paper was sponsored by the Office of Ordnance Research, Contract No. DA-11-022-ORD-1156, Project No. TB2-0001 (570). A more detailed discussion, especially of the experimental phase of the work, is contained in Progress Report No. 3 submitted to OOR under the same contract.

[2] Associate Professor of Engineering Mechanics, University of Michigan, Ann Arbor, Mich.

[3] Assistant Professor of Civil Engineering, Illinois Institute of Technology, Chicago, Ill.

[4] Numbers in parentheses refer to the Bibliography at the end of the paper.

Presented at the National Applied Mechanics Conference, Urbana, Ill., June 14–16, 1956, of The American Society of Mechanical Engineers.

Discussion of this paper should be addressed to the Secretary, ASME, 29 West 39th Street, New York, N. Y., and will be accepted until October 10, 1956, for publication at a later date. Discussion received after the closing date will be returned.

Note: Statements and opinions advanced in papers are to be understood as individual expressions of their authors and not those of the Society. Manuscript received by ASME Applied Mechanics Division, May 19, 1955. Paper No. 56—APM-8.

If the structure is statically redundant, however, Equation [4] determines uniquely only that value of λ at which buckling commences, since in the prebuckling range the parameters λ_r remain equal to their initial prestressing values λ_r^* and are therefore presumed to be known. In the postbuckling range, however, the curvature of the buckled members affects the condition of compatible deformations in such a way that a redistribution of axial forces takes place. The parameters λ_r are now governed by the set of compatibility equations

$$\lambda_r - \lambda_r^* = 1/2\,\theta' A_{,r}\theta \qquad (r = 1, 2, \ldots m) \ldots\ldots [5]$$

In Equations [5] and in what follows, a subscript preceded by a comma represents differentiation with respect to the corresponding parameter λ_r, while a primed matrix denotes its transpose.

Equations [5] can be transformed into

$$\lambda_r - \lambda_r^* = (\Sigma A_{ii})^{-1}(\theta'\theta) f_{,r} = (\Sigma A_{ii})^{-1} c^2 f_{,r} \ldots\ldots [6]$$

in which A_{ii} represents the cofactor of a_{ii} in A. As c increases beyond bounds, and if all the parameters λ_r remain finite, λ approaches an ultimate value λ^u which is governed by Equation [4] and the set of equations

$$f_{,r}(\lambda^u, \lambda_1 \ldots \lambda_m) = 0 \qquad (r = 1, 2, \ldots m) \ldots\ldots [7]$$

A Minimum Strain-Energy Principle

Equations [4] and [6] admit an interesting geometric interpretation which is somewhat analogous to that developed for a different loading case in (2). In fact, in the λ_r-space, Equation [4] defines a series of "surfaces of neutral equilibrium" which are convex. If they are closed,[5] they "shrink" for increasing values of the load parameter λ until, for $\lambda = \lambda^u$, a single point is reached which will be designated by P^u (Fig. 2). On the other hand, Equations

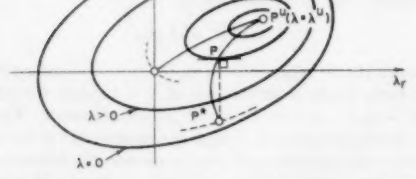

Fig. 2 Geometric Representation of Postbuckling History

[5] or [6] apply to any system which has been "orthonormalized" in the manner described in (1) and (2). For a generic point P, therefore, Equations [6] may be expressed in an (n, t) co-ordinate system, in which n represents the direction normal (in the sense of increasing λ) to the instability surface at P and t is the totality of all the $m - 1$ directions tangent to the surface.[6]

However, $f_{,t}$ obviously vanishes for all the tangential directions. Equations [6] therefore are now transformed into the set of equations

$$\left.\begin{aligned} \lambda_t - \lambda_t^* &= 0 \\ \lambda_n - \lambda_n^* &= (\Sigma A_{ii})^{-1} c^2 f_{,n} \end{aligned}\right\} \ldots\ldots [8]$$

In other words, the vector $\overline{P^*P}$ is normal to the instability surface at P. In view of the convexity of the surface and of the positive definiteness of the coefficient of $f_{,n}$ in Equations [8], it follows that P is that point on the surface of neutral equilibrium which is closest to P^*.

For sufficiently small values of λ, P and the initial point P^* remain coincident so long as the latter is on the concave side of the associated instability surface. After neutral equilibrium is reached, P travels on the sequence of shrinking surfaces as described, and reaches finally (for the closed case) the limiting point P^u. Since the square of the length of the vector $\overline{P^*P}$ is twice the fictitious strain energy associated with axial-bar forces (except for an additive term depending only on the load parameter λ), the following principle is established:

For a given set of loads, the actual bar forces minimize the fictitious strain energy as compared with any other system of bar forces satisfying the equations of equilibrium and corresponding to either stable or neutral equilibrium.

It is interesting to note that this principle is analogous to the one of Haar and von Karman (5) dealing with the state of stress in an elastic-plastic structure, except that in the case under consideration the loading history is immaterial since the unloading path is identical with the loading path (that is, there are no "permanent strains"). For pin-jointed structures this analogy is to be expected on account of the similarity between the "stress-strain" relationship of an Euler column and that of an ideally plastic bar. The corresponding instability surfaces in that case are composed of a number of "planes," while the stress path consists of a sequence of straight lines.

Response to Primary Bending Moments—Singular Case

In this section the theory presented in (2), that is, the response of a redundant structure to applied primary bending moments, is extended to certain singular cases which were excluded in the original development.

Without significant loss of generality it will be assumed that, in addition to a given set of external forces applied at the joints, the structure is subjected only to external joint couples designated by the column vector M. For this loading case, the axial forces and joint rotations are governed by Equations [1], [2], and [5]. For increasing M, the stress point P in the λ_r-space approaches a limiting point P^u which corresponds to the smallest value which the "potential energy" can assume. This potential energy is given by

$$Q = {}^1/_2 \bar{\theta}' A \bar{\theta} \ldots\ldots [9]$$

in which $\bar{\theta}$ is the normalized vector proportional to the vector θ satisfying Equation [2].

The existence of an interior minimum of the Q-surface is predicated on its convexity and on the fact that Q approaches infinity as the stress point P approaches the closed "cylinder" of neutral equilibrium. While the former condition is always satisfied, the latter is true if M is not orthogonal to the buckling mode associated with any point of neutral equilibrium. If, on the other hand, such orthogonality does exist, the stress path may proceed differently as loading continues.

In what follows it will be assumed that at a point P of neutral equilibrium the normalized buckling mode θ_1, which is governed by

$$\left.\begin{aligned} A\theta_1 &= 0 \\ \theta_1'\theta_1 &= 1 \end{aligned}\right\} \ldots\ldots [10]$$

[5] Under special circumstances, open instability surfaces may also converge to a limiting point, which then lies at infinity. In that case, the finite ultimate load is approached without all bar forces remaining finite.

[6] It is presumed that Equation [4] has continuous derivatives with respect to all the parameters λ_r. Actually, it can be shown that the following developments hold true also for sectionally continuous derivatives. The presence of "corners" in the instability surface is therefore admitted.

is orthogonal to M, i.e.

$$M'\theta_1 = 0 \quad \ldots\ldots [11]$$

It will be assumed further that Q has no interior minimum, since otherwise the discussion in (2) applies to this case without modification. In view of Equations [10] and [11], Equations [2] have a solution (in spite of the singularity of A) which can be written as follows

$$\theta = c\theta_1 + \phi \quad \ldots\ldots [12]$$

in which c is an as yet unknown multiplier, while ϕ is determined uniquely by

$$\left.\begin{aligned} A\phi &= M \\ \phi'\theta_1 &= 0 \end{aligned}\right\} \quad \ldots\ldots [13]$$

On the $(m-1)$-dimensional region of neutral equilibrium defined by Equations [10] in the λ_r-space, Equation [11] generally designates a (p)-dimensional subregion, where $0 \leq p \leq m-1$. Since the existence of an interior minimum was precluded for the case under consideration, it follows that, for increasing magnitudes of M, the stress point P approaches a point on the boundary which lies within this subregion. If the direction of the approach path is designated by the subscript s, it can be shown, through a limiting process, that the multiplier c approaches the value

$$c_0 = -\frac{\phi' A_{,s}\theta_1}{\theta'_1 A_{,s}\theta_1} \quad \ldots\ldots [14]$$

It can be shown further, by differentiating Equations [10], [11], [12], and [13] with respect to λ_t, that both the numerator and denominator in Equation [14] vanish for all t-directions for which Equation [11] is identically satisfied. Hence the s-subscripts in Equation [14] may be replaced by n and the value of c_0 is independent of the approach path.

After the stress point P has reached the surface of neutral equilibrium, and as the magnitude of M increases further, P travels on the p-dimensional subregion just defined in such a way as to reduce the value of Q. In view of Equation [12] and of the vanishing of the numerator and denominator in Equation [14] for all t-directions, the equations of compatibility, Equations [5], now assume the form

$$\lambda_n - \lambda_n^* = 1/2c^2\theta_1' A_{,n}\theta_1 + c\phi' A_{,n}\theta_1 + 1/2\phi' A_{,n}\phi \ldots [15n]$$

$$\lambda_t - \lambda_t^* = 1/2\phi' A_{,t}\phi \qquad (t = 1, 2 \ldots p) \ldots\ldots [15t]$$

In this system of equations, the p Equations [15t] define the position of the stress point, while Equation [15n] governs the magnitude of the multiplier c. In the limit, with M passing all bounds, an ultimate point P^u is reached, whose position is governed by

$$\lim_{M \to \infty} \bar{\phi}' A_{,t}\bar{\phi} = 0 \qquad (t = 1, 2 \ldots p) \ldots\ldots [16]$$

in which $\bar{\phi}$ is defined as the normalized vector which is proportional to the vector ϕ satisfying Equations [13]. It is therefore evident that the minimum principles developed in (2) remain valid for singular cases if their scope is extended to include "exterior" minima. For example, the ultimate stress point P^u represents the lowest possible value of Q compared with all points inside, and on the boundary of, the region of stability.

For the special case of $p = 0$ (which corresponds to that of the model structure), only Equation [15n] is available after neutral equilibrium is reached. In other words, for increasing values of the applied couples M, the stress point P remains fixed, thus giving the structure a superficial resemblance to a statically determinate one. It is interesting to note that, in general, for this special case the ultimate state of axial stress is reached for a finite magnitude of M. Owing to the constancy of A, the direction of ϕ also remains unchanged, while its magnitude increases in proportion to that of M. It can be verified readily that if the multiplier c is plotted against the magnitude of M, Equation [15n] defines a hyperbola. In general, for given M, there are two solutions for c and therefore two possible equilibrium configurations. This does not violate the uniqueness theorem developed in (2), however, since the validity of that principle was restricted to the inside of the region of stability.

Discussion of Test Procedure and Results

In order to establish an experimental corroboration of the analytical results contained in (1) and (2) (the latter modified by the discussion of the preceding section), a model structure shown schematically in Fig. 1 was subjected to vertical forces at joint 1 or 3 or to a couple applied at joint 2. The structure is of one degree of redundancy relative to its axial forces. This redundancy can be removed, in order to provide a check with existing linear theories, by releasing joint 5 and by permitting it to slide. Also, by imposing an initial displacement on joint 5, an arbitrary system of prestresses can be introduced.

The members of the truss were fabricated from high-strength strap steel, whose proportional limit was tested at 187,000 psi. The diagonal members were 1 in. wide and 0.032 in. thick and the nondiagonal members were of the same width and 0.062 in. thick. The resulting combination of very large slenderness ratios with a high proportional limit insured the fully elastic behavior of the members well into the nonlinear post-buckling domain. At the same time, the high width-thickness ratio prevented a tendency of the lower chord to buckle laterally.

The joint rotations were measured in the usual fashion by means of attached mirrors. The axial forces were computed from the measured strains on two opposite faces of the members. This presented some difficulty in that relatively small errors in the gage response led to substantial discrepancies in the calculated axial stresses. Also, the stiffness of the strain gages themselves affected the results to an unexpectedly high extent. The effect of these errors was minimized, so far as possible, by placing the gages near the points of contraflexure. The vertical forces were applied through a displacement-type loading device; this was necessary because of the asymptotic character of the displacement-load relationship as the load approaches its ultimate value.

According to the linear theory, a vertical downward force of

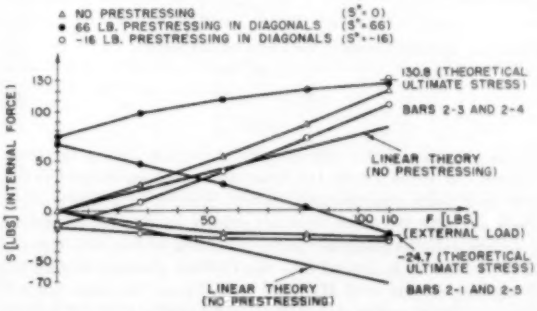

Fig. 3 Stress Histories Versus Load Magnitude

35.5 lb applied at joint 3 causes the structure to collapse as a result of instability. The nonlinear theory predicts collapse at 110.0 lb; during the interval between initial instability and ultimate collapse, the behavior follows a pattern similar to Fig. 3 (reference 1). If the truss is prestressed it may buckle under different loads, but the magnitude of the ultimate load is unaffected. Furthermore, the axial forces in the members, which are linearly related to the

load in the prebuckling range, converge to ultimate values which are independent of the state of initial stress.

These analytical results were largely substantiated by the experiments. The largest recorded vertical load was, in fact, 110 lb, beyond which sharp increases in the joint rotations were accompanied by unappreciably small changes in the load magnitude. This measured value of the collapse load was independent of the initial state of stress; three systems of prestresses were used, as is shown in Fig. 3. Also, the measured axial forces under collapse conditions were reasonably independent of the prestressing systems and in fairly good agreement with the values predicted by the nonlinear analysis.

As was to be expected, however, the precollapse behavior deviated appreciably from the results of the idealized nonlinear theory. In particular, the sharp break between prebuckling (linear) and postbuckling (nonlinear) domains failed to materialize. In fact, joint rotations occurred at load values well below the theoretical buckling load; conversely, the bar force-load relationships were nonlinear from the start (Fig. 3). This discrepancy is readily explicable by virtue of unavoidable initial eccentricities, curvatures, and so on, as well as the fact that the joint translations are disregarded in the moment-rotation relationships at the joints. It can easily be shown analytically that these factors influence the stress and displacement history of the structure, but leave the state of axial stress under collapse conditions as well as the collapse mode itself unaffected. It is of interest to note, however, that the conventional buckling load has become devoid of physical meaning in the indeterminate case. Undoubtedly, the onset of plastic yielding must introduce drastic modifications in the strength analysis; it appears reasonable, however, that in any case the actual load capacity should be computed in terms of the ultimate, rather than of the linear buckling load.

The second part of the experimental program concerned itself with the response of the structure to a couple applied at joint 2. In the absence of any external joint loads, the boundary of the stability range is reached when the force S in the diagonal members equals 67 lb in tension and that in the remaining members 47 lb in compression. Associated with this axial-force system is a buckling mode which, when normalized, is expressed by the vector

$$\theta_1 = \begin{bmatrix} 0.707 \\ 0 \\ -0.707 \end{bmatrix} \quad \ldots\ldots\ldots\ldots\ldots\ldots [17]$$

Since the applied moment vector is of the form

$$M = \begin{bmatrix} 0 \\ M_2 \\ 0 \end{bmatrix} \quad \ldots\ldots\ldots\ldots\ldots\ldots [18]$$

the satisfaction of the orthogonality Equation [11] is therefore evident. In other words, the structure is singular relative to the system of joint couples under study, with $m = 1$ and $p = 0$. Moreover, the Q-surface does not exhibit an interior minimum.

In line with the discussion in the preceding section, the response of the structure is divided into two distinct phases. During the first phase, that is, with $M_2 < M' = 25.7$ in-lb, the stress point P stays inside the region of stability. The rotation vector θ and the axial-force system (identified by λ_1) are governed by Equations [2] and [5]. As P approaches neutral equilibrium, the multiplier c_0 given by Equation [14] vanishes. This follows from the second of Equations [13] and from the fact that the fundamental eigenvector of A (given by Equation [17]) is independent of λ_1. If the structure is prestressed, neutral equilibrium, with $S = 67$ lb, is reached for different values of M'; otherwise, the foregoing discussion is equally applicable.

For $M_2 \geqq M'$, the response of the structure is governed by Equation [15n] (with $n = 1$). The left side of this equation remains constant; this expresses the fact that for increasing moments the axial forces are unaffected. It can be shown that Equation [15n] can be transformed into

$$c = \pm \sqrt{\frac{2(\lambda_1 - \lambda_1^*)\left[\left(\frac{M_2}{M'}\right)^2 - 1\right]}{a_{13,1} - a_{11,1}}} \quad (M_2 \geqq M') \ldots [19]$$

As pointed out before, this defines a hyperbola. On the other hand, the rotation of the center joint, which is independent of c, increases linearly with M_2.

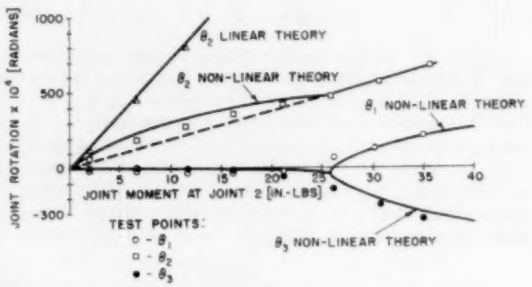

FIG. 4 JOINT ROTATION VERSUS APPLIED COUPLE

Fig. 4 shows the computed and measured values of the joint rotations as functions of the applied moment for the unprestressed case. It is seen that there is good quantitative agreement,[7] especially for large magnitudes of M_2. It is also interesting to note the discontinuous response of the structure as the critical moment M' is reached. The solid straight line corresponds to the center-joint rotation predicted by the linear theory; this was experimentally verified by permitting joint 5 to slide freely and by thus rendering the truss statically determinate. As far as joint 2 is concerned, the introduction of the nonlinear terms amounts to a "stiffening" effect which reduces the joint rotations to 34.9 per cent of those anticipated by the linear theory. Of course it is not to be inferred that all structures, or even the same structure under all loading conditions, display the same degree of stiffening;[8] to some extent, however, the same effect is common in all cases.

ACKNOWLEDGMENT

The authors wish to acknowledge gratefully the help of L. Mente, who was in charge of the very extensive computational phase of the work. Thanks are also due L. H. Donnell, who served as a consultant during the preliminary part of the experimental program.

BIBLIOGRAPHY

1 "Post-Buckling Strength of Redundant Trusses," by E. F. Masur, Trans. ASCE, vol. 119, 1954, p. 699.

2 "A Large Deflection Theory of Redundant Structures," by E. F. Masur, Proceedings of the Second U. S. National Congress of Applied Mechanics, ASME, 1955, pp. 427–436.

3 "Stability of Structural Members Under Axial Load," by E. E. Lundquist, NACA TN 617, 1937.

4 "Buckling of Rigid-Jointed Plane Trusses," by N. J. Hoff, B. A. Boley, S. V. Nardo, and Sara Kaufman, Trans. ASCE, vol. 116, 1951, p. 958.

5 "Zur Theorie der Spannungszustaende in plastischen und sandartigen Medien," by A. Haar and Th. von Karman, Goettingen Nachrichten, Math.-Phys. Kl. 1909, p. 204.

[7] The presence of primary bending moments sharply reduces the effect of initial curvatures, etc., which were mentioned previously.

[8] An almost identical structure subjected to a different (nonsingular) set of joint couples in (2) exhibits hardly any stiffening effect.

The Propagation of Fatigue Cracks

By A. K. HEAD,[1] MELBOURNE, AUSTRALIA

A theory of the rate of growth of fatigue cracks is extended to the case of large stresses. Recent measurements of McClintock and Ryan are discussed.

Introduction

McCLINTOCK and Ryan[2] have recently presented the results of an experiment designed to test a theoretical analysis of the rate of growth of fatigue cracks,[3] in particular, the dependence of rate of growth on stress. While finding agreement with some predictions of the theory, they also point out apparent discrepancies. These will be discussed. In order to do so, it is first necessary to extend the analysis to large stresses, the PM theory being an approximation for small stresses. A résumé of the relevant parts of PM is given and the same notation will be used, except to write a for a_0.

Résumé of PM Theory

The growth of a fatigue crack is visualized as follows: If the crack were in a purely elastic solid then the applied stress would generate a high stress at the tip of the crack, as a result of the large stress concentration there. In a metal this high stress would be above the yield stress and so a plastic region would be created ahead of the tip of the crack. This has three consequences:

(a) As the plastic region yields, it work hardens.

(b) The plastic region is constrained by its elastic surroundings which, as yielding occurs, take up some of the load, thus reducing the stress in the plastic region.

(c) This increase in stress in the surrounding regions will cause some parts, which in the purely elastic case carried a stress less than the yield stress, to be subjected to a large enough stress to become plastic.

On reversing the applied stress, reverse plastic flow will occur, again governed by the three effects mentioned. Continual application of an alternating stress will cause a continual work hardening at the tip of the crack, leading to one or other of the following possibilities:

1 If the peak stress at the tip of the crack in an elastic medium is less than the fracture stress, then the work hardening will tend to a limit after which the applied stress causes elastic deformation only. In this case the crack does not spread.

2 If this peak stress under purely elastic deformation is greater than the fracture stress, then it is impossible for the material to work-harden sufficiently to produce a purely elastic state. Fracture in the neighborhood of the tip of the crack will occur after a number of cycles. The crack then starts to spread with the same process being repeated at the new tip of the crack.

Consider the history of a small volume of metal in the line of advance of the crack. When the crack is far away the stress in the volume is essentially equal to the applied stress and the deformation is elastic. As the crack approaches, the stress rises. When it rises to the initial yield stress the volume becomes plastic and then describes a hysteresis loop, gradually work hardening. When its ductility is exhausted, it fractures and becomes part of the crack.

This process by which a fatigue crack is visualized to extend is too complicated for solution by present methods of mathematical plasticity. So a model of the process was proposed which was simplified sufficiently to be tractable yet retained the essential features. The material is idealized into a chain of three types of mechanical elements:

1 Plastic elements of length a with linear work hardening from yield stress Σ_0 to fracture stress Σ_1. The work-hardening modulus is F so the fracture strain is $(\Sigma_1 - \Sigma_0)/F$.

2 Elastic elements of Young's modulus E through which the stress is applied to the plastic elements. These represent the constraint of the surrounding material. If the length of these elements is taken as half the current length of the crack then it can be shown that certain properties of the model crack correspond closely with a real crack, in particular, the amount the crack opens up under stress and the stress concentration at the tip of the crack.

3 Elastic-shear elements which transfer stress down the chain of elements.

The growth of the model crack leads to the following mathematical problem: Suppose the crack is growing along the x-axis and the center of the crack is at $x = 0$. By symmetry we need only consider one half of the crack, say, that half for x positive. After n cycles of alternating stress $\pm\Sigma$ let the (half) crack extend from $x = 0$ to $x = b(n)$ and the plastic region ahead of the crack extend from $x = b(n)$ to $x = c(n)$.

Let $\sigma(n, x)$ be the yield stress to which the plastic element at x has work hardened and define

$$f(n, x) = \frac{4}{Ea}\,[\sigma(n, x) - \Sigma] \qquad [1]$$

Then in the plastic region ahead of the crack $f(n, x)$ must satisfy[4]

$$\frac{\partial f(n, x)}{\partial n} = \frac{16F}{Ea^2k}\int_{c(n)}^{x} f(n, t)\,\sinh\,[k(x - t)]dt \qquad [2]$$

with boundary conditions

$$f[n, x = b(n)] = \frac{4}{Ea}\,(\Sigma_1 - \Sigma) \qquad [3]$$

$$f[n, x = c(n)] = \frac{4}{Ea}\,(\Sigma_0 - \Sigma) \qquad [4]$$

---

[1] Senior Scientific Officer, Aeronautical Research Laboratories, Department of Supply.

[2] "On the Rate of Growth of Fatigue Cracks," by F. A. McClintock and F. J. Ryan, Journal of Applied Mechanics, Trans. ASME, vol. 76, 1954, pp. 296–297.

[3] "The Growth of Fatigue Cracks," by A. K. Head, *Philosophical Magazine*, seventh series, vol. 44, 1953, pp. 925–938. This paper will be referred to as PM.

Presented at the National Applied Mechanics Conference, Urbana, Ill., June 14–16, 1956, of The American Society of Mechanical Engineers.

Discussion of this paper should be addressed to the Secretary, ASME, 29 West 39th Street, New York, N. Y., and will be accepted until October 10, 1956, for publication at a later date. Discussion received after the closing date will be returned.

Note: Statements and opinions advanced in papers are to be understood as individual expressions of their authors and not those of the Society. Manuscript received by ASME Applied Mechanics Division, July 18, 1955. Paper No. 56—APM-15.

[4] An error was made in PM (17). This is corrected if $4F$ is substituted for F in PM (17), et seq.

$$\frac{kb\Sigma}{E} = \int_b^c f(n, t) \exp\,[k(t-b)]dt \ldots\ldots\ldots [5]^a$$

where

$$k = 2/(ab)^{1/2} \ldots\ldots\ldots [6]$$

The difficulty of the analysis lies in the fact that it is a floating boundary problem; i.e., the positions of the boundary curves $x = b(n)$ and $x = c(n)$ are not given but are to be found from the excess boundary conditions. An approximate solution for the case $\Sigma << \Sigma_0$ was given in PM. A better approximation for this case and also a solution for the case $\Sigma \geq \Sigma_0$ is given here.

Solution for Small Stresses

Formally integrating Equation [2] with respect to n gives

$$f(n, x) = \frac{4}{Ea}(\Sigma_0 - \Sigma) + \frac{16F}{Ea^2k}\int\int f(u, t)\sinh\,[k(x-t)]dt\,du \ldots\ldots [7]$$

where the arbitrary function of integration becomes the constant $4(\Sigma_0 - \Sigma)/Ea$, i.e., the value of $f(n, x)$ for $x = c(n)$, provided the double integral is taken over the region in the $x - n$ plane indicated by shading in Fig. 1.

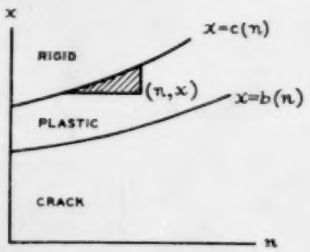

Fig. 1 Region of Integration for Equation [7]

We now assume that the applied stress Σ is small and that the crack is growing slowly, so that over this region of integration the curve $x = c(n)$ can be taken as a straight line of gradient $dc/dn = c'$. Then Equation [7] can be written

$$f(n, x) = \frac{4}{Ea}(\Sigma_0 - \Sigma) + \frac{16F}{Ea^2k}\int_{u=n-\frac{c-x}{c'}}^{u=n}\int_{t=c-c'(n-u)}^{t=x} f(u, t)\sinh\,[k(x-t)]dt\,du \ldots\ldots [8]$$

We now find by iteration an approximate solution to this integral equation for $f(n, x)$. From the Boundary Conditions [3] and [4] we know that $f(n, x)$ increases from

$$4(\Sigma_0 - \Sigma)/Ea \quad \text{for} \quad x = c(n)$$

to

$$4(\Sigma_1 - \Sigma)/Ea \quad \text{for} \quad x = b(n)$$

so as a first approximation take

$$f(n, x) = \frac{4}{Ea}(\Sigma_0 - \Sigma)$$

Substituting this in the right-hand side of Equation [8] and evaluating the integral gives as a second approximation

$$f(n, x) = \frac{4}{Ea}(\Sigma_0 - \Sigma)\left[1 + \frac{16F}{Ea^2k^2c'}\{\sinh\,[k(c-x)] - [k(c-x)]\}\right] \ldots [9]$$

This satisfies the Boundary Condition [4] and to satisfy Equation [3] we must have

$$\frac{dc}{dn} = c' = \frac{16F}{Ea^2k^2}\frac{\Sigma_0 - \Sigma}{\Sigma_1 - \Sigma_0}\{\sinh\,[k(c-b)] - [k(c-b)]\} = \frac{2F}{E}\frac{b^{1/2}}{a^{1/2}}\frac{\Sigma_0 - \Sigma}{\Sigma_1 - \Sigma_0}\{\sinh\,[k(c-b)] - [k(c-b)]\}$$

where we have substituted for k from Equation [6].

Substituting this value of c' in Equation [9] gives

$$f(n, x) = \frac{4}{Ea}\left\{(\Sigma_0 - \Sigma) + (\Sigma_1 - \Sigma_0)\frac{\sinh\,[k(c-x)] - [k(c-x)]}{\sinh\,[k(c-b)] - [k(c-b)]}\right\}$$

and using this, the final Boundary Condition [5] becomes, on writing $z = k(c-b)$

$$\Sigma = (\Sigma_0 - \Sigma)(e^z - 1) + (\Sigma_1 - \Sigma_0)(\sinh z - z)^{-1}\left(\frac{1}{2}ze^z - \frac{5}{4}e^z + \frac{1}{4}e^{-z} + z + 1\right) \ldots\ldots [10]$$

From Equation [10] we see that z is a function of stress only and remains constant during the growth of the crack. Since

$$c - b = z/k = z(ab)^{1/2}/2$$

we have

$$\frac{dc}{dn} - \frac{db}{dn} = \frac{z}{4}\left(\frac{a}{b}\right)^{1/2}\frac{db}{dn}$$

and so

$$\frac{db}{dn} = \left[1 + \frac{z}{4}\left(\frac{a}{b}\right)^{1/2}\right]^{-1}\frac{dc}{dn} \simeq \frac{dc}{dn} = \frac{2F}{E}\frac{b^{1/2}}{a^{1/2}}\frac{\Sigma_0 - \Sigma}{\Sigma_1 - \Sigma_0}(\sinh z - z) \ldots\ldots [11]$$

where the approximation is good for $b >> a$, i.e., for a long thin crack.

Integrating Equation [11] gives

$$b^{-1/2} = \frac{F}{Ea^{1/2}}g(\Sigma)(N - n) \ldots\ldots [12]$$

as the law connecting b the half length of the fatigue crack, with n the number of cycles of applied stress. In Equation [12] N is an arbitrary constant of integration and

$$g(\Sigma) = \frac{\Sigma_0 - \Sigma}{\Sigma_1 - \Sigma_0}(\sinh z - z) \ldots\ldots [13]$$

where z is a function of Σ, Σ_0, and Σ_1 given implicitly by Equation [10]. If $\Sigma << \Sigma_0$ this reduces to

[a] This is a better approximation than the corresponding PM(20) which it replaces.

$$g(\Sigma) = \frac{\Sigma^3}{3(\Sigma_1 - \Sigma_0)(\Sigma_0 - \Sigma)^2} \quad [14]$$

as given in PM.[4]

Solution for Large Stresses

We now consider the case where the applied stress Σ is greater than, or equal to, the initial yield stress of the material Σ_0. Bullen, Head, and Wood[6] have shown that under these conditions there is rapid work hardening throughout the bulk of the metal and after the first few hundred cycles the static yield stress has been raised and is essentially equal to the peak value of the applied stress; so a fatigue crack would be growing in a medium with yield stress equal to the applied stress.

This tends to simplify the analysis of the model crack. For as the bulk of the material is just stressed to the yield stress, the stress concentration of the crack causes the plastic region to extend from the tip of the crack to infinity; i.e., in this case $c(n) = \infty$. So the basic Equation [2] becomes

$$\frac{\partial f(n, x)}{\partial n} = \frac{16F}{Ea^2k} \int_x^\infty f(n, t) \sinh [k(x - t)]dt \quad [15]$$

which is to be solved with the following boundary conditions. From Equation [3]

$$f[n, b(n)] = \frac{4}{Ea} (\Sigma_1 - \Sigma) \quad [16]$$

From Equation [4]

$$f(n, \infty) = 0 \quad [17]$$

From Equation [5]

$$\frac{kb\Sigma}{E} = \int_b^\infty f(n, t) \exp [k(t - b)]dt \quad [18]$$

It will be found that the function

$$f(n, x) = Ae^{\alpha n - \beta x} \quad [19]$$

with A, α, β constants, satisfies Equation [15] provided that

$$\alpha = \frac{16F}{Ea^2(\beta^2 - k^2)} \quad [20]$$

A solution of this form satisfies Equation [17] for positive values of β. Substituting Equation [19] in [16] gives

$$Ae^{\alpha n - \beta b(n)} = \frac{4}{Ea} (\Sigma_1 - \Sigma) \quad [21]$$

and this can only be satisfied strictly if $b(n)$ is a linear function of n with

$$\frac{db}{dn} = \frac{\alpha}{\beta} = \frac{16F}{Ea^2\beta(\beta^2 - k^2)} \quad [22]$$

We now assume that locally the boundary $x = b(n)$ can be regarded as straight and that the foregoing expressions are good approximations. The local gradient of the boundary is given by Equation [22] where β is to be determined from the remaining Condition [18].

Substituting Equation [19] in [18] gives

$$\frac{kb\Sigma}{E} = \frac{A}{\beta - k} e^{\alpha n - \beta b} \quad [23]$$

Eliminating $A \exp(\alpha n - \beta b)$ between Equations [21] and [23] and substituting for k from Equation [6] gives

$$\beta = \frac{2}{(ab)^{1/2}} \frac{\Sigma_1}{\Sigma} \quad [24]$$

and so from Equation [22]

$$\frac{db}{dn} = \frac{2F}{E} \frac{b^{1/2}}{a^{1/2}} \frac{\Sigma^3}{\Sigma_1(\Sigma_1^2 - \Sigma^2)} \quad [25]$$

which on integration becomes

$$b^{-1/2} = \frac{F}{Ea^{1/2}} \frac{\Sigma^3}{\Sigma_1(\Sigma_1^2 - \Sigma^2)} (N - n) \quad [26]$$

where N is an arbitrary constant of integration.

Solution for All Stresses

On comparing Equations [12] and [26] it will be seen that the laws of crack growth for both small and large stresses are of the same form, namely

$$b^{-1/2} = \frac{F}{Ea^{1/2}} g(\Sigma) (N - n) \quad [27]$$

where

$$g(\Sigma) = \frac{\Sigma^3}{\Sigma_1(\Sigma_1^2 - \Sigma^2)} \quad \text{for } \Sigma \geq \Sigma_0 \quad [28]$$

$$= \frac{\Sigma_0 - \Sigma}{\Sigma_1 - \Sigma_0} (\sinh z - z) \quad \text{for } \Sigma \ll \Sigma_0 \quad [29]$$

with z given by Equation [10].

It is a reasonable assumption that at intermediate stresses the crack-growth law will still be of the same form as Equation [27] with an intermediate function $g(\Sigma)$ connecting the upper and lower forms, Equations [28] and [29]. In Fig. 2, Equations [28] and [29] are shown by solid curves (for the case $\Sigma_0 = 2/3\Sigma_1$). It will be seen that there can be but little uncertainty in connecting the two. The dashed connection is the continuation of Equation [28] which is seen to provide a good approximation to $g(\Sigma)$ for all values of Σ. Now Equation [28] would be strictly true for all stresses for a material with zero initial yield stress. So the rate of growth of a crack in this material is only slightly faster than in a similar material with an initial yield stress, even though the plastic region is infinite in one case and finite in the other.

The explanation of this insensitivity to the value of Σ_0 follows from the foregoing analysis. From Equation [1], $f(n, x)$ is proportional to the excess of local stress over applied stress. From Equation [19] this difference exponentially decreases ahead of the crack with decay length

$$\frac{1}{\beta} = \frac{(ab)^{1/2}}{2} \frac{\Sigma}{\Sigma_1}$$

by Equation [24]. Thus the significant work hardening is occurring in a region ahead of the crack, of length of order $(ab)^{1/2}$, and this is the same order as the size of the finite plastic region in the case where the material has an initial yield stress. Thus the work hardening is mainly near the tip of the crack in both cases and the rate of crack growth depends mainly on Σ and Σ_1 and is little affected by the value of Σ_0.

[6] "Structural Changes During the Fatigue of Metals," by F. P. Bullen, A. K. Head, and W. A. Wood, Proceedings of the Royal Society of London, England, series A, vol. 216, 1953, p. 332.

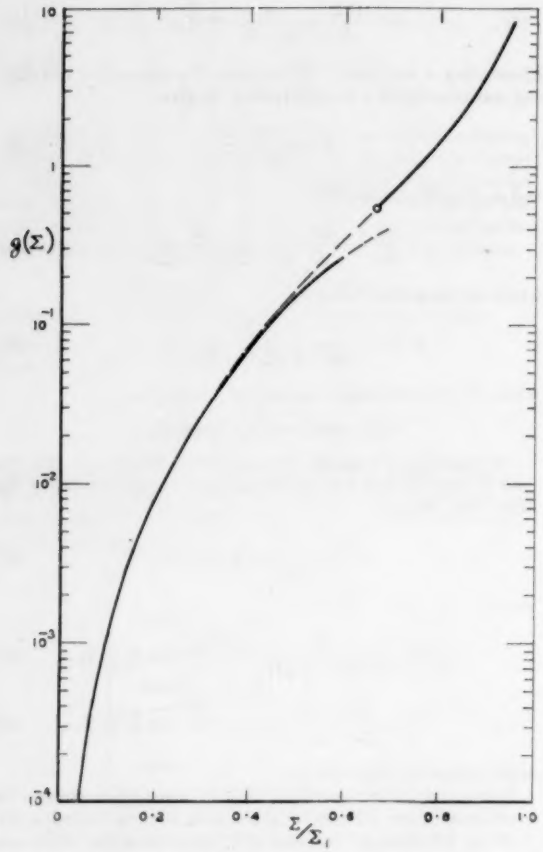

FIG. 2 DEPENDENCE OF $g(\Sigma)$ ON Σ FOR THE CASE $\Sigma_0 = {}^2/_3\Sigma$

CONCLUSION

McClintock and Ryan[3] have pointed out that the PM theory predicts an infinite rate of growth when the applied stress is equal to the yield stress. This follows from Equation [14] and is now seen to be due to the approximations used which restrict the validity of this equation to $\Sigma << \Sigma_0$. For $\Sigma = \Sigma_0$ there is a definite finite rate of growth given by Equation [26].

They also point out that their measurements imply that F must be from one hundred to one thousand times smaller than its value as measured in a tensile test. A similar difference was found for the data analyzed in PM. An alternative way of expression is that the ductility of the metal under fatigue conditions must be 100 to 1000 times greater than that measured under unidirectional loading. This is discussed in PM where it was pointed out that the total plastic strain to fracture for cyclic stressing can be expected to be much larger than for static stressing. This is verified by measurements of the hysteresis loop during fatigue. For example, measurements have been made in the author's laboratories which show that, for copper under a push-pull stress of 11,000 psi, the average plastic strain per cycle is approximately equal to the elastic strain ($\sim$0.1 per cent). For a life of 10^4 cycles this gives a total plastic strain of 1000, which is of the right order of magnitude.

McClintock and Ryan also have suggested a number of additional properties the model might have which would make it closer to a real crack. These are interesting, particularly the suggestion that the crack should be able to carry a compressive load, as it appears to do in practice. One improvement was considered, namely, to allow the plastic elements to be elastic plastic instead of rigid plastic. This leads to a floating-boundary problem (as indeed all models should since the problem of the real crack is one) with a more complicated set of equations. These could be solved only by making further mathematical approximations and the final result was not essentially different from that for rigid-plastic elements. Any inherent improvements were apparently lost by the more drastic approximations necessary to find a solution. It would appear that to introduce, and retain, improvements in the model is essentially a mathematical problem calling for a more exact analysis than has been used so far.

ACKNOWLEDGMENTS

This paper is based on an internal report,[7] and is published by permission of the Chief Scientist, Department of Supply.

[7] "Growth of Fatigue Cracks," by A. K. Head, Report Met. 5, Department of Supply, Commonwealth of Australia, July, 1954.

Impact With Finite Acceleration Time of Elastic and Elastic-Plastic Beams[1]

By R. C. ALVERSON,[2] PROVIDENCE, R. I.

The purpose of the work described in this paper was to provide information on the elastic and plastic deformation of steel beams subjected to transverse impact. The particular impact problem treated was chosen to correspond to conditions in tests in which a beam initially at rest is struck by a massive hammer, so that a specified change of velocity is imposed at a certain cross section in a small time interval. In the present analysis the initial elastic and subsequent elastic-plastic motions were obtained by methods similar to those used by Bleich and Salvadori (3).[3] As in (3), it is assumed that plastic deformation occurs only at a single stationary plastic hinge (in this case at the struck cross section). Results obtained are compared with those of a "rigid-plastic" solution of the same problem, in which plasticity conditions are correctly taken into account but elastic vibrations are not included.

Introduction

VARIOUS problems of impact and dynamic loading of beams have been considered previously by several authors. Using the rigid-plastic hypothesis, Symonds and Leth (1) have obtained the solution for a finite beam whose mid-section acquires a given velocity in zero time; and Green (2), has modified their solution to include the finite acceleration time. Experiments have been conducted at Brown University to check the ranges of the parameters involved for which the plastic deformations predicted in (1) and (2) are good approximations.

A previous study of elastic-plastic deformations of beams was made by Bleich and Salvadori (3), who gave a method for the mathematical analysis of elastic-plastic beams subjected to impulsive loading. They applied their method to obtain the motion and the final deformation of a free-free beam with a given symmetric initial velocity distribution. Thomson (4) has also obtained solutions of several elastic-plastic beam problems by analog-computing methods.

In this paper is presented a solution for the elastic-plastic motion of a uniform beam of length $2l$ subjected to a specified impact condition, in which the middle cross section is forced to move with velocity Vt/τ in the time interval $0 < t \leq \tau$, and with velocity V = const for $t > \tau$. The acceleration time τ is taken to be small but finite. In particular, the permanent angle of rotation at the struck cross section is computed on the assumption that only one plastic hinge is present. The results are compared with those obtained by use of the rigid-plastic hypothesis (1, 2). The range of validity of the present results is determined by examining the bending-moment distribution along the beam.

The mathematical solution of the problem is sketched in the Appendix. The following section summarizes the results of main interest, and presents a discussion of their significance.

Principal Results and Discussion

The physical quantities involved in the analysis, in addition to the half length of the beam l, the velocity V, and acceleration time τ, are mass per unit length m, elastic flexural rigidity EI, and limit moment M_p. The curve representing the moment-curvature relation is assumed to consist of two straight lines as shown in Fig. 1. Results are best presented in terms of certain

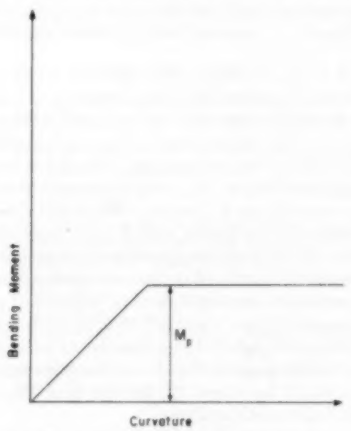

FIG. 1 BENDING-MOMENT CURVATURE RELATION ASSUMED IN THIS REPORT

dimensionless combinations; namely, $ml^2V/M_p\tau$, τ/T, and $M_p\theta_b/mlV^2$, where $T_1 = 1.79l^2\sqrt{m/EI}$ denotes the fundamental period of vibration of the elastic beam, and θ_b is the permanent angle of rotation of the mid-point.

In the first stage of the motion the beam behaves wholly elastically. The solution for the displacement $y(x, t)$ of the beam in this phase is given by Equation [5] in the Appendix. This phase ends at a time t_1 when the moment M_0 at the mid-section becomes equal to M_p. Fig. 2 shows how the moment M_0 builds up with time, since it is a plot of $M_0\tau/ml^2V$ as a function of t/T_1 from Equation [6]. By setting $M_0 = M_p$ and $t = t_1$, this curve furnishes the time ratio t_1/T_1 at which the wholly elastic phase terminates. For example, if $M_p\tau/ml^2V = 0.02$, the corresponding value of t_1/T_1 is about 0.0125. In this paper only the case where $t_1 < \tau$ is considered.

For $t > t_1$ it is necessary to solve a new boundary-value problem, in which the condition of slope continuity at the mid-section, which holds in the wholly elastic phase, is replaced by the condition for a plastic hinge, namely, $M_0 = M_p$ = const, while the

---

[1] The results presented in this paper were obtained in the course of research sponsored by the Office of Naval Research under Contract N7onr-35801.

[2] Instructor in Engineering, Division of Engineering, Brown University.

[3] Numbers in parentheses refer to the Bibliography at the end of the paper.

Presented at the National Applied Mechanics Conference, Urbana, Ill., June 14-16, 1956, of THE AMERICAN SOCIETY OF MECHANICAL ENGINEERS.

Discussion of this paper should be addressed to the Secretary, ASME, 29 West 39th Street, New York, N. Y., and will be accepted until October 10, 1956, for publication at a later date. Discussion received after the closing date will be returned.

NOTE: Statements and opinions advanced in papers are to be understood as individual expressions of their authors and not those of the Society. Manuscript received by ASME Applied Mechanics Division, July 12, 1955. Paper No. 56—APM-14.

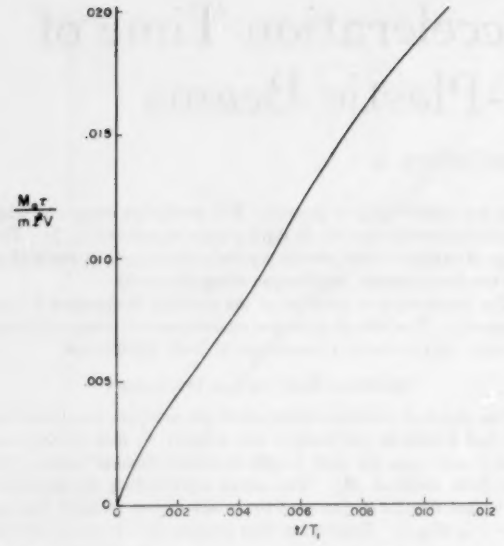

FIG. 2 BENDING MOMENT AT MID-POINT OF BEAM AS A FUNCTION OF TIME UP TO END OF WHOLLY ELASTIC STAGE

slope angle θ is unprescribed. The solution for $y(x, t)$ in this phase is given by Equation [7] of the Appendix.

It should be emphasized that the solution presented for the second phase is valid only so long as the beam is wholly elastic everywhere except at the mid-section. On this assumption the solution applies so long as the rate of increase $\dot{\theta}$ of the slope angle at the plastic hinge is positive. When this rate vanishes a new wholly elastic phase begins, with $\dot{\theta} = 0$; otherwise the rotation at a plastic hinge would be opposite in sense to the moment.

The slope angle θ_0 calculated at the instant when $\dot{\theta}$ becomes zero is thus the permanent angular deflection, which is of practical interest as a measure of the "damage" done to the beam in the impact. The plot of $M_p\theta_0/mlV^2$ as a function of $ml^2V/M_p\tau$ for the case $\tau/T_1 = 0.02$ is given in Fig. 3. In the same figure is drawn the curve obtained by Green (2) for the final slope angle predicted by the rigid-plastic analysis.

The particular value $\tau/T_1 = 0.02$ for which computations were made was chosen as representative of values used in experiments at Brown University, to be described elsewhere (5). For the same reason computations were made only for $ml^2/V/M_p\tau$ in the range between 50 and 250. In this range the effect of varying the time ratio τ/T_1 from 0.02 to 0.08 was found to be small; the reduction of $M_p\theta_0/mlV^2$ was found to be of the order of 10 per cent at $ml^2V/M_p\tau = 50$, and less than 1 per cent for $ml^2V/M_p\tau \geq 150$. In the calculation of the curve in Fig. 3 only the first two terms of the series were retained; for the range of variables considered the effects of additional terms would not have been visible in the curve as plotted. Furthermore, the possibility of successive elastic and elastic-plastic stages beyond the first elastic-plastic phase has been neglected.

It is noteworthy that the permanent angular deflections predicted by the present analysis are much less than those predicted by the rigid-plastic solution. The latter type of analysis has been proposed as a suitable one for cases in which the ratio of the energy spent in plastic-deformation greatly exceeds the maximum elastic-strain energy that could be stored in the beam. The ratio R of these two energies can be taken as $R = 2M_p\theta_0/(M_p^2l/EI)$, since M_p^2l/EI is the elastic strain energy of the beam loaded to the limit moment throughout. Thus when $R \gg 1$ it is

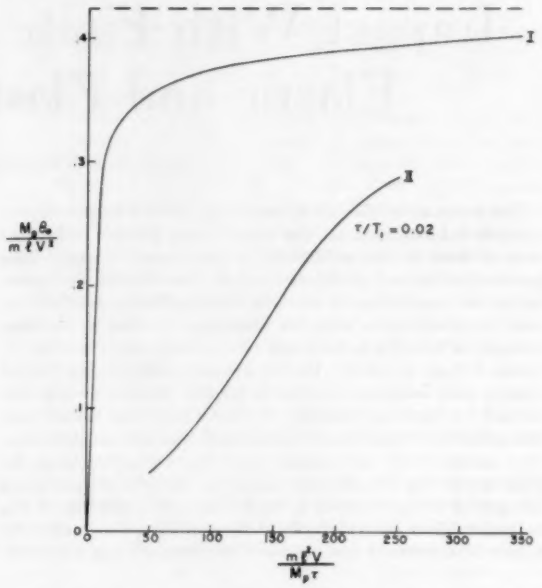

Curve I, Nondimensional angular-deflection curve—rigid-plastic analysis (2)

Curve II, Nondimensionalized deflection curve from present analysis

FIG. 3 NONDIMENSIONAL DEFLECTION CURVES

reasonable to expect that deformations predicted by the plastic-rigid type of analysis will be satisfactory at least so far as the neglect of elastic deformation is concerned; for example, if $R \geq 10$ the plastic-rigid analysis should give results agreeing closely with those furnished by an elastic-plastic solution of a given problem. However at $ml^2V/M_p\tau = 150$, where $2M_p\theta_0$ from the rigid-plastic solution is about $0.80mlV^2$, we have $R \simeq 10$, but the angular deformation predicted by the rigid-plastic analysis is about 2 times that predicted by the present solution. However, the permanent deformation predicted in the present analysis generally exceeds that observed in experiments (5).

Investigation of the bending-moment distribution along the beam at various times after the beginning of the plastic hinge at the mid-section yields some significant information concerning the validity of the curve in Fig. 3. Calculations for particular cases show that at a short distance from the mid-section the bending moment first decreases and then increases and attains a maximum in the vicinity of $x = 0.4l$. For $ml^2V/M_p\tau = 65$, of $R = 0.85$,[4] the bending moment near $x = 0.4l$ reaches M_p at nearly the same time that the deformation predicted in Fig. 3 is attained. For values of $ml^2V/M_p\tau$ greater than about 65, the yield moment is exceeded in the vicinity before the deformation predicted in Fig. 3 is reached.

Further calculations show that for still higher values of $ml^2V/M_p\tau$, a negative yield moment (opposite in sense to the moment at the mid-section) in the vicinity of $x = 0.4l$ is attained before the deformations predicted in Fig. 3 are reached, and if the solution obtained in this paper were still valid, a positive yield moment would later be attained. The value of $ml^2V/M_p\tau$ for which the negative yield moment is first attained is about 80, corresponding to R equal to about 1.3. Plots of these results are shown in Figs. 4 and 5, where only the first two terms of the series have been re-

[4] The R-values quoted here are based on the angular deformation computed according to the present elastic-plastic analysis.

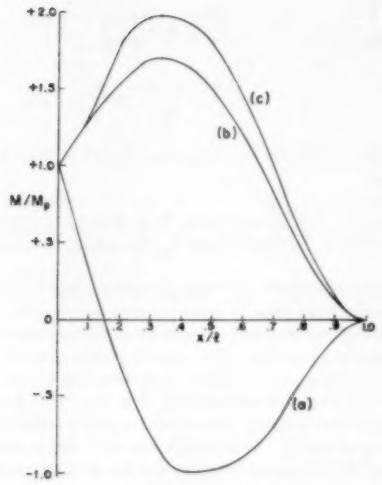

(*a*) at $t/T_1 = 0.070$
(*b*) at $t/T_1 = 0.140$
(*c*) at $t/T_1 = 0.185$

FIG. 4 BENDING DISTRIBUTION ALONG BEAM FOR $ml^2V/M_p\tau = 80$, $R = 1.3$

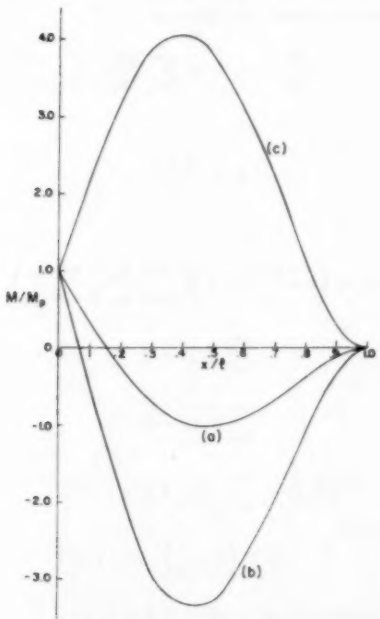

(*a*) at $t/T_1 = 0.020$
(*b*) at $t/T_1 = 0.070$
(*c*) at $t/T_1 = 0.180$

FIG. 5 BENDING-MOMENT DISTRIBUTION ALONG BEAM FOR $ml^2V/M_p\tau = 200$, $R = 25.0$

tained in the calculations. The negative bending at outer hinges has been observed in experiment (5), and is predicted in the rigid-plastic analysis of the problem.

SUMMARY

To summarize, it has been found that the prediction of angular deformation given by the plastic-rigid analysis exceeds that of the present elastic-plastic solution by a factor ranging from 6 at $ml^2V/M_p\tau = 50$ to 1.4 at $ml^2V/M_p\tau = 250$. In this comparison the ratio τ/T_1 (of the impact duration to the fundamental period of the elastic beam) has the constant value 0.02, but the results otherwise are in general nondimensional form. As $ml^2V/M_p\tau$ varies from 50 to 250 the ratio R of the work done at plastic hinges to the maximum possible elastic-strain energy increases from 0.70 to 35.

The present elastic-plastic solution is known to satisfy the plasticity condition throughout the beam only in the range $ml^2V/M_p\tau < 65$. Hence the angular deformations predicted by this solution are strictly correct only in this range, which corresponds to $R \leq 0.85$. If $ml^2V/M_p\tau$ exceeds 65 by an amount which is not very large, the present results will probably be reasonable approximations. However, if $ml^2V/M_p\tau$ is much greater than 80, gross violations of the plasticity condition occur, as indicated by Fig. 5. No validity can then be claimed for this elastic-plastic solution in this range, and the results, unfortunately, cannot be used to test the validity of the rigid-plastic solution. The latter solution is presumably accurate at large enough values of $ml^2V/M_p\tau$. However, an estimate of the particular value of this parameter above which the error of the rigid-plastic solution is less than, say, 10 per cent, can only be obtained by a complete elastic-plastic solution which takes proper account of the plasticity condition throughout the beam.

BIBLIOGRAPHY

1 "Impact of Finite Beams of Ductile Metal," by P. S. Symonds and C. F. A. Leth, *Journal of the Mechanics and Physics of Solids*, vol. 2, 1954, p. 92.

2 "The Effect of Acceleration Time on Plastic Deformation of Beams Under Transverse Impact Loading," by D. S. Green, Report No. A11-112 of Brown University to the Office of Naval Research under Contract N7-onr-35801.

3 "Impulsive Motion of Elasto-Plastic Beams," by H. H. Bleich and M. G. Salvadori, Proceedings of the American Society of Civil Engineers, Separate No. 287, September, 1953.

4 "Impulsive Response of Beams in the Elastic and Plastic Regions," by W. T. Thomson, JOURNAL OF APPLIED MECHANICS, Trans. ASME, vol. 76, 1954, p. 271.

5 "Plastic Deformation of Beams in Impact—Theory and Preliminary Tests," by T. J. Mentel, D. S. Green, and P. S. Symonds, Report of Brown University to Office of Naval Research under Contract N7-onr-35801, in preparation.

Appendix

The problem considered in this paper is to obtain the elastic and elastic-plastic motion of a free-free beam which undergoes impact loading at its mid-point for a finite period of time. The beam is supposed initially at rest and the mid-section acquires a velocity V in a small finite period of time τ, for all subsequent time the velocity of the mid-point is assumed constant and equal to V.

The origin of co-ordinates is taken at the mid-point of the beam at $t = 0$. The distance along the central axis of the beam is denoted by the variable x, and y denotes the lateral displacement of the beam at any point x, and for each value of time t.

From the symmetry of the problem it is only necessary to obtain the solution of the equation of motion in $0 \leq x \leq l$ for all t.

The differential equation to be satisfied is

$$\frac{\partial^4 y}{\partial x^4} + a^2 \frac{\partial^2 y}{\partial t^2} = 0 \qquad a^2 = \frac{m}{EI} \qquad [1]$$

where m is mass per unit length and EI is the flexural rigidity, which is assumed constant.

The boundary conditions are

$$y_x(0, t) = y_{xx}(l, t) = y_{xxx}(l, t) = 0$$

and

$$y(0, t) = \frac{Vt^2}{2\tau} \quad \text{for } 0 \leq t \leq \tau$$

$$= V\left(t - \frac{\tau}{2}\right) \quad \text{for } t \geq \tau$$

and the two initial conditions are

$$y(x, 0) = y_t(x, 0) = 0$$

Equation [1] is transformed by use of the Laplace integral and becomes

$$d^4 \frac{Y(x, s)}{dxt} - q^4 Y(x, s) = 0 \quad \ldots\ldots\ldots\ldots [2]$$

where

$$q^4 = -a^2 s^2$$

and

$$Y(x, s) = \int_0^\infty e^{-st} y(x, t)dt$$

The most general solution of Equation [2] is

$$Y(x, s) = C_1 \cosh qx + C_2 \sinh qx + C_3 \sin qx + C_4 \cos qx$$

where the C's are arbitrary functions of the parameter s. When the boundary conditions are satisfied, $Y(x, s)$ becomes

$$Y(x, s) = \frac{\alpha(s)}{2}(\cosh qx + \cos qx)$$

$$+ \frac{\alpha(s)}{2} \frac{\sinh ql \sin ql}{(1 + \cosh ql \cos ql)}(\cosh qx - \cos qx)$$

$$- \frac{\alpha(s)}{2} \frac{(\cosh ql \sin ql + \sinh ql \cos ql)}{(1 + \cosh ql \cos ql)}(\sinh qx - \sin qx)$$

$$\ldots\ldots [3]$$

When this solution is inverted to x and t and after some manipulation

$$y(x, t) = \frac{V}{2\tau}[t^2 - (t - \tau)^2]$$

$$+ \frac{2Va^2l^4}{\tau} \sum_{n=1}^{\infty} \left[\cos \frac{\mu_n^2 t}{al^2} - \cos \frac{\mu_n^2}{al^2}(t - \tau)\right] \Gamma_n \varphi_n, \ldots [4]$$

where $\Gamma_n = \dfrac{\sinh \mu_n - \sin \mu_n}{\mu_n^5}$

$$\varphi_n = \frac{\cosh \mu_n \frac{x}{l} - \cos \mu_n \frac{x}{l}}{\cosh \mu_n + \cos \mu_n} - \frac{\sinh \mu_n \frac{x}{l} - \sin \mu_n \frac{x}{l}}{\sinh \mu_n + \sin \mu_n}$$

$$(t - \tau) = 0 \quad \text{when } t \leq \tau$$

$$= t - \tau \text{ for } t > \tau$$

and the μ_n are the solutions of $\cos ql \cosh ql = -1$.

It is readily verified that this solution for $y(x, t)$ satisfies the differential equation together with the boundary and initial conditions.

The case of practical interest is when the yield bending moment at the mid-section is reached for $t < \tau$. The solution for $y(x, t)$ for $t < \tau$ can be written

$$y(x, t) = \frac{V}{2\tau}\left(t^2 - \frac{a^2x^4}{12} - \frac{a^2l^2x^2}{2} + \frac{a^2x^2l}{3}\right)$$

$$+ \frac{2Va^2l^4}{\tau} \sum_{n=1}^{\infty} \cos \frac{\mu_n^2 t}{al^2} \Gamma_n \varphi_n \ldots\ldots [5]$$

Letting M_0 denote the bending moment at $x = 0$, in nondimensional form

$$\frac{M_0 \tau}{ml^2 V} = \frac{1}{2} - 4 \sum_{n=1}^{\infty} \cos \frac{\mu_n^2 t}{al^2} \frac{1}{\mu_n^3}\left(\frac{\sinh \mu_n - \sin \mu_n}{\cosh \mu_n + \cos \mu_n}\right) \ldots [6]$$

The quantity $M_0\tau/ml^2V$ has been plotted against t/T_1 in Fig. 2. T_1 denotes the fundamental period of vibration of the beam and only the first three terms of the series have been retained.

Assuming then that the yield moment has occurred at the mid-point for a value of $t_1 < \tau$, a new boundary-value problem must be solved. It is also assumed that after the yield moment has occurred that the bending moment at the mid-point remains constant and equal to M_p. It is further assumed that a plastic hinge develops at the mid-point and that this hinge is infinitely thin.

For $t > t_1$ where $t_1 < \tau$, the differential equation to be satisfied is still

$$\frac{\partial^4 y}{\partial x^4} + a^2 \frac{\partial^2 y}{\partial t^2} = 0$$

But the boundary conditions are now

$$(a) \qquad \frac{\partial^2 y}{\partial x^2}(0, t) = B \sum_{n=1}^{\infty} \frac{2A_n}{\mu_n^3}$$

where

$$B = \frac{2Va^2l^2}{\tau}$$

and

$$A_n = \left(\cos \frac{\mu_n^2 t_1}{al^2} - 1\right)\left(\frac{\sinh \mu_n - \sin \mu_n}{\cosh \mu_n + \cos \mu_n}\right)$$

$$(b) \qquad \frac{\partial^2 y}{\partial x^2}(l, t) = 0$$

$$(c) \qquad \frac{\partial^3 y}{\partial x^3}(l, t) = 0$$

$$(d) \qquad y(0, t) = \frac{Vt^2}{2\tau} \quad \text{for} \quad t \leq \tau$$

$$= V\left(t - \frac{\tau}{2}\right) \quad \text{for} \quad t \geq \tau$$

and the conditions to be satisfied at $t = t_1$ are

$$(1) \qquad y(x, t_1) = \frac{V}{2\tau} t_1^2 + \frac{2Va^2l^4}{\tau} \sum_{n=1}^{\infty} \frac{1}{\mu_n^5} B_n \varphi_n$$

$$= \frac{V}{2\tau} t_1^2 + Bl^2 \sum_{n=1}^{\infty} \frac{1}{\mu_n^5} B_n \varphi_n$$

where

$$B_n = (\cosh \mu_n + \cos \mu_n)A_n$$

and B, A_n, and φ_n are as previously defined.

$$\frac{\partial y}{\partial t}(x, t_1) = \frac{Vt_1}{\tau} - \frac{B}{a}\sum_{n=1}^{\infty}\frac{1}{\mu_n^3}C_n\varphi_n \qquad (2)$$

where

$$C_n = \sin\frac{\mu_n^2 t_1}{al^2}(\sinh\mu_n - \sin\mu_n)$$

Upon changing to the new time $u = t - t_1$, the Laplace integral with respect to u yields an ordinary differential equation in the (x, s)-plane. Solution of this equation together with its boundary conditions gives $Y(x, s)$.

Then, after applying the complex inversion integral

$$\left.\begin{aligned} y(x,u) &= \frac{V}{2\tau}\left(1-\frac{3x}{2l}\right)[u^2-(u-\gamma)^2] \\ &+ \frac{B}{2}l^2\sum_{m=1}^{\infty}\frac{1}{V_m^5}\left(\cos\frac{V_m^2 u}{al^2}-\cos\frac{V_m^2(u-\gamma)}{al^2}\right)\left(\frac{1}{\sin V_m}-\frac{1}{\sinh V_m}\right)\theta_m \\ &- \frac{6B}{al}xu\sum_{n=1}^{\infty}\frac{D_n}{\mu_n^5} + 6Blx\sum_{n=1}^{\infty}\frac{A_n}{\mu_n^7} \\ &+ B\left(x^2-\frac{x^3}{2l}+\frac{6x^5}{l_5^3}-\frac{3xu^2}{a^2l^2}\right)\sum_{n=1}^{\infty}\frac{A_n}{\mu_n^3} \\ &- \frac{33}{70}Blx\sum_{n=1}^{\infty}\frac{A_n}{\mu_n^3} \\ &- 2Bl^3\sum_{m=1}^{\infty}\sum_{n=1}^{\infty}\frac{D_n}{\mu_n V_m(\mu_n^4-V_m^4)}\left(\frac{1}{\sinh V_m}+\frac{1}{\sin V_m}\right)\frac{\sin V_m^2\mu}{a^2}\theta_m \\ &+ 2Bl^3\sum_{m=1}^{\infty}\sum_{n=1}^{\infty}\frac{A_n\mu_n}{V_m^2(\mu_n^4-V_m^4)}\left(\frac{1}{\sinh V_m}+\frac{1}{\sin V_m}\right)\cos\frac{V_m^2\mu}{al^2}\theta_m \\ &+ \frac{Vt_1^2}{2\tau}+\frac{Vt_1}{\tau} \end{aligned}\right\} \ldots [7]$$

$$\ldots [7] \text{ (continued)}$$

where $\tan V_m = \tanh V_m$

$$\theta_m = \frac{\sinh\frac{V_m x}{l}}{\sinh V_m} + \frac{\sin\frac{V_m x}{l}}{\sin V_m}$$

$$\gamma = \tau - t_1 \qquad D_n = \frac{c_n}{\cosh\mu_n + \cos\mu_n}$$

and

$$\begin{aligned} (u-\gamma) &= 0 \quad \text{for} \quad u \le \gamma \\ &= u-\gamma \quad \text{for} \quad u > \gamma \end{aligned}$$

It is easily verified that this solution satisfies the differential equation, the boundary conditions, and the initial conditions.

On the Determination of a Viscoelastic Model for Stress Analysis of Plastics[1]

By D. R. BLAND[2] and E. H. LEE[3]

A method of assessing whether or not the measured variation of complex compliance with frequency for a viscoelastic material is consistent with a four-element model is presented. The four-element model was chosen since it is relatively simple to analyze, and exhibits the three main types of viscoelastic response; namely, instantaneous elasticity, viscous flow, and delayed elasticity. If the compliance measurements are found to conform with the behavior of a four-element model over the whole or part of the frequency range studied, a graphical method of determining the model constants is presented. The significance of the application of such a model to stress analysis under transient loading is discussed.

Introduction

THE determination of the stresses in a viscoelastic body subjected to transient loading is considerably simplified (1)[4] if the stress-strain, $\sigma - \epsilon$, relation can be represented by a linear operator equation of the form

$$P(\sigma) = Q(\epsilon) \quad \ldots\ldots [1]$$

where P and Q are polynomials in the operator $\partial/\partial t$, t denoting time. In this paper we consider single components of stress and strain, which could, for example, be shear, or simple tension. The lower the order of these polynomials which will adequately reproduce the response of the material to stress, the simpler the analysis becomes. We therefore seek a method of assessing how well experimental measurements can be reproduced by means of a four-element model, Fig. 1, which corresponds to quadratic polynomials, or by means of simpler models.

The experimental measurements of the viscoelastic properties of the material are considered to be in the form of the steady-state response with periodic variation of stress and strain of angular frequency ω, which can be represented in the complex form

$$\frac{\epsilon}{\sigma} = J'(\omega) - iJ''(\omega) \quad \ldots\ldots [2]$$

where the time dependence of both ϵ and σ is of the form $e^{i\omega t}$. This ratio is known as the complex compliance, and nonzero imaginary part, $J''(\omega)$, implies a phase difference between the oscillations of stress and strain. Both J' and J'' are functions of ω which can be determined experimentally over the frequency range of interest.

If the viscoelastic properties of the material are governed by Equation [1], substitution of steady-state sinusoidal variation of stress and strain determines

$$\frac{\epsilon}{\sigma} = \frac{P(i\omega)}{Q(i\omega)} = J'(\omega) - iJ''(\omega) \quad \ldots\ldots [3]$$

Thus, given P and Q, J' and J'' can be found. In this paper we are concerned with the deduction of P and Q, for prescribed J' and J'' as functions of ω.

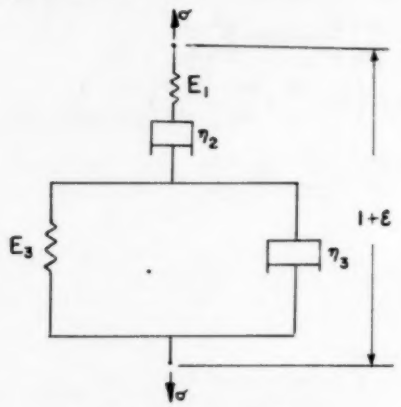

Fig. 1 Four-Element Model

For many problems of transient loading with a limited loading duration, which is also of the order of the time during which stress analysis is of interest, the load variation is dominated by a relatively narrow spectrum of frequencies. These are dominant frequencies in a Fourier-series expansion of the loading function. Within this range of frequencies, it may be possible adequately to reproduce the variation of complex compliance with an equation of the type of Equation [1], corresponding to a four-element model. This model can only be expected to be satisfactory within the particular time range of interest and for the type of loading function for which it was devised, and a more complicated law probably would be necessary to represent the viscoelastic behavior of the material over a wider frequency range. Moreover, the model will represent the material at a prescribed temperature, and the values of the material constants, and possibly the type of model, may be temperature-dependent.

The foregoing limitations emphasize the contrast between the objectives of this paper and, for example, the work of Leaderman and Marvin (2), who sought a viscoelastic model to reproduce approximately the response of a material over a very wide range of frequencies. In that paper close agreement with measured compliances was not sought, and the general form of the complex compliance function could be reproduced by a six-element model, which was equivalent to the four-element model of Fig. 1, with an

[1] This work was sponsored under a Department of Defense Contract NOrd 11496, with the Bureau of Ordnance, Navy Department.

[2] Imperial Chemical Industries Research Fellow, King's College, London, England.

[3] Professor of Applied Mathematics, Brown University, Providence, R. I.

[4] Numbers in parentheses refer to the Bibliography at the end of the paper.

Presented at the National Conference of the Applied Mechanics Division, Urbana, Ill., June 14–16, 1956, of The American Society of Mechanical Engineers.

Discussion of this paper should be addressed to the Secretary, ASME, 29 West 39th Street, New York, N. Y., and will be accepted until October 10, 1956, for publication at a later date. Discussion received after the closing date will be returned.

Note: Statements and opinions advanced in papers are to be understood as individual expressions of their authors and not those of the Society. Manuscript received by ASME Applied Mechanics Division, January 3, 1956. Paper No. 56—APM-26.

additional Voigt unit of spring and dashpot in parallel placed in series. The frequency range was so wide, of the order 10^{15}, that, in determining the model constants, the individual Voigt units and the spring and dashpot in series could be considered independently, leading to compliance curves with two regions of variation separated by plateaus of essentially constant compliance. For the objective of the present paper, the accuracy required of the model and the narrow frequency range considered involve the interaction of the elements of the model, so that the combined response must be studied throughout the investigation, and the influences of the individual groups of elements cannot be considered separately.

The Four-Element Model

The four-element model shown in Fig. 1 offers the possibility of representing material behavior adequately since it exhibits the three main types of deformation found in viscoelastic materials:

(*a*) Instantaneous elastic response associated with the spring element E_1.

(*b*) Viscous flow associated with the dashpot η_2.

(*c*) Delayed elastic response associated with the Voigt unit of spring and dashpot in parallel, $E_3\ \eta_3$

It is the simplest model which exhibits all three phenomena.

Let us derive the relation of the type 1 corresponding to this model. Let ϵ_1, ϵ_2, and ϵ_3 be the strain components in the spring, dashpot, and Voigt unit, respectively; then the total strain ϵ is given by

$$\epsilon = \epsilon_1 + \epsilon_2 + \epsilon_3 \quad \ldots\ldots [4]$$

The stress σ is the same through each of these units, giving

$$\sigma = E_1\epsilon_1 = \eta_2 \frac{\partial \epsilon_2}{\partial t} = E_3\epsilon_3 + \eta_3 \frac{\partial \epsilon_3}{\partial t} \quad \ldots\ldots [5]$$

Operating formally with the operator $D = \partial/\partial t$, Equation [5] substituted into Equation [4] gives

$$\epsilon = \left(\frac{1}{E_1} + \frac{1}{\eta_2 D} + \frac{1}{E_3 + \eta_3 D}\right)\sigma \quad \ldots\ldots [6]$$

To express this in the form of Equation [1] we must remove the D from the denominator by multiplying throughout by

$$D\left(D + \frac{E_3}{\eta_3}\right)$$

giving

$$\left[\frac{1}{E_1}D^2 + \left(\frac{E_3}{E_1\eta_3} + \frac{1}{\eta_2} + \frac{1}{\eta_3}\right)D + \frac{E_3}{\eta_2\eta_3}\right]\sigma = \left[D^2 + \frac{E_3}{\eta_3}D\right]\epsilon \quad \ldots [7]$$

or

$$(p_2D^2 + p_1D + p_0)\sigma = (D^2 + q_1D)\epsilon \quad \ldots\ldots [8]$$

It is thus seen that Equation [1] for the four-element model of Fig. 1 consists of derivatives of σ and ϵ up to the second in both cases, but with the constant multiplier of ϵ equal to zero.

The simpler models of a simple spring, simple dashpot, Voigt unit, and Maxwell unit of a spring and dashpot in series, and three-element models can be included as special cases of the four-element model by making certain of the element parameters infinite. The present analysis thus applies to these models as special cases.

Reaction of Four-Element Model to Sinusoidal Stress

As detailed in the foregoing, the complex compliance represents the response of the material to steady-state sinusoidal stress when initial transients have died away. Using the complex representation $e^{i\omega t}$, the operator D is replaced by $i\omega$, and the compliance is given directly by Equations [2] and [6]

$$J'(\omega) - iJ''(\omega) = \frac{\epsilon}{\sigma} = \frac{1}{E_1} + \frac{1}{\eta_2\omega i} + \frac{1}{E_3 + \eta_3\omega i} \quad \ldots [9]$$

Equating real and imaginary parts

$$J'(\omega) = \frac{1}{E_1} + \frac{E_3}{E_3^2 + \eta_3^2\omega^2} \quad \ldots\ldots [10]$$

$$J''(\omega) = \frac{1}{\eta_2\omega} + \frac{\eta_3\omega}{E_3^2 + \eta_3^2\omega^2} \quad \ldots\ldots [11]$$

From Equation [11]

$$\omega J''(\omega) = \frac{1}{\eta_2} + \frac{1}{\eta_3} - \frac{E_3^2/\eta_3}{E_3^2 + \eta_3^2\omega^2} \quad \ldots\ldots [12]$$

Multiplying Equation [10] by E_3/η_3 and adding to Equation [12] gives

$$\frac{E_3}{\eta_3}J'(\omega) + \omega J''(\omega) = \frac{E_3}{E_1\eta_3} + \frac{1}{\eta_2} + \frac{1}{\eta_3} \quad \ldots\ldots [13]$$

It is thus seen from Equation [13] that, for the four-element model of Fig. 1, $\omega J''(\omega)$ plotted against $J'(\omega)$ gives a straight line of slope $-E_3/\eta_3$ and with intercept on

$$J'(\omega) = 0 \text{ of } E_3/E_1\eta_3 + 1/\eta_2 + 1/\eta_3$$

This provides the basis for the assessment of measured compliances detailed in the following.

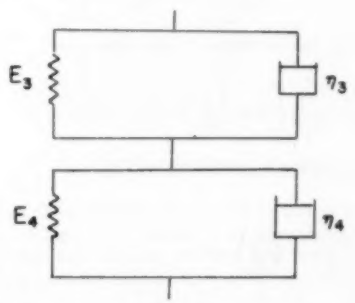

Fig. 2 Two Voigt Elements in Series

A linear relation between $J'(\omega)$ and $\omega J''(\omega)$ is both a necessary and sufficient condition that the corresponding model is of the type shown in Fig. 1, or a special case of this. It is known (3) that any linear model, neither included in nor reducible to the four-element model of Fig. 1 can be represented by a model of the type of Fig. 1 with additional Voigt units in series. The simplest such model, and one which is included in all other such models, is that which consists only of two Voigt elements in series, Fig. 2. By an analysis similar to the foregoing it can be shown that, for such a model

$$J'(\omega) = \frac{E_3}{E_3^2 + \eta_3^2\omega^2} + \frac{E_4}{E_4^2 + \eta_4^2\omega^2}$$

$$\omega J''(\omega) = \frac{1}{\eta_3} + \frac{1}{\eta_4} + \frac{E_3^2/\eta_3}{E_3^2 + \eta_3^2\omega^2} + \frac{E_4^2/\eta_4}{E_4^2 + \eta_4^2\omega^2} E_4$$

$$\frac{E_3}{E_3^2 + \eta_3^2\omega^2} \text{ and } \frac{E_4}{E_4^2 + \sigma_4^2\omega^2}$$

cannot both be eliminated from the last two equations to leave a linear equation between $J'(\omega)$ and $\omega J''(\omega)$ unless $E_3/\eta_3 = E_4/\eta_4$. But in this case the model would be reducible to one Voigt unit, contrary to hypothesis. So we have proved that any linear model, neither included in nor reducible to a four-element model of the type shown in Fig. 1, cannot produce a linear relationship between $J'(\omega)$ and $\omega J''(\omega)$. The same argument applies with additional terms which cannot be eliminated if additional Voigt elements in series are considered.

Fitting of Experimental Data by a Four-Element Model

Given experimentally determined values of $J'(\omega)$ and $J''(\omega)$ for a linear viscoelastic material, can this material be represented by a four-element model? This question can be answered by plotting $\omega J''(\omega)$ against $J'(\omega)$. If the plot is linear, the answer is in the affirmative. If only a "best" straight line can be drawn through the experimental points, then the model will be only an approximation. If no straight line fits reasonably well, the answer is in the negative. If the plot is linear over a certain range of ω, then the behavior of the material in that range can be represented by a four-element model.

Let us assume that a straight line, exact or approximate, can be drawn through the experimental points. How do we now obtain the constants of the relevant four-element model?

From Equation [13] the slope of the line is $-E_3/\eta_3$ and the intercept with the axis

$$J'(\omega) = 0 \text{ is } \frac{E_3}{E_1\eta_3} + \frac{1}{\eta_2} + \frac{1}{\eta_3}$$

Equation [10] can be written in the form

$$J'(\omega) = \frac{1}{E_1} + \frac{1}{E_3}\left[1 + \left(\frac{\eta_3}{E_3}\right)^2 \omega^2\right]^{-1} \quad [14]$$

Since η_3/E_3 is known, $J'(\omega)$ can be plotted against

$$\left[1 + \left(\frac{\eta_3}{E_3}\right)^2 \omega^2\right]^{-1}$$

The points will lie on a straight line, exact or approximate according to whether the former straight line was exact or approximate. From Equation [14] the slope of this second line will be $1/E_3$ and its intercept with

$$\left[1 + \left(\frac{\eta_3}{E_3}\right)^2 \omega^2\right]^{-1} = 0$$

will be $1/E_1$. The four constants E_1, η_2, E_3, and η_3 can now be evaluated from the values of the two slopes and the two intercepts.

Example. The values of J' and J'' found by Fitzgerald, Grandine, and Ferry (4) for polyisobutylene at 25 C are used in this example. In Fig. 3, J' is plotted against $J''f$, the frequency f being used instead of ω for convenience, without essential change in the analysis. Over the whole range, 30 to 4000 cycles/sec, a four-element model is clearly not adequate. However, as the two straight lines in the figure show, for each of the two separate ranges 30 to 300 cycles/sec and 600 to 4000 cycles/sec, a four-element model represents a good approximation to the behavior of the polyisobutylene. From each of these straight lines values of

$$E_3/\eta_3 \text{ and } \frac{E_3}{E_1\eta_3} + \frac{1}{\eta_2} + \frac{1}{\eta_3}$$

are determined. In Fig. 4, J' is plotted against

$$\left[1 + \left(\frac{\eta_3}{E_3}\right)^2 \omega^2\right]^{-1}$$

making use of the values of E_3/η_3 just found. From the best straight line, $1/E_3$ and $1/E_1$ are evaluated. Values E_1, E_3, η_2, and η_3 can now be calculated. They are given in Table 1.

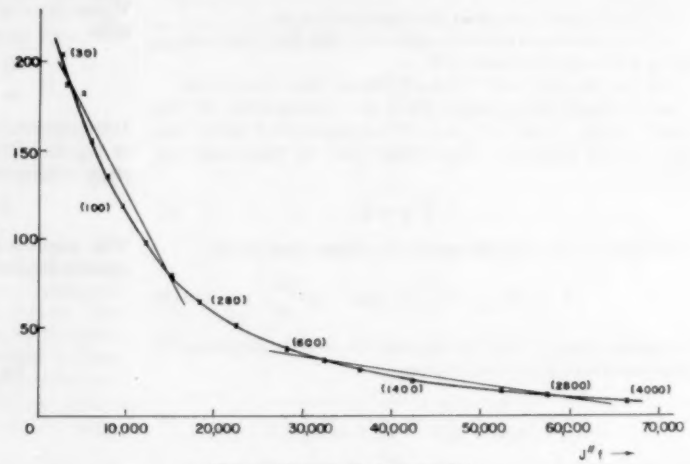

Fig. 3 Plot of J' Against $J''f$
(Numbers in brackets are frequencies at points alongside.)

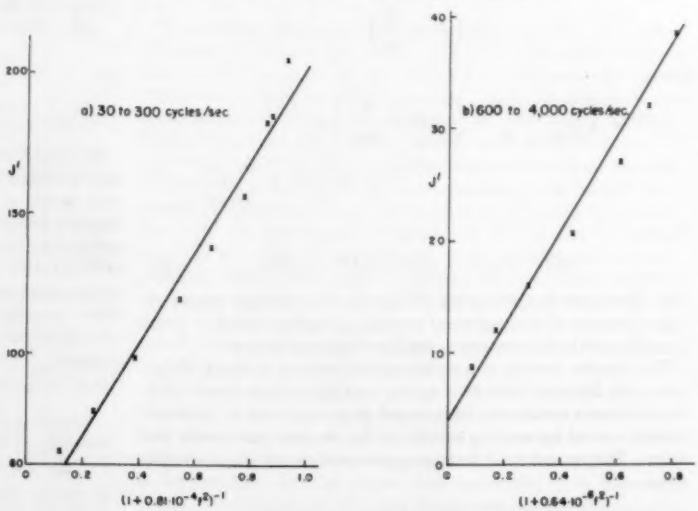

Fig. 4 Plots of J' Against $\left[1 + \left(\frac{\eta_3}{E_3}\right)^2 \omega^2\right]^{-1}$

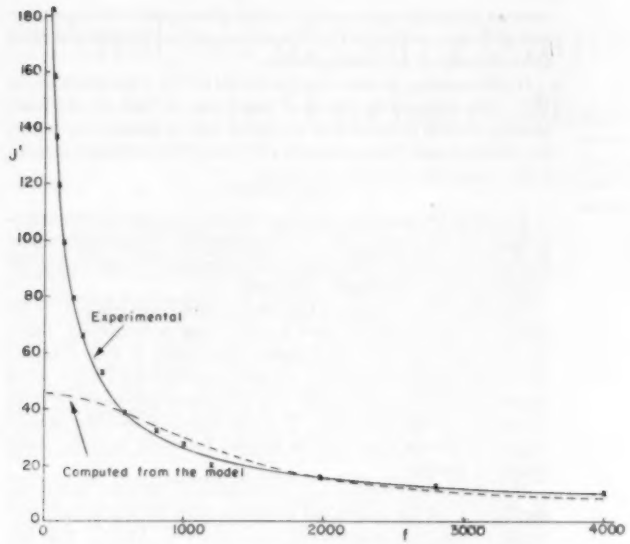

FIG. 5 COMPARISON OF VARIATION OF J' WITH FREQUENCY MEASURED EXPERIMENTALLY AND CORRESPONDING TO FOUR-ELEMENT MODEL

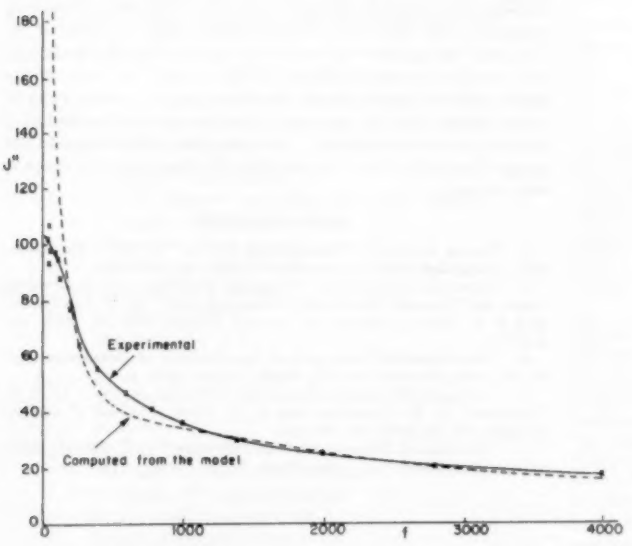

FIG. 6 COMPARISON OF VARIATION OF J'' WITH FREQUENCY MEASURED EXPERIMENTALLY AND CORRESPONDING TO FOUR-ELEMENT MODEL

TABLE 1 VALUES OF E_1, E_2, η_2, η_3 FOR POLYISOBUTYLENE AT 25 C, CGS UNITS

Frequency range	E_1	E_2	η_2	η_3
30 to 300 cps	$2.8 \cdot 10^7$	$6.1 \cdot 10^8$	$7.6 \cdot 10^4$	$8.7 \cdot 10^8$
600 to 4000 cps	$2.6 \cdot 10^6$	$2.4 \cdot 10^7$	$1.1 \cdot 10^4$	$3.0 \cdot 10^8$

Figs. 5 and 6 show the resulting values for J' and J'' in the high-frequency range plotted against frequency and compared with the measured values. It is seen that over a frequency range with a ratio of about 10 to 1, adequate agreement with the measured compliance values is obtained by means of a four-element model.

EXTENSION TO MAXWELL TYPE MODELS

We have considered Voigt type models of units in series for which the total strain is the sum of the component strains, and the stress is the same through each unit. For such models the compliance ϵ/σ, which is the sum of the individual compliances, prescribes the viscoelastic behavior in a particularly convenient form for analysis. Alternatively, Maxwell type units of a spring and dashpot in series can be arrayed in parallel to provide equivalent models. The four-element case shown in Fig. 7, which contains degenerate Maxwell units of a single spring, and a single dashpot, exhibits a certain duality with the four-element model of Fig. 1. If the complex modulus, σ/ϵ, for sinusoidal loading is considered, the modulus for the model is the sum of the moduli of the individual units in parallel, and relations analogous to those presented in earlier sections can be developed. They are described briefly in the following. It can be shown that for appropriate choice of constants the model of Fig. 7 is equivalent to that of Fig. 2, so that a convenient method of treating that model is available.

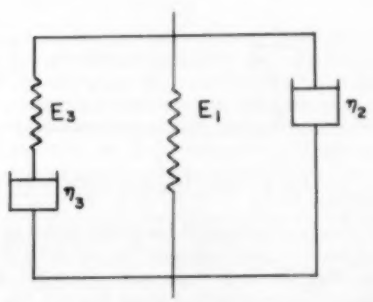

FIG. 7 FOUR-ELEMENT MAXWELL TYPE MODEL

To emphasize the duality in analyzing the model of Fig. 7, the corresponding equation numbers of the previous analysis will be used with primes. The complex modulus is given by

$$\frac{\sigma}{\epsilon} = G'(\omega) + iG''(\omega) = E_1 + i\omega\eta_2 + \frac{1}{\left(\frac{1}{E_3} + \frac{1}{i\omega\eta_3}\right)} \quad [9']$$

Separating real and imaginary parts, we have

$$G'(\omega) = E_1 + E_3 - \frac{E_3^2}{E_3^2 + \omega^2\eta_3^2} \quad [10']$$

$$G''(\omega)/\omega = \eta_2 + \frac{\eta_3 E_3^2}{E_3^2 + \omega^2\eta_3^2} \quad [12']$$

Thus

$$G'(\omega) + \frac{E_3}{\eta_3}\frac{G''(\omega)}{\omega} = E_1 + E_3 + \frac{E_3\eta_2}{\eta_3} \quad [13']$$

Thus if the plot of $G'(\omega)$ against $G''(\omega)/\omega$ is linear, a model of this type represents the experimental results, and determines E_3/η_3

and $E_1 + E_3 + E_3\eta_2/\eta_3$. A plot of G' against

$$\left[1 + \omega^2\left(\frac{\eta_2}{E_2}\right)^2\right]^{-1}$$

determines E_3 and $E_1 + E_3$, and so all the model constants. As in the earlier work, this necessary condition of linearity for the four-element model can be shown to be sufficient. For any Maxwell-type model which cannot be reduced to the foregoing must have at least two Maxwell units in parallel, as shown in Fig. 8, and for this

$$G'(\omega) = \frac{-E_2^2}{E_2^2 + \omega^2\eta_2^2} + \frac{-E_4^2}{E_4^2 + \omega^2\eta_4^2} + E_3 + E_4$$

$$G''(\omega)/\omega = \frac{\eta_2 E_2^2}{E_2^2 + \omega^2\eta_2^2} + \frac{\eta_4 E_4^2}{E_4^2 + \omega^2\eta_4^2}$$

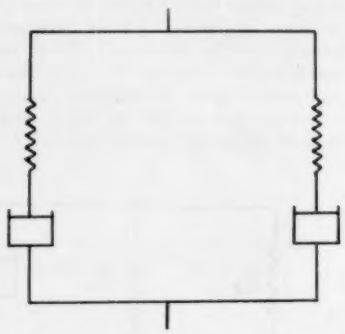

FIG. 8 TWO MAXWELL UNITS IN PARALLEL

The terms in ω on the right-hand sides cannot all be eliminated to give a linear relation between $G'(\omega)$ and $G''(\omega)/\omega$ unless $E_4/\eta_4 = E_4/\eta_4$, when the model degenerates into a simple Maxwell unit.

Thus a Maxwell type four-element model, Fig. 7, can readily be assessed against complex modulus measurements. In practice this is probably not as useful as the model shown in Fig. 1 since it exhibits neither instantaneous elasticity nor permanent viscous flow.

It has been pointed out that the model of Fig. 7 is equivalent to that of Fig. 2 for appropriate choice of constants. For zero values of E_4 or η_4 in Fig. 2, the three-element models considered previously as special cases of Fig. 1 are again reproduced, so that a necessary and sufficient condition for these models to represent sinusoidal stress-strain measurements is that both J' against $\omega J''$ and G' against G''/ω give linear plots. The same applies to three-element Maxwell type models, so that this supplies the necessary and sufficient condition that the corresponding model be at most three-element of any configuration.

It is interesting to note that the model of Fig. 8 is equivalent to Fig. 1 for appropriate choice of constants, so that all the four-element models illustrated in the paper can be assessed by linearity relations, and these comprise all types of four-element models.

CONCLUSIONS

A method for assessing whether complex compliance versus frequency curves correspond to a four-element viscoelastic model has been presented, with a practical process for determining the corresponding viscoelastic constants.

The example given shows that such a model is in general too restricted to be applicable over a wide range of frequency, but a useful range could be encompassed adequately in that case. A ten-to-one range of frequency will give a satisfactory Fourier series representation of a force pulse if it has a reasonably smooth form in the time range of interest. It seems therefore that the method suggested in this paper can be applied for stress analysis under transient loading.

If such a model applies only over a limited frequency range, the significance of the individual elements must be interpreted correctly as has been pointed out by Alfrey (5). Over a wide frequency range a material will in general correspond to a series of Voigt elements with a wide range of delay times. In the four-element model which we have determined, the elements of delay times short compared with our time range of interest will be lumped with the instantaneous spring E_1, and those with delay times long compared with this time will be lumped with the dashpot η_2. Thus the "permanent" viscous flow computed from this model will only remain if the stress falls to zero for times of the order of the period of the lowest frequency considered, and may relax away in longer times. In the same way, instantaneous response has a similarly restricted meaning. However, these restrictions do not impair the application of the model in the time range for which it was devised.

BIBLIOGRAPHY

1 "Stress Analysis in Visco-Elastic Bodies," by E. H. Lee, *Quarterly of Applied Mathematics*, vol. 13, 1955, pp. 183–190.

2 "Dynamic Compliance, Dynamic Modulus, and Equivalent Voigt and Maxwell Models for Polyisobutylene," by H. Leaderman and R. S. Marvin, *Journal of Applied Physics*, vol. 24, 1953, pp. 812–813.

3 "Mathematical Structures of the Theories of Viscoelasticity," by B. Gross, Hermann et Cie, Paris, France, 1953, p. 63.

4 "Dynamic Mechanical Properties of Polyisobutylene," by E. R. Fitzgerald, L. D. Grandine, and J. D. Ferry, *Journal of Applied Physics*, vol. 24, 1953, pp. 650–655.

5 "Mechanical Behavior of High Polymers," by T. Alfrey, Interscience Publishers, Inc., New York, N. Y., 1948, p. 166.

Analysis of Slip Damping With Reference to Turbine-Blade Vibration

By L. E. GOODMAN[1] and J. H. KLUMPP,[2] MINNEAPOLIS, MINN.

Energy of vibration may be dissipated by microscopic slip-on interfaces where machine elements are joined in a press fit. In this paper slip damping is studied as an agent in reducing turbine-blade resonant stresses and prolonging turbine life. A general theory of slip damping is developed and an expression for the energy loss per cycle of oscillation is found. The predictions of the theory are compared with the results of controlled experiments. It appears that the theory is in satisfactory agreement with experiment and with measurements made on turbine blades elsewhere in this country and abroad. The implications of the general theory in the design of turbine blades are discussed. It appears that slip damping is capable of being an effective agent in reducing resonant stresses, especially in the "stall-flutter" condition where aerodynamic damping is inadequate. The design of a slip-damping joint which would achieve theoretically possible energy decrements much larger than are present in existing commercial construction is shown to depend on the maintenance of an optimum contact pressure.

Nomenclature

The following nomenclature is used in the paper. Symbols are defined where first introduced in the text. They are listed here in the order of their appearance:

x, y, z = Cartesian co-ordinates
p = $p(x, y)$ pressure clamping joint faces together
E = Young's modulus of elasticity
ν = Poisson's ratio
u, v = displacements in directions x and y, respectively
σ_x, τ_{xy} = components of stress
ξ = a dummy variable
u_1, v_1 = $u(x, 0+)$, $v(x, 0+)$
u_2, v_2 = $u(x, 0-)$, $v(x, 0-)$
Δu = $u_2 - u_1$, $\Delta v = v_2 - v_1$
$(\sigma_x)_1$ = $\sigma_x(x, 0+)$
$(\sigma_x)_2$ = $\sigma_x(x, 0-)$
$\Delta\sigma_x$ = $(\sigma_x)_2 - (\sigma_x)_1$
t = thickness of joint in z-direction
μ = coefficient of Coulomb friction
D_0 = energy dissipated per cycle
l = length of slipped region
h = half-depth of blade in flexure, see Fig. 2
F = cyclic exciting force
F_m = peak exciting force
F_s = exciting force required to initiate slip
k^{-1} = exciting force required to produce unit deflection at the point l, 0 prior to slip; $k = 2Eth^3l^{-3}$
ω_{n2} = lowest natural frequency of blade for case of infinite friction on mating surfaces, rad/sec
ϕ = phase angle between exciting force and excited displacement
ω_ϕ = frequency at which $\phi = \pi/2$ radians, rad/sec
σ_m = maximum value of extreme fiber stress at built-in end of blade
C = compliance of joint; displacement per unit exciting force, at l, 0

Introduction

Service failures of gas-turbine blades in many cases can be attributed to the high stresses accompanying resonant vibration. These stresses reduce the fatigue life of the blading. Failures so induced have been matters of concern to the designers of aircraft power plants and it has been thought that any significant increase in the damping present in the blade structure would operate to reduce vibration stresses and to increase turbine life. Apart from aerodynamic damping, the mechanisms of energy dissipation available to the designer may be considered under two headings, (*a*) internal damping inherent in the metal or cermet, and (*b*) slip damping which, in present industrial designs is usually associated with the mounting of the blade in its holder. In this paper slip damping is considered from a comprehensive point of view. A general theory of the energy-dissipation properties of press-fit joints in the presence of Coulomb friction is developed and its predictions compared with the results of experiment. It appears from our investigation that, under favorable circumstances, the energy dissipated in slip damping may be quite large, not only compared with that dissipated in internal friction, but also when compared with the total strain energy stored in the blade.

The importance of damping in reducing the incidence of turbine failures has been generally recognized in this country and abroad since about 1940. General discussions of the blade-design problem as well as experimental evidence to which later reference is made may be found in the reports of Kroon (1),[3] Shannon (2), and Schnittger (3). Manson, Meyer, Hanson, and Calvert (4, 5, 6) have measured the total damping present in turbines of prototype dimensions. The measurements of slip damping reported by these investigators are in agreement with the theory developed here.

A theory of structural damping in a built-up beam has been described by Pian and Hallowell (7, 8). They have considered a beam fabricated in two parts connected by riveted cover plates. While useful in connection with the structural problems for which it was developed, their analysis is limited by idealized properties attributed to the riveted connections and the cover plates. It cannot successfully be applied to turbine blades.

---

[1] Professor of Mechanics, Department of Mechanics and Materials, University of Minnesota. Assoc. Mem. ASME.

[2] Research Fellow, Department of Mechanics and Materials, University of Minnesota. Assoc. Mem. ASME.

Contributed by the Applied Mechanics Division and presented at the Diamond Jubilee Annual Meeting, Chicago, Ill., November 13–18, 1955, of The American Society of Mechanical Engineers.

Discussion of this paper should be addressed to the Secretary, ASME, 29 West 39th Street, New York, N. Y., and will be accepted until October 10, 1956, for publication at a later date. Discussion received after the closing date will be returned.

Note: Statements and opinions advanced in papers are to be understood as individual expressions of their authors and not those of the Society. Manuscript received by ASME Applied Mechanics Division, June 15, 1955. Paper No. 55—A-80.

[3] Numbers in parentheses refer to the Bibliography at the end of the paper.

Internal or material damping has been the subject of intensive study in recent years. For the purposes of the present paper, we are concerned with this aspect of the damping problem only to the extent of making comparisons between the amount of energy loss available from this source and from slip. Detailed information on the present status of technical research in the field of material damping may be found in the survey monograph of Lazan (9) or by reference to the bibliography contained in ATI 6174 (10).

General Theory of Energy Dissipation in Slip Joints

We consider two mating parts, e.g., blade root and hub, which have a common interface or joint. The part of the interface which is to be investigated is taken to lie in the plane $y = 0$ and the structure as a whole is taken to be in a state of plane stress in the x-y plane. The most general joint would have a doubly curved mating surface and a three-dimensional state of stress. We do not consider this more general type in the present paper; it is felt that the possible advantages of complete generality would not be in proportion to the increased complexity of the analysis, at least in the present stage of its development. In practice the mating surface is usually built up of planes or cylinders for simplicity of fabrication. The contemplated applications to turbine-blade vibration all fall within the scope of a two-dimensional theory.

The joint is shown schematically in Fig. 1. The region $y > 0$ is designated as region 1 and the region $y < 0$ as region 2. The two regions are held in contact along the interface by static pressures $p = p(x, y)$ which may include concentrated forces. Now suppose that in addition to the pressures p a further set of loads is

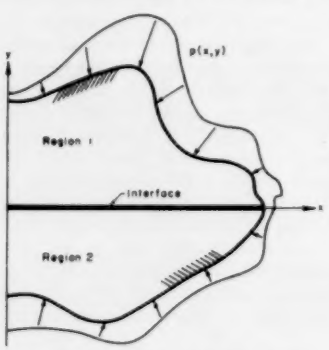

Fig. 1 Co-Ordinate System

applied, either in the form of direct external excitation or in the form of a distributed "inertia" loading, and that this second set first increases in magnitude to a peak positive value, then decreases to a value equal in magnitude but opposite in sign to the first peak and finally returns to zero. At the beginning of the cycle, which may be repeated many times, the structure behaves as a solid elastic body. When the shear stress acting on the plane $y = 0$ exceeds a limiting value, microscopic slip occurs and there is a relative displacement of points on opposite sides of the interface in the slipped region. This relative displacement is parallel to the interface since the pressures p are assumed large enough to maintain contact. Corresponding to the discontinuity in displacement there is a discontinuity in the component of direct stress parallel to the interface.

As the variable part of the external load increases, the slipped region grows in length and the magnitude of the relative slip at any point also increases. It must be assumed, of course, that slip does not propagate along the entire plane, otherwise gross motion will occur. On decreasing the load from its peak value there is no change in the relative slip until the load has been reduced twice the amount required to produce initial slip. After this stage, slip again occurs, reversed in direction.

Using conventional notation (see nomenclature) we have, at any place in the structure

$$E(\partial u/\partial x) = \sigma_x - \nu\sigma_y \quad [1]$$

Here E and ν are Young's modulus and Poisson's ratio, respectively, u is the component of displacement in the x-direction, and σ_x and σ_y are components of direct stress.

Equation [1] is true on either side of the interface, that is

$$E\frac{\partial u(x, 0)}{\partial x} = \sigma_x(x, 0) - \nu\sigma_y(x, 0) \quad [2]$$

Integrating both sides of this expression we have

$$Eu(x, 0) = \int_0^x \sigma_x(\xi, 0)d\xi - \nu\int_0^x \sigma_y(\xi, 0)d\xi + K \quad [3]$$

In this equation ξ plays the role of a dummy variable which disappears on integration. We choose the origin of x at the point where slip originates and measure displacement from that point. This imposes no loss of generality and it conveniently makes $u(0, 0) = 0$ so that the constant of integration disappears. Now let

$$\Delta u = u_2 - u_1 = \text{relative slip at interface} \quad [4a]$$

$$\Delta\sigma_x = (\sigma_x)_2 - (\sigma_x)_1 = \text{discontinuity in } \sigma_x \quad [4b]$$

Here

$$u_1 = u(x, 0+),\ u_2 = u(x, 0-) \quad [5a]$$

$$(\sigma_x)_1 = \sigma_x(x, 0+),\ (\sigma_x)_2 = \sigma_x(x, 0-) \quad [5b]$$

Since Equation [3] holds in both region 1 and region 2

$$\Delta u = E^{-1}\int_0^x \Delta\sigma_x(\xi)d\xi \quad [6]$$

Use has here been made of the fact that σ_y must be continuous across the interface. The frictional force acting on the interface, per unit of length, is taken to be

$$\mu t\sigma_y(x, 0) \quad [7]$$

where μ is the coefficient of (Coulomb) friction, and t is the thickness of the joint in the z-direction; σ_y is the compression holding the two regions in contact. The energy dissipated by the forces acting on either of the two surfaces which comprise the interface is the integral of the products of relative slip and frictional force taken along the length l of the slipped region. Energy is dissipated during intervals in which relative slip takes place, both when the load is increasing and when it is decreasing. Since the loading cycle is one of complete reversal, the graph of Δu versus σ_y at any point will be a single-valued function of Δu (except at $\Delta u = 0$) symmetrical about $\Delta u = 0$. The energy dissipated per cycle D_0 will be four times the energy dissipated as the load increases from zero to its maximum value

$$D_0 = 4\mu t E^{-1}\int_0^l \left[\sigma_y(x, 0)\int_0^x \Delta\sigma_x(\xi)d\xi\right]dx \quad [8]$$

In view of the implications of Equation [8], the assumptions involved in its derivation deserve explicit statement. Apart from the assumption that the blade material behaves elastically, the principal limitations of this treatment are implicit in the simple form of Coulomb friction embodied in Expression [7].

In practice the friction characteristics will be velocity dependent

to a certain degree and may be expected to change somewhat with increase in the number of cycles of stress reversal to which the blade is subjected. No allowance has been made for a difference between static and kinetic coefficients of friction, although this difference can be incorporated in the theory at the expense of a slight additional complexity. In mitigation of the deficiencies of these assumptions it may be noted that after a relatively small number of slip cycles (2×10^3 in the case of the steels employed in the experiments described in the section Comparison of Slip and Material Damping) the coefficient of friction tends to stabilize. The difference between static and kinetic coefficients of friction has been detected by means of careful measurements described in the section mentioned, but it does not appear to be a serious factor in the estimation of energy loss due to slip damping. It is not detectable in any but the slowest slip cycles.

It is believed that the generality of Equation [8] compensates to some degree for the fact that it is based on what may be described as a first-order theory. Certain conclusions of a general nature can be drawn directly from the form of the expression. At zero clamping pressure the integrand vanishes and the energy dissipation is zero, as it should be under these circumstances. At high clamping pressures the maximum length of the slipped region l also approaches zero and the energy dissipation again vanishes. This is less obvious from the form of Equation [8], but it should be noted that $\Delta\sigma_x$ also approaches zero with l. It follows that there is always an intermediate clamping pressure at which the energy dissipation per cycle is a maximum. The existence of an optimum pressure has interesting confirmation in technical experience with torsional dampers in the form of press-fit rings used to deaden gear noise (11).

Equation [8] gives the energy dissipation per cycle whether the stresses rise from external forces or from dynamic (inertia) loadings. Of course, the stress distributions to be used in the application of the equation may be quite different in the two cases. An "exact" stress analysis is not required for the technical application of Equation [8]. An approximate or experimental analysis such as may, for example, be obtained by a photoelastic investigation will serve. In checking the predictions of the theory we have, however, preferred to restrict consideration to a joint for which a theoretical analysis is obtainable, with the object of limiting the possible sources of discrepancy between slip theory and experiment.

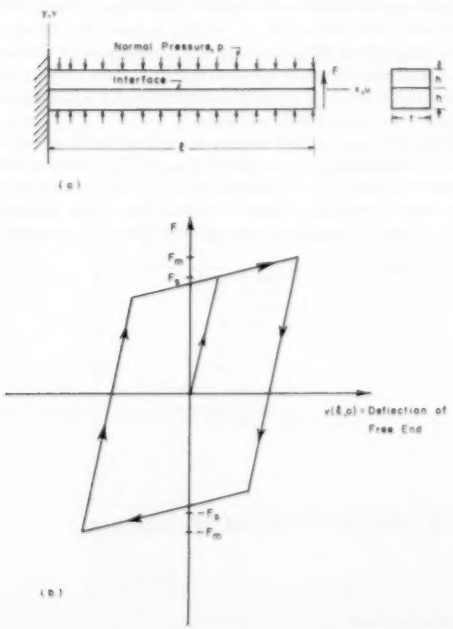

FIG. 2 UNIFORM-PRESSURE JOINT, SCHEMATIC

ANALYSIS OF THE UNIFORM-PRESSURE JOINT

A simple joint geometry, chosen primarily for the purpose of checking the theory developed in the preceding section, is shown in Fig. 2. It consists of two identical regions of constant depth h held in contact by a uniform pressure p applied to the upper and lower boundaries. The extent of the interface is limited by a massive clamp at one end of the joint; the cyclic force F is applied at the other end in a direction at right angles to the interface. In appearance the joint resembles a cantilevered beam, the interface lying at mid-depth.

The choice of this joint for an initial study has been motivated by the fact that an exact analysis of the postslip stress distribution is relatively simple. Proceeding by a semi-inverse method, we take $\sigma_y = -p$, a constant. In view of the conditions of plane stress, $\sigma_z = \tau_{yz} = \tau_{zx} = 0$. The stress equations of equilibrium (12) reduce to two

$$(\partial\sigma_x/\partial x) + (\partial\tau_{xy}/\partial y) = 0 \text{ and } (\partial\tau_{xy}/\partial x) = 0 \ldots [9]$$

For the upper region of the joint in the postslip condition the boundary conditions on stress are

$$\left.\begin{aligned} \sigma_y(x, h) &= -p, \quad \tau_{xy}(x, h) = 0 \\ \tau_{xy}^2(x, 0) &= \mu^2\sigma_y^2(x, 0) \\ \int_0^h \tau_{xy}(l, y)dy &= F/2t \\ \int_0^h \sigma_x(l, y)dy &= \int_0^h y\sigma_x(l, y)dy = 0 \end{aligned}\right\} \ldots [10]$$

According to the second equation of equilibrium, the shear distribution may vary through the thickness but not along the length of the blade. The simplest such shear distribution which will satisfy the second, third, and fourth boundary conditions is

$$\tau_{xy} = +\mu p + [-(4\mu p/h) + (3F/th^2)]y + [(3\mu p/h^2) - (3F/th^3)]y^2 \ldots [11]$$

On substituting this expression into the first equation of equilibrium and solving for the remaining unknown stress, we have

$$\sigma_x = -(6F/th^3)\,x\,(y - h/2) - (\mu p/h^2)(6y - 4h)x + Y \ldots [12]$$

where the symbol Y represents an arbitrary function of y. The choice of this function is determined by the last of the boundary conditions, Equation [10], which is satisfied by making σ_x vanish identically at the end of the blade

$$\sigma_x = (x - l)[(6F/th^3)(y - h/2) - (6\mu p/h^2)(y - 2h/3)] \ldots [13]$$

In order to establish the validity of this solution it is necessary first to investigate the displacements to which these stresses correspond. This may be done in the usual way by converting from stresses to strains and then integrating the strain-displacement relations. Denoting the displacement parallel to the interface by u_1 and the displacement in the direction of the depth of the blade by v_1 we find, on the interface $y = 0$

$$Eu_1 = \nu px - [(3F/th^2) - (4\mu p/h)](x^2/2 - lx) \ldots [14]$$

$$Ev_1 = [(F/th^3) - (\mu p/h^2)](3lx^2 - x^3) \ldots [15]$$

Since the complete expressions for the displacements are polynomials in x, y, no further investigation of compatibility is required.

The foregoing stress analysis may be repeated, with obvious modifications, in the lower half of the blade shown in Fig. 2. Corresponding to Fig. 1, this is region 2. The significant stress and displacement components in this region are found to be

$$\tau_{xy} = +\mu p - [-(4\mu p/h) + (3F/th^3)]y - [(3F/th^3) - (3\mu p/h^2)]y^2 \quad [16]$$

$$\sigma_x = (x - l)[(6F/th^3)(y + h/2) - (6\mu p/h^2)(y + 2h/3)] \quad [17]$$

$$Eu_2 = \nu px + [(3F/th^3) - (4\mu p/h)](x^2/2 - lx) \quad [18]$$

$$Ev_2 = [(F/th^3) - (\mu p/h^2)](3lx^2 - x^3) \quad [19]$$

We note that the displacements on the interface in a direction normal to it (v_1 and v_2) match, indicating that contact is maintained in the postslip condition. This is a condition which the stress analysis must satisfy.

The displacement discontinuity at the interface does not correspond to a rigid-body motion of the classic type formulated by Weingarten and by Volterra. This dislocation is a member of the more general class recently described by E. H. Mann (14) and by J. L. Bogdanoff (15). From Equations [13] and [17] we have

$$\Delta\sigma_x = +[(8\mu pl/h) - (6Fl/th^2)](1 - x/l) \quad [20]$$

This dislocation is contained in the first two terms of equation [4.23] of reference (15).

For purposes of future reference we note displacement discontinuity and the load-deflection relationship in the postslip condition

$$\Delta u = -E^{-1}[(3Fl^2/th^3) + (4\mu pl^2/h)][(2x/l) - (x/l)^2] \quad [21]$$

$$v(l, 0) = 2E^{-1}[(Fl^3/th^3) - (\mu l^3 p/h^2)] \quad [22]$$

The application of the results of the stress analysis to the computation of energy dissipation per cycle is quite straightforward. Since slip is instantaneous and extends the length of the joint and since σ_y is constant, Equation [8] takes the form

$$D_0 = (4\mu tp/E)[(6F/th^2) - (8\mu p/h)] \int_0^l \int_0^x (l - \xi)d\xi dx \quad [23]$$

$$= (4/3)(\mu tpl^2/E)[(6Fl/th^2) - (8\mu pl/h)] \quad [24]$$

The optimum pressure is

$$p_0 = (3/8)F/\mu lh \quad [25]$$

and the corresponding energy dissipation per cycle is

$$D_0 = \frac{32}{3}\mu^2 p_0^2(tl^3/Eh) \quad [26]$$

The value of F to be used in Equations [24] and [25] is that corresponding to the peak applied force. The expression may be simplified in appearance by introducing the notation

F_m = peak exciting force
F_s = exciting force required to initiate slip = $(4/3)\mu pth$
k^{-1} = exciting force required to produce unit deflection at point l, 0 prior to slip
$k = 2Eth^3/l^3$

In terms of these symbols Equation [24] becomes

$$D_0 = (12F_s^3/k)(F_m/F_s - 1) \quad [27]$$

Experiments With Uniform-Pressure Joint

As a necessary preliminary to the design and testing of a uniform-pressure joint, some of the frictional characteristics of lubricated mild steel were checked carefully. The requirement imposed upon the experiment by the theory developed in the previous sections of this work is the maintenance of a Coulomb type of friction with a coefficient essentially constant for a large number of cycles and independent of normal pressure over a usable range. Ideally, static and kinetic coefficients of friction would be equal in magnitude.

It was found that flat ground-steel surfaces which were roughened with an 80-grade emery paper and lubricated with a commercial mixture of MoS_2 and oil would approximately meet these requirements. The asperities produced by the emery paper penetrate the lubricant and produce an over-all dry-friction characteristic with an average kinetic coefficient equal to 0.14, while the lubricant partially inhibits fretting or mechanical wear. The preliminary tests in which the coefficient of friction was studied have been reported previously (16). Briefly, they consisted in rubbing carefully prepared essentially identical surfaces under known normal pressure by means of a controlled tangential force. Appropriate instrumentation provided an oscilloscope display of frictional force versus time, frictional force versus velocity, and velocity versus time for the purpose of monitoring the change in frictional characteristics throughout the tests. Final results of these tests are shown in Fig. 3. It may be seen that for pressures in the range 40 to 200 psi the kinetic coefficient of friction stabilized after approximately 2×10^3 cycles. The rubbing velocity in these tests varied in amplitude between 4.0 and 10.0 ips and was found not to be a critical factor.

Details of the joint and test setup used to study the theory of the preceding section are shown in Fig. 4. The uniform pressure was approximated by 25 calibrated aluminum clamps set 1/2 in. apart and alternately staggered about the center line so as to assist in distributing the screw applied force. A pressure range

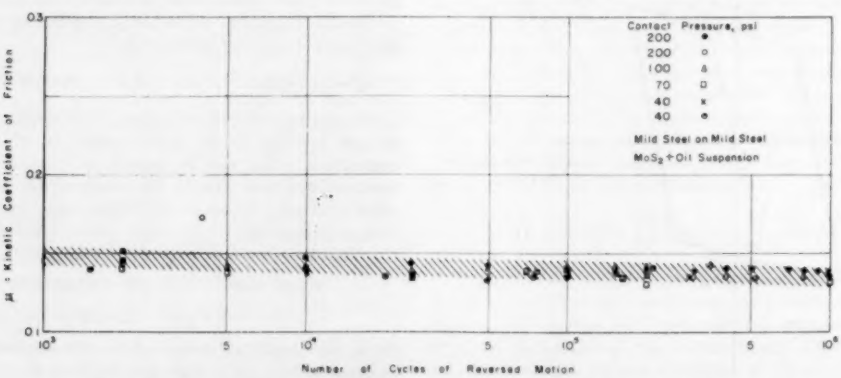

Fig. 3 Coefficient of Friction Versus Number of Cycles of Operation

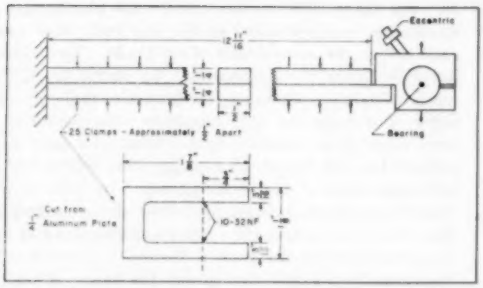

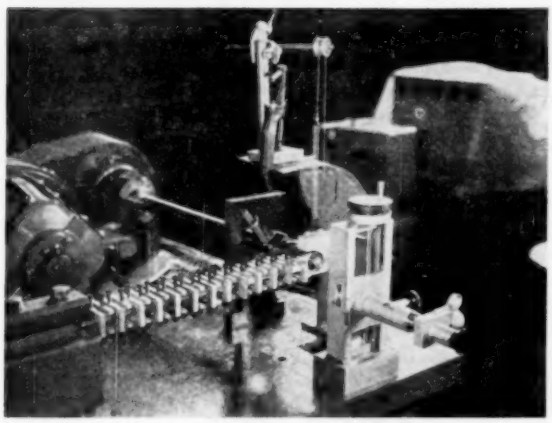

FIG. 4 DETAIL OF UNIFORM-PRESSURE JOINT AND CLAMP

of 20 to 200 psi was available through an individual clamp range of 5 to 50 lb. Micrometer measurements of clamp-tip separation enabled the clamp load to be set to within 2 psi at any given setting.

The joint was made of flat ground steel prepared as just described and the test setup was adapted to both static and dynamic measurements. The joint was mounted on a heavy, seismically sprung table, a part of a vibration exciter and controller described elsewhere (17). The weight of the beam, clamps, shaft, eccentric, and other attachments was counterbalanced by dead weight acting through a soft spring. This arrangement established the zero initial load condition postulated by the theory. In addition, the soft springs served to isolate the joint from abrupt changes which occurred during the "static" tests.

There was a minor deviation from the theory in that the end load was applied to the lower half of the end face instead of being distributed over the entire end face. The effects of this departure from theory were not observable except at low pressures, and even then they were quite small.

Dead-weight loading was used in the static tests with a maximum applied tip load F_m of 4 lb in the case of hysteresis-loop measurements. Deflection and relative slip were measured with a micrometer microscope. Maximum stress in all tests was less than 5000 psi. A typical hysteresis loop obtained in this fashion is illustrated in Fig. 5. The stepped, fine structure, there shown, is caused by the small difference in static and kinetic coefficients of friction which produces a slight effect each time the load is changed. This phenomenon accounts in part for measured compliances slightly lower than the theoretically computed ones (see Table 1). It also accounts for a small difference between calculated and measured maximum deflection at the end of the beam.

A rough check of the coefficient of friction is provided by the value of load at slip initiation, $\mu = 0.75F_s/pth$. While a variable slip distribution existed in the joint (see Fig. 6), the coefficient of friction measured in the joint tests corresponded closely with that obtained in the preliminary friction tests. A measurement of slip distribution at a relatively high load showed good agreement with Equation [21], as is illustrated in Fig. 6. It may be worth while to mention again that a minimum of 2000 cycles of motion were applied to the joint before measurements were made.

A group of hysteresis loops plotted from measured data is shown in Fig. 7. The loop area, a measure of energy loss per cycle, varies in accordance with Equation [24], small area at low and high pressures with a maximum (heavy lines) near $p =$ 80 psi. The theoretical optimum pressure is 86 psi. Values of energy loss per cycle as obtained from the loop area are plotted in Fig. 8 as a function of pressure for the purpose of comparison with the theoretical predictions (see also Table 1). Agreement between theory and experiment is within 5 per cent in most cases. The elastic strain energy of flexure which appears in the denominator of the ordinate is that which would be developed in the absence of friction; it has been introduced in order to obtain a dimensionless plot.

Dynamic loading was obtained by means of an adjustable-while-running eccentric. At a frequency corresponding to a 90-

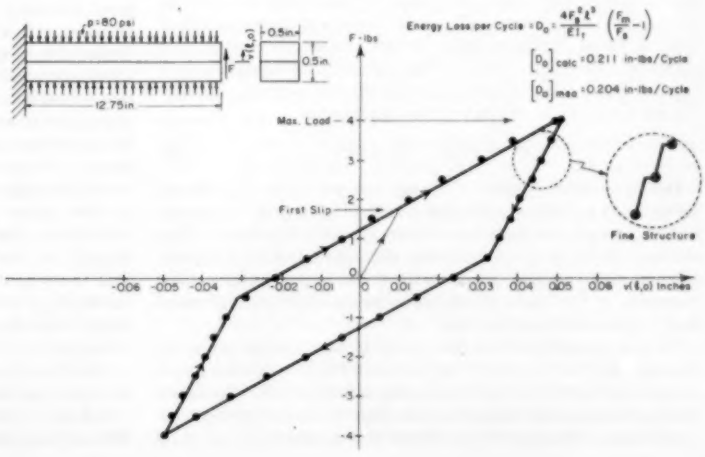

FIG. 5 TYPICAL STATIC HYSTERESIS LOOP

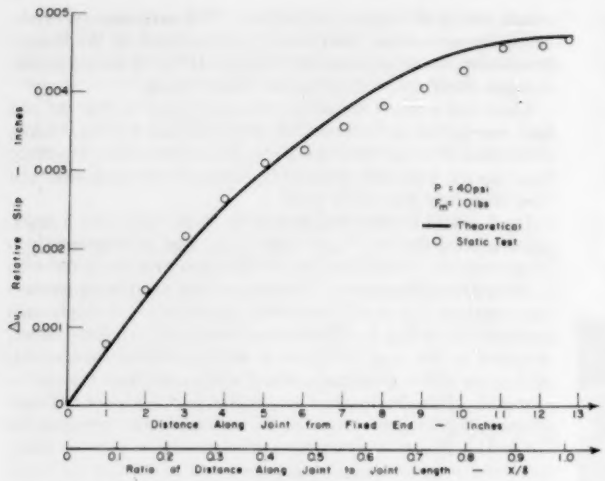
0.005
0.004
0.003
0.002
0.001
0
Δ_R, Relative Slip — Inches
P = 40psi
F_m = 10 lbs
Theoretical
Static Test
0 1 2 3 4 5 6 7 8 9 10 11 12 13
Distance Along Joint from Fixed End — Inches
0 0.1 0.2 0.3 0.4 0.5 0.6 0.7 0.8 0.9 1.0
Ratio of Distance Along Joint to Joint Length — x/ℓ

FIG. 6 RELATIVE SLIP AT INTERFACE

lb. For the relative motion versus time photograph, the strain gage was positioned so that one knife edge was on each side of the neutral axis of the blade. Two identical low-pass filters were introduced to eliminate high-frequency "noise." However, the filter also probably eliminates or distorts the high-frequency components of the force signal to a certain extent. Additional error is also possible because five pressure clamps were removed to permit installation of the strain pickup. In spite of these possible sources of experimental error, the photographs of Fig. 10 further confirm the static measurements and fulfill the predictions of the general theory. A parallelogram hysteresis loop exists throughout the range of test frequencies. The strain, which is proportional to the excited force-time trace, shows the effect of slip by the sharply slanted portion just prior to the peak force and peak displacement. The displacement-time relationship measured at the blade tip is sinusoidal.

The relative slip-time relationship illustrates the predicted flat-topped wave form. The flat portion relates to nonslip conditions and the remainder indicates relative motion between the two mating surfaces.

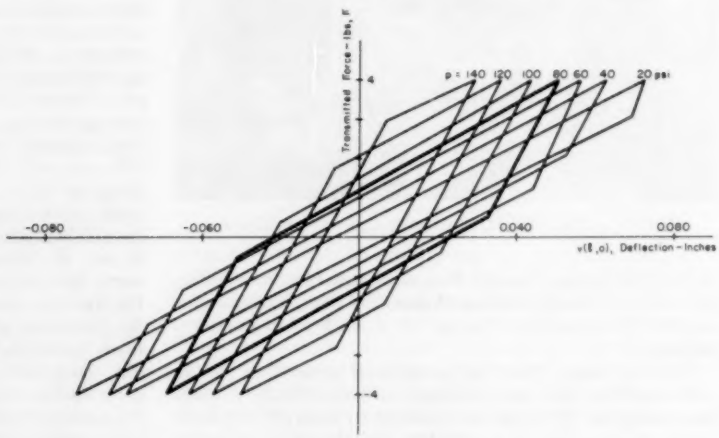

FIG. 7 MEASURED HYSTERESIS LOOPS FOR UNIFORM-PRESSURE JOINT

deg phase angle between force and displacement, the exciting force was adjusted so as to produce approximately (peak to peak) the same amplitude that was measured previously for a static loop at the same pressure. The phase angle was measured with a General Radio Strobotac and checked against the output of a phase-discriminating circuit in the controller. Vibration amplitude was again measured with a micrometer microscope. Energy loss per cycle can be computed from the relation

$$D_\theta = \pi F_m v(l, 0)_{\max} \sin \varphi \quad \ldots\ldots\ldots\ldots [28]$$

Dynamic measurements of energy loss per cycle are given in Table 1 and plotted as solid circles in Fig. 8. Again, correlation with static and with theoretical results is within 5 per cent. This also may be taken as an indication that, provided the frequency of excitation does not greatly exceed the fundamental natural frequency of the blade, the dynamic stress distribution is essentially similar to the static one.

To provide additional verification of the theory of the preceding section, the joint was instrumented as in Fig. 9 to obtain records of dynamic hysteresis loops, strain versus time, relative slip versus time, and displacement versus time. Fig. 10 shows typical photographs taken at a pressure of 120 psi and an exciting force of 1.8

COMPARISON OF SLIP AND MATERIAL DAMPING

Useful comparisons of the relative magnitudes of slip and material damping are inherently elusive, owing to physical differences in the ways in which energy is dissipated in the two cases. Material (internal) damping is, from a phenomenological point of view, a function of the mean stress amplitude, material constitution, stress history, and temperature. In general, specific damping energy increases markedly at stresses exceeding the so-called cyclic stress-sensitivity limit which is approximately 0.8 of the fatigue strength at 2×10^7 cycles of reversed stress. While material damping depends on volume-averaged properties of the turbine blade, slip damping depends upon the local stress distribution in the vicinity of the surface on which slip occurs. It depends on the mean coefficient of friction, the clamping stress, and the magnitude of the stress discontinuity at the interface. As has been shown in preceding two sections of this paper, the latter two effects are interrelated so that there is an optimum pressure at which their product is a maximum.

Since one form of damping is proportional to a volume and the other to a surface effect, it is always possible to conceive joints in which one or the other mode of energy dissipation will dominate. The uniform-pressure joints discussed in the preceding two sec-

TABLE 1 MEASURED AND CALCULATED JOINT PROPERTIES AT VARIOUS PRESSURES

F_m = 4 lb, μ = 0.14, ω_{nt} = 1450 rpm

Pressure, psi	Slip Load, F_s		Compliance, C			Energy loss per cycle			ω_ϕ	Exciting force, $\phi = 90°$	$\left[\frac{v(l,0)_{max}}{v(l,0)_{stat}}\right]_{\phi=90°}$	Stress-amplification factor, $\phi = 90°$
	Calc.	Meas.	Preslip	Postslip	Ratio	Calc.	Stat.	Dynamic				
20	0.467	0.45	235	49.8	4.72	0.087	0.095	0.115	790	0.610	23.1	6.57
40	0.933	0.93	195	51.8	3.78	0.152	0.150	0.157	850	0.833	14.1	4.80
60	1.400	1.36	222	50.8	4.37	0.193	0.207	0.189	900	1.11	10.8	3.61
80	1.867	1.75	186	54.9	3.38	0.211	0.204	0.210	1030	1.385	6.48	2.89
100	2.333	2.24	200	48.7	4.12	0.206	0.194	0.196	1060	1.440	6.00	2.78
120	2.800	2.85	196	52.0	3.77	0.178	0.179	0.146	1230	1.142	6.93	3.51
140	3.267	3.45	197	49.5	4.00	0.127	0.122	0.129	1310	1.057	7.30	3.79
180	4.2	...	198	...	...	...	...	0.00144	1450	0.0229	175	174.8
Theoretical values			226.5	56.65	4.00	...	...					

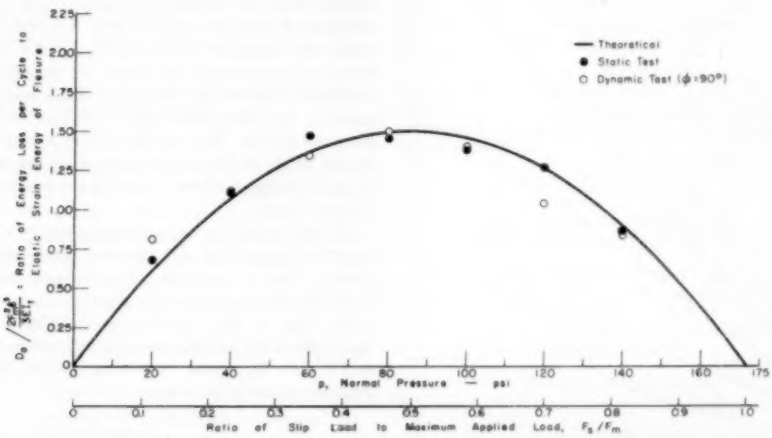
Theoretical
Static Test
Dynamic Test (φ=90°)
Ratio of Energy Loss per Cycle to Elastic Strain Energy of Flexure
p, Normal Pressure — psi
Ratio of Slip Load to Maximum Applied Load, F_s/F_m

FIG. 8 VARIATION OF ENERGY LOSS PER CYCLE WITH JOINT NORMAL PRESSURE

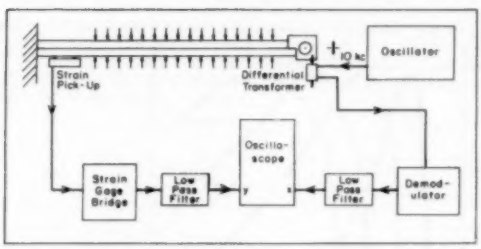

FIG. 9 SCHEMATIC OF INSTRUMENTATION FOR DYNAMIC MEASUREMENTS

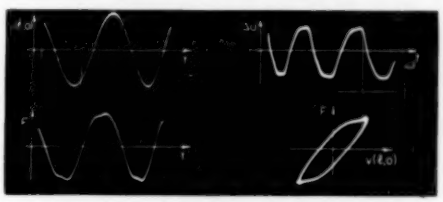

FIG. 10 PHOTOGRAPHS SHOWING $v(l, 0)$, F, Δu VERSUS TIME AND F VERSUS $v(l, 0)$

tions of this paper were chosen for analysis partly because it was anticipated, on the basis of the general theory developed in the third section, that slip damping would be large. There was, therefore, a reasonable expectation of making measurements accurate enough to test the theory. For these joints the energy dissipated per cycle of oscillation is shown in the straight lines of Fig. 11 as a function of σ_m, the maximum value of the extreme fiber stress excited at the built-in end of the blade. These curves are derived directly from Equation [26]. They have been placed on a dimensionless basis by dividing abscissas by 36,000 psi, the fatigue strength at 2×10^7 cycles of reversed stress, and dividing ordinates by the elastic strain energy which would be stored in the blade if it were loaded axially to a uniform stress equal to the fatigue strength. The straight lines intersect the axis of abscissas to the right of the origin, a reflection of the fact that a certain minimum excited stress, depending on the clamping pressure p, is required to initiate slip. For purposes of comparison, a curve which represents an estimate of the magnitude of material damping in a solid blade of the same dimensions has been drawn in Fig. 11. This curve has been computed by means of the procedure suggested in reference (9), making use of a specific damping relationship (18) representative of a wide range of technically important materials. The curves afford a direct comparison between material and slip damping only for uniform-pressure joints.

It is in some respects more revealing to use as ordinates the ratio of the slip-energy loss per cycle to the maximum strain energy which would be stored in the vibrating blade in the absence of any friction. Fig. 12 drawn with these ordinates reveals that at low excited stresses slip damping predominates over material damping. The experiments described in the preceding section were conducted in this low-stress region in order to avoid any possibility of confusing the two effects.

The general picture presented by Figs. 11 and 12 is one in which energy dissipation due to slip exceeds that due to material damping except at excited stresses which probably must be regarded as excessive from a design point of view. This conclusion is supported by measurements made by Shannon (2) on turbine blades of British H1A design. He reports a 5:1 ratio between slip and

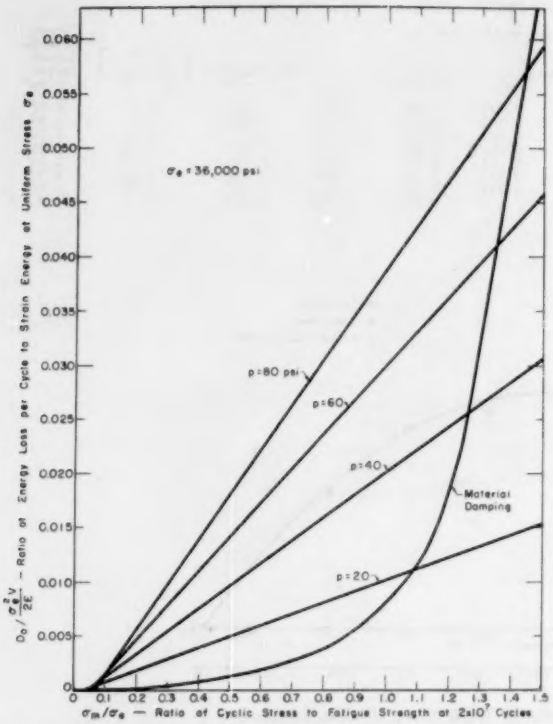
σ_e = 36,000 psi
p=80 psi
p=60
p=40
p=20
Material Damping
$D_0/\frac{\sigma_e^2 V}{2E}$ — Ratio of Energy Loss per Cycle to Strain Energy at Uniform Stress σ_e
σ_m/σ_e — Ratio of Cyclic Stress to Fatigue Strength at 2×10^7 Cycles

FIG. 11 COMPARISON OF SLIP AND MATERIAL DAMPING FOR UNIFORM-PRESSURE JOINT (COMPARISON A)

agreement with the measurement reported by Shannon for a "fir-tree" joint.

The very high theoretically possible values of slip damping are, however, never achieved in present-day fir-tree, "dovetail," or "ball-and-socket" root designs. This has been brought out by the work of Hanson, Meyer, and Manson (6) who have shown, furthermore, that the damping decreases with rotor speed. These results are understandable in the light of the general theory developed in this paper. With high centripetal accelerations the blade root is forced against the hub and the optimum pressure is exceeded almost from the start. As speeds increase, one departs further from the optimum pressure. (In regard to this point, reference should be made to Fig. 8 rather than to Fig. 12, in which the abscissas refer to the excited stresses.) Matters are somewhat improved if the blades are assembled initially loose, as is current fabricating practice in some assembly plants in this country, but the advantages of initial looseness disappear at elevated speeds. The proper course of improved design would appear to lie in the arrangement of a joint embodying radial interfacial surfaces whose contact pressures would not be affected by axial stress.

Corrosion fretting accompanying slip has been suggested as a possible deterrent to the effective use of slip damping. In the present state of engineering knowledge it does not seem possible to decide this question dogmatically. But it should be borne in mind that in the troublesome stall-flutter condition aerodynamic damping is inadequate and if turbine blades were brazed to the hub to prevent corrosion fretting, large resonant stress amplifications would occur.

CONCLUSIONS

Over a cycle of load or displacement a turbine blade dissipates energy due to microscopic slip of the blade root along its mating

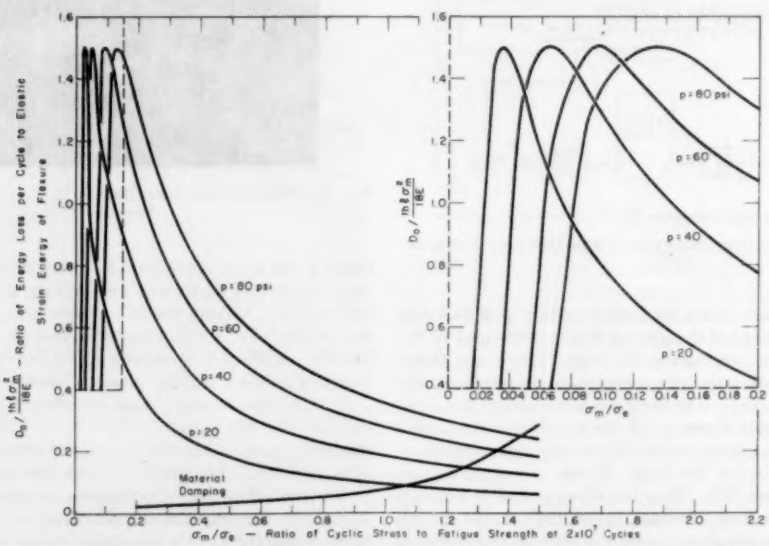
p=80 psi
p=60
p=40
p=20
Material Damping
$D_0/\frac{\pi k \sigma_m^2}{16E}$ — Ratio of Energy Loss per Cycle to Elastic Strain Energy of Flexure
σ_m/σ_e — Ratio of Cyclic Stress to Fatigue Strength at 2×10^7 Cycles

FIG. 12 COMPARISON OF SLIP AND MATERIAL DAMPING FOR UNIFORM-PRESSURE JOINT (COMPARISON B)

material damping at a cyclic stress equal to about 90 per cent of the fatigue limit. The ordinates of Fig. 12 are essentially equal to twice the logarithmic decrement. If proper allowance is made for differences in the contact areas in the two cases, the quantitative value of decrement predicted by theory is in satisfactory

surface with the hub. An explicit formula for the energy dissipated per cycle of vibration has been developed, Equation [8]. Notwithstanding the limitations of the analysis, which arise primarily from the assumption of a Coulomb friction effect at the interface, it appears that energy losses capable of providing a

highly beneficial reduction in resonant stresses can be achieved by means of slip damping. To achieve this maximum energy loss, joints must be designed so as to maintain a particular value of clamping pressure at the interface. In joints of conventional design the energy loss due to slip is inhibited by the high centrifugal pressures associated with full rotor speeds. Even in the case of these joints, however, slip damping may be expected to play a role as important as that of material damping in the minimization of stall-flutter effects.

The stress analysis of a plane interface under uniform pressure, but with variable slip, has been carried out. The predictions of the theory have been confirmed by experiment in this case. Other investigators working with prototype turbine blades have reported experimental results which are in satisfactory agreement with the theory.

Computations of the magnitudes of slip and material damping have been worked out for the uniform-pressure joint.

Acknowledgment

The work described in this paper was performed in the laboratories of the Department of Mechanics and Materials, University of Minnesota. It was sponsored by the United States Air Force and was administered under the direction of the Materials Laboratory, Directorate of Research, Wright Air Development Center, Mr. W. J. Trapp acting as project engineer.

In addition to the authors, the following personnel of the University of Minnesota contributed to the work: Technician, A. R. Magnuson; drafting and manuscript preparation, B. Gulbrandson, D. Schultz, and H. Thomas.

The authors' thanks are due Prof. B. J. Lazan, University of Minnesota, for advice concerning the comparisons between material and slip damping embodied in this paper.

BIBLIOGRAPHY

1 "Turbine-Blade Vibration Due to Partial Admission," by R. P. Kroon, Journal of Applied Mechanics, Trans. ASME, vol. 62, 1940, pp. A-161–A-165.

2 "Vibration Problems in Gas Turbines, Centrifugal and Axial Flow Compressors," by J. F. Shannon, R & M No. 226, Aeronautical Res. Council, Great Britain, 1945.

3 "The Stress Problem of Vibrating Compressor Blades," by J. F. Schnittger, Journal of Applied Mechanics, Trans. ASME, vol. 77, January, 1955, pp. 57–64.

4 "Factors Affecting Vibration of Axial Flow Compressor Blades," by S. S. Manson, A. J. Meyer, H. F. Calvert, and M. P. Hanson, Proceedings of the Society for Experimental Stress Analysis, vol. 7, no. 2, 1949, p. 1.

5 "Stress Investigation in Gas Turbine Disks and Blades," by S. S. Manson, SAE Quarterly Trans., vol. 3, no. 2, April, 1949, p. 229.

6 "A Method of Evaluating Loose-Blade Mounting as a Means of Suppressing Turbine and Compressor Blade Vibrations," by M. P. Hanson, A. J. Meyer, and S. S. Manson, Proceedings of the Society for Experimental Stress Analysis, vol. 10, no. 2, 1953, p. 103.

7 "Investigation of Structural Damping in Simple Built-Up Beams," by T. H. H. Pian and F. C. Hallowell, Jr., Technical Report, Contract N5ori-07833 to ONR, Aeroelastic and Structures Laboratory, Massachusetts Institute of Technology, Cambridge, Mass., February, 1950.

8 "A Study of the Structural Damping of a Simple Built-Up Beam With Riveted Joints in Bending," by T. H. H. Pian, Technical Report, Contract N5ori-07833 to ONR, Aeroelastic and Structures Laboratory, Massachusetts Institute of Technology, Cambridge, Mass., May, 1954.

9 "Fatigue Failure Under Resonant Vibration Conditions," by B. J. Lazan, ASM Symposium on Fatigue, Cleveland, Ohio, October, 1953.

10 "Advisory Report on Bibliography of Damping of Metals," by H. C. Cross, ATI 6174, Central Air Documents Office, Dayton, Ohio, 1946.

11 "Frictional Phenomena," by A. Gemant, Chemical Publishing Company, Brooklyn, N. Y., 1950, p. 449.

12 "Theory of Elasticity," by S. P. Timoshenko and J. N. Goodier, McGraw-Hill Book Company, Inc., New York, N. Y., second edition, 1951, p. 229.

13 Ibid., p. 6.

14 "An Elastic Theory of Dislocations," by E. H. Mann, Proceedings of the Royal Society of London, England, series A, vol. 199, no. 1058, 1949, p. 376.

15 "On the Theory of Dislocations," by J. L. Bogdanoff, *Journal of Applied Physics*, vol. 21, 1950, p. 1258.

16 "Frictional Damping and Resonant Vibration Characteristics of an Axial Slip Lap Joint," by J. H. Klumpp and B. J. Lazan, WADC TR 54-64, March, 1954.

17 "Dynamic Testing of Materials and Structures With a New Resonance Vibration Exciter and Controller," by B. J. Lazan, J. Brown, A. Gannet, P. Kirmser, and J. Klumpp, Proceedings of the ASTM, vol. 52, 1952, p. 858.

18 Reference (9), pp. 55–57.

Flexural Vibrations of Rectangular Plates[1]

By R. D. MINDLIN,[2] A. SCHACKNOW,[3] and H. DERESIEWICZ,[4] New York, N. Y.

The influence of rotatory inertia and shear deformation on the flexural vibrations of isotropic, rectangular plates is investigated. Three independent families of modes are possible when the edges are simply supported. Coupling of the modes is studied for the case of one pair of parallel edges free and the other pair simply supported. The development of the coupling is traced by means of a solution for elastically supported edges. Special attention is given to the higher modes and frequencies of vibration which are beyond the range of applicability of the classical theory of thin plates.

Plate Equations

When shear deformation and rotatory inertia terms are included, the flexural vibrations of a plate are governed by three differential equations each of which contains the deflection (w) and the two components of rotation (ψ_x, ψ_y). It was shown in a previous paper (1)[5] that the equations can be uncoupled by expressing ψ_x, ψ_y, and w in terms of three potentials (w_1, w_2, H). Thus, omitting factors $\exp(ip_jt)$, $j = 1, 2, 3$, from w_1, w_2, and H, respectively

$$\left.\begin{aligned} \psi_x &= (\sigma_1 - 1)\partial w_1/\partial x + (\sigma_2 - 1)\partial w_2/\partial x + \partial H/\partial y \\ \psi_y &= (\sigma_1 - 1)\partial w_1/\partial y + (\sigma_2 - 1)\partial w_2/\partial y - \partial H/\partial x \\ w &= w_1 + w_2 \end{aligned}\right\} \quad \ldots [1]$$

and

$$(\nabla^2 + \delta_1^2)w_1 = 0, \quad (\nabla^2 + \delta_2^2)w_2 = 0, \quad (\nabla^2 + \omega^2)H = 0 \quad \ldots [2]$$

where

$$\left.\begin{aligned} \delta_j^2 &= 6F_j^2[1 + g - (-1)^j Q_j]h^{-2}, \quad j = 1, 2 \\ \sigma_j &= 2[1 + g - (-1)^j Q_j]^{-1}, \quad j = 1, 2 \\ Q_j &= [(1 - g)^2 + 4gF_j^{-2}]^{1/2}, \quad j = 1, 2 \\ F_j &= p_j/p_0, \quad j = 1, 2, 3, \quad p_0^2 = \pi^2 G/\rho h^2 \\ \omega^2 &= \pi^2(F_3^2 - 1)h^{-2}, \quad g = \kappa^2(1 - \nu)/2 \end{aligned}\right\} \quad \ldots [3]$$

In Equations [3], G is the shear modulus, ν is Poisson's ratio, ρ is the density, h is the thickness of the plate, and p_0 is the frequency of simple thickness-shear vibration of an infinite plate. The symbols δ_j, ω, and σ_j have the same significance as in reference (1), but here they are expressed in terms of the frequency ratios F_j. The constant κ^2, for which alternative values were given in reference (1), has the value $\pi^2/12$ here.

The bending moments, twisting moment, and shearing forces, per unit of length, are given by

$$\left.\begin{aligned} M_x &= D\left(\frac{\partial \psi_x}{\partial x} + \nu\frac{\partial \psi_y}{\partial y}\right), \quad M_y = D\left(\frac{\partial \psi_y}{\partial y} + \nu\frac{\partial \psi_x}{\partial x}\right) \\ M_{xy} &= \frac{D(1 - \nu)}{2}\left(\frac{\partial \psi_y}{\partial x} + \frac{\partial \psi_x}{\partial y}\right) \\ Q_x &= \kappa^2 Gh\left(\psi_x + \frac{\partial w}{\partial x}\right), \quad Q_y = \kappa^2 Gh\left(\psi_y + \frac{\partial w}{\partial y}\right) \end{aligned}\right\} \quad \ldots [4]$$

where

$$D = Gh^3/6(1 - \nu)$$

is the plate flexure modulus.

Boundary conditions sufficient to assure a unique solution of Equations [2] are set by specifying, at each point of the edge of the plate, one member of each of the three products

$$M_\nu \partial\psi_\nu/\partial t, \quad M_{\nu s}\partial\psi_s/\partial t, \quad Q_\nu \partial w/\partial t \quad \ldots [5]$$

where ν and s are co-ordinates normal and tangential, respectively, to the edge.

Simply Supported Rectangular Plate

The boundary conditions of a simply supported rectangular plate of length $2a$ and width $2b$ are taken to be

$$\left.\begin{aligned} M_x &= 0, \quad \partial\psi_y/\partial t = 0, \quad \partial w/\partial t = 0 \quad \text{on} \quad x = \pm a \\ M_y &= 0, \quad \partial\psi_x/\partial t = 0, \quad \partial w/\partial t = 0 \quad \text{on} \quad y = \pm b \end{aligned}\right\} \quad \ldots [6]$$

It may be seen from Equation [5] that the conditions on ψ_x and ψ_y could be replaced by conditions on M_{yx}, but the former are chosen because they lead to simple modes analogous to those of the classical theory of thin plates.

Equations [2] have solutions

$$\left.\begin{aligned} w_1 &= A_1 \sin \xi_1 x \sin \eta_1 y \\ w_2 &= A_2 \sin \xi_2 x \sin \eta_2 y \\ H &= A_3 \cos \xi_3 x \cos \eta_3 y \end{aligned}\right\} \quad \ldots [7]$$

provided that

$$\xi_1^2 + \eta_1^2 = \delta_1^2, \quad \xi_2^2 + \eta_2^2 = \delta_2^2, \quad \xi_3^2 + \eta_3^2 = \omega^2 \quad \ldots [8]$$

Substituting Equations [7] in [4] (where necessary) and [6], we find

$$\xi_j = r_j\pi/2a, \quad \eta_j = s_j\pi/2b, \quad j = 1, 2, 3 \quad \ldots [9]$$

where r_j and s_j are even integers. The first two of Equations [7] represent deflections odd in both x and y. Although H generates no deflection, it produces rotations with the same symmetry as those derived from w_1 and w_2. Hence all three of Equations [7] will be termed modes odd in x and y. For modes even in x, $\sin \xi_j x$ and $\cos \xi_j x$ are interchanged in all three of Equations [7]

---

[1] This investigation was supported by the Office of Naval Research and the Signal Corps Engineering Laboratories.

[2] Professor of Civil Engineering, Columbia University. Mem. ASME.

[3] Supervisor, Engineering Computing Section, Republic Aviation Corporation, Long Island, N. Y.

[4] Assistant Professor of Civil Engineering, Columbia University. Assoc. Mem. ASME.

[5] Numbers in parentheses refer to the Bibliography at the end of the paper.

Contributed by the Applied Mechanics Division and presented at the Diamond Jubilee Annual Meeting, Chicago, Ill., November 13–18, 1955, of The American Society of Mechanical Engineers.

Discussion of this paper should be addressed to the Secretary, ASME, 29 West 39th Street, New York, N. Y., and will be accepted until October 10, 1956, for publication at a later date. Discussion received after the closing date will be returned.

Note: Statements and opinions advanced in papers are to be understood as individual expressions of their authors and not those of the Society. Manuscript received by ASME Applied Mechanics Division, July 9, 1955. Paper No. 55—A-78.

and the r_j are odd integers. Similarly, for modes even in y, sin $\eta_j y$ and cos $\eta_j y$ are interchanged and the s_j are odd integers.

Substituting Equations [9] in [8] and solving for the frequency ratios F_j, we find

$$\left.\begin{aligned} 2F_j^2 &= 1 + k\psi_j^2 + (-1)^j\Omega_j, \quad j = 1, 2 \\ F_3^2 &= 1 + \psi_3^2 \end{aligned}\right\} \quad \ldots\ldots [10]$$

where

$$\left.\begin{aligned} \psi_j^2 &= (r_j h/2a)^2 + (s_j h/2b)^2, \quad j = 1, 2, 3 \\ \Omega_j &= [(1 + k\psi_j^2)^2 - 4\kappa^4\psi_j^4/g]^{1/2}, \quad j = 1, 2, 3 \\ k &= \kappa^2(1 + g)/g \end{aligned}\right\} \quad [11]$$

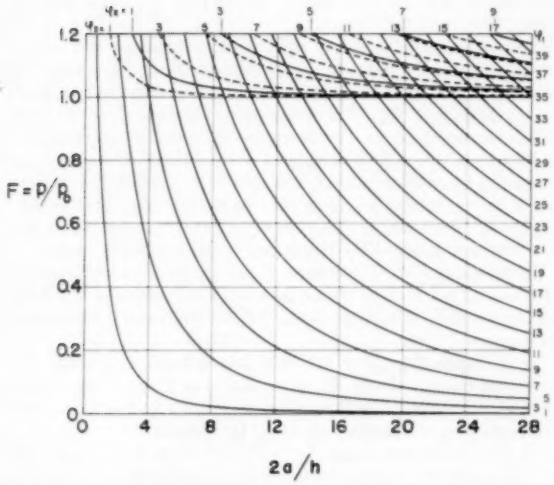

FIG. 1 CHART FOR ESTIMATING FREQUENCIES OF VIBRATION OF SIMPLY SUPPORTED RECTANGULAR PLATES

The three sets of frequency ratios are plotted against the length-thickness ratio, in Fig. 1, with

$$\varphi_j = (r_j^2 + s_j^2 a^2/b^2)^{1/2}, \quad j = 1, 2, 3 \ldots\ldots [12]$$

as parameters and $\nu = 0.312$.

For given length-width-thickness ratios and order of mode, the frequencies of the three types of motion satisfy the inequalities $p_1 < p_3 < p_2$. The lowest of these derives from the potential w_1; its mode shape, as calculated from Equations [1], is illustrated in Fig. 2(*a*). Of the three types of motion, this is the one that corresponds most closely to that of the classical theory. In fact, for the lower modes of large, thin plates, this mode shape approaches that of classical theory, in which

$$\psi_x = -\partial w/\partial x \text{ and } \psi_y = -\partial w/\partial y$$

as illustrated in Fig. 3. Also, as p_1 diminishes, it approaches

$$p_0\psi_1^2\kappa^2/g^{1/2}$$

the frequency obtained from the classical theory. The other two frequencies are very much higher than p_1 and their mode shapes are quite different. In the case of p_2, which is associated with the potential w_2, the thickness-shear deformation predominates over the flexural deformation, as illustrated in Fig. 2(*b*). The remaining mode shape, Fig. 2(*c*), contains no deflection and the two components of rotation are so related in phase as to form a twist about

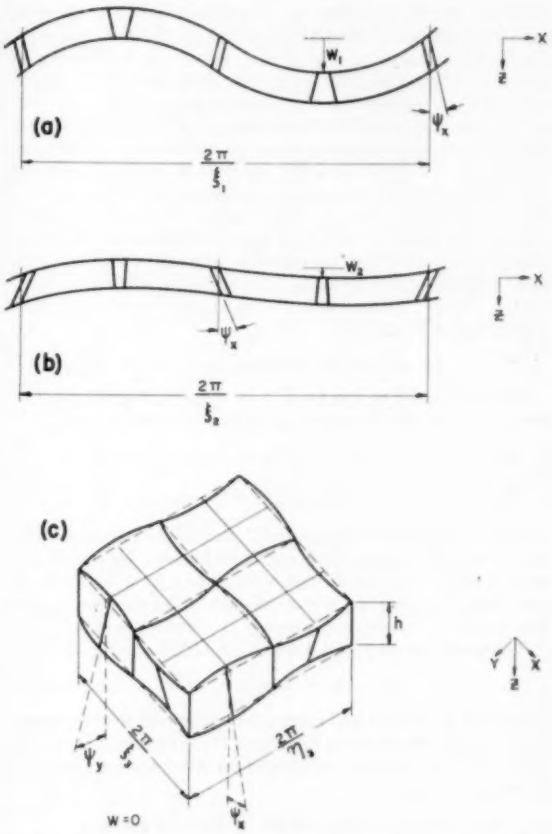

FIG. 2 THE THREE TYPES OF VIBRATIONAL MODES OF SIMPLY SUPPORTED RECTANGULAR PLATES WHEN ROTATORY INERTIA AND SHEAR DEFORMATION ARE TAKEN INTO ACCOUNT
(*a*, Flexural; *b*, thickness-shear; *c*, thickness-twist.)

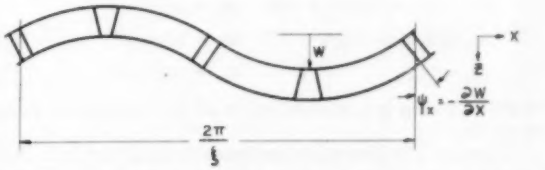

FIG. 3 VIBRATIONAL MODE OF A SIMPLY SUPPORTED RECTANGULAR PLATE ACCORDING TO THE CLASSICAL THEORY OF THIN PLATES

the normal to the plate. For convenience of reference, the types of motion generated by w_1, w_2, and H are called flexural, thickness-shear, and thickness-twist, respectively.

Although Fig. 1 is convenient for the rapid estimation of the three frequencies for wide ranges of modes and dimensional ratios, it will be found useful to plot Equations [10] for a fixed ratio, $s_j h/2b$, of thickness to nodal spacing along the direction of the width. In this case, each type of motion has a low-frequency cut-off given by

$$\left.\begin{aligned} 2(F_j^*)^2 &= 1 + (\psi_j^*)^2 + (-1)^j\Omega_j^*, \quad j = 1, 2 \\ (F_3^*)^2 &= 1 + (\psi_3^*)^2 \end{aligned}\right\} \quad \ldots [13]$$

where ψ_j^* and Ω_j^* are given by Equations [11] with $r_j h/2a = 0$. Equations [10] are plotted in Fig. 4 for $s_j h/2b = 0.2$ and $\nu = 0.312$. In this figure, $r_1 = m$, $r_2 = n$, and $r_3 = q$; i.e., the curves m, n, q = constant give the frequencies of the flexural, thickness-shear, and thickness-twist modes, respectively. Odd and even values of m, n, q identify modes even and odd, respectively, in x. All the curves apply to modes either odd or even in y. The range of F in Fig. 4 is 1.0198 to 1.20. Above 1.20 the results are not very reliable, as the theory does not contain the effects of vibrations having more than one nodal surface parallel to the faces $z = \pm h/2$. Below $F = 1.0198$ (the thickness-twist cutoff frequency for $s_j h/2b = 0.2$) the curves m = constant look much the same as those derived from the classical theory, but the frequencies are lower. The two sets of curves coalesce as F_1 diminishes to its cutoff value 0.0578.

One Pair of Parallel Edges Free

When the plate is free along $x = \pm a$ and simply supported along $y = \pm b$ the boundary conditions become

$$\left.\begin{aligned} &M_x = 0, \quad M_{yz} = 0, \quad Q_z = 0 \qquad \text{on} \quad x = \pm a \\ &M_y = 0, \quad \partial\psi_z/\partial t = 0, \quad \partial w/\partial t = 0 \quad \text{on} \quad y = \pm b \end{aligned}\right\} \ldots [14]$$

The solutions given by Equations [7] and [8] are applicable again, but w_1, w_2, and H cannot each satisfy all the boundary conditions, as they did for the simply supported plate. This is because, on incidence at a free edge, a wave of each of the three types gives rise, in general, to reflected waves of all three types (2).

The conditions on $y = \pm b$ are satisfied if

$$\eta_1 = \eta_2 = \eta_3 = \eta = s\pi/2b \ldots\ldots\ldots\ldots [15]$$

where s is an even or odd integer for modes odd or even, respectively, in y. Substituting Equations [7] successively in [1], [4], and [14], the boundary conditions on $x = \pm a$ are satisfied if $p_1 = p_2 = p_3$ and

$$\left.\begin{aligned} &A_1\alpha_{11}\sin\xi_1 a + A_2\alpha_{12}\sin\xi_2 a + A_3\alpha_{13}\sin\xi_3 a = 0 \\ &A_1\alpha_{21}\cos\xi_1 a + A_2\alpha_{22}\cos\xi_2 a + A_3\alpha_{23}\cos\xi_3 a = 0 \\ &A_1\alpha_{31}\cos\xi_1 a + A_2\alpha_{32}\cos\xi_2 a + A_3\alpha_{33}\cos\xi_3 a = 0 \end{aligned}\right\} \ldots [16]$$

where, with $j = 1, 2$

$$\left.\begin{aligned} &\alpha_{1j} = (\sigma_j - 1)(\xi_j^2 + \nu\eta^2), \quad \alpha_{13} = -(1-\nu)\xi_3\eta \\ &\alpha_{2j} = 2(\sigma_j - 1)\xi_j\eta, \qquad \alpha_{23} = \xi_3^2 - \eta^2 \\ &\alpha_{3j} = \sigma_j\xi_j, \qquad \alpha_{33} = -\eta \end{aligned}\right\} \ldots [17]$$

For modes even in x, sine and cosine are interchanged in Equations [16].

Equations [16] determine amplitude ratios $A_1 : A_2 : A_3$ so that, except for special cases to be considered later, all three types of motion must be present when a pair of edges is free. For a non-trivial solution the determinant of the coefficients of the A_j in Equations [16] must vanish. This leads to the equation

$$M_1 \tan\gamma - M_2 \tan\alpha\gamma + M_3 \tan\beta\gamma = 0 \ldots\ldots [18]$$

where

$$\left.\begin{aligned} M_1 &= \xi_3(\sigma_1 - 1)(\xi_1^2 + \nu\eta^2)(\sigma_2\omega^2 - 2\eta^2) \\ M_2 &= \xi_1(\sigma_2 - 1)(\xi_2^2 + \nu\eta^2)(\sigma_1\omega^2 - 2\eta^2) \\ M_3 &= 2(1-\nu)\xi_1\xi_2\xi_3\eta^2(\sigma_1 - \sigma_2) \\ \gamma &= \xi_1 a, \quad \alpha = \xi_2/\xi_1, \quad \beta = \xi_3/\xi_1 \end{aligned}\right\} \ldots [19]$$

The frequency spectrum may be computed as follows: For a given Poisson ratio (which fixes g) and a given ratio, $sh/2b$, of thickness to nodal spacing along y, a choice of F fixes α, β, and $M_j h^3$. Equation [18] then has γ as the only variable and a set of roots may be computed by successive approximations. For the chosen frequency, to each root γ there corresponds a length-thickness ratio

$$2a/h = \gamma(h^2\delta_1^2 + h^2\eta^2)^{-1/2} \ldots\ldots\ldots\ldots [20]$$

as obtained from the first of Equations [8]. Since $h\delta_1$ is fixed by the choice of F and g, see Equations [3], and since $h\eta$ is fixed by the choice of $sh/2b$, all the quantities on the right-hand side of Equation [20] are known. Thus a set of values of $2a/h$ is obtained for the chosen F. This procedure was followed for a number of suitably spaced values of F, with $\nu = 0.312$ and $sh/2b = 0.2$, sufficient to enable plotting of the curves shown in Fig. 5. The dashed and full lines are for modes odd and even, respectively, in x.

The difference in character of the spectrum above and below each frequency F_j^* is due to the fact that ξ_1, ξ_2, and ξ_3 are real or imaginary as δ_1, δ_2, and ω, respectively, are greater or less than η, see Equations [8]. The changes occur when $\xi_j = 0$; but this is the condition used to determine the cutoff frequencies F_j^* in the case of the simply supported plate. Hence there are four frequency ranges, separated by the three F_j^*, in which the character of the frequency spectrum may be expected to be different, since one, two, or three of the transcendental functions in Equation [18] are hyperbolic, depending on the frequency range.

In the range $F < F_1^*$, all three ξ_j are imaginary and Equation [18] has no real roots. Hence there are no frequencies of vibration below F_1^*. For $sh/2b = 0.2$, $F_1^* = 0.0578$ and is not shown in Fig. 5.

In the range $F_1^* < F < F_2^*$, only ξ_1 is real and, as a result, the spectrum has the simple character shown in Fig. 5. The lower part of this range ($F \to F_1^*$) is not shown in Fig. 5 as it is given adequately by the classical theory of thin plates.

In the next higher range, $F_2^* < F < F_3^*$, ξ_1 and ξ_2 are real and ξ_3 is imaginary. This results in a more complicated spectrum but also in some simple solutions, which may be found by noting that, with ξ_1 and ξ_2 real, Equations [16] are satisfied by

$$\cos\xi_1 a = 0, \quad \cos\xi_2 a = 0, \quad A_3 = 0 \ldots\ldots\ldots [21]$$

Thus the thickness-shear type of motion is absent and Equation [18] has roots

$$\xi_1 = m\pi/2a, \quad \xi_2 = q\pi/2a, \quad m, q \text{ odd} \ldots\ldots\ldots [22]$$

These roots, and the condition $F_1 = F_3$, determine the co-ordinates of the white squares in both Figs. 4 and 5. Hence, for a given nodal spacing in the direction of the width (for modes odd or even in y) points on the frequency spectrum of a simply supported plate, where flexural and thickness-twist modes even in x have the same frequencies, are also points on the spectrum, for modes odd in x, of a plate with a pair of parallel edges free. Accordingly, the curves of F versus $2a/h$, determined by Equation [18], (the dashed curves), pass through the white squares in Fig. 5. However, the dashed curves (modes odd in x) do not pass through the black squares since these are intersections of curves m even, q even, and these points are not solutions of Equations [21]. The converse is true for modes even in x, of the plate with a pair of edges free. Thus the full curves in Fig. 5 pass through the black squares but not the white squares. Points on the curves m = constant, q = constant, Fig. 4, lying between their intersections are not points on the spectrum shown in Fig. 5, as only the intersections satisfy the condition $F_1 = F_3$ which is required for free edges.

It is interesting to observe the behavior of the lowest mode as a/h approaches zero. In this case Equation [18] becomes an

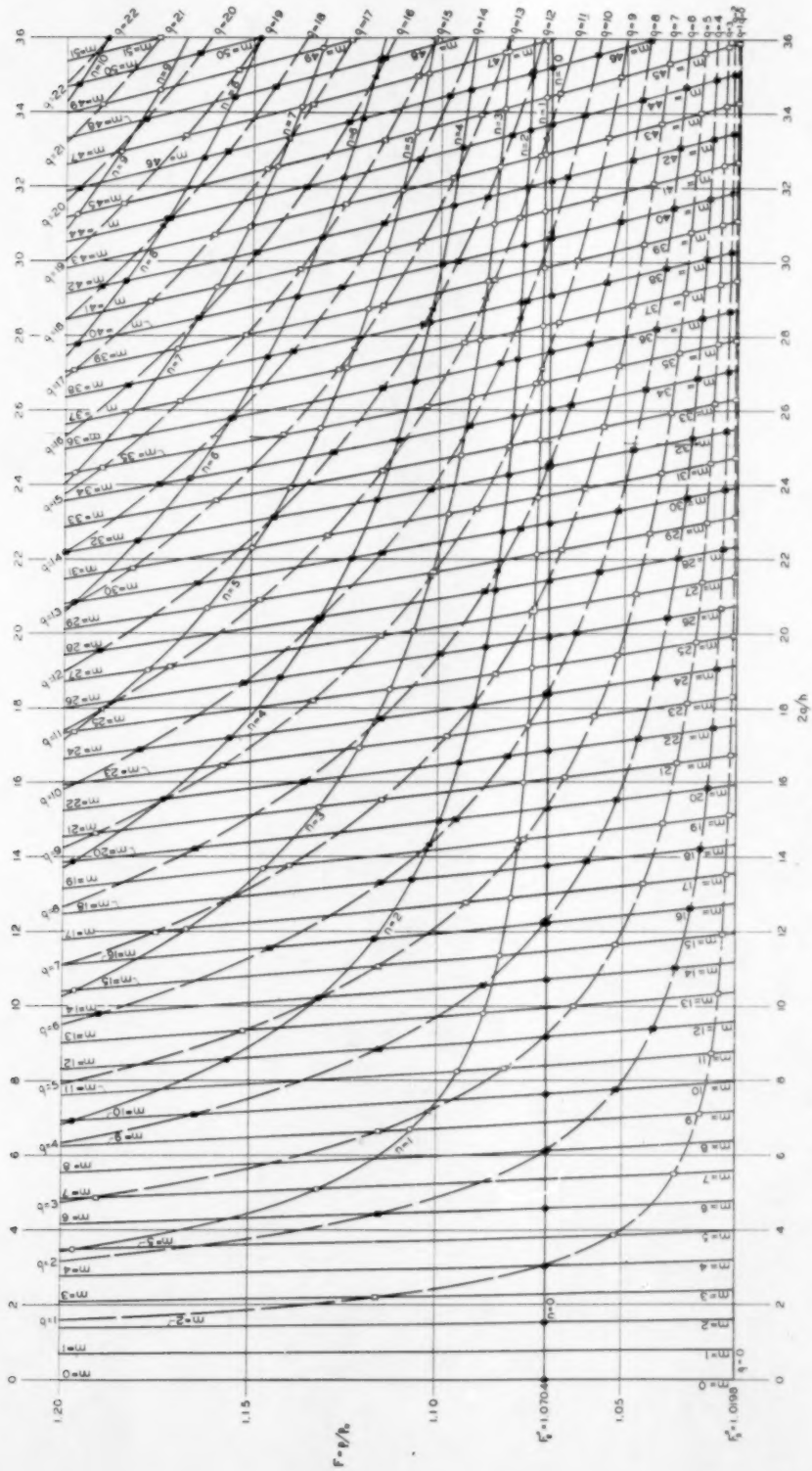

FIG. 4 FREQUENCIES OF VIBRATION OF SIMPLY SUPPORTED RECTANGULAR PLATES ($\nu = 0.312$) WHEN THE DISTANCE BETWEEN NODES ALONG THE WIDTH IS FIVE TIMES THE THICKNESS

(Curves m, n, q = constant give frequencies of flexural, thickness-shear, and thickness-twist modes, respectively. m, n, q even and odd are modes odd and even, respectively, in x. All modes may be odd or even in y.)

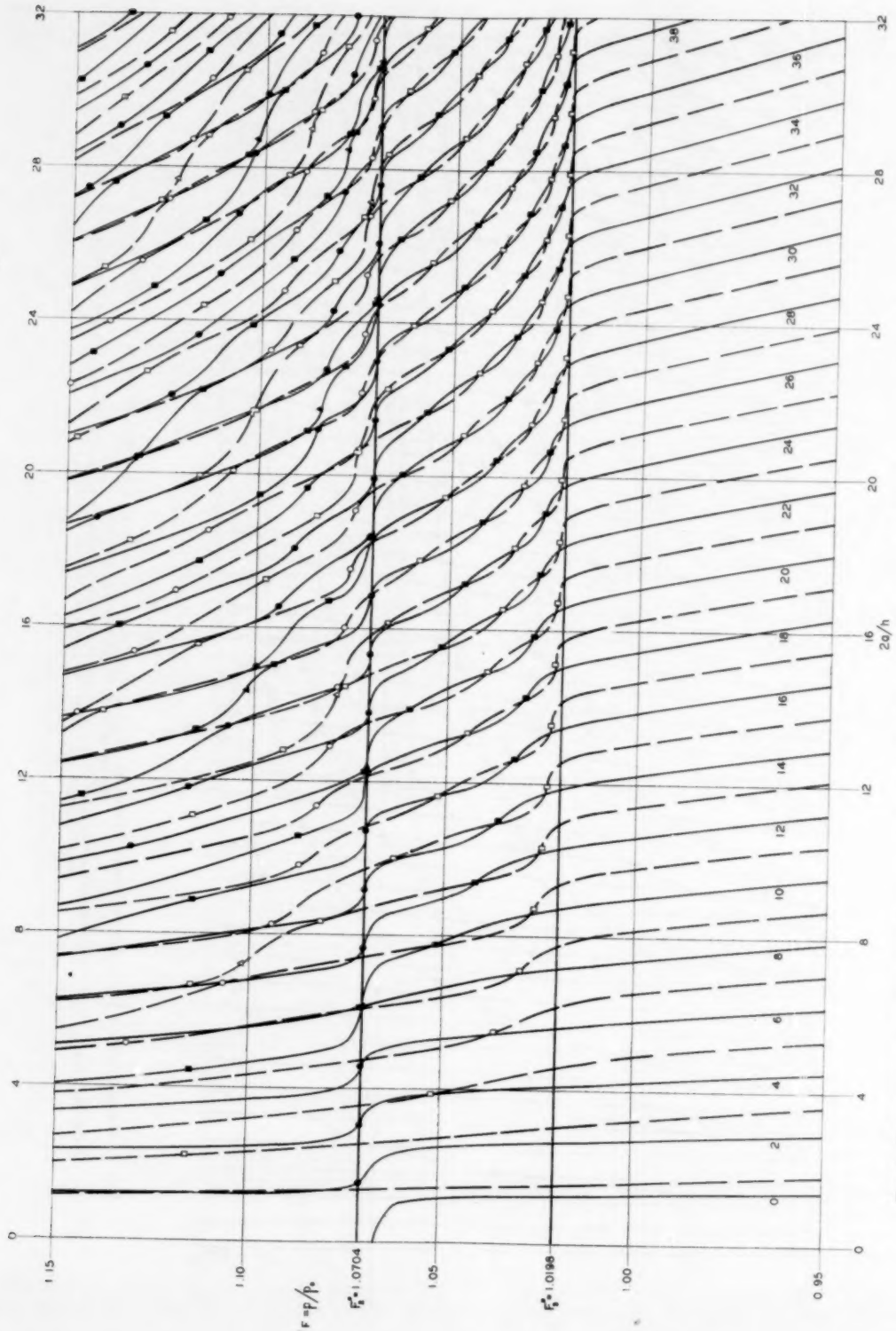

FIG. 5 FREQUENCIES OF VIBRATION OF RECTANGULAR PLATES WITH ONE PAIR OF PARALLEL EDGES FREE AND THE OTHER PAIR SIMPLY SUPPORTED
(Dashed and full lines are for modes odd and even, respectively, in z.)

indeterminate form, but the limiting frequency may be found readily by recognizing that the lowest mode is even in x and that, as $a/h \to 0$, the plate degenerates to a beam, of narrow rectangular section, simply supported at $y = \pm b$. Hence the limiting frequency is given by the formula for F_2^* in Equations [13], except that $1 - \nu$, in the expression for g, must be replaced by $(1 + \nu)^{-1}$ in order to account for the difference between the modulus of elasticity E of a beam and the corresponding quantity $E/(1 - \nu^2)$ for a plate. With $sh/2b = 0.2$, the result is $F = 1.0666$.

In the highest frequency range ($F > F_2^*$) all three ξ_j are real. Hence what was said of the case ξ_1, ξ_3 real and the points identified by white and black squares applies again in this range. Similar conclusions are reached for the combinations ξ_1, ξ_2 and ξ_2, ξ_3. In the former case, the curves of the coupled spectrum, for modes odd in x, pass through the intersections of m odd, n odd (white circles) but not through m even, n even (black circles) and at these intersections the thickness-twist mode is absent. In the latter case the common intersections are n odd, q odd (white triangles) and the flexural mode is absent. For the description of the coupled spectrum of modes even in x, "odd" and "even," "black" and "white" should be interchanged.

Development of Coupling

The difference between the simple spectrum of the simply supported plate, Fig. 4, and the complicated spectrum of the plate with a pair of edges free, Fig. 5, is due to the absence, in the former, and presence, in the latter, of coupling between the three types of motion. The development of the coupling, and hence the transition from one spectrum to the other, may be traced continuously by considering a case of elastically supported edges.[6] In order to simplify the discussion, the special case $\eta_j = 0$ will be considered, so that the mode shapes are independent of y and only the flexural and thickness-shear modes can couple. Then, from the first two of Equations [7] and [8]

$$w_1 = A_1 \sin \delta_1 x, \quad w_2 = A_2 \sin \delta_2 x \ldots\ldots\ldots [23]$$

and the boundary conditions are

$$M_x = 0, \quad Q_x = \mp K w \qquad \text{on } x = \pm a \ldots\ldots [24]$$

where K is the spring constant of the elastic support. Substituting Equations [23] successively in Equations [4] and [24], we obtain

$$\left.\begin{aligned} &(\sigma_1 - 1)\delta_1^2 A_1 \sin \delta_1 a + (\sigma_2 - 1)\delta_2^2 A_2 \sin \delta_2 a = 0 \\ &\kappa^2 G h(\sigma_1 \delta_1 A_1 \cos \delta_1 a + \sigma_2 \delta_2 A_2 \cos \delta_2 a) \\ &\qquad = -K(A_1 \sin \delta_1 a + A_2 \sin \delta_2 a) \end{aligned}\right\} \ldots [25]$$

When $K = \infty$, the edges are simply supported and Equations [25] reduce to

$$A_1 \sin \delta_1 a = 0, \quad A_2 \sin \delta_2 a = 0 \ldots\ldots [26]$$

Thus, the modes w_1 and w_2 are not coupled and the roots of Equations [26] are

$$\delta_1 = m\pi/2a, \quad \delta_2 = n\pi/2a, \quad m, n \text{ even} \ldots\ldots [27]$$

In the case of modes even in x the roots have the same form but m and n are odd. A typical portion of the frequency spectrum in the range $F > 1$ is shown in Fig. 6 by the curves m = constant, n = constant. (Note that, when $\eta = 0$, $F_2^* = F_3^* = 1$, $F_1^* = 0$.)

When $K = 0$, the edges are free and Equations [25] reduce to

$$\left.\begin{aligned} &(\sigma_1 - 1)\delta_1^2 A_1 \sin \delta_1 a + (\sigma_2 - 1)\delta_2^2 A_2 \sin \delta_2 a = 0 \\ &\sigma_1 \delta_1 A_1 \cos \delta_1 a + \sigma_2 \delta_2 A_2 \cos \delta_2 a = 0 \end{aligned}\right\} \ldots [28]$$

[6] This was suggested by E. Sternberg.

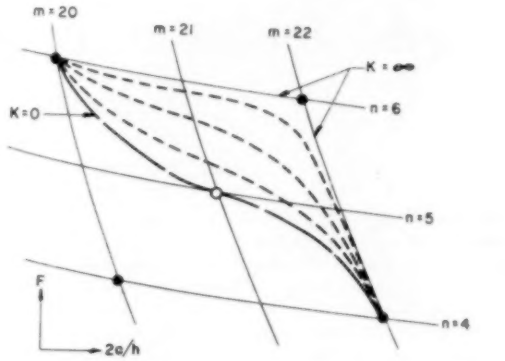

Fig. 6 Illustrating the Development of Coupling Between Flexural and Thickness-Shear Modes as the Stiffness of Elastic Support of Edges Is Diminished From $K = \infty$ (Simply Supported) to $K = 0$ (Free)

These are the same as the first and third of Equations [16] for the limiting case $\eta = 0$. It will be observed that Equations [28] have the solutions [27] for m and n both odd and even. Hence the spectral curves for modes odd in x and free edges must pass through the intersections of the spectral curves both for modes odd in x (black circles) and modes even in x (white circles) with simply supported edges. A typical curve ($K = 0$) is shown[7] in Fig. 6.

When $0 < K < \infty$, Equations [25] still have the roots determined by Equations [26], so that the curves giving the frequencies of modes odd in x pass through the intersections of m even, n even (black circles in Fig. 6). The portions of the curves between the black circles do not, however, pass through the intersections m odd, n odd (white circles) because Equations [25] are not satisfied by $\cos \delta_1 a = 0$, $\cos \delta_2 a = 0$. These portions pass above the white circles because the introduction of the elastic support is an additional constraint which serves to raise the frequencies above those for free edges, as shown by the dashed curves lying between $K = 0$ and $K = \infty$ in Fig. 6. As the support is stiffened indefinitely, these curves approach, asymptotically, the curves m even, n even. Similar results apply to modes even in x, but odd and even, black and white are interchanged.

If $\eta \neq 0$, the situation is somewhat more complicated because there are no common points such as the black circles in Fig. 6. For example, in the limiting case $K = 0$, for modes odd in x, the curves pass through the intersections m odd, n odd but not through the intersections m even, n even; and similarly, for the networks n, q and q, m, as explained in the discussion of Equations [16] and [18].

Construction of Approximate Coupled Spectrum

The co-ordinates of the points marked by circles, squares, and triangles in Figs. 4 and 5 are easy to calculate, as they are given by explicit algebraic formulas obtained by eliminating F and $2a/h$, in turn, from Equations [10], taken two at a time. Since the curves m, n, q = constant, for the simply supported plate, are monotonic, they may be drawn with little error through the

[7] More extensive sets of curves for modes both odd and even in x are given in references (3) and (4). In these, problems of crystal plates are treated; but when $\eta = 0$ the transition from crystalline to isotropic requires only a change in the definition of g. It may also be observed that Equations [23] to [28] apply equally well to beams. It is only necessary to replace $1 - \nu$ by $1/(1 + \nu)$ in the expression for g given in Equation [3]. With $\kappa^2 = \pi^2/12$ the solutions then apply to beams of narrow rectangular section. For beams of other cross sections, appropriate values of κ are given in reference (5).

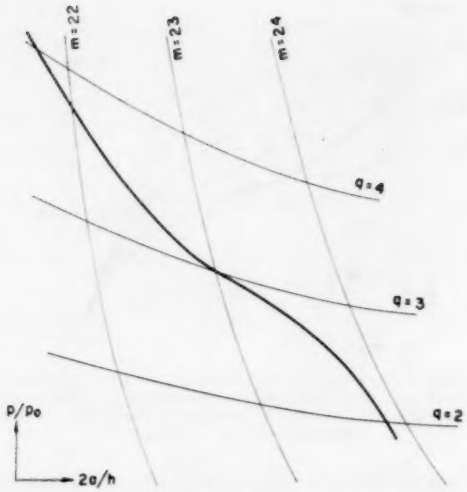

FIG. 7 CONSTRUCTION OF TYPICAL PORTION OF COUPLED SPECTRUM FOR A MODE ODD IN x. FREQUENCY RANGE $F_3^* < F < F_3^*$

plotted points, Fig. 4. On the other hand, the calculation of the complicated curves of Fig 5 is a long and tedious process, involving the determination of the roots of a transcendental equation. However, if only qualitative information is required, the spectrum may be sketched approximately, on the network of curves for the simply supported plate, in accordance with the following rules. The rules are given for modes odd in x. For modes even in x, odd and even are interchanged.

1 Starting in the low-frequency range of the spectrum, proceed to sketch a line upward. (The line should tend to the left, since, for a given mode, increasing frequencies correspond to decreasing length-thickness ratios.)

2 The line cannot cross a curve m, n, or q odd except at the intersection with another curve m, n, or q odd.

3 On approaching a curve m, n, or q odd, either from below or from the right, the line must bear upward and to the left, so that it converges, with the curve, to the nearest intersection with a second curve m, n, or q odd, at which point the crossing is made.

4 The line may cross curves m, n, or q even, but must not pass through intersections of curves m, n, or q even.

Typical applications of these rules are illustrated in Figs. 7 and 8.

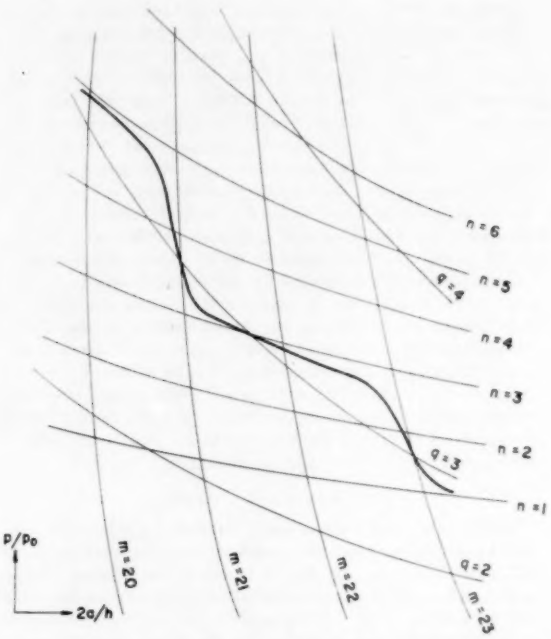

FIG. 8 CONSTRUCTION OF TYPICAL PORTION OF COUPLED SPECTRUM FOR A MODE ODD IN x. FREQUENCY RANGE $F > F_3^*$

BIBLIOGRAPHY

1 "Influence of Rotatory Inertia and Shear on Flexural Motions of Isotropic, Elastic Plates," by R. D. Mindlin, JOURNAL OF APPLIED MECHANICS, Trans. ASME, vol. 73, 1951, pp. 31–38.

2 "Reflection of Flexural Waves at the Edge of a Plate," by T. R. Kane," JOURNAL OF APPLIED MECHANICS, Trans. ASME, vol. 76, 1954, pp. 213–220.

3 "Thickness-Shear and Flexural Vibrations of Crystal Plates," by R. D. Mindlin, *Journal of Applied Physics*, vol. 22, 1951, pp. 316–323.

4 "Forced Thickness-Shear and Flexural Vibrations of Piezoelectric Crystal Plates," by R. D. Mindlin, *Journal of Applied Physics*, vol. 23, 1952, pp. 83–88.

5 "Timoshenko's Shear Coefficient for Flexural Vibrations of Beams," by R. D. Mindlin and H. Deresiewicz, Proceedings of the Second U. S. National Congress of Applied Mechanics, 1954, pp. 175–178.

Momentum Diffusion From a Slot Jet Into a Moving Secondary[1]

By A. S. WEINSTEIN,[2] J. F. OSTERLE,[3] AND W. FORSTALL,[4] PITTSBURGH, PA.

Results are presented for an experimental, impact-tube study of the diffusion of momentum for the isothermal, incompressible, turbulent mixing of a slot jet issuing into a slower moving secondary region. The symmetric spread of the jet into a uniformly flowing secondary stream of low initial turbulence is well correlated by phenomenological expressions based on assumptions suggested by the Engineering Experiment Station of the University of Illinois and extended in this paper to include the case of the slot jet issuing into a moving secondary. The single parameter upon which this correlation is based, the spreading coefficient, is shown to have an interesting interpretation in terms of the diffusion of a stream of fluid "particles" into uniformly flowing fields of homogeneous isotropic turbulence.

Introduction

THE diffusion of momentum from jets discharging into regions of the same fluid has been examined both theoretically and experimentally by many investigators over the past three decades. Principally, the past work has been concerned with the diffusion process occurring when jets discharge into stationary media. Only in recent years has the problem of jets issuing into moving secondaries been considered.

Forstall (1)[5] conducted an experimental investigation of the diffusion of material and momentum when a round jet issues into a moving secondary stream. However, no similar work with slot jets is known. Förthmann (3) has studied experimentally the diffusion of momentum from a slot jet issuing into a stationary secondary but a bibliography on jets compiled by Forstall (1) and a more recent one by v. Krzywoblocki (2) do not show any references to the problem of a slot jet issuing into a moving secondary.

This paper attempts to provide these data by presenting the results of an experimental impact-tube study of the turbulent, isothermal, incompressible mixing of two streams of the same fluid at different velocities when one stream issues from a slot.

No attempt was made in this work to study the nature of the turbulence inherent in this model of free-jet mixing. This remains as a task for the future, when it should fit in with studies now being made elsewhere in this country and abroad on the structure of turbulence in free boundary layers. In the meanwhile, as will be shown, the results of this two-dimensional jet mixing can be nicely correlated by phenomenological considerations.

The correlation theory employed is based upon certain assumptions suggested by the work of the Engineering Experiment Station of the University of Illinois (6, 7, 8) and leads to an expression for the velocity distributions which can be applied to stationary as well as moving secondaries. It is therefore used to correlate not only the present measurements but also the data of Förthmann (3) as further evaluated by Reichardt (4).

Comparisons made between the slot-jet and round-jet diffusion processes indicate a relationship between the two mixing phenomena. Finally, the diffusion processes occurring when jets discharge into stationary secondaries suggest an interesting interpretation of the spreading coefficient in terms of the diffusion of a stream of fluid particles into a region of homogeneous, isotropic turbulence.

Experimental Equipment and Measurements

A rectangular nozzle, $^1/_2$ in. $\times$ 12 in. in cross section, furnished a primary air stream which issued into a test section, or mixing chamber, $10^3/_4$ in. $\times$ 12 in. in cross section. The nozzle was located centrally in the test section and its 24:1 length-to-width ratio was sufficiently large to achieve the effect of two-dimensional flow. A centrifugal blower at the exit of the apparatus drew room air through the test section for a secondary stream. Another centrifugal blower with a plenum chamber ahead of the nozzle supplied the slot jet or primary air. Fig. 1 shows the general arrangement of the apparatus.

The pitot-static probe and its micrometer-screw traversing mechanism were both specially designed for this apparatus. The probe was 0.065-in-OD stainless steel with an impact hole 0.020 in. diam and four static holes of 0.010 in. diam. It could be positioned laterally (y-direction) to within $\pm$0.0005 in. and axially (x-direction) to within $\pm$0.005 in. For the range of velocities used, the error in static pressure was less than 0.005 of the velocity pressure and the pitot-static tube factor was considered unity. By means of an inclined-tube manometer, pressures could easily be read to within 0.005 in. of water.

The secondary stream was parallel to the primary stream to within $\pm$0.25 deg (determined by a claw-type directional probe) for the largest secondary velocity used and this error was even less with the lower secondary velocities.

The variation in the primary and secondary velocities in the z-direction, see Fig. 1, was found to be slight, no more than $^1/_2$ per cent for the primary and 1 per cent for the secondary, to within $^1/_2$ in. of the upper and lower boundaries of the test section. This uniformity indicates that the desired two-dimensionality of the flow was obtained.

The outer boundary of mixing was always far enough away from the side walls of the test section so that the appropriate model was a slot jet issuing into a moving secondary of infinite extent.

[1] The research underlying this paper was partially supported by the U. S. Air Force under Contract AF 18(600)-969, and was done in part by Alvin Weinstein in partial fulfillment of the requirements for the degree of Doctor of Philosophy at the Carnegie Institute of Technology.

[2] Assistant Professor, Department of Mechanical Engineering, Carnegie Institute of Technology. Assoc. Mem. ASME.

[3] Associate Professor, Department of Mechanical Engineering, Carnegie Institute of Technology. Assoc. Mem. ASME.

[4] Associate Professor, Department of Mechanical Engineering, Carnegie Institute of Technology. Mem. ASME.

[5] Numbers in parentheses refer to the Bibliography at the end of the paper.

Contributed by the Applied Mechanics Division and presented at the Diamond Jubilee Annual Meeting, Chicago, Ill., November 13–18, 1955, of The American Society of Mechanical Engineers.

Discussion of this paper should be addressed to the Secretary, ASME, 29 West 39th Street, New York, N. Y., and will be accepted until October 10, 1956, for publication at a later date. Discussion received after the closing date will be returned.

Note: Statements and opinions advanced in papers are to be understood as individual expressions of their authors and not those of the Society. Manuscript received by ASME Applied Mechanics Division, May 31, 1955. Paper No. 55—A-60.

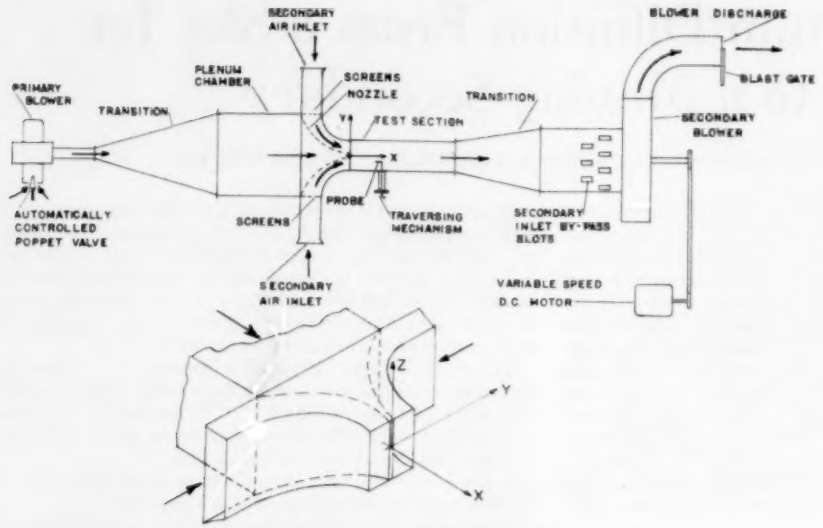

FIG. 1 PLAN VIEW OF TEST APPARATUS AND NOZZLE DETAIL

TABLE 1 CONDITIONS OF TESTS

Series	Primary velocity U_p, fps	Secondary velocity U_s, fps	$\lambda = \frac{U_s}{U_p}$	$e = \frac{U_p - U_s}{2U_s}$
I	140	70	0.50	0.50
II	120	80	0.67	0.25
III	120	40	0.33	1.00
IV	100	50	0.50	0.50

The velocities were kept low so that the air streams could be treated as incompressible. As shown in Table 1, four series were run, with the velocities chosen to provide three different velocity ratios.

The velocities of Series I and IV were chosen to show that the turbulent mixing is dependent on the velocity ratio and independent of the absolute velocities.

The primary blower, taking its supply from the room, slightly heated the air issuing from the slot, so that its density was on the average about 2.6 per cent less than the secondary stream. It was deemed unnecessary to go to the complication of a refrigerated primary air source since Corrsin (5) points out that the density of the primary stream in a circular jet can be as much as 23 per cent lower than the secondary before the total head profiles depart appreciably from the equal density case. However, the actual density is important in calculating local velocity. Exploratory temperature runs were made for each of the four series and proper corrections were introduced into the velocity calculations wherever the temperature effect on density was greater than 0.5 per cent.

Uncertainties in the measured quantities lead to an average uncertainty in the calculated velocity of ±0.5 per cent. Any error due to the effect of velocity fluctuations on the manometer reading is believed small and has been ignored.

THEORY OF CORRELATION

In order that the data obtained in the experimental portion of this report may be an effective contribution to the present knowledge of the jet-mixing problem, it is necessary to correlate the results.

The Engineering Experiment Station of the University of Illinois was quite successful in correlating the round-jet problem for both moving and stationary secondaries by use of the Reichardt hypothesis (6, 7, 8). A correlation for the slot-jet data was attempted along the same lines.

Use of the Reichardt hypothesis involves making certain assumptions about the mixing process and determining what restrictions these assumptions place on the mean velocity distribution. On this basis, the Engineering Experiment Station was able to correlate the round-jet problem in terms of a single parameter, called the spreading coefficient, which was evaluated from the experimental data. This paper presents a similar correlation for the slot-jet problem with a moving secondary.

The necessary assumptions concerning the mixing process are:

1 The diffusion of momentum from a point source into a region of the same fluid is described by the Gaussian probability function.

2 There are no external forces (pressure gradients, wall shear, etc.).

3 Momentum from individual point sources treated as infinitesimal area sources may be superimposed to give the momentum diffusion from a source of finite area.

For a stationary secondary, assumption 1 leads to

$$\overline{\rho U(x, r)^2} = K(x)e^{-\left(\frac{r}{b(x)}\right)^2} \quad \ldots\ldots\ldots\ldots [1]$$

for the velocity U at any point x, r in the fluid flow due to a point source of momentum flux. The quantity ρ is the fluid density. The factor K and the quantity b (called the spreading coefficient) are considered to be functions of x only. Equation [1] represents the momentum flux per unit area.

It is assumed that

$$\overline{\rho U^2} = \overline{\rho}\,\overline{U^2} = \rho\overline{U^2}$$

where the bar denotes time average.

By assumption 2, the momentum flux across all planes normal to the x-axis must be the same. The factor $K(x)$ in Equation [1] may be evaluated from this condition

$$\overline{\rho U_0^2}\Delta A = \int_0^\infty \rho\overline{U^2} 2\pi r\, dr \quad \ldots\ldots\ldots\ldots [2]$$

where $\overline{\rho U_0^2}$ is the momentum flux issuing from a jet source of area ΔA. Substituting Equation [1] into [2] leads to

$$K(x) = \frac{\overline{\rho U_0^2}\Delta A}{\pi[b(x)]^2} \quad \ldots\ldots\ldots\ldots [3]$$

Equation [1] now becomes

$$\frac{\overline{U^2}}{\overline{U_0^2}} = \frac{\Delta A}{\pi b^2} e^{-\left(\frac{r}{b}\right)^2} \quad \ldots\ldots\ldots\ldots [4]$$

Equation [4] represents the distribution of the axial component of momentum flux downstream from a point source issuing into a stationary secondary. To apply this result to a point source

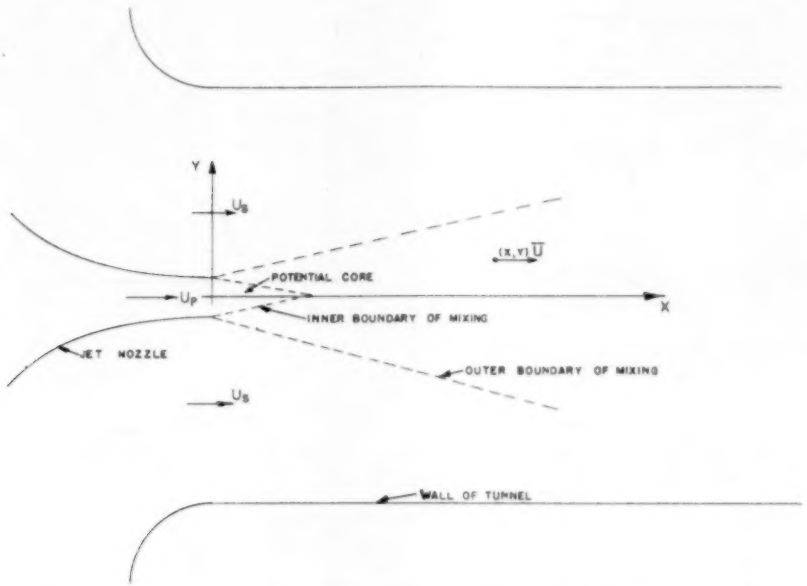

FIG. 2 MIXING REGION IN RELATION TO APPARATUS FOR SLOT JET ENTERING MOVING REGION OF SAME FLUID

issuing into a moving secondary, it is further assumed that the axial component of momentum flux at any point relative to the momentum flux of the secondary is conserved. Equation [4] then becomes, see Fig. 2

$$\frac{\overline{U^2} - \overline{U_s^2}}{\overline{U_p^2} - \overline{U_s^2}} = \frac{\Delta A}{\pi b^2}\, e^{-\left(\frac{r}{b}\right)^2} \quad \ldots\ldots\ldots\ldots [5]$$

where $\overline{U^2}$ is the axial component of momentum flux at any point; $\overline{U_p^2}$ is the discharge momentum flux from the point source; $\overline{U_s^2}$ is the momentum flux of the secondary stream.

On the basis of assumption 3, the plane of the slot is presumed to be composed of a number of sources of very small area. The total relative momentum-flux distribution from these sources comprising the slot on a normal plane downstream is given by the superposition of the relative momentum flux from each source. If the source areas become infinitesimal, the total relative momentum flux from the slot is given by, see Fig. 3

$$\frac{\overline{U^2} - \overline{U_s^2}}{\overline{U_p^2} - \overline{U_s^2}} = \frac{1}{\pi b^2} \int_{-a}^{a} \int_{-\infty}^{\infty} \exp\left[-\frac{(y-\eta)^2 + (z-\zeta)^2}{b^2}\right] d\eta d\zeta \quad \ldots\ldots [6]$$

assuming that $\overline{U_p}$ is constant over the entire plane of the slot exit, a is half the nozzle width D, and η, ζ are the co-ordinates of any point source of area $d\eta d\zeta$ in the plane of the slot. Equation [6] integrates to

$$\frac{\overline{U^2} - \overline{U_s^2}}{\overline{U_p^2} - \overline{U_s^2}} = \frac{1}{2}\left\{\operatorname{erf}\left[\frac{a}{b}\left(\frac{y}{a}+1\right)\right] - \operatorname{erf}\left[\frac{a}{b}\left(\frac{y}{a}-1\right)\right]\right\} \quad \ldots\ldots [7]$$

where $$\operatorname{erf}(t) \equiv \frac{2}{\sqrt{\pi}} \int_0^t e^{-t^2} dt$$

a well-tabulated function.

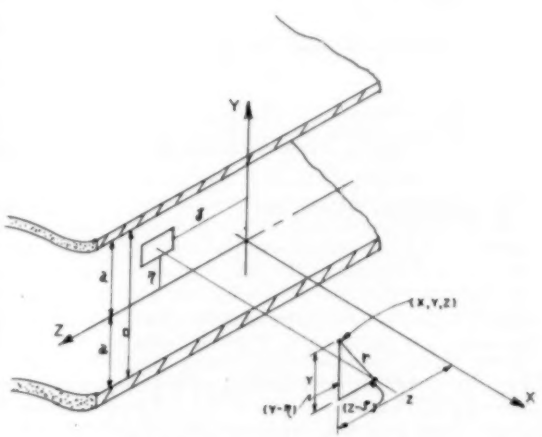

FIG. 3 AXES AND NOTATION FOR INFINITESIMAL AREA SOURCES IN PLANE OF SLOT DISCHARGE

If the velocity fluctuations are neglected, a simple algebraic manipulation leads to

$$\frac{\overline{U} - \overline{U_s}}{\overline{U_p} - \overline{U_s}} = \left\{\left(\frac{1}{2\epsilon}\right)^2 + \frac{1+\epsilon}{2\epsilon}\left[\operatorname{erf}\left\{\frac{a}{b}\left(\frac{y}{a}+1\right)\right\} - \operatorname{erf}\left\{\frac{a}{b}\left(\frac{y}{a}-1\right)\right\}\right]\right\}^{1/2} - \frac{1}{2\epsilon} \quad \ldots\ldots [8]$$

where

$$\epsilon = \frac{\overline{U_p} - \overline{U_s}}{2\overline{U_s}} = \frac{1}{2}\left(\frac{1}{\lambda} - 1\right)$$

a constant for any given initial velocity ratio.

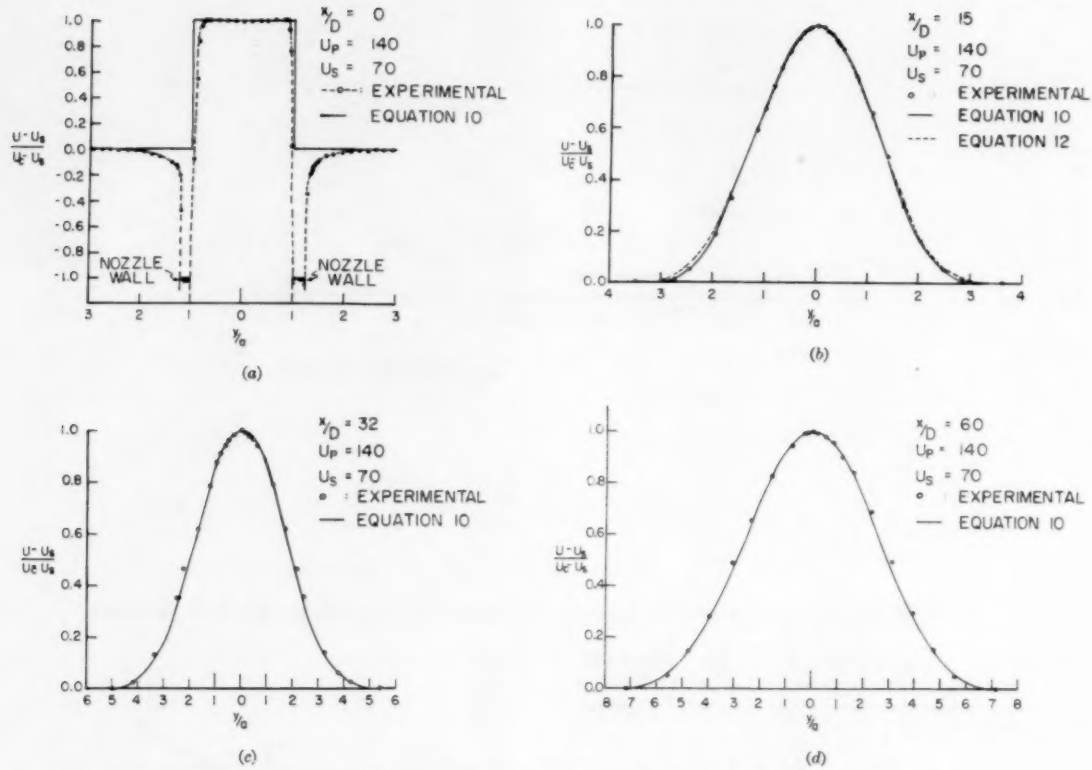

FIG. 4 MEASURED POINTS OF VELOCITY PROFILES FOR SERIES I COMPARED WITH PREDICTED CURVES

The characteristic velocity ratio

$$\frac{\overline{U} - \overline{U}_s}{\overline{U}_c - \overline{U}_s}$$

where $\overline{U}_c$ is the velocity at the jet center line ($y = 0$) is obtained by first setting $y = 0$ in Equation [8] which results in

$$\frac{U_c - U_s}{U_p - U_s} = \left\{\left(\frac{1}{2\epsilon}\right)^2 + \left(\frac{1+\epsilon}{\epsilon}\right)\operatorname{erf}\left(\frac{a}{b}\right)\right\}^{1/2} - \frac{1}{2\epsilon} \quad \ldots [9]$$

Here, and in what follows, the bars denoting time average are omitted for convenience.

Equation [9], the dimensionless expression for the center-line velocity decay, is divided into Equation [8] yielding

$$\frac{U - U_s}{U_c - U_s} = \frac{\left\{1 + 2\epsilon(1+\epsilon)\left[\operatorname{erf}\left\{\frac{a}{b}\left(\frac{y}{a}+1\right)\right\} - \operatorname{erf}\left\{\frac{a}{b}\left(\frac{y}{a}-1\right)\right\}\right]\right\}^{1/2} - 1}{\left[1 + 4\epsilon(1+\epsilon)\operatorname{erf}\left(\frac{a}{b}\right)\right]^{1/2} - 1} \quad \ldots [10]$$

Equations [9] and [10] are the desired phenomenological expressions for the center-line velocity decay and the transverse velocity profile in terms of the single unknown parameter b, the spreading coefficient.

Far downstream from the slot exit it may be expected that the velocity distributions obtained from the finite-width slot would be very nearly the same as the distributions obtained from a line source of the same strength.

If, in Equations [9] and [10], regions far downstream are considered where the ratio a/b is very small (in effect suggesting a line-source distribution for which the nozzle half-width a becomes infinitesimal), the following simplified expressions are obtained for the center-line velocity decay and transverse velocity profile, respectively

$$\frac{U_c - U_s}{U_p - U_s} = \left[\left(\frac{1}{2\epsilon}\right)^2 + \left(\frac{1+\epsilon}{\epsilon}\right)\frac{2}{\sqrt{\pi}}\left(\frac{a}{b}\right)\right]^{1/2} - \frac{1}{2\epsilon} \quad \ldots [11]$$

$$\frac{U - U_s}{U_c - U_s} = \frac{\left[1 + \frac{8\epsilon(1+\epsilon)}{\sqrt{\pi}}\left(\frac{a}{b}\right)e^{-\left(\frac{y}{a}\frac{a}{b}\right)^2}\right]^{1/2} - 1}{\left[1 + \frac{8\epsilon(1+\epsilon)}{\sqrt{\pi}}\left(\frac{a}{b}\right)\right]^{1/2} - 1} \quad \ldots [12]$$

Equations [11] and [12] may also be derived directly, of course, by assuming that beyond the core region the velocity profiles are effectively those occurring when the primary stream issues from a line source rather than a slot.

CORRELATION OF EXPERIMENTAL RESULTS

In order to employ Equation [10] for predicting the transverse velocity profile beyond the core region for some given value of the

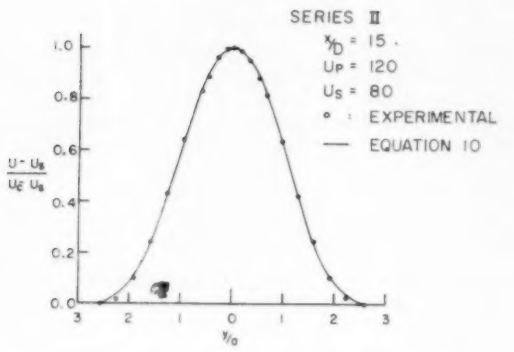

FIG. 5 MEASURED POINTS OF VELOCITY PROFILES AT $x/D = 15$ FOR SERIES II, III, AND IV COMPARED WITH PREDICTED CURVES

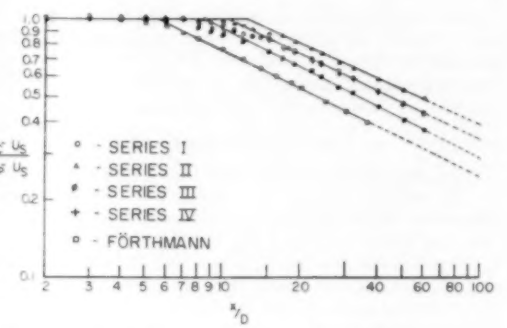

FIG. 6 CENTER-LINE VELOCITY DECAY FOR ALL SERIES, INCLUDING STATIONARY SECONDARY

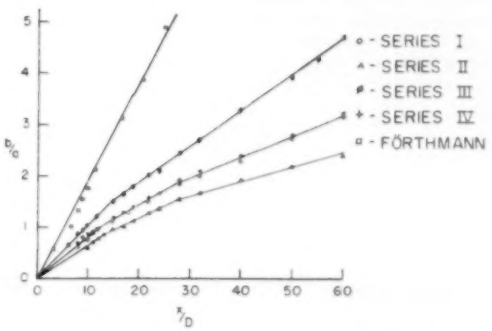

FIG. 7 VARIATION OF SPREADING COEFFICIENT WITH AXIAL DISTANCE FOR ALL SERIES, INCLUDING STATIONARY SECONDARY

initial velocity ratio, the spreading coefficient b must be known for any desired transverse plane. For a particular velocity ratio, b as a function of x must be determined experimentally. The method employed here was to use the experimentally found center-line velocity to determine the spreading coefficient b by means of Equation [9]. With b thus determined Equation [10] was plotted and the measured data compared with it. These results are shown in Fig. 4 for Series I, the solid line in each representing Equation [10]. In general, the agreement is quite good. The results for Series II, III, and IV at an x/D of 15 are shown in Fig. 5.

The dotted line in Fig. 4(b) is the profile predicted by a Gaussian distribution from a line source as given by Equation [12]. Up to approximately 30 slot widths, the profiles given by the more exact analysis, Equation [10], are a better fit for the observed data than those given by Equation [12]. Beyond 30 slot widths, however, the simpler analysis yields profiles almost identical with the more exact theory which takes into account the finite slot width.

Fig. 6 shows experimentally determined values for the center-line velocities from the four series of this investigation and from Förthmann's data for a stationary secondary. Straight lines through the data on this logarithmic plot have nearly equal slopes, with Förthmann's measurements fitting in nicely as the limiting case of zero velocity ratio. Fig. 6 also shows that the results of Series I and IV, with the same velocity ratio but differing absolute velocities, are almost identical.

Reichardt (4) has indicated that for the slot jet issuing into a stationary secondary the velocity on the center line beyond the core region should vary inversely as the square root of the axial distance. The best fit to the data of Fig. 6 for both moving and stationary secondary is given by

$$\frac{U_c - U_s}{U_p - U_s} = \left(\frac{L}{x/D}\right)^{0.49} \quad \ldots\ldots\ldots\ldots [13]$$

where

$$L = 5.5 + 10\lambda = 5.5 + \frac{10}{2\epsilon + 1} \quad \ldots\ldots\ldots [14]$$

which differs from Reichardt's prediction by less than the experimental uncertainty.

Equations [9] and [10] have also been utilized for the correlation of Förthmann's data for a slot jet issuing into a stationary secondary by setting $U_s = 0$ and $1/\epsilon = 0$. The transverse profiles predicted by Equation [10] for this limiting case agree quite well with the data presented by Förthmann.

The Spreading Coefficient

Fig. 7 shows the spreading coefficient as determined from Equation [9] using the data of this investigation. The spreading coefficient for the slot jet issuing into a stationary secondary as determined from Förthmann's data using Equation [9] with $U_s = 0$, $1/\epsilon = 0$ is also presented. In this plot of spreading coefficient against axial distance, the data for any given velocity ratio are well fitted (as far as 60 slot widths downstream) by successive straight-line segments.

Since the center-line velocities beyond the core region vary inversely very nearly as the square root of the dimensionless axial distance, an attempt was made to obtain, from Equation [11], a simple analytical expression for the variation of the spreading coefficient far downstream.

From Equation [11], for the slot jet issuing into a stationary secondary ($U_s = 0$, $1/\epsilon = 0$)

$$\frac{U_c}{U_p} = \left[\frac{2}{\sqrt{\pi}}\,\frac{a}{b}\right]^{1/2} \qquad [15]$$

also

$$\frac{U_c}{U_p} \approx \left(\frac{L}{x/D}\right)^{1/2} \qquad [16]$$

Substituting Equation [16] into [15], squaring and solving for b/a

$$\frac{b}{a} \approx \left[\frac{2}{L\sqrt{\pi}}\right]\frac{x}{D} \qquad [17]$$

Equation [17] indicates the linear variation of the spreading coefficient with axial distance.

Substituting $L = 5.5$ from Equation [14]

$$\frac{b}{a} = 0.205\,\frac{x}{D} \qquad [18]$$

The coefficient of x/D given by the approximate relationship, Equation [18], compares quite well with the value 0.190 obtained by Reichardt (4) in another manner. For the region of Förthmann's data $x/D \leq 25$ the slope 0.190 is a better fit for the calculated values of b/a.

For the moving secondary, it is not possible to reduce Equation [11] to a simpler form for the range of experimental data presented in this report.

For the region

$$2 + 39\lambda \leq \frac{x}{D} \leq 60$$

the graphical results of Fig. 7 may be generalized somewhat. If the abscissa intercepts and the slopes of the lines in this region, including the results obtained from Förthmann, are each plotted versus $\lambda = U_s/U_p$, the curves shown in Fig. 8 are determined. From these curves, the variation of the spreading coefficient with axial distance may be found for values of $\lambda \leq 5/6$ by inserting the proper values of slope r and intercepting R into the equation

$$\frac{b}{a} = r\left(\frac{x}{D} + R\right) \qquad [19]$$

For $\lambda = 1$, the condition, for which theoretically no mixing occurs, the spreading coefficient b, must be infinite for all values of x/D. In Fig. 8 the slope curve (r versus λ) is zero at this point and the intercept R approaches infinity as λ approaches unity.

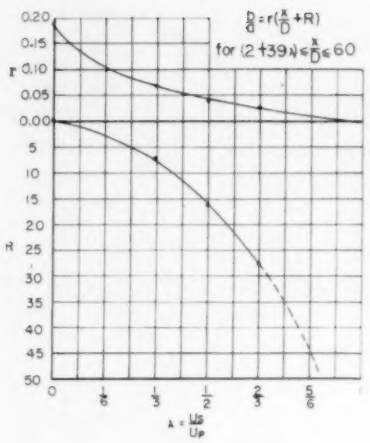

Fig. 8 Correlation for Spreading Coefficient

Interpretation of Spreading Coefficient

It has already been pointed out from the data of this experiment and the data of Förthmann, see Fig. 6, that the center-line velocity for the slot jet varies very nearly as the square root of the axial distance beyond the core region. It has also been shown, see Equation [17], that for the Gaussian diffusion this variation implies a linear relationship between the spreading coefficient and axial distance.

Baron and Alexander (6, 7) and Forstall (1) have observed that for the round jet the center-line velocity varies inversely as the axial distance beyond the core region. It can easily be shown that for Gaussian diffusion from a round jet this variation also implies a linear relationship between the spreading coefficient and axial distance.

Frenkiel (10), in analytically treating Gaussian diffusion of fluid particles from point and line sources into fields of homogeneous isotropic turbulence, also predicted a linear relationship between the term analogous to the spreading coefficient and axial distance, for axial distances comparable to those examined in the various experiments. Thus it would appear that jet diffusion is characterized by this linearity. Frenkiel was able further to express the predicted linearity constant in terms of properties of the turbulence as follows

$$c = \frac{\sqrt{2}\,T}{UL_h}$$

where T is the intensity of turbulence, L_h is the Lagrangian scale of turbulence, and U is the mean velocity of the flow into which the particles are emitted. These quantities are constants for the chosen diffusion model.

Therefore the spreading coefficient is given by

$$b = \frac{\sqrt{2}\,T}{UL_h}\,x \qquad [20]$$

Equation [20] can be interpreted as indicating the dependence of the spreading coefficient on certain mean properties of the turbulent characteristics of the flow.

Conclusions

1 The phenomenological expression for the transverse velocity profile, Equation [10], based upon a finite-area slot was shown to be in excellent agreement with the experimental data. This agreement between predicted and experimental results justifies the single-parameter (spreading-coefficient) representation of the mixing process.

2 The spreading coefficient was observed to be well represented by a series of straight-line segments up to 60 slot widths, and may be readily correlated as a function of the initial velocity ratio in this range.

3 The expression for the transverse velocity profile may be applied to the slot jet issuing into a stationary secondary as a limiting case of the slot jet issuing into a moving secondary.

4 The spreading coefficients for round and slot jets indicate a linear dependence on axial distances analogous to that obtained when a particle stream issues from point or line sources into fields of homogeneous isotropic turbulence. For the latter, the proportionality constant is a function of the turbulent intensity, the Lagrangian scale of turbulence, and the velocity of the flow field.

BIBLIOGRAPHY

1 "Material and Momentum Transfer in Coaxial Gas Streams," by W. Forstall, Jr., ScD thesis, Massachusetts Institute of Technology, Cambridge, Mass., 1949.

2 "Jets," by M. Z. v. Krzywoblocki, U. S. Naval Ordnance Test Station TM No. 1576, 1953.

3 "Über Turbulente Strahlausbreitung," by E. Förthmann, *Ingenieur Archiv*, vol. 5, 1934, p. 42.

4 "Gesetzmassigkeiten der Freien Turbulenz," by H. Reichardt, VDI-Forschungsheft, series B, vol. 13, May-June, 1942, p. 414.

5 "Further Experiments on the Flow and Heat Transfer in a Heated Turbulent Air Jet," by S. Corrsin and M. S. Uberoi, NACA TN 1865.

6 "Transport of Momentum, Mass and Heat in Turbulent Jets," by L. G. Alexander, T. Baron, and E. W. Comings, University of Illinois Engineering Experiment Station, Bulletin Series No. 413.

7 "An Ad Hoc Theory of Free Turbulent Jets," by L. G. Alexander, University of Illinois Engineering Experiment Station Technical Report No. 13, August 5, 1952.

8 "Application of the Reichardt Hypothesis to the Transport of Momentum and Mass in Coaxial Jets," by A. Kivnick and H. F. Johnstone, University of Illinois Engineering Experiment Station, Technical Report CML-2, June 15, 1952.

9 "Investigations of Free Turbulent Mixing," by H. W. Liepmann and J. Laufer, NACA TN 1257, August, 1947.

10 "Turbulent Diffusion: Mean Concentration Distribution in a Flow Field of Homogeneous Turbulence," by F. N. Frenkiel, "Advances in Applied Mechanics," vol. 3, 1953, p. 62, Academic Press, Inc., New York, N. Y.

11 "Fluid Dynamics of Jets," by S. I. Pai, D. Van Nostrand Company, Inc., New York, N. Y., 1954.

Studies on Plastic Flow of Anisotropic Metals

By L. W. HU,[1] UNIVERSITY PARK, PA.

This investigation deals with a study of the plastic behavior of anisotropic metals. By extending Hill's theory of plastic flow of anisotropic metals, plastic stress-strain relations for anisotropic materials with strain hardening are developed. Applications of these relations are also made to plane-stress and plane-strain problems with anisotropy. The effect of anisotropy on the stress distribution and on the pressure to produce yielding in a thick-walled cylinder under internal pressure is discussed. The influence of anisotropy on the interpretation of conventional biaxial tension-tension and tension-torsion tests is also considered in this study.

Introduction

By assuming that a material is isotropic, various theories of plasticity have been proposed and many problems on stress-strain determination in plastically deformed bodies have been investigated for both ideally plastic and strain-hardening materials (1, 2, 3, 4).[2] However, it is a well-known fact that engineering materials are anisotropic to various degrees. Some of them, such as sheet metals, fabricated forms, do manifest predominant directional properties. In studying the plastic flow of such materials, it is necessary to consider the effect of anisotropy. The significance of the effect of anisotropy on the plastic behavior of materials has been emphasized in recent years. Since 1939, when Reuss (5) first considered the formulation of anisotropic loading functions, considerable attention has been given to the study of the plastic flow of anisotropic bodies. In 1948 a theory of plastic flow of an initially anisotropic metal was suggested by Hill (6). At the same time, similar stress-strain relations for anisotropic materials with strain hardening were proposed by Jackson, Smith, and Lankford (7), Dorn (8), Prager (5), and Fisher (9). Relatively little work has been done in the field of plasticity utilizing the plastic stress-strain relations for anisotropic bodies. Hill has studied several problems in plastic torsion of anisotropic bodies (1, 6, 10); the plastic flow of a thick-walled cylinder under internal pressure with a certain degree of anisotropy has been investigated by Fisher (9); the theory of slip-line fields for anisotropic metals has been presented by Hill (11); the effect of anisotropy of metals on the "earing" of deep-drawn cups has been solved by Bourne and Hill (12); and the necking of an anisotropic tension specimen has been investigated by Hill (6, 13).

Using the experimental facts available, an extension of Hill's theory of plastic flow of anisotropic metals will be given in this paper. Such an extended theory will be shown to be applicable to the analysis of plastic flow of anisotropic bodies with strain hardening. The effects of anisotropy on various problems will also be discussed.

Fundamental Equations

The assumption will be made that the principal axes of anisotropy form an orthogonal set, which may or may not bear any relationship to the geometrical configuration of the anisotropic body considered. If the physical properties of materials are considered, this assumption can be justified. For instance, the state of anisotropy in a laminated plastic tube can be properly described only by a system of cylindrical co-ordinates; the directional properties of sheet metals can be described by a system of Cartesian co-ordinates. Depending upon the mode of stressing, the directions of the principal axes of anisotropy may, or may not, remain unchanged. However, the plastic stress-strain relations referred to the principal axes of anisotropy are assumed not to be affected by the change of the directions of the principal axes.

Defining the plastic potential or the effective stress $\bar{\sigma}$ in a similar manner as in the theory of plasticity for isotropic materials (1)

$$f = \bar{\sigma}^2 = [\alpha_{12}(\sigma_{11} - \sigma_{22})^2 + \alpha_{23}(\sigma_{22} - \sigma_{33})^2 + \alpha_{31}(\sigma_{33} - \sigma_{11})^2 + 3\alpha_{44}\tau_{12}^2 + 3\alpha_{55}\tau_{23}^2 + 3\alpha_{66}\tau_{31}^2] \quad [1]$$

where the σ's are stress components, α's are parameters of anisotropy which may be functions of the state of stress and plastic deformation, and the subscripts 1, 2, 3 refer to the directions of the three principal axes of anisotropy. By analogy with the Levy-Mises plastic stress-strain relations for isotropic materials, the plastic stress-strain relations for anisotropic materials are then

$$\left.\begin{aligned} d\epsilon_{11} &= [\alpha_{11}\sigma_{11} - \alpha_{12}\sigma_{22} - \alpha_{31}\sigma_{33}]d\lambda \\ d\epsilon_{22} &= [\alpha_{22}\sigma_{22} - \alpha_{23}\sigma_{33} - \alpha_{12}\sigma_{11}]d\lambda \\ d\epsilon_{33} &= [\alpha_{33}\sigma_{33} - \alpha_{31}\sigma_{11} - \alpha_{23}\sigma_{22}]d\lambda \\ d\epsilon_{12} &= \frac{1}{2}\,d\gamma_{12} = \frac{3}{2}\,\alpha_{44}\tau_{12}d\lambda \\ d\epsilon_{23} &= \frac{1}{2}\,d\gamma_{23} = \frac{3}{2}\,\alpha_{55}\tau_{23}d\lambda \\ d\epsilon_{31} &= \frac{1}{2}\,d\gamma_{31} = \frac{3}{2}\,\alpha_{66}\tau_{31}d\lambda \end{aligned}\right\} \quad \ldots\ldots [2]$$

where the $d\epsilon$'s are plastic strain-increment components, and

$$\left.\begin{aligned} \alpha_{11} &= \alpha_{12} + \alpha_{31} \\ \alpha_{22} &= \alpha_{23} + \alpha_{12} \\ \alpha_{33} &= \alpha_{31} + \alpha_{23} \end{aligned}\right\} \quad \ldots\ldots [3]$$

In this paper, the α's will be considered as constant during plastic deformation. This can be justified by the experimental results obtained by Hazlett, Robinson, and Dorn (14). In their investigation on the plastic flow of anisotropic sheet metals, both the ratio of axial plastic strain to lateral plastic strain and the

[1] Associate Professor of Engineering Mechanics, Department of Engineering Mechanics, The Pennsylvania State University.

[2] Numbers in parentheses refer to the Bibliography at the end of the paper.

Contributed by the Applied Mechanics Division and presented at the Diamond Jubilee Annual Meeting, Chicago, Ill., November 13–18, 1955, of The American Society of Mechanical Engineers.

Discussion of this paper should be addressed to the Secretary, ASME, 29 West 39th Street, New York, N. Y., and will be accepted until October 10, 1956, for publication at a later date. Discussion received after the closing date will be returned.

Note: Statements and opinions advanced in papers are to be understood as individual expressions of their authors and not those of the Society. Manuscript received by ASME Applied Mechanics Division, November 8, 1954. Paper No. 55—A-79.

ratio of axial plastic strain to plastic shear strain are found to remain constant during the simple tension tests of steel, aluminum alloys, and magnesium alloys. In other words, the anisotropy factors α's can be considered as constant and can be directly determined by means of simple stress tests.

For perfectly plastic materials, the effective stress $\bar{\sigma}$ will have a value equal to K when materials are deformed plastically. From Equation [1], the anisotropy factors α's can be found by alternatively letting all stress components be equal to zero except one

$$\left.\begin{aligned} \alpha_{11} &= \alpha_{12} + \alpha_{31} = (K/Y_{11})^2 \\ \alpha_{22} &= \alpha_{23} + \alpha_{12} = (K/Y_{22})^2 \\ \alpha_{33} &= \alpha_{31} + \alpha_{23} = (K/Y_{33})^2 \\ \alpha_{44} &= \frac{1}{3}\,(K/Y_{12})^2 \\ \alpha_{55} &= \frac{1}{3}\,(K/Y_{23})^2 \\ \alpha_{66} &= \frac{1}{3}\,(K/Y_{31})^2 \end{aligned}\right\} \quad \ldots\ldots\ldots\ldots [4]$$

It was in this manner that the characteristic parameters of anisotropy were defined in Hill's theory of plastic flow for anisotropic bodies (1).

For a body deformed plastically, the increment of plastic work per unit volume is

$$dW = \sigma_{11}d\epsilon_{11} + \sigma_{22}d\epsilon_{22} + \sigma_{33}d\epsilon_{33} + 2\tau_{12}d\epsilon_{12} + 2\tau_{23}d\epsilon_{23} + 2\tau_{31}d\epsilon_{31} \ldots [5]$$

Substituting the values of strain increments from Equations [2] into [5], and using Equations [1] and [3]

$$dW = (\bar{\sigma})^2 d\lambda \ldots\ldots\ldots\ldots\ldots\ldots [6]$$

By means of Equations [2] and [3], it can be shown that

$$\frac{\alpha_{23}d\epsilon_{11} - \alpha_{31}d\epsilon_{22}}{G(\sigma_{11} - \sigma_{22})} = \frac{\alpha_{31}d\epsilon_{22} - \alpha_{12}d\epsilon_{33}}{G(\sigma_{22} - \sigma_{33})} = \frac{\alpha_{12}d\epsilon_{33} - \alpha_{23}d\epsilon_{11}}{G(\sigma_{33} - \sigma_{11})}$$

$$= \frac{2d\epsilon_{12}}{3\alpha_{44}\tau_{12}} = \frac{2d\epsilon_{23}}{3\alpha_{55}\tau_{23}} = \frac{2d\epsilon_{31}}{3\alpha_{66}\tau_{31}} = d\lambda \ldots\ldots [7]$$

where $G = \alpha_{12}\alpha_{23} + \alpha_{23}\alpha_{31} + \alpha_{31}\alpha_{12}$

Substituting the values of stresses from Equations [7] into Equation [1]

$$\frac{\alpha_{12}}{G^2}\,[\alpha_{23}d\epsilon_{11} - \alpha_{31}d\epsilon_{22}]^2 + \frac{\alpha_{23}}{G^2}\,[\alpha_{31}d\epsilon_{22} - \alpha_{12}d\epsilon_{33}]^2 + \frac{\alpha_{31}}{G^2}\,[\alpha_{12}d\epsilon_{33} - \alpha_{23}d\epsilon_{11}]^2 + 3\alpha_{44}\left[\frac{2d\epsilon_{12}}{3\alpha_{44}}\right]^2 + 3\alpha_{55}\left[\frac{2d\epsilon_{23}}{3\alpha_{55}}\right]^2 + 3\alpha_{66}\left[\frac{2d\epsilon_{31}}{3\alpha_{66}}\right]^2 = [\bar{\sigma}d\lambda]^2 \ldots\ldots [8]$$

Defining the increment of effective strain $d\bar{\epsilon}$ as

$$(d\bar{\epsilon})^2 = \frac{1}{G^2}\,[\alpha_{12}(\alpha_{23}d\epsilon_{11} - \alpha_{31}d\epsilon_{22})^2 + \alpha_{23}(\alpha_{31}d\epsilon_{22} - \alpha_{12}d\epsilon_{33})^2 + \alpha_{31}(\alpha_{12}d\epsilon_{33} - \alpha_{23}d\epsilon_{11})^2] + \frac{4}{3}\left[\frac{(d\epsilon_{12})^2}{\alpha_{44}} + \frac{(d\epsilon_{23})^2}{\alpha_{55}} + \frac{(d\epsilon_{31})^2}{\alpha_{66}}\right] \ldots\ldots [9]$$

Therefore the quantity $d\lambda$ is found from Equations [8] and [9] to be

$$d\lambda = \frac{d\bar{\epsilon}}{\bar{\sigma}} \ldots\ldots\ldots\ldots\ldots\ldots [10]$$

Substituting the value of $d\lambda$ from Equation [10] into Equation [6], the increment of unit plastic work is

$$dW = \bar{\sigma}d\bar{\epsilon} \ldots\ldots\ldots\ldots\ldots\ldots [11]$$

Therefore, if there is a functional relation that exists between the plastic work and the effective stress, there must be a functional relation between the effective stress and the effective strain $\int d\bar{\epsilon}$ as pointed out by Hill (1).

Placing the value of $d\lambda$ from Equation [10] into Equations [2], the stress-strain-increment relations for plastic flow of anisotropis bodies become

$$\left.\begin{aligned} d\epsilon_{11} &= [\alpha_{11}\sigma_{11} - \alpha_{12}\sigma_{22} - \alpha_{31}\sigma_{33}]\,\frac{d\bar{\epsilon}}{\bar{\sigma}}, & d\epsilon_{12} &= \frac{3}{2}\,\alpha_{44}\tau_{12}\,\frac{d\bar{\epsilon}}{\bar{\sigma}} \\ d\epsilon_{22} &= [\alpha_{22}\sigma_{22} - \alpha_{23}\sigma_{33} - \alpha_{12}\sigma_{11}]\,\frac{d\bar{\epsilon}}{\bar{\sigma}}, & d\epsilon_{23} &= \frac{3}{2}\,\alpha_{55}\tau_{23}\,\frac{d\bar{\epsilon}}{\bar{\sigma}} \\ d\epsilon_{33} &= [\alpha_{33}\sigma_{33} - \alpha_{31}\sigma_{11} - \alpha_{23}\sigma_{22}]\,\frac{d\bar{\epsilon}}{\bar{\sigma}}, & d\epsilon_{31} &= \frac{3}{2}\,\alpha_{66}\tau_{31}\,\frac{d\bar{\epsilon}}{\bar{\sigma}} \end{aligned}\right\} \ldots [12]$$

Combining Equations [12] with Equations [1], [3], and [9] a system of fundamental equations for determining the plastic stress-strain distributions in anisotropic bodies is obtained.

If the effective strain $\int d\bar{\epsilon}$ can be assumed to be a function of the effective stress $\bar{\sigma}$ only, the relation between the effective strain $\int d\bar{\epsilon}$ and the effective stress $\bar{\sigma}$ can be determined from a simple tension test in which the axis of loading coincides with one of the principal axes of anisotropy of the specimen. Consider that a simple tension test is conducted by loading the specimen along the axis of anisotropy 1-1, and that the plastic stress-strain relation is found to be

$$\epsilon_{11} = k\sigma_{11}^n \ldots\ldots\ldots\ldots\ldots\ldots [13]$$

where k and n are material constants. Substituting the value of ϵ_{11} from Equation [13] into Equations [12]

$$d\epsilon_{11} = kn\sigma_{11}^{n-1}d\sigma_{11} = \alpha_{11}\sigma_{11}\,\frac{d\bar{\epsilon}}{\bar{\sigma}} \ldots\ldots [14]$$

But from Equation [1], the effective stress $\bar{\sigma}$ for simple tension is

$$\bar{\sigma} = \sqrt{\alpha_{11}}\,\sigma_{11} \ldots\ldots\ldots\ldots\ldots\ldots [15]$$

Placing the value of σ_{11} from Equation [15] into Equation [14] and integrating

$$\sqrt{\alpha_{11}}\,\bar{\epsilon} = k\left(\frac{\bar{\sigma}}{\sqrt{\alpha_{11}}}\right)^n \ldots\ldots\ldots\ldots [16]$$

By assuming $\alpha_{11} = 1.0$, the effective stress strain relation becomes

$$\bar{\epsilon} = k\bar{\sigma}^n \ldots\ldots\ldots\ldots\ldots\ldots [17]$$

Placing the value of $\bar{\epsilon}$ from Equation [17] into Equation [12] and taking $\alpha_{11} = 1.0$

$$\left.\begin{aligned} d\epsilon_{11} &= kn[\sigma_{11} - \alpha_{12}\sigma_{22} - \alpha_{31}\sigma_{33}]\bar{\sigma}^{n-2}d\bar{\sigma} \\ d\epsilon_{22} &= kn[\alpha_{22}\sigma_{22} - \alpha_{23}\sigma_{33} - \alpha_{12}\sigma_{11}]\bar{\sigma}^{n-2}d\bar{\sigma} \\ d\epsilon_{33} &= kn[\alpha_{33}\sigma_{33} - \alpha_{31}\sigma_{11} - \alpha_{23}\sigma_{22}]\bar{\sigma}^{n-2}d\bar{\sigma} \\ d\epsilon_{12} &= \frac{1}{2}\,d\gamma_{12} = \frac{3}{2}\,kn\,[\alpha_{44}\tau_{12}]\bar{\sigma}^{n-2}d\bar{\sigma} \\ d\epsilon_{23} &= \frac{1}{2}\,d\gamma_{23} = \frac{3}{2}\,kn[\alpha_{55}\tau_{23}]\bar{\sigma}^{n-2}d\bar{\sigma} \\ d\epsilon_{31} &= \frac{1}{2}\,d\gamma_{31} = \frac{3}{2}\,kn[\alpha_{66}\tau_{31}]\bar{\sigma}^{n-2}d\bar{\sigma} \end{aligned}\right\} \quad \ldots [18]$$

The plastic stress-strain-increment relation for an anisotropic body with strain hardening can now be determined by Equations [18]. In using Equations [18] the material constants k and n in simple tension for direction 1-1 are employed.

For isotropic materials $\alpha_{11} = \alpha_{22} = \alpha_{33} = \alpha_{44} = \alpha_{55} = \alpha_{66} = 1$ and $\alpha_{12} = \alpha_{23} = \alpha_{31} = 1/2$, the flow rule Equations [7] will reduce to the well-known rule of plastic flow

$$\frac{d\epsilon_{11} - d\epsilon_{22}}{\sigma_{11} - \sigma_{22}} = \frac{d\epsilon_{22} - d\epsilon_{33}}{\sigma_{22} - \sigma_{33}} = \frac{d\epsilon_{33} - d\epsilon_{11}}{\sigma_{33} - \sigma_{11}} \quad \ldots [19]$$

From Equation [19] the Lode's variables for isotropic materials can be obtained

$$\left.\begin{aligned} \mu &= \frac{2\sigma_{22} - (\sigma_{33} + \sigma_{11})}{\sigma_{33} - \sigma_{11}} \\ \nu &= \frac{2d\epsilon_{22} - (d\epsilon_{33} + d\epsilon_{11})}{d\epsilon_{33} - d\epsilon_{11}} \end{aligned}\right\} \quad \ldots [20]$$

and

$$\mu = \nu \quad \ldots [21]$$

The validity of the μ-ν relationship, Equation [21], has been studied experimentally and is considered as a means to check various theories of plasticity. However, no good agreement has been found between the experimental results and theoretical prediction (1, 2).

If the anisotropy of materials is considered, a new variable ν^* should be defined by using the flow rule Equation [7]

$$\nu^* = \frac{2\alpha_{23}d\epsilon_{22} - (\alpha_{22}d\epsilon_{11} + \alpha_{12}d\epsilon_{33})}{\alpha_{12}d\epsilon_{33} - \alpha_{23}d\epsilon_{11}} \quad \ldots [22]$$

For materials which can be dealt with by the plastic stress-strain relations for anisotropic bodies given in this paper, it can be shown that

$$\mu = \nu^* \quad \ldots [23]$$

In other words, the μ-ν^* relationship can be employed as a means to check the validity of the plastic stress-strain-increment relations for anisotropic metals given in this paper.

Plane-Strain Problems

In plane-strain problems, consider one of the principal axes of anisotropy normal to the planes of plastic flow which remain plane during deformation. Then

$$d\epsilon_{33} = 0 \quad \ldots [24]$$

From Equations [12] and [24], the normal stress σ_{33} becomes

$$\sigma_{33} = \frac{\alpha_{23}\sigma_{22} + \alpha_{31}\sigma_{11}}{\alpha_{33}} \quad \ldots [25]$$

Equation [25] was first derived by Hill (11) in his theory of plane strain for anisotropic metals. Assuming ideally plastic materials, he gave a detailed discussion on the slip-line field in plane-strain problems.

Substituting the value of σ_{33} from Equation [25] into Equation [1] and considering $\tau_{23} = \tau_{31} = 0$, the effective stress $\bar{\sigma}$ is found to be

$$\bar{\sigma} = \sqrt{\frac{G}{\alpha_{33}}\,[\sigma_{11} - \sigma_{22}]^2 + 3\alpha_{44}\tau_{12}^2} \quad \ldots [26]$$

Similarly, the stress-strain-increment relations are obtained from Equation [12] or

$$\left.\begin{aligned} d\epsilon_{11} &= \frac{G}{\alpha_{33}}\,(\sigma_{11} - \sigma_{22})\,\frac{d\bar{\epsilon}}{\bar{\sigma}} \\ d\epsilon_{22} &= \frac{G}{\alpha_{33}}\,(\sigma_{22} - \sigma_{11})\,\frac{d\bar{\epsilon}}{\bar{\sigma}} \\ d\epsilon_{12} &= \frac{1}{2}\,d\gamma_{12} = \frac{3}{2}\,\alpha_{44}\tau_{12}\,\frac{d\bar{\epsilon}}{\bar{\sigma}} \end{aligned}\right\} \quad \ldots [27]$$

where G is equal to $\alpha_{12}\alpha_{23} + \alpha_{22}\alpha_{31} + \alpha_{31}\alpha_{12}$. An examination of Equations [26] and [27] shows that both the effective stress and the stress-strain-increment relations for plane-strain problems are quite similar to those for isotropic materials, but Equation [25] shows that the stress distribution in the direction normal to the plane of plastic flow is characteristically different.

To illustrate the effect of anisotropy on plastic flow in a state of plane strain, the stress distribution in a thick-walled cylinder of ideally plastic material will be discussed.

Consider a long cylinder of outside diameter b and inside diameter a subjected to an internal pressure p. In cylindrical co-ordinates, the equation of equilibrium is

$$r\,\frac{d\sigma_r}{dr} = \sigma_t - \sigma_r \quad \ldots [28]$$

The well-known solution for the plastic flow of a thick-walled cylinder of an ideally plastic isotropic material was obtained by Nadai (2) as

$$\left.\begin{aligned} \sigma_r &= -\frac{2Y}{\sqrt{3}}\ln\left[\frac{b}{r}\right] \\ \sigma_t &= \frac{2Y}{\sqrt{3}}\left[1 - \ln\left(\frac{b}{r}\right)\right] \\ \sigma_z &= \frac{2Y}{\sqrt{3}}\left[\frac{1}{2} - \ln\left(\frac{b}{r}\right)\right] \end{aligned}\right\} \quad \ldots [29]$$

where Y is the yield stress in simple tension. In obtaining Equations [29], the assumption was made that there was no initial deformation. The pressure p under which the cylinder yields is found to be

$$p = \frac{2Y}{\sqrt{3}}\ln\left(\frac{b}{a}\right) \quad \ldots [30]$$

Now, in contrast, consider a thick-walled cylinder of anisotropic material. It must be assumed that the principal axes of anisotropy form an orthogonal set which coincide with the cylindrical co-ordinates of the cylinder and that the material of the cylinder is ideally plastic with yield stresses in the axial, tangential, and radial directions of Y_a, Y_t, and Y_r, respectively. By

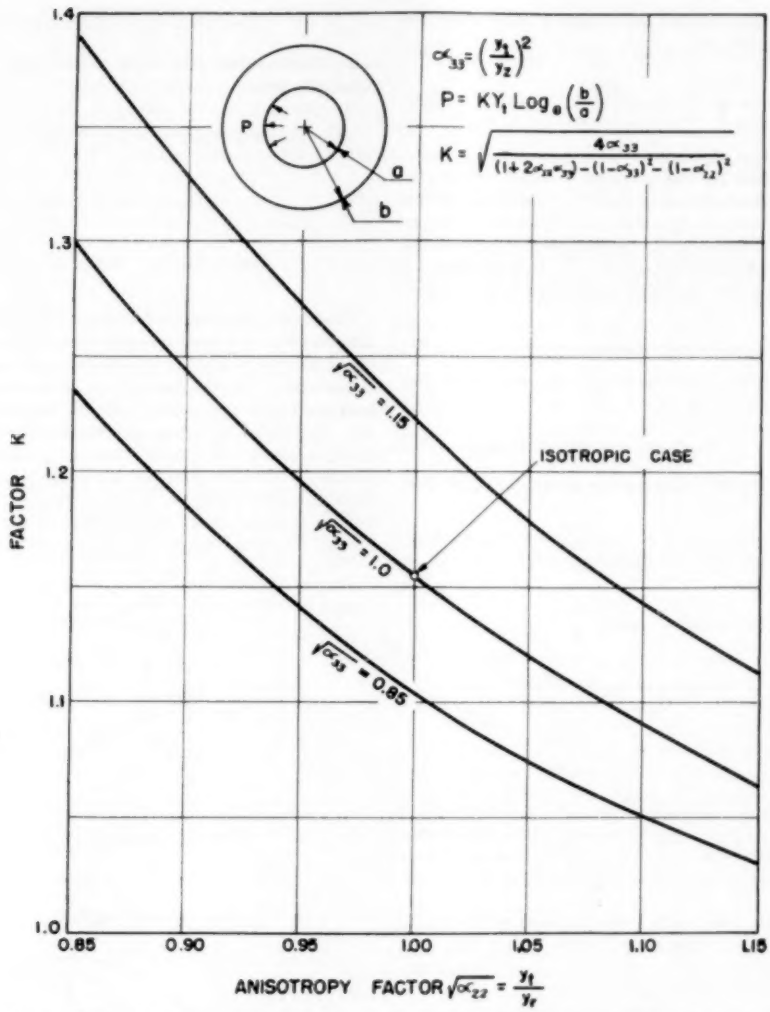

FIG. 1 EFFECT OF ANISOTROPY ON STRENGTH OF THICK-WALLED CYLINDER UNDER INTERNAL PRESSURE P

combining Equations [4], [26], and [27], the effective stress $\bar{\sigma}$ and the stress-strain-increment relations are found to be, respectively

$$\bar{\sigma} = Y_t = \sqrt{\frac{\overline{G}}{\alpha_{33}}}\,(\sigma_t - \sigma_r) \qquad [31]$$

and

$$\left.\begin{aligned} d\epsilon_t &= \sqrt{\frac{\overline{G}}{\alpha_{33}}}\,(\sigma_t - \sigma_r)d\lambda \\ d\epsilon_r &= \sqrt{\frac{\overline{G}}{\alpha_{33}}}\,(\sigma_r - \sigma_t)d\lambda \\ d\epsilon_z &= 0 \end{aligned}\right\} \qquad [32]$$

where

$$\alpha_{11} = 1,\ \alpha_{22} = (Y_t/Y_r)^2,\ \alpha_{33} = (Y_t/Y_z)^2$$

and $$G = \frac{1}{4}\,[1 + 2\alpha_{22}\alpha_{33} - (1 - \alpha_{22})^2 - (1 - \alpha_{33})^2]$$

Substituting the difference of $\sigma_t - \sigma_r$ from Equation [31] into Equations [28], the stress components become

$$\left.\begin{aligned} \sigma_r &= -\sqrt{\frac{\overline{\alpha_{33}}}{G}}\;Y_t \ln\left(\frac{b}{r}\right) \\ \sigma_t &= \sqrt{\frac{\overline{\alpha_{33}}}{G}}\;Y_t\left[1 - \ln\left(\frac{b}{r}\right)\right] \\ \sigma_z &= \sqrt{\frac{\overline{\alpha_{33}}}{G}}\;Y_t\left[\frac{1 - \alpha_{22} + \alpha_{33}}{2\alpha_{33}} - \ln\left(\frac{b}{r}\right)\right] \end{aligned}\right\} \qquad [33]$$

When Equations [33] are compared with Equations [29], it can be seen that the distributions of radial and tangential stress in an anisotropic cylinder are entirely similar to those in an isotropic cylinder but the characteristics of the distribution of axial stress are changed by the anisotropy.

Using the first of Equations [33], the pressure p under which the cylinder yields is found to be

$$p = \sqrt{\frac{\alpha_{33}}{G}}\, Y_t \ln\left(\frac{b}{a}\right) \quad \ldots\ldots\ldots\ldots\ldots [34]$$

In other words, the state of anisotropy in a thick-walled cylinder has a prominent effect on the pressure p under which the cylinder yields. The effect of various degrees of anisotropy on the yield pressure p as given by Equation [34] is plotted in Fig. 1. The significant result obtained is that the yield pressure p can be increased by reducing the axial yield stress Y_a, or by increasing the radial yield stress Y_r, if the tangential yield stress Y_t is kept constant.

Plane-Stress Problems

For plane-stress problems in which $\sigma_{33} = \tau_{23} = \tau_{31} = 0$, the effective stress $\bar{\sigma}$ is found to be

$$\bar{\sigma} = \sqrt{\alpha_{11}\sigma_{11}^2 - 2\alpha_{12}\sigma_{11}\sigma_{22} + \alpha_{22}\sigma_{22}^2 + 3\alpha_{44}\tau_{12}^2} \ldots [35]$$

The stress-strain-increment relations given by Equation [12] then become

$$\left.\begin{aligned} d\epsilon_{11} &= [\alpha_{11}\sigma_{11} - \alpha_{12}\sigma_{22}]\,\frac{d\bar{\epsilon}}{\bar{\sigma}} \\ d\epsilon_{22} &= [\alpha_{22}\sigma_{24} - \alpha_{12}\sigma_{11}]\,\frac{d\bar{\epsilon}}{\bar{\sigma}} \\ d\epsilon_{33} &= -[\alpha_{23}\sigma_{22} + \alpha_{31}\sigma_{11}]\,\frac{d\bar{\epsilon}}{\bar{\sigma}} \\ d\epsilon_{12} &= \frac{1}{2}\,d\gamma_{12} = \frac{3}{2}\,\alpha_{44}\tau_{12}\,\frac{d\bar{\epsilon}}{\bar{\sigma}} \end{aligned}\right\} \quad \ldots\ldots\ldots [36]$$

where 1, 2, 3 are the principal directions of an orthogonal set of axes of anisotropy. This set of axes of anisotropy may change orientation during straining. The effect of the rotation of axes of anisotropy on plastic flow of anisotropic bodies was first considered by Hill (1).

In this section, only two special topics in plane stress dealing with the plastic flow of anisotropic bodies will be discussed, namely, plastic behavior of thin-walled tubes under biaxial tension-tension and under biaxial tension-torsion.

In attempting to verify the validity of various theories of plasticity, biaxial-stress tests have been conducted for several decades (2). In such tests, the biaxial-stress state is generally produced by subjecting a thin-walled tubular specimen to either axial load and internal pressure or axial load and torsion. Although the anisotropy of tubular materials caused by fabrication processes has long been realized, isotropy is usually assumed in the interpretation of test results. In the following paragraphs, the effect of anisotropy on the interpretation of biaxial-stress tests will be considered.

The assumption will be made that the principal axes of anisotropy initially coincide with the cylindrical co-ordinates describing the thin-walled tube considered. For biaxial tension-tension cases, it is reasonable to consider that the principal axes of anisotropy do not rotate during deformation. For biaxial tension-torsion cases, it is easy to visualize that the principal axes of anisotropy will rotate as the angle of twist increases, as shown in Fig. 2.

Consider a thin-walled tube subjected to axial load and internal pressure. For the biaxial tension-tension state produced, the axes of principal stresses coincide with the axes of anisotropy. From Equation [1], the effective stress is

$$\bar{\sigma} = \sqrt{\alpha_{11}\sigma_{11}^2 - 2\alpha_{12}\sigma_{11}\sigma_{22} + \alpha_{22}\sigma_{22}^2} \quad \ldots\ldots\ldots [37]$$

and the stress-strain-increment relations are found, from Equations [12], to be

$$\left.\begin{aligned} d\epsilon_{11} &= d\epsilon_t = [\alpha_{11}\sigma_{11} - \alpha_{12}\sigma_{22}]\,\frac{d\bar{\epsilon}}{\bar{\sigma}} \\ d\epsilon_{22} &= d\epsilon_a = [\alpha_{22}\sigma_{22} - \alpha_{12}\sigma_{11}]\,\frac{d\bar{\epsilon}}{\bar{\sigma}} \\ d\epsilon_{33} &= d\epsilon_r = -[\alpha_{31}\sigma_{11} + \alpha_{23}\sigma_{22}]\,\frac{d\bar{\epsilon}}{\bar{\sigma}} \end{aligned}\right\} \quad \ldots\ldots [38]$$

The plastic stress-strain-increment relations for an anisotropic tube under biaxial tension are characteristically the same as those for an isotropic one (15). For conventional constant and variable stress-ratio tests, the methods of interpretation suggested for isotropic bodies are equally valid for anisotropic materials (1, 2, 15). Furthermore, for constant stress-ratio tests where $\sigma_{11}/\sigma_{22} = \sigma_t/\sigma_a = \text{const}$, the ratio of strain increments $d\epsilon_{11}/d\epsilon_{22} = d\epsilon_t/d\epsilon_a$ obtained from Equations [38] is a constant during the test. This is the condition under which the deformation theory of plasticity is valid. In other words, the deformation theory of plasticity can be used for the interpretation of the constant stress-ratio tests in

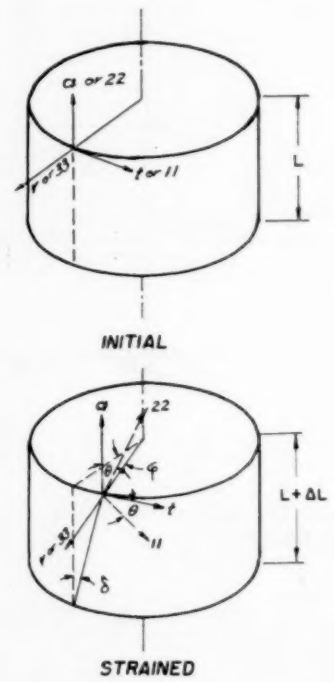

Fig. 2 Rotation of Principal Axes of Anisotropy

biaxial tension in the case of anisotropic materials as well as for isotropic ones.

Now consider the case of thin-walled tubes under biaxial tension-torsion. Assume that the principal axes of anisotropy initially coincide with the cylindrical co-ordinate system describing the thin-walled tube under consideration as shown in Fig. 2. From Equations [1] and [12], the effective stress and the plastic stress-strain-increment relations are, respectively

$$\bar{\sigma} = \sqrt{\alpha_{11}\sigma_{11}^2 - 2\alpha_{12}\sigma_{11}\sigma_{22} + \alpha_{22}\sigma_{22}^2 + 3\alpha_{44}\tau_{12}^2} \quad \ldots [39]$$

and

$$\left.\begin{aligned} d\epsilon_{11} &= [\alpha_{11}\sigma_{11} - \alpha_{12}\sigma_{22}]\,\frac{d\bar{\epsilon}}{\bar{\sigma}} \\ d\epsilon_{22} &= [\alpha_{22}\sigma_{22} - \alpha_{12}\sigma_{11}]\,\frac{d\bar{\epsilon}}{\bar{\sigma}} \\ d\epsilon_{12} &= \frac{1}{2}\,[d\gamma_{12}] = \frac{3}{2}\,\alpha_{44}\tau_{12}\,\frac{d\bar{\epsilon}}{\bar{\sigma}} \end{aligned}\right\} \quad \ldots\ldots [40]$$

Suppose the thin-walled tube is subjected to an axial stress σ and shear stress τ, and that the axial extension is found to be ΔL and the angle of twist is φ. At any point on the tube there is a rotation of the axes of anisotropy due to this deformation. Consider that the angle of rotation of the axes of anisotropy is equal to θ as shown in Fig. 2. It can be shown that the stress components along the principal axes of anisotropy are (16)

$$\left.\begin{aligned} \sigma_{11} &= \sigma \sin^2\theta - \tau \sin 2\theta \\ \sigma_{22} &= \sigma \cos^2\theta + \tau \sin 2\theta \\ \tau_{12} &= \tau \cos 2\theta - \frac{1}{2}\,\sigma \sin 2\theta \end{aligned}\right\} \quad \ldots\ldots [41]$$

Using Equations [40], the stress-strain-increment relations referred to the principal axes of anisotropy become

$$\left.\begin{aligned} d\epsilon_{11} &= [\sigma(\alpha_{11}\sin^2\theta - \alpha_{12}\cos^2\theta) \\ &\qquad - \tau(\alpha_{11} + \alpha_{12})\sin 2\theta]\,\frac{d\bar{\epsilon}}{\bar{\sigma}} \\ d\epsilon_{22} &= [\sigma(\alpha_{22}\cos^2\theta - \alpha_{12}\sin^2\theta) \\ &\qquad + \tau(\alpha_{12} + \alpha_{22})\sin 2\theta]\,\frac{d\bar{\epsilon}}{\bar{\sigma}} \\ d\epsilon_{12} &= \frac{d\gamma_{12}}{2} = \frac{3}{2}\,\alpha_{44}\left[\tau\cos 2\theta - \frac{\sigma}{2}\sin 2\theta\right]\frac{d\bar{\epsilon}}{\bar{\sigma}} \end{aligned}\right\} \quad \ldots [42]$$

Using Equations [42], the axial strain and shear deformation referred to the axes of loading are found by conventional procedure of strain transformation

$$\left.\begin{aligned} d\epsilon &= \sin^2\theta\, d\epsilon_{11} + \cos^2\theta\, d\epsilon_{22} - \sin 2\theta\, d\epsilon_{12} \\ &= [\phi_1\sigma + \phi_2\tau]\,\frac{d\bar{\epsilon}}{\bar{\sigma}} \\ d\gamma &= \sin 2\theta(d\epsilon_{22} - d\epsilon_{11}) + 2\cos 2\theta\, d\epsilon_{12} \\ &= [\phi_2\sigma + \phi_3\tau]\,\frac{d\bar{\epsilon}}{\bar{\sigma}} \end{aligned}\right\} \quad \ldots [43]$$

and the effective stress is obtained by substituting the values of stress components from Equations [41] into Equation [39]

$$\bar{\sigma} = \sqrt{\phi_1\sigma^2 + 2\phi_2\sigma\tau + \phi_3\tau^2} \quad \ldots\ldots [44]$$

where

$$\phi_1 = [(\alpha_{11} + 2\alpha_{12} + \alpha_{22} - 3\alpha_{44})\sin^4\theta + (3\alpha_{44} - 2\alpha_{12} - 2\alpha_{22})\sin^2\theta + \alpha_{22}]$$

$$\phi_2 = \frac{1}{2}\sin 2\theta[(2\alpha_{22} + 2\alpha_{12} - 3\alpha_{44}) - 2(\alpha_{11} + \alpha_{22} + 2\alpha_{12} - 3\alpha_{44})\sin^2\theta]$$

$$\phi_3 = [3\alpha_{44} + (\alpha_{11} + 2\alpha_{12} + \alpha_{22} - 3\alpha_{44})(\sin 2\theta)^2]$$

Therefore the plastic behavior of a thin-walled tube with given anisotropy under biaxial tension-torsion is completely defined by Equations [43] and [44], provided the relationship between the angle of twist φ and the angle of rotation of the principal axes of anisotropy θ is specified.

The ratio of strain increments from Equations [43] is

$$\frac{d\epsilon}{d\gamma} = \frac{\phi_1\sigma + \phi_2\tau}{\phi_2\sigma + \phi_3\tau} \quad \ldots\ldots [45]$$

For isotropic materials

$$\alpha_{11} = \alpha_{22} = \alpha_{44} = 1; \qquad \alpha_{12} = \frac{1}{2} \quad \ldots\ldots [46]$$

Substituting the values of α's from Equations [46] into Equation [44], the ratio of the strain increments becomes

$$\frac{d\epsilon}{d\gamma} = \frac{\sigma}{3\tau} \quad \ldots\ldots [47]$$

This result checks with the value obtained in the theory of plasticity for isotropic materials (2). However, since the angle of rotation of the axes of anisotropy θ changes with the angle of twist φ of the tube during plastic deformation, the ratio of strain increments $d\epsilon/d\gamma$ given in Equation [45] will not remain constant, even though the stress ratio σ/τ is kept a constant during loading. Therefore the deformation theory of plasticity cannot be applied to interpret the conventional constant stress-ratio tests in biaxial tension-torsion if the material under consideration is anisotropic. For the conventional variable stress-ratio tests in biaxial tension-torsion, in which either σ or τ is kept constant and the other stress varies during the test, the methods of interpretation suggested by Shepherd (17), and Hu and Marin (15) are no longer valid for anisotropic materials because of the presence of variable θ in the plastic stress-strain-increment relations given by Equations [43]. Probably this may account for the poor agreement between theoretical predictions and experimental results for some of the published biaxial tension-torsion test data (18). Thus, in interpreting test results of biaxial tension-torsion experiments, the flow theory of plasticity for anisotropic materials must be used.

Conclusion

Based on Hill's theory of plasticity for anisotropic metals, the plastic stress-strain-increment relations were derived for materials with strain hardening.. The influence of anisotropy on the plastic behavior of metals in a state of plane strain or plane stress was discussed. For a thick-walled cylinder under internal pressure, it was found that the pressure-carrying capacity can be increased by decreasing the axial strength. For conventional biaxial-stress tests, it was found that the existing methods of interpretation of test results are valid for biaxial tension-tension tests of anisotropic materials but not valid for biaxial tension-torsion tests.

Acknowledgment

The analysis given in this paper was prepared as part of a project on "Plastic Flow of Metals," sponsored by the Office of Ordnance Research.

BIBLIOGRAPHY

1 "The Mathematical Theory of Plasticity," by R. Hill, Oxford University Press, London, England, 1950.

2 "Theory of Flow and Fracture of Solids," by A. Nadai, McGraw-Hill Book Company, Inc., New York, N. Y., 1950.

3 "Theory of Perfectly Plastic Solids," by W. Prager and P. G. Hodge, Jr., John Wiley & Sons, Inc., New York, N. Y., 1951.

4 "Introduction to the Theory of Plasticity for Engineers," by G. Sachs and O. Hoffman, McGraw-Hill Book Company, Inc., New York, N. Y., 1953.

5 "Recent Developments in the Mathematical Theory of Plasticity," by W. Prager, *Journal of Applied Physics*, vol. 20, March, 1949, pp. 234–241.

6 "A Theory of Yielding and Plastic Flow of Anisotropic Metals," by R. Hill, Proceedings of the Royal Society of London, series A, vol. 193, 1948, p. 281.

7 "Plastic Flow in Anisotropic Sheet Metal," by L. R. Jackson, K. F. Smith, and W. T. Lankford, *Metals Technology*, T. P. 2440, August, 1948.

8 "Stress-Strain Relations for Anisotropic Plastic Flow," by J. E. Dorn, *Journal of Applied Physics*, vol. 20, January, 1949, pp. 15–20.

9 "Anisotropic Plastic Flow," by J. C. Fisher, Trans. ASME, vol. 71, 1949, pp. 349–356.

10 "The Plastic Torsion of Anisotropic Bars," by R. Hill, *Journal of Mechanics and Physics of Solids*, vol. 2, 1954, pp. 87–91.

11 "The Theory of Plane Plastic Strain for Anisotropic Metals," by R. Hill, Proceedings of the Royal Society of London, series A, vol. 198, 1949, pp. 428–437.

12 "On the Correlation of the Directional Properties of Rolled Sheet in Tension and Cupping Tests," by L. Bourne and R. Hill, *Philosophical Magazine*, vol. 41, 1950, p. 671.

13 "A New Method for Determining the Yield Criterion and Plastic Potential of Ductile Metals," by R. Hill, *Journal of Mechanics and Physics of Solids*, vol. 1, 1953, p. 271.

14 "An Evaluation of a Theory for Plastic Flow in Anisotropic Sheet Metals," by T. H. Hazlett, A. T. Robinson, and J. E. Dorn, Trans. ASM, vol. 42, 1950, pp. 1326–1356.

15 "Determination of Theoretical Plastic Stress-Strain Relations for Variable Combined Stress Ratios," by L. W. Hu and J. Marin, JOURNAL OF APPLIED MECHANICS, Trans. ASME, vol. 74, 1952, pp. 485–488.

16 "A Treatise on the Mathematical Theory of Elasticity," by A. E. H. Love, Dover Publications, New York, N. Y., 1944.

17 "Plastic Stress-Strain Relations," by W. M. Shepherd, Proceedings of The Institution of Mechanical Engineers, vol. 159, 1948, pp. 95–99.

18 "Preliminary Experiments for Testing Basic Assumptions of Plasticity Theories," by R. W. Peters, N. F. Dow, and S. B. Batdorf, Proceedings of the Society for Experimental Stress Analysis, vol. 7, no. 2, 1950.

"Plastic Stress-Strain Relations for Combined Tension and Compression," by J. Marin and H. A. B. Wiseman, NACA TN 2737, July, 1952.

A Method for Calculating Stress-Concentration Factors[1]

By M. HETÉNYI[2] and T. D. LIU[3]

It is shown in this paper that along the root sections of filleted or notched bars there is a rapid rise in the transmitted shearing forces, and this may be regarded as the principal reason for the occurrence of stress peaks under these circumstances. By making a few assumptions concerning the distribution of these shear loads, the stress-concentration factors can be calculated with satisfactory accuracy for such cases which have been heretofore analytically intractable.

Introduction

LET us consider a filleted-plane tension bar, as shown in Fig. 1. If the two shoulder parts of this bar are removed and their effect is replaced along the lines of separation by corresponding normal and shearing stresses, the stress distribution in the remaining net section of constant width will evidently remain the same as before, when this strip formed a contingent part of the original piece. The state of stress may then be calculated at any point of this center strip by regarding the above-mentioned normal and shearing stresses as external loads applied normally and tangentially along the straight boundary lines of separation.

Though the exact distribution of these boundary loads is unknown, of course, for the type of problems which will be considered here, there are some pointers which will enable us to make satisfactory approximations as regards their nature. We know, for instance, that the shearing-load curve will rise rapidly in the neighborhood of the fillet, and the sharper the fillet the more rapid this rise will be. Also, the total amount of transmitted shear loading will have to be the same on each side as the load carried by the respective shoulder portion of the filleted bar, that is, $\sigma_1(D-d)/2$ in the notation of Fig. 1. The effect of the normal loads on the straight boundaries will be comparatively small. This follows from two considerations: The normal load on each boundary will be equivalent to a zero resultant force, since there is no transverse external load present. Furthermore, since the stresses in the boundary layer of an elastic half-plane will never exceed the intensity of the applied normal loading within the loaded region and will vanish outside that region, we may conclude that for tension pieces that are wide in terms of fillet radii, and which consequently give the highest concentrations of stress, the effect of the normal loads will become small.

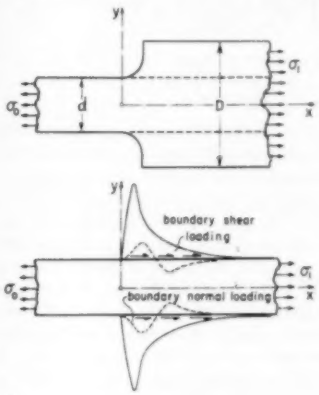

Fig. 1

On the basis of these considerations we will proceed in calculating the stresses at the boundaries of the net section by taking into account only the shearing loads and disregarding the normal forces. In this analysis the shear-load distribution will be assumed in the form of triangles, which seems to be the simplest approximation permissible in these cases, as will be shown in the next section by means of curves derived from existing solutions for stress-concentration problems. In a similar manner it would be possible to take into account in some simple form the effect of the normal forces also, though these were found entirely dispensable in all cases investigated here. There is one particular omission involved in this approximate analysis, however, which it may be well to point out now; namely, the calculation will give the stress distribution only in the net section, while in the original problem the maximum stress is known to occur at a short distance within the fillet, at a point where the tangent to the boundary includes about 10 deg with the horizontal (as indicated in Fig. 6). This small gap of separation between the true location of the stress peak and the point where the approximate stress peak is obtained on the straight boundary is entirely disregarded in the present calculation. It should be noted, however, that this deviation is present only in case of filleted members. In grooved tension bars the maximum stress occurs at the bottom of the grooves, that is, at points which lie directly on the straight boundaries of the net section. These cases, therefore, will not involve any approximation as far as the location of the stress peaks are concerned. It naturally follows that boundary loadings in the analysis of notched bars will be assumed to consist of shear forces distributed symmetrically with respect to the axis of the notch, just as if the right side of Fig. 1 would be reproduced on the left by a mirror reflection around the y-axis.

Shear-Load Distribution in Known Cases

To provide foundation for subsequent simplifying assumptions, the distribution of shearing stresses has been calculated first for cases of stress concentration for which the exact analytical solu-

---

[1] The contents of this paper was first presented at the Eighth International Congress on Theoretical and Applied Mechanics, Istanbul, Turkey, August, 1952. The results were obtained in the course of an investigation conducted for the Office of Naval Research under Contract N7onr-45009.

[2] Walter P. Murphy Professor of Engineering Science, The Technological Institute, Northwestern University, Evanston, Ill. Mem. ASME.

[3] Research Engineer, California Research Corporation, La Habra, Calif.; formerly, Research Assistant at The Technological Institute of Northwestern University, Evanston, Ill.

Contributed by the Applied Mechanics Division and presented at the Diamond Jubilee Annual Meeting, Chicago, Ill., November 13–18, 1955, of The American Society of Mechanical Engineers.

Discussion of this paper should be addressed to the Secretary, ASME, 29 West 39th Street, New York, N. Y., and will be accepted until October 10, 1956, for publication at a later date. Discussion received after the closing date will be returned.

Note: Statements and opinions advanced in papers are to be understood as individual expressions of their authors and not those of the Society. Manuscript received by ASME Applied Mechanics Division, June 27, 1955. Paper No. 55—A-81.

tions are known. This has been done on the basis of H. Neuber's formulas (1)[4] for tension bars with hyperbolic notches and elliptic holes. Since the original solutions of these problems are in terms of curvilinear co-ordinates u and v the derivation of the Cartesian τ_{xy} component required rather lengthy transformations, the details of which will be omitted here.

The co-ordinates

$$x = c \sinh u \cos v \quad \text{and} \quad y = c \cosh u \sin v$$

provide a convenient system to describe elliptic holes as well as hyperbolic notches. Since

$$\left(\frac{x}{c \sinh u}\right)^2 + \left(\frac{y}{c \cosh u}\right)^2 = 1$$

and

$$\left(\frac{y}{c \sin v}\right)^2 - \left(\frac{x}{c \cos v}\right)^2 = 1$$

it is evident that the lines u = const will be confocal ellipses and the lines v = const will be confocal hyperbolas, as indicated in Fig. 2. The constant c denotes one half of the common focal length of this system and, in the following, this c will be taken equal to unity with the dimension of length. In this scale for any assigned value of $u = u_0$ we will have an ellipse of a particular size and shape, with a certain value for the major diameter $2t$ and a radius of curvature ρ at the end of the major axes, as shown in Fig. 2. Similarly, for any particular value of $v = v_0$ we will have a hyperbolic contour of certain proportions, with a net diameter of $2a$ and minimum root radius of curvature ρ. The symbols a, t, and ρ, as well as x and y, denote here absolute numbers, that is, ratios referred to $c = 1$ as a basis of unit length.

It was not possible to obtain an explicit expression for the required τ_{xy} in terms of the Cartesian co-ordinate x. Instead, for each particular contour, the τ_{xy}-values for the root section have been calculated in successive steps by means of the formulas given in the following:

Hyperbolic Notch ($v = v_0$)

Half-diameter of net section: $$[y]_{\substack{u=0 \\ v=v_0}} = \sin v_0 = a \quad \ldots [1a]$$

Minimum radius of curvature: $$\rho = a/\tan^2 v_0 \ldots [1b]$$

Fillet ratio: $$a/\rho = \tan^2 v_0 \ldots [1c]$$

For any assigned value of the x-co-ordinate, the corresponding u and v-values can be calculated from

$$\cos^2 v = \frac{1}{2}(1 - a^2 - x^2) + \frac{1}{2}\sqrt{(1 - a^2 - x^2) + 4x^2} \ldots [1d]$$

and

$$\sinh u = x/\cos v_0 \ldots [1e]$$

In terms of these, the shearing stress along the root section of the notched bar is obtained as

$$[\tau_{xy}]_{y=a} = \frac{x\sigma_0 \sin v_0}{v_0 + \sin v_0 \cos v_0} \cdot \frac{(a^2 - \sin^2 v)^2 \tan v - a^2 \cot v\,(a^2 - \sin^2 v - 2a^2 \cot^2 v)}{(\sinh^2 u + \cos^2 v)^2} \ldots [1f]$$

where σ_0 is the average stress in the net section.

Elliptic Hole ($u = u_0$)

Half major diameter of hole: $$[y]_{\substack{u=u_0 \\ v=\pi/2}} = \cosh u_0 = t \ldots [2a]$$

Minimum radius of curvature: $$\rho = t \sinh^2 u_0/\cosh^2 u_0 \ldots [2b]$$

[4] Numbers in parentheses refer to the Bibliography at the end of the paper.

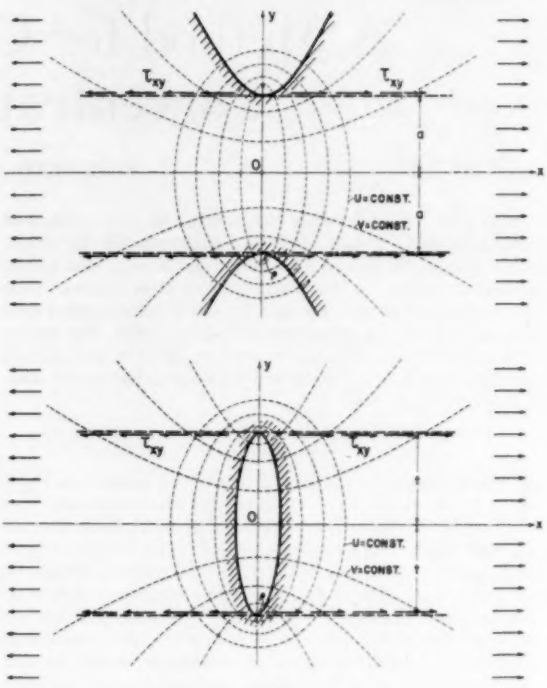

FIG. 2

Fillet ratio: $$t/\rho = \coth^2 u_0 \ldots [2c]$$

For any assigned value of the x-co-ordinate, the corresponding u and v-values may be obtained from

$$\sinh^2 u = \frac{1}{2}(x^2 + t^2 - 1) + \frac{1}{2}\sqrt{(x^2 + t^2 - 1) + 4x^2} \ldots [2d]$$

and

$$\cos v = x/\sinh u_0 \ldots [2e]$$

In terms of these, and of the average stress σ_0, the shearing-stress values along the root sections through the ends of the major axes (as indicated in Fig. 2), may be calculated from the following formula

$$[\tau_{xy}]_{y=t} = -\frac{xt\sigma_0}{4(\sinh^2 u + \cos^2 v)^2} \Big\{(\sinh^2 u + \cos^2 v)\frac{\sinh u}{\cosh u}[A + 2C + 6(C - B)e^{-2u}] + (\cos^2 v - 3\sinh^2 u)\frac{1}{\sinh u}[A \cosh u + e^{-u}(2B + 4C\sinh^2 u)] - 4Be^{-3u}\sinh^2 u\Big\} + \frac{x^2 t\sigma_0}{2(\sinh^2 u + \cos^2 v)^2} \Big\{\frac{\sinh^2 u + \cos^2 v}{\sinh^2 u \cosh u}[2(C - B)e^{-u} + C\sinh u] - \frac{\cos^2 v + 5\sinh^2 u}{\sinh^3 u}[(2B - C)e^{-u} + C\sinh u]\Big\} \ldots [2f]$$

where

$$A = -(1 + \cosh 2u_0)$$
$$B = 1/4(2e^{2u_0} - 4e^{4u_0} + 3)$$
$$C = 1 + e^{2u_0}$$

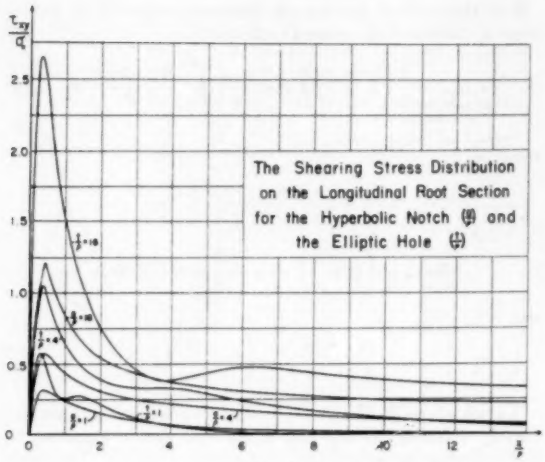

FIG. 3

The τ_{xy}/σ_0 curves, calculated from Equations [1*a*] to [1*f*] and Equations [2*a*] to [2*f*] for three ratios of the hyperbolic notch ($a/\rho = 1, 4, 16$) and of the elliptic hole ($t/\rho = 1, 4, 16$), are shown in Fig. 3. It is seen that in every case the τ_{max} occurs very nearly at $x/\rho = 1/2$. Furthermore, we find that for elliptic holes the τ_{max}/σ_0 values vary about linearly with the t/ρ ratios, while for hyperbolic notches a nearly linear relationship is obtained if τ_{max}/σ_0 is plotted against the corresponding $\sqrt{a/\rho}$ values, as shown in Fig. 4.

These conclusions provide us with sufficient information for making quantitative assumptions concerning the shear-load distribution in the root section of any filleted or notched tension bar. In this approximate analysis the difference between the stress maxima for elliptical holes and semielliptical notches will be disregarded.[5] The τ_{max}/σ_0 values for elliptical holes in Fig. 4 will be used for "shallow" fillets or notches, while the τ_{max}/σ_0 ratios obtained for hyperbolic contours will be used in the analysis of bars with "deep" notches or fillets. Before specifying the distinction between these two classes, we must recall that three quantities are needed for identifying the shape of a filleted or notched tension bar (namely major diameter D, net diameter d, and fillet radius r), while the analytical solutions discussed for elliptical holes or hyperbolic notches involve only two variables in each case (t and ρ, or a and ρ). It is seen that the a in the latter case is actually the same as $d/2$ (that is, the half-diameter of the net section), while t will correspond to $1/2(D - d)$, that is, the one shoulder depth. Through the equivalence of these quantities, the border line between shallow and deep notches or fillets will be defined by a bar of such proportions that the τ_{max}/σ_0 value for this bar will be the same, no matter whether it is taken from Fig. 4 on the basis of $\sqrt{d/2r}$ (that is, $\sqrt{a/\rho}$), or according to $(D - d)/2r$ (or t/ρ). Bars having a smaller D/d than this limiting case will be regarded as having shallow notches or fillets and will be analyzed on the basis of the τ_{max}/σ_0 values obtained for elliptic holes. On the other hand, bars with larger D/d ratios than this borderline case will be classified in the deep notch or fillet class and in their calculation the τ_{max}/σ_0 values will be used which were obtained for hyperbolic contours.

In each case τ_{max} will be assumed to occur as $x = r/2$, and the rest of the τ-diagram will be completed in the form of a triangle,

[5] This difference is likely to be about the same as that between the stress-concentration factors for circular holes and semicircular notches in an infinitely wide bar, which is known to be 2½ per cent.

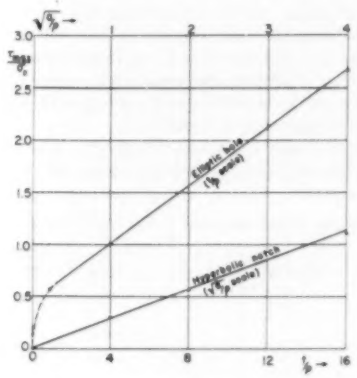

FIG. 4

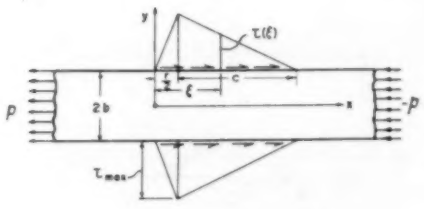

$$(\sigma_x)_{y=\pm b} = \frac{2}{\pi}\int_0^\infty \frac{\cosh 2bz + 1}{\sinh 2bz + 2bz}\cos xz\,dz \int_{-\infty}^{\infty}\tau(\xi)\sin x\xi\,d\xi$$
$$-\frac{2}{\pi}\int_0^\infty \frac{\cosh 2bz + 1}{\sinh 2bz + 2bz}\sin xz\,dz \int_{-\infty}^{\infty}\tau(\xi)\cos x\xi\,d\xi$$

FIG. 5

the area of which has to be the same as the total load carried by the shoulder section of the bar. These conditions define the shear-loading diagram completely in every case.[6]

CALCULATION OF STRESS MAXIMA AT BOUNDARIES OF NET SECTIONS

On the basis of the previous considerations, the problem of filleted or notched tension bars is reduced to the calculation of stresses in an infinite strip of constant width, the boundaries of which are subjected to specified surface shear loadings. A general solution for an infinite strip under any type of boundary loads was presented by L. N. G. Filon (3). When the two boundaries are subjected to shearing forces that are symmetrically distributed with respect to the center line of the strip of width $d = 2b$, Filon's solution can be written in the form

$$[\sigma_x]_{y=\pm b} = \frac{2}{\pi}\int_0^\infty \frac{\cosh 2bz + 1}{\sinh 2bz + 2bz}\cos xz\,dz \int_{-\infty}^{\infty}\tau(\xi)\sin z\xi\,d\xi$$
$$-\frac{2}{\pi}\int_0^\infty \frac{\cosh 2bz + 1}{\sinh 2bz + 2bz}\sin xz\,dz \int_{-\infty}^{\infty}\tau(\xi)\cos z\xi\,d\xi \quad [3]$$

This corresponds to the case shown in Fig. 5, which represents the equivalent shear loadings for filleted bars and can be obtained as a sum of an odd and an even function, as indicated in Equation

[6] E. Weinel (2) appears to have been the first to propose that stress-concentration problems may be analyzed by means of equivalent shearing loads. His suggestion, however, that for symmetrically notched tension bars the transmitted shearing loads may be assumed to vary as the slope of the notch contour, leads to an entirely unrealistic distribution and was found by the authors to give erroneous results for the type of problems investigated here.

[3]. The situation will be simpler in case of symmetrically notched bars, when the shear-load distribution will be an odd function of x, the left side of which is a mirror image of the loading diagram in Fig. 5 around the y-axis and, consequently, the expression for σ_x at the boundaries will contain in that case only the first half of the right side of Equation [3].

In order to make Equation [3] directly applicable to the analysis of filleted bars, the following substitutions and alterations will be made:

1 According to the assumed linear variation in $\tau(\xi)$, we put

$$\tau(\xi) = \frac{\tau_{max}}{r/2}\,\xi, \quad \text{for} \quad 0 \leqslant \xi \leqslant r/2$$

and

$$\tau(\xi) = -\frac{\tau_{max}}{c}\,\xi + \frac{\tau_{max}(c + 1/2\,r)}{c}, \quad \text{for} \quad \frac{r}{2} \leqslant \xi \leqslant \frac{r}{2} + c$$

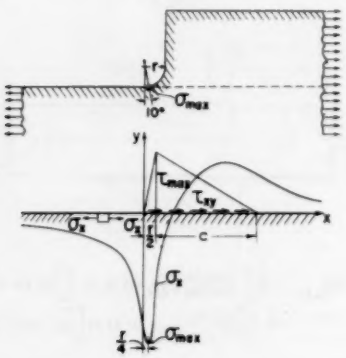

FIG. 6

The value for τ_{max} is to be taken out of the graph in Fig. 4, according to the rule previously described, and c is defined by the equilibrium condition

$$^1/_2(r/2 + c)\tau_{max} = {}^1/_2(D - d)\sigma_1 = {}^1/_2 d(1 - d/D)\sigma_0$$

since $\sigma_1 = \sigma_0 d/D$ according to the notation in Fig. 1.

2 According to Equation [3] the total axial load on the strip $(r/2 + c)\tau_{max}$ is balanced by a uniform compressive stress at $x = \infty$ and a uniform tension stress at $x = -\infty$, as indicated in Fig. 5, the magnitude of which is

$$p = \frac{(r/2 + c)\tau_{max}}{2}\,\frac{1}{d} = \frac{1}{2}\left(1 - \frac{d}{D}\right)\sigma_0$$

In order to satisfy the conditions existing in a filleted bar, that is, to make the normal stress equal to σ_0 in the net section, it is seen that a uniform normal stress of the intensity

$$\frac{1}{2}\left(1 + \frac{d}{D}\right)\sigma_0$$

will have to be superimposed on the results of Equation [3].

3 By plotting the variation of σ_x at the boundary for triangularly distributed shear loadings of various proportions, it has been found that the maximum stress occurs in every case within the steep rise of the τ-diagram, about halfway between the points of $\tau = 0$ and $\tau = \tau_{max}$, as shown in Fig. 6. Hence a good approximation for the required σ_{max}-value may be obtained by putting simply $x = r/4$ into Equation [3].

With the outlined changes, the final formula for the maximum stress in filleted bars is reduced to the form

$$[\sigma_x]_{\substack{max \\ \text{at } x = r/4 \\ y = \pm d/2}} = \frac{1}{2}\left(1 + \frac{d}{D}\right)\sigma_0 + \frac{\tau_{max}}{\pi}\int_0^\infty \frac{\Phi_1(z)\Phi_2(z)}{z^2}\,dz \ldots . [4]$$

where

$$\Phi_1(z) = \frac{\cosh 4(d/r)z + 1}{\sinh 4(d/r)z + 4(d/r)z}$$

$$\Phi_2(z) = \left(2 + \frac{1}{n}\right)\sin z - \frac{1}{n}\sin(1 + 2n)z$$

and

$$n = \frac{c}{r/2} = \frac{2d}{r}\,\frac{\sigma_0}{\tau_{max}}\left(1 - \frac{d}{D}\right) - 1$$

A similar expression may be obtained for symmetrically notched bars by doubling the first half of the right side of Equation [3] and omitting the second half, as mentioned before. The conditions at $x = \pm\infty$ will require now only the addition of a uniform stress $\sigma_1 = \sigma_0 d/D$ to the expression in Equation [3], while the maximum stress will occur in this case at $x = 0$, on account of symmetry.

This leads to the following formula for the maximum stress in symmetrically notched bars

$$[\sigma_x]_{\substack{max \\ \text{at } x = 0 \\ y = \pm d/2}} = \sigma_0\,\frac{d}{D} + \frac{4\tau_{max}}{\pi}\int_0^\infty \frac{\Psi_1(z)\Psi_2(z)}{z^2}\,dz \ldots . [5]$$

where

$$\Psi_1(z) = \frac{\cosh 2(d/r)z + 1}{\sinh 2(d/r)z + 2(d/r)z}$$

$$\Psi_2(z) = \left(1 + \frac{1}{n}\right)\sin z - \frac{1}{n}\sin(1 + n)z$$

and

$$n = \frac{c}{r/2} = \frac{2d}{r}\,\frac{\sigma_0}{\tau_{max}}\left(1 - \frac{d}{D}\right) - 1$$

The stress-concentration factors $k = \sigma_{max}/\sigma_0$, calculated for a series of filleted and notched bars from Equations [4] and [5], are shown in Figs. 7 and 8. It is seen that the results agree very well with the experimental values obtained photoelastically by M. M. Frocht (4) and Charles Lipson (5).

The procedure used in the numerical evaluation of the formulas in Equations [4] and [5] is illustrated by two examples given in the Appendix.

Effect of Stress-Relieving Notches

Perhaps the most interesting feature of the foregoing method is that it provides an easy understanding and quantitative explanation for the so-called stress-relieving effect of closely spaced notches and grooves. This will be illustrated now by means of an example shown in Fig. 9, where a row of equally spaced semicircular notches is assumed along the edge of a tension bar of unlimited depth.

In accordance with our basic rule, the maximum value of the shearing load will be assumed to occur for each notch at an $r/2$ distance from the bottom of the notch. For a circular contour, corresponding to an ellipse of $t/\rho = 1$ ratio, we have from Fig. 4, $\tau_{max} = 0.570\sigma_0$. The rest of the triangular loading diagram, that

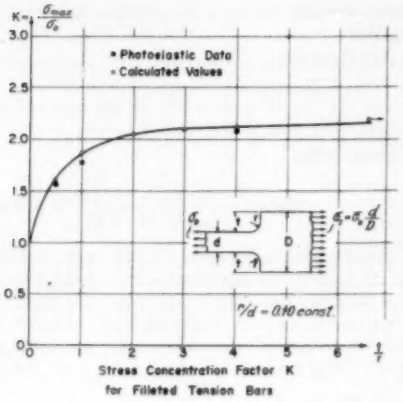

FIG. 7

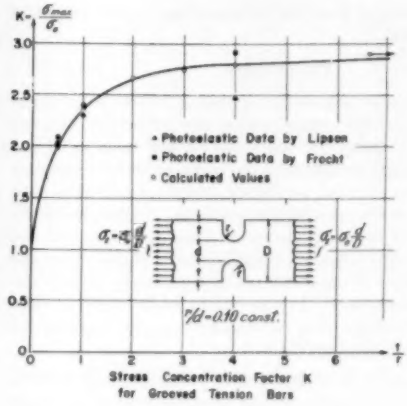

FIG. 8

is, the dimension c in Fig. 6, is determined from the condition of equilibrium. For a single notch of r depth, this can be stated as

$$\frac{1}{2}\tau_{max}(r/2 + c) = r\sigma_0$$

which gives, on substituting the foregoing value for τ_{max}, the equivalent distance $c = 3.00r$. The total length of the base of the loading triangle will be thus $3.50r$ for a single notch, from which it follows that semicircular notches spaced at $7r$ center distance from each other will hardly interfere and, therefore, will not produce any noticeable amount of stress relief.

In order to calculate the stress relief for more closely spaced notches, let us assume a spacing of $4r$, for which particular ratio an approximate value for the stress-concentration factor was derived analytically by C. Weber (6). The equivalent shear-load distribution in this case will have the pattern shown in Fig. 9 where, for reason of symmetry, the shear loads are assumed to vanish at the mid-points between two neighboring notches. The base of each of these triangles will be, therefore, $2r$ or $c = 1.5r$, which means that the transmitted shear load will be now only about one half of the value transmitted through the root section in case of a single notch. In the calculation of the peak stresses in this instance, use will be made of the following formulas for the boundary stress σ_x in a semi-infinite plate subjected to triangularly distributed shearing loads. Following the notation in Fig. 6, and putting $n = c/\frac{1}{2}r$ as before, we have the following:

For values of $x > (r/2 + c)$, that is, outside and to the right of the loading diagram in Fig. 6

$$\sigma_x = -\frac{2\tau_{max}}{\pi}\left[\frac{nx - c(1+n)}{nc}\log\frac{2x - r(1+n)}{2x - r} + \frac{2x}{r}\log\frac{2x}{2x - r}\right] \quad [6a]$$

To the left of the loading diagram in Fig. 6, measured from point O with positive values for x

$$\sigma_x = \frac{2\tau_{max}}{\pi}\left[\frac{2x}{r}\log\frac{2x}{2x + r} + \frac{nx + c(1+n)}{nc}\log\frac{2x + r(1+n)}{2x + r}\right] \quad [6b]$$

The latter formula gives for $x = 0$, that is, at the toe of the loading diagram

$$\sigma_x = \frac{2\tau_{max}}{\pi}\left(1 + \frac{1}{n}\right)\log(1+n) \quad [6c]$$

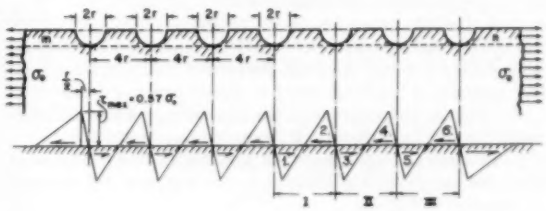

At Center Groove:

$$\sigma_{max} = \sigma_0 + \frac{2\tau_{max}}{\pi}\left(\underbrace{3.0526}_{I} + \underbrace{0.1376}_{II} + \underbrace{0.0469}_{III}\right) - \sigma_0(1 + 1.1748) = 2.18\,\sigma_0$$

At End Groove:

$$\sigma_{max} = \sigma_0 + \frac{\tau_{max}}{\pi}4.5442 + \frac{1}{2}1.1760\,\sigma_0 = \sigma_0(1 + 1.4125) = 2.41\sigma_0$$

FIG. 9

By means of these formulas the maximum stress at the center notch is obtained as

$$\sigma_{max} = \sigma_0 + \frac{2\tau_{max}}{\pi}(3.697 - 0.644 + 0.417 - 0.279 + 0.227 - 0.180)$$

where the six terms in the parentheses represent the effect of the six loading triangles, numbered in Fig. 9. Out of these, the second, fourth, and sixth terms were calculated from Equation [6a], the third and the fifth from Equation [6b], and the first one from Equation [6c]. The total effect is doubled, of course, on account of the symmetry with respect to the center notch.

Putting $\tau_{max} = 0.570\sigma_0$ into the foregoing equation we get a stress-concentration factor

$$k = \sigma_{max}/\sigma_0 = 2.175$$

which is in good agreement with the value, also approximate, of $k = 2.13$ obtained by C. Weber (6) for an infinite row of semicircular notches with this spacing.

However, the present method has one advantage over Weber's analysis; namely, it provides an explanation of the fact that in case of a finite number of equally spaced notches, the stress at the end notch will be somewhat higher than the rest. Since on the one side of the end notch the shear-load diagram is fully developed, while on the other side the foregoing calculated sequence effect is in force, we have for the end notch by means of Equation [6c]

$$\sigma_{max} = \sigma_0 + \frac{\tau_{max}}{\pi}4.544 + \frac{1}{2}1.175\sigma_0 = 2.41\sigma_0$$

which is indeed greater than the value obtained in the foregoing for the endless row.

Conclusion

Though it has been demonstrated that satisfactory quantitative values for the stress-concentration factors can be obtained in this manner, the greatest virtue of this method seems to be that it provides a physical insight into the origin of stress concentrations, which is not afforded by formal analytical solutions, such as those derived by means of stress functions. A great deal of information is available on the nature of stress concentrations and it is well established, chiefly by experimental means, how the place and magnitude of the stress peaks are affected by the proportions of the specimens. In conclusion, we list some of these established relationships, showing that they can all be explained by the present method of approach.

1 As r gets smaller, the ratio $n = c/\frac{1}{2}r$ increases and leads to higher stresses. It is shown in the simplest way in Equation [6c] that the increase is nonlinear and nonasymptotic. If $r \to 0$, $\sigma_{max} \to \infty$ at any value of σ_0.

2 If the shoulder depth $(D - d)$ is increased in a tension bar, while d and r are kept the same, the area of the τ-diagram gradually approaches the limit when it equals one half of the total load. (See second example in the Appendix.) This increase is nonlinear, but asymptotic. If $D \to \infty$, $\sigma_{max} \to$ const.

3 In filleted tension bars the maximum stress occurs at a small distance within the fillet (at $x = r/4$ or at a 10-deg angle, as indicated in Fig. 6).

4 The stress increase in symmetrically notched bars will be less than twice the stress increase produced in a filleted bar of the same proportions. This is evident from the curve in Fig. 6. The value at $x = 0$ is less than the maximum.

5 It has been shown in the last section that the effect of stress-relieving notches and the somewhat less favorable condition at the last notch in a row can all be explained by this method.

BIBLIOGRAPHY

1 "Kerbspannungslehre," by H. Neuber, Julius Springer, Berlin Germany, 1937; (American edition: "Theory of Notch Stresses," translation by F. A. Raven and J. S. Brock, David Taylor Model Basin, 1946).

2 "Über die Spannungserhoehung in Kerbstaeben," by E. Weinel, Proceedings of the Fifth International Congress of Applied Mechanics, Cambridge, Mass, 1938, pp. 51–53.

3 "On an Approximate Solution for the Bending of a Beam of Rectangular Cross Section Under any System of Load, With Special Reference to Points of Concentrated or Discontinuous Loading," by L. N. G. Filon, Philosophical Transactions of the Royal Society of London, England, series A, vol. 201, 1903, pp. 72–76.

4 "Factors of Stress Concentration Photoelastically Determined," by M. M. Frocht, Journal of Applied Mechanics, Trans. ASME, vol. 57, 1935, pp. A-67 and A-68.

5 "Stress and Strength of Manufactured Parts," by C. Lipson, G. C. Noll, and L. S. Clock, McGraw-Hill Book Company, Inc., New York, N. Y., 1950, p. 85.

6 "Halbebene mit periodisch gewelltem Rand," by Constantin Weber, *Zeitschrift für angewandte Mathematik und Mechanik*, vol. 22, February, 1942, pp. 29–33.

Appendix

The procedure used in the evaluation of Equations [4] and [5] will be illustrated here by two numerical examples, one for a filleted and one for a symmetrically notched tension bar.

Filleted Tension Bar of Proportions: $r/d = 0.1$ and $D/d = 1.10$

This is obviously a case of shallow fillets and, therefore, the data obtained in Fig. 4 for elliptical holes will be used in the analysis.

For the ratio

$$\frac{D-d}{2r} = \frac{t}{\rho} = 0.5, \text{ we get } \tau_{max} = 0.459\sigma_0$$

This gives for

$$n = \frac{2d}{r}\frac{\sigma_0}{\tau_{max}}\left(1 - \frac{d}{D}\right)^{-1} = 2.9612$$

The integral in Equation [4] will be evaluated numerically up to the value of the argument $4(d/r)z = 10$, which corresponds to $z = 0.25$ for this particular d/r ratio. At this limit it is permissible to put $\Phi_1(z) = 1$, which simplification makes it possible to obtain an analytical expression for the remaining part of the integral. Thus writing

$$\frac{\tau_{max}}{\pi}\int_0^\infty \frac{\Phi_1(z)\Phi_2(z)}{z^2}\,dz = \frac{\tau_{max}}{\pi}\left[\int_0^{0.25}\frac{\Phi_1(z)\Phi_2(z)}{z^2}\,dz + \int_{0.25}^\infty \frac{\Phi_1(z)\Phi_2(z)}{z^2}\,dz\right]$$

and denoting the first integral on the right side by $I_1(z)$ and the second one by $I_2(z)$, we have by Simpson's rule

$$I_1(z) = (0.025/3)\{0.4570 + 4 \times 0.5702 + 2 \times 0.7708 + 4 \times 1.1531 + 2 \times 1.6147 + 4 \times 2.0896 + 2 \times 2.5329 + 4 \times 2.9357 + 2 \times 3.2989 + 4 \times 3.6251 + 3.9160\} = 0.5192$$

where the ordinates have been taken from Table 1.

TABLE 1

z	$4(d/r)z$	$\Phi_1(z)$	$\Phi_2(z)$	$\Phi_1(z)\Phi_2(z)/z^2$
0.000				0.4570[a]
0.025	1.00	1.1691	0.0003	0.5702
0.050	2.00	0.8463	0.0023	0.7708
0.075	3.00	0.8502	0.0076	1.1531
0.100	4.00	0.9047	0.0178	1.6147
0.125	5.00	0.9496	0.0344	2.0896
0.150	6.00	0.9759	0.0584	2.5329
0.175	7.00	0.9892	0.0909	2.9357
0.200	8.00	0.9953	0.1326	3.2989
0.225	9.00	0.9980	0.1839	3.6251
0.250	10.00	0.9992	0.2450	3.9160

[a] This limiting value was obtained as

$$\lim_{z \to 0}\frac{\Phi_1(z)\Phi_2(z)}{z^2} = \frac{1}{6}\frac{r}{d}(2n+1)(n+1)$$

Putting $\Phi_1(z) = 1$, the second integral becomes

$$I_2(z) = \left(2 + \frac{1}{n}\right)\left\{-\left[\frac{\sin z}{z}\right]_{0.25}^{\infty} - Ci(z)_{z=0.25} + \left[\frac{\sin(1+2n)z}{(1+2n)z}\right]_{0.25}^{\infty} + Ci(z)_{z=0.25(1+2n)}\right\}$$

where the symbols $Ci(z)$ denote cosine integral functions and their numerical values can be taken out of available tables. The result in this case $I_2(z) = 3.9932$.

Substituting the foregoing values into Equation [4] we have

$$\sigma_{max} = \frac{1}{2}\left(1 + \frac{1}{1.10}\right)\sigma_0 + \frac{0.459\sigma_0}{\pi}(0.5192 + 3.9932) = 1.6138\sigma_0$$

which is equivalent to a stress-concentration factor

$$k = \sigma_{max}/\sigma_0 = 1.61$$

SYMMETRICALLY NOTCHED BAR OF PROPORTIONS: $r/d = 0.1$ AND $D/d = \infty$

This is an extreme case of a deep notch and, consequently, the data obtained in Fig. 4 for hyperbolic notches will be used in the calculation.

For the ratio $d/2r = a/\rho = 5.0$, we get $\tau_{max} = 0.626\sigma_0$, which gives for

$$n = \frac{2d}{r}\frac{\sigma_0}{\tau_{max}}\left(1 - \frac{d}{D}\right) - 1 = 30.9489$$

In the evaluation of the integral in Equation [5] the limiting value for the argument $2(d/r)z = 10$ will now correspond to $z = 0.50$ and, consequently, the calculation will be carried out in two parts

$$\frac{4\tau_{max}}{\pi}\int_0^\infty \frac{\Psi_1(z)\Psi_2(z)}{z^2}\,dz = \frac{4\tau_{max}}{\pi}\left\{\int_0^{0.50}\frac{\Psi_1(z)\Psi_2(z)}{z^2}\,dz + \int_{0.50}^\infty \frac{\Psi_1(z)\Psi_2(z)}{z^2}\,dz\right\}$$

where the first integral on the right side will be denoted by $K_1(z)$ and the second by $K_2(z)$.

By means of Simpson's rule we get for the first integral

$$K_1(z) = (0.05/3)\{8.7723 + 4 \times 9.0230 + 2 \times 8.8674 + 4 \times 7.0461 + 2 \times 4.5609 + 4 \times 3.3938 + 2 \times 3.3638 + 4 \times 3.1148 + 2 \times 2.4582 + 4 \times 2.0583 + 2.0123\} = 2.4638$$

where the ordinates have been taken from Table 2.

TABLE 2

z	$2(d/r)z$	$\Psi_1(z)$	$\Psi_2(z)$	$\Psi_1(z)\Psi_2(z)/z^2$
0.00				8.7723
0.05	1.00	1.1691	0.0133	9.0230
0.10	2.00	0.8463	0.1048	8.8674
0.15	3.00	0.8502	0.1865	7.0461
0.20	4.00	0.9047	0.2016	4.5609
0.25	5.00	0.9496	0.2234	3.3938
0.30	6.00	0.9759	0.3102	3.3638
0.35	7.00	0.9892	0.3857	3.1148
0.40	8.00	0.9953	0.3952	2.4582
0.45	9.00	0.9980	0.4176	2.0583
0.50	10.00	0.9992	0.5035	2.0123

Putting $\Psi_1(z) = 1$, the second integral can be written as

$$K_2(z) = \left(1 + \frac{1}{n}\right)\left\{-\left[\frac{\sin z}{z}\right]_{0.50}^\infty - Ci(z)_{z=0.50} + \left[\frac{\sin(1+n)z}{(1+n)z}\right]_{0.50}^\infty + Ci(z)_{z=0.50(1+n)}\right\}$$

Substituting here the corresponding numerical values from tables we have $K_2(z) = 1.1777$.

With the foregoing values, we get from Equation [5] for the peak stress, $\sigma_0 d/D$ being zero now

$$\sigma_{max} = \frac{4 \times 0.626\sigma_0}{\pi}(2.4638 + 1.1777) = 2.9025\sigma_0$$

that is, a stress-concentration factor $k = \sigma_{max}/\sigma_0 = 2.90$.

In this limiting case the conditions are nearly the same as those assumed in Neuber's solution for an infinitely deep hyperbolically notched bar, in which instance the exact formula for an $a/\rho = 5.0$ ratio gives

$$k = \frac{2(a/\rho + 1)\sqrt{a/\rho}}{(a/\rho + 1)\tan^{-1}\sqrt{a/\rho} + \sqrt{a/\rho}} = 2.93$$

Critical Thickness of Surface Film in Boundary Lubrication

By I-MING FENG[1] and C. M. CHANG[2]

When the combined equivalent thickness of the surface film approaches and finally becomes greater than the critical value, the weakening of the interlocking effect of the plastic roughening results in rapid decrease in wear and ultimately reduces wear to practically zero. This is verified by experimental results of wear of pure metals with controlled surface film thickness in the region near the critical thickness.

Introduction

THE effect of the thickness of surface film on friction, metal transfer, and wear has been brought out based upon the plastic roughening mechanism in papers by one of the authors.[3,4] The plastic roughening mechanism suggested in footnote 3 is summarized as follows.

The inherent nature of plastic deformation involving abrupt movement along crystallographic planes causes roughening of the interface of actually contacting high spots which, in carrying the normal load, are usually plastically deformed. The plastically roughened mating high spots create an interlocking effect. When a pair of firmly interlocked high spots is forced to move apart, breakage will occur. Most of the energy dissipated during the process of breaking the high spots is transformed into heat which causes a temperature flash throughout the interface, resulting in momentary diffusion. If the diffusion process is rapid enough to cause welding of the sheared-off piece to the opponent high spot metal transfer take splace. If the conditions are such that no appreciable diffusion occurs, the adhesive force, if present, may keep the metal blob on the opposite high spot. When both diffusion and adhesion are weak, the small piece of sheared metal becomes a loose wear particle.

The significance of the thickness of surface film in its effect on friction, metal transfer, and wear is obvious. The presence of a surface film has little effect on the roughened interface in resisting tangential motion, unless its thickness is comparable to or greater than the average depth of plastic roughening, as illustrated in Figs. 1(*a* and *b*). The thickness of surface film when it just exceeds the average depth of plastic roughening will be called the critical thickness.

When weak surface films are purposely introduced to the rubbing surfaces as in the case of boundary lubrication, increase in the film thickness from thicknesses smaller than the critical value to thicknesses greater than the critical value makes a great difference in the wear characteristics. The case of film thickness smaller than the critical value has been analyzed.[5] The major conclusions reached are (1) that the total damage, which is equal to the sum of metal transfer and wear, is not influenced by the film thickness; and (2) that only the distribution of the total damage between metal transfer and wear is affected by the film thickness, a thicker film causing a larger amount of wear. These conclusions are well supported by experimental results.[6] When the film thickness approaches the critical value, the mechanical interlocking effect of the plastic roughening is greatly weakened and, consequently, wear drops rapidly to zero. For film thickness greater than the critical value, shear takes place inside the film and little damage is done to the surface. The present paper reports the experimental investigation of wear of pure metals with controlled surface-film thickness in the region near the critical value.

(*a*) (*b*)

Fig. 1 Sketches Illustrating the Roughened Interface of a Pair of Actually Contacting High Spots Covered With Surface Film

(*a*, Thin surface film as compared to the average depth of roughening of interface; *b*, film thickness is close to or greater than the average depth of roughening of the interface.)

Combined Equivalent Thickness

The surface film is usually composite in nature, e.g., a layer of adsorbed gas, grease on top of an oxide scale. The oxide scale affects the tangential resistance of the plastically roughened interface in two different ways. If the oxide scale is much weaker than the bulk metal, shear takes place inside the surface film when the total thickness of the oxide scale and the adsorbed gas layer exceeds the critical thickness. If it is stronger than the bulk metal, the oxide scale tends to inhibit the plastic roughening. The thicker the oxide scale, the greater is its effect in reducing the plastic roughening of the interface. The combined effect of a composite surface film is, therefore, equivalent to a weak film of a certain thickness called the combined equivalent thickness. The combined equivalent thickness will be equal to the sum of the thicknesses of each individual layer in a composite film in case the layers are all weaker than the bulk metal.

[1] Research Laboratories Division, Bendix Aviation Corporation, Detroit, Mich.

[2] Electronics Division, Sylvania Electric Products, Inc., Woburn, Mass.

[3] "Metal Transfer and Wear," by I-M. Feng, *Journal of Applied Physics*, vol. 23, 1952, pp. 1011-1019.

[4] "New Theory of Metal Transfer and Wear," by I-M. Feng, *Lubrication Engineering*, vol. 10, 1954, pp. 34-38.

Contributed by the Applied Mechanics Division and presented at the Diamond Jubilee Annual Meeting, Chicago, Ill., November 13-18, 1955, of The American Society of Mechanical Engineers.

Discussion of this paper should be addressed to the Secretary, ASME, 29 West 39th Street, New York, N. Y., and will be accepted until October 10, 1956, for publication at a later date. Discussion received after the closing date will be returned.

Note: Statements and opinions advanced in papers are to be understood as individual expressions of their authors and not those of the Society. Manuscript received by ASME Applied Mechanics Division, February 7, 1955. Paper No. 55—A-84.

[5] "An Analysis of the Effect of Various Factors on Metal Transfer and Wear Between Specimen Pairs of Same Metal and Same Shape II. Effect of the Surrounding Atmosphere," by I-M. Feng, *Journal of Applied Physics*, vol. 26, January, 1955, pp. 28-32.

[6] "Effect of the Surrounding Atmosphere on Wear of Pure Copper," by I-M. Feng and C. M. Chang, Technical Report No. 1 on DIC Project No. 5-7021, under OOR Contract No. DA-19-020-ORD-1767.

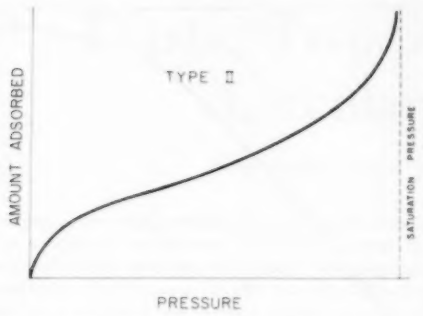

FIG. 2 TYPE II ISOTHERM (PHYSICAL ADSORPTION)

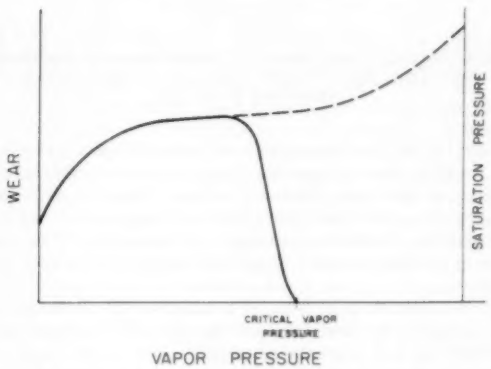

FIG. 3 CURVES ILLUSTRATING THE EFFECT OF SURFACE-FILM THICKNESS ON WEAR WHEN THE CRITICAL THICKNESS IS APPROACHED

SHAPE OF WEAR VERSUS VAPOR-PRESSURE CURVES

The variation of the amount of physically adsorbed gas on a solid surface at constant temperature as a function of its vapor pressure is described by the adsorption isotherm. Fig. 2 shows a Type II isotherm. Almost all isotherms for physical adsorption of gases on metal are of this type. When the film present on the surface has a combined equivalent thickness smaller than the critical thickness, variation in the film thickness does not affect the total damage, the sum of metal transfer, and wear. The surface film increases the barrier to metal transfer and hence gives less metal transfer and more wear. Thus the wear versus vapor-pressure curve is expected to have a similar shape to that of the adsorption isotherm.

Since the combined equivalent thickness of the surface film increases with increasing vapor pressure, the critical film thickness corresponds to a critical vapor pressure. The wear versus vapor-pressure curve will follow the S-shape (shown by dotted curve in Fig. 3), until the critical vapor pressure is approached when wear drops rapidly and becomes practically zero at vapor pressures higher than the critical value, as shown by the solid curve in Fig. 3.

WEAR-TEST ARRANGEMENT

The experimental setup for wear tests is briefly described as follows: Two cylindrical specimens which are counterbored to leave an annular surface at the end are placed end to end with the annular surfaces in contact. One of them is rotating at a constant speed and the other is stationary. The load is applied normal to the annular surface. The amount of wear is measured by

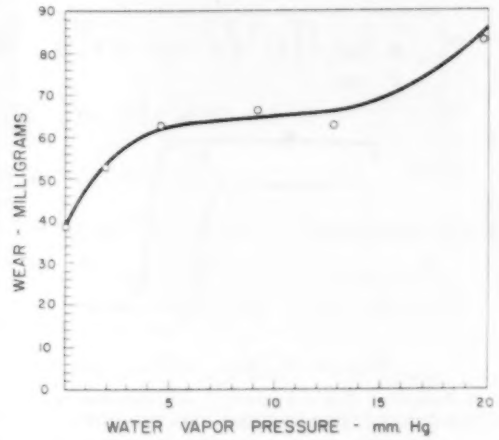

FIG. 4 EFFECT OF WATER-VAPOR PRESSURE IN AIR ON WEAR OF PURE COPPER SPECIMENS—1100-G LOAD

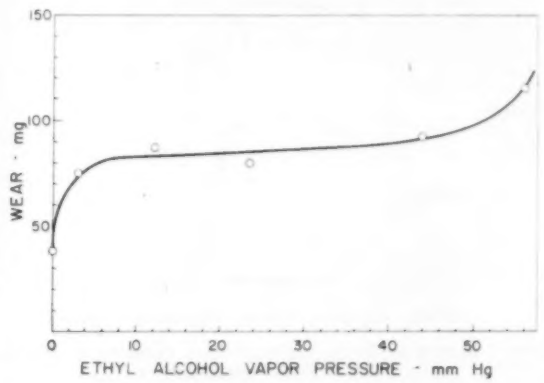

FIG. 5 EFFECT OF ETHYL-ALCOHOL VAPOR PRESSURE IN AIR ON WEAR OF PURE COPPER SPECIMENS—1100-G LOAD

the average weight loss of the two mating specimens. The testing surfaces are finished by polishing with No. 1 emery paper. Before they are put together, the specimens are thoroughly cleaned in two steps, primary cleaning with benzene followed by final cleaning in boiling distilled benzene. All experiments are carried out at room temperature, with a sliding speed of 4.5 cm/sec and for a total distance of travel of 307.5 m. The thickness of adsorbed layer and hence the combined equivalent thickness of the composite surface film are controlled by regulating the temperature of alcohol through which air bubbles.

EXPERIMENTAL RESULTS

The experimental wear versus water-vapor-pressure curve (1100-g load)[8] has a shape similar to that of the Type II adsorption isotherm. It is reproduced in Fig. 4. As shown in Fig. 5, additional wear results of pure copper (electrolytic tough pitch), obtained under 1100-g load in air containing various amounts of ethyl-alcohol vapor, ranging from 0 to ca. 56-mm Hg vapor pressure, further substantiate the parallelism between the adsorption isotherm and the wear versus vapor-pressure curve.

When the normal load is reduced, the average depth of plastic roughening is decreased and, consequently, the critical thickness of surface film is also decreased. With a load of 50 g, the critical

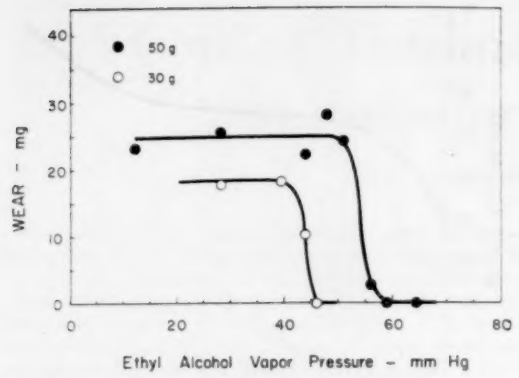

FIG. 6 EFFECT OF ETHYL-ALCOHOL VAPOR PRESSURE IN AIR ON WEAR OF PURE COPPER SPECIMENS NEAR THE CRITICAL VALUE

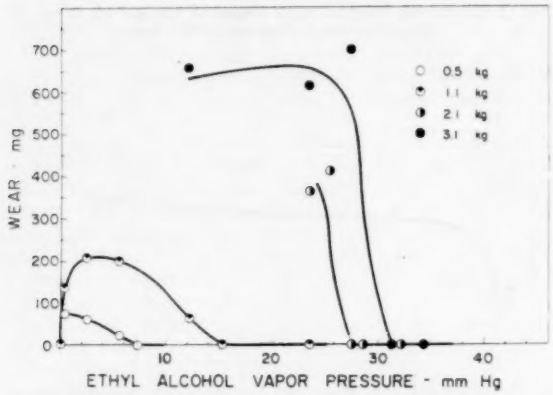

FIG. 7 EFFECT OF ETHYL-ALCOHOL VAPOR PRESSURE IN AIR ON WEAR OF PURE IRON SPECIMENS

thickness becomes smaller than the maximum combined equivalent thickness at ca. 56-mm Hg alcohol vapor pressure. Wear data plotted in Fig. 6 demonstrate the sudden drop in wear near the critical vapor pressure for two different loads—30 g and 50 g.

Results of wear experiments with pure iron which contains C and O_2 as low as only 0.003 and 0.0053 per cent, respectively, under various loads, in air containing various amounts of ethyl-alcohol vapor, are summarized in Fig. 7. These curves also show the sudden decrease in wear near the critical vapor pressure and the vanishing of wear above the critical vapor pressure.

DISCUSSION

Although no weight loss of the rubbing specimens is detected above critical point, yet a small amount of superficial impairment to the surface is still present. This is because contacting high spots are not roughened to the same degree by plastic deformation.

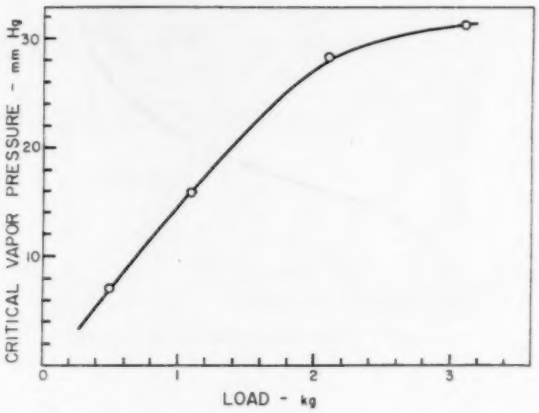

FIG. 8 CRITICAL VAPOR PRESSURE VERSUS LOAD CURVE DEMONSTRATING THAT THE AVERAGE DEPTH OF PLASTIC ROUGHENING INCREASES WITH LOAD

When the film thickness exceeds the statistical average value of the depth of plastic roughening, the great majority of contacting high spots lose their interlocking effect. However, there may still remain a few high spots which are roughened to an extent greater than the statistical average. This accounts for the presence of a small amount of superficial damage above the critical point.

The sudden drop of wear to practically zero at the critical point leads to the possibility of studying the effect of load on the average depth of plastic roughening by determining the critical thickness of surface film at various loads. A qualitative picture of the variation of the average depth of plastic roughening with the normal load can be obtained by using critical vapor pressure to represent the critical film thickness. The critical vapor pressure, as determined from Fig. 7, is plotted against the normal load in Fig. 8, from which one can conclude indirectly that a larger load causes greater plastic roughening.

The rapid rise of the wear versus ethyl-alcohol vapor-pressure curve in the region just below the critical point explains why boundary lubricated parts can be ruined or seized together so quickly during a momentary, unfavorable change in the operating conditions. To avoid such serious difficulties caused by load fluctuation or the variation of other operating conditions which influence the film thickness, the film thickness must be kept well above the critical value.

ACKNOWLEDGMENT

The authors are indebted to Prof. Brandon G. Rightmire of the Lubrication Laboratory, Massachusetts Institute of Technology, for his encouragement and interest.

The work was performed under the auspices of the project sponsored by the Office of Ordnance Research, U. S. Army, with Mr. M. Petronio of the Frankford Arsenal as the technical supervisor.

Plastic Twisting of Thick-Walled Circular Ring Sectors[1]

By W. FREIBERGER[2] and W. PRAGER,[3] PROVIDENCE, R. I.

The paper presents a graphical method of determining the fully plastic stress distribution in a twisted circular ring sector with hollow cross section and the warping of the cross sections of this ring in the ensuing plastic flow. The ring is assumed to consist of a rigid, perfectly plastic material.

Introduction

THE plastic twisting of circular ring sectors has been discussed by several authors. Freiberger (1)[4] gave an analytical treatment of the solid circular cross section. For an arbitrary solid section, Wang and Prager (2) developed a graphical method based on Freiberger's characteristic equation. Whereas these papers were concerned with rings made of perfectly plastic materials, the plastic twisting of a thin-walled circular ring sector made of a work-hardening material was discussed by Wang (3).

In the present paper, the graphical method of Wang and Prager is extended to the plastic twisting of a thick-walled circular ring sector made of a perfectly plastic material. Aside from the possible application to overstressed helical springs of small pitch, the solution of this problem is of interest because it illustrates the important role of discontinuities in the theory of perfectly plastic solids (4).

Stresses

Fig. 1 shows a thick-walled ring sector, the loads acting on it, and the system of cylindrical co-ordinates r, z, θ used in the following text. For the fully plastic stress distribution considered here, the stress transmitted across a generic element of cross-sectional plane θ = const is a shear stress of the intensity k, the yield stress in simple shear. If the angle between the stress vector and the positive r-direction is denoted by ψ, the components of the stress vector with respect to the axes of r and z are given by

$$\tau_r = k \cos \psi, \quad \tau_z = k \sin \psi \ldots\ldots\ldots\ldots [1]$$

When these expressions are substituted into the equation of equilibrium

$$\frac{\partial}{\partial r}(r^2\tau_r) + \frac{\partial}{\partial z}(r^2\tau_z) = 0 \ldots\ldots\ldots\ldots [2]$$

the following differential equation is obtained for the angle ψ

$$\frac{\partial \psi}{\partial r} \sin \psi - \frac{\partial \psi}{\partial z} \cos \psi - \frac{2}{r} \cos \psi = 0 \ldots\ldots\ldots [3]$$

The characteristic equations of [3] are

$$\frac{dr}{ds} = \sin \psi, \quad \frac{dz}{ds} = -\cos \psi, \quad \frac{d\psi}{ds} = \frac{2}{r} \cos \psi \ldots\ldots [4]$$

where ds is the line element of the characteristic. The first two Equations [4] show that the characteristic through a generic point Q of the cross section is normal to the stress vector at Q. The positive direction of the characteristic is obtained by rotating the stress vector by a right angle in the sense which transforms the positive z-direction into the positive r-direction. The last Equation [4] shows then that the radius of curvature of the characteristic is given by

$$\rho = \frac{r}{2} \sec \psi \ldots\ldots\ldots\ldots [5]$$

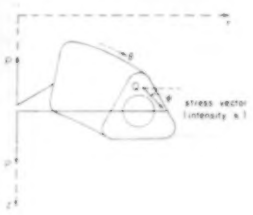

Fig. 1

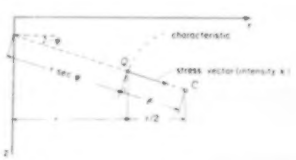

Fig. 2

Fig. 2 indicates how the center of curvature C at a point Q of the characteristic is found when the stress vector at Q is known. C lies on the line of action of the stress vector, and its distance from the z-axis equals 1.5 times the distance of Q from this axis.

As in the case of a solid section, characteristics are constructed starting from a number of suitably chosen points on the exterior boundary of the cross section. At a point Q on this boundary, the stress vector is tangential to the boundary. The center of curvature of the characteristic through Q can, therefore, be determined in the manner indicated in Fig. 2. In the neighborhood of Q, the characteristic can be approximated by a short arc QQ' of its circle of curvature. The stress vector at Q' has the line of action $Q'C$. The center of curvature C' at Q' can, therefore, be determined as before. Proceeding in this manner, one approximates the characteristic by a sequence of short circular arcs.

Characteristics starting from different parts of the boundary of the cross section may intersect in the points of a line of discontinuity of the stress field. This phenomenon is well known from the theory of plastic torsion of a prismatic bar, where the characteristics are the projections, on the cross-sectional plane, of the

---

[1] The results presented in this paper were obtained in the course of research work sponsored by Watertown Arsenal Laboratories, under Contract DA-19-020-ORD-2598.

[2] Assistant Professor of Applied Mathematics, Brown University.

[3] Chairman, Physical Sciences Council, Brown University. Mem. ASME.

[4] Numbers in parentheses refer to the Bibliography at the end of the paper.

Contributed by the Applied Mechanics Division and presented at the Diamond Jubilee Annual Meeting, Chicago, Ill., November 13–18, 1955, of The American Society of Mechanical Engineers.

Discussion of this paper should be addressed to the Secretary, ASME, 29 West 39th Street, New York, N. Y., and will be accepted until October 10, 1956, for publication at a later date. Discussion received after the closing date will be returned.

Note: Statements and opinions advanced in papers are to be understood as individual expressions of their authors and not those of the Society. Manuscript received by ASME Applied Mechanics Division, July 11, 1955. Paper No. 55—A-85.

lines of steepest descent on Nadai's sand hill (5), and the lines of discontinuity are the projections of the ridges of the sand hill.

For the plastic torsion of a prismatic bar as well as the plastic twisting of a circular ring sector, the line of discontinuity bisects the angles formed by the characteristics meeting on it. Fig. 3 shows how this property is used to construct lines of discontinuity.

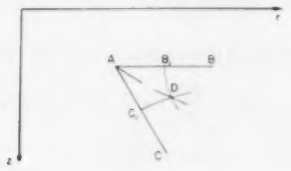

FIG. 3

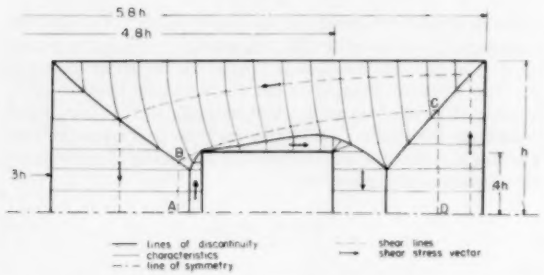

FIG. 4 RING SECTOR OF RECTANGULAR CROSS SECTION WITH SYMMETRICAL RECTANGULAR HOLE. CASE I

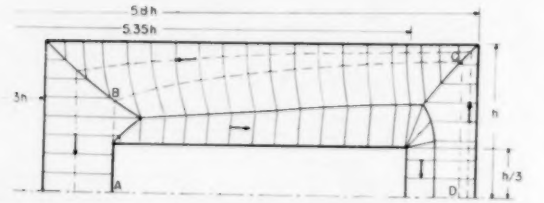

FIG. 5 RING SECTOR OF RECTANGULAR CROSS SECTION WITH SYMMETRICAL RECTANGULAR HOLE. CASE II

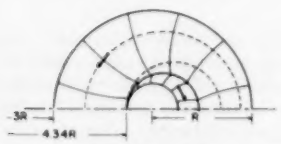

FIG. 6 RING SECTOR OF CIRCULAR CROSS SECTION WITH CONCENTRIC CIRCULAR HOLE

Let B-A-C be part of the boundary of the cross section. A line of discontinuity then starts from the corner A in the direction of the bisector of the angle B-A-C. The characteristics B_1D and C_1D starting from generic points on A-B and A-C, respectively, are constructed in the manner indicated in Fig. 2. At their intersection D, the bisector of the angle formed by these characteristics is marked. As the positions of B_1 and C_1 are varied, a directional field is obtained in this manner. The line of discontinuity is the integral curve of this field that passes through A.

As the characteristics are extended from the exterior boundary into the cross section, the shear lines can be drawn as the orthogonal trajectories of the characteristics. If the interior boundary of the cross section happens to coincide with one of these shear lines, the determination of the stress field is complete. In general, however, the procedure leads eventually to a shear line that has a point or an arc in common with the interior boundary, but does not coincide with it. Figs. 4 and 5 illustrate these possibilities. In each case the last shear line that is exclusively determined by the exterior boundary is A-B-C-D. In Fig. 4 this line contains only a corner of the interior boundary; in Fig. 5 it contains an entire side of the interior boundary.

In each case, the construction of characteristics and shear lines is continued by envisaging the area enclosed by the last shear line A-B-C-D and the interior boundary as a solid cross section. In Fig. 6 the method is applied to a circular cross section with a concentric circular hole.

STRESS RESULTANT

Since the shearing stresses satisfy the condition of equilibrium, Equation [2], they can be derived from a stress function $\varphi(r, z)$ according to

$$\tau_r = \frac{1}{r^2}\frac{\partial \varphi}{\partial z}, \quad \tau_z = -\frac{1}{r^2}\frac{\partial \varphi}{\partial r} \qquad [6]$$

At a generic point of the boundary of the cross section, the resultant shearing stress is tangential to the boundary, i.e.

$$\tau_r dz - \tau_z dr = 0 \qquad [7]$$

Substitution of the Expressions [6] into the Boundary Condition [7] shows that the stress function must be constant along each boundary. For one of the boundaries, e.g., the exterior boundary B_e, the constant value of the stress function may be taken as zero. The constant value of this function on the interior boundary B_i will be denoted by φ_i.

At a line of discontinuity of the stress field, the stress function and its tangential derivative are continuous, but the normal derivative is discontinuous.

The resultant P of the shearing stresses transmitted in a cross section of the ring is most conveniently evaluated in terms of the stress function. The resultant of the radial shearing stresses is given by

$$P_r = \int\int \tau_r \, dr \, dz = \int\int \frac{1}{r^2}\frac{\partial \varphi}{\partial z} \, dr \, dz \qquad [8]$$

where the integration is extended over the entire cross section. In view of the boundary and continuity conditions on φ, the last integral in Equation [8] can be transformed into the following line integral along B_i

$$P_r = \varphi_i \int_{B_i} d\left(\frac{1}{r}\right) = 0 \qquad [9]$$

since the integrand is single-valued and bounded on the closed curve B_i.

The resultant moment of the shearing stresses with respect to the origin of the r, z-plane is given by

$$M = \int\int (r\tau_z - z\tau_r) dr \, dz = -\int\int \left(\frac{1}{r}\frac{\partial \varphi}{\partial r} + \frac{z}{r^2}\frac{\partial \varphi}{\partial z}\right) dr \, dz \qquad [10]$$

With $f(r, z) = z/r$, Equation [10] can be written in the form

$$M = -\int\int \left(\frac{\partial \varphi}{\partial r}\frac{\partial f}{\partial z} - \frac{\partial \varphi}{\partial z}\frac{\partial f}{\partial r}\right) dr \, dz \qquad [11]$$

In view of the boundary and continuity conditions on φ, the inte-

gral in Equation [11] can be transformed into the following line integral along B_i

$$M = \varphi_i \int_{B_i} df = 0 \quad \ldots\ldots\ldots\ldots\ldots [12]$$

The vanishing of R and M establishes the fact that the resultant of the shearing stresses in the cross section is a force acting along the z-axis. According to Equation [1] this force is given by

$$P_z = P = \int\int \tau_z \, dr \, dz = k \int\int \sin \psi \, dr \, dz \ldots\ldots [13]$$

When ψ has been determined by the graphical method described in the section under Stresses, the integral in Equation [13] is best evaluated graphically.

Velocities

For all strain rates except the shear rates $\gamma_{r\theta}$ and $\gamma_{z\theta}$ to vanish, the velocities of the plastic flow must be of the form

$$v_r = 0, \quad v_z = a\theta, \quad v_\theta = aw(r, z) \ldots\ldots\ldots\ldots [14]$$

where a is an arbitrary velocity and w the rate of warping of the cross section when $a = 1$. Since the perfectly plastic material is inviscid, the velocities are determined only to within the arbitrary factor a.

The determination of the warping function $w(r, z)$ follows the same lines for a hollow as for a solid cross section. As Wang and Prager (2) have shown, the variation of w along a line of discontinuity is given by

$$dw = \frac{1}{r} (w \, dr - dz) \ldots\ldots\ldots\ldots\ldots [15]$$

When the value of w has been assumed at one point of a line of discontinuity, graphical integration of Equation [15] furnishes w along this line. Since the circumferential velocity v_θ is determined only to within an arbitrary constant corresponding to a rigid-body rotation about the z-axis, w may be assumed to be zero at an arbitrarily chosen point of the line of discontinuity.

As for a solid cross section, the variation of w along a characteristic is given by

$$\frac{dw}{ds} = \frac{1}{r} (w \sin \psi + \cos \psi) \ldots\ldots\ldots\ldots [16]$$

Since r and ψ are known along each characteristic, graphical integration of Equation [16] furnishes w along any characteristic that intersects the line of discontinuity, along which w has been determined by the graphical integration of Equation [15]. Fig. 7 shows the contour lines of $w(r, z)$ obtained in this manner for the cross section in Fig. 4.

A difficulty not encountered with solid cross sections arises when the last shear line that is exclusively determined by the exterior boundary has an arc in common with the interior boundary (see Figs. 5 and 8). The warping function $w(r, z)$ then is not uniquely determined in the domain of the cross section that is bounded by this common arc, the characteristics through its end points, and part of the exterior boundary. Therefore, in Fig. 8, no contour lines have been indicated in this domain. The indeterminacy of the warping function in this domain is a special case of the indeterminacy of plastic deformation that is encountered in many problems concerning perfectly plastic solids; homogeneous plastic stress, for instance, does not require homogeneous velocity strain. The introduction of a small amount of work hardening could be expected to remove this indeterminacy of the warping function.

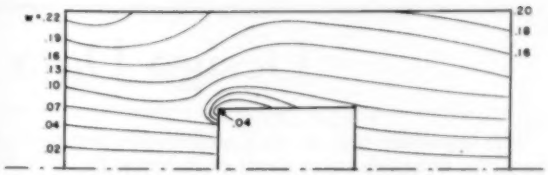

Fig. 7 Warping of Cross Section. Case I

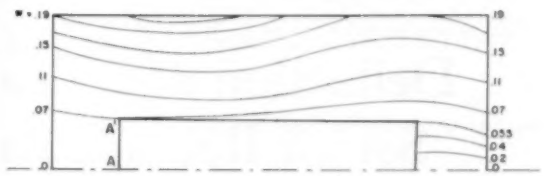

Fig. 8 Warping of Cross Section. Case II

Bibliography

1 "The Uniform Torsion of a Perfectly Plastic Circular Ring," by W. Freiberger, Commonwealth of Australia, Aeronautical Research Laboratories, Report ARL SM 213, 1953.

2 "Plastic Twisting of a Circular Ring Sector," by A. J. Wang and W. Prager, *Journal of Mechanics and Physics of Solids*, vol. 3, 1955, pp. 169–175.

3 "Twisting of a Circular Ring Sector of Hollow Cross Section," by A. J. Wang, submitted to the Journal of Applied Mechanics.

4 "Discontinuous Fields of Plastic Stress and Flow," by W. Prager, General Lecture, Proceedings of the Second U. S. Congress of Applied Mechanics, Ann Arbor, Mich., 1954, pp. 21–32.

5 "Der Beginn des Fliessvorgangs in einem tordierten Stab," by A. Nadai, *Zeitschrift für angewandte Mathematik und Mechanik*, vol. 3, 1923, pp. 442–454.

Design Data and Methods

It is important that the data contained in technical papers be made readily available to designing engineers. In order to satisfy these needs of industry, this section of the Journal includes a concise presentation of data and information drawn chiefly from papers previously published by the Applied Mechanics Division of The American Society of Mechanical Engineers.

Deflection of a Beam Referred to Any Set of Rectangular Centroidal Axes

By J. C. LEVY,[1] LONDON, ENGLAND

An expression is developed for the deflection of a straight beam subjected to unsymmetrical bending which eliminates the necessity of first finding the principal axes and principal moments of inertia of the section. Since it is already possible[2] to calculate the position of the neutral axis and also the stress distribution without referring to principal axes, the present work offers one method of completing such a solution for the class of problems where deflections besides stresses are required.

Nomenclature

The following nomenclature is used in the paper:

OX, OY = any pair of rectangular axes through the centroid of the cross section of the beam

I_x, I_y = moments of inertia of the beam section about OX and OY, respectively

I_{xy} = product of inertia about OX, OY

OU, OV = principal axes through centroid of cross section of beam. OU is always taken in the first and third quadrants with respect to OX, OY when I_x is greater than I_y

I_u, I_v = principal moments of inertia of beam section through centroid; i.e., $I_{uv} = 0$

θ = angle between OX and OU or between OY and OV

φ = angle between loading plane and OY-axis

α = angle between OX and neutral axis

δ_u = deflection in direction perpendicular to axis OU

δ_v = deflection in direction perpendicular to axis OV

δ = actual deflection = $\sqrt{\delta_u^2 + \delta_v^2}$

K = deflection coefficient for section at which deflection is required (see Equation [1])

K_x = component of K in direction perpendicular to OX

K_y = component of K in direction perpendicular to OY

Introduction

When calculating the deflection of a beam which is subjected to unsymmetrical bending, it is usual to split the loading system into components, parallel to each of the two principal axes through the centroid of the cross section. Deflections about each of these axes are then calculated independently by ordinary bending theory and the results combined vectorially to give the required deflection. Provided the loads pass through the shear center, the direction of this deflection is always normal to the neutral axis of the beam.

The foregoing procedure entails arbitrary selection of rectangular axes through the centroid of the section, the computation of the moments of inertia and product of inertia for these axes and the subsequent numerical or graphical evaluation of the directions of the principal axes and the principal moments of inertia through the centroid.

In the following work an expression for the deflection is deduced in terms of the original arbitrarily selected axes, the necessity for reference to principal axes and moments of inertia being eliminated.

The procedure is to resolve the loading system, in the general case, into directions parallel to the selected axes and then to resolve these components themselves into the directions of the principal axes. The consequent expression for deflection is reduced algebraically and geometrically to a relation between the moments and product of inertia about the arbitrary axes, and constants depending upon the system of loading and upon the length and material of the beam.

Attention will be confined to straight beams having constant cross section and constant Young's modulus.

Definition of a "Deflection Coefficient"

It will be convenient when dealing with the deflection problem to designate a deflection coefficient which will incorporate in one symbol the material, longitudinal dimensions, manner of support, and load distribution of a particular beam. Thus

$$\delta = K/I \quad \ldots\ldots [1]$$

where

[1] Lecturer, Northampton Polytechnic; formerly Research Assistant, Department of Theoretical and Applied Mechanics, University of Illinois, Urbana, Ill.

[2] "Advanced Mechanics of Materials," by F. B. Seeley and J.O. Smith, John Wiley & Sons, Inc., New York, N. Y., second edition, 1952, p. 128.

Discussion of this paper should be addressed to the Secretary, ASME, 29 West 39th Street, New York, N. Y., and will be accepted until October 10, 1956, for publication at a later date. Discussion received after the closing date will be returned.

Note: Statements and opinions advanced in papers are to be understood as individual expressions of their authors and not those of the Society. Manuscript received by ASME Applied Mechanics Division, October 14, 1954.

K = deflection coefficient
δ = deflection due to bending about appropriate axis
I = moment of inertia about that axis

For example, if a beam simply supported at the ends of a span L carries a central, concentrated load W

$$\delta = \frac{WL^3}{48EI}$$

so

$$K = \frac{WL^3}{48E}$$

Similarly, for a cantilever with distributed load w/unit length

$$K = \frac{wL^4}{8E}$$

It is important to note that K will vary from point to point along any particular beam and its value must be freshly calculated for each section at which it is desired to find the deflection.

Theory

Reference is made to Fig. 1. For bending about axis OU

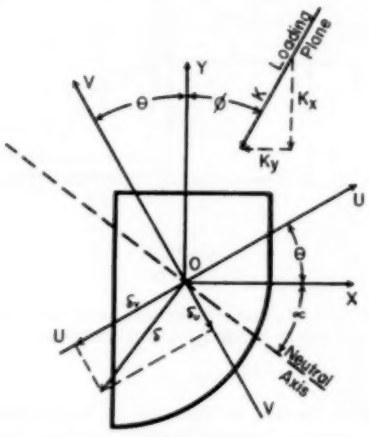

Fig. 1

$$\delta_u = \frac{K_x \cos\theta}{I_u} - \frac{K_y \sin\theta}{I_u} \quad \ldots\ldots [2]$$

For bending about axis OV

$$\delta_v = \frac{K_x \sin\theta}{I_v} + \frac{K_y \cos\theta}{I_v} \quad \ldots\ldots [3]$$

Also $$\delta = \sqrt{\delta_u^2 + \delta_v^2} \quad \ldots\ldots [4]$$

Substituting into Equation [4] from Equations [2] and [3]

$$\delta = \frac{\sqrt{I_v^2(K_x \cos\theta - K_y \sin\theta)^2 + I_u^2 (K_x \sin\theta + K_y \cos\theta)^2}}{I_u I_v} \quad \ldots\ldots [5]$$

There is also the following relationship between the selected axes and the principal axes

$$I_u, I_v = \frac{I_x + I_y}{2} \pm \frac{1}{2}\sqrt{(I_x - I_y)^2 + 4I_{xy}^2} \quad \ldots\ldots [6]$$

By substituting from Equation [6] into Equation [5], a value of δ may evidently be obtained which is independent of I_u and I_v. It happens that such a substitution also eliminates θ but, in order to accomplish this, it is first necessary to determine how to allocate to I_u and I_v the positive and negative values of the square root in Equation [6] when I_x is greater than I_y. Two cases will be considered by use of the Mohr-Land circle,[3] a graphical construction representing Equation [6]. Fig. 2(a) shows a positive value of I_{xy} and Fig. 2(b) a negative value of I_{xy}. I_x is assumed to be greater than I_y so the principal axis in the first quadrant is designated OU.

In Fig. 2(a) $OC = I_x$, $CD = I_y$, $CT = I_{xy}$.
In Fig. 2(b) $OC' = I_x$, $C'D' = I_y$, $C'T' = I_{xy}$.

(a) I_{xy} positive

$$HT = I_v,\ TE = I_u \text{ in Fig. 2}(a)$$

which means that I_v is greater than I_u. Now

$$\tan 2\theta = -\frac{2I_{xy}}{I_x - I_y}$$

As $I_x > I_y$, a positive value of I_{xy} means θ is greater than 45 deg.

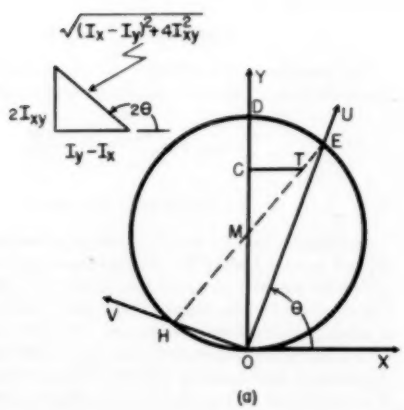

Fig. 2

Hence $\sin 2\theta$ is positive and equals

$$\frac{2I_{xy}}{\sqrt{(I_x - I_y)^2 + 4I_{xy}^2}}$$

and $\cos 2\theta$ is negative and equals

$$\frac{I_y - I_x}{\sqrt{(I_x - I_y)^2 + 4I_{xy}^2}} \quad \text{..... [7]}$$

Substituting Equation [6] in [5], I_v taking the positive sign in [6]

$$\delta = \frac{1}{I_u I_v}\sqrt{\left\{\frac{I_x^2 + I_y^2}{2} + I_{xy}^2 + \frac{I_x + I_y}{2}\sqrt{(I_x - I_y)^2 + 4I_{xy}^2}\right\}\{K_x^2\cos^2\theta + K_y^2\sin^2\theta - K_xK_y\sin 2\theta\} + \left\{\frac{I_x^2 + I_y^2}{2} + I_{xy}^2 - \frac{I_x + I_y}{2}\sqrt{(I_x - I_y)^2 + 4I_{xy}^2}\right\}\{K_x^2\sin^2\theta + K_y^2\cos^2\theta + K_xK_y\sin 2\theta\}}$$

$$= \frac{1}{I_u I_v}\sqrt{K_x^2\left(\frac{I_x^2 + I_y^2}{2} + I_{xy}^2\right) + K_x^2\sqrt{(I_x - I_y)^2 + 4I_{xy}^2}(\cos 2\theta)\frac{I_x + I_y}{2} + K_y^2\left(\frac{I_x^2 + I_y^2}{2} + I_{xy}^2\right) - K_y^2\sqrt{(I_x - I_y)^2 + 4I_{xy}^2}(\cos 2\theta)\frac{I_x + I_y}{2} - K_xK_y(\sin 2\theta)(I_x + I_y)\sqrt{(I_x - I_y)^2 + 4I_{xy}^2}}$$

Substituting in here for $\sin 2\theta$ and $\cos 2\theta$ from Equations [7]

$$\delta = \frac{1}{I_u I_v}\sqrt{(K_x^2 + K_y^2)\left(\frac{I_x^2 + 2I_{xy}^2 + I_y^2}{2}\right) + (K_y^2 - K_x^2)(I_x - I_y)\frac{(I_x + I_y)}{2} - 2K_xK_yI_{xy}(I_x + I_y)}$$

$$= \frac{1}{I_u I_v}\sqrt{K_x^2I_y^2 + K_x^2I_{xy}^2 + K_y^2I_x^2 + K_y^2I_{xy}^2 - 2K_xK_yI_{xy}(I_x + I_y)}$$

$$= \frac{1}{I_u I_v}\sqrt{(K_yI_x - K_xI_{xy})^2 + (K_xI_y - K_yI_{xy})^2} \quad \text{..... [8]}$$

Now from Equation [6], $I_u I_v = I_x I_y - I_{xy}^2$

Substituting this value into Equation [8]

$$\delta = \frac{\sqrt{(K_yI_x - K_xI_{xy})^2 + (K_xI_y - K_yI_{xy})^2}}{I_xI_y - I_{xy}^2} \quad \text{..... [9]}$$

(*b*) I_{xy} negative

$$H'T' = I_u,\ T'E' = I_v \text{ in Fig. 2(}b\text{)}$$

which means that I_u is greater than I_v and, since the previous expression for $\tan 2\theta$ is still valid, a negative value of I_{xy} means θ is less than 45 deg. Hence $\sin 2\theta$ is positive and equals

$$\frac{-2I_{xy}}{\sqrt{(I_x - I_y)^2 + 4I_{xy}^2}}$$

and $\cos 2\theta$ is positive and equals

$$\frac{I_x - I_y}{\sqrt{(I_x - I_y)^2 + 4I_{xy}^2}} \quad \text{..... [10]}$$

Substituting Equation [6] in [5], I_u this time taking the positive sign in Equation [6], and using values of $\sin 2\theta$ and $\cos 2\theta$ from Equations [10] instead of from Equations [7], the expression for δ is still found to be Equation [9], which therefore gives the deflection irrespective of the sign of I_{xy}. (However, the correct sign of I_{xy} must, of course, be used when substituting in Equation [9].)

Special Cases

As a check on Equation [9], let us take some special cases in which it may be reduced as follows:

Suppose OX and OY are themselves principal axes, then $I_{xy} = 0$. Equation [9] then reduces to

$$\delta = \sqrt{\frac{(K_y)^2}{(I_y)^2} + \frac{(K_x)^2}{(I_x)^2}} \quad \text{..... [11]}$$

Suppose now, bending takes place about only one of these axes, then either

$$K_x \text{ or } K_y = 0$$

If $K_x = 0$

$$\delta = \frac{K_y}{I_y} \quad \text{..... [12]}$$

If $K_y = 0$

$$\delta = \frac{K_x}{I_x} \quad \text{..... [13]}$$

Equations [11], [12], and [13] are seen to be correct results from the theory of simple bending and the definitions of K_x and K_y.

Signs

Considering the form of Equation [9], correct results will be given if K_x is always reckoned positive, but K_y is reckoned negative if the loading plane is in the second and fourth quadrants instead of in the first and third as assumed in the theory.

Direction of Deflection

The direction of the deflection is always normal to the neutral axis of the beam. The neutral axis direction is given by[2]

$$\tan\alpha = \frac{I_{xy} - I_x\tan\varphi}{I_{xy}\tan\varphi - I_y} \quad \text{..... [14]}$$

Numerical Example

An example will be worked both by substituting in Equation [9] and by first finding the principal axes and moments of inertia so that the identity of results may be seen and the lengths of solution compared. The beam section chosen is shown in Fig. 3 and is taken as being simply supported on a span, length L, of 24 in. with a uniformly distributed load of $w = 500$ lb per in. of length, the plane of loading being inclined 50 deg to the plane of the web. $E = 10^7$ lb per sq in. and it is required to find the central deflection.

OY is chosen on the center line of the web and the section constants are found to be

$$I_x = 25.32 \text{ in.}^4, I_y = 9.11 \text{ in.}^4, I_{xy} = 11.5 \text{ in.}^4$$

By the method proposed in this paper

$$K = \frac{5}{384}\frac{wL^4}{E} = \frac{5}{384} \times \frac{500 \times 24^4}{10^7} = 0.216 \text{ in.}^3$$

$$K_x = 0.216 \cos 50° = 0.139 \text{ in.}^3$$

$$K_y = 0.216 \sin 50° = 0.165 \text{ in.}^3$$

$$\therefore \delta = \frac{\sqrt{(0.165 \times 25.32 - 0.139 \times 11.5)^2 + (0.139 \times 9.11 - 0.165 \times 11.5)^2}}{25.32 \times 9.11 - 11.5^2}$$

$$= \frac{\sqrt{2.593^2 + 0.637^2}}{98.42} = 0.0271 \text{ in.}$$

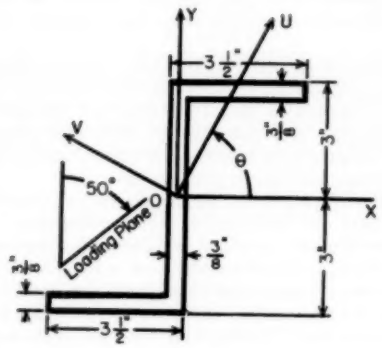

FIG. 3

By conventional method

$$\tan 2\theta = -\frac{2 \times 11.5}{25.32 - 9.11} = -1.419$$

$\therefore 2\theta = 125° 10'$

$\therefore \theta = 62° 35'$

$\therefore$ Angle between loading plane and $OU = 22° 25'$

$$I_u = I_x \cos^2\theta + I_y \sin^2\theta - 2I_{xy} \sin\theta \cos\theta$$
$$= 25.32 \times 0.212 + 9.11 \times 0.788 - 2 \times 11.5 \times 0.887 \times 0.460$$
$$= 5.368 + 7.178 - 9.401 = 3.145 \text{ in.}^4$$

$$I_v = I_x \sin^2\theta + I_y \cos^2\theta + 2I_{xy} \sin\theta \cos\theta$$
$$= 19.952 + 1.931 + 9.401 = 31.284 \text{ in.}^4$$

$$\therefore \delta_u = \frac{5 \times 500 \times 24^4}{384 \times 10^7} \times \frac{\sin 22° 25'}{3.145} = 0.0264 \text{ in.}$$

$$\delta_v = \frac{5 \times 500 \times 24^4}{384 \times 10^7} \times \frac{\cos 22° 25'}{31.284} = 0.0064 \text{ in.}$$

$$\therefore \delta = \sqrt{0.0264 + 0.0064} = 0.0271 \text{ in.}$$

CONCLUSION

Equations [9] and [14] give a complete solution for the magnitude and direction of the deflection of a straight, uniform beam with reference to any set of rectangular, centroidal axes. The necessity for calculating the directions of the principal centroidal axes and moments of inertia is thus eliminated.

When using Equation [9], K_x may always be taken as positive, but a negative value of K_y must be used when the loading plane is in the second and fourth quadrants of OX, OY.

ACKNOWLEDGMENT

The author wishes to thank Prof. J. O. Smith for the suggestion that this problem would be worthy of solution.

Rational Analysis of Heat-Exchanger Tube-Sheet Stresses

By YI-YUAN YU,[1] SYRACUSE, N. Y.

The paper presents a rational method of analysis of heat-exchanger tube-sheet stresses. While the tube sheet is taken to be a perforated plate on an elastic foundation in the manner of Gardner and Miller, it is also considered as part of an integrated indeterminate structure, and the interaction between the tube sheet and the connecting cylindrical shells and flange of the exchanger is determined so that a condition may be formulated which the edge rotation and edge moment of the tube sheet must satisfy. In general, neither the edge rotation nor the edge moment is zero; the edge of a tube sheet is therefore neither clamped nor simply supported. Application of the present method to four different types of heat exchangers is described in detail. To illustrate the method, Gardner's example of a fixed-tube-sheet exchanger is recalculated. While Gardner's method yields only the two limiting values of the maximum stress in the tube sheet, which differ by more than 100 per cent, the present method makes it possible to determine the exact value of this maximum stress. By means of the present method, the stresses in the other parts of the heat exchanger, namely, the tubes, shell, head, and flange, also can be calculated. As a consequence of the present analysis, it is found that, in the external-floating-head type of exchanger, the tube-sheet stress is not independent of the shell-side pressure, which is contrary to Gardner's and Miller's conclusions.

Introduction

RATIONAL methods of design of the various parts of a heat exchanger are given in the ASME Code (1)[2] and API-ASME Code (2) for unfired pressure vessels. The design of tube sheets, however, is not covered in either code. Empirical formulas now in use by the manufacturers of heat exchangers (3) give the maximum stress in the tube sheet in terms of only its radius and thickness and the pressure acting on it. In 1947 the problem was considered on a semirational basis by Gardner (4, 5), who first proposed a plate-on-elastic-foundation analysis for the tube sheet, with the action of the tube bundle considered as that of an elastic foundation, and with the effect of perforation in the tube sheet taken care of by the so-called deflection and ligament efficiencies. These efficiencies were proposed originally by Gardner in a somewhat empirical manner, but one of these, the deflection efficiency, was later put on a rational basis by Malkin (6) and Horvay (7). The same approach as Gardner's also was used by Miller (8) more recently in England.

One of the main shortcomings of Gardner's analysis is that no consideration has been given to the interaction between the tube sheet and the connecting shell and flange. While Gardner assumes the edge condition of the tube sheet to be either simply supported or clamped, the actual edge condition lies somewhere between the two. Since, in general, the tube sheet has a higher maximum stress in the clamped case and the tube has a higher maximum stress in the simply supported case, and the maximum stresses in the two cases of different edge conditions may differ by more than 100 per cent, it is clearly desirable to determine the exact edge condition, so that the exact value of the maximum stress may be calculated, which is the main theme of the present paper.

The typical arrangement of a tube sheet in a heat exchanger is given in Fig. 1 in which a longitudinal cross section of part of the exchanger is shown. Although the shell and head are usually cylindrical shells of the same diameter, their thicknesses may be different. Sometimes the flange may be absent, and the tube sheet is welded to the shell directly in such a case.

Four different types of heat exchangers will be discussed in this paper; namely, (*a*) U-tube type, (*b*) fixed-tube-sheet type, (*c*) external-floating-head type, and (*d*) internal-floating-head type. In the U-tube type the tube sheet shown in Fig. 1 is the only one in the exchanger. In the fixed-tube-sheet type there is a second tube sheet at the other end of the exchanger, which is usually identical to the first. A second tube sheet also exists in both the external- and internal-floating-head type of exchangers, but the arrangement for this second tube sheet is always different from that shown in Fig. 1. However, for simplicity's sake, both tube sheets in all of the last three types of exchangers will be assumed to be identically built. Since the second tube sheet in the floating-head-type exchangers is usually smaller in diameter than the first, any design based upon this assumption probably will be on the safe side. An analysis of two tube sheets of different construction in a heat exchanger is also possible but will not be considered here.

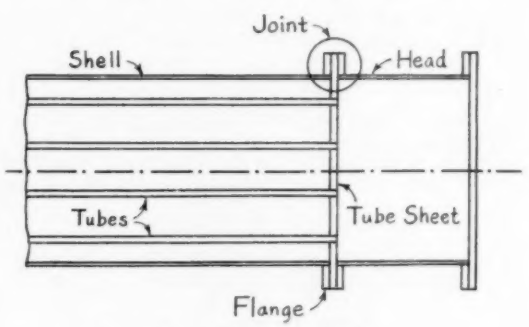

Fig. 1 Tube Sheet in Heat Exchanger

In the following the action of the cylindrical shells and flange will be discussed first. The condition at the joint where the edge of the tube sheet, the edges of the shell and head, and the flange meet together will next be formulated, based upon the fact that the sum of the moments acting on various parts at the joint must

---

[1] Associate Professor of Mechanical Engineering, L. C. Smith College of Engineering, Syracuse University. Assoc. Mem. ASME.

[2] Numbers in parentheses refer to the Bibliography at end of paper.

Discussion of this paper should be addressed to the Secretary, ASME, 29 West 39th Street, New York, N. Y., and will be accepted until October 10, 1956, for publication at a later date. Discussion received after the closing date will be returned.

Note: Statements and opinions advanced in papers are to be understood as individual expressions of their authors and not those of the Society. Manuscript received by ASME Applied Mechanics Division, August 25, 1955.

be equal to zero. This condition will replace the usual one of zero edge moment for a simply supported tube sheet or one of zero edge rotation for a clamped tube sheet. The tube-sheet problem will then be solved by making use of this condition at the joint.

While the problem for a U-tube-type exchanger will be discussed separately, those for the other three types of exchangers will be investigated together on a more or less common basis.

Notations will be defined as they are first introduced.

Shell, Head, and Flange

Since the effect of bending is concentrated in a region very near the supporting edge for a cylindrical shell subjected to uniform pressure, the shell and head of a heat exchanger will be assumed to be semi-infinite cylindrical shells with their supportng edges at the joint. The edge rotation of a hinged semi-infinite cylindrical shell subjected to uniform pressure may be shown to be (9)

$$\theta = \frac{3^{1/4}(1-\nu^2)^{1/4}p}{E}\left(\frac{a}{t}\right)^{3/2}$$

where p is the uniform pressure, E Young's modulus, ν Poisson's ratio, a the radius of shell, and t the thickness of shell. A counterclockwise rotation at the upper joint in Fig. 1 will be considered positive. When this rule and the foregoing formula are applied to the shell and head, as shown in Fig. 2, their edge rotations are

$$\theta_s = \frac{3^{1/4}(1-\nu_s^2)^{1/4}p_s}{E_s}\left(\frac{a}{t_s}\right)^{3/2}, \quad \theta_h = \frac{3^{1/4}(1-\nu_h^2)^{1/4}p_t}{E_h}\left(\frac{a}{t_h}\right)^{3/2} \qquad \text{.....[1]}$$

where the subscript s refers to the shell, subscript h refers to the head, and p_s and p_t are, respectively, the shell-side and tube-side pressures.

Fig. 2 Edge Rotations of Shell and Head at Joint

The term "rotation stiffness" will now be introduced. The rotation stiffness of the edge of a semi-infinite cylindrical shell is defined to be the moment applied at the edge which will rotate the edge through a unit angle. This may be shown to be (10)

$$\left.\begin{aligned} K_s &= \frac{E_s}{2\times 3^{3/4}(1-\nu_s^2)^{3/4}}\frac{t_s^{3/2}}{a^{1/2}} \\ K_h &= \frac{E_h}{2\times 3^{3/4}(1-\nu_h^2)^{3/4}}\frac{t_h^{3/2}}{a^{1/2}} \end{aligned}\right\} \qquad \text{.....[2]}$$

for the shell and head, respectively.

Similarly, the rotation stiffness of a flange is defined to be the moment applied at the inside edge of the flange which will rotate the cross section of the flange through a unit angle. Here it is assumed that the cross section will rotate rigidly, and the rotation stiffness is seen to be equal to the reciprocal of Horvay and Clausen's "flexibility" of the flange (11); accordingly, the rotation stiffness of a flange is

$$K_f = \frac{E_f I_f}{Ra}, \quad I_f = \frac{bc^3}{12} \qquad \text{.....[3]}$$

where E_f is Young's modulus of the flange material and I_f is the moment of inertia of the flange cross section. The various dimensions are shown in Fig. 3, in which the shaded area represents the cross section of the flange. It is seen that the portion of the tube sheet which lies outside the shell is considered to be part of the flange and any irregularity in the cross section is rounded off by the straight sides. When the various parts of the flange are of

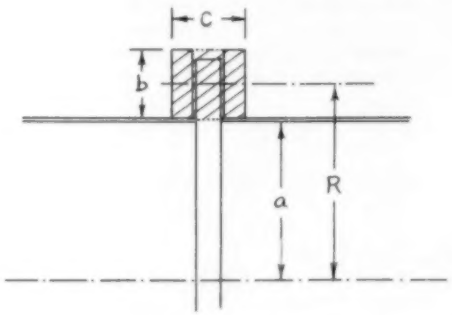

Fig. 3 Flange

different materials, an estimated average value for E_f is to be used. All these simplifications together with the one that the cross section of the flange rotates rigidly are justified on the basis of the assumption that the cross-sectional dimensions of the flange are small compared with its radius, which is most often the case. When the cross-sectional dimensions are not small, some refinement may be necessary.

Condition at Joint

Let M_a and θ_a be the as yet undetermined edge moment and edge rotation of the tube sheet, both considered positive when counterclockwise at the upper joint in Fig. 1. If the joint is a rigid one, as is assumed to be the case, all other elements meeting at the joint will finally be rotated through the same angle θ_a at the joint from their undeformed configurations. The edge moments needed to bring about such a rotation are

$K_s(\theta_a+\theta_s)$	for the shell
$K_h(\theta_a-\theta_h)$	for the head
$K_f\theta_a$	for the flange

as may be seen from Fig. 4 in which the dotted lines represent the deflected positions of the edges of the shell and head, if hinged, under the action of shell-side and tube-side pressures, respectively.

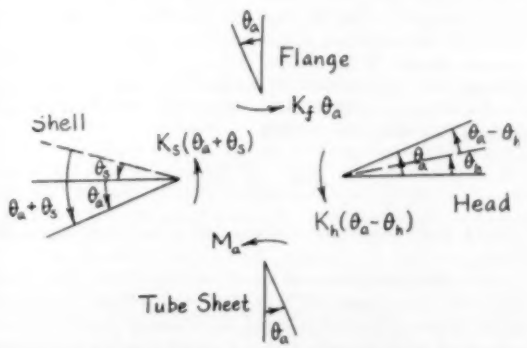

Fig. 4 Edge Rotations and Moments at Joint

Since the four edge moments must balance each other at the joint, there results immediately, according to Fig. 5

$$M_a + K_s(\theta_a + \theta_s) + K_h(\theta_a - \theta_h) + K_f\theta_a = 0$$

or

$$M_a + (K_s + K_h + K_f)\theta_a = K_h\theta_h - K_s\theta_s \quad \ldots\ldots [4]$$

which is the condition to replace the one of zero moment for a simply supported edge or one of zero rotation for a clamped edge. In general neither M_a nor θ_a vanishes, and the two must be related to one another in such a manner as to satisfy Equation [4].

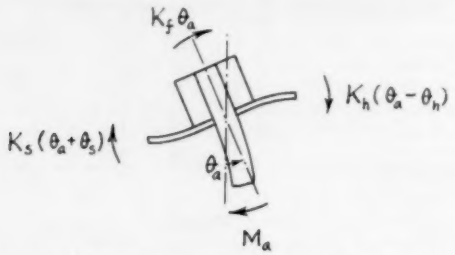

FIG. 5 BALANCE OF MOMENTS AT JOINT

When a flange is absent, the value of K_f is taken equal to zero in the equation.

U-TUBE-TYPE EXCHANGERS

The analysis is the simplest for this type of exchanger, since the tube bundle does not act as an elastic foundation.

The general solution for the deflection of a circular plate under uniform pressure is

$$w = \frac{q(r^4 - a^4)}{64D} + \frac{C_1(r^2 - a^2)}{4} + C_2 \log \frac{r}{a}$$

where q is the uniform pressure, r the radial co-ordinate, a the radius of plate, D the flexural rigidity of plate, and C_1 and C_2 are constants. When the solution is applied to the tube sheet, the uniform pressure on the plate takes the form

$$q = f_t p_t - f_s p_s$$

$$f_t = 1 - \frac{N}{4}\left(\frac{d - 2t}{a}\right)^2, \quad f_s = 1 - \frac{N}{4}\left(\frac{d}{a}\right)^2$$

where f_t is the fraction of tube-side face of the tube sheet including tube ends on which the tube-side pressure acts directly, f_s the fraction of shell-side face of tube sheet on which shell-side pressure acts directly. N the number of tubes, d the outside diameter of tubes, and t the tube-wall thickness. The worst case in which either p_t or p_s acts alone should be considered. The flexural rigidity for a tube sheet has the form

$$D = \frac{Eh^3\eta_w}{12(1 - \nu^2)}$$

where h is the tube-sheet thickness and η_w is the deflection efficiency.

The deflection efficiency of a uniformly perforated plate, such as the tube sheet is assumed to be, is the ratio between the flexural rigidity of the perforated plate and that of a solid plate of identical dimensions without perforation. Working formulas based upon the results of Malkin, Horvay, and Miller (12) are, respectively

$$\eta_w = 0.35\left(1 - 0.908\,\frac{d^2}{P^2}\right)$$

$$\eta_w = 0.50\left(1 - 0.952\,\frac{d}{P}\right)$$

and

$$\eta_w = 1 - \frac{\pi\sqrt{3}}{6}\,\frac{d^2}{P^2}$$

where d is the outside diameter of tube and P is the tube pitch. The second formula was derived on a more sound basis than the other two.

The slope and radial moment for the tube sheet are

$$\left.\begin{aligned} \theta &= \frac{dw}{dr} = \frac{qr^3}{16D} + \frac{C_1 r}{2} \\ M_r &= D\left(\frac{d^2w}{dr^2} + \frac{\nu}{r}\,\frac{dw}{dr}\right) = \frac{(3 + \nu)qr^2}{16} \\ &\qquad + D(1 + \nu)\,\frac{C_1}{2} \end{aligned}\right\} \quad \ldots [5]$$

The presence of C_2 in these expressions would make θ and M_r equal to infinity at the center of the tube sheet; C_2 must therefore be set equal to zero. To determine C_1, the edge values θ_a and M_a of the slope and moment are obtained from Equations [5] and substituted into the edge condition, Equation [4]; the result yields

$$C_1 = \frac{2(K_h\theta_h - K_s\theta_s)}{D(1 + \nu) + a(K_s + K_h + K_f)} - \frac{qa^2 D(3 + \nu) + a(K_s + K_h + K_f)}{8D\,D(1 + \nu) + a(K_s + K_h + K_f)}$$

The maximum moment $(M_r)_{max}$ occurs either at the center or at the edge, and the maximum bending stress is given by

$$\sigma_{max} = \frac{6(M_r)_{max}}{h^2\eta_\sigma}$$

where η_σ, the ligament efficiency, is in essence the reciprocal of a stress-concentration factor due to the perforation in the tube sheet. The following formulas for η_σ are available at the present time

$$\eta_\sigma = 1 - \frac{4}{\pi}\sin^{-1}\left(\frac{\sqrt{2}}{2}\,\frac{d}{P}\right) \quad \text{(square pitch)}$$

$$\eta_\sigma = 1 - \frac{3}{\pi}\sin^{-1}\left(\frac{\sqrt{2}}{2}\,\frac{d}{P}\right) \quad \text{(triangular pitch)}$$

$$\eta_\sigma = 1 - \frac{\pi\sqrt{3}}{6}\,\frac{d^2}{P^2} \quad \text{(triangular pitch)}$$

The first two are due to Gardner (4); the last one is due to Miller (8) and is the same as his formula for the deflection efficiency. Horvay (7) also has indicated how stresses in the ligament of a tube sheet may be computed. In spite of these existing results, the determination of the ligament efficiency still seems to be an open question.

OTHER THREE TYPES OF EXCHANGERS

The tube bundle in these types of exchangers acts as an elastic foundation to the tube sheet. The governing differential equation and its solution are[2]

[2] Horvay (13) pointed out that for tube sheets of square layout the bending becomes anisotropic; the present solution, as also used by Gardner, therefore holds strictly for only tube sheets with triangular layout.

$$x^4\frac{d^4q}{dx^4} + 2x^3\frac{d^3q}{dx^3} - x^2\frac{d^2q}{dx^2} + x\frac{dq}{dx} + x^4q = 0$$

$$q = A \operatorname{ber} x + B \operatorname{bei} x \quad [6]$$

$$w = \frac{1}{\beta^4 D}\left[A(\operatorname{ber} x_a - \operatorname{ber} x) + B(\operatorname{bei} x_a - \operatorname{bei} x)\right] \quad [7]$$

$$\theta = -\frac{1}{\beta^3 D}(A \operatorname{ber}' x + B \operatorname{bei}' x) \quad [8]$$

$$M_r = \frac{1}{\beta^2}\left[A\left(\operatorname{bei} x + \frac{1-\nu}{x}\operatorname{ber}' x\right) - B\left(\operatorname{ber} x - \frac{1-\nu}{x}\operatorname{bei}' x\right)\right] \quad [9]$$

$$x = \beta r = \left(\frac{2k}{D}\right)^{1/4} r, \quad x_a = \beta a$$

$$k = \frac{Nt(d-t)E_t}{a^2L}$$

where k is the tube-bundle modulus, E_t Young's modulus of the tube material, L the tube length, and A, B are constants. The positive directions of θ and M_r in these equations are in agreement with those of their edge values θ_a and M_a specified before; namely, positive when counterclockwise at the upper joint in Fig. 1. The nonuniform effective pressure on the tube sheet is, for the fixed-tube-sheet-type exchanger (5)

$$q = (f_t p_t - f_s p_s) + k(m - \alpha_t T_t L - 2w) \quad [10a]$$

or, for the internal- or external-floating-head-type exchanger (4)

$$q = (f_t p_t - f_s p_s) + k(m - 2w) \quad [10b]$$

where m is the distance the tube-sheet edges move with respect to each other under load, α_t the linear coefficient of thermal expansion of tube, and T_t the tube temperature.

Three conditions are needed for the determination of the three constants m, A, and B. The condition at the joint given in Equation [4] constitutes the first one. The edge values θ_a and M_a of the slope and moment are first obtained from Equations [8] and [9] and substituted into Equation [4], which then yields

$$A\left[\operatorname{bei} x_a + \left(\frac{1-\nu}{x_a} - \frac{K_s + K_h + K_f}{\beta D}\right)\operatorname{ber}' x_a\right] - B\left[\operatorname{ber} x_a - \left(\frac{1-\nu}{x_a} - \frac{K_s + K_h + K_f}{\beta D}\right)\operatorname{bei}' x_a\right] = \beta^2(K_h\theta_h - K_s\theta_s) \quad [11]$$

Since the deflection w has been chosen to be zero at the edge of the tube sheet, the edge value of q is, according to Equations [6] and [10]

$$q_a = A \operatorname{ber} x_a + B \operatorname{bei} x_a = km + f_t p_t - f_s p_s - k\alpha_t T_t L \quad [12a]$$

for the fixed-tube-sheet-type exchanger, or

$$q_a = A \operatorname{ber} x_a + B \operatorname{bei} x_a = km + f_t p_t - f_s p_s \quad [12b]$$

for the floating-head-type exchangers. Equation [12a] or [12b] represents the second required condition. The third and last condition deals with the balance of forces on the tube sheet. In the case of the fixed-tube-sheet-type exchanger this is given by (5)

$$\int_0^a 2\pi r q\, dr = \frac{2\pi a^2}{x_a}(A \operatorname{bei}' x_a - B \operatorname{ber}' x_a) = \pi a^2 p_t - \frac{2\pi a E_s t_s}{L}(m - \alpha_s T_s L)$$

where α_s is the linear coefficient of thermal expansion of shell and T_s is the shell temperature. Denoting

$$K = \frac{2E_s t_s}{akL}$$

we have

$$\frac{2}{x_a}(A \operatorname{bei}' x_a - B \operatorname{ber}' x_a) = p_t - Kkm + Kk\alpha_s T_s L \quad [13a]$$

The corresponding condition[4] for the internal-floating-head-type exchanger is

$$\frac{2}{x_a}(A \operatorname{bei}' x_a - B \operatorname{ber}' x_a) = p_t - p_s \quad [13b]$$

and that for the external-floating-head-type exchanger is

$$\frac{2}{x_a}(A \operatorname{bei}' x_a - B \operatorname{ber}' x_a) = p_t \quad [13c]$$

The constant m is nonessential for the calculation of q, w, θ, and M_r. For the floating-head-type exchangers the constants A and B may be determined directly from Equations [11] and [13b] or [13c]. For the fixed-tube-sheet-type exchanger, m has to be eliminated first from Equations [12a] and [13a]; thus

$$A\left(K \operatorname{ber} x_a + \frac{2 \operatorname{bei}' x_a}{x_a}\right) + B\left(K \operatorname{bei} x_a - \frac{2 \operatorname{ber}' x_a}{x_a}\right) = p_t + K(f_t p_t - f_s p_s) + KkL(\alpha_s T_s - \alpha_t T_t) \quad [14]$$

The constants A and B may then be solved from Equations [11] and [14] in this case.

Once A and B are determined, the quantities q, w, θ, and M_r may all be computed according to Equations [6] to [9], for various locations in the tube sheet defined by r, and for various combinations of the independent effects due to tube-side pressure, shell-side pressure, and thermal expansion. However, there will be no straightforward procedure for the determination of the location and the combination of the three elements for which the stresses in the tube sheet and tubes would be the most critical. Calculation of these stresses will be illustrated by the numerical example given later.

It is noteworthy that A and B and consequently the tube-sheet moment and stress in the external-floating-head type of exchanger are not zero if p_t is zero but p_s is not, for the right-hand side of Equation [11] will be nonvanishing in such a case. Both Gardner and Miller arrived at the erroneous conclusion that in this type of exchanger the tube-sheet stress was independent of p_s and would be zero if only p_t should vanish, which was due to their overlooking the interaction between the tube sheet and the shell.[5]

Example

Gardner's example of a fixed-tube-sheet exchanger (5) will be recalculated by using the foregoing results. The example will be taken as one of analyzing the stresses rather than one of design.

The exchanger has a 20-in. ID, with 260 $^3/_4$-in. 18-BWG steel tubes 12 ft long on 1-in. triangular pitch, and 5 semi-support plates on 27-in. centers. The shell thickness is $^3/_8$ in., which will be taken to be the thickness also of the head. Young's modulus for all parts

[4] The difference between the two floating-head types of exchangers was not made clear by Gardner but was indicated by Miller (8).

[5] Gardner in his 1952 paper (5) seems to have erred further in considering the design pressure to be independent of the shell-side pressure also in an internal-floating-head exchanger. He obviously did not consider so in his 1948 paper (4), for the design pressure used in his example was the shell-side pressure.

is 30×10^6 psi, Poisson's ratio is 0.3, and the coefficient of thermal expansion is 6.7×10^{-6} per deg F. The design conditions are

$$p_i = 150 \text{ psi} \qquad p_s = 400 \text{ psi}$$
$$T_i = 300^\circ \text{ F} \qquad T_s = 290^\circ \text{ F}$$

The stresses in a $1^1/_4$-in. tube sheet will be computed.

The values of the following constants are taken from Gardner's calculations:

$$f_i = 0.723 \qquad K = 0.84$$
$$f_s = 0.635 \qquad D = 0.915 \times 10^6$$
$$k = 1.86 \times 10^4 \qquad \beta = 0.449$$
$$\eta_w = 0.171 \qquad x_a = 4.49$$
$$\eta_\sigma = 0.3$$

Other constants are computed as follows: By Equations [1]

$$\theta_s = 2360 \times 10^{-6} \qquad \theta_h = 885 \times 10^{-6}$$

By Equations [2]

$$K_s = K_h = 0.1922 \times 10^6$$

and, since there is no flange

$$K_f = 0$$

The quantities on the right-hand sides of Equations [11] and [14] become, respectively

$$\beta^3(K_h\theta_h - K_s\theta_s) = 34.3 - 91.5 + 0$$

$$p_i + K(f_i p_i - f_s p_s) + KkL(\alpha_s T_s - \alpha_i T_i) = 241 - 213 - 151$$

which are written with the respective contributions of the tube-side pressure, shell-side pressure, and thermal expansions kept separated. Equations [11] and [14] are now

$$4.63\,A + 5.83\,B = 34.3 - 91.5 + 0$$
$$-4.48\,A + 3.10\,B = 241 - 213 - 151$$

from which

$$\left.\begin{aligned} A &= -32.1 + 23.7 + 21.8 \\ B &= 31.4 - 34.5 - 17.3 \end{aligned}\right\} \quad \ldots\ldots\ldots [15]$$

These are also written with the respective contributions kept separated.

To determine the tube-sheet stress, an expression for the radial moment is first obtained according to Equation [9], which becomes for the present example

$$M_r = (-159.6 + 118.0 + 108.4)\left(\text{bei } x + \frac{1-\nu}{x}\,\text{ber}'\,x\right)$$
$$+ (-156.2 + 171.5 + 86.0)\left(\text{ber } x - \frac{1-\nu}{x}\,\text{bei}'\,x\right)$$

The values of M_r for various ratios of x/x_a are next computed and are given in Table 1.

TABLE 1 VALUES OF M_r FOR VARIOUS RATIOS OF x/x_a

	M_r due to		
x/x_a	p_i	p_s	Thermal expansion
0	−101	+111	+56
0.2	−127	+130	+73
0.4	−184	+164	+115
0.6	−206	+148	+141
0.8	−62	−36	+72
1.0	+437	−544	−218

It is clear now that the maximum radial moment occurs at the edge of the tube sheet when the tube-side pressure is absent. Its value is

$$(M_r)_{max} = M_a = -544 - 218 = -762 \text{ in-lb}$$

The corresponding maximum bending stress is then

$$\sigma_{max} = \frac{6M_a}{h^2\eta_\sigma} = \frac{6 \times 762}{(1.25)^2 \times 0.3} = 9750 \text{ psi}$$

as compared with the following results of Gardner's

$$\sigma_{max} = 14{,}300 \text{ psi (clamped)}$$

$$\sigma_{max} = 6450 \text{ psi (simply supported)}$$

To see the shell action at the joint, the edge rotation θ_a of the tube sheet is calculated according to Equation [8]

$$\theta_a = -\frac{1}{(0.449)^3 \times 0.915 \times 10^6}$$
$$[(23.7 + 21.8)(-3.75) + (-34.5 - 17.3)(-2.01)]$$
$$= +803 \times 10^{-6} \text{ radian}$$

in which the contribution of p_i to A and B has been put equal to zero due to the absence of p_i. The moments acting on the edges of the shell and the head are, respectively

$$K_s(\theta_a + \theta_s) = +608 \text{ in-lb}$$
$$K_h(\theta_a - \theta_h) = +154 \text{ in-lb}$$

in which θ_h is zero since p_i is absent. The sum of the three moments at the joint is obviously equal to zero, as it should be.

The tube stresses are next computed. To determine the direct stress in the tube, the effective pressure will be found first. Substitution of A and B from Equation [15] into [6] yields

$$q = (-32.1 + 23.7 + 21.8)\,\text{ber } x + (31.4 - 34.5 - 17.3)\,\text{bei } x$$

The load on any tube is then given by (5)

$$W_i = \frac{\pi a^2}{N}(q - f_i p_i + f_s p_s)$$
$$= \frac{\pi \times 100}{260}(q - 0.723 \times 150 + 0.635 \times 400)$$

which is computed for various ratios of x/x_a (Table 2).

TABLE 2 VALUES OF W_t FOR VARIOUS RATIOS OF x/x_a

	W_t due to		
x/x_a	p_i	p_s	Thermal expansion
0	−170	+336	+26
0.2	−162	+327	+22
0.4	−133	+298	+5
0.6	−75	+243	−30
0.8	+12	+170	−86
1.0	+100	+114	−148

The maximum tensile load is seen to be

$$W_t = +336 + 26 = +352 \text{ lb}$$

which acts on the tube at the center when the tube-side pressure fails. The maximum compressive load is

$$W_t = -170 \text{ lb}$$

which also acts on the tube at the center, but now when the tube-side pressure alone is acting. The maximum direct tube stress is therefore

$$\sigma_{max} = \frac{(W_t)_{max}}{\pi t(d - t)} = \frac{+352}{\pi \times 0.049(0.75 - 0.049)} = +3350 \text{ psi}$$

Possible failure of the tube as a result of buckling under the maximum compressive load also may be investigated (5). The bending stress in the tube at this location is zero since the slope of the tube sheet vanishes at the center.

The stresses introduced in the shell, head, and flange also may be computed if desired.

Discussion

Any motion of the joint in a direction normal to the shell axis has been neglected in the present treatment. The inclusion of this translation in the problem would result in great complication, for, in such a case, the tube sheet will be subjected to forces in its middle plane, and the problem becomes one of a circular plate under the simultaneous action of lateral pressures, forces in its middle plane, and an elastic foundation. Not only is the plate problem itself much complicated (14), but also the application of its solution to the design of tube sheet will not be so straightforward owing to the fact that the force in the middle plane of the plate will not appear linearly in the solution.

Computations have been carried out on the basis of the assumption that the force in the middle plane does not affect bending. Results show that the force induced is of such a magnitude that the stresses caused by it in the tube sheet are much smaller than the bending stresses; therefore the error introduced by neglecting the translation of the joint and thus the force in the middle plane is probably small. However, since a thorough investigation of the effect of the forces in the middle plane of the tube sheet is essential to a fuller understanding of the problem, it is expected to be carried out in the future.

Acknowledgment

The author wishes to express his sincere appreciation to Mr. W. Kenneth Bodger, formerly of Carrier Corporation, for having introduced him to the study of heat-exchanger tube-sheet design problems.

Bibliography

1 "Rules for Construction of Unfired Pressure Vessels," The American Society of Mechanical Engineers, New York, N. Y., 1952.

2 "API-ASME Code for the Design, Construction, Inspection, and Repair of Unfired Pressure Vessels for Petroleum Liquids and Gases," American Petroleum Institute and The American Society of Mechanical Engineers, New York, N. Y., fifth edition, 1951.

3 "Standards of Tubular Exchanger Manufacturer's Association," New York, N. Y., second edition, 1949, pp. 13 and 28.

4 "Heat-Exchanger Tube-Sheet Design," by K. A. Gardner, Journal of Applied Mechanics, Trans. ASME, vol. 70, 1948, pp. 377–385.

5 "Heat-Exchanger Tube-Sheet Design 2—Fixed Tube Sheets," by K. A. Gardner, Journal of Applied Mechanics, Trans. ASME, vol. 74, 1952, pp. 159–166.

6 "Notes on a Theoretical Basis for Design of Tube Sheets of Triangular Layout," by I. Malkin, Trans. ASME, vol. 74, 1952, pp. 387–396.

7 "Bending of Honeycombs and of Perforated Plates," by G. Horvay, Journal of Applied Mechanics, Trans. ASME, vol. 74, 1952, pp. 122–123, 406–407.

8 "The Design of Tube Plates in Heat Exchangers," by K. A. G. Miller, Proceedings of The Institution of Mechanical Engineers, London, England, Series B, vol. 1, 1952, pp. 215–231.

9 "Theory of Plates and Shells," by S. Timoshenko, McGraw-Hill Book Company, Inc., New York, N. Y., 1940, p. 399.

10 Ibid., p. 392.

11 "Stresses and Deformations of Flanged Shells," by G. Horvay and I. M. Clausen, Jr., Journal of Applied Mechanics, Trans. ASME, vol. 76, 1954, p. 112.

12 "Heat-Exchanger Tube-Sheet Design 2—Fixed Tube-Sheets," by K. A. Gardner, Journal of Applied Mechanics, Trans. ASME, vol. 74, 1952, p. 574 (author's closure).

13 "Heat-Exchanger Tube-Sheet Design 2—Fixed Tube Sheets," by K. A. Gardner, Journal of Applied Mechanics, Trans. ASME, vol. 74, 1952, pp. 572–573 (discussion).

14 "Axisymmetrical Bending of Circular Plates Under Simultaneous Action of Lateral Loads, Forces in the Middle Plane and Elastic Foundation," by Yi-Yuan Yu, to be published.

Brief Notes*

On the recommendations of the Executive Committee of the ASME Applied Mechanics Division, it has been decided to initiate a section devoted to brief notes on technical matters in mechanics. These notes must not be longer than 750 words (about 2½ double-spaced typewritten pages, including figures) and will be subject to the usual review procedure prior to publication. After approval such notes will be published in the next issue of the Journal. The notes should be submitted to the Secretary of the ASME Applied Mechanics Division.

Theory of Fatigue Fracture

By A. Ali Kheiralla,[1] Boston, Mass.

A theory of fatigue fracture based on a reaction kinetic argument has been proposed by T. Yokobori.[2] It is the purpose of this note to point out a fundamental difficulty therein which leads to an unacceptable conclusion and also to indicate how this may be overcome.

With minor changes in notation the argument as originally presented may be summarized as follows: The equilibrium number of nuclei (aggregating to form a crack) per unit volume is given by

$$Z_e = Z_p \operatorname{nexp}(F/kT) \quad [1]$$

where

Z_p = number of preferred nucleation sites per unit volume
F = free energy necessary for nucleus formation
nexp = negative exponential of

The net forward rate of the crack-nucleation reaction (reverse rate is neglected) is given by

$$I = Z_e \left(\frac{kT}{h}\right) \operatorname{nexp}\left(f - \frac{vq^2\sigma^2}{2E}\right) \Big/ kT \quad [2]$$

where

v = atomic volume
q = stress-concentration factor
$q\sigma$ = local effective stress
f = free energy necessary for separation of a pair of atoms

The extension from the foregoing static-loading argument to a cyclic-loading one involves averaging the nucleation rate over a half cycle

$$I_e = \frac{\nu}{N\nu} \quad [3]$$

[1] Mathematician-Physicist, Lessells and Associates, Inc.

[2] "The Theory of Fatigue Fracture of Metals," by T. Yokobori, *Journal of the Physical Society of Japan*, vol. 10, May, 1955, p. 368.

* Discussion of papers in Brief Notes should be addressed to the Secretary, ASME, 29 West 39th Street, New York, N. Y., and will be accepted until October 10, 1956, for publication at a later date. Discussion received after the closing date will be returned.

Note: Statements and opinions advanced in papers are to be understood as individual expressions of their authors and not those of the Society. Manuscript received by ASME Applied Mechanics Division, May 3, 1956.

where

ν = loading frequency (cps)
V = volume of specimen
N = number of cycles to fracture

The latter is assumed to be large compared to the number of cycles required to attain the limit of strain hardening.

The fracture criterion adopted is

$$\sigma_1 + n\tau_1 = \text{maximum} \quad [4]$$

where

σ_1 = local tensile stress in direction of slip plane (taken normal to crack)
τ_1 = local shear stress in direction of slip plane
n = number of similar edge dislocations moving on slip plane

and since n is assumed to be proportional to τ_1, Equation [4] becomes

$$\sigma_1 + C_0\tau_1^2 = \text{maximum} \quad [5]$$

The free energy associated with crack formation is approximated as

$$F = 2\pi\rho r^2 - \frac{16(1-\mu^2)r^3q^2}{3E}(\sigma_1 + n\tau_1)^2 \quad [6]$$

where

r = crack radius
ρ = solid surface tension
μ = Poisson's ratio

This has a maximum value of

$$F \frac{\pi^3\rho^3E^2}{24(1-\mu^2)^2q^4(\sigma_1 + n\tau_1)^4} \quad [7]$$

If the stress range is S and σ_1 and τ_1 be replaced by the average value of S over a half cycle, one obtains using Equations [5], [7], [3], and [1] in [2]

$$\frac{\nu q^2}{2\pi^2 E}\left(1 + \frac{C_0}{\pi}S\right)^2 S^2 - \frac{\pi^4 A}{4q^4\left(1 + \frac{C_0}{\pi}S\right)^4 S^4} = f - kT\log\left(\frac{VZ_p kTN}{h\nu}\right) \quad [8]$$

The left-hand side of Equation [8] is then replaced by what the author calls a "rough approximation" $\log (C_1S)^{1/\alpha}$ leading to the result

$$N = \left(\frac{h\nu}{VZ_p kT}\right)(CS)^{-B/T} \quad [9]$$

where

$$B = \frac{1}{\alpha\, k \log_e 10} \text{ and } C = \frac{C_1}{10^{\alpha f}}$$

This completes the summary of Yokobori's paper.

One notices immediately from Equation [9] that the number of cycles to failure N is given as proportional to the loading frequency and that this conclusion in no way depends on the left side of Equation [8]. It stems from the arbitrary assumption that the frequency factor in Equation [2] is (kT/h), a procedure which has been criticized by Zener.[3] Without denying the possibility of the existence of a dependence on loading frequency (particularly at higher frequencies) the common engineering observation is that there is very little or no frequency dependence for the usual low-frequency fatigue tests. It is clear that this undesirable proportionality would be immediately removed by assuming a crack-nucleation frequency in Equation [2] proportional to the loading frequency ν instead of simply introducing the value (kT/h). The assumption suggested amounts to saying that the number of cracks per unit time exceeding a critical size is proportional to the number of cycles per unit time. Utilizing the foregoing assumption, Equation [8] may be rewritten

$$\varphi(S) = kT\log(VZ_p\lambda N) \quad [10]$$

where λ is the ratio of crack-nucleation frequency to loading frequency. Now if we assume λ and Z_p to be independent of temperature the relation between relative change in number of cycles to failure and relative change in (absolute) temperature for any given stress range S is given by

$$\frac{\delta N}{N\log(VZ_p\lambda N)} = -\frac{\delta T}{T} \quad [11]$$

This is independent of the form of $\varphi(S)$.

[3] "The Role of Statistical Mechanics in Physical Metallurgy," by C. Zener, "Thermodynamics in Physical Metallurgy," American Society for Metals, 1950, p. 23.

A Criterion for the Constancy of the Gage Factor of SR-4 Type Strain Gages

By G. C. KUCZYNSKI,[1] NOTRE DAME, IND.

It has been shown that the criterion of the gage-factor constancy of SR-4 type strain gages is that it is equal to 2 or nearly so. The experimental results agree with this theoretical conclusion.

A STRAIN gage is said to be stable if its output is not appreciably changed by changes in temperature, time, humidity, its previous strain history, and so on. In the present note the problem of the stability of an SR-4 type strain gage with respect to its strain history will be discussed. It is desirable that the gage material could be stretched beyond its yield point without changing its gage factor. In other words, a plot of fractional resistance increment $\Delta R/R$ versus strain ϵ for such a material, for tension followed by compression, should consist of two coincident straight lines, even though the yield point has been exceeded. Advance (also called constantan), the alloy used in the SR-4 gage, is precisely such a material. This exceptional behavior of Advance may be contrasted with that of such metals as copper or platinum, whose gage factors decrease as soon as their yield point is exceeded. This decrease causes a permanent change in resistivity, resulting in a hysteresis loop when wires of these metals are cycled between tensile and compressive stresses. The following reasoning will help us to understand the peculiar gage-factor constancy of the Advance alloy used in the SR-4 strain gages and derive a general criterion for this phenomenon.

After the yield stress is exceeded the wire will be permanently deformed and the permanent strain is $\epsilon - \epsilon_1$ (Fig. 1) where ϵ is the total strain at the stress σ, and ϵ_1 the elastic strain at the same stress. The electrical resistance of the wire increases linearly with elastic strain; i.e., for strains less than the yield strain ϵ_0 (Fig. 1). The resistance R will therefore follow the equation

$$R = R_0(1 + g\epsilon)$$

[1] Professor of Metallurgy, University of Notre Dame.

Manuscript received by ASME Applied Mechanics Division, April 21, 1955.

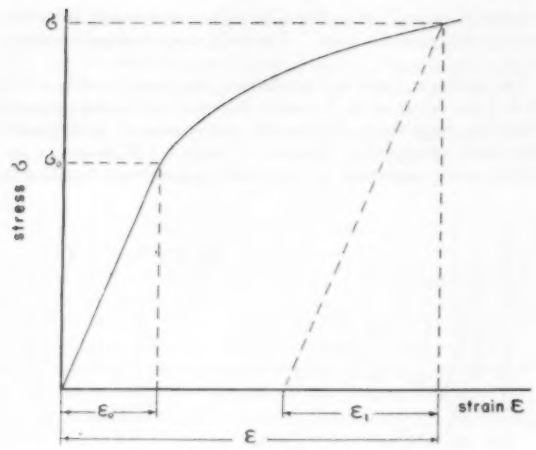

FIG. 1

where R_0 is the resistance at $\epsilon = 0$, and g is the gage factor for elastic strains defined as follows

$$g = \frac{dR}{R_0 d\epsilon}$$

Two effects are responsible for the value of g.[2] First, the change of length and diameter during stretching contributes the quantity $1 + 2\mu$, where μ is Poisson's ratio for the wire material, and then the changes in atomic and electronic structure manifest themselves in a change of specific resistivity

$$\frac{d\rho}{\rho d\epsilon} = a$$

Both effects are additive and can be conveniently summarized in the following equation

$$g = a + 1 + 2\mu$$

Owing to the continuous relaxation of the material during plastic deformation, its specific resistivity should not change greatly. Indeed, most metals when cold-worked at room temperature change their specific resistivity only by a few per cent, and such changes can be neglected here. There is, however, a permanent change in the resistance of a plastically deformed wire caused by its change in shape. This change of resistance, per unit resistance, per unit strain, is given by the term $(1 + 2\mu)$. During plastic flow the volume remains constant at least to a first approximation, and therefore $\mu = 0.5$ for all materials. It follows that the gage factor for the plastic part of the total strain is equal to 2.0. Let us consider now the change of electrical resistance of a wire which is stretched beyond the yield strain ϵ_0. Its resistance increase, $R - R_0$, is composed of two parts, one due to elastic strain ϵ_1 and the other due to plastic strain $(\epsilon - \epsilon_1)$ (Fig. 1). We shall therefore have

$$R - R_0 = R_0[2(\epsilon - \epsilon_1) + g\epsilon_1]$$

and the gage factor observed, due to this deformation is

$$\frac{dR}{R_0 d\epsilon} = 2\left(1 - \frac{d\epsilon_1}{d\epsilon}\right) + g\frac{d\epsilon_1}{d\epsilon} \quad \ldots\ldots\ldots\ldots [1]$$

[2] "Effect of Elastic Strain on the Electric Resistance of Metals," by G. C. Kuczynski, *Physical Review*, vol. 94, 1954, pp. 61–64.

Because Young's modulus does not change appreciably with cold work

$$\epsilon_1 = \frac{\epsilon_0}{\sigma_0}\sigma$$

where σ_0 is the yield stress of the wire material. We can therefore write

$$\frac{d\epsilon_1}{d\epsilon} = \frac{\epsilon_0}{\sigma_0}\frac{d\sigma}{d\epsilon}$$

which, if introduced into Equation [1] and after slight rearrangement of terms yields

$$\frac{dR}{R_0 d\epsilon} = 2 + \frac{\epsilon_0}{\sigma_0}\frac{d\sigma}{d\epsilon}(g - 2) \quad \ldots\ldots\ldots\ldots [2]$$

This equation is quite general and represents the gage factor in elastic as well as the plastic range. Indeed, for purely elastic deformation

$$\frac{d\sigma}{d\epsilon} = \frac{\sigma_0}{\epsilon_0} \quad \text{and} \quad \frac{dR}{R_0 d\epsilon} = g$$

For plastically deformed metals $(d\sigma/d\epsilon)$ is not constant but some function of ϵ and therefore the gage factor changes with strain unless $g = 2$.

Now it is clear that only for metals and alloys with a gage factor of 2, and Advance is one of them, will the resistance-strain curve remain linear even after the yield point is exceeded (Fig. 2). For

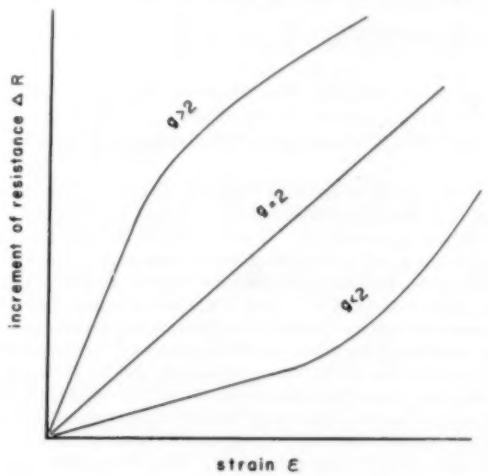

FIG. 2

metals and alloys having gage factors larger or smaller than 2, there will be lesser or greater departures from linearity, depending on the value of $(d\sigma)/(d\epsilon)$. If the stress-strain curve is steep even above the yield stress, the change in $(dR)/(R_0 d\epsilon)$ at the yield point may only be very slight no matter what the value of g. However, in a good many cases the stress-strain curve beyond the yield point is comparatively flat and therefore sharp changes in $(dR)/(R_0 d\epsilon)$ near the yield point should be expected.

Excellent experimental support for the foregoing theoretical conclusions is supplied by the work of Kammer and Pardue,[3] who

[3] "Electric Resistance Changes of Fine Wires During Elastic and Plastic Strains," by E. W. Kammer and T. E. Pardue, Proceedings of the Society for Experimental Stress Analysis, vol. 7, no. 1, 1949, pp. 7–20.

on the basis of their results come to similar conclusions. They investigated the change of resistance as a function of strain of commercial metals and alloys such as Tophet A and C, Nichrome V, iron, and platinum. All these materials have gage factors exceeding 2. Their ΔR versus ϵ curves all resemble the upper curve of Fig. 2. After the yield point is exceeded the gage factors decrease to 2. On the other hand, the curve for Manganin, whose gage factor $g = 0.8$, resembles the lower curve of Fig. 2; i.e., its gage factor increases to 2 in the plastic region.

ACKNOWLEDGMENT

The interest of Baldwin-Lima-Hamilton Corporation in this research is gratefully acknowledged.

New Numerical Results of the Theory of Buckling of Sandwich Cylinders

BY A. C. ERINGEN,[1] LAFAYETTE, IND.

AN IBM card program calculator has been used to obtain numerical results from the theory developed in an earlier paper.[2] Buckling stress σ_{cr} of a sandwich cylinder under axial compressive load is given by

$$\sigma_{cr} = \frac{1}{12} E_f(1-\nu_f^2)^{-1}\tau_f^2 + \frac{1}{2} E_f(\alpha_1^{-2}+\alpha_2^{-2}) + (G_c/2\tau_f)[S_{1m}(\alpha_1)+S_{2m}(\alpha_2)] \mp \left\{\left[\frac{1}{2}E_f(\alpha_1^{-2}-\alpha_2^{-2}) + (G_c/2\tau_f)[S_{1m}(\alpha_1)-S_{2m}(\alpha_2)]\right]^2 + (G_c/\tau_f)^2 S_{1m}(\alpha_2) S_{2m}(\alpha_1)\right\}^{1/2} \quad \ldots\ldots [1]$$

where E_f, ν_f are modulus of elasticity, Poisson's ratio for the faces, G_c is the shear modulus of the core, and $\tau_f = m\pi t_f/L$, $\tau = m\pi t/L$, and $\alpha_i = m\pi a_i/L$. Here t_f, t, L are the face thickness, core thickness, and the length of the cylinder, and $m = 1, 2, \ldots$. Functions S_{im} are given by Equations [33] and [47] of the paper.[2]

In Table 1 and in Figs. 1 and 2, two sets of minimum critical stresses, σ_{cr}^+ and σ_{cr}^-, are given. They are obtained by numerically minimizing Equation [1] with respect to τ_f for fixed values of the parameter τ. In Table 1 there are also shown values of τ_f for which these minimums occur. Of the two critical stresses, σ_{cr}^+ corresponds to Equation [1] with (+) sign before the radical and σ_{cr}^- to that with the (—) sign. The latter stress σ_{cr}^- was not calculated in the previous paper. Also, the present numerical results on σ_{cr}^+ were found to differ considerably from the ones contained in the paper. The early computations contained error.

Physically, σ_{cr}^+ and σ_{cr}^- produce ripple type of buckling with both faces deformed in the same direction and in the opposite direction, respectively. These are the analogs of antisymmetrical and symmetrical buckling of beams. However, completely antisymmetrical or completely symmetrical buckling is

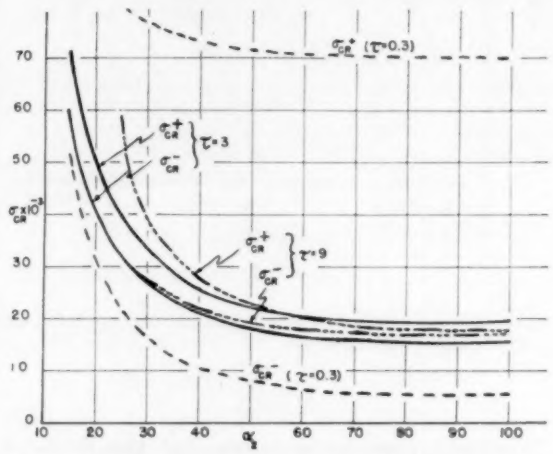

FIG. 1 MINIMUM BUCKLING STRESS FOR 75S-T FACES AND CCA CORE WITH E = 2000 PSI (WITH YIELD CORRECTION)

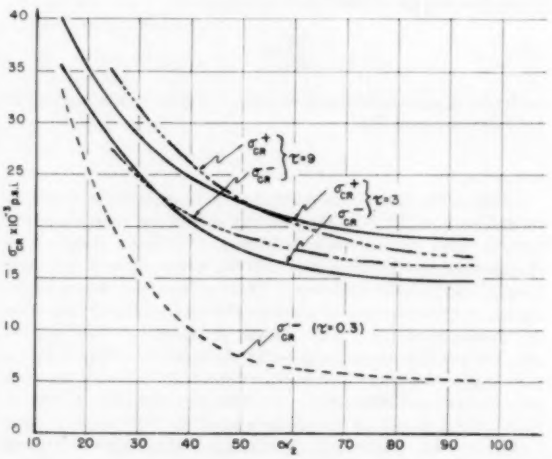

FIG. 2 MINIMUM BUCKLING STRESS FOR 24S-T ALCLAD FACES AND CCA CORE WITH E_c = 2000 PSI (WITH YIELD CORRECTION)

[1] Associate Professor of Engineering Sciences, Purdue University.

[2] "Buckling of a Sandwich Cylinder Under Uniform Axial Compressive Load," by A. C. Eringen, JOURNAL OF APPLIED MECHANICS, Trans. ASME, vol. 73, 1951, pp. 195–202.

Manuscript received by ASME Applied Mechanics Division, September 24, 1954.

TABLE 1 MINIMUM BUCKLING STRESSES FOR 75S-T AND 24S-T ALCLAD FACES AND CCA CORE WITH E_c = 2000 PSI (WITH AND WITHOUT YIELD CORRECTIONS)

		α_1 =	15			25			40			100		
		τ =	0.3	3	9	0.3	3	9	0.3	3	9	0.3	3	9
75S-T	Elastic	σ_{cr}^+	121790	91300	310000	91100	39800	58600	80700	26000	27900	75300	19700	17900
		τ_f	0.16	0.08	0.07	0.16	0.08	0.08	0.16	0.08	0.08	0.17	0.08	0.07
		σ_{cr}^-	51800	61800	61500	22350	31900	32400	10900	21300	22400	5380	15500	17200
		τ_f	0.04	0.08	0.07	0.06	0.07	0.08	0.03	0.07	0.07	0.03	0.07	0.07
	Yield correction	σ_{cr}^+	...	71600	...	75000	39800	58600	73000	26000	27900	70400	19700	17900
		σ_{cr}^-	51800	59200	58000	22350	31900	32400	10900	21300	22400	5380	15500	17200
24S-T Alclad	Yield correction	σ_{cr}^+	...	40200	...	...	32000	35100	...	24700	26300	...	19000	17300
		σ_{cr}^-	33300	35400	...	20300	28600	27800	10200	20100	21300	5200	14900	16700

not possible except for the case of cylinders having infinite radii (i.e., flat columns).

The von Karman-Engesser reduced modulus curves given by Fig. 16 of the paper[2] are used to modify stresses beyond the proportional limit.

Finally, a few errors were discovered in the original manuscript: In Equations [15], [20], [21] m should have the range ($m = 0, 1, 2, \ldots$)

$$w_0(r) = \frac{1}{2}\,[W_m(r)]_{m=0}$$

should be inserted after Equation [15]. In Equation [27], $D_i^j(\alpha_1, \alpha_2)$ should be replaced by $D_i^j(\alpha_2, \alpha_1)$; $(-)^k$ should be placed in front of $\sigma_r(a_k, z)$ in Equation [30] and in front of $R_{im}(\alpha_k)$ in Equation [33]. Incidentally, in σ_z of Equation [42] inside of the radical G_o factors were missing. Equation [1] of this note contains the corrected form of this radical. Further, in Equation [47] $2R_{2m}$ and $2T_{2m}$ (α_1) should replace R_{1m} and T_{1m} (α_1) and $2R_{1m}$, and $2T_{1m}$ (α_2) should replace R_{2m} and T_{2m} (α_2). Finally, T_{1m} (α_2), T_{2m} (α_1) and Δ_1 of Equation [47] should read

$$T_{1m}(\alpha_1) = T_{2m}(\alpha_2) = \Delta_1^{-1}(\cosh 2\tau - 4\tau^2\gamma^{-2} - 1)$$

$$\Delta_1 = \cosh 2\tau - 1 - 2\tau^2\gamma^{-2}$$

respectively.

The author is indebted to J. W. Dunkin for carrying out the computations in the IBM card program calculator.

The Complex-Variable Approach to Stress Singularities—II

By M. L. Williams,[1] Pasadena, Calif.

In a recent note[2] Dr. Huth suggested the application of complex variable techniques as an alternate method for treating the problem of stress singularities at the vertex of an infinite wedge subject to extension in its plane. The method is indeed well suited to this problem and furnishes a concise representation of the phenomenon. In applying the technique to one of the specific problems solved by the more common approach,[3] he has, however, been led to the conclusion that the solutions are not completely compatible. Since apparently this point has not yet been resolved in the literature, it is pertinent to show that the results as obtained by the two methods are identical.

Using the previous notation,[3] the stresses and displacements can be represented in terms of two analytic functions $\Phi(z)$ and $\Psi(z)$ such that

$$\sigma_\theta - i\tau_{r\theta} = \Phi(z) + \overline{\Phi}(\bar{z}) + (\bar{z}/z)\,[z\,\overline{\Phi}'(\bar{z}) + \overline{\Psi}(\bar{z})] \quad \ldots [1]$$

$$2\mu(u_x + iv_x) = k\,\Phi(z) - \overline{\Phi}(\bar{z}) - z\,\Phi'(\bar{z}) - \overline{\Psi}(\bar{z}) \quad \ldots [2]$$

For the case of one radial edge clamped and the other edge free, Huth has transformed the wedge to the half plane and defined $\overline{\Psi}$ such that Φ can be continued analytically across the clamped edge. The condition that the other edge be free results in the cut condition along the negative real axis, Equation [6].[2]

Huth then assumes solutions of the form $\Phi(w) = (a + ib)(-w)^n$ where a, b, and n are real and, after obtaining the eigenequation, finds agreement with the earlier results;[3] but then assuming $\Phi(w) = (a + ib)(-w)^{\gamma+i\beta}$ where a, b, γ, and β are real, is led to the inconsistency that complex roots $\gamma + i\beta$, are inadmissible as postulated previously.[3]

Compatibility of Solutions

The first purpose of this note is to state that functions of the form

$$\Phi(w) = (a + ib)(-w)^{\gamma+i\beta} + (c + id)(-w)^{\gamma-i\beta}$$

resolve the inconsistency and lead to the same eigenequation[3] if λ is identified with $\gamma + i\beta$.

As a second point, it may be mentioned that as the conformal mapping function from the wedge to half plane is a power variation, the use of analytic continuation is not necessary, but one can obtain the proper results by using Equations [1] and [2] and letting

$$\Phi(z) = A'z^\lambda + B'z^{\bar{\lambda}} \quad \ldots [3]$$

$$\Psi(z) = C'z^\lambda + D'z^{\bar{\lambda}} \quad \ldots [4]$$

where $z = re^{i\theta}$, substituting directly into Equations [1] and [2], and requiring $u_x(r, 0) + i\,v_x(r, 0) = 0$ and $\sigma_\theta(r, \alpha) - i\,\tau_{r\theta}(r, \alpha) = 0$. Four complex homogeneous equations in the four (complex) constants A', B', C', and D' are obtained by investigating solutions independent of r^λ and $r^{\bar{\lambda}}$. The use of analytical continuation through an edge with a homogeneous boundary condition merely amounts to providing a simple and convenient method for relating C' and D' to A' and B'. It should be noted that without providing for the possibility of functions varying with $z^{\bar{\lambda}}$ in Equations [3] and [4], the indeterminacy in the eigenvalues observed by Huth results.

Turning now to a specific illustration, consider again the clamped-free case using analytical continuation and Huth's expression (Equation [5]) that

$$\Psi(w) = -\Phi(w) + k\,\overline{\Phi(\bar{w})} - \frac{\pi}{\alpha}\,w\,\Phi'(w) \quad \ldots [5]$$

which when substituted into Equation [1] after using the transformation $w = z^{\pi/\alpha}$, with $w \equiv \rho e^{i\delta}$, gives

$$\sigma_\theta - i\,\tau_{r\theta} = \Phi(w) + ke^{-2i\alpha\delta/\pi}\,\overline{\Phi}(\bar{w}) + (1 - e^{-2i\alpha\delta/\pi})\left[\overline{\Phi}(\bar{w}) + \frac{\pi}{\alpha}\,\bar{w}\,\overline{\Phi}'(\bar{w})\right] \quad \ldots [6]$$

and

$$2\mu(u_x + iv_x) = k[\Phi(w) - \Phi(\bar{w})] + (1 - e^{2i\alpha\delta/\pi})\,\frac{\pi}{\alpha}\,\bar{w}\,\overline{\Phi}'(\bar{w}) \quad \ldots [7]$$

It is observed that $u_x + iv_x = 0$ at the fixed edge, $\delta = 0$, as was required.

Upon setting

$$\Phi(w) = A\,w^\lambda + B\,w^{\bar{\lambda}} \quad \ldots [8]$$

and substituting into Equation [6]

$$\sigma_\theta - i\tau_{r\theta} = w^\lambda\left\{[1 + ke^{-2i(\alpha+\lambda\pi)\delta/\pi}]\,A + (1 - e^{-2i\alpha\delta/\pi})\,[(\lambda\pi/\alpha) + 1]e^{-2i\lambda\delta}\,\overline{B}\right\} + w^{\bar{\lambda}}\left\{[1 + ke^{-2i(\alpha+\bar{\lambda}\pi)\delta/\pi}]\,B + (1 - e^{-2i\alpha\delta/\pi})\,[(\bar{\lambda}\pi/\alpha) + 1]\,e^{-2i\bar{\lambda}\delta}\,\overline{A}\right\}$$

---

[1] Associate Professor of Aeronautics, California Institute of Technology.

[2] "The Complex-Variable Approach to Stress Singularities," by J. H. Huth, Journal of Applied Mechanics, Trans. ASME, vol. 75, 1953, p. 561.

[3] "Stress Singularities Resulting From Various Boundary Conditions in Angular Corners of Plates in Extension," by M. L. Williams, Journal of Applied Mechanics, Trans. ASME, vol. 74, 1952, p. 526.

Manuscript received by ASME Applied Mechanics Division, October 12, 1954.

Evaluating at $\delta = \pi$, $(\theta = \alpha)$ for zero stress on the unloaded edge

$$0 = \rho^{\lambda} e^{i\lambda\pi} \{[1 + ke^{-2i(\alpha+\lambda\pi)}] A + [(\lambda\pi/\alpha) + 1] (1 - e^{-2i\alpha}) e^{-2i\lambda\pi} \bar{B}\} + \rho^{\bar{\lambda}} e^{-i\bar{\lambda}\pi} \{[1 + ke^{-2i(\alpha+\bar{\lambda}\pi)}] B + [(\bar{\lambda}\pi/\alpha) + 1](1 - e^{-2i\alpha}) e^{-2i\bar{\lambda}\pi} \bar{A}\}$$

whereupon, requiring independence of ρ, the determinant of the two (complex) homogeneous equations yields the previous eigenequation[3]

$$\sin^2 (\alpha + \lambda\pi) = \frac{(1 + k)^2}{4k} - \frac{(\alpha + \lambda\pi)^2 \sin^2 \alpha}{k \alpha^2} \quad \ldots\ldots [9]$$

which holds for complex as well as real λ. There results an infinite number of eigenvalues from which an infinite set of eigenfunctions can be generated; the lowest controls a possible stress singularity.[3]

While the main emphasis has been on the stress singularities, a third point should be mentioned. In contrast with the conclusion drawn in the last paragraph of Dr. Huth's paper, the set of functions not only can be used to analyze a finite sector but indeed several applications have been published for sector plates in extension[4] and the closely related problem of bending.[5, 6] From the standpoint of mathematical precision, however, the completeness of the set of functions has not, to the author's knowledge, been established. With standard methods of proof being complicated by the nonorthogonality of the functions it may be that the Fourier integral method used by Brahtz could be applied to guarantee the exactness of the solution in the limit.

Stress-Concentration Factors in Shafts Containing Transverse Holes and Subjected to Bending

By H. ŌKUBO[1] and K. TAKAI,[2] NAGOYA, JAPAN

THE peak stresses in shafts containing transverse holes and subjected to torsion were presented in a previous paper by means of the electroplating method.[3]

The stress concentration arising from bending has been investigated in the same manner and the results are given here. Test pieces used are 15-mm diam with transverse holes, the diameters of which vary from 1.01 mm to 5.06 mm. The stress-concentration factors both in the bore m and at the edge of the hole n, Fig. 1, were obtained for the mentioned values of the hole diameter. Their values based on the nominal stress calculated using the full section of the shaft are shown in Fig. 2, where open circles give the values for the bore and filled circles for the edge of the hole.

With decrease of the hole diameter, the two curves of stress-concentration factors both approach the theoretical value 3 for an infinitely small hole in a tension field. The results of various previous investigators derived from different techniques, such as photoelasticity, mechanical strain gages, and plaster models, are also shown in the same figure.[4] Their results all indicate that there is a comparatively rapid fall in the value of the stress-concentration factor as the hole diameter is increased from zero.

It is interesting, however, to note that the results of Peterson and Wahl are in agreement with those herein obtained within the discrepancy of several per cent. Furthermore, the curve connecting their experimental points runs almost parallel to the present one, as is indicated by the dashed line in Fig. 2.

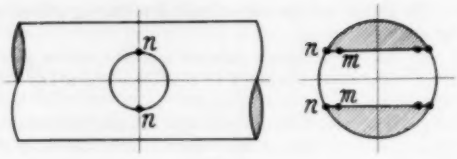

FIG. 1

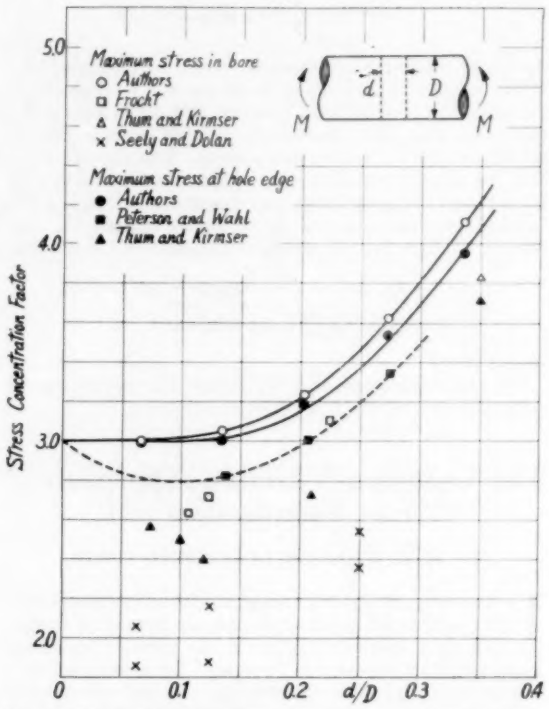

FIG. 2 STRESS-CONCENTRATION FACTORS FOR SHAFTS WITH TRANSVERSE HOLES, SUBJECTED TO BENDING

[4] "Stress Distribution in a Reentrant Corner," by J. H. A. Brahtz, Trans. ASME, vol. 55, paper APM-55-6, 1933.

[5] "Some Problems in the Bending of Thin Plates," by G. F. Carrier and F. S. Shaw, Proceeding of the Symposium on Applied Mathematics, vol. 3, 1950, p. 125.

[6] "Surface Stress Singularities From Various Boundary Conditions in Angular Corners of Plates Under Bending," by M. L. Williams, Proceedings of First U. S. National Congress of Applied Mechanics, 1951, pp. 1–11.

[1] Professor of Applied Mechanics, Nagoya University.

[2] Graduate Student, Nagoya University.

[3] "Stress-Concentration Factors in Shafts With Transverse Holes as Found by the Electroplating Method," by H. Ōkubo and S. Satō, JOURNAL OF APPLIED MECHANICS, Trans. ASME, vol. 77, 1955, p. 193.

[4] "Stress Concentration at Fillets, Holes and Keyways as Found by the Plaster-Model Method," by F. B. Seely and T. J. Dolan, University of Illinois Engng. Experimental Station Bulletin No. 276, 1935.

"Two- and Three-Dimensional Cases of Stress Concentration, and Comparison With Fatigue Tests," by R. E. Peterson and A. M. Wahl, JOURNAL OF APPLIED MECHANICS, Trans. ASME, vol. 58, 1936, p. A-15.

"Tension, Bending and Torsion of Bars Containing a Transverse Hole, and Combinations Thereof," by A. Thum and W. Kirmser, *VDI-Forschungaheft*, No. 419, March–April, 1943.

"Stresses in Bent Circular Shafts With Transverse Holes," by M. M. Frocht, JOURNAL OF APPLIED MECHANICS, Trans. ASME, vol. 66, 1944, p. A-10.

Manuscript received by ASME Applied Mechanics Division, May 9, 1955.

The Bauschinger Effect on Columns

By P. C. PARIS,[1] BETHLEHEM, PA.

Earthquakes or the passing shock wave of an atomic blast may cause tensile yield in members before collapse in compression (1).[2] In order to examine the effect of this reversal, the reduction of compressive properties of structural steel are analyzed after a variety of tensile prestrains and these properties are applied to calculate collapse loads. The calculated maximum loads are then compared with test results to determine a practical method whereby they may be predicted.

Material-Properties Tests

THREE prestrains were chosen to examine the variation of compressive properties from a prestrain just greater than initial yield strain to a prestrain a little less than the strain at which strain hardening commences. The third prestrain was chosen to be a mean of the other prestrains.

The tensile prestrain was applied by putting a 24-in-long, $^1/_8$-in-square bar in the tension grips of a universal testing machine. A 2-in. Metzger strain gage was applied to the center of length of the bar. Its maximum strain reading in tension was recorded as the prestrain.

Compressive properties were examined after prestraining by testing the center portion of the bar, using the same strain gage. This center portion (4 in. long) was cut from the prestrained bar and compressed between surface plates. The compressive properties for each level of prestrain are recorded in Fig. 1 to compare the gradient reduction of these properties.

Column Tests

Column specimens were prestrained in the same manner as in the material-properties tests. The columns were then cut with the gaged portion from the prestrain application comprising the central portion of the column. Cylindrical end fixtures were used to attain a pin-end condition [these fixtures are described in the author's previous works (2, 3)].

A variety of lengths was chosen for the column tests so as to cover the usual design L/r-values for columns (L/r from 21 to 126). Results of column tests are shown in Fig. 2.

[1] Instructor of Mechanics, Lehigh University.

[2] Numbers in parentheses refer to the Bibliography at the end of the note.

Manuscript received by ASME Applied Mechanics Division, December 8, 1954.

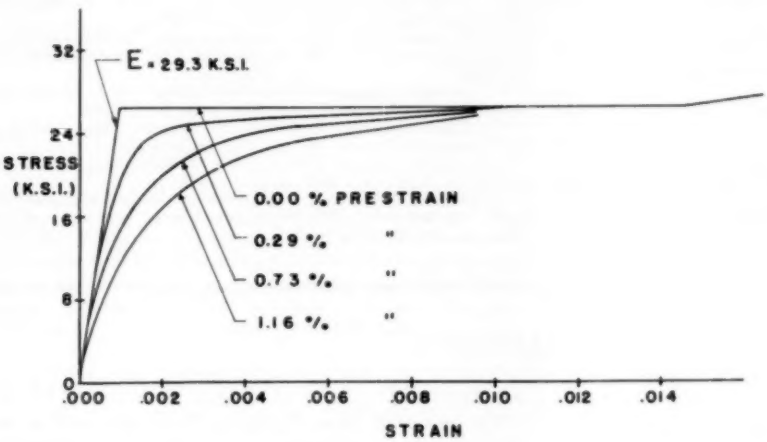

Fig. 1 Compressive Properties of Annealed A-7 Steel With a Given Per Cent of Tensile Prestrain Found by Ordinary Material-Properties Tests

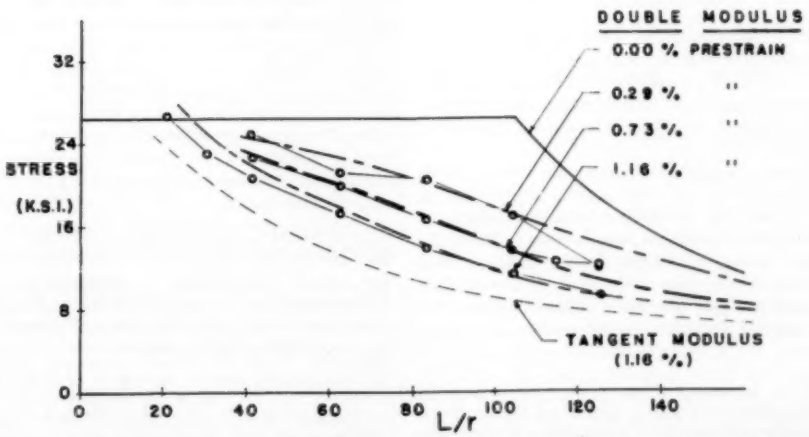

Fig. 2 Column Curves Comparing Column Theories With Experimental Data on Previously Yielded Members

Theory and Comparison With Tests

The Engesser-Shanley theory and the von Karman theory (4), i.e. the tangent modulus and double modulus formulas, respectively, have been discussed at length and are well known as criteria of column strength for materials of variable modulus (5). The conclusion of these discussions is that a column begins to deflect upon reaching the tangent modulus load and reaches its ultimate load between the tangent modulus and the double modulus loads. No simple theory for determining the exact ultimate load has been devised, though a complex method for finding it has been derived (6).

The question of where the ultimate load lies with respect to the tangent modulus and double modulus loads becomes of interest on inspecting Fig. 2. The ultimate loads recorded in the column tests lie close to the double modulus values. Where the test data show scatter, the mean values also seem to indicate correlation with the double modulus theory. The cause of the scatter probably was nonuniform yielding during prestraining, and thus would cause scatter to be both positive and negative. Therefore the mean value should be close to the correct criterion. The data exhibited ultimate loads which seem to correspond to the double modulus theory.

Duberg and Wilder (7) have shown for columns of materials without a well-defined yield point (which do not have a sharp "knee" in their stress-strain curve) that the compressive ultimate load lies considerably above the tangent modulus load. Their conclusion seems well exhibited in the tests recorded in Fig. 2, since the ultimate loads are close to the double modulus curves.

Conclusions

1 Previous tensile yield considerably reduces the buckling properties of steel columns (sometimes greater than 50 per cent).

2 The buckling loads of prestrained columns may be sufficiently predicted from ordinary materials-properties tests of material with the same prestrain history.

3 The tangent-modulus column theory is a conservative criterion for predicting the collapse loads of prestrained structural-steel columns. (Test data show collapse loads closer to the double modulus theory, but scatter of results makes it an unreliable criterion.)

Acknowledgment

The author wishes to express his appreciation for the patient guidance of Dr. J. A. Van den Broek. The program was initiated upon the suggestion of Dr. B. G. Johnston, who also gave the benefit of his experience and time to laying out the initial test program. Thanks also are due to Dr. T. A. Hunter, Dr. B. Thürlimann, and Mr. John Rowley for many helpful suggestions.

The test program was initiated in the Engineering Mechanics Laboratories of the University of Michigan, and the concluding tests were performed in Fritz Engineering Laboratory of Lehigh University.

BIBLIOGRAPHY

1 "Structural Steel Members and Frames," by B. G. Johnston, Symposium on Earthquake and Blast Effects on Structures, University of California, June, 1952.

2 "Testing of Columns With Uniformly Distributed Transverse Loads," by P. C. Paris, *The Engineering Journal* (Canada), vol. 37, 1954, pp. 945–949.

3 "Limit Design of Columns," by P. C. Paris, *Journal of the Aeronautical Sciences*, vol. 21, 1954, pp. 43–49.

4 "Untersuchungen über Knickfestigkeit. Mitteilungen über Forschungsarbeiten," by Th. von Karman, VDI Forschungsheft No. 81, 1910.

5 "Buckling Strength of Metal Structures," by F. Bleich, McGraw-Hill Book Company, Inc., New York, N. Y., 1952.

6 "Inelastic Column Buckling," by Tung-Hua Lin, *Journal of the Aeronautical Sciences*, vol. 17, 1950, pp. 159–172.

7 "Inelastic Column Behavior," by J. E. Duberg and T. W. Wilder III, NACA TN 2267, January, 1951.

8 "Column Formulas for Materials of Variable Modulus," by J. A. Van den Broek, *The Engineering Journal* (Canada), vol. 28, 1945, pp. 772–777, 783.

Discussion

Displacements in an Elastic-Plastic Cylindrical Shell[1]

Eugene Levin.[2] The difficulties involved in solving an elastic-plastic problem are well known, and hence any such solution represents an important addition to the state of the art. The present contribution is particularly welcome since information concerning the displacements is provided for a problem of great practical interest.

Although the paper was primarily concerned with analysis, it should be noted that the results also may be used for design purposes. In particular, Fig. 7, which relates the central displacement to the dimensionless length, may be used to determine the spacing of the reinforcing rings. If the cross-sectional dimensions and physical properties of the shell are known, then the equations preceding Fig. 7 provide a relation between the reinforcement spacing and the maximum deformation which may be tolerated.

The assumption of an idealized sandwich cross section was quite convenient, but it would appear that the description of this cross section is incomplete. In the example considered, the maximum elastic dimensionless load (Equation [18]) was found to be

$$P^* = \frac{\sqrt{3}}{2}$$

Using Equation [6] to relate this result to the actual load p, yields

$$p = 2\sqrt{3}\,\frac{k}{a}\,h$$

Thus it would appear that some knowledge of the thickness h of the "indefinitely thin" outer faces is required in order to perform any actual computation. A particular computation of great interest would be a comparison of this maximum elastic load with the critical buckling load of a long cylindrical shell. This buckling load is given by the formula

$$p_{cr} = \frac{E}{4(1-\nu^2)}\left(\frac{H}{a}\right)^3$$

where H is the equivalent uniform thickness of the shell.

[1] By P. G. Hodge, Jr., published in the March, 1956, issue of the Journal of Applied Mechanics, Trans. ASME, vol. 78, pp. 73–79.

[2] Mathematical Analysis Group, Computer Systems Division, The Ramo-Wooldridge Corporation, Los Angeles, Calif.

Author's Closure

The author would like to thank Dr. Levin for his kind words and interesting comments and questions. If the results are to be used for an actual sandwich shell, then the values of h and t will, of course, be known. On the other hand, if the results are to be applied as an approximation to a uniform shell, it appears reasonable to relate the dimensions so that the maximum pure moment and maximum direct stress are the same. Thus if H is the thickness of the uniform shell and K the yield stress in shear

$$M_0 = (1/2)\,KH^2 = 4\,kht$$

$$N_0 = 2\,KH = 4kh$$

Obviously, then, the equivalent sandwich dimensions are

$$kh = KH/2, \quad t = H/4$$

Therefore, the maximum elastic load for the uniform shell is approximately

$$p^* = \sqrt{3}\,KH/a$$

A comparison of this with the critical buckling load shows that

$$p_{cr}/p^* = \frac{(E/K)\,(H/a)^2}{4\sqrt{3}\,(1-\nu^2)}$$

As an example, if

$$E = 30 \times 10^6$$
$$K = 2 \times 10^4$$
$$\nu = 0.3$$

then

$$p_{cr}/p^* = 238\,(H/a)^2$$

In other words, if H/a is less than 0.065, the shell will buckle before any part of it becomes plastic, while if H/a is greater than 0.065 it will become at least partially plastic at a lower load. For shorter shells the equation for p_{cr} must be modified to account for the built-in ends, while the value of p^* is independent of length. Therefore the shorter a shell is, the smaller is the value of H/a at which plasticity will occur before buckling.

A Matrix Solution for the Vibration Mode of Nonuniform Disks[1]

S. H. Crandall.[2] In extending the methods of Myklestad[3] and Thomson[4] to organize the more involved computations for rotating-disk structures, the author has made a valuable contribution. The separation of the elastic behavior into a primary bending stiffness in the matrix E_k and the secondary stiffnesses due to centrifugal forces and membrane action represented in the matrix L_k is interesting.

Although for simplicity of exposition the author has introduced the summary matrix H, the writer would suppose that in actual calculation one would obtain the X_k in sequence according to Equation [53] of the paper. This would provide a picture of the appropriate mode shape which would be very useful in selecting the next trial ω. In similar computations with the Holzer and Myklestad processes the writer has found it efficient[5] to apply Rayleigh's principle to the approximate mode shape obtained from one calculation in order to get the next trial frequency.

It occurs to the writer that when the matrixes E_k for a particular disk have been obtained, they may be used for other design calculations besides those of natural frequencies. For instance, if when the disk is rotating at speed Ω its axle is tipped at an angular velocity $\dot{\gamma}$ it will be subjected to a gyroscopic force field $2\dot{\gamma}\Omega r\cos(\phi - \Omega t)$ per unit mass. The resulting deformations and stresses could be computed by using the matrixes E_k and L_k for $n = 1$ and $\omega = \Omega$ and the recurrence formula

$$X_{k+1} = E_k(L_kX_k + G_k)$$

where $G_k = (0, 0, 0, 2\mu_k\dot{\gamma}\Omega r_k{}^4)$. For this kind of computation a trial-and-error process would not be necessary but two calculations across the disk would be required. Thus, if the disk were free at the outer edge, the solution would be that linear combination of the results for $X_1 = (1, 0, 0, 0)$ and $X_2 = (0, 1, 0, 0)$ which satisfied the inner-edge boundary conditions.

Author's Closure

Professor Crandall has aptly pointed out that convergence of the successive frequency trials can be speeded by using Rayleigh's principle on the deflection shape generated at any intermediate guess. It should be noted that the deflection shape cannot be calculated directly in the course of calculating the residual determinant. When the calculation is initiated, the relationship between the deflection and slope at the free outer edge (for instance) is unknown. Therefore the calculation is performed in the form

$$\begin{bmatrix} h_{11} & h_{12} \\ h_{21} & h_{22} \\ h_{31} & h_{32} \\ h_{41} & h_{42} \end{bmatrix} = L_KE_{K-1}L_{K-1}\ldots E_kL_k\ldots E_1L_1 \begin{bmatrix} 1 & 0 \\ 0 & 1 \\ 0 & 0 \\ 0 & 0 \end{bmatrix}$$

After testing the residual determinant for zero

$$\epsilon = \begin{vmatrix} h_{11} & h_{12} \\ h_{21} & h_{22} \end{vmatrix} \to 0$$

the actual state of deflection, slope, moment, and force at any intermediate station may be calculated by computing

$$X_k = E_kL_k\ldots E_1L_1 \begin{bmatrix} 1 \\ -h_{11}/h_{12} \\ 0 \\ 0 \end{bmatrix}$$

This would give at the clamped inner edge

$$X_K = \begin{bmatrix} 0 \\ (h_{21}h_{12} - h_{11}h_{22})/h_{12} \\ m_Kr_K{}^2 \\ v_Kr_K{}^3 \end{bmatrix}$$

Unless the residual determinant is zero, the slope at the inner edge will be nonzero and application of the Rayleigh principle must take into account this nonsatisfaction of the boundary conditions.

Professor Crandall points out an interesting extension in the application of the matrix treatment of disk problems in applying it to the problem of gyroscopic moments. The author has been working on a similar extension to the problem of steady-state,

[1] By F. F. Ehrich, published in the March, 1956, issue of the Journal of Applied Mechanics, Trans. ASME, vol. 78, pp. 109–115.

[2] Associate Professor of Mechanical Engineering, Massachusetts Institute of Technology, Cambridge, Mass. Mem. ASME.

[3] "New Method of Calculating Natural Modes of Uncoupled Bending Vibrations," by N. O. Myklestad, *Journal of the Aeronautical Sciences*, vol. 11, 1944, pp. 153–162.

[4] "Matrix Solution for the Vibration of Nonuniform Beams," by W. T. Thomson, Journal of Applied Mechanics, Trans. ASME, vol. 72, 1950, pp. 337–339.

[5] "Iterative Procedures Related to Relaxation Methods for Eigenvalue Problems," by S. H. Crandall, Proceedings of the Royal Society of London, England, series A, vol. 207, 1951, pp. 416–423.

axisymmetric pressure forces acting on disks acting in combination with the stiffening effect of disk rotation. The recurrence formula takes the form (with $\omega = 0$ and $n = 0$)

$$X_{K+1} = E_K(L_K X_K + P_K)$$

where $P_k = (0,0,0,p_k r_k^2)$ where p_k is the pressure force acting at any loading circumference.

In addition to the torsion calculation of Holzer and the beam or shaft calculation of Myklestad,[2] the author has found that the system of successive multiplication of elasticity and loading matrices is a very efficient format for formulation and calculation of a wide variety of one-dimensional problems in elasticity as well as two-dimensional problems reducible to one-dimensional form by separation of variables.

The Stress Distribution in a Strip Loaded in Tension by Means of a Central Pin[1]

G. Mesmer.[2] This contribution to the question of the stresses in a pin-loaded strip is very interesting because of the unusual simplification of the problem; some of its results are encouraging for similar further calculations of loaded pins. Without mentioning it explicitly, the author's calculations are based upon the assumption that the pin (disk, loaded at its center) has the same thickness and equal elastic behavior as the strip, and that the front side of the disk, the pressure side, is rigidly connected with the inner surface of the hole in the strip. This is equivalent to assuming an infinitely high coefficient of friction between disk and hole. As the results are in agreement with some experimental data of similar cases for small values of $\lambda = d_i/d_0$, these assumptions seem to be reasonable, when the relatively wide strip does not deform very much. For larger values of λ, however, this is not valid, and one must assume certain relative tangential displacements between the deformable strip and the more rigid disk. In this case, the pressure distribution on the front half of of the disk changes; its maximum flattens or may even shift to the sides, and the "open slot" behind the disk becomes shorter.

As the directions of the principal stresses σ_1 and σ_2 are only approximately tangential and radial to the pin, their numerical values are not exactly the values of the pressure and the circumferential stress. The integral of $\sigma_1\, dy$ in the horizontal cross section is not necessarily equal to the load but must be larger. This effect may be partly responsible for the errors found by the author.

The writer hesitates to use the expression "exact" solution of a mechanical problem for solutions of this type. Most of them are exact only in the sense that they fulfill the two-dimensional equations for equilibrium and compatibility, assuming certain boundary conditions. These assumptions, however, are quite arbitrary and are, in fact, only approximations of the real physical problem, convenient for a rigorous mathematical treatment.

Author's Closure

The author appreciates the interest of Professor G. Mesmer and his valuable discussion of the paper. As is pointed out, the paper assumes that the diameter of the hole does not exceed the half width of the strip ($\lambda = a/b \leq 0.5$). The reason for this restriction is that the convergence of the series expressing the stress function ceases to be good for values of λ larger than 0.5 and that, in practice, λ would rarely be greater than 0.5.

[1] By P. S. Theocaris, published in the March, 1956, issue of the Journal of Applied Mechanics, Trans. ASME, vol. 78, pp. 85–90.

[2] Head, Department of Applied Mechanics, Washington University, St. Louis, Mo.

It may be of interest to add that experimental data obtained by the author using the methods of photoelasticity and the conducting-paper analogy are in close agreement with the results obtained analytically in the paper.[3] Some discrepancies occurring are always in the neighborhood of the hole's boundary where the assumptions of the theory may not be well justified. They can, however, be explained by the difficulty of making optical measurements very close to the rim of the hole due to the imperfection of the contact between the strip and the pin and the very narrow region in the vicinity of the rim of the hole which is hidden by the deformed pin. It is, therefore, not possible to determine experimentally the stresses at the rim exactly because in this region the stresses vary rapidly.

Studies in Dynamic Photoelasticity[1]

A. J. Durelli.[2] The authors should be congratulated for developing Tuzi and Nisida's method of streak photography. Fig. 7 in their paper shows a striking corroboration of the theoretical thinking on wave reflection. The streak method, however, is subjected to very important limitations. The interpretation of the fringe pattern is complicated and the coverage of the field is restricted to a thin zone. Fig. 3 shows that the authors, with their technique, have not been able to detect the wave-propagation phenomenon in a disk under impact. The reaction at the end of the diameter opposite to the one on which the impact is applied takes place when only the $1^1/_2$-order fringe appears at the point of contact, and the rest of the disk is not stressed sufficiently to produce an optical response.

The writer and some of his associates have developed, in the past year and a half, a "whole field" method of dynamic photoelasticity, in conjunction with a grid method of dynamic-strain measurements. A plastic of the epoxy family, exhibiting a low modulus of elasticity, was especially developed for this purpose, and the photographs were taken using the commercially available Fastax camera. The description of these methods will be submitted for publication shortly. An example of the results that can be obtained is shown in Fig. 1 of this discussion. The point of the disk to which the load is applied shows fringes up to the ninth order before the reaction at the other end begins to develop; and the stress distribution can be seen within the entire field of the disk. The 60-microsec interval shown in the authors' disk-streak photograph is covered by ten frames like the ones shown in the writer's figure. It is obvious that this whole-field technique allows not only a much easier interpretation of the photoelastic patterns, but also a more precise determination of the wave propagation.

Another example of the kind of work that can be conducted using this method is shown in Fig. 2 of this discussion. Here the phenomenon of wave propagation in a rectangular strut, rigidly supported at one end and under a uniformly distributed impact at the other, is illustrated. Both photoelasticity and grids were used in this study of wave propagation. Two fixed wires (shown near the center of each photograph) were placed in the field to be used as a reference for measurements and to correct for film shrinkage. Some features of the wave-propagation phenomenon can be observed in these whole-field photo-

[3] "La Distribution des Tensions autour d'un Trou de Rivet dues à un Effort appliqué sur ce Rivet," by P. S. Theocaris, Doctor's thesis presented at the University of Brussels, Belgium, in March, 1953.

[1] By M. M. Frocht and P. D. Flynn, published in the March, 1956, issue of the Journal of Applied Mechanics, Trans. ASME, vol. 78, pp. 116–122.

[2] Supervisor, Stress Analysis Section, Armour Research Foundation of Illinois Institute of Technology, Chicago, Ill. Assoc. Mem. ASME.

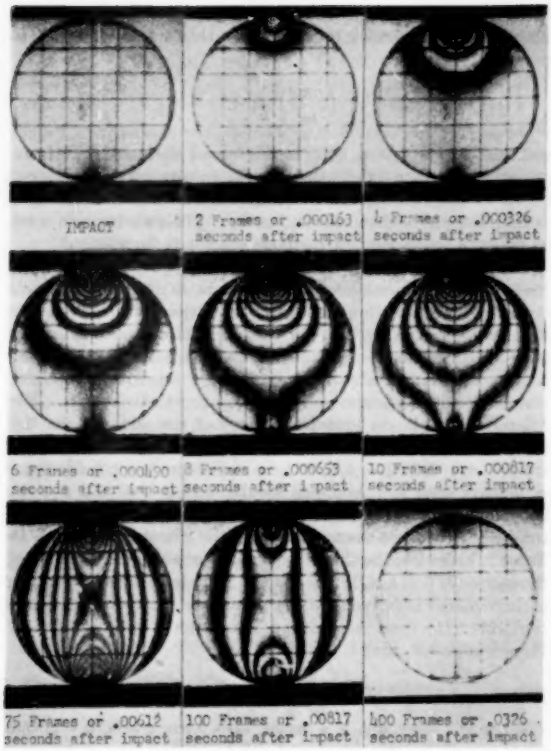
IMPACT
2 Frames or .000163 seconds after impact
4 Frames or .000326 seconds after impact
6 Frames or .000490 seconds after impact
8 Frames or .000653 seconds after impact
10 Frames or .000817 seconds after impact
75 Frames or .00612 seconds after impact
100 Frames or .00817 seconds after impact
400 Frames or .0326 seconds after impact

FIG. 1 ARALDITE EPOXY RESIN DISK 2½ IN. DIAM UNDER IMPACT OF 4-OZ WEIGHT FALLING FROM HEIGHT OF 8 IN.
(Views taken with 8-mm Fastax camera at 12240 frames per sec.)

graphs which would be missed if the streak method of photography were used. It can be seen from the photographs that the impact was essentially uniform over the width of the top end of the strut. (It should be pointed out that the irregular fringes near the bottom of the strut in the first 10 frames are caused by the dead weight of the strut.) At the beginning, the 0.5-order fringe is plane, but since the velocity of propagation of the fringe near the boundaries is higher than at the center, it becomes curved after only a few frames. It also can be observed in the photographs that the higher-order fringes do not propagate at the same velocity as the 0.5-order fringe. The photographs illustrated here show only 18 representative frames out of a total of over 300 which cover the entire event.

AUTHORS' CLOSURE

Dr. Durelli and his associates should be congratulated for having obtained very good full-image dynamic stress patterns. The claim of developing a new "whole field" method for dynamic photoelasticity can refer only to the grid aspect of the method since Perkins, in 1953, published dynamic stress patterns from photoelastic rubber taken with a Fastax camera.[2]

Dr. Durelli makes three criticisms of the method of streak

[2] "Movies of Stress Waves in Photoelastic Rubber," by H. C. Perkins, JOURNAL OF APPLIED MECHANICS, Trans. ASME, vol. 75, 1953, p. 140.

Also, in an unpublished report to the U. S. War Department, Frocht, in 1942, showed full-image dynamic stress patterns from models made of gelatin. Flynn, in 1953, obtained similar patterns from photoelastic rubber.

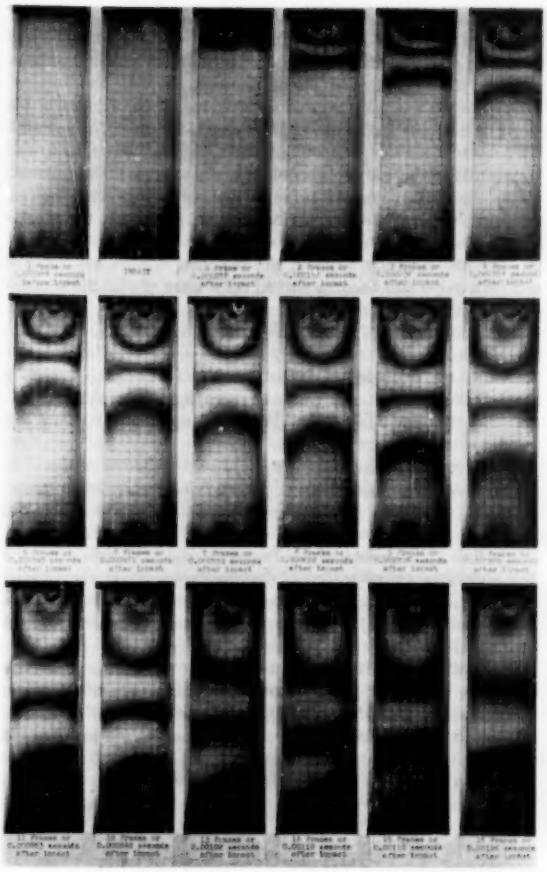

FIG. 2 ARALDITE EPOXY RESIN STRUT 6¾ IN. × 2½ IN. UNDER IMPACT OF 325-GRAM WEIGHT FALLING FROM HEIGHT OF 4 IN.
(Views taken with 8-mm Fastax camera with a 4-in. lens at a speed of 12,720 frames per sec.)

photography: (1) The interpretation of a streak photograph is complicated; (2) the coverage of the field is restricted to a thin zone; and (3) the method is less precise than full-image photography.

The first point is, in our opinion, trivial. The authors have encountered no one who has had difficulty interpreting streak photographs. Furthermore, for a given line of interest the reduction of data from a single streak photograph is, in a way, simpler than from a series of full-image photographs.

The second statement, although true for the image from one lens, is nevertheless misleading. It is possible to build cameras with more than one lens (our camera has two lenses) and to obtain simultaneous streak photographs of several lines. By repeating the experiment as many lines as needed may be covered.

Dr. Durelli seems to base his third statement, regarding precision, on the fact that in our streak photograph of the disk the maximum fringe order at the region of impact is only 1½ when the reaction on the opposite side becomes visible, whereas in his full-image photographs the corresponding fringe order is about nine. This indicates a confusion of ideas. The difference in fringe order at the region of impact has nothing to do with the method of photography. The maximum fringe order in the region of impact is a function of the optical sensitivity of the ma-

terial and of the magnitude of the force employed in impact, and not of the method of photography. Had we used a larger force or a more sensitive material, higher fringe orders would have been obtained from our disk by streak photography.

Dr. Durelli's explanation of the curving of the fringes in his stress patterns of the strut seems to us untenable. The patterns do not show surface effects but effects which penetrate to the very center of the body. Also, since surface waves are the slowest waves, the fringes should curve in a direction opposite to that obtained by Dr. Durelli experimentally. Moreover, the results from our studies with Castolite show that when the hammer and the bar are carefully aligned, the resulting fringes are straight and transverse and become curved only when the load is concentrated or in cases of misalignment.

A salient feature of streak photography is that it yields a continuous time record at extremely short exposures. Also, it is not limited to materials in which the velocity of wave propagation is low. Since the properties of wave propagation vary with the material, it is obviously desirable to have methods which are not restricted to soft materials.

Streak photography has already yielded valuable results. It provided an important tool for the study of the dynamic stress-optic law in elastic materials such as Castolite for which the Fastax camera proved inadequate. Specifically, it furnished a continuous time record of birefringence which could be related to a continuous time record of dynamic strain.[4] It also proved effective in the study of the maximum tensile stresses in beams under central impact.[5] Moreover, the method can be applied with equal ease to the study of more complicated plane structures.

Both streak and full-image photography have their place and use. It is not a matter of "either-or" but, as is generally the case in research, of judiciously utilizing the best features of all available methods which collectively are still inadequate to solve the complex problem of dynamic stresses.

Free Vibrations of Thin Cylindrical Shells Having Finite Lengths With Freely Supported and Clamped Edges[1]

G. B. WARBURTON.[2] The sources of error in deriving the frequencies of vibration of thin cylindrical shells can be divided into three types: (*a*) Approximations in the strain expressions used in the analysis; (*b*) simplifying assumptions made in the analysis; and (*c*) the use of approximate vibration forms for the shell. The effect on frequency of various small approximations in the strain expressions has been shown to be very small for most modes of practical cylinders.[3]

The writer would like to comment on the effect of the two simplifying assumptions used in the author's analysis—the assumptions that

$$\left(\frac{n\pi a}{ml}\right)^2 \ll 1$$

and that the shear term Q_ϕ/a in the second of Equations [1] can be neglected. It is difficult to differentiate between the numerical effects of the two assumptions, but the limitations of the first assumption can be demonstrated easily. (This assumption must be made, if more complex methods are not to be adopted.)

The author gives only one numerical example; it relates to a freely supported shell and the data are taken from Flügge's book.[4] Frequencies are calculated by various methods for the mode $m = 4$, $n = 1$; i.e., the number of circumferential nodes $2m = 8$ and the number of axial half waves $n = 1$. For any nodal pattern m/n there are three frequencies, f_1 ($=\omega_1/2\pi$), f_2, and f_3, of which the lowest f_1 is usually of most practical interest. For Flügge's example the lowest frequency of the shell is f_1 for the mode $m = 3$, $n = 1$. In order of ascending values of f_1 the modes are 3/1, 4/1, 5/1, 2/1, 5/2, 4/2. . . . . (Flügge was considering a cylindrical shell roof, bounded by the lines $\phi = 0$ and $\phi = \pi$. Thus only modes with nodal lines along $\phi = 0$ and $\phi = \pi$ were considered; of these the mode 4/1 has the lowest frequency.) In Table 1, herewith, the three frequencies corresponding to each of the modes 2/1, 3/1, 4/1, and 5/1 are given for Flügge's example; each frequency is derived: (*a*) By the author's method from Equation [21]; (*b*) from Arnold and Warburton's analysis;[5] (*c*) by Flügge's method using Equation [23].

TABLE 1 FREQUENCIES OF CYLINDRICAL SHELL I. VALUES OF ω ($=2\pi f$)

$a = 8.50$ m, $l = 42.30$ m, $h = 9.3$ cm, $\rho g = 2.4$ tons/cu m, $E = 210{,}000$ kg/cm^2, $\mu = 1/6$, $n = 1$

Method		Number of circumferential nodes (2m)			
		4	6	8	10
(*a*) Yu	ω_1	31.05	17.28	19.05	27.58
	ω_2	449	675	901	1128
	ω_3	781	1105	1443	1780
(*b*) Arnold and Warburton	ω_1	27.91	16.36	18.36	26.91
	ω_2	485	695	914	1138
	ω_3	805	1124	1455	1792
(*c*) Flügge	ω_1	27.91	16.36	18.36	26.91
	ω_2	485	696	918	1138
	ω_3	805	1123	1452	1792

From Table 1 it is seen that for these four modes the author's values of ω_1 are from 2.5 to 11.2 per cent higher than those derived from Flügge's or Arnold and Warburton's analyses. The good agreement between frequencies obtained by methods (*b*) and (*c*) again shows that approximations made in some small strain terms have little effect on frequency. For the higher frequencies, ω_2 and ω_3, the percentage differences between the author's values and those of either Flügge or Arnold and Warburton are smaller than the differences for ω_1. The writer considers that the value of ω_1 derived from Arnold and Warburton's equations for the mode 4/1 should be 18.36 and not 18.1 as stated by the author. It should be noted that in deriving the curves showing the variation of frequency factor $\Omega_1^{1/2}$ with nodal pattern, Arnold and Warburton have assumed that Poisson's ratio is 0.29. These curves can be used to find the frequency factors for shells of most metals, as small variations in μ have a negligible effect on frequency factor. Changing μ from 0.29 to 1/6 as in Flügge's example, the frequency factor $\Omega_1^{1/2}$ for the mode 4/1 is increased by only 0.7 per cent.

[4] "The Stress-Optic Law for Castolite Under Impact Loading," by A. A. Betser, P. D. Flynn, and M. M. Frocht, to be presented at the Ninth International Congress of Applied Mechanics, Brussels, Belgium, September 5–13, 1956.

[5] "A Photoelastic Study of Maximum Tensile Stresses in Simply Supported Short Beams Under Central Transverse Impact," by M. M. Frocht and A. A. Betser, Technical Report to the Office of Ordnance Research, U. S. Army, under Contract DA-11-022-ORD-1609, October, 1955.

[1] By Yi-Yuan Yu, published in the December, 1955, issue of the JOURNAL OF APPLIED MECHANICS, Trans. ASME, vol. 77, pp. 547–552.

[2] Lecturer, Department of Engineering, University of Edinburgh, Edinburgh, Scotland.

[3] Contribution by G. B. Warburton to discussion of "Tables for Frequencies and Modes of Free Vibration of Infinitely Long Thin Cylindrical Shells," JOURNAL OF APPLIED MECHANICS, Trans. ASME, vol. 77, 1955, pp. 135–136.

[4] "Statik und Dynamik der Schalen," by W. Flügge, Julius Springer, Berlin, Germany, 1934, pp. 227–232.

[5] "Flexural Vibrations of the Walls of Thin Cylindrical Shells Having Freely Supported Ends," by R. N. Arnold and G. B. Warburton, Proceedings of the Royal Society, London, England, series A, vol. 197, 1949, pp. 238–256.

The author's method depends on the satisfaction of the inequality

$$\left(\frac{n\pi a}{ml}\right)^2 \ll 1$$

Thus the percentage error in the frequencies given by the author's method increases as m decreases. The author writes that his method only applies to comparatively long shells with a fairly large number of circumferential waves. Possibly it is unfair to give values of frequency obtained by his method for $m = 2$ and $m = 3$, but the writer considers that for a method of analysis to have general use it should be possible to apply it to the modes 2/1 and 3/1. Although the author states that his method is applicable to comparatively long shells, it should be stated that it is only applicable to shells with axial wave lengths long compared with the radius; i.e., l/na should be large. Thus for most cylinders the frequencies of the higher modes in which there are several nodal circles along the length cannot be found accurately by his method.

For many cylinders the lowest frequency is the value of $\omega_1/2\pi$ for the mode 2/1. In Table 2 the frequency factors $\Omega_1^{1/3}$, proportional to ω_1, for a cylinder in which $l/a = 4.975$, $h/a = 0.0547$, and $\mu = 1/6$ are given; i.e., a cylinder with freely supported ends and similar to that of Flügge's example but with ratio of thickness to radius increased five times. The errors in values obtained by the author's method are slightly increased and the most important mode—that with the lowest frequency—is now 2/1, for which of course the error is greatest.

TABLE 2 FREQUENCY FACTORS $\Omega_1^{1/3}$ FOR CYLINDER II. $n = 1$

Method	Number of circumferential nodes, 2m.		
	4	6	8
(a) Yu	0.1049	0.1403	0.2464
(b) Arnold and Warburton	0.09195	0.1312	0.2367
(c) Flügge	0.09206	0.1313	0.2367

Thus the necessity of satisfying the inequality

$$\left(\frac{n\pi a}{ml}\right)^2 \ll 1$$

makes the author's method unsuitable for the accurate determination of the frequencies of many modes of all cylindrical shells, including the gravest modes for many shells. All of the foregoing calculations are for shells with freely supported ends, but the limitations associated with this assumption will be similar for the other end conditions.

One effect of the author's second assumption, that the shear term Q_ϕ/a in the second of Equations [1] can be neglected, can be seen by considering a cylindrical shell in which the axial wave length tends to infinity. For this shell the end effects can be neglected and each cross section performs the same inextensional motion. The frequency, as given by Rayleigh,[6] is

$$f = \frac{1}{2\pi}\left[\frac{Eh^2g}{12\rho a^4(1-\mu^2)}\right]^{1/2}\left[\frac{m^2(m^2-1)^2}{m^2+1}\right]^{1/2}$$

Using the frequency factor $\Omega^{1/3}$ of the paper, this can be expressed as

$$\Omega^{1/3} = k^{1/3}\frac{m(m^2-1)}{(m^2+1)^{1/3}}$$

It is possible to obtain this expression, as the limiting value of the lowest root of the frequency equation as $l/n \to \infty$, from Arnold and Warburton's theory and also from Equation [23] based on Flügge's analysis. However, from the author's analysis the corresponding expression is

$$\Omega^{1/3} = k^{1/3}\frac{m^2}{(m^2+1)^{1/3}}$$

Thus for the fundamental frequency (corresponding to $m = 2$) the author's value is 33.3 per cent too high; this error decreases rapidly as m increases. This error, which cannot be caused by the first assumption as

$$\left(\frac{n\pi a}{ml}\right)^2 = 0$$

in this case, occurs because the terms

$$\frac{h^2}{12a^2}\frac{\partial^2 v}{\partial s^2} \quad \text{and} \quad \frac{h^2}{12a}\frac{\partial^3 w}{\partial s^3}$$

in the second of Equations [2] are omitted in Equation [4]; thus it is due to neglecting the term Q_ϕ/a in the second of Equations [1]. As the axial wave length decreases from infinity, the percentage of the strain energy due to stretching increases from zero and the effect on frequency of neglecting Q_ϕ/a decreases.

The vibration form obtained by the author for shells with both ends freely supported is exact, as it satisfies the boundary conditions and the equations of motion of a shell (Equations [2]). However, the forms obtained for shells with either both ends clamped or one end clamped and the other freely supported are only approximate, as they do not satisfy Equations [2]. For these two end conditions the approximate variation of displacement along the axis of the cylinder is found to be the same as that along a beam with similar end conditions undergoing transverse vibrations. For a shell with both ends clamped Arnold and Warburton[7] assumed that the displacement along the axis had the same wave form as that of a beam with clamped ends. The good agreement between theory and experiment suggests that this assumption has little effect on computed frequencies. For shells with one end clamped and the other freely supported the assumption of similar wave forms for the shell and the corresponding beam also should have little effect on computed frequencies.

Possibly frequencies for shells with one or both ends free can be obtained by assuming the wave form in the axial direction to be the same as that of the analogous beam. However, the boundary conditions for a free end of a shell will not be satisfied by this assumption, but experience of the vibration of rectangular plates,[8] for which similar assumptions about the wave form were made and the boundary conditions were not satisfied if one or more of the plate edges was free, suggests that this method may give reasonable values for frequency.

Author's Closure

One has to realize that, from the standpoint of the linear theory of elasticity, all thin-shell theories are approximations. It is then clear that the accuracy of any problem solved on the basis of the thin-shell theory cannot be estimated accurately unless the same or a similar problem is solved, also on the basis of the theory of elasticity. For the problem of vibration of cylindrical shells, the present status of our knowledge is as follows: The frequency equation of the axisymmetrical vibration of infinitely long cylindrical shells has been obtained on the basis of the theory of elasticity by Fay,[9] with an error corrected by Herrmann-

[6] "Theory of Sound," by Lord Rayleigh, Macmillan and Co. Ltd., London, England, second edition, vol. 1, 1894, p. 417.

[7] "The Flexural Vibrations of Thin Cylinders," by R. N. Arnold and G. B. Warburton, Proceedings of The Institution of Mechanical Engineers, series A, vol. 167, 1953, pp. 62–80.

[8] "The Vibration of Rectangular Plates," by G. B. Warburton, Proceedings of The Institution of Mechanical Engineers, vol. 168, 1954, pp. 371–384.

[9] "Waves in Liquid-Filled Cylinders," by R. D. Fay, *Journal of the Acoustical Society of America*, vol. 24, 1952, pp. 459–462.

Mirsky.[10] On the basis of the thin-shell theory including the influence of transverse shear and rotational inertia, the same axisymmetrical problem has also been solved by Lin-Morgan[11] and Hermann-Mirsky.[10] The numerical data given by the latter authors indicate that, while there is a large discrepancy between the usual shell solution (not including transverse shear and rotation) and the elasticity solution for certain range of the wave length, the new shell solution (including transverse shear and rotation) shows very good agreement with the elasticity solution. However, these data are for the lowest mode only and are for a particular shell having the thickness-to-radius ratio equal to 1/30. For higher modes, for other dimensions of the shell, as well as for the more general vibration problems, it is very probable that even this new shell theory will not be accurate enough compared with the elasticity theory.

Recognizing these facts, one would not consider Mr. Warburton's comparison given in the two tables as a means of evaluating the error involved in the author's theory. Instead, the comparison shows only the difference between frequency values calculated from various approximate frequency equations. To show the comparison more effectively, the maximum percentage difference between Row (a) and Row (b) or (c) in each table and the corresponding values of $(n\pi a/ml)^2$ are computed and added to the tables as in Tables 1 and 2 (continued).

TABLE 1 (continued)

	Value of $2m$			
	4	6	8	10
Maximum percentage difference between (a) and (b) or (c)	11.2	5.6	3.8	2.5
Value of $(n\pi a/ml)^2$	0.10	0.044	0.025	0.016

TABLE 2 (continued)

	Value of $2m$		
	4	6	8
Maximum percentage difference between (a) and (b) or (c)	14.0	6.9	4.1
Value of $(n\pi a/ml)^2$	0.10	0.044	0.025

It is seen that, even when $(n\pi a/ml)^2 = 0.10$, for which the author's method was not supposed to be valid, the maximum difference is still only 14 per cent. For values of $(n\pi a/ml)^2$ below 0.05, the difference becomes even smaller and may well be neglected. Thus, on the basis of the calculations made in these tables, we see that, even if the frequency values given by Flügge's equations were exact, those computed by the author's method would still be accurate enough for engineering purposes. In fact, from the engineer's viewpoint, any inaccuracy of the method which might be reflected in these small differences would be more than compensated for by the great simplicity associated with the method, which is therefore suitable for the calculation of frequencies of cylindrical shells and is rather valuable to engineers. The simplicity of the method is also shared by the original Donnell's static equations when applied to bending and buckling problems of cylindrical shells, except that the difference between the results obtained from Donnell's and Flügge's equations for bending problems may at times be as high as 40 per cent, as was recently shown by Hoff.[12] The percentage difference between the frequencies based on the corresponding dynamic equations is thus comparatively much smaller.

[10] "Three-Dimensional and Shell Theory Analysis of Axially-Symmetric Motions of Cylinders," by G. Herrmann and I. Mirsky, Office of Scientific Research Technical Note, April, 1955.

[11] "A Study of Axisymmetric Vibrations of Cylindrical Shells as Affected by Rotatory Inertia and Transverse Shear," by T. C. Lin and G. W. Morgan, JOURNAL OF APPLIED MECHANICS, Trans. ASME, vol. 78, 1956, pp. 255–261.

[12] "The Accuracy of Donnell's Equations," by N. J. Hoff, JOURNAL OF APPLIED MECHANICS, Trans. ASME, vol. 77, 1955, pp. 329–334.

The degenerated limiting case of a shell executing inextensional vibration with a longitudinal wave of infinite length is a very special one to be chosen as a basis for comparing the equations. In this case not only the shell has to behave in the manner of a ring, but it also must be infinitely thin (to be inextensional) as well as infinitely long (to be free from boundary conditions). Some terms have to be omitted from the frequency Equations [21] and [24] for the two values of $\Omega^{1/2}$ given by Mr. Warburton to be deduced. The large discrepancy between the two values when $m = 2$ may hardly be taken as an indication of the accuracy of the original unabridged frequency equations.

The assumption

$$\left(\frac{n\pi a}{ml}\right)^2 \ll 1$$

for the freely supported case implies various conditions. How these conditions are stated depends upon which among the four parameters m, n, a, and l are involved. The parameters which are not involved are considered to be held constant. For instance, when Mr. Warburton states, "Thus the percentage error (which, by the way, should preferably be 'difference') . . . increases as m decreases," it is implied that n, a, and l are held constant, else the statement may always be shown to be untrue by increasing l or decreasing n or a. In entirely the same manner the author's statement "the method is applicable to comparatively long shells" is made, in which the only parameter concerned is l. When the parameter n is singled out, the condition is that the number of longitudinal waves should be fairly small, which was not mentioned in the preprint of the paper but was added to the paper in its final published form.[13] The statement, however, does not mean that the method is necessarily poor for large n, that is, with several or more nodal circles, for the assumption

$$\left(\frac{n\pi a}{ml}\right)^2 \ll 1$$

may still be satisfied provided that the other three parameters are of such values as to make it so. More than one parameter may be included when a condition is stated. Indeed, an example has already been given, although unknowingly, by Mr. Warburton, when he made the statement that the longitudinal wave length should be long compared with the radius, in which three parameters, n, a, and l, were involved. Similarly, we may choose m, a, and l and state that the circumferential wave length should be short compared with the length of the shell. All these should now suffice to emphasize that the primary concern of ours is

$$\left(\frac{n\pi a}{ml}\right)^2 \ll 1$$

in which the four parameters are, strictly speaking, not separable. A most complete statement would be that the circumferential wave length should be short compared with the longitudinal wave length, which is another way of stating the first and second lines of page 550. Needless to say, the present discussion applies equally well to the assumptions for the other two cases in which one or both edges of the shell are clamped.

The fact that, by the author's method, the normal functions of the shell in the longitudinal direction have been shown to be, at least approximately, the same as those for a beam may be considered as the reason why good results are obtainable by assuming so to start with. When the assumed normal functions satisfy only the boundary conditions but not the differential

[13] See p. 550, first line; also footnote 5.

equation, such as in the case of a shell with one or both edges clamped, better results may be obtained by the Galerkin method using a series of functions instead of a single-term function, and then the accuracy of the result may always be improved by taking more terms in the properly chosen series. If the boundary conditions in a problem are "natural boundary conditions," the normal functions need not even satisfy the boundary conditions if the Ritz method is used. Such is the case of cylindrical shells with one or both edges free, for the vibration problem of which the author has proposed to use normal functions of a beam with one or both ends free as normal functions for the shell in the longitudinal direction.[14] Similar procedure has been successfully applied to plate vibration problems by Young.[15]

Theoretical Determination of Rigidity Properties of Orthogonally Stiffened Plates[1]

HENRI MARCUS.[2] The purpose of the very remarkable investigations presented by the author is to demonstrate that the analysis of stress and strain in orthogonally stiffened plates is greatly simplified if the actual plate-stiffener combination can be replaced by an "equivalent" homogeneous orthotropic plate of constant thickness.

The author does not neglect to point out that the "term equivalent requires careful definition since the orthotropic plate obviously cannot be equivalent to the stiffened plate in every respect." One of the criteria of equivalency used in his analysis is based upon the equality of the strain energy of the two systems.

Considering the suitability of the proposed concept, one must keep in mind that the four rigidity constants, D_x, D_y, D_1, D_{xy}, of the homogeneous orthotropic plate have in terms of Timoshenko's notations the respective value

$$D_x = E_x' \frac{h^3}{12}, \quad D_y = E_y' \frac{h^3}{12}, \quad D_1 = E'' \frac{h^3}{12}, \quad D_{xy} = G \frac{h^3}{12} \ldots [1]$$

and that the deflection of this plate is defined by the basic equation

$$E_x' \frac{\partial^4 w}{\partial x^4} + 2(E'' + 2G) \frac{\partial^4 w}{\partial x^2 \partial y^2} + E_y' \frac{\partial^4 w}{\partial y^4} = \frac{12}{h^3} p(x,y) \ldots [2]$$

The elastic moduli E_x', E_y', E'', G are purely physical constants, depending only upon the nature of the material, whereas the rigidity constants D_x, D_y, D_1, D_{xy}, as determined by the author, are dependent not only upon the conventional modulus E and the conventional Poisson's coefficient ν, but also upon the dimensions and spacing of the stiffening ribs and, moreover, upon the span and the support conditions of the whole system.

The application of the principle of equivalent-strain energies leads to a correlation between these numerous factors and the rigidity constants D_x, D_y, D_1, D_{xy}. The equations expressing these correlations are indeed extremely complex in all cases when the spacing of the stiffening ribs is not very small as compared with the spans a and b.

On the contrary, the correlation becomes very simple if the spans are much larger than the spacing of the ribs. In such a case the same correlation has been advanced by other authors who treated the stiffened plate as a wide beam, without any reference to the equivalency of strain energies. In fact, the equations used by the author for a comparison of the theoretical with the experimental values are those so-called asymptotic relations, which are not dependent upon the size of the slab and upon the boundary conditions.

Although the difference between the two sets of values does not appear significant, the justification for substituting an orthotropic plate of constant thickness to a rib-stiffened plate would be more convincing if the tests would have shown that the slab and the ribs are subjected to strains approximately equal to those derived from the analysis of the equivalent orthotropic plate.

It may be noted that the stiffeners have, in the experiments, a spacing of $^3/_4$ in., while the specimens have a width varying between 6 and 12 in. The ratio being very small, one might wonder whether it would be correct to assume that the concept of the equivalent orthotropic plate will give sufficiently reliable results also for relatively greater spacings of the ribs.

The writer would hesitate to apply in such a case a theory, which presupposes an orthotropic material with different moduli E_x', E_y', E'', to a structure which is in reality composed of plates and beams of the same isotropic material. He would prefer to treat the problem more realistically as a problem of the coaction of plates and ribs, according to the classic methods of the theory of isotropic elasticity.

The writer wishes to commend the author for his, in many respects, excellent work. A further development of the experimental investigations covering a wide range of spacing ratios and giving more information on the effect of support conditions on both deflections and stresses is highly desirable and would enhance the merits of the whole research.

H. A. SCHADE.[3] This paper represents an interesting and important extension of previous studies concerning the use of orthotropic-plate theory in describing the behavior of orthogonally stiffened steel plates. The author takes into account the transverse and torsional stiffness of the stiffeners, which usually have been neglected in the simpler theories.

It seems apparent that the maximum uncertainty among the stiffness constants is in the value of D_{xy}. The order of magnitude of the differences among the three values (two calculated, one experimental) for each plate shown in Table 1 of the paper is small. The effect reveals itself when the usual torsion coefficient η is used, where

$$\eta = \frac{D_1 + 2D_{xy}}{\sqrt{D_x D_y}}$$

The values of η are 0.85, 0.89 and 0.84 for the first plate, and the effect of these differences in η upon strains and deflections would be considerably less than the proportionate differences themselves. For the second plate the values of η are 0.88, 0.95, and 1.095, respectively. The last value is interesting, in view of the fact that the value of η for the isotropic unstiffened plate is unity, and this is usually regarded as the upper bound for η in the simpler theories.

At any rate, as the author points out, this is primarily a plate theory, and is not applicable when beam action is predominant. Within this limitation it would be expected that η would never

[14] "Flexural Vibration of Cylindrical Shells With Free and Clamped Edges by the Ritz Method," a research proposal, by Yi-Yuan Yu, Syracuse University Research Institute, Syracuse, N. Y., 1955.

[15] "Vibration of Rectangular Plates by the Ritz Method," by Dana Young, JOURNAL OF APPLIED MECHANICS, Trans. ASME, vol. 72, 1950, pp. 448–453.

[1] By N. J. Huffington, Jr., published in the March, 1956, issue of the JOURNAL OF APPLIED MECHANICS, Trans. ASME, vol. 78, pp. 15–20.

[2] Code 6205, Mechanics Division, Naval Research Laboratory, Washington, D. C.

[3] Professor of Naval Architecture, University of California Berkeley, Calif. Mem. ASME.

depart far from unity. When this is so, as an approximation suitable for many design purposes it can be assumed equal to unity and solutions derived directly from isotropic-plate theory by making a transformation of space co-ordinates based on evaluation of D_x and D_y alone.

C. B. Smith.[4] It is well known that the rigidity properties of a rectangular plate can be considerably increased by attaching stiffeners to the plate perpendicular to an edge. To discuss theoretically the bending and buckling of such a plate is quite difficult in most cases. In the paper the author shows how to determine the rigidity constants for certain types of stiffened plates by replacing the plate-stiffener combination by an "equivalent" homogeneous orthotropic plate of constant thickness. This idea is not new. However, the author's use of this idea together with energy criterion to determine all of the rigidity constants except one, is novel and leads to good results.

It is interesting to note that the ratio a/s (the ratio of the width of the plate parallel to the stiffeners to the width of the space between adjacent stiffeners) plays an important role in the analysis. If this ratio is large the formulas developed for the various rigidity constants to be associated with the stiffened plate reduce to simple ones. Also, as the author points out, it is necessary that this ratio be fairly large in order to permit the use of an "equivalent" orthotropic plate. It seems highly probable then that unless this ratio is large enough to allow the use of the reduced formulas the orthotropic-plate theory will not apply. Hence it appears that the problem involving the bending and buckling of a stiffened plate where the ratio a/s is small (a plate with say two or three stiffeners) is one that needs more discussion. Especially is this true when the stiffeners have large cross-sectional dimensions, as in the case of plywood plates and solid-wood stiffeners.

Author's Closure

The author is deeply indebted to the discussers for their stimulating and thoughtful remarks.

The treatment of a stiffened plate as a problem of coaction of plates and ribs, as preferred by Dr. Marcus, becomes exceedingly complex as the number of stiffeners becomes large. By contrast, this is just the case when orthotropic-plate theory can be expected to give the best results.

Timoshenko's elastic moduli E_x', E_y', E'', G are purely physical constants in the case of a constant-thickness orthotropic plate but their effective values for a stiffened plate also would depend on the geometry of a repeating cross section. The constants D_x, D_y, D_{xy}, D_1 have the advantage that deflections and strains may be determined without consideration of effective thickness of the equivalent orthotropic plate. The treatment of the stiffened plate as a wide beam, which Dr. Marcus correctly attributes to other authors, leads more directly to the author's asymptotic value for D_x, but provides no information regarding the other three orthotropic constants.

The author does not believe that any difficulty will arise with larger stiffener spacings, provided that there is a sufficient number of stiffeners to satisfy the approximate homogeneity condition and that the deflection limitations of classical thin-plate theory are observed. Experimental data on bending strains were not available at the time of submission of this paper but have been reported subsequently.[5] Good agreement with theory was found for the longitudinal bending strains. The transverse bending strains in the plate between stiffeners evidence departures from orthotropic-plate theory which the author hopes to discuss in a future paper.

With respect to Dr. Schade's comments, it appears to the author that there is actually greater uncertainty as to the correct value of the constant D_1 which is a measure of the Poisson cross-contraction effect. However, both D_1 and D_{xy} influence the value of the torsion coefficient η. There are two possible explanations for the value of η greater than unity. First, this value results from use of experimentally determined values of the rigidity constants, one of which, D_1, is potentially much less accurate than the others, since it is based on the difference of approximately equal quantities. Second, the stability condition which requires that $\nu = 1/2$ be the upper bound for Poisson's ratio of an isotropic material yields the following relation when applied to an orthotropic material

$$(1 - \nu_{xy} - \nu_{xx})E_yE_x + (1 - \nu_{yy} - \nu_{yx})E_xE_x + (1 - \nu_{xx} - \nu_{xy})E_xE_y = 0$$

This expression involves six independent constants, only three of which occur in the classical thin-plate problem. While this relation alone does not set the upper bound of the Poisson's ratios of an orthotropic material, it does indicate the possibility that certain of the Poisson's ratios may exceed 0.5 and result in a value of $\eta > 1$.

Since the purpose of this investigation was to devise methods for determining the effective orthotropic constants as accurately as possible, all assumptions which would have reduced the number of independent orthotropic constants were avoided. The author agrees that in certain design applications the rigidity constants may have values such that the transformation mentioned by Dr. Schade would be useful. However, the author does not believe that boundary-value problems of orthotropic-plate theory are sufficiently more difficult than the corresponding ones of isotropic-plate theory to justify any serious approximations in this connection.

The author agrees with Dr. Smith that orthotropic-plate theory may not apply to stiffened plates if the a/s ratio (ratio of

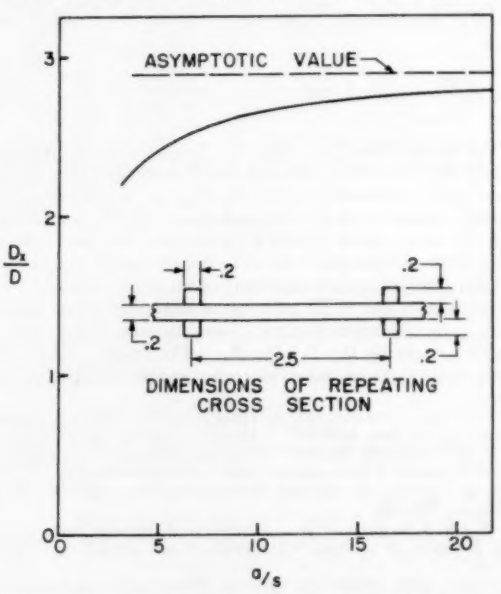

Fig. 1 Variation of Effective Flexural Rigidity With Span

[4] University of Florida, Gainesville, Fla.

[5] "A Study of Orthogonally Stiffened Plates," by W. H. Hoppmann, 2nd, N. J. Huffington, Jr., and L. S. Magness, published in this issue, pp. 343–350.

plate span in the direction of the stiffeners to the stiffener spacing) is too small to permit use of the reduced formulas, since in this event the rigidity properties are dependent on the boundary dimensions. However, as may be seen in Fig. 1 of this closure, the range of applicability of the reduced formulas is principally governed by the degree of precision required. In this figure the variation of D_x/D is plotted against the ratio a/s using values computed from Equation [8] of the paper and compared with the asymptotic value obtained using Equation [10]. These results apply only to a plate-stiffener combination having the repeating cross section shown in the figure which is composed of isotropic materials for which Poisson's ratio $\nu = 0.3$.

Although the theory ideally requires that the number of stiffeners be large, it is believed that the number may become quite small before the validity of the theory is impaired seriously. The actual minimum number of stiffeners, as well as other restrictions on this analytical procedure, can be determined only in the laboratory. Consequently, it is hoped that support can be obtained for a systematic experimental investigation of the range of applicability and the limitations of orthotropic-plate theory in the analysis of stiffened plates.

Analysis of Short Thin Axisymmetrical Shells Under Axisymmetrical Edge Loading[1]

G. D. Galletly.[2] The authors are to be congratulated on extending Geckeler's method to axisymmetrical shells. Their method should be of interest to designers of pressure vessels.

In Section 5 of their paper the authors give limitations on the latitude angle φ, but do not explain how they arrived at these limits. Presumably they made some numerical comparisons with more accurate theories. The writer feels it would be helpful if the authors would give more detail as to how they arrived at these limits, with which theories they compared their approximate method, what criterion of accuracy they were using, how many cases they investigated, and so on.

Authors' Closure

The authors thank Dr. Galletly for his generous comments. They believe, though, that the merit of the paper is due mainly to its consolidating existing methods and ideas into a convenient technique, rather than to its novelty. (There is really little in the paper that is truly new.)

The approximations involved in arriving at Equation [6a] of the text are

$$M_\theta \cos\varphi/rQ \simeq 0, \quad u \cot\varphi/w \simeq 0, \quad \nu N_x/N_\theta \simeq 0 \ldots [A1]$$

where u is the meridional displacement. The first approximation is made in the moment-equilibrium relation, the other two in the stress-strain relation. The last expression may be shown, for conical shells, to be equivalent to

$$\varphi l/\sqrt{2\lambda s} \simeq 0 \ldots [A2]$$

where s represents meridional distance from the apex, λ the meridional distance of the smaller end (of the truncated conical shell) from the apex. The approximation involved in Relations [9] of the text requires the further assumption[3] that

$$\sqrt[4]{12(1-\nu^2)}\ \sqrt{s \tan\varphi/h} \gtrsim 3 \ldots [A3]$$

This is insured by

$$\lambda \gtrsim 2.5l \ldots [A4a]$$

for the truncated cone (l refers to the smaller end), and by

$$\lambda \gtrsim 4l \ldots [A4b]$$

for the untruncated cone (λ and l now refer to the wide end).

The foregoing restrictions appear to be quite drastic, but it also appears from Hetenyi's example[4] and Galletly's[5] that some of the errors are self-canceling and that the formulas may be used safely, down to $\varphi = 45$-deg inclination.

Another question concerns the distance c from the meridional center of the virtual center of a short, cylindrical shell, with linearly varying wall thickness. Letting

$$\eta = h/h_0 = 1 + \alpha x/L \ldots [A5]$$

represent the wall-thickness variation, one obtains, by steps analogous to the case of radius variation (Equations [17], [18], [19] of the paper) that

$$c = -\alpha L/4 \ldots [A6]$$

When there is simultaneous increase of wall thickness and of radius with x, then the two effects—presumed to be small—may be superposed, and one obtains

$$c/L = -\alpha/4 - L\cos\varphi/4r_m \ldots [A7]$$

Bending Creep and Its Application to Beam Columns[1]

Yoh-Han Pao.[2] The authors are to be commended on the refreshingly simple and interesting manner in which they have presented the method of solution of the analytical problem. The experimental method of determining the creep deflection at the free end of the beam-columns by means of an electric-indicator circuit is clever and seems to be free of the faults associated with many of the earlier experimental techniques reported in the literature. The authors are, of course, also to be congratulated on the agreement between theoretical results and experimental data, at least for three of the four cases reported.

The writer was also interested in the fact that the values of the stress indexes a and n are 1.47 and 1.82, respectively, for the magnesium alloy FS1-F investigated. They are sufficiently far from unity so that the theory of viscoelasticity could not be used for this problem. In terms of viscoelasticity, Expression [5] of the paper describes a material with three retardation times, the values being zero, $^1/_3$, and infinite. Further refinement in the direction of considering additional relaxation times was apparently sacrificed in order to take care of the nonlinearity in stress.

Authors' Closure

The authors wish to thank the discusser for his comments and encouragement.

---

[1] By G. Horvay, C. E. Linkous, and J. S. Born, published in the March, 1956, issue of the Journal of Applied Mechanics, Trans. ASME, vol. 78, pp. 68–72.

[2] Shell Development Company, Emeryville, Calif. Assoc. Mem. ASME.

[3] See reference (8) of the Bibliography of the paper, p. 105.

[4] "Theory of Plates and Shells," by S. Timoshenko, McGraw-Hill Book Company, Inc., New York, N. Y., 1940, p. 359.

[5] "Influence Coefficients for Hemispherical Shells With Small Openings at the Vertex," by G. D. Galletly, Journal of Applied Mechanics, Trans. ASME, vol. 77, 1955, pp. 20–24.

[1] By L. W. Hu and N. H. Triner, published in the March, 1956, issue of the Journal of Applied Mechanics, Trans. ASME, vol. 78, pp. 35–42.

[2] Polychemicals Department, Research Division, E. I. du Pont de Nemours and Company, Wilmington, Del.

Book Reviews

High-Temperature Technology

HIGH-TEMPERATURE TECHNOLOGY. Editor-in-Chief I. E. Campbell. Sponsored by The Electrochemical Society, Inc., New York, N. Y. John Wiley & Sons, Inc., New York, N. Y. 1956. Cloth, 6 × 9 in., xiv and 526 pp., illus., $15.

REVIEWED BY B. H. SCHOFIELD[1]

THIS monograph is a collection of the recent developments and progress in the research in high-temperature technology. Presented by 35 active workers in the field, it is primarily intended to acquaint the reader with the present state of the art and the trend of future developments.

The contributors have adhered very closely to the theme. Except for portions of the materials and methods sections, consideration is given to service at temperatures in excess of 2700 F, considerably higher than the temperatures normally associated with the so-called "high-temperature alloys." Lower temperatures are discussed in these two chapters to some extent since the processing of materials for service at the extreme temperatures is done at much lower temperatures.

The book is divided into four sections: Introductory, Materials, Methods, and Measurement.

The introductory section briefly outlines the evolution of modern refractories summarizing the outstanding developments and the general philosophy and importance of high-temperature technology, a field which has received its greatest interest and activity following World War II. Also included is a brief discussion concerning the "reinforcing principle," one of the latest concepts concerning material compositions, and a short outline on the behavior of brittle-state materials.

The materials section discusses in considerable detail the various properties and characteristics of metals, oxides, carbon, and graphite, carbides, borides, silicides, nitrides, sulphides, and the hybrid cermets. Production methods and fabrication techniques are also included.

In the metals chapter there is no discussion on the vast amount of data available concerning the alloys normally referred to as the high-temperature alloys since they are definitely inferior at the temperatures concerned in this book.

Of the several metals discussed it is pointed out that four—tungsten, molybdenum, tantalum, and niobium—are sufficiently abundant and economically and physically suitable for extreme-temperature service except under oxidizing atmospheres. Recent developments in the field of protective coatings indicate that a limited number of metals or metallic alloys may be rendered useful for exposure to oxidizing conditions at temperatures in excess of 2700 F, and it is in this field that considerable attention is being focused.

Information on the strength properties of the materials is meager throughout. Modulus of elasticity, compression strength, and fatigue strength are given for some of the oxides, carbon, and cermets; however, most of the properties tabulated concern chemical, thermal, physical, and electrical properties.

The fundamentals, properties, and most promising compositions of cermets are discussed in considerable detail. No detailed data are presented, however, on the newer intermetallic materials such as the SAP (sintered aluminum powder) and aluminum-aluminum oxide types.

Fluorides, oxyfluorides, oxysulphides, and phosphides are not included due to the small amount of data presently available; however, these may be of interest as further developments are made.

In the methods section an extensive discussion of the sintering mechanism is presented. Although the process is well established it is inserted due to its close relationship to the materials technology. This is followed by a chapter on means of achieving high temperatures and the limitations of such means. Combustion-type furnaces are not included. Newer furnaces of the induction, resistor, and arc-type are presented in detail with brief mention of the conventional means of attaining high temperatures. Two relatively unfamiliar furnace types also included are: the solar furnace and the radio-frequency torch.

The final section is concerned with the various techniques and equipment for making high-temperature measurements, pyrometry, thermocouples, and the noise thermometer, which is yet in the development stage. The chapter on mechanical properties illustrates the types of apparatus employed to test properties such as creep and hot hardness. Mechanical tests to determine ductile to brittle transition are not included.

Techniques for determining physical properties are covered in the last chapter pointing out two special methods; the high-temperature microscope and the x-ray diffraction.

Each chapter of the book is followed by a notably generous list of references.

The book is an extensive study of the present state of high-temperature technology. It is of primary interest to the chemist, physicist, metallurgist, and ceramist, with particular significance to other scientific and engineering branches associated closely with the problems of high temperatures.

[1] Project Engineer, Lessells and Associates, Inc., Boston, Mass.

Plasticity

PROBLEME DER PLASTIZITÄTSTHEORIE. By William Prager. Verlag Birkhäuser, Basel, Switzerland, 1955. Cloth, 6½ × 9½ in., 100 pp., 52 figs., Fr. 12.50 (DM 12.50).

REVIEWED by PAUL M. NAGHDI[2]

THIS lucid and comprehensive presentation of numerous recent achievements in the theory of plasticity is based on a series of lectures delivered by the author at the Federal Polytechnic Institute of Zurich during November and December, 1954. Although the book is concluded with a detailed and accurate summary in English, it seems desirable to indicate briefly the nature of the topics discussed in each of the four chapters of the book: (1) The mechanical behavior of plastic solids, employing dynamic and kinematic models for the rigid, perfectly plastic and the elastic, perfectly plastic solids, as well as a discussion of the theories of plastic potential and generalized plastic potential for an elastic, perfectly plastic continuum; (2) the mechanical behavior of structures in the plastic range, together with the concepts of "load-carrying capacity" and "shake-down"; (3) methods of determining load-carrying capacity of various types of rigid, perfectly plastic structures (limit analysis); (4) finite plastic deformations, with a detailed account of the theory of plane plastic flow.

[2] Professor of Engineering Mechanics, University of Michigan, Ann Arbor, Mich. Mem. ASME.

Various features of the theories are illustrated throughout the book and several useful problems are solved. This collection of topics in the theory of perfectly plastic solids is a welcome addition to the literature on plasticity.

Mathieu Functions and Spheroidal Functions

MATHIEUSCHE FUNKTIONEN UND SPHÄROIDFUNKTIONEN. By Josef Meixner and Friedrich Wilhelm Schäfke. Springer-Verlag, Berlin, Germany, 1954. Cloth, 6 × 9 in., xii and 414 pp., 29 figs., DM 49.—; linen, DM 62.60.

REVIEWED BY ERIC REISSNER[3]

MATHIEU functions and spheroidal wave functions owe a great part of their importance to the fact that they occur in the solution of the so-called wave equation, written in terms of elliptical cylindrical co-ordinates or ellipsoid of revolution co-ordinates. As such they represent natural generalizations of trigonometric and of Bessel functions. An understanding of the properties of Mathieu functions and of spheroidal wave functions and knowledge of their numerical values allow the solution of many interesting problems in elasticity, hydromechanics, electromagnetic theory, and wave mechanics.

The object of the present book is a mathematically satisfactory, well-rounded presentation of the basic theory of these functions. In this way the foundations are being laid for further mathematical research and also for further applications. The book is divided into four chapters. The first chapter concerns itself with relatively more general mathematical developments concerning two-parameter eigenvalue problems for second-order ordinary differential equations. On the basis of these general results the authors deduce in the second and third chapters definitions, main properties, expansion theorems, addition theorems, series expansions, and integral formulas for Mathieu functions and spheroidal wave functions. The final chapter considers numerous applications which are in part new.

As far as the character of this book is concerned it should be considered as a treatise in advanced applied mathematics, more or less on the level of Morse and Feshbach's important "Methods of Theoretical Physics" but perhaps with more emphasis on mathematical rigor. The authors assume that the reader is familiar with the more important properties of Bessel and Legendre functions. Relatively minor emphasis is given to numerical methods, for which reference is made to McLachlan's "Theory and Applications of Mathieu Functions."

Altogether, the book is an authoritative and original treatment of a significant subject in applied mathematics and as such will be welcomed by all who are interested in progress in this field.

Nuclear Reactors

THERMAL POWER FROM NUCLEAR REACTORS. By A. Stanley Thompson and Oliver E. Rodgers. John Wiley & Sons, Inc., New York, N. Y., 1956. Cloth, 6 × 9 in., xiii and 229 pp., figs., $7.25.

REVIEWED BY A. ALI KHEIRALLA[4]

AS A readily assimilable introduction to the study of the engineering problems of reactor design, this book has much to recommend it. The emphasis throughout is on basic principles rather than on specific applications.

The Scylla of vague generality and the Charybdis of irrelevant detail have been largely avoided by the authors and, although extreme simplifications have been introduced in practically every section, the reader is continually apprised of the existence of difficulties and complications in a more exact treatment. The fact that the latter are not pursued is quite consistent with the introductory character of the text.

The chapter (5) on reactor materials is rather apologetic and appears to constitute a lamentation about a purported lack of progress in radiation-damage theory. It may be that this section was especially hampered by security regulations.

Of special interest to students of mechanical engineering will be the chapter on shielding of reactors and the three chapters on thermal stress, power extraction from reactors, and thermal power cycles.

The book should be quite useful as a senior or initial graduate text in nuclear engineering or as a means of orientation for newcomers to the nuclear-engineering field.

Introduction to Plasticity

INTRODUCTION TO PLASTICITY. By Aris Phillips. The Ronald Press Company, New York, N. Y., 1956. Cloth, 9 × 6 in., ix and 230 pp., illus., $7.

REVIEWED BY D. C. DRUCKER[5]

PROFESSOR J. N. Goodier in his foreword states clearly the need for and the scope of Professor Phillips' introduction to plasticity:

"Methods for making engineering calculations of stress and deformation in metal structures loaded beyond their elastic capacity have in the past 30 years, and especially in the past 10, been brought to a stage of definiteness and simplicity which recommends them strongly to practicing engineers. They can, therefore, be presented with confidence to students looking forward to professional practice in aeronautical, civil, and mechanical engineering. There is no longer any reason for letting the academic curtain fall on the subject of strength of materials without some excursion into plasticity, unless it be the obdurate but not permanently valid consideration of the perennial tightness of undergraduate engineering curricula. As the subject is now developed, no break of level need obstruct the excursion, as the reader of this book will see. His preparation need be no more than what the present orthodox undergraduate strength of materials course provides. So, if he is already a practicing engineer, he is already equipped to satisfy for himself his curiosity as to what lies further, and to add to his design resources.

"The reader will be carried forward by this book to the point where other, intermediate and advanced, works serving the needs of the research student will readily draw his further attention."

The text is divided almost half and half between what are termed one-dimensional problems and the more complicated problems of combined stress. Among the topics covered are: trusses, beams and their deflections, frames, axial force plus bending, curved bars, stress-strain relations, torsion, and collapse of structures, rotating disks, tubes, and spherical shells.

Every effort has been made to simplify the presentation by including most of the algebra and by tabulating results for numerous special cases. Even when such complex matters as stress-strain relations, uniqueness, and limit theorem proofs are discussed, elementary mathematics and descriptive material are employed rather than advanced and general techniques.

Perhaps some of the advantages gained by an elementary presentation are lost here and there in obscuring algebra. Also, the

[3] Professor of Mathematics, Massachusetts Institute of Technology, Cambridge, Mass.

[4] Lessells and Associates, Inc., Boston, Mass.

[5] Chairman, Division of Engineering, Brown University, Rhode Island. Mem. ASME.

less elegant approach seems to foster some misstatements. A few are of some importance. For example, it is not true that the collapse mode is unique, although the collapse or limit load is determined uniquely. Also, the simplest stress-strain relation based upon the Mises criterion does not really predict individual strain components very well. Hinges in structures do not necessarily form continuously and remain active; some regions may unload and behave elastically as loading proceeds.

Read with the proper attitude, however, the book under review will provide a good introduction to the simpler and the practical aspects of plastic analysis.

Design of Piping Systems

DESIGN OF PIPING SYSTEMS. By The M. W. Kellogg Company and subsidiaries. John Wiley & Sons, Inc., New York, N. Y., Second Edition, 1956. Cloth, 11 × 8 1/2 in., xiv and 365 pp., charts, tables, and illus., $15.

REVIEWED BY A. M. WAHL[6]

THE present volume, the second edition of a book published under the same title in 1941, comprises primarily a revision and enlargement of the original treatise which dealt with analytical methods of evaluating stresses, reactions, and deflections in irregular piping systems in space. This second edition has been expanded to include not only such analytical methods but also other subjects of vital interest to the piping designer, including such topics as strength and failure of materials, effects of local loadings, branch connections, expansion joints, and vibration.

Contributions to this volume were made by numerous individuals, most of them engineers of The M. W. Kellogg Company. As indicated in the preface, the objective was to supplement Code rules and other readily available information with specific mechanical-design approaches for entire piping systems and to provide background information of assistance in handling the many special situations which may occur in critical piping.

A feature of the book is a chapter by Prof. E. Orowan dealing with the strength and failure of materials. This includes treatments of plastic flow, fracture, creep and fatigue, subjects which are becoming increasingly important in the design of modern piping systems operating at elevated temperatures. Other chapters of particular interest deal with the following subjects: Design assumptions and limits; openings, branch connections, and flanges; flexibility analysis by means of analytical methods including a discussion of the utilization of electronic computers; flexibility analysis by means of model testing; expansion joints; prevention and control of vibration effects. An extensive treatment and bibliography on the history and development of piping flexibility and stress-analysis methods is given in an appendix. Lists of references given after each chapter will be helpful to readers who wish to broaden their knowledge of the subject.

Summing up, it is the reviewer's opinion that this book should be of great interest and value not only to piping designers but also to pressure-vessel designers as well.

[6] Advisory Engineer, Westinghouse Research Laboratories, Pittsburgh, Pa. Fellow ASME.

Applied Mechanics

SELECTED PAPERS ON ENGINEERING MECHANICS. A tribute to Theodore von Kármán from students and associates of the Aachen period. Editors: G. Gabrielli, F. N. Scheubel, and F. L. Wattendorf. Butterworths Scientific Publications, London, England, 1955. Cloth, 8 1/2 × 5 1/2 in., 186 pp., figs., 50s.

REVIEWED BY A. ALI KHEIRALLA[7]

THIS volume constitutes a tribute to the well-known engineer-scientist Theodore von Kármán from his students and associates of the period when he was director of the Aerodynamics Institute at the Technische Hochschule, Aachen. It was conceived by the late Dr. Bernhard G. Dirksen as an anniversary volume for Dr. von Kármán's seventieth birthday, but the former's untimely death delayed publication which was finally effected with the aid of the three editors, G. Gabrielli, F. N. Scheubel, and F. L. Wattendorf.

There are ten papers altogether including contributions from G. Gabrielli, R. Grammel, T. H. Troller, Frank L. Wattendorf, Lorenzo Poggi, F. N. Scheubel, F. Bollenrath and A. Troost, A. Betz, M. Hansen, and finally G. V. Lachmann.

The topics presented cover a wide range of interests. Included are articles on determination of wing area and aspect ratio in aircraft design; theory of self-excited unsymmetrical gyroscopes; three-dimensional flow in turbomachinery; differences between "inertial" and "gravitational" mass; subsonic flow in a supersonic region; heat exchange in blast-furnace stoves; aircraft laminarization; and the effect of size and shape on fatigue strength.

There are summaries in German and Italian at the end of each paper.

Spheroidal Functions

SPHEROIDAL WAVE FUNCTIONS Including Tables of Separation Constants and Coefficients. By J. A. Stratton, P. M. Morse, L. J. Chu, J. D. C. Little, F. J. Corbató. Published jointly by The Technology Press of M.I.T. and John Wiley & Sons, Inc., New York, N. Y., 1956. Cloth, 11 × 8 1/2 in., xiii and 613 pp., $12.50.

REVIEWED BY A. ALI KHEIRALLA[7]

THIS book consists principally of a set of tables of the coefficients in the expansions of oblate and prolate spheroidal wave functions in terms of spherical Bessel functions and associated Legendre functions. There are 550 pages of tables. These are preceded by a chapter (51 pages) by L. J. Chu and J. A. Stratton in which the properties and analytical origin of the functions are discussed. A short introduction to the tables is provided by J. D. C. Little and F. J. Corbató.

It is hoped that the appearance of reliable numerical values for these functions will encourage wider application of them in engineering problems involving spheroidal symmetry. It need hardly be mentioned that these include among others approximations to finite bars and disks *without* sharp edges.

[7] Lessells and Associates, Inc., Boston, Mass.

Announcement by the Executive Committee of the ASME Applied Mechanics Division

On Oct. 1, 1956, technical editorship of the *Journal of Applied Mechanics* will be transferred from J. M. Lessells to D. C. Drucker and Joseph Kestin of Brown University. Dr. Drucker and Dr. Kestin, as technical editors of the Journal, will take over gradually the present duties of the Editorial Board of the Applied Mechanics Division of The American Society of Mechanical Engineers.

Professor Lessells will continue as Honorary Editor, assisting the technical editors in a consulting capacity.

All papers to be sponsored by the ASME Applied Mechanics Division now should be sent to:

Technical Editors
Journal of Applied Mechanics, ASME
Division of Engineering
Brown University
Providence 12, Rhode Island